Journal of Geophysics Zeitschrift für Geophysik

Volume 53 1983

Managing Editors

W. Dieminger, G. Müller, J. Untiedt

Editorial Board

K.M. Creer Edinburgh, Scotland
W. Dieminger Lindau, F.R.G.
C. Kisslinger Boulder, Colorado
Th. Krey Hannover, F.R.G.
G. Müller Frankfurt, F.R.G.
G.C. Reid Boulder, Colorado
U. Untiedt Münster, F.R.G.
S. Uyeda Tokyo, Japan

Advisory Board

G. Angenheister, München
A.A. Ashour, Cairo
H.-J. Burkhardt, Berlin
K. Fuchs, Karlsruhe
N. Fukushima, Tokyo
H. Gebrande, München
V. Haak, Berlin
W. Jacoby, Frankfurt a.M.
T. Kirsten, Heidelberg
I.P. Kosminskaja, Moskwa
G. Kremser, Katlenburg-Lindau
W. Lowrie, Zürich
St. Müller, Zürich
F. Neubauer, Köln
H. Neugebauer, Clausthal-Zellerfeld
F. Rummel, Bochum
S. Saxov, Aarhus
U. Schmucker, Göttingen
M. Siebert, Göttingen
H. Soffel, München
H. Stiller, Potsdam
P. Weidelt, Hannover
J. Zschau, Kiel

Springer International

Journal of Geophysics – Zeitschrift für Geophysik

This journal was founded by the Deutsche Geophysikalische Gesellschaft on the initiative of L. Mintrop in 1924 as the Zeitschrift für Geophysik and edited by G. Angenheister from Vol. 1–18 (1944). It reappeared in 1954 edited by B. Brockamp from Vol. 19–26 (1960), and edited by W. Dieminger from Vol. 27–33 (1961), and from Vol. 34 (1968) edited by W. Dieminger and J. Untiedt. After Vol. 40 (1970) the title was changed to Journal of Geophysics – Zeitschrift für Geophysik.

Published: Vols. 19–39 by Physica-Verlag, Würzburg, from Vol. 40 by Springer Berlin, Heidelberg, New York, Tokyo.

Copyright

Submission of a manuscript implies that the work described has not been published before (except in the form of an abstract or as part of a published lecture, review or thesis), that it is not under consideration for publication elsewhere, that its publication has been approved by all the authors and by the responsible authorities – tacitly or explicitly – in the laboratories where the work was carried out and that, if accepted, it will not be published elsewhere in the same form, in either the same or another language, without the consent of the copyright holders. By submitting a manuscript, the authors agree that the copyright for their article is transferred to the publisher if and when the article is accepted for publication. The copyright covers the exclusive rights to reproduce and distribute the article, including reprints, photographic reproductions, microform, electronic data-base, video-disks, or any other reproductions of similar nature, and translations.

Photographic reproduction, microform, electronic data-base, video-disks, or any other reproduction of text, figures, or tables from this journal is prohibited without permission obtained from the publisher.

The use of general descriptive names, trade names, trade marks, etc., in this publication, even if the former are not specifically identified, is not to be interpreted as exempt from the relevant protective laws and regulations and may accordingly be used freely by anyone.

Special Regulations for the USA

The Article Fee Code on the first page of an article in this journal indicates the copyright owner's consent that in the USA copies may be made for personal or internal use, provided the stated fee for copying beyond that permitted by Section 107 or 108 of the United States Copyright Law is paid through the Copyright Clearance Center, Inc., 21 Congress Street, Salem, Mass. 01970, USA.

If a code does not appear, copies of the article may be made without charge, provided permission is obtained from the publisher.

The copyright owner's consent does not extend to copying for general distribution, for promotion, for creating new works, or for resale. Specific written permission must be obtained from the publisher for such copying.

Other Regulations

Authors of this journal can benefit from library and photocopy fees collected by VG WORT if certain conditions are met. If an author lives in the Federal Republic of Germany or in West Berlin it is recommended that he contact Verwertungsgesellschaft WORT, Abteilung Wissenschaft, Goethestraße 49, D-8000 München 2, for detailed information.

Springer-Verlag Berlin Heidelberg New York Tokyo

Printed in Germany by Universitätsdruckerei H. Stürtz AG Würzburg

© Deutsche Geophysikalische Gesellschaft, Clausthal-Zellerfeld, 1983

Author Index

Arnason, K. 16

Baumjohann, W. 182, 198
Beblo, M. 16
Björnsson, A. 16

Červený, V. 1
Christensen, U. 201
Constable, S.C. 52

Fowler, A.C. 42, 203

Hayakawa, M. 59
Hussain, A.G. 131

Jones, A.G. 72

Kaila, K.U. 182
Kangas, J. 182
Kanngieser, E. 24
Kapička, Aleš 144
Kessels, W. 163
Kind, R. 127

McFadden, P.L. 52
Mohan, N.L. 34
Müller, T. 155

Nevanlinna, H. 149

Odom, R.I. 127
Ohtsu, J. 59

Pellinen, R.J. 182, 198
Pšenčik, I. 1

Ranta, H. 182
Raspopov, O.M. 182

Sergeev, V.A. 182
Seshagiri Rao, S.V. 34
Starkov, G.V. 198
Stein, B. 16
Sundararajan, N. 34

Torge, W. 24
Třísková, L. 68

Uspensky, M.V. 198

Veitch, R.J. 141

Watermann, J. 74
Wolfgram, P. 16

Yahnin, A.G. 182
Yoshida, T. 59

Zürn, W. 155

Subject Index

Archaeomagnetism

Archaeomagnetic Investigations in Egypt: Inclination and Field Intensity Determinations (Hussain A.G.) 131

Aurora

Substorm Time Sequence and Microstructure on 11 November 1976 (Yahnin, A.G., et al.) 182

Auroral Electrojets

A Case Study of the Response of the Magnetosphere to Changes in the Interplanetary Medium (Rostocker, G., et al.) 170

Substorm Time Sequence and Microstructure on 11 November 1976 (Yahnin, A.G., et al.) 182

Borehole Measurements

Determination of the Steady State Temperature Gradient and of the Thermal Diffusivity in a Shallow Borehole near Braunschweig (F.R.G.) (Kessels, W.) 163

Coil Systems

On the Generation of Almost Uniform Magnetic Fields Inside Solenoids (Watermann, J.) 74

Data Analysis

The Estimation and Removal of a Linear Drift from Stacked Data (McFadden, P.L., Constable, S.C.) 52

Drift Removal

The Estimation and Removal of a Linear Drift from Stacked Data (McFadden, P.L., Constable S.C.) 52

Earth's Mantle

On the Thermal State of the Earth's Mantle (Fowler, A.C.) 42

Comments on "On the Thermal State of the Earth's Mantle" by A.C. Fowler (Christensen, U.) 201

Reply (Fowler, A.C.) 203

Egypt

Archaeomagnetic Investigations in Egypt: Inclination and Field Intensity Determinations (Hussain, A.G.) 131

Geomagnetic Field

The 1977–1979 Geomagnetic Impulse: Its Induction Effect and Dependence on Magnetic Activity (Nevanlinna, H.) 149

Geothermal Field

Determination of the Steady State Temperature Gradient and of the Thermal Diffusivity in a Shallow Borehole near Braunschweig (F.R.G.) (Kessels, W.) 163

Gravity

Gravity and Height Variations Connected with the Recent Rifting Process in Northern Iceland 1975–1981 (Torge, W., Kanngieser, E.) 24

Observation of Gravity Changes During the Passage of Cold Fronts (Müller, T., Zürn, W.) 155

Gravity Anomalies

Gravity Interpretation of Two Dimensional Fault Structures Using Hilbert Transforms (Sundararajan, N., et al.) 34

Iceland

Electrical Conductivity Beneath Iceland – Constraints Imposed by Magnetotelluric Results on Temperature, Partial Melt, Crust- and Mantle Structure (Beblo, M., et al.) 16

Gravity and Height Variations Connected with the Recent Rifting Process in Northern Iceland 1975–1981 (Torge, W., Kanngieser, E.) 24

Interplanetary Magnetic Fields

foF2 Response to IMF Sector-Boundary Crossings (Třísková, L.) 68

A Case Study of the Response of the Magnetosphere to Changes in the Interplanetary Medium (Rostocker, G., et al.) 170

Substorm Time Sequence and Microstructure on 11 November 1976 (Yahnin, A.G., et al.) 182

Ionosphere

foF2 Response to IMF Sector-Boundary Crossings (Třísková, L.) 68

Magnetic Fields

On the Generation of Almost Uniform Magnetic Fields Inside Solenoids (Watermann, J.) 74

Magnetotellurics

Electrical Conductivity Beneath Iceland – Constraints Imposed by Magnetotelluric Results on Temperature, Partial Melt, Crust- and Mantle Structure (Beblo, M., et al.) 16

On the Equivalence of the "Niblett" and "Bostick" Transformations in the Magnetotelluric Method (Jones, A.G.) 72

Radar Aurora

Experimental Data on Electric Field and Electron Density Dependence of Auroral E-Region Drift Turbulence and Radar Backscatter (Uspensky, M.V., et al.) 198

Rock Magnetism

Magnetostatic Energy of Spherical Two-Domain Particles and the Upper Single-Domain Particle Size in Magnetite (Veitch, R.J.) 141

Irreversible Changes of Anisotropy of Magnetic Susceptibility of Rocks due to Uniaxial Pressure (Kapička, Al.) 144

Seismic Waves

Gaussian Beams and Paraxial Ray Approximation in Three-Dimensional Elastic Inhomogeneous Media (Červený, V., Pšenčik, I.) 1

Improvements to Layer Matrix Methods (Kind, R., Odom, R.I.) 127

Substorms

A Case Study of the Response of the Magnetosphere to Changes in the Interplanetary Medium (Rostocker, G., et al.) 170

Substorm Time Sequence and Microstructure on 11 November 1976 (Yahnin, A.G., et al.) 182

VLF Emissions

A Study of the Mechanism of Whistler-Triggered VLF Emissions (Yoshida, T., et al.) 59

Whistlers

A Study of the Mechanism of Whistler-Triggered VLF-Emissions (Yoshida, T., et al.) 59

Book Reviews 77, 78, 79, 80, 206, 207

8° Z Nat. 2148
Z 4137 G4

Journal of Geophysics Zeitschrift für Geophysik

Volume 53 Number 1 1983

Original Investigations

V. Červený, I. Pšenčik
Gaussian Beams and Paraxial Ray Approximation in Three-Dimensional Elastic Inhomogeneous Media **1**

M. Beblo, A. Björnsson, K. Arnason, B. Stein, P. Wolfgram
Electrical Conductivity Beneath Iceland – Constraints Imposed by Magnetotelluric Results on Temperature, Partial Melt, Crust- and Mantle Structure **16**

W. Torge, E. Kanngieser
Gravity and Height Variations Connected with the Recent Rifting Process in Northern Iceland 1975–1981 **24**

N. Sundararajan, N.L. Mohan, S.V. Seshagiri Rao
Gravity Interpretation of Two Dimensional Fault Structures Using Hilbert Transforms **34**

A.C. Fowler
On the Thermal State of the Earth's Mantle **42**

P.L. McFadden, S.C. Constable
The Estimation and Removal of a Linear Drift from Stacked Data **52**

T. Yoshida, J. Ohtsu, M. Hayakawa
A Study of the Mechanism of Whistler-Triggered VLF Emissions **59**

L. Třísková
foF2 Response to IMF Sector-Boundary Crossings **68**

Letter to the Editor

A.G. Jones
On the Equivalence of the "Niblett" and "Bostick" Transformations in the Magnetotelluric Method **72**

Short Communication

J. Watermann
On the Generation of Almost Uniform Magnetic Fields Inside Solenoids **74**

Book Reviews **77, 78, 79, 80**

Indexed in Current Contents

Evaluated for Physics Briefs and INKA-PHYS data base

1-3, t, i

Springer International

252 J. Geophys. — ISSN 0340-062X — JGEOD4 53(1) 1–80 (1983) — July 1983

27. Juli 1983
Niedersächsische Staats- und Universitätsbibliothek Göttingen

SD1

Journal of Geophysics – Zeitschrift für Geophysik

Edited for the **Deutsche Geophysikalische Gesellschaft** by **W. Dieminger, G. Müller, and J. Untiedt**

This journal was founded by the Deutsche Geophysikalische Gesellschaft on the initiative of L. Mintrop in 1924 as the Zeitschrift für Geophysik and edited by G. Angenheister from Vol. 1–18 (1944). It reappeared in 1954 edited by B. Brockamp from Vol. 19–26 (1960), and edited by W. Dieminger from Vol. 27–33 (1961), and from Vol. 34 (1968) edited by W. Dieminger and J. Untiedt. After Vol. 40 (1970) the title was changed to Journal of Geophysics – Zeitschrift für Geophysik.

Published: Vols. 19–39 by Physica-Verlag, Würzburg, from Vol. 40 by Springer-Verlag GmbH & Co. KG Berlin, Heidelberg, New York.

Manuscripts may be addressed to any of the Editors. For addresses see last cover page. Manuscripts should conform with the journal's accepted practice as described in the Instructions to Authors.

The Journal accepts

- Review Articles (invited by the Editors)
- Original Papers
- Short Communications
- Letters to the Editors
- Book Reviews

in the field of Geophysics and Space Physics.

Copyright

It is a fundamental condition that submitted manuscripts have not been published and will not be simultaneously submitted or published elsewhere. By submitting a manuscript, the authors agree that the copyright for their article is transferred to the publisher if and when the article is accepted for publication. The copyright covers the exclusive rights to reproduce and distribute the article, including reprints, photographic reproductions, microform or any other reproductions of similar nature, and translations. Photographic reproduction, microform, or any other reproduction of text figures, or tables from this journal is prohibited without permission obtained from the publisher.

The use of general descriptive names, trade names, trade marks, etc., in this publication, even if the former are not specifically identified, is not to be interpreted as exempt from the relevant protective laws and regulations and may accordingly be used freely by anyone.

Special Regulations for the USA

Photocopies may be made for personal or internal use beyond that permitted by Section 107 or 108 of the U.S. Copyright Law, provided a fee is paid. This fee is $0.20 per page or a minimum of $1.00 if an article consists of less than five pages. Please pay this fee to the Copyright Clearance Center, Inc., 21 Congress Street, Salem, MA 01970, USA, stating the ISSN 0340-062X, volume, and first and last page numbers of each article copied.

The copyright owner's consent does not extend to copying for general distribution, for promotion, for creating new works, or for resale. Specific written permission must be obtained from the publisher for such copying.

Other Regulations

Authors of this journal can benefit from library and photocopy fees collected by VG WORT if certain conditions are met. If an author lives in the Federal Republic of Germany or in West Berlin it is recommended that he contact Verwertungsgesellschaft WORT, Abteilung Wissenschaft, Goethestraße 49, D-8000 München 2, for detailed information.

Subscription Information

Volumes 53 + 54 (3 issues each) will appear in 1983. The price of a volume is DM 168,00 or $70.00. Prices for backvolumes are available on request. Correspondence concerning subscriptions should be addressed to the publisher.

Members. Members of the Deutsche Geophysikalische Gesellschaft are entitled to purchase the Journal for their own use at a privilege price of DM 98,00 payable with the Membership dues . Orders should be sent to the Society's office at the following address: Postfach 230, D-3392 Clausthal-Zellerfeld.

North America. Annual subscription rate: $149.00, including carriage charges. Subscriptions are entered with prepayment only. Orders should be addressed to:
Springer-Verlag New York Inc.
Journal Sales Department
44 Hartz Way
Secaucus, NJ 07094, USA
Tel. (201) 348-4033, Telex 0023-125994.

All Other Countries. Annual subscription rate: DM 336,00, plus carriage charges. Airmail delivery on request only. For *Japan,* carriage charges (Surface Airmail Lifted) are DM 45,60; for *India* DM 36,60. Single issue price: DM 67,20 plus carriage charges. Orders can either be placed with your bookdealer or sent directly to:
Springer-Verlag
Heidelberger Platz 3
D-1000 Berlin 33
Tel. (0)30/8207-1, Telex 1-83319.

Changes of Address: Allow six weeks for all changes to become effective. All communications should include both old and new addresses (with Postal Codes) and should be accompanied by a mailing label from a recent issue.

Microform: Microform editions are available from:
University Microfilms International
300 N. Zeeb Road
Ann Arbor, MI 48106, USA

Production

Springer-Verlag
Journal Production Department II
Postfach 105280
D-6900 Heidelberg 1
Federal Republic of Germany
Tel. (0)6221/487-339, Telex 4-61690.

Responsible for Advertisements

Springer-Verlag
G. Sternberg
Kurfürstendamm 237
D-1000 Berlin 15
Tel. (0)30/8821031, Telex 1-85411.

Das Heft enthält eine Beilage des Springer-Verlages Berlin Heidelberg NewYork Tokyo

Springer International

Printers

Universitätsdruckerei H. Stürtz AG Würzburg

© the Deutsche Geophysikalische Gesellschaft, Clausthal-Zellerfeld, 1983

Printed in Germany

J Geophys (1983) 53:1–15

Journal of Geophysics

Gaussian Beams and Paraxial Ray Approximation in Three-Dimensional Elastic Inhomogeneous Media

V. Červený [1] and I. Pšenčík [2]

[1] Institute of Geophysics, Charles University, Ke Karlovu 3, 12116 Praha 2, Czechoslovakia
[2] Geophysical Institute, Czechoslovakian Academy of Sciences, Boční II, 14131 Praha 4, Czechoslovakia

Abstract. The elastodynamic Gaussian beams in 3D elastic inhomogeneous media are derived as asymptotic high-frequency one-way solutions of the elastodynamic equation concentrated close to rays of *P* and *S* waves. In this case, the elastodynamic equation is reduced to a parabolic (Schrödinger) equation which further leads to a matrix Riccati equation and the transport equation. Both these equations can be simply solved along the ray, the first numerically and the other analytically. The amplitude profile of the principal displacement component of the elastodynamic Gaussian beams is Gaussian in the plane perpendicular to the ray, with its maximum at the ray. The Gaussian beams are regular along the whole ray, even at caustics. As a limiting case of infinitely broad Gaussian beams, the paraxial ray approximation is obtained. The properties and possible applications of Gaussian beams and paraxial ray approximations in the numerical modelling of seismic wave fields in 3D inhomogeneous media are discussed.

Key words: Seismic waves – 3D elastodynamic equation – Paraxial ray approximation – Riccati equation – Elastodynamic Gaussian beams

Introduction

To solve various problems of 2D and 3D structural seismology, the high-frequency asymptotic methods, such as the ray method and its modifications, have been found very useful. Numerical procedures and program packages to evaluate rays, travel-times, ray amplitudes and ray synthetic seismograms in rather general 2D media have been developed. These programs, however, have certain limitations regarding their accuracy in singular regions, sensitivity to the fine details of the medium, etc. Moreover, the generalization of the 2D methods to 3D structures is not straightforward, mainly due to difficulties with the time-consuming two point ray tracing.

A powerful generalization of the ray method, based on the procedure of Gaussian beams, was suggested recently. This procedure combines the broad possibilities of the ray method and the accuracy of wave methods. The Gaussian beams represent high-frequency asymptotic solutions of the wave (or elastodynamic) equation, which are concentrated close to rays of *P* or *S* waves. Their properties along the ray are controlled by the parabolic (Schrödinger) equation. The distribution of the amplitude of the principal component of the displacement of the beam in the profile perpendicular to the ray is bell-shaped (Gaussian). The Gaussian beams are regular along the whole ray, even at caustics.

The basic concepts of the solution of the wave equation concentrated close to rays were first suggested by Babich (1968). For other details and references see Babich and Buldyrev (1972), Babich and Kirpichnikova (1979), Červený et at. (1982b). These references consider only the scalar Gaussian beams, which are asymptotic solutions of the scalar wave equation. In seismology, however, we are interested in the solutions of the elastodynamic equation. The high-frequency vectorial solutions of the elastodynamic equation concentrated close to rays of *P* and *S* waves were first investigated from a mathematical point of view by Kirpichnikova (1971), see also Popov (1982). In this paper, we are interested mainly in the seismological aspects of the Gaussian beams and in their relationship to the ray method. Our presentation follows mainly the paper by Červený and Pšenčík (1983) in which the elastodynamic Gaussian beams in two-dimensional elastic inhomogeneous media were investigated. Here the results of that paper are generalized for three-dimensional media. Note that scalar acoustic beams in 3D media were investigated by Babich and Popov (1981).

Gaussian beams can find various applications both in structural seismology and in the investigation of seismic sources. In seismology, as in other branches of physics, the Gaussian beams themselves, as a physical reality, may play an important role. They can, however, also be used to simulate complete wave fields generated by various seismic sources. In the latter case, the complete wave field is evaluated as an integral superposition of Gaussian beams, the relevant integrals being valid asymptotically (for high frequencies). The procedure is as follows: the wave field generated by a source is expanded into Gaussian beams. Each beam is continued along a ray. The properties of Gaussian beams vary along the ray due to diffusion, spreading, and reflection/transmission at interfaces. The final wave field at any point of the medium is then obtained as a superposition of all beams passing in some neighbourhood of the receiver. The procedure based on the

Gaussian beams removes most of the difficulties of the ray method: a) It is uniformly valid everywhere. The singularities at caustics are removed automatically as the Gaussian beams are regular along the whole ray. The integral superposition of beams removes most of the remaining singularities of the wave field associated with interfaces (critical region, etc.). b) The procedure is not so sensitive to the details of the medium as the ray method, mainly due to some frequency-dependent smoothing effect contained in the expansion integrals. c) The procedure does not require the time-consuming two-point ray tracing. As soon as a sufficiently dense system of supporting Gaussian beams covering a region is evaluated, the wave field at any point of this region can be obtained very efficiently, practically without any additional effort.

The procedure based on Gaussian beams may be applied both in the frequency domain and in the time domain. Several approaches can be used to rewrite the final expressions for the wave field from the frequency domain to the time domain. The most efficient of these approaches to evaluating the synthetic seismograms is based on the procedure of wave packets, which propagate along rays. For a detailed description of the evaluation of synthetic seismograms in laterally varying layered structures using the Gaussian beam method see Červený (1983).

The Gaussian beam approach is closely connected with the so-called dynamic ray tracing and the paraxial ray approximation. The paraxial ray approximation offers a possibility to evaluate the travel-time field and ray amplitudes not only directly on the ray (as in the standard ray method) but also in its close neighbourhood. Thus, when we wish to determine the travel-times and ray amplitudes at any point A close to the ray Ω, it is not necessary to seek a new ray which passes through A; the wave field at A can be computed directly from the quantities determined along the ray Ω. The two-point ray tracing is not involved in the procedure. The paraxial ray approximation, however, does not remove the singularities of the ray field, as is done in the Gaussian beam approach. Contrary to the Gaussian beam approach, however, the complete wave field at A is obtained directly, not by expansion integrals. Various modifications of the paraxial ray approximations are possible, see details in Červený (1983). The application of the paraxial ray approximation substantially increases the efficiency of the ray methods. In a 2D medium, it considerably decreases the computing time necessary to evaluate synthetic seismograms. However, it will find applications mainly in 3D media, where the cumbersome and time consuming procedures of two-point ray tracing have prevented the development of effective programs for synthetic seismograms. Program packages based on the paraxial ray approximation are now available to evaluate the synthetic seismograms for 3D media, even if the source is situated outside the profile, see Klimeš (1982a), Červený et al. (1982a). Similarly as in the Gaussian beam approach, the ray synthetic seismograms at any point of a region D on the Earth's surface can be computed easily by the paraxial ray approximation as soon as a system of supporting rays is evaluated which covers the region D at the Earth's surface with a sufficient density.

The above applications of Gaussian beams and paraxial ray approximations show the importance of these approaches. Before they can be fully realized, a detailed study of the behaviour of individual Gaussian beams and paraxial ray approximations must be performed.

In this paper, we study the 3D elastodynamic Gaussian beams and paraxial ray approximations in smooth, infinite 3D inhomogeneous media without interfaces. The behaviour of Gaussian beams and of the paraxial ray approximation in 3D media with curved interfaces will be described elsewhere.

Three-Dimensional Elastodynamic Equation in Ray-Centred Coordinates

Let us consider an isotropic medium described by the Lamé elastic parameters λ and μ and by the density ρ. We assume that λ, μ and ρ are continuous functions of coordinates together with at least the first and the second spatial derivatives.

We shall investigate the solutions of the elastodynamic equation which are concentrated close to a ray of a P or an S wave. For such a purpose it is very useful to introduce a special system of coordinates, which is centred at the specified ray. In the first part of this section, we shall introduce the ray centred coordinate system (s, n, m) and in the second part, we shall express the elastodynamic equation in these coordinates.

Ray-Centred Coordinate System

We consider an arbitrary ray Ω corresponding to a compressional (P) or a shear (S) wave and introduce an orthogonal coordinate system (s, n, m) connected with this ray. The coordinate s measures the arclength along the ray from an arbitrary reference point, n and m form a 2D Cartesian coordinate system in the plane perpendicular to Ω at s, with origin at Ω. In the coordinate system (s, n, m), the equation of the ray Ω is $n=m=0$. The vector basis of the coordinate system is formed by a right-handed system of three unit vectors $\mathbf{t}, \mathbf{e}_n, \mathbf{e}_m$, where $\mathbf{t}$ is the unit tangent to the ray Ω and the vectors $\mathbf{e}_n$ and $\mathbf{e}_m$ are perpendicular to the ray Ω. They are introduced in such a way as to make the ray centred coordinate system orthogonal. It was shown by Popov and Pšenčík (1978a, 1978b) that this condition was satisfied when the vectors $\mathbf{e}_n$ and $\mathbf{e}_m$ were introduced as follows:

$$\mathbf{e}_n = \mathbf{n}\cos\theta - \mathbf{b}\sin\theta, \qquad \mathbf{e}_m = \mathbf{n}\sin\theta + \mathbf{b}\cos\theta, \tag{1}$$

where $\mathbf{n}$ is the unit normal and $\mathbf{b}$ the unit binormal to the ray Ω and $\theta(s) = \int_{s_0}^{s} T(\zeta)\,d\zeta + \theta(s_0)$, T being the torsion of the ray. The integral in the expression for $\theta(s)$ is taken along the ray Ω, s_0 denotes the s-coordinate of a reference point on the ray Ω. The orientation of the mutually perpendicular unit vectors $\mathbf{e}_n, \mathbf{e}_m$ in the plane perpendicular to the ray Ω is controlled by the angle $\theta(s_0)$, which may be chosen arbitrarily.

We shall denote by V_P and V_S the velocities of compressional (P) and shear (S) waves, respectively,

$$V_P(s,n,m)=\left(\frac{\lambda+2\mu}{\rho}\right)^{1/2}, \qquad V_S(s,n,m)=\left(\frac{\mu}{\rho}\right)^{1/2}. \tag{2}$$

Similarly as λ, μ and ρ, the velocities of P and S waves, V_P and V_S, are smooth functions of coordinates s, n, m. In the following equations, we shall often use the velocities of P and S waves directly at the ray Ω, i.e. $V_P(s,0,0)$ and $V_S(s,0,0)$. To simplify the equations, we shall use special symbols for these quantities,

$$\alpha(s)=V_P(s,0,0), \qquad \beta(s)=V_S(s,0,0). \tag{3}$$

A similar notation will be used even for the partial derivatives of V_P and V_S in the direction perpendicular to the ray,

$$\alpha_{,n}(s)=\left[\frac{\partial V_P(s,n,m)}{\partial n}\right]_{n=m=0}, \qquad \beta_{,n}(s)=\left[\frac{\partial V_S(s,n,m)}{\partial n}\right]_{n=m=0}, \tag{4a}$$

$$\alpha_{,nm}(s)=\left[\frac{\partial^2 V_P(s,n,m)}{\partial n\,\partial m}\right]_{n=m=0}, \qquad \beta_{,nm}(s)=\left[\frac{\partial^2 V_S(s,n,m)}{\partial n\,\partial m}\right]_{n=m=0} \tag{4b}$$

(and similarly for $\alpha_{,m}$, $\alpha_{,nn}$, $\alpha_{,mm}$, $\beta_{,m}$, $\beta_{,nn}$, $\beta_{,mm}$).

Thus, all the quantities denoted by symbols with α or β are functions of s only, not of n and m.

In this section and the two following we shall not specify whether the considered ray corresponds to a P wave or an S wave, all the equations in these sections are valid for both waves. The specification will be done only in the fifth section. Therefore, we introduce a special symbol $v(s)$ for the velocity of propagation along the ray Ω. If the ray corresponds to a P wave, we put

$$v=\alpha, \qquad v_{,n}=\alpha_{,n}, \qquad v_{,nm}=\alpha_{,nm}, \quad \text{etc.} \tag{5}$$

Similarly, if the ray Ω corresponds to an S wave, we put

$$v=\beta, \qquad v_{,n}=\beta_{,n}, \qquad v_{,nm}=\beta_{,nm}, \quad \text{etc.} \tag{6}$$

We should also use a special notation for $\rho(s,0,0)$, the density measured directly at the ray Ω. However, we shall use only one symbol ρ for the density throughout the paper, both for $\rho(s,0,0)$ and for $\rho(s,n,m)$. Note that any ρ in this and the next two sections has the meaning of $\rho(s,n,m)$ and any ρ in other sections denotes $\rho(s,0,0)$.

In the ray-centred coordinate system (s,n,m), we can write for the infinitesimal length element dr the expression

$$dr^2=\mathbf{dr}\cdot\mathbf{dr}=h^2\,ds^2+dn^2+dm^2, \tag{7}$$

where h is given by the formula

$$h=1+v^{-1}v_{,n}n+v^{-1}v_{,m}m, \tag{8}$$

see Popov and Pšenčík (1978a, 1978b), Červený and Hron (1980). Equation (7) shows that the ray-centred coordinate system (s,n,m) is orthogonal, with the scale factors

$$h_s=h, \qquad h_n=1, \qquad h_m=1. \tag{9}$$

In the case when the ray Ω is curved, the perpendicular planes to Ω intersect at certain distances from Ω. In other words, the ray centred coordinate system (s,n,m) is not regular at large distances from Ω. In the following, we shall consider only a region along Ω, in which the ray-centred coordinate system (s,n,m) is regular, and we shall call it the regularity region.

Elastodynamic Equation in Ray-Centred Coordinates

Consider a right-handed orthogonal curvilinear coordinate system c_1, c_2, c_3 and denote the corresponding scale factors by h_1, h_2, h_3. (We shall write all indices as subscripts.) The displacement components in a coordinate system c_1, c_2, c_3 are denoted by $u_1(x_i,t)$, $u_2(x_i,t)$, $u_3(x_i,t)$. The elastodynamic equation can be then written in the following form (Aki and Richards, 1980),

$$\rho\frac{\partial^2\mathbf{u}}{\partial t^2}=\frac{1}{h_1h_2h_3}\sum_{p=1}^{3}\sum_{q=1}^{3}\frac{\partial}{\partial c_q}(\tau_{pq}\mathbf{n}_p h_1h_2h_3/h_q). \tag{10}$$

In (10), t is the time and the other symbols have the following meaning:

$$\tau_{pq}=\lambda\delta_{pq}\Theta+2\mu e_{pq}, \qquad \Theta=\sum_{r=1}^{3}e_{rr},$$

$$e_{pq}=\frac{1}{2}\left[\frac{h_p}{h_q}\frac{\partial}{\partial c_q}\left(\frac{u_p}{h_p}\right)+\frac{h_q}{h_p}\frac{\partial}{\partial c_p}\left(\frac{u_q}{h_q}\right)\right]+\frac{\delta_{pq}}{h_q}\sum_{r=1}^{3}\frac{u_r}{h_r}\frac{\partial h_p}{\partial c_r}, \tag{11}$$

$$\mathbf{n}_p=h_p\nabla c_p, \qquad \frac{\partial\mathbf{n}_p}{\partial c_q}=\frac{1}{h_p}\mathbf{n}_q\frac{\partial h_q}{\partial c_p}-\delta_{pq}\sum_{r=1}^{3}\frac{1}{h_r}\mathbf{n}_r\frac{\partial h_p}{\partial c_r}.$$

Here δ_{pq} denotes the Kronecker symbol, $\delta_{pq}=1$ for $p=q$, $\delta_{pq}=0$ for $p\neq q$; $\mathbf{n}_p$ is the unit normal to the surface $c_p=\text{const.}$, τ_{pq} and e_{pq} are the components of the stress and strain tensor, respectively. Body forces are not considered in (10).

To simplify the following equations, we shall use commas between subscripts to denote the derivatives of the vector and tensor components with respect to coordinates c_i and time, e.g.

$$u_{p,tt}=\partial^2u_p/\partial t^2, \qquad u_{p,pq}=\partial^2u_p/\partial c_p\,\partial c_q, \qquad u_{p,q}=\partial u_p/\partial c_q. \tag{12}$$

Similar notation for derivatives will be also used for the derivatives of scalar quantities, e.g.

$$\lambda_{,q}=\partial\lambda/\partial c_q, \qquad \mu_{,q}=\partial\mu/\partial c_q. \tag{12'}$$

Under the coordinates (c_1, c_2, c_3) we shall understand the ray-centred coordinates (s,n,m) introduced above i.e. $c_1=s$, $c_2=n$, $c_3=m$. It is, however, useful to continue to work with the notation (c_1, c_2, c_3) for a while because of the summation convenience. We shall only specify the scale factors according to (9). Then we can rewrite Eqs. (10) and (11) in a component form,

$$\rho u_{p,tt}=\frac{\lambda}{h_p}\Theta_{,p}+2\mu\sum_{q=1}^{3}\frac{1}{h_q}e_{pq,q}+\frac{1}{h_p}\lambda_{,p}\Theta$$
$$-\frac{2\mu}{hh_p}e_{11}h_{,p}+\frac{1}{h}\sum_{q=1}^{3}\frac{e_{pq}}{h_p}(2\mu hh_p/h_q)_{,q}, \tag{13}$$

with

$$e_{pq}=\frac{1}{2}\left(\frac{1}{h_q}u_{p,q}+\frac{1}{h_p}u_{q,p}\right)-\frac{1}{2h_ph_q}(u_ph_{p,q}+u_qh_{q,p})$$
$$+\frac{1}{h_q}\delta_{pq}\sum_{r=1}^{3}\frac{u_r}{h_r}h_{p,r}. \tag{14}$$

Inserting (14) into (13) and separating the terms that contain the second derivatives of the displacement components from other terms yields

$$\rho u_{p,tt}=\sum_{q=1}^{3}\left(\frac{\lambda+\mu}{h_ph_q}u_{q,pq}+\frac{\mu}{h_q^2}u_{p,qq}\right)+C_p, \tag{15}$$

where C_p is given by the relation

$$C_p=\sum_{q=1}^{3}\left(\sum_{r=1}^{3}D_{pqr}u_{q,r}+E_{pq}u_q\right). \tag{16}$$

In expression (16), we have 27 quantities D_{pqr} and nine quantities E_{pq}. In the following, however, we shall need only five of these quantities. All other quantities D_{pqr} and E_{pq} will vanish in the high-frequency ($\omega\to\infty$) approximation of the elastodynamic equation, as will be shown later. We shall therefore specify here only the five quantities D_{pqr} mentioned:

$$D_{111}=h^{-1}[h^{-1}(\lambda+2\mu)]_{,1},\qquad D_{231}=D_{321}=0,$$
$$D_{221}=D_{331}=h^{-1}(\mu/h)_{,1}. \tag{17}$$

Now we shall rewrite the elastodynamic Eq. (15) in the ray-centred coordinate system (s, n, m). Remember that $u_1=u_s$ denotes the component of the displacement vector $\mathbf{u}$ in the direction of $\mathbf{t}$ (along the ray), $u_2=u_n$ the component in the direction of $\mathbf{e}_n$ and $u_3=u_m$ the component in the direction of $\mathbf{e}_m$. We obtain

$$\rho u_{s,tt}=h^{-2}(\lambda+2\mu)u_{s,ss}+h^{-1}(\lambda+\mu)(u_{n,sn}+u_{m,sm})$$
$$+\mu(u_{s,nn}+u_{s,mm})+C_s,$$
$$\rho u_{n,tt}=h^{-2}\mu u_{n,ss}+(\lambda+\mu)(h^{-1}u_{s,sn}+u_{n,nn}+u_{m,nm})$$
$$+\mu(u_{n,nn}+u_{n,mm})+C_n,$$
$$\rho u_{m,tt}=h^{-2}\mu u_{m,ss}+(\lambda+\mu)(h^{-1}u_{s,sm}+u_{n,nm}+u_{m,mm})$$
$$+\mu(u_{m,nn}+u_{m,mm})+C_m. \tag{18}$$

Here we have used the subscripts s, n and m to denote the partial derivatives with respect to s, n and m.

The quantities C_s, C_n and C_m correspond to C_1, C_2 and C_3, respectively, given by (16), where both q and r take values $1=s$, $2=n$, $3=m$.

Equations (18) represent a final form of the elastodynamic Eq. (10), written in the ray-centred coordinates (s, n, m). They are still fully equivalent to (10), as no approximation was used to derive them.

Equations (18) may be used for arbitrary time-dependent displacement vector $\mathbf{u}$. In this paper, however, we consider the time-harmonic solutions. We assume that the time-harmonic factor is $\exp(-i\omega t)$, where ω is the angular frequency.

One-way Elastodynamic Equation

We shall study the solutions of the elastodynamic Eqs. (18), corresponding to the wave propagating along the ray Ω *in the direction of increasing* s. For this purpose, it is suitable to make the following substitution

$$u_j(s,n,m,t)=\exp\left\{-i\omega\left(t-\int_0^s v^{-1}(\xi)\,d\xi\right)\right\}U_j(s,n,m). \tag{19}$$

Here $j=s$, n or m. The integral is taken along the ray Ω. The lower limit in the integral may be an arbitrary real-valued constant; without loss to generality we put the constant equal to zero.

As Eq. (19) describes only the solution of the elastodynamic equation corresponding to the wave which propagates along Ω in the direction of increasing s (not in the opposite direction), we shall call it the *one-way solution.*

Inserting (19) into (18) yields

$$-\rho\omega^2U_s=\frac{\lambda+2\mu}{h^2}\left[\left(-\frac{\omega^2}{v^2}+i\omega\left(\frac{1}{v}\right)_{,s}\right)U_s+\frac{2i\omega}{v}U_{s,s}+U_{s,ss}\right]$$
$$+\frac{\lambda+\mu}{h}\left[\frac{i\omega}{v}(U_{n,n}+U_{m,m})+U_{n,sn}+U_{m,sm}\right]$$
$$+\mu(U_{s,nn}+U_{s,mm})$$
$$+\frac{i\omega}{v}(U_sD_{sss}+U_nD_{sns}+U_mD_{sms})+\tilde{C}_s,$$

$$-\rho\omega^2U_n=\frac{\mu}{h^2}\left[\left(-\frac{\omega^2}{v^2}+i\omega\left(\frac{1}{v}\right)_{,s}\right)U_n+\frac{2i\omega}{v}U_{n,s}+U_{n,ss}\right]$$
$$+(\lambda+\mu)\left(\frac{i\omega}{hv}U_{s,n}+\frac{1}{h}U_{s,sn}+U_{n,nn}+U_{m,nm}\right)$$
$$+\mu(U_{n,nn}+U_{n,mm})$$
$$+\frac{i\omega}{v}(U_sD_{nss}+U_nD_{nns})+\tilde{C}_n. \tag{20}$$

The third equation (for U_m) is not written here as it is obtained from the second equation merely by interchanging the indices n and m. The quantities $\tilde{C}_s$, $\tilde{C}_n$ and $\tilde{C}_m$ are again given by (16), where $u_{q,r}$ are replaced by $U_{q,r}$ and u_q by U_q. We must, of course, again consider $1\to s$, $2\to n$, $3\to m$ in the relevant indices.

High-frequency Approximation of One-way Elastodynamic Equation

It is well known that the high-frequency elastic wave field propagates mostly along rays. In this and the next sections, we shall show that the one-way elastodynamic equation reduces to the parabolic equation in the high-frequency approximation. This will give us a possibility to study the high-frequency elastic wave field concentrated close to the ray by the parabolic equation method.

We shall assume that ω is high and keep only the terms containing the highest degrees of ω in Eqs. (20). We shall retain only the terms of the order ω^{δ}, with $\delta \geqq 1$, and neglect all the terms of the order ω^{δ}, $\delta < 1$.

Before doing that, we shall assume that $n = O(\omega^{-\gamma})$, $m = O(\omega^{-\gamma})$ with $\gamma = \frac{1}{2}$. This assumption expresses the fact that for large ω the investigation of the wave field can be restricted to a "boundary layer" along Ω. It is then suitable to introduce new variables ν, η instead of n, m:

$$\nu = \omega^{1/2} n, \qquad \eta = \omega^{1/2} m. \tag{21}$$

Note that $\nu = O(1)$, $\eta = O(1)$ with respect to the frequency $\omega \to \infty$. Substituting (21) into (20), dividing the equations by ρ and neglecting the terms with lower powers of ω (i.e., with $\omega^{1/2}$, ω^{0}, $\omega^{-1/2}$, ...), we obtain

$$\begin{aligned}
-\omega^2 U_s = & \frac{\lambda+2\mu}{\rho h^2}\left[\left(-\frac{\omega^2}{v^2} + i\omega\left(\frac{1}{v}\right)_{,s}\right) U_s + \frac{2i\omega}{v} U_{s,s}\right] \\
& + \frac{i\omega^{3/2}}{\rho h v}(\lambda+\mu)(U_{n,\nu} + U_{m,\eta}) + \frac{\mu\omega}{\rho}(U_{s,\nu\nu} + U_{s,\eta\eta}) \\
& + \frac{i\omega}{\rho v}(U_s D_{sss} + U_n D_{sns} + U_m D_{sms}),
\end{aligned}$$

$$\begin{aligned}
-\omega^2 U_n = & \frac{\mu}{\rho h^2}\left[\left(-\frac{\omega^2}{v^2} + i\omega\left(\frac{1}{v}\right)_{,s}\right) U_n + \frac{2i\omega}{v} U_{n,s}\right] \\
& + \frac{\lambda+\mu}{\rho}\frac{i\omega^{3/2}}{hv} U_{s,\nu} + \frac{\lambda+\mu}{\rho}\omega(U_{n,\nu\nu} + U_{m,\nu\eta}) \\
& + \frac{\mu}{\rho}\omega(U_{n,\nu\nu} + U_{n,\eta\eta}) + \frac{i\omega}{\rho v}(U_s D_{nss} + U_n D_{nns}).
\end{aligned} \tag{22}$$

The third equation for U_m is again obtained from the second equation by interchanging the indices n with m and ν with η. It would be simple to show that the expressions $\tilde{C}_s$, $\tilde{C}_n$ and $\tilde{C}_m$ are of the order $\omega^{1/2}$ and less so that they do not contribute to (22).

We shall now expand U_i into asymptotic series in inverse powers of $\omega^{1/2}$,

$$U_i = U_i^0 + \omega^{-1/2} U_i^1 + \omega^{-1} U_i^2 + \ldots, \tag{23}$$

for $i = s$, n or m. Inserting (23) into (22) and keeping only the terms which contain the factors ω^2, $\omega^{3/2}$ and ω^1, we get

$$\begin{aligned}
& -\omega^2\left(\frac{\lambda+2\mu}{\rho h^2 v^2} - 1\right)(U_s^0 + \omega^{-1/2} U_s^1 + \omega^{-1} U_s^2) + \frac{i\omega^{3/2}(\lambda+\mu)}{h v \rho} \\
& \cdot [U_{n,\nu}^0 + U_{m,\eta}^0 + \omega^{-1/2}(U_{n,\nu}^1 + U_{m,\eta}^1)] \\
& + \omega\left\{ i\frac{\lambda+2\mu}{\rho h^2}\left[\left(\frac{1}{v}\right)_{,s} U_s^0 + \frac{2}{v} U_{s,s}^0\right]\right. \\
& + \frac{\mu}{\rho}(U_{s,\nu\nu}^0 + U_{s,\eta\eta}^0) \\
& \left. + \frac{i}{v\rho}(U_s^0 D_{sss} + U_n^0 D_{sns} + U_m^0 D_{sms})\right\} = 0,
\end{aligned}$$

$$\begin{aligned}
& -\omega^2\left(\frac{\mu}{\rho h^2 v^2} - 1\right)(U_n^0 + \omega^{-1/2} U_n^1 + \omega^{-1} U_n^2) \\
& + \frac{i\omega^{3/2}(\lambda+\mu)}{h v \rho}(U_{s,\nu}^0 + \omega^{-1/2} U_{s,\nu}^1) \\
& + \omega\left\{ i\frac{\mu}{\rho h^2}\left[\left(\frac{1}{v}\right)_{,s} U_n^0 + \frac{2}{v} U_{n,s}^0\right]\right. \\
& + \frac{\lambda+\mu}{\rho}(U_{n,\nu\nu}^0 + U_{m,\nu\eta}^0) + \frac{\mu}{\rho}(U_{n,\nu\nu}^0 + U_{n,\eta\eta}^0) \\
& \left. + \frac{i}{v\rho}(U_s^0 D_{nss} + U_n^0 D_{nns})\right\} = 0.
\end{aligned} \tag{24}$$

The third equation can be again obtained from the second equation by interchanging the indices n with m and ν with η.

This is the final form of the high-frequency approximation of the one-way elastodynamic equation, valid for solutions concentrated close to the rays of both P wave and S wave. Let us note that all the functions λ, μ, ρ and h in (24) depend generally an all the three coordinates s, n, m. To simplify further the above equations, we must consider the cases of P and S waves separately.

Parabolic Equations

It is now easy to specify the asymptotic high-frequency elastodynamic equations separately for the rays of P waves and S waves. In this section, we shall derive these equations and show that they correspond to the well-known parabolic equations.

For simplicity, we shall use the term "component of the displacement vector" not only for u_s, u_n and u_m, but also for the quantities U_s, U_n, U_m, see (19).

Parabolic Equation for a P Wave

In the zero-order approximation of the ray method, the only non-vanishing component of the displacement vector of a P wave has a direction tangent to the ray. The components perpendicular to the ray vanish. From this we can expect that in our case also the component along the ray Ω will be more important. Thus we shall call the component U_s *the principal component* and the components U_n and U_m *the additional components.*

To find the components U_s, U_n and U_m, we shall specify Eqs. (24) for case that the ray Ω corresponds to a P wave, i.e. for $\nu = \alpha$. Since the coefficients in (24) depend generally on n and m, we shall expand them in terms of n and m. As $n = \omega^{-1/2}\nu$, $m = \omega^{-1/2}\eta$, these expansions automatically represent the expansions in $\omega^{-1/2}$. In all cases, we shall again keep in (24) only the terms with powers of ω higher or equal to ω^1.

First let us expand the most important coefficient in (24), $(\lambda+2\mu)/(\rho h^2 \alpha^2) - 1$. We can write

$$\frac{\lambda+2\mu}{\rho h^2 \alpha^2} - 1 = \frac{V_P^2(s,n,m)}{h^2\alpha^2} - 1,$$

where $V_P(s, n, m)$ is given by (2). Expanding V_P in powers of n and m, we get

$$\begin{aligned}
V_P(s,n,m) \sim & \alpha(s) + \alpha_{,n} n + \alpha_{,m} m \\
& + \tfrac{1}{2}(n^2 \alpha_{,nn} + 2nm\alpha_{,nm} + m^2 \alpha_{,mm}).
\end{aligned}$$

This can be rewritten in a more convenient matrix form

$$V_P(s,n,m)\sim\alpha(s)+\alpha_{,n}n+\alpha_{,m}m+\tfrac{1}{2}q^T\mathbf{V}^\alpha q, \tag{25}$$

where

$$\mathbf{V}^\alpha=\begin{pmatrix}\alpha_{,nn} & \alpha_{,nm}\\ \alpha_{,nm} & \alpha_{,mm}\end{pmatrix},\qquad q=\begin{pmatrix}n\\ m\end{pmatrix},\qquad q^T=(n\ m). \tag{26}$$

Thus, $\mathbf{V}^\alpha$ is a 2×2 real-valued symmetric matrix of second derivatives of the velocity of compressional waves in the plane perpendicular to the ray Ω. From (25) we easily get

$$V_P(s,n,m)\sim\alpha h\left(1+\frac{1}{2\alpha h}q^T\mathbf{V}^\alpha q\right),$$

where h is given by (8). This gives

$$\frac{\lambda+2\mu}{\rho h^2\alpha^2}-1\sim\frac{1}{\alpha h}q^T\mathbf{V}^\alpha q. \tag{27}$$

We shall now use the coordinates v and η instead of n and m in (27). Let us denote

$$g=\omega^{1/2}q=\begin{pmatrix}v\\ \eta\end{pmatrix},\qquad g^T=\omega^{1/2}q^T=(v\ \eta). \tag{28}$$

Then we get finally

$$\frac{\lambda+2\mu}{\rho h^2\alpha^2}-1\sim\frac{1}{\alpha h\omega}g^T\mathbf{V}^\alpha g. \tag{29}$$

Thus, we can see that the first term in the first equation of (24) is not of the order ω^2, but of the order ω. The situation is different for the first term in the second equation of (24). Similarly we get

$$\frac{\mu}{\rho h^2\alpha^2}-1=\frac{\beta^2-\alpha^2}{\alpha^2}-\omega^{-1/2}H_1^\alpha+\omega^{-1}H_2^\alpha+\dots \tag{30}$$

where

$$H_1^\alpha=\frac{2\beta^2}{\alpha^2}\left[\left(\frac{\alpha_{,n}}{\alpha}-\frac{\beta_{,n}}{\beta}\right)v+\left(\frac{\alpha_{,m}}{\alpha}-\frac{\beta_{,m}}{\beta}\right)\eta\right]. \tag{31}$$

The expressions $\alpha_{,n}$, $\beta_{,n}$, $\alpha_{,m}$ and $\beta_{,m}$ are given by (4a). The expression for H_2^α is not given here as we shall not need it.

Now we insert (29) and (30) into (24) and keep only the terms of the order ω^γ, $\gamma\geqq1$. After some simple manipulations, we obtain

$$\begin{aligned}&\frac{i\omega^{3/2}}{\alpha}(U^0_{n,v}+U^0_{m,\eta})+\frac{\omega}{\alpha^2-\beta^2}\left\{U^0_s\left[i\rho^{-1}(\rho\alpha)_{,s}-\frac{1}{\alpha}g^T\mathbf{V}^\alpha g\right]\right.\\&+2i\alpha U^0_{s,s}+\beta^2(U^0_{s,vv}+U^0_{s,\eta\eta})\\&+\frac{i}{\alpha}(\alpha^2-\beta^2)(U^1_{n,v}+U^1_{m,\eta})\\&\left.+\frac{i}{\alpha\rho}(U^0_nD_{sns}+U^0_mD_{sms})\right\}=0,\end{aligned}$$

$$\omega^2\frac{\alpha^2-\beta^2}{\alpha^2}U^0_n+\omega^{3/2}\left\{\frac{\alpha^2-\beta^2}{\alpha}\left(\frac{1}{\alpha}U^1_n+iU^0_{s,v}\right)+H_1^\alpha U^0_n\right\}=0,$$

$$\omega^2\frac{\alpha^2-\beta^2}{\alpha^2}U^0_m+\omega^{3/2}\left\{\frac{\alpha^2-\beta^2}{\alpha}\left(\frac{1}{\alpha}U^1_m+iU^0_{s,\eta}\right)+H_1^\alpha U^0_m\right\}=0. \tag{32}$$

In the second and the third equation of (32), we did not write the last terms (with ω), as we shall not need them in the following. Note that the first equation was multiplied by $\rho h/(\lambda+\mu)$. In the second terms of all the three equations, only the following approximations were used:

$$\begin{aligned}&(\lambda+2\mu)/\rho\sim\alpha^2,\qquad \mu/\rho\sim\beta^2,\qquad \rho(s,n,m)\sim\rho(s,0,0),\\&h\sim1,\qquad h_{,s}\sim0.\end{aligned} \tag{33}$$

They correspond to the first terms of Taylor expansions of the relevant quantities in powers of $1/\omega^{1/2}$. Thus, the density ρ in (32) does not depend on the coordinates n, m; $\rho=\rho(s,0,0)$, see the discussion above. The corresponding approximation for the quantity $D_{sss}(=D_{111})$ was $(\rho\alpha^2)_{,s}$, see (17). The quantities D_{sns} and D_{sms} are not specified in (32), as they will not contribute to the final results.

From the last two equations in (32) we simply obtain

$$\begin{aligned}&U^0_n=0,\qquad U^1_n=-i\alpha U^0_{s,v},\\&U^0_m=0,\qquad U^1_m=-i\alpha U^0_{s,\eta}.\end{aligned} \tag{34}$$

Thus, the first terms of the asymptotic series for both the additional components (perpendicular to Ω) vanish, and the leading terms are U^1_n and U^1_m. The additional components are given by relations, see (23) and (34),

$$U_n=-i\alpha\omega^{-1/2}U^0_{s,v},\qquad U_m=-i\alpha\omega^{-1/2}U^0_{s,\eta}. \tag{35}$$

Now we return to the first equation of (32). From the first term we immediately obtain $U^0_{n,v}+U^0_{m,\eta}=0$. This relation, however, does not give us anything new, it follows immediately from (34). More important is the second term, with ω. Multiplying the term by α^{-2}, inserting $U^0_n=0$, $U^0_m=0$ and $U^1_{n,v}+U^1_{m,\eta}=-i\alpha(U^0_{s,vv}+U^0_{s,\eta\eta})$, see (34), we obtain

$$\begin{aligned}&\frac{2i}{\alpha}U^0_{s,s}+U^0_{s,vv}+U^0_{s,\eta\eta}\\&+U^0_s\left\{i\alpha^{-1}[\ln(\alpha\rho)]_{,s}-\frac{1}{\alpha^3}g^T\mathbf{V}^\alpha g\right\}=0.\end{aligned} \tag{36}$$

This is the parabolic equation for U^0_s we have sought. The Eq. (36) can be further simplified by the substitution

$$U^0_s(s,v,\eta)=[\alpha(s)\rho(s)]^{-1/2}W^\alpha(s,v,\eta). \tag{37}$$

Inserting (37) into (36) we obtain the final form of the *parabolic equation for P waves*,

$$\frac{2i}{\alpha}W^\alpha_{,s}+W^\alpha_{,vv}+W^\alpha_{,\eta\eta}-\frac{1}{\alpha^3}(g^T\mathbf{V}^\alpha g)W^\alpha=0. \tag{38}$$

In the conclusion of this section we shall write the

final expression for the vectorial time-harmonic solution of the three-dimensional elastodynamic equation, concentrated close to a ray of a P wave. It reads

$$\mathbf{u}(s,v,\eta,t)=u_s(s,v,\eta,t)\,\mathbf{t}+u_n(s,v,\eta,t)\,\mathbf{e}_n +u_m(s,v,\eta,t)\,\mathbf{e}_m, \tag{39}$$

where

$$u_s(s,v,\eta,t)=\frac{1}{\sqrt{\alpha(s)\,\rho(s)}}\exp\left\{-i\omega\left[t-\int_0^s\frac{d\zeta}{\alpha(\zeta)}\right]\right\}W^\alpha(s,v,\eta),$$

$$u_n(s,v,\eta,t) =-i\omega^{-1/2}\sqrt{\frac{\alpha(s)}{\rho(s)}}\exp\left\{-i\omega\left[t-\int_0^s\frac{d\zeta}{\alpha(\zeta)}\right]\right\}\frac{\partial W^\alpha(s,v,\eta)}{\partial v},$$

$$u_m(s,v,\eta,t) =-i\omega^{-1/2}\sqrt{\frac{\alpha(s)}{\rho(s)}}\exp\left\{-i\omega\left[t-\int_0^s\frac{d\zeta}{\alpha(\zeta)}\right]\right\}\frac{\partial W^\alpha(s,v,\eta)}{\partial \eta}, \tag{40}$$

and where $W^\alpha(s,v,\eta)$ is a solution of the parabolic Eq. (38). Note that the function W^α depends on frequency ω, as $v=\omega^{1/2}n$, $\eta=\omega^{1/2}m$.

Parabolic Equation for an S Wave

In case of vectorial solutions of the 3D elastodynamic equation concentrated close to a ray Ω of an S wave, the components of the displacement vector U_n and U_m will be referred to as the principal components, the component U_s as the additional component. Thus, the principal components are perpendicular to the ray, and the additional component is parallel to the ray.

As the derivation of all the equations is now very similar to that above, we shall be brief. We put $v=\beta$ and get approximately

$$\frac{\mu}{\rho h^2\beta^2}-1\sim\frac{1}{\beta h\omega}\,g^T\mathbf{V}^\beta g, \tag{41}$$

$$\frac{\lambda+2\mu}{\rho h^2\beta^2}-1\sim\frac{\alpha^2-\beta^2}{\beta^2}+\omega^{-1/2}H_1^\beta+\omega^{-1}H_2^\beta, \tag{42}$$

where $H_1^\beta=(\alpha/\beta)^4H_1^\alpha$. The expression for H_2^β is not presented here as it does not influence the final results. The symbol $\mathbf{V}^\beta$ denotes the 2×2 real-valued matrix of the second derivatives of the velocities of shear waves in the plane perpendicular to the ray Ω

$$\mathbf{V}^\beta=\begin{pmatrix}\beta_{,nn} & \beta_{,nm}\\ \beta_{,nm} & \beta_{,mm}\end{pmatrix}, \tag{43}$$

see (4b).

Inserting (41) and (42) into (24) and using similar approximations as above we obtain

$$-\omega^2\frac{\alpha^2-\beta^2}{\beta^2}U_s^0 +\omega^{3/2}\left\{\frac{\alpha^2-\beta^2}{\beta}\left[i(U_{n,v}^0+U_{m,\eta}^0)-\frac{1}{\beta}U_s^1\right]-H_1^\beta U_s^0\right\}=0,$$

$$\frac{i\omega^{3/2}}{\beta}U_{s,v}^0+\frac{\omega}{\alpha^2-\beta^2}\left\{U_n^0\left[\frac{i}{\rho}(\beta\rho)_{,s}-\frac{1}{\beta}g^T\mathbf{V}^\beta g\right]+2i\beta U_{n,s}^0 +(\alpha^2-\beta^2)(U_{n,vv}^0+U_{m,\eta v}^0)+\beta^2(U_{n,vv}^0+U_{n,\eta\eta}^0) +\frac{i}{\beta\rho}U_s^0D_{nss}+\frac{i}{\beta}U_{s,v}^1(\alpha^2-\beta^2)\right\}=0,$$

$$\frac{i\omega^{3/2}}{\beta}U_{s,\eta}^0+\frac{\omega}{\alpha^2-\beta^2}\left\{U_m^0\left[\frac{i}{\rho}(\beta\rho)_{,s}-\frac{1}{\beta}g^T\mathbf{V}^\beta g\right] +2i\beta U_{m,s}^0+(\alpha^2-\beta^2)(U_{n,\eta v}^0+U_{m,\eta\eta}^0) +\beta^2(U_{m,vv}^0+U_{m,\eta\eta}^0)+\frac{i}{\beta\rho}U_s^0D_{mss} +\frac{i}{\beta}U_{s,\eta}^1(\alpha^2-\beta^2)\right\}=0. \tag{44}$$

It immediately follows from the first equation in (44)

$$U_s^0=0,\qquad U_s^1=i\beta(U_{n,v}^0+U_{m,\eta}^0). \tag{45}$$

Likewise, from the second and third equation we obtain identical equations for U_n^0 and U_m^0,

$$U_n^0(s,v,\eta)=\frac{1}{\sqrt{\beta(s)\,\rho(s)}}W_n^\beta(s,v,\eta), \tag{46}$$

$$U_m^0(s,v,\eta)=\frac{1}{\sqrt{\beta(s)\,\rho(s)}}W_m^\beta(s,v,\eta),$$

where $W_n^\beta(s,v,\eta)$ and $W_m^\beta(s,v,\eta)$ are solutions of the *parabolic equation for S waves*,

$$\frac{2i}{\beta}W_{,s}^\beta+W_{,vv}^\beta+W_{,\eta\eta}^\beta-\frac{1}{\beta^3}(g^T\mathbf{V}^\beta g)\,W^\beta=0. \tag{47}$$

The final expressions for the vectorial time-harmonic solutions of the three-dimensional elastodynamic equation concentrated close to a ray Ω of an S wave are again given by (39), where u_s, u_n and u_m are given by equations

$$u_s(s,v,\eta,t)=i\omega^{-1/2}\sqrt{\frac{\beta(s)}{\rho(s)}}\exp\left\{-i\omega\left[t-\int_0^s\frac{d\xi}{\beta(\zeta)}\right]\right\} \times\left(\frac{\partial W_n^\beta(s,v,\eta)}{\partial v}+\frac{\partial W_m^\beta(s,v,\eta)}{\partial\eta}\right),$$

$$u_n(s,v,\eta,t) =\frac{1}{\sqrt{\beta(s)\,\rho(s)}}\exp\left\{-i\omega\left[t-\int_0^s\frac{d\zeta}{\beta(\zeta)}\right]\right\}W_n^\beta(s,v,\eta),$$

$$u_m(s,v,\eta,t) =\frac{1}{\sqrt{\beta(s)\,\rho(s)}}\exp\left\{-i\omega\left[t-\int_0^s\frac{d\zeta}{\beta(\zeta)}\right]\right\}W_m^\beta(s,v,\eta), \tag{48}$$

and W_n^β and W_m^β are solutions of (47).

Solutions of the Parabolic Equation

As we have seen, the parabolic equation for both P and S waves can be written in the same form

$$\frac{2i}{v} W_{,s} + W_{,vv} + W_{,\eta\eta} - \frac{1}{v^3}(g^T \mathbf{V} g)\, W = 0. \tag{49}$$

For P waves, we must insert $v = \alpha$, $\mathbf{V} = \mathbf{V}^\alpha$ and $W = W^\alpha$. Similarly, for S waves, we put $v = \beta$, $\mathbf{V} = \mathbf{V}^\beta$ and $W = W^\beta$. Thus, we investigate the solution of the parabolic equation for both P and S waves together.

We shall seek the solution of (49) in the following form

$$W(s, v, \eta) = A(s) \exp\left[\frac{i}{2}(g^T \mathbf{M}(s)\, g)\right], \tag{50}$$

where $\mathbf{M}(s)$ is a 2×2 generally complex-valued symmetric matrix, and $A(s)$ a complex-valued scalar. A similar form of the solution of the parabolic equation is known from quantum mechanics and was also used by Kirpichnikova (1971). We assume that both A and $\mathbf{M}$ depend on s only, not on v and η. For the derivatives of W we simply obtain

$$W_{,s} = \left[\frac{dA}{ds} + \frac{iA}{2}\left(g^T \frac{d\mathbf{M}}{ds} g\right)\right] \exp\left[\frac{i}{2}(g^T \mathbf{M} g)\right],$$

$$W_{,vv} + W_{,\eta\eta} = [iA \operatorname{tr}(\mathbf{M}) - A(g^T \mathbf{M}^2 g)] \exp\left[\frac{i}{2}(g^T \mathbf{M} g)\right].$$

Inserting these expressions into (49) yields

$$\left(\frac{2}{v}\frac{dA}{ds} + A \operatorname{tr}(\mathbf{M})\right) + iA\, g^T \left(\frac{1}{v}\frac{d\mathbf{M}}{ds} + \mathbf{M}^2 + \frac{1}{v^3}\mathbf{V}\right) g = 0. \tag{51}$$

The simplest possibility to satisfy Eq. (51) is to put

$$\frac{d}{ds}\mathbf{M} + v\,\mathbf{M}^2 + \frac{1}{v^2}\mathbf{V} = \mathbf{0}, \tag{52}$$

where $\mathbf{0}$ is a 2×2 null matrix, and

$$\frac{d}{ds} A + \tfrac{1}{2} A\, v \operatorname{tr}(\mathbf{M}) = 0. \tag{53}$$

When $\mathbf{M}$ satisfies Eq. (52) and A Eq. (53), then the function W given by (50) is a solution of the parabolic equation (49). Note that more general solutions of the parabolic equation (49) (higher modes) contain Hermite polynomials. Due to this fact, the corresponding beams are called the Hermite-Gaussian beams. The complete system of linearly independent solutions of (49), i.e. the complete system of Hermite-Gaussian beams is derived and discussed in Klimeš (in press 1982b). Here we shall pay attention only to the Gaussian beams (50), which correspond to the zeroth mode in the above described complete system of solutions.

Equation (52) for $\mathbf{M}$ is a matrix non-linear ordinary differential equation of the first order of the Riccati type. This equation is of basic importance in investigating the solutions concentrated close to rays. Equation (53) can be used to evaluate $A(s)$ as soon as $\mathbf{M}(s)$ is known. Similarly as in the ray method, we shall call it the transport equation. We shall now investigate both Eqs. (52) and (53) in greater detail.

Solution of the Matrix Riccati Equation

It is simple to rewrite the non-linear equation (52) as linear equations. We shall derive several linear forms of (52) in the following.

Let us put

$$\mathbf{M} = v^{-1} \frac{d\mathbf{Q}}{ds} \mathbf{Q}^{-1}, \tag{54}$$

where $\mathbf{Q}$ is a new 2×2 matrix. It will be shown later that this matrix is regular along the whole ray Ω, if the initial conditions for (52) are properly chosen. Taking into account that $\frac{d}{ds}\mathbf{Q}^{-1} = -\mathbf{Q}^{-1}\frac{d\mathbf{Q}}{ds}\mathbf{Q}^{-1}$, we get from (52),

$$v \frac{d^2}{ds^2}\mathbf{Q} - v_{,s}\frac{d}{ds}\mathbf{Q} + \mathbf{V}\mathbf{Q} = \mathbf{0}. \tag{55}$$

Thus, we have obtained a matrix linear ordinary differential equation of the second order. It can be rewritten as a system of two matrix linear ordinary differential equations of the first order. We put

$$\mathbf{P} = v^{-1}\frac{d}{ds}\mathbf{Q}. \tag{56}$$

Then we get from (55) and (56) the system

$$\frac{d}{ds}\mathbf{Q} = v\,\mathbf{P}, \quad \frac{d}{ds}\mathbf{P} = -v^{-2}\mathbf{V}\mathbf{Q}. \tag{57}$$

When we determine $\mathbf{P}$ and $\mathbf{Q}$ from (57), the matrix $\mathbf{M}$ is given by the relation, see (56) and (54),

$$\mathbf{M} = \mathbf{P}\mathbf{Q}^{-1}. \tag{58}$$

The system (57) seems to be most effective form of the equations which can be used to find $\mathbf{M}$. It has also some other advantages, as we shall see later.

Let us now denote by $\mathbf{X}$ a 2×4 matrix

$$\mathbf{X} = \begin{pmatrix} \mathbf{Q} \\ \mathbf{P} \end{pmatrix}. \tag{59}$$

Then the system (57) can be rewritten in the form

$$\frac{d}{ds}\mathbf{X} = \mathbf{H}\mathbf{X}, \tag{60}$$

where $\mathbf{H}$ is a 4×4 real-valued matrix, given by the relation,

$$\mathbf{H} = \begin{pmatrix} \mathbf{0} & v\mathbf{I} \\ -v^{-2}\mathbf{V} & \mathbf{0} \end{pmatrix} = \begin{pmatrix} 0 & 0 & v & 0 \\ 0 & 0 & 0 & v \\ -v^{-2}V_{11} & -v^{-2}V_{12} & 0 & 0 \\ -v^{-2}V_{12} & -v^{-2}V_{22} & 0 & 0 \end{pmatrix}. \tag{61}$$

Here $\mathbf{0}$ is again a 2×2 null matrix and $\mathbf{I}$ the 2×2 identity matrix. The solutions of the above system of equations (60) will be discussed in greater detail later.

The ordinary differential equations derived above may be simplified if we introduce a new variable σ along the central ray Ω instead of s;

$$d\sigma = v\,ds, \quad \text{i.e.} \quad \sigma = \sigma_0 + \int_{s_0}^{s} v(\zeta)\,d\zeta. \tag{62}$$

Then Eq. (55) takes the form of a matrix one-dimensional Helmholtz equation

$$\frac{d^2}{d\sigma^2}\mathbf{Q} + v^{-3}\mathbf{V}\mathbf{Q} = 0. \tag{63}$$

Similarly, (57) yields

$$\frac{d}{d\sigma}\mathbf{Q} = \mathbf{P}, \quad \frac{d}{d\sigma}\mathbf{P} = -v^{-3}\mathbf{V}\mathbf{Q}. \tag{64}$$

Finally, (60) gives

$$\frac{d}{d\sigma}\mathbf{X} = \tilde{\mathbf{H}}\mathbf{X}, \quad \tilde{\mathbf{H}} = \begin{pmatrix} \mathbf{0} & \mathbf{I} \\ -v^{-3}\mathbf{V} & \mathbf{0} \end{pmatrix}. \tag{65}$$

The new coordinate σ has no simple physical meaning, but it may be useful to use it instead of s in numerical computations. In the following, however, we shall use only the differential equations with the variable s, as they have a straightforward physical meaning.

Equations (52), (55) and (57) have been well known for some time in the ray method, especially in the evaluation of geometrical spreading. For details see Popov and Pšenčík (1978a, 1978b), Červený and Hron (1980), Červený et al. (1977), Hubral (1979, 1980), etc. In the ray method we consider **M**, **Q**, **P** to be real-valued, but here we allow **M, Q, P** to be complex-valued.

Transport Equation

Using (54), we can easily prove the relation

$$\mathrm{tr}(\mathbf{M}) = v^{-1}\frac{d}{ds}[\ln(\det \mathbf{Q})]. \tag{66}$$

Then the transport equation (53) takes the form

$$\frac{d}{ds}A + \tfrac{1}{2}A\frac{d}{ds}[\ln(\det \mathbf{Q})] = 0. \tag{67}$$

The transport equation (67) can be solved to give

$$A(s) = \frac{\Psi}{(\det \mathbf{Q}(s))^{1/2}}, \tag{68}$$

where Ψ is generally a complex-valued constant, independent of s.

Gaussian Beams and Paraxial Approximation

Inserting (68) into (50), we obtain the solution of the parabolic equation in the following form

$$W(s, v, \eta) = \frac{\Psi}{(\det \mathbf{Q}(s))^{1/2}} \exp[\tfrac{1}{2}i(g^T\mathbf{M}(s)\,g)], \tag{69}$$

or, using (58),

$$W(s, v, \eta) = \frac{\Psi}{(\det \mathbf{Q}(s))^{1/2}} \exp\left[\frac{i}{2}g^T\mathbf{P}\mathbf{Q}^{-1}g\right]. \tag{70}$$

Here **M** is a solution of the Riccati equation (52), **Q** and **P** are solutions of Eqs. (57). All the matrices **M**, **Q**, **P** are generally complex-valued. Thus we can rewrite (69) in the form

$$W(s, v, \eta) = \frac{\Psi}{(\det \mathbf{Q}(s))^{1/2}} \cdot \exp\left[\frac{i}{2}g^T(\mathrm{Re}\,\mathbf{M}(s))\,g - \tfrac{1}{2}g^T(\mathrm{Im}\,\mathbf{M}(s))\,g\right]. \tag{71}$$

For *complex-valued* **Q, P** *and* **M**, the solutions may, under certain conditions, represent Gaussian beams. We shall call these conditions *the existence conditions of Gaussian beams*. There are three existence conditions:

1) The condition of the concentration of the Gaussian beam: $\mathrm{Im}\,\mathbf{M}(s)$ must be a positive definite matrix along the whole ray Ω. When the condition is satisfied, the solution (71) is concentrated close to Ω.

2) The condition of symmetry of the matrix **M**: The matrix $\mathbf{M}(s)$ must be symmetrical along the whole ray, even though both **Q** and **P** may be non-symmetrical.

3) The condition of regularity of the Gaussian beam: The matrix $\mathbf{Q}(s)$ must be regular along the whole ray, i.e.,

$$\det \mathbf{Q}(s) \neq 0. \tag{72}$$

Thus, the matrix $\mathbf{M}(s) = \mathbf{P}\mathbf{Q}^{-1}$ exists and the solution (71) is regular along the whole ray, even at caustics and a point source.

We shall show in the next section that the existence conditions of Gaussian beams are fulfilled along the whole ray Ω as soon as they are satisfied at any point $s = s_0$ of the ray Ω. This will help us to choose properly the initial conditions for the system of differential equations given above.

For *real-valued solutions* **Q, P** *and* **M**, we have $\mathrm{Im}\,\mathbf{M}(s) = 0$. In this case we shall call the solutions (69)–(71) the *paraxial ray solutions* or *paraxial ray approximations*. The real-valued matrix $\mathbf{M}(s)$ represents the matrix of the second derivatives of the travel-time field and $(\det \mathbf{Q})^{1/2}$ gives the geometrical spreading. Note that the geometrical spreading vanishes at caustics, so that the solution $W(s, v, \eta)$ is singular there. There is only one condition for the existence of the paraxial ray solution: the real-valued matrix **M** must be symmetrical.

Gaussian Beams

By the term Gaussian beams we shall understand the solutions concentrated close to rays which satisfy the existence conditions of Gaussian beams, specified above. The purpose of this section is to show how to select the initial conditions for (60) or (57) at $s = s_0$ to obtain the Gaussian beams.

Matrix of Initial Parameters of Gaussian Beams

Let us rewrite the 2×4 matrix **X** given by (59) in the following form

$$\mathbf{X}=(\mathbf{X}_1\,\mathbf{X}_2) \tag{73}$$

where $\mathbf{X}_1$ and $\mathbf{X}_2$ are the column 1×4 matrices. Both $\mathbf{X}_1$ and $\mathbf{X}_2$ satisfy the same system of differential equations

$$\frac{d\mathbf{X}_i}{ds}=\mathbf{H}\mathbf{X}_i, \tag{74}$$

where $i=1,2$, see (60). We shall consider, for a while, one of these systems. It has four linearly independent real-valued solutions. Let us denote these solutions by $\boldsymbol{\Pi}_i$ $(i=1,2,3,4)$, where $\boldsymbol{\Pi}_i$ is again a 1×4 column matrix. The fundamental 4×4 real-valued matrix of linearly-independent solutions of (74) can be then introduced as follows

$$\boldsymbol{\Pi}(s)=(\boldsymbol{\Pi}_1\,\boldsymbol{\Pi}_2\,\boldsymbol{\Pi}_3\,\boldsymbol{\Pi}_4). \tag{75}$$

We shall specify the fundamental matrix at a reference point $s=s_0$ of the ray Ω by the relation

$$\boldsymbol{\Pi}(s_0)=\begin{pmatrix}1&0&0&0\\0&1&0&0\\0&0&1&0\\0&0&0&1\end{pmatrix}. \tag{76}$$

According to Liouville's theorem (see Kamke, 1959), $\det\boldsymbol{\Pi}(s)=\det\boldsymbol{\Pi}(s_0)$ for arbitrary s, since $\operatorname{tr}\mathbf{H}(s)=0$. Moreover, as all the elements of the matrix $\mathbf{H}$ are continuous functions of s (including the second derivatives of velocity, $v_{,ij}$), the solutions $\mathbf{X}_1$ and $\mathbf{X}_2$ exist for arbitrary s.

Any real or complex solution of (74) can be then expressed as a linear combination of linearly independent solutions $\boldsymbol{\Pi}_1,\boldsymbol{\Pi}_2,\boldsymbol{\Pi}_3,\boldsymbol{\Pi}_4$, multiplied by arbitrary real or complex constants. Thus, we can write

$$\mathbf{X}(s)=\boldsymbol{\Pi}(s)\,\mathbf{C}, \tag{77}$$

where $\mathbf{C}$ is a 2×4 matrix of constants. As we shall consider here the Gaussian beams, we must consider complex-valued constants. We shall call these constants the initial parameters of Gaussian beams and call matrix $\mathbf{C}$ *the matrix of the initial parameters of Gaussian beams.*

We introduce the notation

$$\boldsymbol{\Pi}(s)=\begin{pmatrix}\boldsymbol{\Pi}_{11}&\boldsymbol{\Pi}_{12}\\\boldsymbol{\Pi}_{21}&\boldsymbol{\Pi}_{22}\end{pmatrix},\qquad \mathbf{C}=\begin{pmatrix}\mathbf{C}_1\\\mathbf{C}_2\end{pmatrix}, \tag{78}$$

where $\boldsymbol{\Pi}_{ij}$ and $\mathbf{C}_i$ $(i,j=1,2)$ are 2×2 regular matrices. Then Eq. (77) can be rewritten in the following form

$$\begin{aligned}\mathbf{Q}(s)&=\boldsymbol{\Pi}_{11}\mathbf{C}_1+\boldsymbol{\Pi}_{12}\mathbf{C}_2,\\ \mathbf{P}(s)&=\boldsymbol{\Pi}_{21}\mathbf{C}_1+\boldsymbol{\Pi}_{22}\mathbf{C}_2.\end{aligned} \tag{79}$$

Note that both the matrices $\mathbf{P}(s)$ and $\mathbf{Q}(s)$ exist for arbitrary s. For the matrix $\mathbf{M}$ we then obtain

$$\mathbf{M}=\mathbf{P}\mathbf{Q}^{-1}=(\boldsymbol{\Pi}_{21}\mathbf{C}_1+\boldsymbol{\Pi}_{22}\mathbf{C}_2)(\boldsymbol{\Pi}_{11}\mathbf{C}_1+\boldsymbol{\Pi}_{12}\mathbf{C}_2)^{-1}. \tag{80}$$

It is easy to see that the matrix $\mathbf{M}(s)$ is not changed when both $\mathbf{P}$ and $\mathbf{Q}$ are multiplied from the RHS by a non-singular 2×2 constant matrix $\tilde{\mathbf{C}}$. Let us put, e.g., $\tilde{\mathbf{C}}=\mathbf{C}_1^{-1}$. For simplicity, denoting the matrix $\mathbf{C}_2\tilde{\mathbf{C}}$ again by $\mathbf{C}_2$, we get for $\mathbf{M}$

$$\mathbf{M}=(\boldsymbol{\Pi}_{21}\mathbf{I}+\boldsymbol{\Pi}_{22}\mathbf{C}_2)(\boldsymbol{\Pi}_{11}\mathbf{I}+\boldsymbol{\Pi}_{12}\mathbf{C}_2)^{-1}. \tag{81}$$

We shall now give the interpretation of $\mathbf{C}_2$. At $s=s_0$, we have $\boldsymbol{\Pi}_{11}=\boldsymbol{\Pi}_{22}=\mathbf{I}$, $\boldsymbol{\Pi}_{12}=\boldsymbol{\Pi}_{21}=\mathbf{0}$, see (76). Then Eq. (81) gives

$$\mathbf{C}_2=\mathbf{M}(s_0), \tag{82}$$

and the matrix of the initial parameters of Gaussian beams $\mathbf{C}$ is given as follows

$$\mathbf{C}=\begin{pmatrix}\mathbf{I}\\\mathbf{M}(s_0)\end{pmatrix}. \tag{83}$$

We assume that $\mathbf{M}(s_0)$ is a regular symmetrical matrix with a positive-definite imaginary part.

In the same way, when we put $\tilde{\mathbf{C}}=\mathbf{C}_2^{-1}$, we get $\mathbf{C}_1=\mathbf{M}^{-1}(s_0)$, $\mathbf{C}_2=\mathbf{I}$, and

$$\mathbf{C}=\begin{pmatrix}\mathbf{M}^{-1}(s_0)\\\mathbf{I}\end{pmatrix}. \tag{84}$$

It is our choice which matrix of initial parameters $\mathbf{C}$ will be used in the following. In this section, we shall use Eq. (83).

Note that the special choice of the matrix $\mathbf{C}$ does not influence the matrix $\mathbf{M}(s)$, but it changes separately the matrices $\mathbf{Q}(s)$ and $\mathbf{P}(s)$, see (79). We can see from (69) that the solution of the parabolic equation contains only the matrix $\mathbf{M}$ and the factor $\det\mathbf{Q}$. Since $\det(\mathbf{Q}\tilde{\mathbf{C}})=(\det\mathbf{Q})\,(\det\tilde{\mathbf{C}})$, the special choice of the matrix $\mathbf{C}$ introduces only the multiplicative constant factor $(\det\tilde{\mathbf{C}})^{-1/2}$ into the solution (69). Without any loss of generality, the factor $(\det\tilde{\mathbf{C}})^{-1/2}$ may be included into the constant Ψ, see (69). Thus, the special choice of $\mathbf{C}$ does not influence the expressions for Gaussian beams.

As $\mathbf{M}(s_0)$ is a regular symmetrical 2×2 matrix with a positive-definite imaginary part, it is fully specified by three complex-valued constants. In other words, the Gaussian beam is fully specified by three complex-valued initial parameters, i.e. by six real-valued initial parameters. The imaginary parts of the complex-valued parameters are not quite arbitrary, they must form a *positive-definite* matrix $\operatorname{Im}\mathbf{M}(s_0)$.

Invariant Expressions along the Central Ray

It is not difficult to show that certain expressions formed from the matrices $\mathbf{Q}$ and $\mathbf{P}$ do not change along the ray Ω. We shall consider two such expressions, viz., $\mathbf{Q}^*\mathbf{P}-\mathbf{Q}\mathbf{P}^*$ and $\mathbf{Q}^T\mathbf{P}-\mathbf{Q}\mathbf{P}^T$, where the asterisk denotes the Hermitian conjugate and T the transpose.

From (57) we easily get

$$\frac{d}{ds}(\mathbf{Q}^*\mathbf{P}-\mathbf{P}^*\mathbf{Q})=-v^{-2}(\mathbf{Q}^*\mathbf{V}\mathbf{Q}-\mathbf{Q}^*\mathbf{V}^*\mathbf{Q})=\mathbf{0},$$

as $\mathbf{V}$ is a real symmetric matrix, so that $\mathbf{V}=\mathbf{V}^*$. Similarly,

$$\frac{d}{ds}(\mathbf{Q}^T\mathbf{P}-\mathbf{P}^T\mathbf{Q})=\mathbf{0}.$$

We determine the values of both the invariants at $s = s_0$, considering (83). In this way we obtain

$$\mathbf{Q}^* \mathbf{P} - \mathbf{P}^* \mathbf{Q} = 2i \operatorname{Im} \mathbf{M}(s_0) \tag{85}$$

and

$$\mathbf{Q}^T \mathbf{P} - \mathbf{P}^T \mathbf{Q} = \mathbf{0}. \tag{86}$$

Note that the Eqs. (85) and (86) are valid even for the paraxial ray approximation.

Existence Conditions of Gaussian Beams

In this section, we shall prove that the three existence conditions of Gaussian beams presented above are satisfied along the whole Gaussian beam as soon as they are satisfied at one arbitrary point $s = s_0$ of the beam.

The Condition of Regularity

We wish to prove that the matrix $\mathbf{Q}$ is regular, i.e. that $\det \mathbf{Q}(s) \neq 0$ along the whole ray Ω. We assume that $\operatorname{Im} \mathbf{M}(s_0)$ is a positive definite matrix.

If the matrix $\mathbf{Q}$ is singular, then a non-zero vector $\mathbf{b}$ exists, for which

$$\mathbf{Q}\mathbf{b} = 0. \tag{87}$$

Multiplying (85) by $\mathbf{b}$ from the RHS and by $\mathbf{b}^*$ from the LHS, we get

$$(\mathbf{Q}\mathbf{b})^* \mathbf{P}\mathbf{b} - (\mathbf{P}\mathbf{b})^* \mathbf{Q}\mathbf{b} = 2i \mathbf{b}^* (\operatorname{Im} \mathbf{M}(s_0)) \mathbf{b}. \tag{88}$$

The LHS of (88) vanishes because of (87). The RHS, however, is positive for any choice of $\mathbf{b}$, since $\operatorname{Im} \mathbf{M}(s_0)$ is positive definite. From this it immediately follows that the non-zero vector $\mathbf{b}$ does not exist and that the matrix $\mathbf{Q}$ is regular.

Note that this condition is not satisfied for the paraxial ray approximation.

The Condition of Symmetry of the Matrix $\mathbf{M}$

We multiply (86) by $(\mathbf{Q}^T)^{-1}$ from the LHS and by $\mathbf{Q}^{-1}$ from RHS. This gives

$$(\mathbf{Q}^T)^{-1} \mathbf{Q}^T \mathbf{P} \mathbf{Q}^{-1} - (\mathbf{Q}^T)^{-1} \mathbf{P}^T \mathbf{Q} \mathbf{Q}^{-1} = \mathbf{0},$$

which yields

$$\mathbf{P}\mathbf{Q}^{-1} - (\mathbf{P}\mathbf{Q}^{-1})^T = \mathbf{0}. \tag{89}$$

From Eq. (89) it immediately follows that the matrix $\mathbf{M} = \mathbf{P}\mathbf{Q}^{-1}$ is symmetrical.

Note that this condition is satisfied even for the paraxial ray approximation.

The Condition of the Concentration of the Gaussian Beam

We multiply (85) by $(\mathbf{Q}^*)^{-1}$ from the LHS and by $\mathbf{Q}^{-1}$ from the RHS. It gives

$$\mathbf{P}\mathbf{Q}^{-1} - (\mathbf{P}\mathbf{Q}^{-1})^* = 2i (\mathbf{Q}^*)^{-1} (\operatorname{Im} \mathbf{M}(s_0)) \mathbf{Q}^{-1}. \tag{90}$$

As

$$\operatorname{Im} \mathbf{M}(s) = \frac{1}{2i} [\mathbf{P}\mathbf{Q}^{-1} - (\mathbf{P}\mathbf{Q}^{-1})^*],$$

Eq. (90) yields

$$\operatorname{Im} \mathbf{M}(s) = (\mathbf{Q}^*)^{-1} (\operatorname{Im} \mathbf{M}(s_0)) \mathbf{Q}^{-1}. \tag{91}$$

We shall now show that $\operatorname{Im} \mathbf{M}(s)$ is positive definite for any s. We take into account that $\mathbf{Q}^{-1}$ is regular as the matrix $\mathbf{Q}$ exists for arbitrary s.

As $\operatorname{Im} \mathbf{M}(s_0)$ is positive definite, it can be factorized in the following form: $\operatorname{Im} \mathbf{M}(s_0) = \mathbf{N}_0^T \mathbf{N}_0$. Then we can write

$$\operatorname{Im} \mathbf{M}(s) = (\mathbf{Q}^*)^{-1} \mathbf{N}_0^T \mathbf{N}_0 \mathbf{Q}^{-1} = (\mathbf{N}_0 \mathbf{Q}^{-1})^* (\mathbf{N}_0 \mathbf{Q}^{-1}).$$

It follows from the above equation that $\operatorname{Im} \mathbf{M}(s)$ is positive definite, as the product $\mathbf{A}^* \mathbf{A}$ is positive definite for any regular matrix $\mathbf{A}$.

Note that this condition is not satisfied for the paraxial ray approximation.

Properties of 3D Elastodynamic Gaussian Beams and of the Paraxial Ray Approximation

We shall now discuss the properties of Gaussian beams. As a limiting case of Gaussian beams, we shall also shortly discuss the paraxial ray approximation.

We shall return from the variables (v, η) to the length variables (n, m). For simplicity, we shall call the Gaussian beam concentrated close to a ray of a P wave the compressional Gaussian beam (or P-Gaussian beam), and the beam concentrated close to a ray of an S wave the shear Gaussian beam (or S-Gaussian beam). In both cases, we can write for the displacement vector $\mathbf{u}(s, n, m, t)$ the expression

$$\begin{aligned} \mathbf{u}(s, n, m, t) = {} & u_s(s, n, m, t)\, \mathbf{t} + u_n(s, n, m, t)\, \mathbf{e}_n \\ & + u_m(s, n, m, t)\, \mathbf{e}_m, \end{aligned} \tag{92}$$

see (39). We shall also introduce the notation

$$u_\perp(s, n, m, t) = \begin{pmatrix} u_n(s, n, m, t) \\ u_m(s, n, m, t) \end{pmatrix}. \tag{93}$$

Compressional Gaussian Beams

Inserting the solutions W of the parabolic equation (49) into (40) yields

$$\begin{aligned} u_s(s, n, m, t) = {} & \frac{\Psi_P}{[\alpha(s)\, \rho(s) \det \mathbf{Q}(s)]^{1/2}} \\ & \cdot \exp\left\{ -i\omega \left[t - \int_0^s \frac{d\zeta}{\alpha(\zeta)} \right] + \frac{i\omega}{2} q^T \mathbf{M}(s)\, q \right\}, \\ u_n(s, n, m, t) = {} & \Psi_P \left[\frac{\alpha(s)}{\rho(s) \det \mathbf{Q}(s)} \right]^{1/2} (M_{11} n + M_{12} m) \\ & \cdot \exp\left\{ -i\omega \left[t - \int_0^s \frac{d\zeta}{\alpha(\zeta)} \right] + \frac{i\omega}{2} q^T \mathbf{M}(s)\, q \right\}, \\ u_m(s, n, m, t) = {} & \Psi_P \left[\frac{\alpha(s)}{\rho(s) \det \mathbf{Q}(s)} \right]^{1/2} (M_{12} n + M_{22} m) \\ & \cdot \exp\left\{ -i\omega \left[t - \int_0^s \frac{d\zeta}{\alpha(\zeta)} \right] + \frac{i\omega}{2} q^T \mathbf{M}(s)\, q \right\}. \end{aligned} \tag{94}$$

Here Ψ_P denotes a complex-valued quantity which is constant along the ray Ω. The principal component $u_s\mathbf{t}$ has a direction parallel to the central ray Ω. The additional components $u_n\mathbf{n}$ and $u_m\mathbf{m}$ are perpendicular to the ray Ω; they vanish at the central ray. Their importance increases with the increasing distance from the ray Ω.

Using notation (93), the expressions for the additional components can be written in a more compact form,

$$u_\perp(s,n,m,t)=\Psi_P\left[\frac{\alpha(s)}{\rho(s)\det\mathbf{Q}(s)}\right]^{1/2}\mathbf{M}(s)q \cdot \exp\left\{-i\omega\left[t-\int_0^s\frac{d\zeta}{\alpha(\zeta)}\right]+\frac{i\omega}{2}q^T\mathbf{M}(s)q\right\}. \tag{95}$$

Shear Gaussian Beams

Inserting (69) into (48) yields

$$u_s(s,n,m,t)=-\left[\frac{\beta(s)}{\rho(s)\det\mathbf{Q}(s)}\right]^{1/2} \cdot[\Psi_n(M_{11}n+M_{12}m)+\Psi_m(M_{12}n+M_{22}m)] \cdot\exp\left\{-i\omega\left[t-\int_0^s\frac{d\zeta}{\beta(\zeta)}\right]+\frac{i\omega}{2}q^T\mathbf{M}(s)q\right\},$$

$$u_n(s,n,m,t)=\frac{\Psi_n}{[\beta(s)\rho(s)\det\mathbf{Q}(s)]^{1/2}} \cdot\exp\left\{-i\omega\left[t-\int_0^s\frac{d\zeta}{\beta(\zeta)}\right]+\frac{i\omega}{2}q^T\mathbf{M}(s)q\right\},$$

$$u_m(s,n,m,t)=\frac{\Psi_m}{[\beta(s)\rho(s)\det\mathbf{Q}(s)]^{1/2}} \cdot\exp\left\{-i\omega\left[t-\int_0^s\frac{d\zeta}{\beta(\zeta)}\right]+\frac{i\omega}{2}q^T\mathbf{M}(s)q\right\}. \tag{96}$$

Here Ψ_n and Ψ_m are some complex-valued quantities which are constant along the ray Ω. Let us denote

$$\Psi=\begin{pmatrix}\Psi_n\\ \Psi_m\end{pmatrix}. \tag{97}$$

Using (97) and (93), Eqs. (96) can be then written in a more compact form

$$u_s(s,n,m,t)=-\left[\frac{\beta(s)}{\rho(s)\det\mathbf{Q}(s)}\right]^{1/2}(\Psi^T\mathbf{M}(s)q) \cdot\exp\left\{-i\omega\left[t-\int_0^s\frac{d\zeta}{\beta(\zeta)}\right]+\frac{i\omega}{2}q^T\mathbf{M}(s)q\right\},$$

$$u_\perp(s,n,m,t)=\frac{\Psi}{[\beta(s)\rho(s)\det\mathbf{Q}(s)]^{1/2}} \cdot\exp\left\{-i\omega\left[t-\int_0^s\frac{d\zeta}{\beta(\zeta)}\right]+\frac{i\omega}{2}q^T\mathbf{M}(s)q\right\}. \tag{98}$$

The principal components $u_n\mathbf{n}$ and $u_m\mathbf{m}$ have a direction perpendicular to the central ray Ω. The additional component $u_s\mathbf{t}$ is parallel to the ray Ω; it vanishes directly at the central ray. Its importance increases with increasing distance from the ray Ω.

Paraxial Ray Approximation

As shown above, the solutions (92)–(98) include as a limiting case the paraxial ray solution for real-valued **M**, **Q**, **P**. In other words, the paraxial ray solution is obtained if the matrix of the initial parameters **C** in (78) is chosen real-valued. In some special cases of practical interest, it is not necessary to evaluate all four linearly independent solutions Π_i ($i=1, 2, 3, 4$). For example, for the point source solutions, we can evaluate only Π_3 and Π_4, and for the plane source solutions we can evaluate only Π_1 and Π_2. The paraxial ray approximation for arbitrary other initial conditions (arbitrarily curved wavefront at $s=s_0$) can be then obtained as a linear combination of these two solutions.

We can easily see from the above equations that they give standard ray solutions at the central ray Ω for real-valued **M**, **Q** and **P**. The above equations, however, describe the wave field even in some neighbourhood of the central ray Ω (i.e., for $n\neq0$ and/or $m\neq0$). To determine the wave field at a point A close to the central ray Ω, it is not necessary to evaluate a new ray which passes through the point A, but we can compute the wave field at A by the paraxial ray approximation corresponding to the ray Ω.

The quantity $[\det\mathbf{Q}(s)]^{1/2}$ is real-valued in the paraxial ray approximation and has the meaning of geometrical spreading, well-known in the ray method, see Červený et al. (1977), Popov and Pšenčík (1978a, b), Červený and Hron (1980). It vanishes at caustics and causes infinite ray amplitudes there. Thus, the paraxial ray approximation has the same singularity at caustics as the standard ray method.

In the paraxial ray approximation, the real-valued matrix $\mathbf{M}(s)$ represents *the matrix of the second derivatives of the travel-time field* and the real-valued matrix $\mathbf{K}(s)=v(s)\mathbf{M}(s)$ is called the *curvature matrix*, see Červený and Hron (1980). The matrix $\mathbf{M}(s)$ fully describes the travel-time field in the vicinity of Ω accurate up to the second order terms in n and m. The matrix $\mathbf{K}(s)$ describes the geometric properties of the wavefront in the same vicinity of the ray Ω. As the matrices $\mathbf{M}(s)$ and $\mathbf{K}(s)$ are symmetric, they have real eigenvalues. For simplicity, we shall consider only the matrix $\mathbf{K}(s)$ in the following. (Similar conclusions regarding the matrix $\mathbf{M}(s)$ are straightforward.) Let us denote the eigenvalues of $\mathbf{K}(s)$ by $K_1(s)$ and $K_2(s)$. They represent the principal curvatures of the wavefront on Ω at s. The principal directions of the curvature of the wavefront are determined by the corresponding eigenvectors, $\mathbf{e}_1^K$ and $\mathbf{e}_2^K$. The three unit vectors $\mathbf{t}$, $\mathbf{e}_1^K$, $\mathbf{e}_2^K$ are mutually orthogonal. Instead of the principal curvatures $K_1(s)$ and $K_2(s)$ we can also introduce the principal radii of the curvature of the wavefront on Ω at s, $R_1=1/K_1$ and $R_2=1/K_2$. The quantities $K_{1,2}$ and $R_{1,2}$ may attain arbitrary real values, including 0 and ∞. For $K_{1,2}\neq0$ and $R_{1,2}\neq0$, the wavefront is ellipsoidal (for $K_1K_2>0$) or hyperboloidal (for $K_1K_2<0$) in the vicinity of Ω at s. The

quadratic curve $q^T \mathbf{K}(s) q = 1$ is an ellipse or a hyperbola. We shall call it the wavefront ellipse or the wavefront hyperbola. The main axes of the *wavefront ellipse* (or *hyperbola*) are determined by the eigenvectors $\mathbf{e}_1^K$ and $\mathbf{e}_2^K$. Along the wavefront ellipse (hyperbola) the travel time is constant, the travel-time difference with respect to the relevant point s at Ω equals $(2v(s))^{-1}$.

For $K_1(s) = K_2(s) = 0$, the wavefront is a plane, perpendicular to Ω at s. Similarly, for $R_1(s) = R_2(s) = 0$, we get a point source singularity on Ω at s. The 2D cylindrical wavefronts are described by $K_1(s) = 0$ or $K_2(s) = 0$. For $K_1(s) = 0$ and $R_2(s) = 0$ or $K_2(s) = 0$ and $R_1(s) = 0$ we get a line source singularity on Ω at s.

It is not difficult to see that the displacement vector $\mathbf{u}$ of the paraxial ray approximation for the P wave is *linearly polarized*, even for $n, m \neq 0$. It is approximately perpendicular to the wavefront at a given point (s, n, m) in the close vicinity of the central ray Ω. Thus, the additional components u_n and u_m in (94) represent corrections to the principal component u_s which keep the displacement vector $\mathbf{u}$ perpendicular to the wavefront for $n \neq 0$ and/or $m \neq 0$.

The polarization of $\mathbf{u}$ of the paraxial ray approximation for an S wave is, however, more complicated. Let us first consider the situation directly at the central ray Ω ($n = m = 0$), where the additional component u_s vanishes. In this case the displacement vector $\mathbf{u}$ is generally *elliptically polarized*, the polarization ellipse being perpendicular to Ω, i.e., tangent to the wavefront. The elliptical polarization degenerates into the linear polarization only if the phases of complex-valued constants Ψ_n and Ψ_m differ by $k\pi$, where k is an arbitrary integer (e.g. if both Ψ_n and Ψ_m are real-valued). The parameters of the polarization ellipse can be simply determined by well-known methods, see Born and Wolf (1959), Kravcov and Orlov (1980). The orientation of the polarization ellipse is controlled mainly by the phase difference between Ψ_n and Ψ_m. As this phase difference does not change along a smooth ray (even if it touches a caustic), the polarization ellipse does not change its orientation with respect to $\mathbf{e}_n$ and $\mathbf{e}_m$ along the ray. (It may change its orientation only if the ray impignes supercritically at an interference, but the interfaces are not considered in this paper.)

It is obvious that the vector $\mathbf{u}$ is elliptically polarized even for $n \neq 0$ and/or $m \neq 0$. The polarization ellipse is approximately tangent to the wavefront at the relevant point. The polarization ellipse of the S wave degenerates into linear polarization even for $n \neq 0$ and/or $m \neq 0$, if the phases of Ψ_n and Ψ_m differ by $k\pi$, where k is an integer, e.g. if both Ψ_n and Ψ_m are real-valued, see Eqs. (96).

Thus, we have four significant pairs of unit vectors in the plane perpendicular to the ray Ω at any point of Ω in the paraxial ray approximation. Each of these pairs is formed by two mutually orthogonal unit vectors and determines two specific directions. They are as follows:

1) The unit normal $\mathbf{n}$ and binormal $\mathbf{b}$ to the ray Ω.

2) The unit vectors $\mathbf{e}_n$ and $\mathbf{e}_m$, which form (together with $\mathbf{t}$) the basis of the ray-centred coordinate system (s, n, m). The unit vectors $\mathbf{e}_n$ and $\mathbf{e}_m$ rotate with respect to $\mathbf{n}, \mathbf{b}$ along a 3D ray with a torsion as the wave progresses, see (1). For plane rays (without torsion), the mutual orientation of both systems remains preserved.

3) The eigenvectors of the curvature matrix $\mathbf{e}_1^K$ and $\mathbf{e}_2^K$, which determine the principal curvature directions of the wavefront. They generally rotate both with respect to $\mathbf{e}_n, \mathbf{e}_m$ and with respect to $\mathbf{n}, \mathbf{b}$ as the wave progresses.

4) The directions of the main axes of the polarization ellipse of S waves at Ω. The polarization ellipse does not change its orientation with respect to $\mathbf{e}_n$, $\mathbf{e}_m$ in a smooth medium. It rotates, however, with respect to $\mathbf{n}, \mathbf{b}$, and with respect to $\mathbf{e}_1^K$ and $\mathbf{e}_2^K$ at the same rate as $\mathbf{e}_n$ and $\mathbf{e}_m$ as the wave progresses.

Complex Curvature Matrix of Gaussian Beams

The behaviour of Gaussian beams is controlled by the matrix $\mathbf{M}(s)$. In the case of Gaussian beams, the matrices $\mathbf{M}$, $\mathbf{Q}$ and $\mathbf{P}$ are complex-valued. We shall call $\mathbf{M}$ the *complex matrix of the second derivatives of the travel-time field*. We again introduce a complex-valued 2×2 symmetric matrix $\mathbf{K}(s) = v(s)\,\mathbf{M}(s)$ and call it the *complex curvature matrix*. A similar notation was used by Arnaud and Kogelnik (1969) in the case of light Gaussian beams in optical systems.

Both the matrices $\mathbf{M}(s)$ and $\mathbf{K}(s)$ can be formally divided into the real and imaginary parts. For simplicity, we shall use the following notations

$$\mathbf{M}(s) = \mathbf{M}^R(s) + i\mathbf{M}^I(s), \qquad \mathbf{K}(s) = \mathbf{K}^R(s) + i\mathbf{K}^I(s). \tag{99}$$

The interpretation of matrices $\mathbf{M}^R(s)$ and $\mathbf{K}^R(s)$ is quite similar to the interpretation of matrices $\mathbf{M}(s)$ and $\mathbf{K}(s)$ in the paraxial ray approximation. For example, $\mathbf{K}^R(s)$ describes the geometric properties of the wavefront of the Gaussian beam. The eigenvalues K_1^R, K_2^R of the matrix $\mathbf{K}^R$ and the eigenvalues M_1^R, M_2^R of the matrix $\mathbf{M}^R$ are always real. K_1^R and K_2^R determine the principal curvatures of the wavefront of the Gaussian beam on Ω at s. For finite $K_{1,2}^R \neq 0$, the wavefront of the Gaussian beam is ellipsoidal (when $K_1^R K_2^R > 0$) or hyperboloidal (when $K_1^R K_2^R < 0$). The principal directions of the curvature of the wavefront are determined by the corresponding eigenvectors of $\mathbf{K}^R(s)$, $\mathbf{e}_1^R$ and $\mathbf{e}_2^R$. The quadratic curve $q^T \mathbf{K}^R(s) q = 1$ will be called the *phase ellipse* or *phase hyperbola*. All other conclusions regarding the phase front can be obtained in the same way as above.

Now we shall consider the symmetric 2×2 real-valued positive-definite matrices $\mathbf{M}^I(s)$ and $\mathbf{K}^I(s)$. They are of basic importance in the investigation of Gaussian beams. They control the amplitude profile of the Gaussian beam in a cross-section orthogonal to Ω at s. The amplitude profile of the principal component of the displacement vector is controlled by the factor

$$\exp\left\{-\frac{\omega}{2} q^T \mathbf{M}^I q\right\}$$
$$= \exp\left\{-\frac{\omega}{2}\left(n^2 M_{11}^I(s) + 2nm M_{12}^I(s) + m^2 M_{22}^I(s)\right)\right\}. \tag{100}$$

A similar factor can be written in terms of $\mathbf{K}^I(s)$, using $\mathbf{M}^I(s) = v^{-1}(s)\,\mathbf{K}^I(s)$. Thus, we can see that the amplitude profile in any plane section containing the tangent

to Ω at s is bell-shaped (Gaussian). This is the reason why these solutions are called Gaussian beams.

The width of the beam depends on the frequency; it decreases with increasing frequency. Note that the bell-shaped Gaussian profile is generally deformed by the additional components of the displacement vector, mainly at larger distances from Ω. For simplicity, we shall speak about Gaussian bell-shaped profiles in the following.

As the matrices $\mathbf{K}^I(s)$ and $\mathbf{M}^I(s)$ are positive definite, they have real-valued positive eigenvalues, K_1^I, K_2^I and M_1^I, M_2^I, where $K_{1,2}^I = vM_{1,2}^I$. The principal directions are determined by the corresponding unit eigenvectors $\mathbf{e}_1^I$ and $\mathbf{e}_2^I$ (which are the same for $\mathbf{K}^I$ and $\mathbf{M}^I$). The three unit vectors $\mathbf{t}, \mathbf{e}_1^I, \mathbf{e}_2^I$ are mutually orthogonal.

We can again use any of the two matrices $\mathbf{K}^I(s)$ and $\mathbf{M}^I(s)$ to investigate the amplitude profiles. We shall call the matrix $\mathbf{M}^I(s)$ the matrix of the amplitude profile of the Gaussian beam, or shortly the amplitude profile matrix. The quadratic curve $q^T\mathbf{K}^I(s)\,q=1$ always represents an ellipse, with axes $2/K_1^I$ and $2/K_2^I$. Following Arnaud and Kogelnik (1969), we shall call it the *spot ellipse*. The amplitude of the principal component of the Gaussian beam is constant along this ellipse and equals $\exp[-\frac{1}{2}\omega v^{-1}(s)]\,A(s)$. We can also introduce the frequency-dependent spot ellipse by the relation $q^T\mathbf{K}^I(s)\,q=2\omega^{-1}v(s)$, or equivalently by $q^T\mathbf{M}^I(s)\,q=2\omega^{-1}$. The amplitude along this frequency-dependent spot ellipse is $e^{-1}A(s)$. The dimensions of the frequency dependent spot ellipse decrease with increasing frequency.

Generally speaking, the Gaussian beam is more concentrated to the ray Ω for larger eigenvalues K_1^I and K_2^I. To describe this property, it may be useful to introduce a new matrix $\mathbf{L}(s)$ by the relation

$$\mathbf{L}(s)=\left[\frac{\omega}{2}\mathbf{M}^I(s)\right]^{-1/2}=\left[\frac{\omega}{2v(s)}\mathbf{K}^I(s)\right]^{-1/2}. \tag{101}$$

We shall call $\mathbf{L}(s)$ the matrix of the half-width of the Gaussian beam, or shortly *the half-width matrix*. Its eigenvalues L_1 and L_2 (always real and positive) are given by the relation,

$$L_{1,2}(s)=\left[\frac{\omega}{2}M_{1,2}^I(s)\right]^{-1/2}=\left[\frac{\omega}{2v(s)}K_{1,2}^I(s)\right]^{-1/2}. \tag{102}$$

It is obvious that the quantities $2L_1$ and $2L_2$ measure the length of axes of the frequency dependent spot ellipse. Thus, they determine the minimum and maximum distances from Ω at which the amplitude drops from $A(s)$ on the central ray Ω to $e^{-1}A(s)$. Thus, the Gaussian beam is more concentrated close to Ω for smaller L_1 and L_2.

The matrix $\mathbf{L}$ introduced above and its eigenvalues L_1, L_2 depend on frequency. We can also introduce a *frequency-independent half-width matrix*, namely the half-width matrix for the frequency $f=1$ Hz. We denote it by $\mathbf{L}^0(s)$,

$$\mathbf{L}^0(s)=[\pi\mathbf{M}^I(s)]^{-1/2}=\left[\frac{\pi}{v(s)}\mathbf{K}^I(s)\right]^{-1/2}. \tag{103}$$

The matrix $\mathbf{L}^0(s)$ has the eigenvalues $L_1^0(s)$ and $L_2^0(s)$ given by the relation

$$L_{1,2}^0(s)=[\pi M_{1,2}^I(s)]^{-1/2}=\left[\frac{\pi}{v(s)}K_{1,2}^I(s)\right]^{-1/2}. \tag{104}$$

The half-widths for the frequency $f=1$ Hz, L_1^0 and L_2^0, complemented by an angle which specifies the orientation of the spot ellipse, can be suitably chosen as the initial parameters of the Gaussian beam to characterize the matrix $\operatorname{Im}\mathbf{M}(s_0)$.

Polarization of Gaussian Beams

The displacement vectors $\mathbf{u}$ of both P and S Gaussian beams are generally elliptically polarized. The only exception is the linear polarization of $\mathbf{u}$ of the P Gaussian beam directly on the central ray. Outside the central ray, however, even $\mathbf{u}$ for the P Gaussian beam is elliptically polarized (in contradiction to the paraxial approximation of P-wave). The parameters of the polarization ellipse depend generally on all the three coordinates (s, n, m). The polarization ellipse of the S Gaussian beam directly on the ray is again perpendicular to the central ray Ω, similarly as in the ray approximation.

Astigmatism of Gaussian Beams

It was shown earlier in this section that four significant pairs of unit vectors perpendicular to the ray Ω could be introduced in the paraxial ray approximation. In case of Gaussian beams, an additional pair of unit vectors perpendicular to Ω plays an important role, namely the eigenvectors $\mathbf{e}_1^I$ and $\mathbf{e}_2^I$. They specify the orientation of the spot ellipse.

Generally, the unit vectors $\mathbf{e}_1^I$ and $\mathbf{e}_2^I$ rotate with respect to $\mathbf{e}_n$, $\mathbf{e}_m$ and with respect to $\mathbf{n}$, $\mathbf{b}$ as the wave progresses. They do not coincide (except for certain limiting situations) with the unit vectors $\mathbf{e}_1^R$ and $\mathbf{e}_2^R$, which specify the orientation of the phase ellipse. Thus, the orientation of the spot ellipse is generally different from the orientation of the phase ellipse. Such Gaussian beams are called *astigmatic Gaussian beams*, see Arnaud and Kogelnik (1969). When the unit vectors $\mathbf{e}_1^R$, $\mathbf{e}_2^R$ and $\mathbf{e}_1^I$, $\mathbf{e}_2^I$ coincide along the whole ray Ω (i.e., the spot ellipse and the phase ellipse keep the same orientation along the whole ray), the beam is called *the Gaussian beam with a simple astigmatism*. When the spot ellipse and the phase ellipse are circular along the whole ray Ω, the Gaussian beam is called *stigmatic* (*or circular*).

The stigmatic Gaussian beams and the beams with simple astigmatism are common in homogeneous media. In homogeneous media, we have

$$\mathbf{M}^{-1}(s)=\mathbf{M}^{-1}(s_0)+\mathbf{I}\int_{s_0}^{s}v(\zeta)\,d\zeta.$$

Hence it simply follows that the Gaussian beam remains stigmatic along the whole ray if it is stigmatic at least at one point of the ray. The same is valid for the Gaussian beam with simple astigmatism.

Such Gaussian beams, however, are only of limited significance in general 3D laterally inhomogeneous me-

dia. Even if we locally specify the Gaussian beam by the initial conditions as stigmatic, it becomes astigmatic due to inhomogeneities.

References

Aki, K., Richards, P.: Quantitative seismology. San Francisco: Freeman 1980

Arnaud, J.A., Kogelnik, H.: Gaussian light beams with general astigmatism. Applied Optics **8**, 1687–1693, 1969

Babich, V.M.: Eigenfunctions, concentrated in the vicinity of closed geodesics. In: Mathematical problems of theory of propagation of waves, Vol. 9, V.M. Babich, ed.: pp. 15–63. Leningrad: Nauka 1968 (in Russian)

Babich, V.M., Buldyrev, N.J.: Asymptotic methods in problems of diffraction of short waves. Moscow: Nauka 1972

Babich, V.M., Kirpichnikova, N.Y.: The boundary layer method in diffraction problems. Berlin: Springer 1979

Babich, V.M., Popov, M.M.: Propagation of concentrated acoustical beams in three-dimensional inhomogeneous media. Akust. Zh. **27**, 828–835, 1981 (in Russian)

Born, M., Wolf, E.: Principles of optics. New York: Pergamon Press 1959

Červený, V.: Synthetic body wave seismograms for laterally varying layered structures by the Gaussian beam method. Geophys. J.R. Astron. Soc., **73**, 389–426, 1983

Červený, V., Hron, F.: The ray series method and dynamic ray tracing systems for 3D inhomogeneous media. Bull. Seismol. Soc. Am. **70**, 47–77, 1980

Červený, V., Klimeš, L., Pšenčík, I.: Synthetic seismic wave fields in 2D and 3D inhomogeneous structures. In: Proc. of the 27th Int. Geophysical Symposium, Bratislava 198, Vol. A(I), G. Plíva, ed.: pp. 17–28. Brno: N.E. Geofyzika 1982a

Červený, V., Molotkov, I.A., Pšenčík, I.: Ray method in seismology. Praha: Universita Karlova 1977

Červený, V., Popov, M.M., Pšenčík, I.: Computation of wave fields in inhomogeneous media – Gaussian beam approach. Geophys. J.R. Astron. Soc., **70**, 109–128, 1982b

Červený, V., Pšenčík, I.: Gaussian beams in two-dimensional elastic inhomogeneous media. Geophys. J.R. Astron. Soc., **72**, 417–433, 1983

Hubral, P.: A wave front curvature approach to computing ray amplitudes in inhomogeneous media with curved interfaces. Stud. Geophys. Geod. **23**, 131–137, 1979

Hubral, P.: Wave front curvatures in 3D laterally inhomogeneous media with curved interfaces. Geophysics **45**, 905–913, 1980

Kamke, E.: Differentialgleichungen. Lösungsmethoden und Lösungen. Vol. 1: Gewöhnliche Differentialgleichungen. Leipzig: 1959

Kirpichnikova, N.J.: Construction of solutions concentrated close to rays for the equations of elasticity theory in an inhomogeneous isotropic space. In: Mathematical problems of theory of diffraction and propagation of waves, Vol. 1, V.M. Babich, ed.: pp. 103–113. Leningrad: Nauka 1971 (in Russian, English translation by American Mathematical Society, 1974)

Klimeš, L.: Mathematical modelling of seismic wave fields in 3D laterally inhomogeneous media. Research Report No. 63, Institute of Geophysics, Charles University, Prague 1982a (in Czech)

Klimeš, L.: Hermite-Gaussian beams in inhomogeneous elastic media. Studia Geophys. Geod., in press 1982b

Kravcov, Y.A., Orlov, Y.I.: Geometrical optics of inhomogeneous media. Moscow: Nauka 1980 (in Russian)

Popov, M.M.: Method of composition of Gaussian beams in isotropic theory of elasticity. Preprint LOMI AN SSSR, P-3-82, Leningrad, 1982

Popov, M.M., Pšenčík, I.: Ray amplitudes in inhomogeneous media with curved interfaces. In: Geofys. Sb., Vol. 24, A. Zátopek, ed.: pp. 111–129. Praha: Academia 1978a

Popov, M.M., Pšenčík, I.: Computation of ray amplitudes in inhomogeneous media with curved interfaces. Stud. Geophys. Geod. **22**, 248–258, 1978b

Received December 17, 1982; Accepted March 21, 1983

J Geophys (1983) 53:16–23

Journal of Geophysics

Electrical Conductivity Beneath Iceland – Constraints Imposed by Magnetotelluric Results on Temperature, Partial Melt, Crust- and Mantle Structure

M. Beblo[1], A. Björnsson[2], K. Arnason[1], B. Stein[1] and P. Wolfgram[1,3]

[1] Institut für Allgemeine und Angewandte Geophysik, Universität München, Theresienstrasse 41/IV, 8000 München 2, Federal Republic of Germany

[2] National energy authority, Grensasvegi 9, 108 Reykjavik, Iceland

[3] Department of Physics, University of Toronto, Toronto M5S 1A7, Canada

Abstract. Magnetotelluric results from 38 sites in North Iceland yield a detailed spatial distribution of conductivity versus depth. A high-conductivity layer, about 10 Ωm, marking the transition between crust and upper mantle is detected throughout the surveyed area, its depth increases from 10 km within the zones of present tectonic activity to 20–30 km at a 50–100 km distance from the rift axis. The high conductivity layer indicates some basaltic melt fraction at temperatures around 1,000 °C. The calculated average crustal temperature gradients are 100–150 °C/km at the rift axis and 50–70 °C/km at about 100 km distance. Below this anomalous zone, down to 150 km depth, the conductivity decreases to 100 Ωm due to the ultrabasic chemical composition of the upper mantle and a possible decrease of melt content with increasing depth. The temperature gradient within the upper mantle cannot be more than a few °C/km. However, a highly conducting asthenosphere exists below 150 km depth.

The following petrological model for Iceland is suggested: Diapiric updoming of the asthenosphere leads to partial fusion of parent ultrabasic mantle material, resulting in segregation and upward migration of basaltic melt. Lower density, lower viscosity and higher mobility relative to the solid phase causes the melt to rise faster than the ultrabasic material. This melt fraction then forms the basaltic crust of Iceland which is thickening away from the ridge axis with increasing age.

Key words: Iceland – Magnetotellurics – High-conductivity layer – Temperature – Partial melt – Petrological model

Introduction

Correlation between electrical conductivity and temperature offers a unique chance to infer the temperature distribution in the Earth's interior from magnetotelluric data. Therefore, the magnetotelluric method is applicable to quantitative geodynamic modeling of the Icelandic rift zone.

In 1977 and 1980 magnetoelluric surveys in North and East Iceland were realized in a joint effort of the University of Munich, Germany, and the National Energy Authority, Iceland. A total of 38 magnetotelluric sites were occupied as shown on the simplified geological map (Fig. 1), partially preceded by geological investigations and shallow resistivity soundings. High-energy source fields at the high geomagnetic latitude of Iceland and the absence of technical noise made short recording times possible and high-quality data were obtained.

Mobile magnetotelluric equipment comprising 2-component electric-field amplifiers, 3-component flux-gate mangetometers, 3-component induction-coil magnetometers for shorter periods (6 s–1 h), and digital tape recorders were employed. In addition a line of 6 Askania variographs combined with long period electric field recorders (1 h–1 d) worked simultaneously at six sites during the 1977 survey. For more detailed information on the experiments and the geology, the reader is referred to Beblo and Björnsson (1978), and Beblo and Björnsson (1980), where first results and interpretations along with a description of data analysis and numerical modeling are presented.

Magentotelluric Results, Resistivity Models and Interpretation

Source Field Geometry and Geomagnetic Depth Sounding

According to Haak (1978), an inhomogeneous source field causes the MT response to be different from the zero-wavenumber response only if the skin depth is on the order of the spatial dimensions of the source. The longest periods used for our magnetotelluric modeling were 1,000 s corresponding to a skin-depth of about 50–100 km. This is small compared with the 400–500 km half-width of the polar electrojet, therefore the influence of its inhomogeneity is small enough to be negligible. However, complicated source fields during auroral substorms may have the same spatial dimensions as our profile of the Askania variographs (about 200 km).

Wolfgram (1980) concluded that the disturbed-time magnetic variations in the period range 200 s to a few h were dominated by the source-field geometry. The long-period magnetic data could not be used for geomagnetic

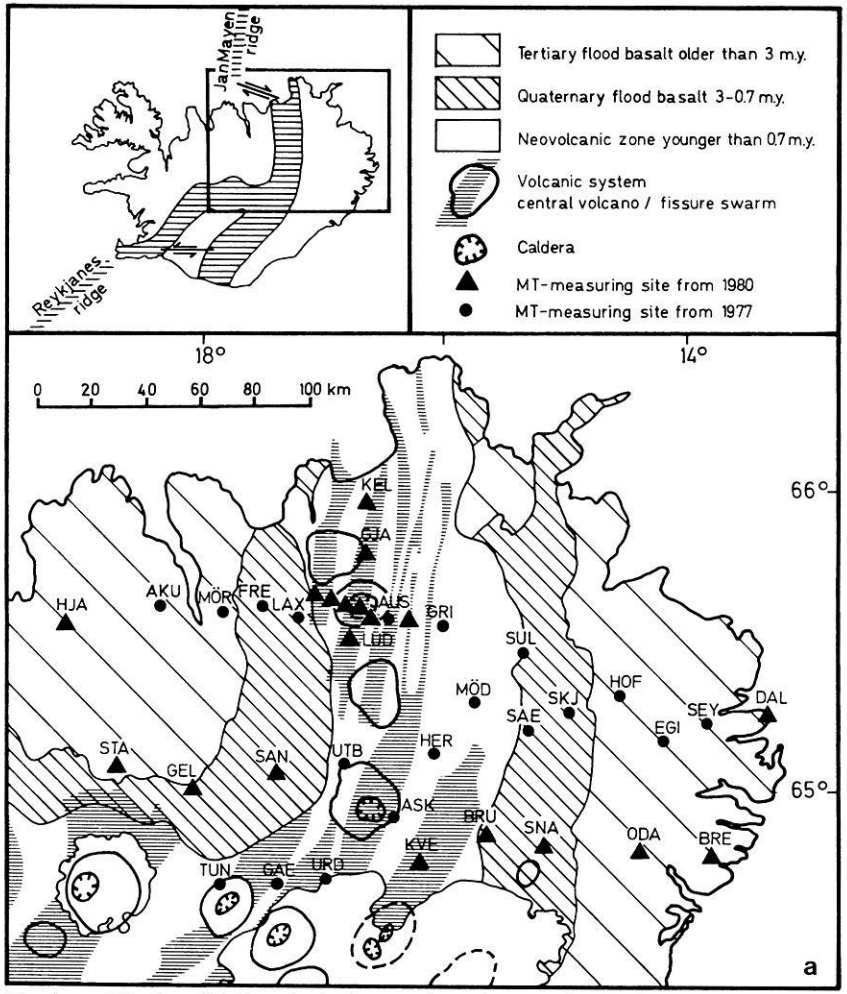

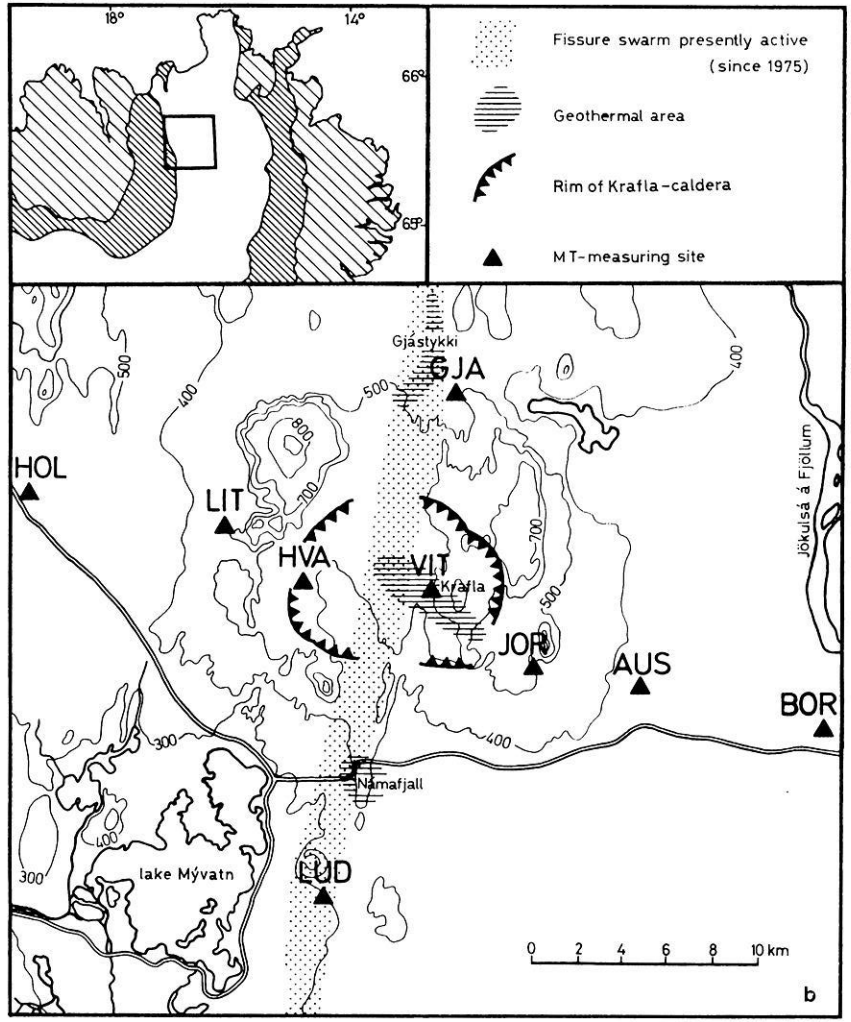

Fig. 1 a and b. Simplified geological map of northeast Iceland, showing locations of magenetotelluric measuring sites

depth sounding because they contained too few variations with a vertical magnetic field component free of source effects. However, it was possible, on the basis of these data, to exclude a very pronounced, two-dimensional conductivity anomaly beneath Iceland at greater depth, that would caused transfer functions between vertical and horizontal magnetic variations to be larger than 0,1.

Interpretation of the Magnetotelluric Data

Using electric (E) and magnetic (B) fields recorded simultaneously one can determine a complex transfer function, the tensor $z\ (i,j) = E(i)/B(j)$. The elements of z depend on the conductivity distribution and on the orientation of the measuring coordinate system. As a first step in data processing the "preference direction" of the electric field was determined as the angle of coordinate rotation at which the two orthogonal electric field components are least coherent. The preference direction indicates lateral variations of the electric conductivity near to the measuring site. For a laterally uniform distribution of the conductivity (one-dimensional case) no preference direction exists. In the case of considerable variations of the conductivity in one horizontal direction (two-dimensional case) the electric field will be strongly polarized giving a well determined preference direction (Kemmerle 1977).

Within the Tertiary flood basalt areas the computed preference direction of the electric field indicates horizontal variations of the conductivity at crustal depths, whereas the preference direction disappears within the Quaternary flood basalt areas and within the Neovolcanic zone. For depths greater than 5 km these areas show approximately a one-dimensional conductivity distribution, i.e. a variation of conductivity with depth only.

Shallow resistivity soundings (Björnsson, 1976) show conductivities down to 2 km depth within the Tertiary flood basalt area distinctly lower than those below the Neovolcanic zone. This indicates that the Neovolcanic zone can be treated as a conductivity anomaly with a pronounced strike direction.

For a two-dimensional structure it is possible to rotate the coordinate system until one axis is parallel to the strike direction. Two independent systems of equations are then obtained to calculate the apparent resistivity ρ_a and the phase φ from the tensor z. The solutions are:

a) $\rho_{a_\parallel} = \frac{\mu_0 T}{2\pi} |z_\parallel|^2$; $\varphi_\parallel = \arg(z_\parallel)$ E-Polarisation, TE-mode,

b) $\rho_{a_\perp} = \frac{\mu_0 T}{2\pi} |z_\perp|^2$; $\varphi_\perp = -\arg(z_\perp)$ B-Polarisation, TM-mode.

In the case of a one-dimensional conductivity distribution both TE-mode and TM-mode, give identical solutions. This is more or less the case for all sites within the Neovolcanic zone.

Apparent resistivity and phase curves were obtained for all sites; some examples of the 1980 th survey are shown in Fig. 2. Small error bars of the 68% confidence interval reflect the high quality of the data. The scattering increases slightly at periods above 1,000 s because of

a) numerical corrections for the slope of the electronic high-pass filter,

b) lesser degrees of freedom for spectral averages at longer periods, and

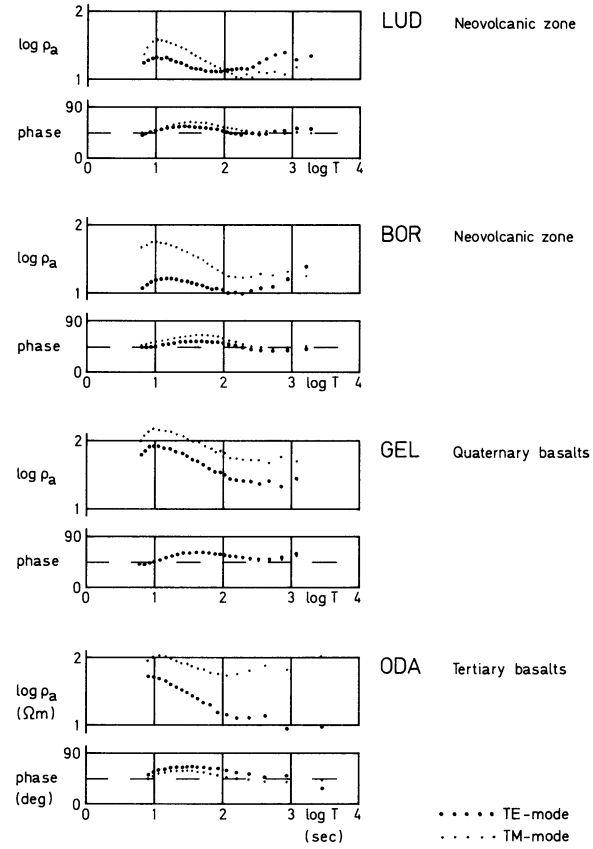

Fig. 2. Examples for apparent resistivities and phase differences, seperated in TE-mode ($\rho_{a_\parallel}$, $\varphi_\parallel$) and TM-mode ($\rho_{a_\perp}$, $\varphi_\perp$). Due to high data quality error bars are too small to be drawn for periods shorter than about 1,000 s. The shift of minimum $\rho_{a_\parallel}$ toward longer periods in correspondence to an increase in depth to the highly conducting layer with increasing distance from the rift axis is clearly seen

c) the spatially inhomogeneous source fields (polar electrojet) being non-stationary.

For a first interpretation of the data, models of one-dimensional conductivity distribution versus depth were fitted to the TE-mode curve of apparent resistivity and phase at each site using the psi-algorithm of Schmucker (Schmucker, 1974). Due to the continuity of the parallel electric field across the boundaries of the two-dimensional anomaly the TE-mode curves are weakly distorted by horizontal near-surface inhomogeneities and reflect mainly the conductivity structure in greater depth.

At all sites the best fit was obtained with three-layer-models of the type: a good conductor for the second layer, poor conductivity below and above.

The results of the numerical modeling were assembled into some east-west sections (Figs. 3a–3d) across the rift axis and a north-south section (Fig. 3e) along it. They clearly show the zone of enhanced electrical conductivity throughout North Iceland dipping from about 10 km to 20–30 km depth with increasing distance from the rift axis. The sites LIT, HVA, and VIT on the rift axis exhibit an extremely shallow conductor (Fig. 3b) at about 5 km depth (Arnason, 1981). These sites are located within the Krafla central volcano where active rifting is taking place.

The results from a seismic refraction measurement near Krafla (Zverev et al., 1980) are superimposed onto the magnetotelluric results in Fig. 3b. Seismic reflecting horizons

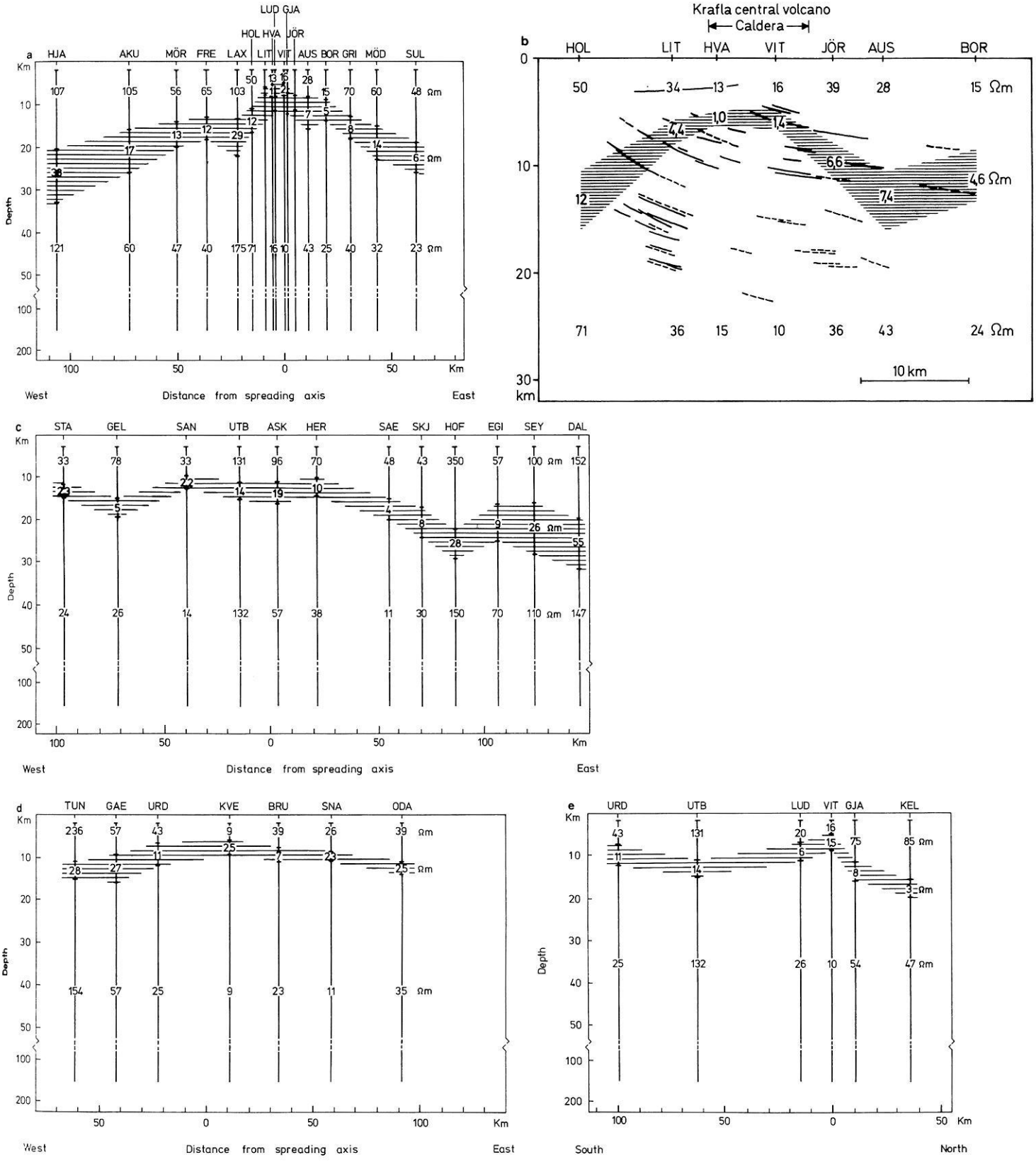

Fig. 3a–e. Models of one-dimensional conductivity distribution at all sites, calculated from apparent resistivities and phases of the *TE*-mode, and assembled into profiles. The hatched areas show a continous high conductivity layer with a mean resistivity of 10–15 Ωm. The numbers indicate resistivities in Ωm. **a, c and d** East-west magnetotelluric cross-sections perpendicular to the strike and centered at the spreading axis showing significant updoming of the high conductivity layer within the Neovolcanic zone. **b** Magnetotelluric cross-section through the currently active Krafla central volcano region (inner part of Fig. 3a) showing extremly high conductivities of 1–5 Ωm (hatched area) at only 5 km depth within the Krafla region. The high conductivity is very likely caused by deep circulating geothermal fluids, high-level melt accumulation and magma chamber below HVA and VIT. A seismic cross-section (Zverev et al., 1980) has been superimposed onto the magentotelluric results. **e** North-south magnetotelluric cross-section along the strike of the rift zone, centered on the Krafla central volcano

are absent below the rift axis at 10–15 km depth suggesting homogeneity in the physical properties at these depths. This seismically homogeneous body is interpreted by Zverev et al. (1980) as being a magma chamber. Microearthquake observations in the Krafla area indicate a confined magma chamber at 3–7 km depth (Einarsson, 1978) below the MT-stations HVA and VIT.

An shallow conductor was also found at the site KVE (Fig. 3d) located in the vicinity of the Kverkfjoell central volcano. The conductivity sections in Fig. 3c and Fig. 3e show an updoming of the conductor at the rift axis and a nearly horizontal position at about 10 km depth within the Neovolcanic zone, which is in agreement with seismic observations which indicate that no continous partially molten layer can be present above 10 km depth within the crust in NE-Iceland (Sanford and Einarsson, 1982).

The subsidence of the good conductor to the north of site KEL in Fig. 3e might be a result of thicker crust within and north of the Tjoernes fracture zone connecting the rift axis to the Kolbeinsey (Iceland-Jan Mayen) ridge.

The Coast Effect

Considerable horizontal changes in electrical conductivity near the coast affect the electromagnetic recordings. Stein (1982) computed and compared numerical modeling results with the two-dimensional distribution of conductivity with the magnetotelluric results of Iceland. The numerical modeling revealed two effects:

a) The coast effect is significantly enhanced if the horizontal gradient of conductivity increases. The influence of the coast effect increases with increasing period of the electromagnetic field variations.

b) Strong lateral gradients of the conductivity distribution, representing a more complicated geological structure, may conceal the coast effect.

Apparent resistivity and phase results at some magnetotelluric sites were chosen for comparison with the coast effect modeling results. The coast effect should be visible within the range SNA-ODA-BRE where BRE is located close to the coast line (cf. Fig. 1). The *TM*-mode fields may be affected when approaching the coast whereas the *TE*-mode fields do not show a coast effect.

In general, the coast effect was found to have less influence than expected. The preference direction of the electric field, the polarisation $p=(Z_{\|}/Z_{\perp})-1$, and the scewness $S=(Z_{xy}-Z_{yx})/(Z_{\|}-Z_{\perp})$ (Reddy et al., 1977) are better indicators for the presence of a coast effect. They indicate an effect at the site ODA and BRE which are nearest to the coast whereas no coast effect is indicated at SNA. On the other hand the Neovolcanic zone as a shallow conductive structure clearly dominates at the sites west of SNA. The northern sites (DAL-SKJ, Fig. 1) are affected by local, shallow contrasts in conductivity; their results could not be explained with the coast effect modeling.

Electrical Conductivity, Temperature, and Petrological Conditions in Crust and Mantle

An importand aim of magnetotelluric investiagtions of subsurface electrical conductivity distribution is to get some knowledge about temperature and petrology in the Earth's interior. The key to this is the change in the electrical conductivity of various rock types with temperature, pressure, oxygen fugacity and other parameters. These parameters have been investigated by several authors, and were complied and interpreted recently by Haak (1980). The usual petrological model for asthenospheric geodynamics (Ringwood, 1969; Waff, 1974) consists of an ultrabasic-peridotitic mantle with solid olivine and liquid basalts.

The average conductivity of basalts is one order of magnitude higher than that of peridotite at the same temperature. Either material is partially molten above 1,000 °C and liquid above 1,400 °C. This relation between electrical conductivity and temperature is valid only for almost dry rocks at depths greater than about 10 km. The conductivity in the uppermost kilometers of the Earth's crust depends mostly on the porosity and permeability of the rock matrix as the amount and chemical condition of the interstitial water.

A Petrological Model for Iceland

The shallow zone of enhanced electrical conductivity as inferred from our magnetotelluric numerical modeling (Fig. 3) is not limited to Northern Iceland since Hermance and Grillot (1970) found a shallow high conductivity layer at a site located within the Neovolcanic zone of Southern Iceland. Recently, Hersir et al. (1982) found a shallow zone of enhanced conductivity in Southern Iceland at a depth increasing with distance from the rift axis. Apparently, the magnetotelluric method does give the same conductivity distribution for North Iceland as it does for South Iceland, which is encouraging for the construction of a petrological model for Iceland.

Iceland's crust is manly build up of flood-basalt layers and basltic intrusions. If the basaltic crust reaches down to the depth of the 10–15 Ωm conductor, temperatures around 1,000 °C must be present. For detailed discussion on this point see Beblo and Björnsson (1980). At this temperature the basalts will already contain some melt fraction. If we assume the basaltic material to extend below the anomalous zone then the increased average resistivity of 100 Ωm at greater depth (Fig. 3) would indicate a decrease in temperature. This would not be in agreement with the geodynamic processes in rifting zones. In a rifting region an upward flow of material is conncected with an upward dragging of isotherms, i.e. an increase in temperature with depth. Consequently, the pronounced change in conductivity is a result of the change in chemical composition below the anomalous layer. We conclude that the material below the zone of enhanced conductivity is of ultrabasic composition, i.e. mantle material. For ultrabasites, a resistivity value of 100 Ωm gives a temperature of 1,000 °C at which partial melting is expected. The melt content is highest in the basaltic high conductivity layer – the base of the crust – and decreases with increasing depth within the upper mantle. These results – indicating a differentiating process in the mantle – are supported by seismic refraction experiments (Gebrande et al., 1980). They concluded a 17–23% melt fraction at depths between about 10–20 km, decreasing with increasing depth. An estimate of the amount of melt fraction from the magentotelluric results is difficult. Waff (1974) showed that two different models may describe the relation between electrical conductivity and melt fraction:

Model 1: Isolated, electrically conducting tubes and pockets of molten basalt are contained in a highly resistant matrix

of solid olivine yielding an effective conductivity σ which is approximately that of the solid phase σ_s, where N is the percent melt fraction.

$$\sigma = \frac{1-2N}{1-N}\,\sigma_s.$$

A melt fraction of about 30% is required for a two-fold to three-fold increase of the electrical conductivity.

Model 2: Isolated, electrically resistant olivines are coated with a highly conductive, basaltic melt resulting in an effective conductivity which is approximately that of the liquid phase σ_l, where N is the percent melt fraction.

$$\sigma = \frac{2N}{3}\,\sigma_l.$$

A melt fraction of around 5% is sufficient to increase the effective conductivity by a factor 10 to 100 beyond the conductivity of the solids.

Hermance (1981) and Thayer et al. (1981) discuss the same facts by interpreting their magnetotelluric field observations in Iceland. Melt pillows (model 1) are not likely to be detected by magnetotelluric measurements because they increase the apparent conductivity only slightly. The zones of enhanced conductivity within the asthenosphere are on the other hand explainable with a continuously connected melt over large areas (model 2).

Shankland and Waff (1977) calculated the changes of temperature and melt fraction with varying electrical conductivity for the crust-mantle boundary. The melt fraction decreases with depth and is probably not more than 5% at about 100 km (30 kbar). Shankland and Waff showed that water contents as low as 0.1% H_2O do not significantly increase the melt fraction or, respectively, decrease the temperature.

Long-period (1,000 s–30,000 s) magnetotelluric results obtained by Haak and Damaske (1980) for the sites AUS and FRE (Fig. 1) fit consistently with our results. Their model shows a pronounced second increase in conductivity for the asthenosphere at 150–170 km depth. This deep-seated conductor shows up in the apparent resistivities above 10,000 s. The phase already exceeds 45° above 1,000 s and increases with increasing periods (Fig. 2), a sign of an increase in conductivity at greater depths.

It is interesting to compare the Mid-Atlantic-Ridge conductivity model for Iceland to MT-data measured in the Pacific-Rise crest by Filloux (1981, 1982). In Fig. 4 the conductivity models are shown for site FRE (Iceland) and station 1A (Pacific-Rise) which are at an equivalent distance from the spreading center. In both models the similarity of a pronounced high conductivity layer is evident at the base of the crust. Electrical conductivities for the asthenosphere from 100–200 km depth are also quite similar. In both places a systematic change of conductivity with crustal age seems to be evolved.

In conclusion, the model for the Earth's crust and mantle beneath Iceland based on the subsurface electrical conductivity distribution may be viewed as follows:

Beneath the rift axis diapiric-type motion in the updoming asthenosphere leads to partial fusion of mantle material, resulting in the segregation and upward migration of a basaltic melt. The melt fraction tends to escape due to its lower density, lower viscosity, and higher mobility as compared with the solid phase. Consequently, a chemical differentiation between melt fraction and rock matrix occurs whereby basaltic melt with a high electrical conductivity is "sweated out" from the olivine-ultrabasite-basalt multiphase system of the mantle. The melt fraction rises faster than the remining solid phase and creates a zone of magma accumulation from which Iceland's basaltic crust is generated, thickening away from the ridge with increasing age.

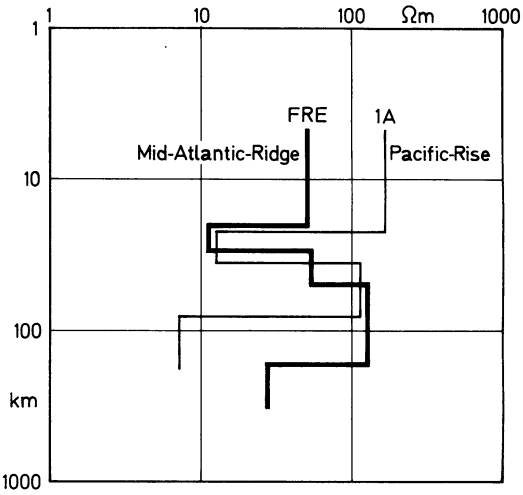

Fig. 4. The Mid-Atlantic-Ridge conductivity model for Iceland (Beblo and Björnsson, 1979, Haak and Damaske, 1980) compared to MT-results in the Pacific-Rise-Crest (Filloux, 1981, 1982). The conductivity models are shown for site FRE (Iceland) and station 1A (Pacific Rise). These sites are at the same distance from the spreading axis. The similarity of a pronounced high conductivity layer at the base of the crust is evident. The electrical conductivity from 100–200 km depth is also quite similar

This model developed from electrical conductivity is consistent with theoretical convection-models for the sub-ocean lithosphere (Bottinga and Allegre, 1976; Bottinga and Steinmetz, 1979). They started from a two-phase system composed of 75% peridotite and 25% basalt with a 1 cm/year drift rate which is in good agreement with assumed drift rates of Iceland. Their final model exhibits a zone enriched with basalt at depths of 15–20 km. The zone of enhanced electrical conductivity beneath Iceland encloses the calculated isotherms 1,000 °C and 1,100 °C entirely.

The Temperature Gradient Beneath Iceland

The MT-results suggest temperatures of 1,000 °C to 1,100 °C for the region of enhanced electrical conductivity. An average value for the temperature gradient in the Icelandic crust can be obtained by dividing these temperatures by the depth to the conductor. The temperature gradients obtained this way reach values as high as 150–180 °C/km at the rift axis and about 60 °C/km at a distance of 100 km (Fig. 5). However, the values at the rift axis scatter considerably. The reason for this is very likely irregular distribution of deep circulating geothermal fluids and magma accumulation in the crust of the active spreading zone. Hydrothermal alteration and circulation of saline geothermal water within the fractured Neovolcanic zone in Iceland may raise the conductivity considerably. Below about 5 km depth most cracks and pores are probably closed. Electrolytic conduction is thus not likely in the depth range greater 5 km, and therefore the high conductivity requires high tempera-

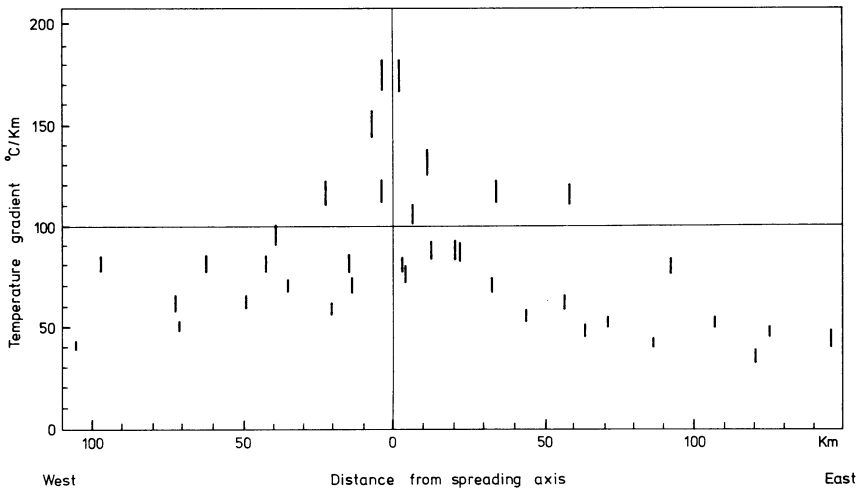

Fig. 5. Thermal gradients for the Icelandic crust, centered on the spreading axis, as inferred from the magnetotelluric results. The vertical bars show the mean temperature gradient at each site assuming a temperature range of 1,000–1,100 °C in the centre of the highly conducting layer

tures caused by magmatic intrusions, dykes or sills and high level magma chambers.

The temperature gradients obtained from magnetotellurics are consistent with borehole temperature measurements from Iceland (Palmason et al. , 1979) as well as from measurements on the Mid-Atlantic Ridge south of Iceland (Bram, 1980).

The conductivity models (Fig. 3) show values of 100 Ωm or even more for the deep layer. In the case of constant increase in temperature with depth the conductivity of ultramafic rocks should be about 10 Ωm, an order of magnitude lower than measured by magnetotellurics. Therefore the temperature gradient must be much lower within the upper mantle than in the crust. According to Shankland and Waff (1977) a theoretical mantle geotherm of 3–4 °C/km may be possible. Hermance and Grillot (1970) as well as Haak and Damaske (1980) inferred mantle geotherms of 2 °C/km from their long-period magnetotelluric results.

Acknowledgements. We thank all who made this research possible by assisting in field work as well as in data interpretation. We are grateful to Professor Dr. G. Angenheister, Munich for his personal interest and support. We thank the unknown reviewers of the initial manuscript for valuable criticisms and constructive suggestions. The financal support of the Deutsche Forschungsgemeinschaft and of the Deutscher Akademischer Austauschdienst is gratefully acknowledged.

References

Arnason, K.: Magnetotellurische Messungen auf einem Profil über den Zentralvulkan Krafla in Nord-Ost-Island. Dipl.-Arbeit, Univ. München, 1981

Beblo, M., Björnsson, A.: Magnetotelluric investigation of the lower crust and upper mantle beneath Iceland. J Geophys. **45,** 1–16, 1979

Beblo, M., Björnsson, A.: A model of electrical resistivity beneath NE-Iceland, correlation with temperature. J. Geophys. **47,** 184–190, 1980

Björnsson, A.: Electrical resistivity of layer 3 in the Icelandic crust. Soc. Sci. Islandica, Greinar 5, 7–23, 1976

Bottinga, Y., Allegre, C.: Geophysical, petrological and geochemical models of the oceanic lithosphere. Tectonophysics **32,** 9–59, 1976

Bottinga, Y., Steinmetz, L.: A geophysical, geochemical, petrological model of the sub-marine lithosphere. Tectonophysics **55,** 311–347, 1979

Bram, K.: New heat flow observations on the Reykjanes ridge. J. Geophys. **47,** 86–90, 1980

Einarsson, P.: S-wave shadows in the Krafla caldera in NE-Iceland, evidence for a magma chamber in the crust. Bull. Volcanol. **41,** 1–9, 1978

Filloux, J.H.: Magnetotelluric exploration of the North Pacific: Progress report and preliminary soundings near a spreading ridge. Phys. Earth Planet. Int. **25,** 187–195, 1981

Filloux, J.H.: Electrical conductivity structure of the seafloor beneath the North Pacific. Proceedings Symp. on Electromagn. in the Transition zone between ocean and continent. Earthquake Research Institute. The University of Tokyo, 1982

Gebrande, H., Miller, H., Einarsson, P.: Seismic structure of Iceland along the RRISP-profile. J. Geophys. **47,** 239–249, 1980

Haak, V.: Interpretations-Verfahren für die Magnetotellurik unter besonderer Berücksichtigung lateral variierender elektrischer Leitfähigkeit im Erdinnern und eines räumlich inhomogenen induzierenden Magnetfeldes. München: Bayerische Akademie der Wissenschaften 1978

Haak, V.: Relations between electrical conductivity and petrological parameters of the crust and upper mantle. Geophysical Surveys **4,** 57–69, 1980

Haak, V., Damaske, D.: Erste Ergebnisse aus den langperiodischen Magnetotellurik-Messungen in Island. Prot. Erdmagn. Tiefenforschung. Berlin-Lichtenrade, 61–67, 1980

Hermance, J.F.: Crustal genesis in Iceland: Geophysical constraints on crustal thickening with age. Geophys. Res. Lett. **8,** 203–206, 1981

Hermance, J.F., Grillot, L.R.: Correlation of magnetotelluric, seismic and temperature data from southwest Iceland. J. Geophys. Res. **75,** 6582–6591, 1970

Hersir, G.P., Björnsson, A., Pedersen, L.B.: Magnetotelluric survey across the active spreading zone on South west Iceland. J. Volcanol. Geotherm. Res., in press, 1983

Kemmerle, K.: Magnetotellurik am Alpen-Nordrand mit Diskussion der lokalen Effekte und Darstellung einer Einzeleffekt-Auswertung. Univers. München: Diss. Fak. Geowiss. 1977

Palmason, G., Arnorsson, S., Fridleifsson, I.B., Kristmannsdottir, H., Saemundsson, K., Stefansson, V., Steingrunsson, B., Tomasson, J., Kristjansson, L.: The Iceland crust: Evidence from drillhole data on structure and processes. In: Deep drilling results in the Atlantic Ocean. Ocean crust. M. Talwani, C.G. Harrison, D.E. Hayes eds. Am. Geophys. Union. Maurice Ewing Series 2, 43–65, 1979

Reddy, J.K., Rankin, D., Phillips, R.J.: 3-dimensional models in magnetotelluric and magnetic variational sounding. Geophys. J.R. Astron. Soc. **51,** 313–325, 1977

Ringwood, A.E.: Composition and evolution of the upper mantle. In: The earth's crust and upper Mantle. P.J. Hart, ed.: pp. 1–17. Am. geophys. Union, Monogr. 13, 1969

Sanford, A., Einarsson, P.: Magma chambers in rifts. In: Continental and oceanic rifts. G. Palmason, ed. Am. Geophys. Union. Geodynamic Series 8, 147–168, 1982

Schmucker, U.: Erdmagnetische Tiefensondierung mit langperiodischen Variationen. Prot. Erdmagn. Tiefensondierung Grafrath, 313–342, München, 1974

Shankland, T.J., Waff, H.S.: Partial melting and electrical conductivity anomalies in the upper mantle. J. Geophys. Res. **82,** 5409–5417, 1977

Stein, B.: Modellrechnungen zum Küsten-Effekt in der Magnetotellurik; Anwendung auf die Messungen in Nord-Island (1977 and 1980) Dipl.-Arbeit, Univ. München, 1982

Thayer, R.E., Björnsson, A., Alvarez, L., Hermance, J.F.: Magma genesis and crustal spreading in the northern neovolcanic zone of Iceland: telluric-magnetotelluric constraints. Geophys. J.R. Astron. Soc. **65,** 423–442, 1981

Waff, H.S.: Theoretical considerations of electrical conductivity in a partially molten mantle and implications for geothermometry. J. Geophys. Res. **79,** 4003–4010, 1974

Wolfgram, P.: Zeitvariationen des Erdmagnetfeldes, gemessen auf einem Profil durch Nordost-Island, 1977. Dipl.-Arbeit, Univ. München, 1980

Zverev, S.M., Litvinenko, I.V., Palmason, G., Yaroshevskaya, G.A., Osokin, N.N., Akhmetjev, M.A.: A seismic study of the rift zone in the northern Iceland. J. Geophys. **47,** 191–201, 1980

Received June 21, 1982; Revised January 17, 1983
Accepted February 17, 1983

J Geophys (1983) 53:24–33

Journal of Geophysics

Gravity and Height Variations Connected with the Recent Rifting Process in Northern Iceland 1975–1981

W. Torge and E. Kanngieser*
Institut für Erdmessung, Universität Hannover, Nienburger Str. 6, D-3000 Hannover, Federal Republic of Germany

Abstract. In 1975 rifting started in northern Iceland along the supramarine part of the constructive plate boundary. Regional gravity and height variations have been observed across the neovolcanic zone and the adjoining western and eastern Pleistocene and Tertiary basalt zones. The center of activity is in the Krafla caldera and the rifting has affected the 100 km long and 5 km wide fissure swarm associated with the central volcano. Local gravity and height variations have been investigated by annually re-observing transverse profiles in the Námafjall area (approx. 10 km south of Krafla) and in the Gjástikki area (approx. 15 km north of Krafla), and additional gravity stations in the northern part of the fissure swarm. The observations which have been performed at an accuracy level of better than $\pm 10 \times 10^{-8}$ ms^2 ($= \pm 0.01$ mGal) and $\pm 0{,}03$ m, respectively, give significant information about vertical mass shifts during the rifting process. The recent rifting process is characterized by shifting of activity with gravity decrease and uplift at the flanks and gravity increase and subsidence at narrow central parts of the Krafla fissure swarm. The annual variations reach $\pm 100 \times 10^{-8}$ ms^{-2} and ± 0.5 m or more, respectively. Since 1978 the activity has been concentrated in the Gjástikki region with the variations decreasing in the southern and northern parts of the fissure swarm.

Key words: Iceland rift zone – Recent gravity and height variations – High precision gravity measurements

Introduction

High precision gravity measurements and technical levelings have been carried out in the axial rift zone of northeastern Iceland since 1965, in order to investigate vertical mass shift along this part of the plate boundary between the American and the Eurasian tectonic plates (e.g. Jacoby et al., 1980; Pálmason and Saemundsson, 1974). The investigations continue the pioneering work of Alfred Schleusener who in 1938 established a number of gravity stations in that area (Schleusener, 1943). As, on the average, secular gravity and height variations will not exceed a few 10^{-8} ms^{-2} (10^{-8} ms$^{-2} = 1$ μGal) and a few centimeters per year, respectively, high precision techniques have to be used especially in gravimetry and systematic influences have to be carefully controlled in both methods. The observations during the last 16 years fall into a non-active tectonic epoch between 1965 and 1975 (Torge and Drewes, 1977) and an active rifting episode since 1975. Preliminary results of the observation epochs 1976, 1977 and 1978 are given in Torge and Kanngieser (1980a). This report contains the final results of the investigations obtained at the recent rifting process between 1979 and 1981. The results of all observation epochs before 1979 are given by Kanngieser (1982a).

These investigations are related to other geodectic research programs, carried out by different Icelandic (see below), German and Austrian groups in nothern Iceland: Horizontal movements are controlled by the Institut für Vermessungskunde, Technische Universität Braunschweig, by a regional network based on the special geodetic network set up by Niemczyk and Emschermann in 1938 (Möller and Ritter, 1980). High precision levelings have been performed by the Institut für Markscheide- und Bergschadenkunde, Montanuniversität, Leoben (Spickernagel, 1980), while local strain and tilt measurements were carried out by the Geodätisches Institut, Universität Hannover, and the Institut für Physikalische Geodäsie, Technische Hochschule Darmstadt (Pelzer and Gerstenecker, 1980).

High Precision Gravity and Height Measurements 1979–1981

The schematic location of the gravity, and partly also height, profiles established in northeastern Iceland is shown in Fig. 1 (Kanngieser, 1982a). Repeated surveys before the rift process were carried out especially along the west-east main profile at 65°40′ latitude. This profile crosses the neovolcanic zone and the adjoining western and eastern Pleistocene and Tertiary basalt zones. Gravity and height have been observed in 5-year intervals, 1965, 1970/71, 1975, and 1980. The small gravity increase, indicated in the axial rift zone between 1965 and 1970 (Schleusener and Torge, 1971), was confirmed in the following observation epoch 1975–1970/71 (Torge and Drewes, 1977); it resulted in a gravity change of approx. $+50 \times 10^{-8}$ ms^{-2}/10 years with respect to the western Tertiary basalt zone. The maximum horizontal gradient of gravity change (70×10^{-8} ms^{-2}/10 years) occurred across approx. 15 km in the Námafjall area south of the Krafla caldera. In today's view, this variation may have been a kind of precursor of the recent rift process.

* Since May 1983: Katasteramt Brake, Schrabberdeich 43, D-2880 Brake, Federal Republic of Germany

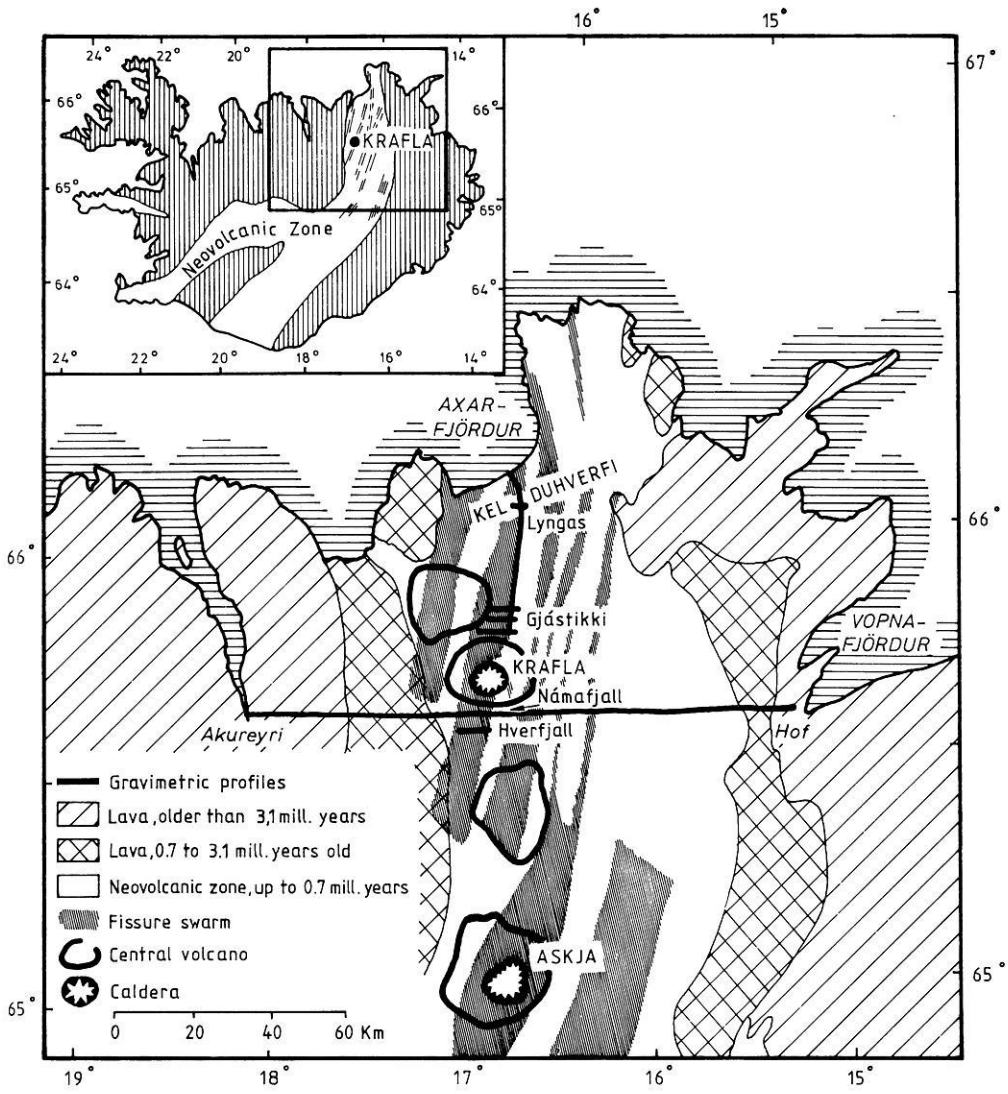

Fig. 1. Location of gravity profiles observed in northern Iceland between 1975 and 1981

Table 1. Statistics of gravity observations

Profile	Epoch	Observation period	Number of stations	LCR gravity meters	Number of observations per station
West-east main profile	1980	28.6.–30.8.	165	G79, G85	7 ... 8
Hverfjall profile	1980	19.8.–20.8.	4	G79, G85, G298, D14	4
	1981	13.7.–22.7.	4	G79, G298, D14	4
Námafjall profile	1979	16.7.–20.7.	19	G79, G85, D14	8
	1980	9.7.– 9.8.	18	G79, G85, G298, D14	8 ... 9
	1981	13.7.–22.7.	18	G79, G298, D14	6
Southern Gjástikki profile	1980	21.7.–24.8.	7	G79, G85, G298, D14	6
	1981	18.7.–30.7.	4	G79, G298, D14	6
Central Gjástikki profile	1979	22.7.–25.7.	14	G79, G85, D14	5
	1980	20.7.–22.8.	14	G79, G85, G298, D14	4 ... 5
	1981	17.7.–29.7.	12	G79, G298, D14	5 ... 6
Northern Gjástikki profile	1980	23.8.	5	G85, G298, D14	3 ... 4
	1981	18.7.–28.7.	5	G79, G298, D14	6
Lyngás profile	1979	24.7.	6	G79, G85, D14	2 ... 3
	1980	24.8.	5	G79, G85, G298, D14	3
	1981	21.7.–28.7.	6	G79, G298, D14	5 ... 6
Gjástikki Kelduhverfi profile	1979	22.7.–23.7.	12	G79, G85, D14	4
	1980	24.7.–24.8.	12	G79, G298, D14	5 ... 6
	1981	18.7.–28.7.	12	G79, G298, D14	6 ... 7

Table 2. R.m.s. errors (10^{-8} ms^{-2}) of one observed gravity difference

Epoch	G79	G85	G298	D14
1979	±25	±21	–	±11
1980	± 8	±11	±15	±15
1981	± 9	–	±13	±12

Table 3. Calibration terms of LCR gravimeters

Instr.	Epoch	Linear factor	Quadratic factor
G79	1979	0.99959	0.00000008
		±15	±2
	1980	0.99893	0.00000013
	1981	±36	±3
G85	1979	0.99750	0.00000044
	1980	±40	±4
G298	1980	1.00014	0.00000007
	1981	±14	±1
D14	1979	0.99994	
	1980	±3	
	1981		

Table 4. Results of the gravity connection continent (Hannover) – south-west Iceland (Reykjavik), Hannover fixed $g = 9.81262376$ ms^{-2}

Epoch	LCR gravity meters	Number of connections	Gravity value of Reykjavik 21941 K (Keflavik) (10^{-5} ms^{-2})	R.m.s. error of the gravity value (10^{-5} ms^{-2})
1965	G79, G85	5	982 259.394	±0.036
1967	G79, G85	7	259.354	±0.024
1970	G79, G85	6	259.401	±0,015
1971	G79, G85	4	259.412	±0.013
1975	G79, G85			
	G87, G298	8	259.410	±0.011
1976	G79, G85	4	259.389	±0.014
1977	G298	2	259.362	±0.022
1978	G79	2	259.400	±0.013
1979	G79, G85	4	259.384	±0.011
1980	G79, G85,			
	G298	6	259.394	±0.014
1981	G79, G298	4	259.373	±0.015
1965–				
1980		48	259.392	±0.007

Table 5. Results of the gravity connection southwest Iceland (Reykjavik) – northeast Iceland (Akureyri); Reykjavik fixed $g = 9.82259392$ ms^{-2}

Epoch	LCR gravity meters	Number of connections	Gravity value of Akureyri 60932 (10^{-5} ms^{-2})	R.m.s. error of the gravity value (10^{-5} ms^{-2})
1965	G79	10	982 333.399	±0.028
1970	G85	2	333.423	±0.021
1971	G79, G85	4	333.405	±0.020
1975	G79, G85			
	G87, G298, D14	10	333.380	±0.014
1976	G79, G85,			
	D14	5	333.387	±0.014
1977	G298, D14	2	333.395	±0.023
1978	G79, D14	4	333.365	±0.015
1979	G79, G85,			
	D14	6	333.389	±0.014
1980	G79, G85,			
	G298, D14	8	333.398	±0.014
1981	G79, G298,			
	D14	6	333.405	±0.012
1965–				
1980		51	333.382	±0.008

Table 6. R.m.s. errors (10^{-8} ms^{-2}) of final gravity values in single observation epochs

Profile	1979	1980	1981
West-east main profile	–	±3 ... ± 8	–
Hverfjall profile	–	±6	±6
Námafjall profile	± 6 ... ±10	±3 ... ± 6	±3 ... ±7
Southern Gjástikki profile	–	±6 ... ± 7	±5 ... ±6
Central Gjástikki profile	± 8 ... ±11	±5 ... ±10	±5 ... ±7
Northern Gjástikki profile	–	±7 ... ± 8	±5 ... ±7
Lyngás profile	±10 ... ±11	±6 ... ± 9	±6 ... ±8
Gjástikki-Kelduhverfi profile	±10 ... ±13	±7 ... ± 9	±4 ... ±7

Since December 1975, the Krafla fissure swarm has shown tectonic and volcanic activity with the Krafla caldera as the activity center. Here rapid subsidence lasting a few hours to a few days occurs, episodically interrupted by uplift intervals lasting several months. During the subsidence events brittle deformation occurs at different parts of the fissure swarm (Pálmason, 1981). These short period variations are carefully monitored by Icelandic geoscientists (Björnsson et al., 1979; Johnson et al., 1980), whereas our Institute has measured gravity and height variations at different parts of the fissure swarm in one-year intervals between 1975 and 1981 (Torge and Kanngieser, 1980a; Torge and Kanngieser, 1981; Torge, 1981). Altogether six transverse profiles (Hverfjall; Námafjall; Gjástikki south, central, north; Lyngás) crossing, and one profile (Gjástikki-Kelduhverfi) running along, the fissure zone have been established (see Fig. 1), with the observations concentrated on the Námafjall and the central Gjástikki profiles, located approx. 10 km south and 15 km north of the Krafla caldera, respectively.

Some statistics of the *gravity observations* are given in Table 1. The r.m.s. errors of single observed gravity differences have been derived from the adjustments of the different epochs and are given in Table 2. The r.m.s. errors of LaCoste-Romberg (LCR) gravity meters G79 and G85 in 1979 result mainly from reading errors caused by the optical readout system and the galvanometer. The high accuracy of LCR D14 in 1979 and of the gravimeters since 1980

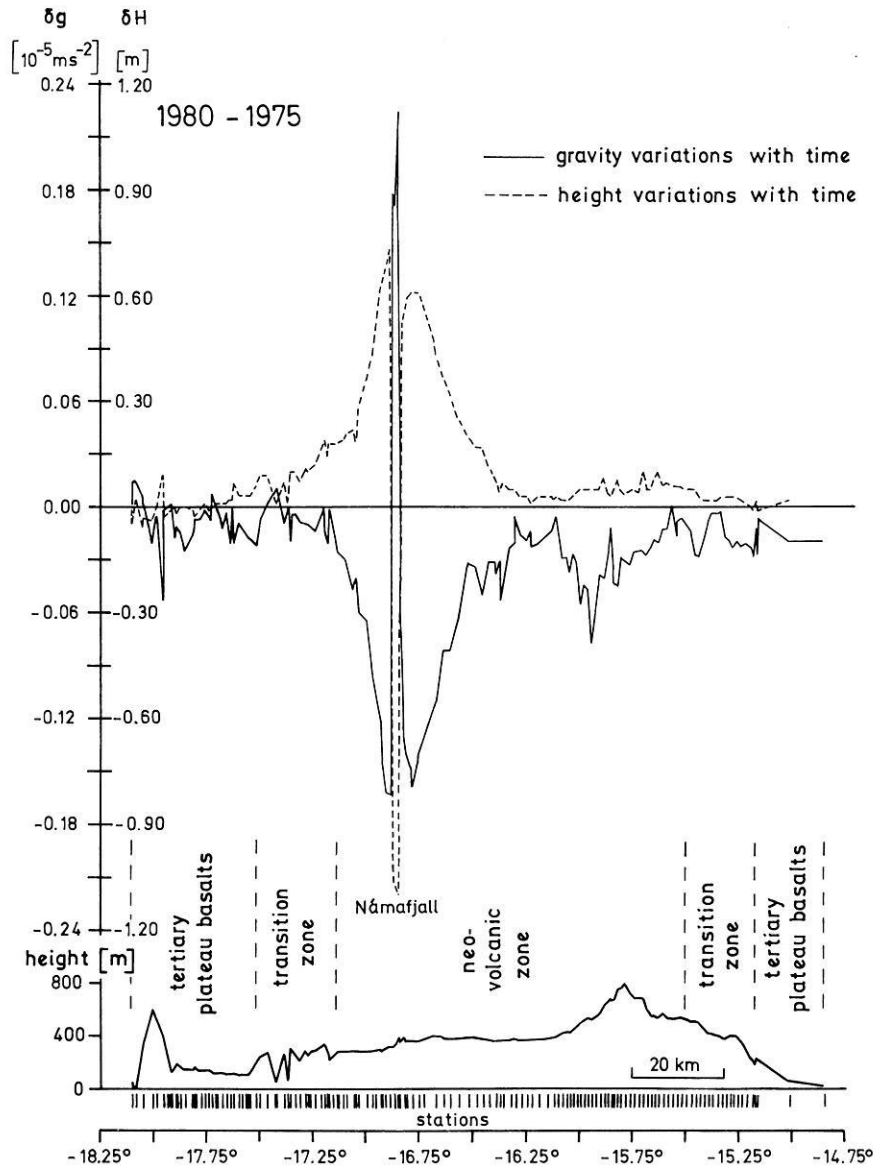

Fig. 2. West-east main profile, northern Iceland: Gravity and height variations 1980–1975

under the difficult environmental conditions in Iceland results from the following developments

- reduction of reading errors: digital voltmeter reading,
- protection against transportation shocks; shock suppressing transport case (Kanngieser, 1982b),
- protection against wind disturbance: wind shelter,
- control of instrumental drift and error accumulation within the gravity network: establishment of a base network with overlapping ties (accuracy 1980: $\pm 3 \times 10^{-8}$ ms^{-2}) and frequent connections to the base stations,
- gravimetric earth tide reduction: introduction of regional tidal parameters observed at a temporary tidal station in northern Iceland (Torge and Wenzel, 1976),
- determination of linear and quadratic calibration terms: back and forth measurements along the European absolute calibration line between Munich and Hammerfest reduce the corresponding calibration errors to $\pm 3 \times 10^{-5}$ (Kanngieser and Torge, 1981). Due to the installation of a capacitive readout system in LCR G 79 (December, 1979) the calibration changed. Quadratic calibration terms have been determined significantly for LCR D 14 on the Hannover-Harz calibration line, but not in northern Iceland. The calibration terms in Table 3 have been introduced in the adjustment,
- determination of periodic calibration terms: measurements along the 0.2, 2, 20 and 200×10^{-5} ms^{-2} (10^{-5} ms^2 = 1 mGal) calibration lines of the Hannover calibration system (accuracy $\pm 1 \times 10^{-8}$ ms^{-2}) reduce periodic errors to the $\pm 1 \times 10^{-8}$ ms^{-2} level (Torge and Kanngieser, 1980b; Kanngieser et al., 1983).

As measurements with static gravimeters give only gravity differences, the problem of the *absolute gravity reference* arises. The networks of each measuring epoch have always been tied to the gravity base station Akureyri 60932 located in the Tertiary plateau basalts at the western edge of the west-east main profile, about 60 km from the activated Krafla fissure zone. Numerous gravity connections between the continent (Hannover) and southwest Iceland (Reykjavik) and between Reykjavik and northeast Iceland (Akureyri) indicated that the gravity values of Reykjavik relative to the continent and of Akureyri relative to Reykjavik had not changed significantly between 1965 and 1981; thus sta-

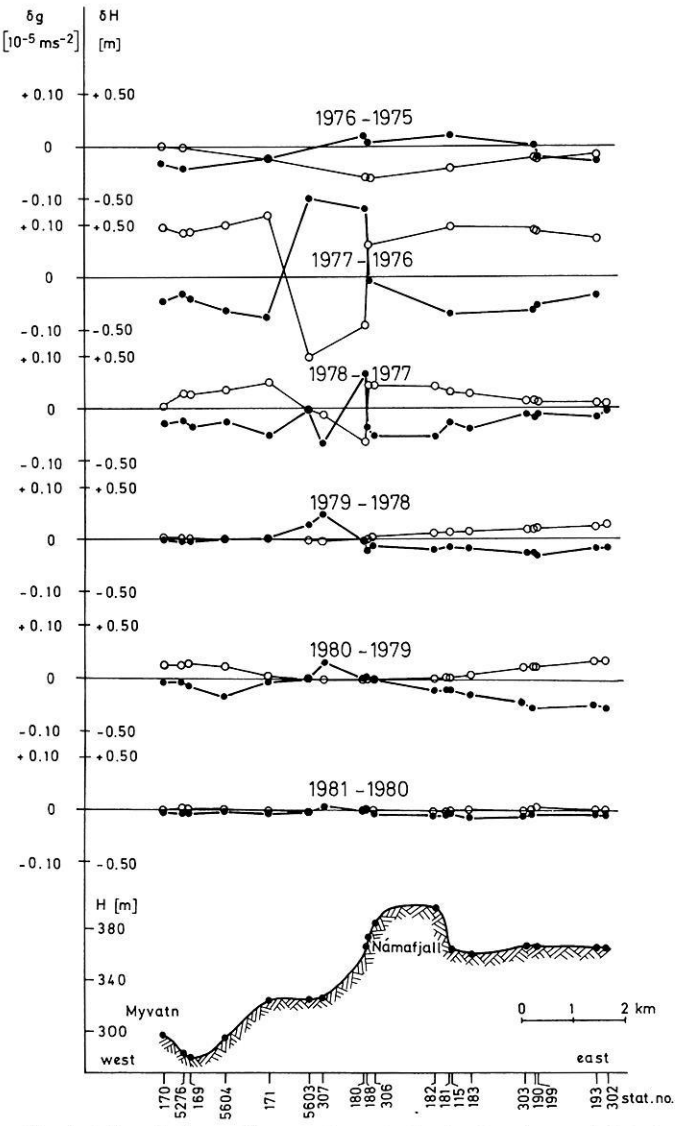

Fig. 3. Námafjall profile, northern Iceland: Gravity and height variations between 1975 and 1981; closed circles = gravity variation δg, open circles = height variation δH

bility is $\pm 10 \ldots \pm 20 \times 10^{-8}$ ms^{-2}/16 years (Table 4 and 5). Consequently the gravity value of Akureyri has been kept fixed since 1965. The absolute gravity level of the gravity system in northern Iceland was derived from the European absolute calibration line (Cannizzo et al., 1978) by means of repeated gravity connections between Akureyri and Hannover, with an accuracy of better than 10×10^{-8} ms^{-2} (Kanngieser, 1982a). The gravity system is compatible with the IGSN 71 (Morelli et al., 1974).

The *adjustment* follows the least squares method with gravity differences as observations and introduction of empirical correlations of sequential gravity differences. The gravity values at the single epochs, referring to the base station Akureyri, are given in Appendices 1–5, their r.m.s. errors are given in a generalized manner in Table 6.

Height determination was performed by technical leveling using automatic levels. From double leveling, either back and forth or by double turning points and connections to mean sea level the accuracy of the height differences is estimated to be better than $\pm 0.01 \times \sqrt{\text{distance (km)}}$ (m). The height reference of the different epochs has been derived by leveling connections to the stable station Akureyri (west-east main profile 1980) or by using stations with small gravity changes as reference, converting significant gravity variations with the factor -0.2×10^{-5} ms^{-2}/m (Torge, 1981) into height variations (Námafjall profile 1979 and 1981, central Gjástikki profile 1979, 1980, 1981).

The *height datum* in the Námafjall profile is
- 1979: profile station no. 143, about 10 km southwest of the starting point of the Námafjall profile, connected by geometric leveling,
- 1980: base station Akureyri no. 60932, which is not affected by the recent activity; its height is given in the height system introduced by Spickernagel (1966),
- 1981: profile station no. 143, connected to the starting point of the Námafjall profile by hydrostatic leveling via the level of the lake Mývatn.

The height datum in the central Gjástikki profile is profile station no. 548 in 1979, no. 556 in 1980 and no. 704 in 1981. The accuracy of the reference height fixed by this method, has been estimated by applying the law of error propagation (Kanngieser, 1982a). For the small gravity variations used for transformation, we obtain ± 0.1 m. This value corresponds to the error, which can be suspected if the height reference is derived from leveling to the base station Akureyri. The reference height error of ± 0.1 m adds to the observation error as a systematic bias, affecting all height variations of one period in the same sense (Torge, 1981).

The results of the height measurements are given in Appendices 1–3.

Comparison of the Gravity and Height Observations 1975–1981

The gravity and height variations (δg and δH) 1980 – 1975 for the *west-east main profile* are given in Appendix 1; Fig. 2 shows the variations along the profile. The comparison contains the regional long-term effect of the recent rifting episode. An extended region of approximately 70 km width is affected by gravity decrease and correlated uplift, with a maximum of -0.16×10^{-5} ms^{-2}/5 years and $+0.7$ m/5 years, respectively, at the activated Krafla fissure zone. The central part of this zone is characterized by short-period variations, which accumulated to $+0.2 \times 10^{-5}$ ms^{-2}/5 years in gravity, and -1.1 m/5 years in elevation, respectively. The stations of this central part of the west-east main profile and some adjacent stations form the *Námafjall profile* and have been observed in one-year intervals between 1975 and 1981. The results are given in Appendix 2 and Fig. 3. We recognize a small gravity increase (20×10^{-8} ms^{-2}) and a correlated subsidence (-0.3 m) at the western edge of the Námafjall ridge and a gravity decrease (up to -50×10^{-8} ms^{-2}) at the flanks in the first observation period (1976–1975). Gravity and height variations enlarged in the next period (1977–1976). The maximum gravity increase (160×10^{-8} ms^{-2}) and subsidence (-0.8 m) concentrated in a narrow, 1.5 km wide part, slightly shifted westward. The flanks of this subsidence area are characterized by uplift ($+0.3$ to $+0.6$ m) and gravity decrease (-30 to -70×10^{-8} ms^{-2}). In the following period (1978–1977) the variations diminished, although the tendencies continued, resulting in a gravity increase (60×10^{-8} ms^{-2}) and subsidence (-0.3 m) at the central part, and gravity decrease

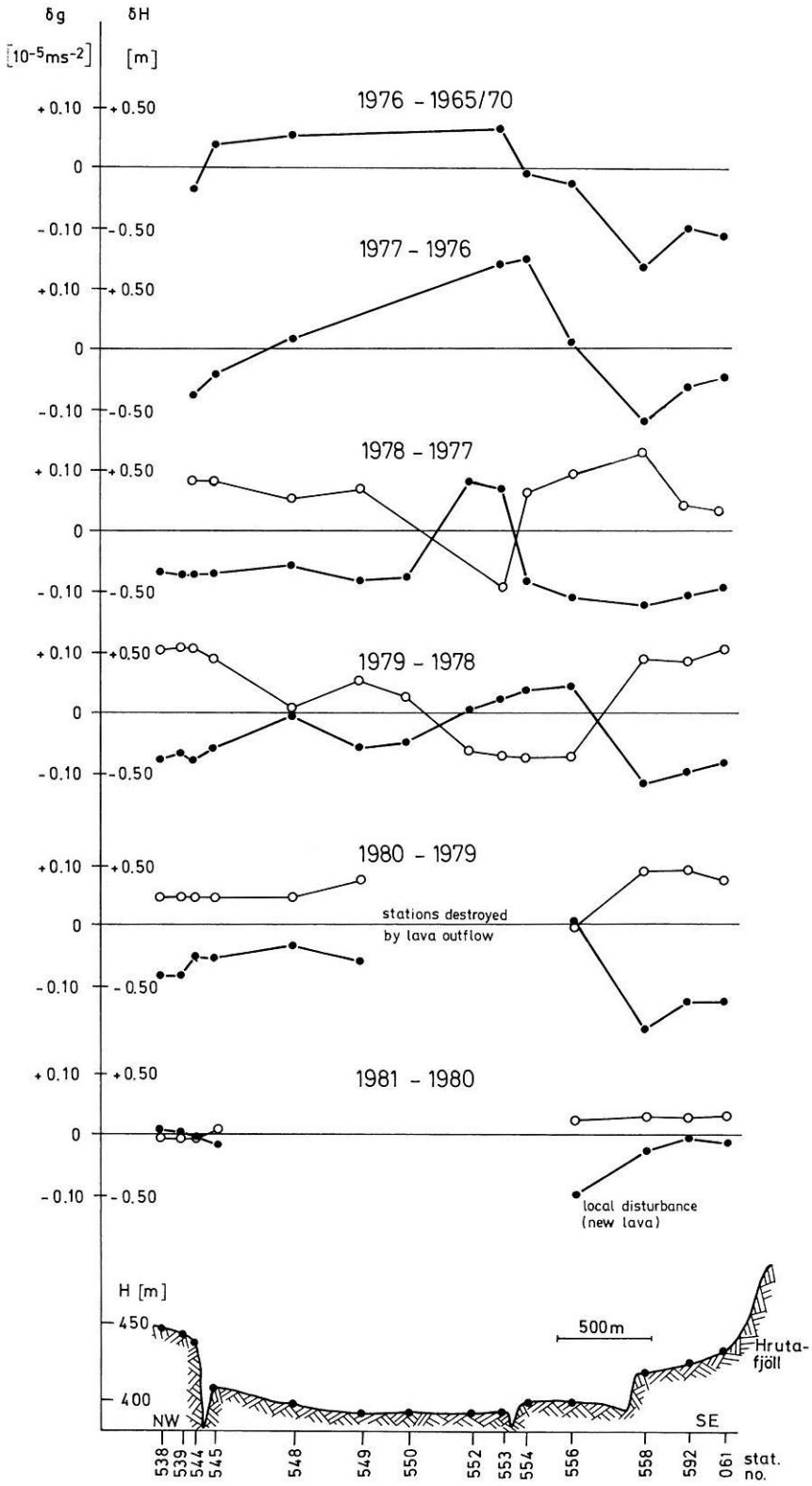

Fig. 4. Central Gjástikki profile, northern Iceland: Gravity and height variations between 1965/70 and 1981; closed circles = gravity variation δg, open circles = height variation δH.

(up to -70×10^{-8} ms^{-2}) and uplift (+0.2 m) at the flanks. West of Námafjall, an abnormal correlation between gravity and height change can be recognized, in the area of new fissure formation and thermal activity. The next two observation periods (1979–1978, 1980–1979) reveal a strongly reduced activity, with small gravity increase (20 to 40×10^{-8} ms^{-2}) and subsidence (<0.1 m) at the center and gravity decrease (up to -60×10^{-8} ms^{-2}) and uplift (<0.2 m) at the flanks. The last observation period (1981–1980) indicates the end of the activity along this profile.

For the *central Gjástikki profile* (Fig. 4), the first gravity

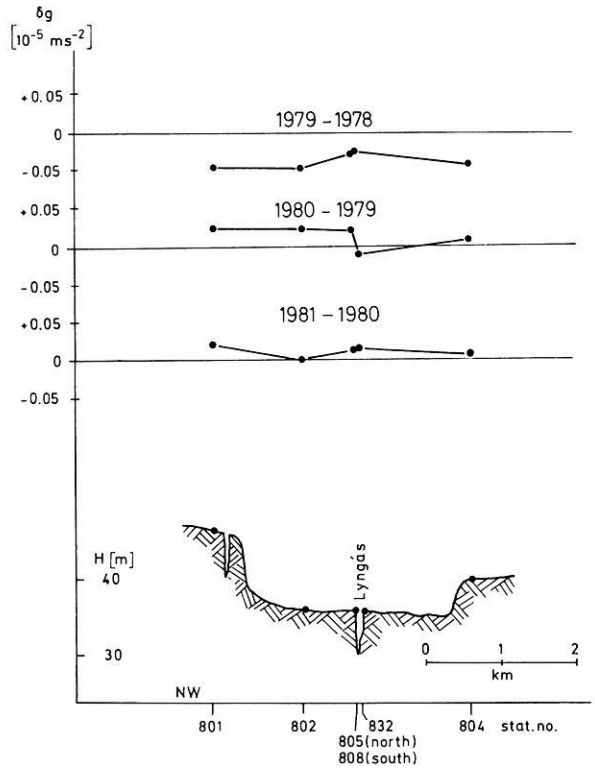

Fig. 5. Lyngás profile, northern Iceland: Gravity variations between 1978 and 1981

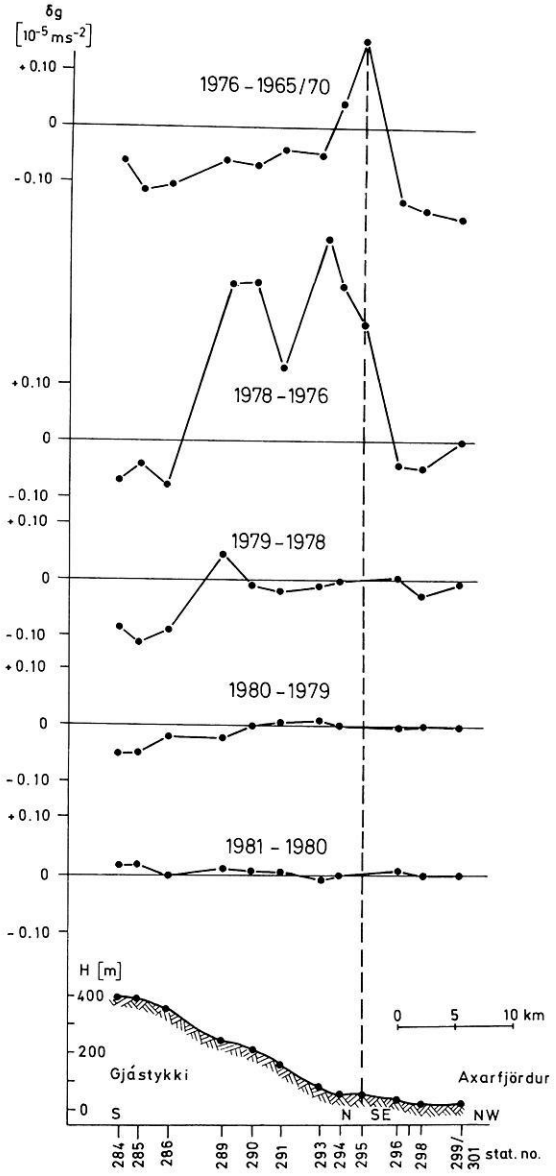

Fig. 6. Gjástikki-Kelduhverfi profile, northern Iceland: Gravity variations between 1965/70 and 1981.

reference epoch is 1965/70. We may assume that larger variations occured only after the end of 1975. The comparison 1976–1965/70 shows a gravity increase (40 to 60×10^{-8} ms^{-2}) in a broad central part and a decrease (up to -160×10^{-8} ms^{-2}) at the flanks. In the following periods, these trends continued. In 1977–1976, the gravity increase ($> 100 \times 10^{-8}$ ms^{-2}) concentrated in a smaller area, while the decrease at the edges kept the same order as before. New stations give for the 1978–1977 period a more detailed picture of the narrow, approx. 300 m wide, central part. We find again a gravity increase ($> 50 \times 10^{-8}$ ms^{-2}) and subsidence (-0.4 m) in this zone and a gravity decrease (up to -110×10^{-8} ms^{-2}) correlated with an uplift (up to 0.6 m) at the flanks. The period 1979–1978 is characterized by an intensified thermal activity in the central part; subsidence (-0.4 m) and gravity increase (50×10^{-8} ms^{-2}) is slightly shifted to the southeast. Uplift (up to 0.6 m) and gravity decrease (-100×10^{-8} ms^{-2}) at the flanks are similar as before, with a more complex picture in the northwestern part. The central part of this profile has been covered by lava flows in 1980 and more extensively in 1981. Therefore in the period (1980–1979) only the gravity decrease (up to -180×10^{-8} ms^{-2}) and uplift (0.5 m) at the flanks could be determined. The variations are decreasing since 1980. Only the gravity of station no. 556 changed strongly (-100×10^{-8} ms^{-2}) because of large new basalt lava masses near the station.

At the *Lyngás profile* (Fig. 5), a gravity decrease (up to -40×10^{-8} ms^{2}) has been observed between 1978 and 1979. This tendency did not continue in the following periods (1980–1979, 1981–1980).

Along the *Gjástikki-Kelduhverfi profile* (Fig. 6), we may again assume that larger variations occured only after the end of 1975. The comparison 1976–1965/70 gives a significant gravity increase (up to 160×10^{-8} ms^{-2}) about 20 km north of Gjástikki and a gravity decrease (up to -160×10^{-8} ms^{-2}) north and south of the maximum. The next period (1978–1976) is characterized by 3 minima (-80×10^{-8} ms^{-2}) and 2 maxima ($< 350 \times 10^{-8}$ ms^{-2}) with wavelengths of approx. 10 km. The great variations north of Gjástikki reduced to approximately zero after 1978. The southern part of the profile (northern Gjástikki region) remained active until 1980 with gravity decrease up to 100×10^{-8} ms^{-2}/year.

Conclusions

From the gravity and height measurements during the recent rifting process in northern Iceland, we arrive at the following conclusions:

– an extended region (70 km) is affected by gravity decrease and correlated uplift during the rifting process;

– the areas south and north of the activity center in the Krafla-caldera show a systematic trend characterized by gravity decrease and correlated uplift at the flanks of the fissure swarm, and gravity increase and subsidence in a narrow central 'graben' with maximum values of $\pm 100 \times 10^{-8}\,ms^{-2}$/year and ± 0.5 m/year, respectively;
– the observed annual variations change their magnitude with time, but generally proceed in the same sense, thus indicating the long-term behaviour of the mass shifts;
– the observations reveal the regional wandering of the swarm activity, from the north (1975/76) to the south (Námafjall 1977/78), concentrated since 1976 in the Gjástikki area;
– activated areas along the fissure swarm show large gravity variations of $200 \times 10^{-8}\,ms^{-2}$/a and more;
– according to the 1981 survey, the gravity and height variations are decreasing.

These results, and hopefully also future observations, will contribute to the understanding of the mass movements in time and space which are related to the present rifting episode. For geophysical model calculations of the subsurface mass shifts, continuous time-space models of the gravity and height variations have been developed, using least squares collocation techniques (Kanngieser, 1980, 1982a, c).

Acknowledgements. The authors thank the National Research Council of Iceland for permission to carry out the gravity surveys in northern Iceland. Fruitful discussions took place with Dr. Axel Björnsson and Dr. Gudmundur Pálmason, National Energy Authority, and Dr. Eysteinn Tryggvason, Nordic Volcanologic Institute, Reykjavik. LCR-gravity meter No. 85 has been kindly lent by the Institut für Geodäsie und Photogrammetrie, Technische Universität Berlin. Computations have been carried out on the CDC 73/76 of the Regional Computing Centre of Niedersachsen. In addition to the authors, the following persons participated in the field surveys 1979–1981. J. Baumgarten (1980), H. Geisendorf (1981), F.H. Jahn (1979), C. Jochheim (1981), B. Kalwar (1980), H.H. Köther (1980), H. Lange (1981), H. Lehrke (1979, 1980), S. Liebig (1980), R. Röder (1980, 1981), U. Stampa (1980), M. Thieme (1979, 1980, 1981), A. Weise (1979). The authors are very grateful to Deutsche Forschungsgemeinschaft for their financial support.

References

Björnsson, A., Johnson, G., Sigurdsson, S., Thorbergsson, G., Tryggvason, E.: Rifting of the plate boundary in North Iceland 1975–1978. J. Geophys. Res. **84**, 3029–3038, 1979

Cannizzo, L., Cerutti, G., Marson, J.: Absolute gravity measurements in Europe. Il Nuovo Cimento, C no. **1**, 39–86, 1978

Jacoby, W.R., Björnsson, A., Möller, D.: Iceland: Evolution, active tectonics, and structure. A Preface. J. Geophys. **47**, 1–6, 1980

Johnson, G.V., Björnsson, A., Sigurdsson, S.: Gravity and elevation changes caused by magma movement beneath the Krafla caldera, northeast Iceland. J. Geophys. **47**, 132–140, 1980

Kanngieser, E.: Common modeling of repeated gravity and height measurements, applied to the recent rifting episode in northern Iceland. Proc. of the second Intern. Symp. on Problems Related to the Redefinition of North American Vertical Geodetic Networks, Ottawa, 343–351, 1980

Kanngieser, E.: Untersuchungen zur Bestimmung tektonisch bedingter zeitlicher Schwere- und Höhenänderungen in Nordisland. Wiss. Arb. der Fachr. Vermessungswesen, Univ. Hannover, no. 114, 1982a

Kanngieser, E.: Investigations of calibration functions, temperature and transportation effects at LaCoste-Romberg gravity meters. J. Geod. Soc. Japan, Spec. Iss., 385–396, Tokyo, 1982b

Kanngieser, E.: Application of least squares collocation to gravity and height variations associated with a recent rifting process. Presented to General Meeting of I.A.G., Tokyo 1982c

Kanngieser, E., Kummer, K., Torge, W., Wenzel, H.-G.: Das Gravimeter-Eichsystem Hannover. Wiss. Arb. der Fachrichtung Vermessungswesen, Universität Hannover, Nr. 120, 1983

Kanngieser, E., Torge, W.: Calibration of LaCoste-Romberg gravity meters model G and D. B.G.I., Bull. d'Inf. no. **49**, 50–63, Toulouse 1981

Möller, D., Ritter, B.: Geodetic measurements and horizontal crustal movements in the rift zone of NE-Iceland. J. Geophys. **47**, 110–119, 1980

Morelli, C., Gantar, C., Honkasalo, T., McConnel, R.K., Szabo, B., Tanner, J.G., Uotila, U., Whalen, C.T.: The International Gravity Standardization Net 1971 (IGSN 71), Association Internationale de Géodésie, Publication Spéciale no. **4**, Paris 1974

Pálmason, G.: Crustal rifting and related thermo-mechanical processes in the lithosphere beneath Iceland. Geol. Rundschau **70**, 244–260, 1981

Pálmason, G., Saemundsson, K.: Iceland in relation to the Mid-Atlantic-Ridge. Ann. Rev. Earth Planet. Sci. **2**, 25–50, 1974

Pelzer, H., Gerstenecker, C.: Measurements of distance and tilt changes in fissures in Northern Iceland. J. Geophys. **47**, 166–170, 1980

Schleusener, A.: Die Gravimetermessungen. In: Spalten auf Island, O. Niemczyk, ed.: pp. 124–175, Stuttgart: K. Wittwer 1943

Schleusener, A., Torge, W.: Investigations of secular gravity variations in Iceland. Z. Geophys. **37**, 679–701, 1971

Spickernagel, H.: Höhenmessungen in Nord-Island. Mitt. aus dem Markscheidewesen **73**, 139–152, 1966

Spickernagel, H.: Results of height measurements in Northern Iceland 1965/1977. J. Geophys. **47**, 120–124, 1980

Torge, W.: Gravity and height variations connected with the current rifting episode in northern Iceland. Tectonophysics **71**, 227–240, 1981

Torge, W., Drewes, H.: Gravity variations with time in northern Iceland 1965–1975. J. Geophys. **43**, 771–790, 1977

Torge, W., Kanngieser, E.: Gravity and height variations during the present rifting episode in nothern Iceland. J. Geophys. **47**, 125–131, 1980a

Torge, W., Kanngieser, E.: Periodic calibration errors of LaCoste-Romberg model G and D gravity meters. In: Deutsche Geod. Komm., Reihe B, no. **252**, 81–93, München 1980b

Torge, W., Kanngieser, E.: Current observations of gravity variations and vertical crustal movements during the recent rifting process in northern Iceland. B.G.I. Bull. d'Inf. no. **49**, 141–150, Toulouse 1981

Torge, W., Wenzel, H.-G.: Gravimetric earth tide observations in Iceland. Bull. d'Inf. marées terr. no. **74**, 4312–4318, Bruxelles 1976

Received December 2, 1982; Revised version March 27, 1983
Accepted March 30, 1983

Appendix 1. Gravity and height values[a] of the west-east main profile between Akureyri and Hof, 1980, gravity and height variations 1980–1975

Station no.	ϕ (°)	λ west (°)	g(80) (10^{-5} ms^{-2})	g(80)−g(75) (10^{-5} ms^{-2})	H(80) (m)	H(80)−H(75) (m)
			982 ...			
60932	65.676	18.098	333.382	0.000	49.11	0.00
60936	65.680	18.098	338.267	0.013	24.00	−0.05
5218	65.655	18.079	337.431	0.015	2.11	0.02
1	65.739	18.046	281.787	0.006	350.33	−0.06
9	65.739	18.046	281.841	0.002	350.12	−0.03
2	65.732	18.003	232.608	−0.020	594.26	−0.04
3	65.737	17.983	248.882	−0.005	520.04	−0.01
18	65.733	17.952	274.847	−0.053	384.59	0.09
10	65.732	17.952	275.201	−0.001	382.32	−0.04
11	65.733	17.933	301.690	−0.001	247.21	−0.02
12	65.734	17.912	326.499	0.002	121.47	−0.01
20	65.738	17.893	317.856	−0.018	168.84	0.00
29	65.740	17.887	310.808	−0.011	198.21	−0.02
21	65.739	17.873	314.120	−0.014	173.21	0.00
22	65.734	17.849	315.626	−0.025	141.43	0.00
24	65.728	17.812	315.344	−0.015	138.25	−0.01
34	65.722	17.807	310.371	−0.008	159.06	−0.01
33	65.723	17.803	311.103	−0.007	154.19	−0.03
35	65.717	17.778	316.429	−0.007	130.86	−0.01
36	65.710	17.754	314.689	−0.002	139.22	0.01
48	65.712	17.726	314.246	−0.007	137.62	−0.02
41	65.714	17.723	314.479	0.008	132.42	0.00
43	65.705	17.708	317.648	0.000	117.67	0.01
50	65.709	17.699	316.587	−0.003	120.87	0.00
59	65.711	17.699	316.209	0.001	121.74	0.01
51	65.707	17.674	314.450	−0.013	121.24	0.01
52	65.705	17.655	316.400	−0.003	112.37	0.01
68	65.697	17.638	316.499	−0.021	112.90	0.02
62	65.696	17.625	316.416	0.000	117.15	0.02
61	65.696	17.621	316.894	−0.020	116.08	0.07
78	65.697	17.596	321.003	−0.009	106.00	0.03
73	65.693	17.564	320.369		114.81	
88	65.687	17.545	321.812	−0.018	111.90	0.03
89	65.685	17.545	321.230	−0.011	114.35	0.03
81	65.681	17.514	304.916	−0.022	205.13	0.06
82	65.678	17.497	295.522	−0.006	253.45	0.09
90	65.677	17.463	291.522	0.003	280.14	0.09
83	65.742	17.419	341.934	0.011	49.36	0.01
92	65.660	17.382	291.683	−0.009	269.24	0.07
93	65.720	17.365	338.550	0.000	55.22	0.01
100	65.655	17.355	282.667	−0.020	312.76	0.10
109	65.655	17.354	282.251	−0.004	314.43	0.10
			982 ...			
101	65.654	17.331	291.819	−0.004	260.03	0.10
102	65.648	17.308	302.948	−0.009	206.89	0.07
119	65.650	17.279	286.303	−0.010	291.92	0.11
110	65.649	17.270	293.799	−0.010	253.09	0.10
111	65.643	17.259	287.491	−0.012	281.02	0.11
113	65.621	17.235	283.322	−0.014	292.70	0.12
129	65.635	17.193	274.681	0.000	337.23	0.18
120	65.634	17.190	275.201	−0.015	334.02	0.19
123	65.593	17.178	280.045	−0.021	284.20	0.14
121	65.630	17.172	297.659	0.000	216.08	0.18
124	65.596	17.132	279.347	−0.026	280.86	0.18
132	65.604	17.104	279.067	−0.027	281.57	0.19
133	65.619	17.086	279.992	−0.032	282.53	0.21
148	65.617	17.057	280.125	−0.046	281.34	0.22
140	65.617	17.052	280.688	−0.047	280.31	0.22
143	65.569	17.045	270.554	−0.040	287.68	0.18
141	65.621	17.031	280.656	−0.060	279.51	0.28
142	65.632	16.992	281.563	−0.064	279.16	0.36
150	65.631	16.966	280.836	−0.097	281.31	0.43
151	65.657	16.951	283.278		286.59	
170	65.631	16.927	277.343	−0.123	296.28	0.62
5276	65.645	16.923	282.004	−0.122	284.81	0.64
169	65.642	16.920	283.007		279.70	
5604	65.641	16.904	279.427		295.40	
171	65.641	16.886	274.103	−0.163	321.87	0.73
5603	65.639	16.869	274.331		319.42	
307	65.639	16.863	272.742		325.68	
180	65.642	16.846	265.170	0.225	363.15	−1.10
306	65.644	16.841	259.730		389.72	
188	65.639	16.840	267.498	−0.048	349.88	0.24
182	65.646	16.819	258.969		394.38	
115	65.644	16.812	266.981		359.65	
181	65.645	16.812	266.975	−0.117	359.74	0.56
183	65.645	16.803	266.555		362.30	
303	65.646	16.781	266.931		358.97	
190	65.649	16.778	266.546	−0.159	359.73	0.61
193	65.650	16.752	267.160	−0.145	359.29	0.61
302	65.649	16.748	267.015		359.61	
200	65.652	16.673	256.546	−0.112	404.00	0.47
209	65.650	16.670	257.469	−0.114	397.84	0.44
202	65.653	16.634	257.490	−0.081	391.89	0.37
201	65.649	16.634	258.966		383.41	
			982 ...			
203	65.656	16.602	259.852	−0.081	374.84	0.32
210	65.662	16.563	259.054	−0.064	377.40	0.25
211	65.660	16.519	258.395	−0.031	387.82	0.20
229	65.657	16.482	257.950	−0.033	386.87	0.17
220	65.659	16.480	258.537	−0.035	384.08	0.17
221	65.655	16.452	261.150	−0.050	371.16	0.17
222	65.655	16.425	262.247	−0.031	369.17	0.12
239	65.650	16.391	262.915	−0.031	360.34	0.08
230	65.650	16.391	264.159	−0.038	354.64	0.08
233	65.640	16.372	260.295	−0.031	366.64	0.06
234	65.640	16.371	261.798	−0.053	360.31	0.04
231	65.647	16.357	261.679	−0.044	363.56	0.07
232	65.644	16.322	262.466	−0.022	365.26	0.05
248	65.637	16.299	259.286	−0.020	377.70	0.05
249	65.638	16.299	259.958	−0.005	375.11	0.05
241	65.638	16.271	262.132	−0.016	362.56	0.03
242	65.637	16.244	259.799	−0.019	368.21	0.03
250	65.639	16.224	260.222	−0.013	366.43	0.01
258	65.641	16.224	260.079	−0.023	366.59	0.01
251	65.626	16.192	259.012	−0.021	371.09	0.03
252	65.641	16.149	262.281	−0.016	376.77	0.03
263	65.644	16.122	261.107	−0.013	384.31	0.03
300	65.648	16.103	259.872	−0.005	392.77	0.03
310	65.653	16.079	256.361	−0.029	412.61	0.02
320	65.657	16.057	253.379	−0.028	429.65	0.02
330	65.663	16.042	253.185	−0.037	428.98	0.02
340	65.668	16.027	251.084	−0.026	440.94	0.03
350	65.673	16.009	245.764	−0.032	470.42	0.04
360	65.680	15.993	240.829	−0.055	496.46	0.05
370	65.687	15.974	239.148	−0.044	507.84	0.05
380	65.693	15.957	232.650	−0.047	536.80	0.05
390	65.699	15.941	235.333	−0.077	525.15	0.05
400	65.700	15.923	233.341	−0.061	534.36	0.05
410	65.703	15.900	226.548	−0.039	567.47	0.05
420	65.705	15.879	212.009	−0.040	630.61	0.08
430	65.706	15.863	205.755	−0.031	658.49	0.04
440	65.710	15.844	202.543	−0.011	680.78	0.03
450	65.710	15.834	204.283	−0.035	669.36	0.05
459	65.710	15.834	203.613	−0.036	672.89	0.04
458	65.710	15.834	203.783	−0.043	671.85	0.04
460	65.709	15.817	186.312	−0.044	756.87	0.08
			982 ...			
470	65.711	15.804	186.237	−0.028	758.83	0.05
480	65.711	15.783	178.419	−0.030	799.30	0.04
490	65.712	15.760	197.834	−0.033	720.06	0.05
500	65.714	15.740	206.254	−0.025	682.55	0.05
510	65.716	15.717	205.666	−0.024	686.50	0.04
520	65.715	15.697	205.887	−0.024	680.94	0.10
530	65.712	15.678	227.565	−0.027	579.87	0.05
540	65.708	15.659	235.036	−0.023	542.14	0.05
550	65.705	15.642	233.248	−0.018	551.54	0.08
560	65.701	15.623	236.917	−0.020	534.89	0.10
570	65.697	15.602	229.669	−0.012	567.40	0.06
580	65.695	15.582	236.202	−0.012	532.57	0.07
590	65.693	15.559	238.160	0.001	528.54	0.06
608	65.692	15.538	238.959	−0.016	531.20	0.06
600	65.692	15.538	239.041	−0.017	530.88	0.05
609	65.691	15.538	238.876	−0.008	531.68	0.06
610	65.689	15.517	237.597	−0.006	538.47	0.06
620	65.687	15.495	239.684	−0.010	529.52	0.05
630	65.686	15.473	243.687	−0.014	509.77	0.05
640	65.684	15.451	242.871	−0.027	511.64	0.05
650	65.682	15.431	245.753	−0.028	495.90	0.03
660	65.679	15.410	252.709	−0.019	455.51	0.02
670	65.677	15.390	260.930	−0.008	415.09	0.02
680	65.676	15.373	262.232	−0.003	408.26	0.02
690	65.676	15.347	264.142	−0.003	402.14	0.02
700	65.673	15.328	265.086	−0.002	395.23	0.03
710	65.669	15.308	269.310	−0.017	371.53	0.03
720	65.665	15.289	264.840	−0.019	394.63	0.03
730	65.661	15.274	262.552	−0.023	406.97	0.03
740	65.659	15.256	263.671	−0.019	401.65	0.03
750	65.656	15.236	270.540	−0.022	361.66	0.02
760	65.657	15.212	286.463	−0.020	280.57	0.01
770	65.659	15.185	301.674	−0.023	207.23	0.00
780	65.659	15.175	304.883	−0.028	193.59	−0.01
790	65.658	15.165	306.746	−0.011	184.32	0.01
798	65.656	15.162	304.186	−0.027	198.86	0.02
799	65.653	15.159	295.969	−0.006	233.78	−0.01
99010	65.656	15.010	339.476	−0.020	54.24	0.02
99011	65.655	15.010	339.015	−0.019	53.86	0.02
5227	65.758	14.849	368.862	−0.019	14.91	

[a] The gravity values refer to the gravity datum introduced by Kanngieser (1982a). The gravity system is compatible with the IGSN 71. The gravity and height values before 1980 are given in Torge and Drewes (1977)

Appendix 2. Gravity and height values[b, c] 1978, 1979 and 1981 along the Námafjall profile (part of the west-east main profile)

Station no.	ϕ (°)	λ west (°)	g(78) (10^{-5} ms^{-2})	g(79) (10^{-5} ms^{-2})	g(81) (10^{-5} ms^{-2})	H(78) (m)	H(79) (m)	H(81) (m)
			982...	982...	982...			
60932	65.676	18.098	333.382	333.382	333.382			
93	65.720	17.365	338.543	338.547	338.544			
143	65.569	17.045	270.572	270.559	270.545		287.66	287.67
170	65.631	16.927	277.354	277.352	277.332	296.16	296.16	296.29
5276	65.645	16.923	282.021	282.014	281.992	284.67	284.69	284.83
169	65.642	16.920	283.028	283.026	282.997	279.55	279.56	279.71
5604	65.641	16.904	279.458	279.455	279.424	295.28	295.29	295.42
171	65.641	16.886	274.116	274.115	274.087	321.82	321.83	321.87
5603	65.639	16.869	274.304	274.327	274.330	319.42	319.40	319.40
307	65.639	16.863	272.658	272.702	272.749	325.74	325.70	325.65
180	65.642	16.846	265.163	265.165	265.167	363.16	363.17	363,16
306	65.644	16.841	259.736	259.725	259.715	389.72	389.75	389.74
188	65.639	16.840	267.509	267.490	267.503	349.87	349.88	349.89
182	65.646	16.819	259.003	258.985	258.954	394.30	394.35	394.39
181	65.645	16.812	267.015	266.998	266.963	359.63	359.67	359.76
115	65.644	16.812	267.024	267.008	266.971	359.56	359.60	359.69
183	65.645	16.803	266.598	266.576	266.538	362.16	362.21	362.33
303	65.646	16.781	267.006	266.976	266.918	358.80	358.85	359.02
190	65.649	16.778	266.630	266.599	266.538	359.55	359.60	359.79
199	65.648	16.776	266.370	266.338		359.80	359.86	
193	65.650	16.752	267.228	267.207	267.150	359.08	359.14	359.35
302	65.649	16.748	267.092	267.070	267.005	359.40	359.47	359.67
234	65.640	16.371	261.836	261.807	261.802			
263	65.644	16.122	261.115	261.127	261.119			

[b] All values refer to the datum introduced by Kanngieser (1982a). The gravity system is compatible with the IGSN 71
[c] The values before 1978 are given in Kanngieser (1982a)

Appendix 3. Gravity and height values[b, c] 1978, 1979, 1980 and 1981 along the central Gjástikki profile

Station no.	ϕ (°)	λ west (°)	g(78) (10^{-5} ms^{-2})	g(79) (10^{-5} ms^{-2})	g(80) (10^{-5} ms^{-2})	g(81) (10^{-5} ms^{-2})	H(78) (m)	H(79) (m)	H(80) (m)	H(81) (m)
			982...	982...	982...	982...				
704	65.847	16.822			258.981	258.977			477.77	477.79
703	65.845	16.813			263.472	263.480			462.80	462.82
702	65.843	16.804			265.417	265.424			454.72	454.73
701	65.842	16.798			266.804	266.820			447.37	447.36
538	65.840	16.793	268.486	268.407	268.325	268.333	438.60	439.15	439.40	439.39
539	65.840	16.792	269.221	269.148	269.066	269.068	434.94	435.50	435.75	435.74
544	65.840	16.791	268.583	268.495	268.433	268.428	434.97	435.53	435.78	435.77
545	65.840	16.790	275.116	275.053	274.991	274.971	407.06	407.53	407.78	407.83
548	65.838	16.781	278.347	278.340	278.304		394.54	394.58	394.82	
549	65.837	16.776	278.715	278.652	278.590		391.61	391.89	392.27	
550	65.836	16.771	278.250	278.194			392.79	392.95		
552	65.835	16.763	278.164	278.174			389.58	389.30		
553	65.834	16.759	278.150	278.175			389.20	388.86		
554	65.834	16.758	275.806	275.849			399.06	398.70		
556	65.833	16.753	275.055	275.101	275.108	275.008	401.93	401.57	401.53	401.66
558	65.831	16.745	271.219	271.087	270.908	270.883	417.37	417.89	418.34	418.50
592	65.830	16.741	270.193	270.092	269.963	269.958	422.45	422.94	423.38	423.54
61	65.829	16.736	266.733	266.648	266.523	266.509	430.92	431.47	431.85	432.02

Appendix 4. Gravity values[b] along the Hverfjall profile (800... 840), the northern (850... 880 and 284) and southern (399... 601) Gjástikki profile and Lyngás profile (801–832)

Station no.	ϕ (°)	λ west (°)	g(78) (10^{-5} ms^{-2})	g(79) (10^{-5} ms^{-2})	g(80) (10^{-5} ms^{-2})	g(81) (10^{-5} ms^{-2})
			982...	982...	982...	982...
800	65.611	16.921			277.103	277.098
820	65.606	16.897			277.096	277.103
830	65.611	16.855			263.612	263.627
840	65.603	16.805			261.724	261.733
850	65.857	16.790			266.634	266.650
860	65.859	16.768			274.184	274.126
870	65.860	16.756			271.590	271.610
880	65.862	16.744			273.774	273.792
284	65.866	16.705			276.182	276.198
399	65.820	16.742			264.776	264.759
401	65.821	16.746			268.895	268.860
499	65.825	16.759			272.431	
501	65.827	16.770			274.664	
502	65.829	16.782			275.564	
599	65.831	16.796			269.313	269.225
601	65.832	16.801			269.452	269.447
801	66.049	16.637	376.298	376.253	376.263	376.283
802	66.043	16.608	377.604	377.559	377.571	377.570
808	66.040	16.594	376.148	376.126	376.136	376.147
805	66.041	16.593	377.035	377.000		376.576
832	66.041	16.590	376.687	376.661	376.655	376.669
804	66.037	16.570	376.593	376.551	376.555	376.562

Appendix 5. Gravity values[b, c] 1978, 1979, 1980 and 1981 along the Gjástikki-Kelduhverfi profile

Station no.	ϕ (°)	λ west (°)	g(78) (10^{-5} ms^{-2})	g(79) (10^{-5} ms^{-2})	g(80) (10^{-5} ms^{-2})	g(81) (10^{-5} ms^{-2})
			982...	982...	982...	982...
284	65.866	16.705	276.322	276.234	276.182	276.198
285	65.885	16.674	283.304	283.190	283.139	283.155
286	65.904	16.678	292.251	292.152	292.125	292.123
289	65.948	16.662	320.667	320.701	320.676	320.687
290	65.971	16.660	331.023	331.010	331.007	331.015
291	65.992	16.655	345.415	345.389	345.395	345.405
293	66.022	16.637	367.436	367.424	367.437	367.430
294	66.040	16.627	374.391	374.385	374.383	374.388
295	66.056	16.643	374.554			
296	66.074	16.689	382.581	382.582	382.575	382.590
297	66.076	16.716	382.181	382.169	382.165	382.168
298	66.099	16.689	383.707	383.679	383.680	383.685
299	66.123	16.730	389.373			
301	66.123	16.730	389.282	389.271	389.274	389.273

J Geophys (1983) 53:34–41

Journal of Geophysics

Gravity Interpretation of Two Dimensional Fault Structures Using Hilbert Transforms

N. Sundararajan, N.L. Mohan, and S.V. Seshagiri Rao
Centre of Exploration Geophysics, Osmania University, Hyderabad-500007, India

Abstract. The Hilbert Transform of the second order horizontal gradient of the gravity effect of a two dimensional dipping fault is derived. Using the derivatives of the horizontal gradient of the gravity effect and the Hilbert Transform, the parameters of the dipping fault, namely the dip, the depths to the top and bottom and the density contrast, are obtained. The gravity effect of the vertical fault has also been analysed treating it as a particular case of the dipping fault. The validity of the method is exemplified with theoretical and field examples in either cases.

Key words: Gravity anomaly – Horizontal derivative – Fault structure – Fourier transform – Discrete Hilbert transform – Points of intersection – Density contrast

Introduction

In recent years, Hilbert transformation techniques (Nabighian, 1972; Stanley and Green, 1976; and Stanley, 1977) have assumed importance in the quantitative interpretation of gravity and magnetic data. Nabighian's (1972) work was confined to the transformation of vertical gradients (vertical magnetic field) into horizontal gradients (horizontal magnetic field) and vice-versa with the help of the Hilbert transform. But Mohan et al. (1982) have devised a novel interpretation technique making use of the Hilbert transform to analyse vertical magnetic anomalies due to some two dimensional bodies, through which the parameters of the causative body are determined by means of simple mathematical expressions. The very same approach has been extended in the present paper for determining the parameters of two dimensional fault structures. Since the gravity effect and its Hilbert transformation are in the space domain, the kind of assumptions which are necessary in frequency domain techniques, (Bhimasankaram et al., 1977) are no longer required.

Gravity Effect of a Dipping Fault

For a semi infinite dipping fault block of finite throw (Fig. 1a), the gravity effect is given by (Jung, 1961):

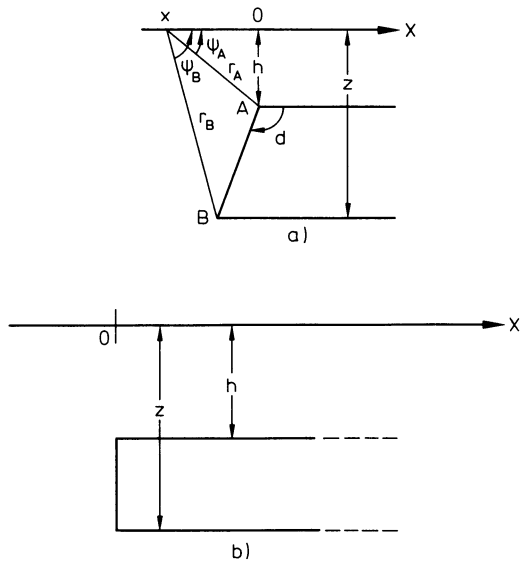

Fig. 1. a Geometry of the two dimensional dipping fault. **b** Geometry of the two dimensional vertical fault

$$g(x)=2G\sigma\sin d[(x+h\cot d)\cdot\sin d\{\sin d\ln(r_B/r_A)-\cos d(\varphi_B-\varphi_A)\}+(Z\varphi_B-h\varphi_A)] \quad (1)$$

where

G – is the gravitational constant.
σ – is the density contrast.
d – is the dip of the fault.
h – is the depth to the top of the fault.
and
Z – is the depth to the bottom of the fault.

Differentiating Eq. (1) with respect to x twice, we obtain,

$$g''(x)=2G\sigma\sin d\left[\frac{h\cos d-x\sin d}{r_A^2}-\frac{(2Z-h)\cos d-x\sin d}{r_B^2}\right]. \quad (2)$$

Equation (2) can be rewritten as,

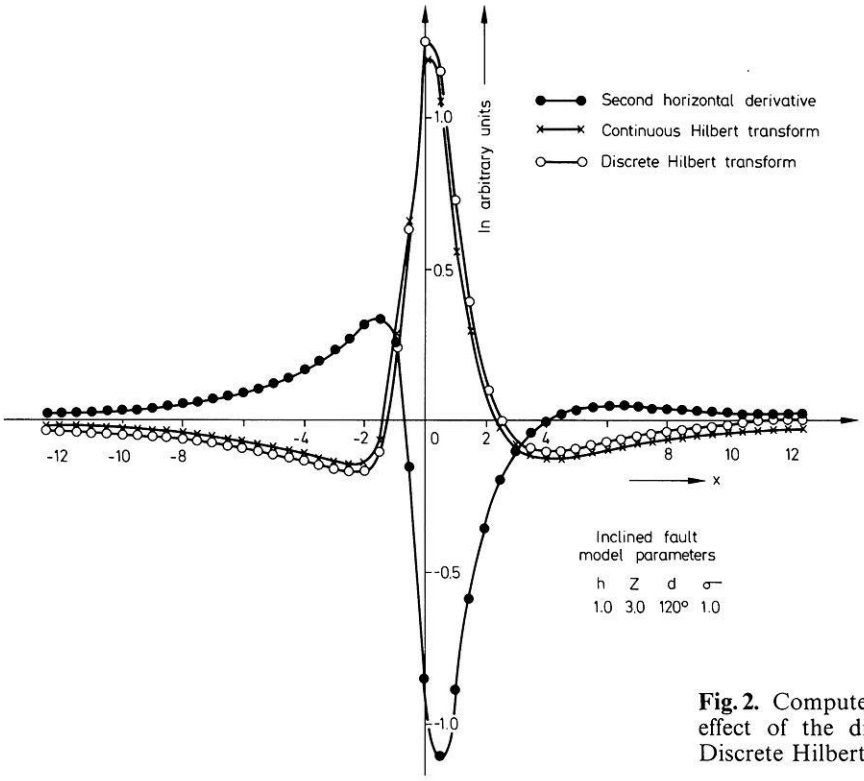

Fig. 2. Computed second horizontal gradient of the gravity effect of the dipping fault, the Hilbert transform and the Discrete Hilbert transform. (Model I)

$$g''(x)=2G\sigma\sin d\left[\frac{h\cos d-x\sin d}{x^2+h^2}+\frac{(x-D)\sin d-Z\cos d}{(x-D)^2+Z^2}\right] \quad (3)$$

where $D=(Z-h)\cot d$.

The Fourier transform of $g''(x)$ is given by,

$$F(\omega)=\int_{-\infty}^{\infty} g''(x)\,e^{-i\omega x}\,dx. \quad (4)$$

Substituting for $g''(x)$ from Eq. (3) in Eq. (4) and evaluating the integral, the real and imaginary components of the Fourier transform are obtained as:

$$\mathrm{Re}\,F(\omega)=2\pi G\sigma\sin d\,[e^{-\omega h}\cos d-\cos(d-\omega D)\,e^{-\omega Z}] \quad (5)$$

and

$$\mathrm{Im}\,F(\omega)=2\pi G\sigma\sin d\,[e^{-\omega h}\sin d-\sin(d-\omega D)\,e^{-\omega Z}]. \quad (6)$$

Hilbert Transform

The Hilbert transform of $g''(x)$ is defined as (Thomas, 1969):

$$H(x)=\frac{1}{\pi}\int_0^{\infty}[\mathrm{Im}\,F(\omega)\cos\omega x-\mathrm{Re}\,F(\omega)\sin\omega x]\,d\omega. \quad (7)$$

Substituting Eqs. (5) and (6) in Eq. (7), and then integrating, the Hilbert transform is obtained as,

$$H(x)=2G\sigma\sin d\left[\frac{h\sin d-x\cos d}{x^2+h^2}+\frac{(x-D)\cos d-Z\sin d}{(x-D)^2+Z^2}\right]. \quad (8)$$

Evaluation of Parameters

Following Nabighian (1972) we determine the origin by considering the maxima of,

$$A(x)=\sqrt{[g''(x)]^2+[H(x)]^2}. \quad (9)$$

Then the approximate dip of the fault block is determined (see Appendix) using the relation,

$$d=\cot^{-1}\left[\frac{g''(0)}{H(0)}\right]. \quad (10)$$

For $g''(0)=0$, d becomes 90 degrees which is the case of a vertical fault. The graphs of the second horizontal derivative of the gravity effect of an inclined fault block $g''(x)$, and its Hilbert transform, $H(x)$, are found to intersect on either side of the origin (Figs. 2 and 3).

If the abscissa of the points of intersection are x_1 and x_2 then,

$$g''(x_{1,2})=H(x_{1,2})$$

(i.e.)

$$x_1^2(h-Z-D)+x_1(D^2+Z^2-h^2-2hD)=Zh^2-hZ^2-h^2D-hD^2 \quad (11)$$

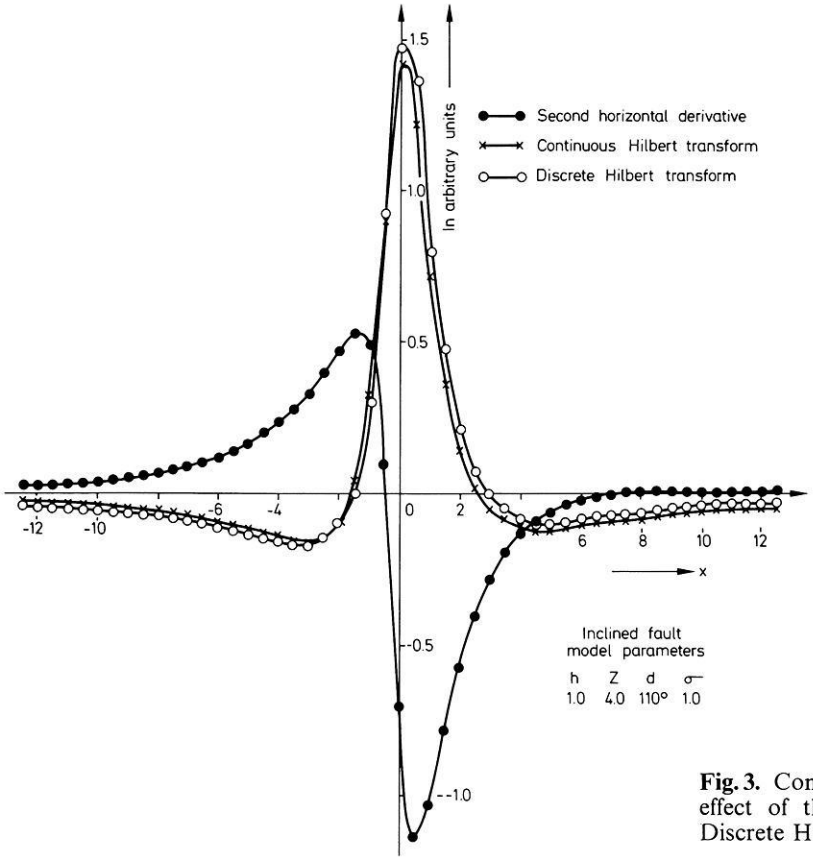

Fig. 3. Computed second horizontal gradient of the gravity effect of the dipping fault, the Hilbert transform and the Discrete Hilbert transform. (Model II)

and

$$x_2^2(h-Z-D)+x_2(D^2+Z^2-h^2-2hD) = Zh^2-hZ^2-h^2D-hD^2. \tag{12}$$

Solving equations (11) and (12), the depths to the top h, and bottom Z are obtained as,

$$h=\frac{(x_1+x_2)\pm\sqrt{(x_1+x_2)^2+4x_1x_2(K_2+K_3)}}{2(K_2+K_3)} \tag{13}$$

and

$$Z=\frac{K_3h^2-x_1x_2}{K_1h} \tag{14}$$

where

$$K_1=\frac{(1+P^2)}{1-P},$$

$$K_2=\frac{1+2P-P^2}{1-P},$$

$$K_3=\frac{P(1+P)}{1-P}$$

and

$$P=\cot d.$$

Finally the density contrast σ is determined from,

$$\sigma=\frac{1}{2G\sin d}\sqrt{\frac{[g''(0)]^2+[H(0)]^2}{A+B+C}} \tag{15}$$

where

$$A=\frac{1}{h^2},$$

$$B=\frac{D^2+Z^2+4DZ\cos d\sin d}{(Z^2+D^2)^2},$$

$$C=-\frac{2(Z+2D\sin d\cos d)}{h(Z^2+D^2)}.$$

Thus, the above analysis facilitates the determination of all the parameters of the dipping fault.

Vertical Fault

The semi infinite vertical fault block (Fig. 1b) is just a particular case of the dipping fault with d assuming the value $\pi/2$.

Correspondingly the second horizontal derivative of the vertical fault and its Hilbert transform are obtained by substituting $d=\pi/2$ in Eqs. (3) and (8).

Thus,

$$g_1''(x)=2G\sigma\left[\frac{x}{x^2+Z^2}-\frac{x}{x^2+h^2}\right] \tag{16}$$

and

$$H_1(x)=2G\sigma\left[\frac{h}{x^2+h^2}-\frac{Z}{x^2+Z^2}\right]. \tag{17}$$

Table 1. Theoretical Examples (* In arbitrary units)

	Parameters	d	h^*	Z^*	σ^*
Dipping fault					
Model I	Assumed values	120.0°	1.00	3.00	1.00
	Evaluated values	123.8°	1.11	3.14	1.03
Model II	Assumed values	110.0°	1.00	4.00	1.00
	Evaluated values	114.6°	0.97	3.90	1.11
Vertical fault					
Model I	Assumed values	-	0.50	1.00	1.00
	Evaluated values	-	0.56	0.99	1.28
Model II	Assumed values	-	1.00	3.00	1.00
	Evaluated values	-	1.00	2.71	0.95

Evaluation of Parameters

As in the earlier case the graphs of $g_1''(x)$ and $H_1(x)$ are found to intersect on either side of the origin (Figs. 4 and 5). The parametric evaluation in the case of a vertical fault can be made simple by substituting $d=\pi/2$ in Eqs. (13), (14) and (15) which yield the depth to the top and bottom and the density contrast as follows:

$$h=\frac{(x_1+x_2)\pm\sqrt{(x_1+x_2)^2+4x_1x_2}}{2}, \tag{18}$$

$$Z=\frac{-x_1x_2}{h} \tag{19}$$

and

$$\sigma=\frac{hZ\sqrt{[g''(0)]^2+[H(0)]^2}}{2G(Z-h)}. \tag{20}$$

Theoretical Examples

The theoretical procedures developed earlier as expressions of continuous variables can be made applicable to the field data which is discrete, by using the Discrete Fourier Transform (DFT) and the Discrete Hilbert Transform (DHT).

The real and imaginary components of the DFT are given by (Gold and Radar, 1969),

$$\mathrm{Re}\,F(n\omega_0)=\sum_{l=0}^{N-1} g''(l\cdot\Delta x)\cos(n\omega_0\cdot l\cdot\Delta x) \tag{21}$$

and

$$\mathrm{Im}\,F(n\omega_0)=\sum_{l=0}^{N-1} g''(l\cdot\Delta x)\sin(n\omega_0\cdot l\Delta x). \tag{22}$$

The discrete Hilbert Transform is defined as,

$$H(l\cdot\Delta x)=\frac{1}{\pi}\left[\sum_{n=0}^{\frac{N}{2}-1}\mathrm{Im}\,F(n\omega_0)\cos(n\omega_0\cdot l\Delta x)-\sum_{n=0}^{\frac{N}{2}-1}\mathrm{Re}\,F(n\omega_0)\sin(n\omega_0\cdot l\Delta x)\right]. \tag{23}$$

Where $\omega_0=2\pi/N\cdot\Delta x$ (radians per unit length) is the fundamental frequency, Δx is the station spacing and N is the total number of observed values.

Dipping Fault

Two theoretical models (Table 1) are analysed to examine the applicability of the procedure. With the help of Eqs. (3) and (8), the second horizontal derivative of the gravity effect and its Hilbert transform are computed in each case and shown in Figs. (2) and (3). The Discrete Hilbert Transform, $H(l\cdot\Delta x)$, is also computed in each case using (23) and they are also shown in the same Figures.

Using the Eqs. (10), (13), (14) and (15) the parameters, namely the dip d, the depth to the top h, the depth to the bottom Z and the density contrast σ are evaluated and presented (Table 1).

Vertical Fault

In the case of a vertical fault also, two theoretical models are computed using the corresponding equations and are shown in Figs. 4 and 5. The parameters of the causative body are evaluated using the procedure given for the vertical fault, and are presented in Table 1.

Field Examples

Dipping Fault

A profile of residual Bouger gravity anomaly (Fig. 6) across the Garber structure, Garber County, Oklahoma (Grant and West, 1965) is considered for interpretation. The entire profile is digitized into 64 equal parts such that it yields a station spacing of 121 m. The second horizontal derivative of the anomaly is computed numerically, and smoothed. Using an FFT algorithm the real and imaginary components of the DFT are computed and then the DHT is computed and plotted with the second horizontal derivative of the anomaly (Fig. 7). It is seen that these two curves intersect at $x_1=20.0$ and $x_2=-2.9$. The parameters of the causative body are evaluated and compared with that of Grant and West (Table 2).

Vertical Fault

Gravity data collected over a fault structure near Adilabad (at latitude 19°42′ N and longitude 78°33′ E), Andhra Pradesh, India, has been analysed (Fig. 8). From the shape of the anomaly it is assumed to be a vertical fault. The area of investigation forms a part of

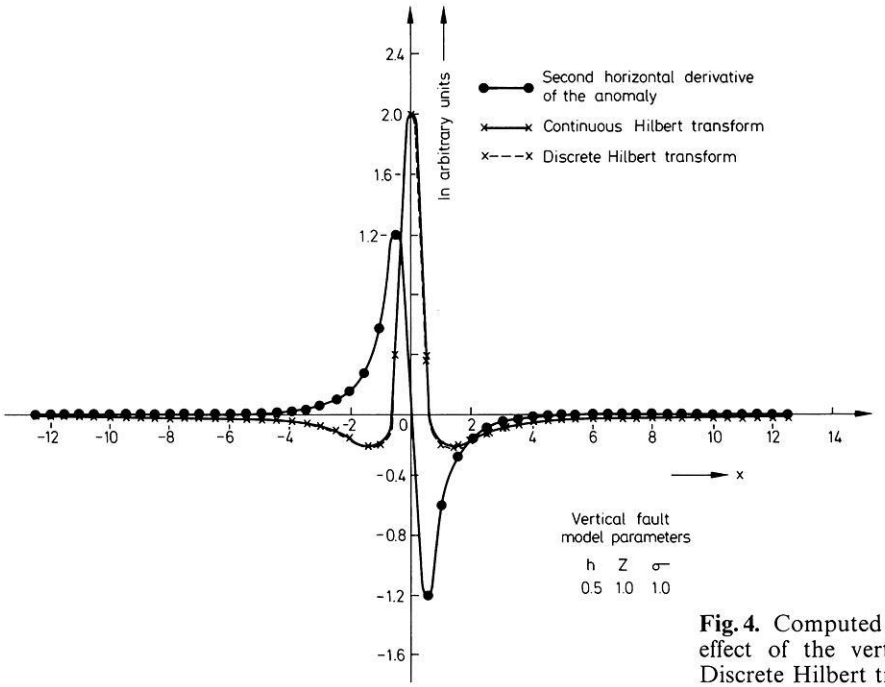

Fig. 4. Computed second horizontal gradient of the gravity effect of the vertical fault, the Hilbert transform and the Discrete Hilbert transform. (Model I)

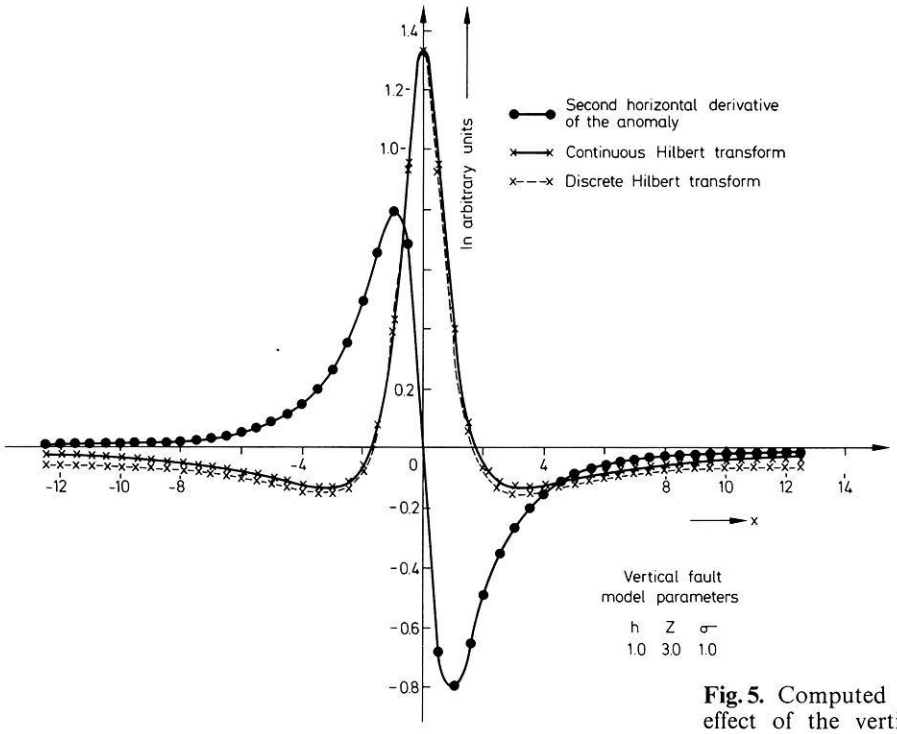

Fig. 5. Computed second horizontal gradient of the gravity effect of the vertical fault, the Hilbert transform and the Discrete Hilbert transform. (Model II)

the Penganga basin of precambrian sedimentary formation. It consists of two successions of alternating limestones and shales with basal quartzites. The stratigraphy sequence is as follows:

Precambrian sedimentaries	Penganga group	Shale Limestone Quartzite -Non-confirmity -
		.....
		Shale[2]
		Limestone[2]

The length of the profile considered is 6.4 km and the station interval is 100 m. The computed second horizontal derivative of the anomaly and its DHT are

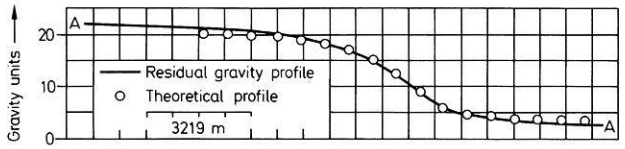

Fig. 6. Bouger gravity anomaly across the Garber structure, Garber County, Oklahoma

Table 2. Field Example (Dipping fault)

Parameters	d	h	Z	σ
Hilbert transform method	73.5°	327 m	2816 m	17.6 kg/m^3
Grant and West method	50°–70°	366 m	2804 to 4328 m	16.0 kg/m^3 to 22.0

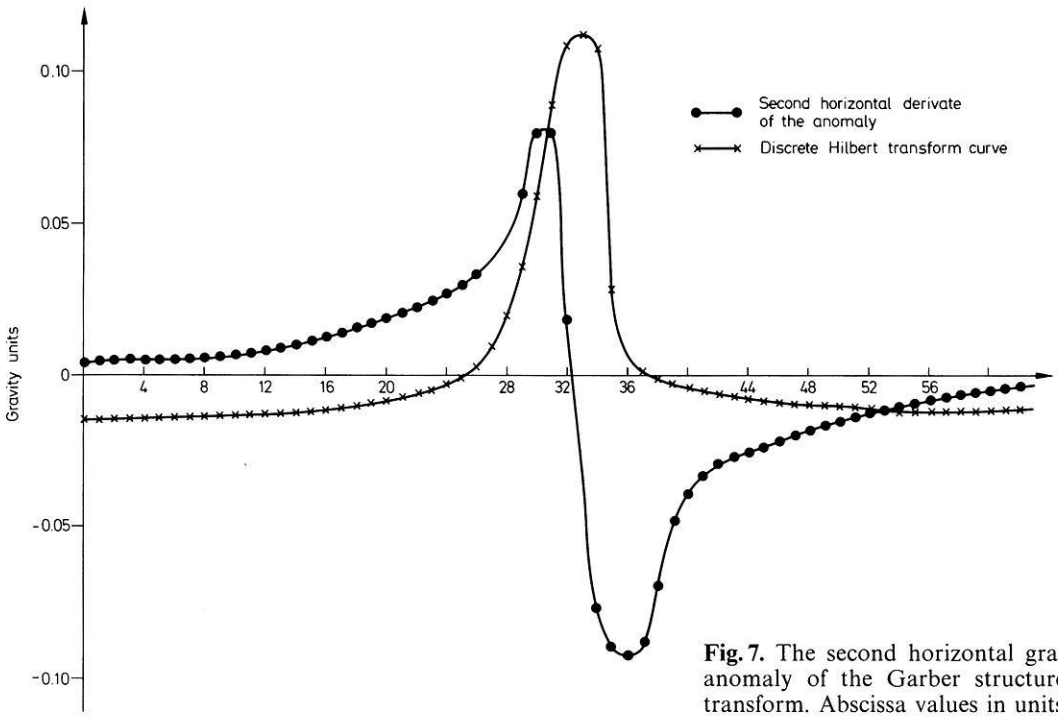

Fig. 7. The second horizontal gradient of the Bouger gravity anomaly of the Garber structure and the Discrete Hilbert transform. Abscissa values in units of 121 m

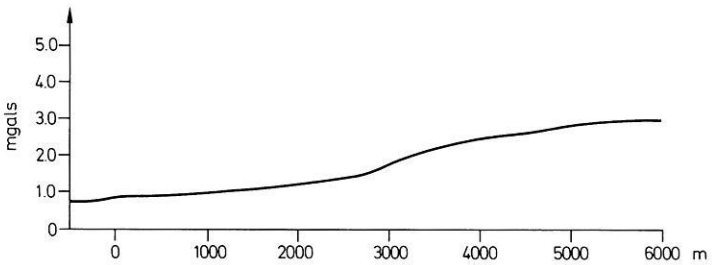

Fig. 8. Gravity anomaly over a vertical fault near Adilabad, Andhra Pradesh, India

plotted and shown (Fig. 9). It is observed that these two curves intersect at $x_1 = 7.6$ and $x_2 = -1.2$. Using the procedure detailed in the text, the results obtained are presented in Table 3.

Discussion

In this method differentiation of $g(x)$ with respect to x introduces a certain amount of error, consequently the Hilbert transform $H(x)$ is affected. The computation of the discrete Hilbert transform is further affected while taking the Fourier transform and its value depends upon the FFT algorithm. The sampling distances and the sampling rate used to digitize the measured potential gradients play an important role in minimising errors. It may be mentioned here that differentiation may be carried out effectively and more accurately in the frequency domain where, controlled by a dense sampling rate, the errors may be reduced sufficiently to obtain a reliable second derivative profile.

It may be pointed that the amount of error in the evaluation of parameters depends on the measurement of the gravity field and the computation of derivatives. We presume that an error of 0.1 units has been made in the measurement of $g(x)$ and the combined gradient value can be expressed as follows:

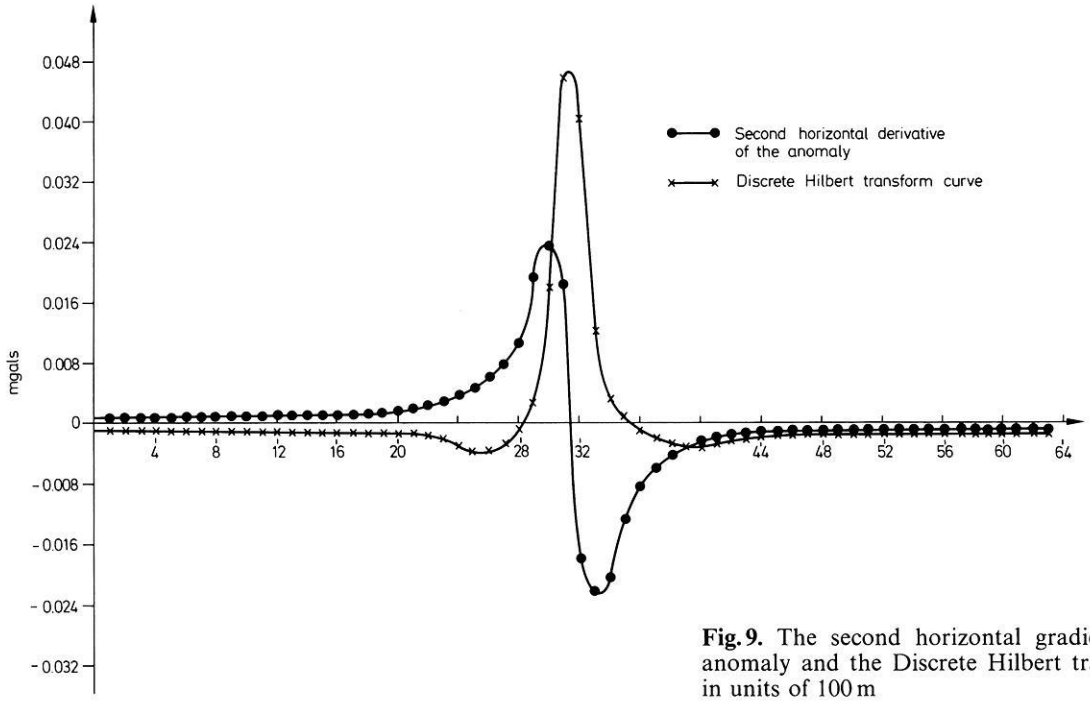

Fig. 9. The second horizontal gradient of the vertical fault anomaly and the Discrete Hilbert transform. Abscissa values in units of 100 m

Table 3. Field Example (Vertical fault)

Parameters	h	Z	σ
Hilbert transform method	214 m	426 m	122.2 kg/m^3

$g(x)=g(x)+0.1\,g(x)$.

The Fourier transform of the above relation can be written as,

$$F(\omega)=F\left[\frac{d^2}{dx^2}\{g(x)\}+\frac{d^2}{dx^2}\{0.1\,g(x)\}\right]$$
$$=1.1\,F[g''(x)].$$

Consequently, the Hilbert transform can be written as:

$$H(x)=H[1.1\,F\{g''(x)\}]+\varepsilon$$

where ε is a small amount of error introduced during the computation of Hilbert transform.

Hence, it is seen that the error in calculating the dip of the fault structure is

$$d=\tan^{-1}\left[\frac{1.1\,H(0)+\varepsilon}{1.1\,g''(0)}\right].$$

Therefore, it could be concluded that when $\varepsilon\to 0$, the dip of the fault is affected little by errors in the measurement and computation of the gravity field. However, the approximation made in determining the dip affects the subsequent evaluation of other parameters.

Appendix

At $x=0$, the Eqs. (3) and (8) reduce to,

$$g''(0)=2G\sigma\cdot\sin d\left[\cos d\left(\frac{1}{h}-\frac{Z}{D^2+Z^2}\right)-\frac{D\cdot\sin d}{D^2+Z^2}\right], \quad (A.1)$$

$$H(0)=2G\sigma\cdot\sin d\left[\sin d\left(\frac{1}{h}-\frac{Z}{D^2+Z^2}\right)-\frac{D\cdot\cos d}{D^2+Z^2}\right]. \quad (A.2)$$

From Eqs. (A.1) and (A.2) we have,

$$\frac{g''(0)}{H(0)}=\frac{M\cdot\cot d-N}{M-N\cdot\cot d}. \quad (A.3)$$

Where,

$$M=\left(\frac{1}{h}-\frac{Z}{D^2+Z^2}\right)$$

and

$$N=\frac{D}{D^2+Z^2}.$$

For large values of Z, N approaches zero. So for many practical purposes, Eq. A-3 can be approximated to

$$\cot d=\frac{g''(0)}{H(0)}.$$

Acknowledgements. The authors thank the referees for their useful suggestions. Our thanks are also due to Professor M.S. Vijaya Raghava, Messrs. P.V. Harinath Baba and V. Veerabhadrappa, Centre of Exploration Geophysics, Osmania University, Hyderabad for providing the field data from the Adilabad area. Also one of the authors (N. Sundararajan) is grateful to the Council of Scientific and Industrial Research, Government of India for the financial help received. N.L. Mohan records his thanks to UGC for the financial grant.

References

Bhimasankaram, V.L.S., Mohan, N.L., Seshagiri Rao, S.V.: Analysis of the gravity effect of two dimensional trapezoidal prisms using Fourier Transform. Geophysical Prospecting, **35**, 334–341, 1977

Gold, B., Rader, C.M.: Digital processing of signals. New York: McGraw-Hill Co. 1969

Grant, F.S., West, G.F.: Interpretation theory in applied Geophysics. New York: McGraw-Hill Book Company 1965

Jung, K.: Schwerkraftverfahren in der angewandten Geophysik. Geest and Portig, 1961

Mohan, N.L., Sundararajan, N., Seshagiri Rao, S.V.: Interpretation of some two dimensional magnetic bodies using Hilbert transforms. Geophysics **47**, 376–387, 1982

Nabighian, I.N.: The analytic signal of two dimensional magnetic bodies with polygonal cross section, its properties and use for automated anomaly interpretation. Geophysics **37**, 507–512, 1972

Stanley, J.M., Green, R.: Gravity gradients and the interpretation of the truncated plate. Geophysics **41**, 1270–1276, 1976

Stanley, J.M.: Simplified gravity interpretation by gradients – The geological contact. Geophysics **42**, 1230–1235, 1977

Thomas, J.B.: An introduction to statistical communication theory. New York: John-Wiley and Sons, Inc. 1969

Received October 1, 1980; Revised version December 10, 1982; Accepted March 30, 1983

J Geophys (1983) 53:42–51

Journal of Geophysics

On the Thermal State of the Earth's Mantle

A.C. Fowler
Department of Mathematics, Room 2-336, Massachusetts Institute of Technology, Cambridge, MA 02139, USA

Abstract. An apparent paradox is discussed, arising from the contrast between an inferred constant mantle viscosity profile and theoretical and experimental rheological flow laws, which predict a mantle viscosity function varying strongly as a function of both temperature and pressure. One can explain the paradox by a particular choice of material parameters, but then mantle temperatures (computed adiabatically) are too low; increasing the temperature by inserting compensatory thermal boundary layers is considered to be dynamically unfeasible, again because of the flow law. We consider this an impasse, and to resolve it, we suggest that old dogmas concerning boundary layers and adiabats need to be critically re-examined, to understand their basis. When this is done, we find that the observed constant viscosity is, in effect, *demanded* by the interplay of the rheology with the convective process, the mantle temperature is not necessarily adiabatic, and some form of layering effect may be expected, although the ideas presented here are virtually independent of the precise dynamical style of the convective motion. A consequence of these results is that explanations and extrapolations taken from constant-viscosity convection models are, a priori, unjustifiable. (Specifically, a constant viscosity mantle is a fundamental consequence of the state of flow together with the fluid parameters and rheology: it is not a passive coincidence, which may *then* be used to deduce the flow state, etc.)

Key words: Mantle temperatures – Mantle convection – Rheology

Introduction

Fifteen years after the pioneering theoretical paper of Turcotte and Oxburgh (1967), our understanding of the nature of the convective flow in the Earth's mantle is in a somewhat confusing state. Although both theoretical (Stocker and Ashby, 1973) and experimental (Goetze, 1978) work on mantle-type minerals show that the effective viscosity is a strongly varying function of both temperature and pressure (which is why the lithosphere is 'rigid', i.e. does not deform significantly on convective time scales of interest (at least away from trenches)), there have been relatively few really serious attempts at modelling the mantle as a fluid with such a viscosity, and where this has been done (Parmentier and Turcotte, 1978; Schmeling and Jacoby, 1981; Kopitzke, 1979; Christensen, 1982), various stop-gap measures have to be introduced in order to simulate the real earth. Particularly, the vital issue of subduction of the lithosphere at oceanic trenches has either been treated kinematically, or simply ignored; this has serious consequences since it is precisely the subduction which causes the active style of convection in the mantle: without subduction, numerical models have a tendency to exhibit a rigid, passive, conducting lid (Daly, 1980; Schmeling, 1980; Schmeling and Jacoby, 1981) as they (obviously) should. Turcotte et al. (1977) propose an elastic transverse buckling of the lithosphere to explain subduction, and if we follow this idea, one should really study viscoelastic convection of the mantle, a proposal which has not been previously considered, except in the recent paper by Ivins et al. (1982).

On the other hand, many workers have used models of high-Rayleigh-number, constant-viscosity convection to study various features of interest (McKenzie et al., 1974; Hewitt et al., 1981; Olson and Corcos, 1980; Elsasser et al., 1979): a recent paper in this style is that of Jarvis and Peltier (1982). One can argue variously about the merits of such models: on the one hand, the inference of a relatively constant sub-lithospheric viscosity (Cathles, 1975; Peltier, 1980) supports their usefulness, but this inference is something which itself needs to be explained, and can lead to apparently circular arguments (Elsasser et al., 1979), or misconceived analogies (Hewitt et al., 1981).

In any case, difficulties remain with the formulation of the problem. Recent geochemical evidence (De Paolo, 1981) supports circumstantially the notion that there is a chemical layering of the mantle across the transition zone. This is plausibly explained by a convective layering, which may also be consistent with the cessation of deep earthquakes at ~ 700 km, and the existence of a seismic discontinuity there. While none of these observations has irrefutable implications, they are self-consistent, and there is no countering evidence in support of whole-mantle convection, other than dynamical reasoning (Schubert and Spohn, 1981) (again on the basis of constant viscosity convection). It would be worthwhile seeing if these dynamic objections stand up in the context of a temperature and pressure dependent rheology.

This paper will not be overtly concerned with the specific issue of a layered convection, but will address directly the issue of a constant viscosity distribution in the mantle, and study how it may be reconciled with the expected rheology of the real Earth. In so doing, we shall infer some characteristics of the style of convection, and will thus be led to a new proposal for the mantle geotherm.

On the face of it, constant viscosity observations from post-glacial uplift (Cathles, 1975; Peltier, 1980) or polar wander (Yuen et al., 1982) do not appear likely if the effective viscosity (Goetze, 1978) based on dislocation creep, is of the form

$$\eta = \frac{A}{\tau^2} \exp\left[\frac{E^* + pV^*}{RT}\right]; \tag{1.1}$$

here, τ is the second stress invariant, T is temperature, p is pressure, E^* is activation energy, V^* is activation volume, and R is the gas constant. For any acceptable temperature in the mantle, one finds $E^*/RT \gg 1$ (e.g. ~ 30) using laboratory measurements of E^*, and the exponent is far and away the most important part of determining the viscosity. In particular, isoviscous temperatures are those for which the exponent is approximately constant, i.e. $T \propto E^* + pV^*$; for constant E^* and V^*, this would imply that isoviscous temperature profiles are essentially linear with pressure, and hence depth. With commonly quoted values $E^* \sim 125$ kcal/mode, $V^* \sim 11$ cm^3/mole, such isoviscous profiles have temperature gradients $dT_{iso}/dz \sim 0.7$ K km^{-1}: here z is the depth coordinate. On the other hand, the internal temperatures (i.e. away from boundary layers) of a vigorously convecting fluid should be approximately adiabatically related (see further discussion of this below), that is $dT_{ad}/dz \approx \alpha g T_{ad}/c_p$. Using values $c_p \sim 0.27$ cal gm^{-1} K^{-1}, $g \sim 10^3$ cm s^{-2}, $\alpha \sim 3 \times 10^{-5}$ K^{-1}, $T_{ad} \sim 2{,}000$ K (a mean value) we obtain $dT_{ad}/dz \sim 0.5$ K km^{-1} as a reasonable estimate. These fairly roughly calculated values show that adiabatic and isoviscous temperature profiles have gradients differing by probably no more than a factor of two. Nevertheless, a difference of 0.2 K km^{-1} in the mean temperature gradient across the mantle would imply a difference of these two profile temperatures at the core-mantle boundary of 600 K, and in view of the largeness of E^*/RT, this could correspond to a viscosity differing from that in the asthenosphere by at least four orders of magnitude: the viscosity law is very sensitive to changes in temperature.

This discrepancy led Weertman (1978) to suggest that transient creep processes in the mantle might explain the apparent viscosity, even though the long term behaviour would be governed by thermally activated steady state processes. Indeed, extrapolation of experimental results of Goetze and Brace (1972) to mantle strain rates $\sim 10^{-15}$ s^{-1} would suggest a time-scale for transient creep of $\sim 10{,}000$ years, just that over which post-glacial rebound occurs. Peltier et al. (1980) examined the data for transient rheologies, and did not find any need to include such effects. In any case, transient creep should also be thermally activated, and Weertman's motivation would disappear.

O'Connell (1977) and Sammis et al. (1977) have proposed that other factors may contribute to the resolution of the isoviscosity problem. It is plausible (see also Karato, 1981) that the activation volume V^* decreases by up to a factor of about 4 as p increases through the mantle. Such a decrease is able to offset the slower than isoviscous increase in temperature due to adiabaticity, and it becomes possible to accommodate the observations with plausible Earth parameters. On the other hand Jaoul et al. (1981) show that E^* for forsterite increases with temperature: this would act in the opposite direction to decreasing V^*. Further, if one appeals to variation of V^* with p, consistency demands adoption of the best constraints available on thermodynamic parameters. From results of Dziewonski and Anderson (1981), Anderson and Sumino (1980) and Stacey (1977), we can infer that the thermal expansion coefficient α decreases (a factor of about 3) with pressure in the mantle. If we adopt these various results, one can compute an adiabatic temperature which (given the largeness of E^*/RT) to all intents and purposes gives a relatively uniform mantle viscosity (see Table 1); obviously by adjustment of dK/dp, dV^*/dp, etc., one could tune the viscosity to be absolutely constant. However, more importantly, the resultant adiabatic temperature only reaches a temperature of $\sim 2{,}400$ K at the base, about 800 K less than the constrained value due to extrapolation of the FeS solidus to core pressures (Stacey, 1977). One could again remedy this by fiddling with parameters until both adiabatic and constant viscosity temperatures overlap: this is a philosophically unsatisfactory and academically unsound procedure, amounting to no more than curve-fitting, and the remedy should lie elsewhere. In fact, Jeanloz and Richter (1979) noted the same difficulty and suggested that the temperature deficit could be made up by one or more thermal boundary layers at the base of the mantle, and at the transition zone (670 km) if layered convection occurs: they do not consider that temperature jumps at phase changes can amount to more than about 100 K in total.

This proposal sounds reasonable provided one accepts boundary layers as inevitable, and indeed, this is exactly what constant viscosity convection leads us to expect. However, it is not a priori obvious in what manner boundary layers, in which the temperature jumps $\gtrsim 500$ K, can and will occur in a temperature-dependent viscous fluid: in fact, more recent consideration of this proposition suggests that boundary layers in convection of such fluids become asymmetric, the bulk of the temperature jump occurring across the cold, upper thermal boundary layer: this is evident in numerical studies (Schmeling, 1980), experimental studies (Nataf and Richter, 1982), and may be understood in terms of a marginal stability criterion of boundary layers (Howard, 1966); one can easily compute the order of magnitude temperature jump that basal boundary layers can sustain, from linear stability results of Schubert et al. (1969): when $E^*/RT \gg 1$ (as for the mantle), this temperature jump is $O[RT_b^2/(E^* + pV^*)]$, where T_b is the basal temperature (see also Fowler, 1982b; Morris, 1980); when $T_b \sim 3{,}000$ K, this is ~ 100 K at the core-mantle boundary, with reasonable estimates for E^* and V^*. Thus one should not expect a temperature jump of ~ 800 K in the D'' layer: this would entail

Table 1. Values of α, p, ρ, g, V^*, T_{ad}, η and K computed using the formulae $K = K_0 + K_1 p$, $\alpha = \gamma \rho c_p / K$, $\rho = \rho_0 [1 - \alpha(T - T_0)] \exp\left[\int_0^p dp/K(p)\right]$, $V^* = V_0^*/(K/K_0)$, $\eta = (A/\tau^2)\exp[E^* + pV^*)/RT]$. The lithostatic pressure p and gravity g are calculated after solving Poisson's equation for the gravitational potential. For the results here, we have used $\rho_0 = 3.8\,\mathrm{gm\,cm^{-3}}$, $T_0 = 273\,\mathrm{K}$, $K_0 = 131\,\mathrm{GPa}$ ($1\,\mathrm{GPa} = 10^4\,\mathrm{bar}$), $K_1 = 4.0$, $\gamma = 1.0$ (Gruneisen parameter), $\tau = 10\,\mathrm{bars}$, $A = 1/70\,\mathrm{bar^3\,s}$, $c_p = 1.26\,\mathrm{kJ\,kg^{-1}\,K^{-1}}$, $V_0^* = 11\,\mathrm{cm^3/mol}$, $E^* = 122\,\mathrm{kcal/mol}$, $R = 8.3\,\mathrm{J\,mol^{-1}\,K^{-1}}$, and the adiabatic temperature is determined from $dT_{ad}/dp = \gamma T_{ad}/K$, where also $T_{ad}(0) = 1{,}550\,\mathrm{K}$ here. These values are either taken from commonly quoted values ($V^*, E^* \ldots$) or induced from Earth models such as that of Dziewonski and Anderson (1981). With the chosen values of K_0, K_1, γ, ρ_0, we see that p, ρ, g and K look pretty much like their inferred values from the above Earth model, V^* decreases in line with inferences of Sammis et al. (1977), and α decreases as expected. The computed adiabatic temperature fails to approach the constrained value of $\gtrsim 3{,}000\,\mathrm{K}$ at the core mantle boundary, whereas the viscosity is *relatively* uniform over the whole sub-lithospheric mantle, though still varying by a factor of fifty or so. We emphasise that the point of this table is not to predict anything precisely (viscosity or temperature) but rather to show the qualitative results which may *reasonably* be expected

depth (km)	α ($\mathrm{K^{-1}}$)	p (k bar)	ρ ($\mathrm{gm\,cm^{-3}}$)	g ($\mathrm{ms^{-2}}$)	V^* ($\mathrm{cm^3\,mole^{-1}}$)	T_{ad} (K)	η (poise)	K (GPa)
100.0	$0.32E-04$	36.1	3.7	9.81	9.9	1,591.1	$0.15E+21$	145.5
200.0	$0.30E-04$	73.3	3.8	9.81	9.0	1,630.3	$0.52E+21$	160.3
300.0	$0.28E-04$	111.3	3.9	9.81	8.2	1,667.7	$0.13E+22$	175.5
400.0	$0.26E-04$	150.3	4.0	9.80	7.5	1,703.5	$0.24E+22$	191.1
500.0	$0.25E-04$	190.0	4.1	9.79	7.0	1,737.9	$0.37E+22$	207.0
600.0	$0.24E-04$	230.6	4.2	9.78	6.5	1,771.0	$0.49E+22$	223.2
700.0	$0.22E-04$	271.9	4.3	9.77	6.0	1,802.9	$0.59E+22$	239.8
800.0	$0.21E-04$	313.9	4.3	9.75	5.6	1,833.7	$0.64E+22$	256.6
900.0	$0.20E-04$	356.6	4.4	9.74	5.3	1,863.5	$0.65E+22$	273.7
1,000.0	$0.19E-04$	400.0	4.5	9.72	5.0	1,892.4	$0.64E+22$	291.0
1,100.0	$0.19E-04$	444.0	4.6	9.72	4.7	1,920.3	$0.58E+22$	308.6
1,200.0	$0.18E-04$	488.6	4.6	9.70	4.4	1,947.5	$0.52E+22$	326.4
1,300.0	$0.17E-04$	533.8	4.7	9.68	4.2	1,973.9	$0.45E+22$	344.5
1,400.0	$0.17E-04$	579.6	4.8	9.67	4.0	1,999.7	$0.39E+22$	362.8
1,500.0	$0.16E-04$	625.9	4.8	9.66	3.8	2,024.7	$0.32E+22$	381.4
1,600.0	$0.15E-04$	672.8	4.9	9.66	3.6	2,049.2	$0.27E+22$	400.1
1,700.0	$0.15E-04$	720.3	4.9	9.65	3.4	2,073.1	$0.22E+22$	419.1
1,800.0	$0.14E-04$	768.3	5.0	9.66	3.3	2,096.4	$0.18E+22$	438.3
1,900.0	$0.14E-04$	816.9	5.1	9.66	3.1	2,119.3	$0.14E+22$	457.8
2,000.0	$0.14E-04$	866.1	5.1	9.67	3.0	2,141.7	$0.11E+22$	477.5
2,100.0	$0.13E-04$	916.0	5.2	9.69	2.9	2,163.7	$0.92E+21$	497.4
2,200.0	$0.13E-04$	966.4	5.2	9.71	2.8	2,185.3	$0.73E+21$	517.6
2,300.0	$0.12E-04$	1,017.5	5.3	9.75	2.7	2,206.6	$0.59E+21$	538.0
2,400.0	$0.12E-04$	1,069.3	5.3	9.79	2.6	2,227.6	$0.47E+21$	558.7
2,500.0	$0.12E-04$	1,121.9	5.4	9.84	2.5	2,248.2	$0.37E+21$	579.8
2,600.0	$0.11E-04$	1,175.3	5.4	9.90	2.4	2,268.7	$0.30E+21$	601.1
2,700.0	$0.11E-04$	1,229.5	5.5	9.98	2.3	2,288.9	$0.24E+21$	622.8
2,800.0	$0.11E-04$	1,284.8	5.5	10.07	2.2	2,308.9	$0.19E+21$	644.9
2,900.0	$0.11E-04$	1,341.1	5.6	10.18	2.2	2,328.8	$0.15E+21$	667.4

a viscosity *decrease* with depth on the order of a factor 10^3, which I suggest would be wildly unstable (Howard, 1966; Schubert et al., 1969). Alternatively, as Jeanloz and Richter (1979) suggest, one could have two layered convection cells, so that the temperature jump necessary could be accommodated by smaller boundary layers at the base of the lower and upper mantle. However, one would still have temperature jumps ~ 400 K, and consequently the lower mantle would have a viscosity say 10^2 times that of the upper mantle. According to rotation and uplift data (Peltier, 1980; Yuen et al., 1982) this is not possible. We think that Jeanloz and Richter found a real problem, but that their solution is not feasible - the problem remains. Note that we are not saying that a geochemical *layering* is impossible: simply that large internal or basal temperature jumps are improbable, for *dynamical reasons.*

If we accept the premises (constant sub-asthenospheric viscosity and thermally activated creep), apparently we still have a dilemma on our hands. One can always escape by choosing not to believe either the reasoning or the results, but it is also worth pursuing the logic of the argument, to see if it is truly self-consistent. The impasse we have is that a feasible adiabatic temperature for an internal (i.e. away from boundary layers) isoviscous flow is too low for the core-mantle boundary constraint ($T_b \gtrsim 3{,}000$ K). The implication is simply that the internal temperature variation with depth is faster than adiabatic. The description of the temperature of convecting fluids in terms of boundary layers and adiabats is usually taken for granted, but it may be worthwhile to examine these concepts in a little more detail, to understand under what circumstances such a description is appropriate, since there is a tendency in the geophysical literature to misconstrue the mathematical significance of boundary layers, and to put them in freely whenever there is a temperature deficit to be made up.

Boundary Layers and Adiabats

For the purposes of this section, we require only an energy equation

$$\rho c_p \frac{dT}{dt} - \alpha T \frac{dp}{dt} = k \nabla^2 T, \tag{2.1}$$

in which T is temperature, p is pressure, ρ is density, c_p is specific heat, α is thermal expansion coefficient, k is thermal conductivity, and $d/dt = \mathbf{q} \cdot \nabla$ in the steady state. We can also define the Grüneisen parameter

$$\gamma = \alpha K / \rho c_p, \tag{2.2}$$

where K is the (adiabatic or isothermal) bulk modulus, and can be indirectly estimated from seismic and mean density data. The equation of state may then be written (Bullen, 1975)

$$\rho = \rho(p, T) \quad \text{and} \quad \frac{\partial \rho}{\partial p} = \frac{\rho}{K}, \quad \frac{\partial \rho}{\partial T} = -\alpha \rho, \tag{2.3}$$

and $K = K(p)$, $\alpha = \alpha(p)$ (dependence on T is weak). We will consider a viscosity in the form

$$\eta = \eta_0 \exp\left[\frac{E^* + pV^*}{RT}\right], \tag{2.4}$$

where really $\eta_0 = A/\tau^2$ (Goetze, 1978), or perhaps $\eta_0 = A/\tau^2 + B$ to include diffusion creep, but we suppress dependence on τ to emphasise the strong exponential variation of η with T and p.

We must scale the variables; thus we write

$$T = T_a \theta, \; p = \rho_0 g d p^*, \; x = l x^*, \; y = d y^*,$$
$$t = (l/U) t^*, \; u = U u^*, \; v = (dU/l) v^*, \tag{2.5}$$

where g is gravity, $\mathbf{q} = (u, v)$ is the velocity, T_a is the sub-lithospheric temperature (this will be made more specific in due course), d and l are vertical and horizontal scale heights, and U is a horizontal velocity scale. Adoption of (2.5) then leads to the following dimensionless equations, where we drop asterisks on the variables:

$$\frac{d\theta}{dt} - D\theta \frac{dp}{dt} = \delta^2 \nabla^2 \theta \equiv \delta^2 [\theta_{yy} + v^2 \theta_{xx}],$$
$$\eta = \eta_a \exp\left[\frac{1 + \mu p - \theta}{\varepsilon \theta}\right], \tag{2.6}$$

where $\eta_a = \eta_0 \exp(1/\varepsilon)$ is (roughly) the sub-lithospheric viscosity ($\theta = 1$, $p \approx 0$). In (2.6) there are five dimensionless parameters

$$v = d/l, \tag{2.7}$$

$$\delta^2 = \frac{\kappa l}{U d^2} \tag{2.8}$$

(κ is the thermal diffusivity $k/\rho c_p$),

$$D = \alpha g d / c_p, \tag{2.9}$$

$$\mu = \rho_0 g \, dV^*/E^*, \tag{2.10}$$

and

$$\varepsilon = RT_a/E^*. \tag{2.11}$$

If we are being realistic, then all these are functions of p and T: particularly $D = D(p)$, $\mu = \mu(p)$ (both decreasing). If we define a stress scale

$$[\tau] = \eta_a U/d, \tag{2.12}$$

and non-dimensionalise the stress components with $[\tau]$, the dimensionless constitutive law may be written

$$\tau_2 = \eta^*(u_y + v^2 v_x),$$
$$\tau_1 = 2v\eta^* u_x, \tag{2.13}$$

where η^* is the dimensionless viscosity $= \eta/\eta_a$.

We have some comments. We are now going to choose 'representative' values of the various parameters, and examine the analytical implications of these choices for the possible temperature field. Our discussion will use *asymptotic* orders of magnitude for the various quantities δ, etc., and to this (mathematical) extent, such discussion will be reasonably general. However, in attempting to make an application to one particular planet at one particular epoch (the present Earth), we are naturally forced to consider whether the *quantitative* values of δ, etc., that we adopt can be construed as having a realistic bearing on this one sample.

Being biased in favour of the views promoted here, it is natural that the scales so chosen will happen to give a satisfactory explanation of some observed features of the mantle. However, one should be aware that, even where the scaling analysis is *qualitatively* valid, precise numerical estimates depend on numerical evaluation of fixed 'order one' constants, whose actual magnitude can vary substantially.

As an example, consider the well-known boundary layer analysis (Turcotte and Oxburgh, 1967) of isoviscous convection at high Rayleigh number, *Ra*. Scaling alone (for stress free boundary conditions) suggests that the Nusselt number $Nu \sim Ra^{1/3}$ as $Ra \to \infty$, whereas experiments and analysis give the more accurate $Nu \sim 0.1 Ra^{1/3}$: here 0.1 (an order of magnitude) arises as a coefficient of "$O(1)$". In fact, one can understand the appearance of such a factor by writing $Nu \sim (Ra/Ra_c)^{1/3}$, where Ra_c is the critical value at the onset of convection; this form is suggested by Howard's (1966) marginal stability argument, where $Ra_c = 27\pi^4/4 \approx 657$ is "$O(1)$"! Thus, one should beware of treating approximate scaling results in an exact manner.

One might argue as a result of the caveat above that these kind of arguments are of little use, but the success of such techniques in many areas of applied mathematics belies this statement, and in any case the main thrust of such arguments is in suggesting the possible (or plausible) *structure* of solutions: precise quantitative results require a detailed numerical solution.

One might also then ask for such a numerical solution, but this inverts the argument: one can hardly give a numerically parameterised result (e.g. the factor 0.1 referred to above) without a previous analysis of the boundary layer structure.

As an illustration of these comments, consider the parameter δ^2 in (2.8). Below we shall find $\delta^2 \sim 10^{-2}$, and this will fit nicely with the inferred viscosity of the mantle. However, if δ^2 is much smaller (say, $<10^{-3}$), then this nice correspondence becomes less tenable. Now the obvious choice of $d=l=3{,}000$ km for the whole mantle and $U=10$ cm yr^{-1} leads to $\delta^2 \sim 10^{-4}$, too low for our needs. However, the same parameters with a viscosity $\eta_m \sim 10^{22}$ Poise define a stress scale $[\tau] = \eta_m U/d \sim 10$ bars, much less than the negative buoyancy in a down-going slab would suggest [~ 500 bars]. Alternatively, if we supposed layered convection can occur, then a more appropriate choice of d is 700 km, so that then $\delta^2 \sim 10^{-3}$, and the 10 bar figure (modified by d but also (probably) by η_a) becomes more recognisable as an inferred sub-lithospheric stress. But if shallow convection is considered, then more typically $l \sim 7{,}000$ km than 700 km, and $\delta^2 \sim 10^{-2}$! The important point to note is that in any case $\delta^2 \ll 1$, and that the subsequent discussion of this paper relies only on *asymptotic* estimates $1 \gg \delta^2 \gg \exp[-1/\varepsilon]$, which are in any case qualitatively applicable. Since a result of this analysis will be that the effective depth of vigorous convection is generally less than that of the whole mantle (see also Fowler, 1982a), we will simply anticipate this below in choosing d.

To proceed, however: in principle, scaling of the entire system of equations (not all given here) should rationally be done in terms only of the actual inputs to the model (basal temperature, depth, etc.) (Fowler, 1982b). This is not our present concern, and we simply use observation to choose

$$U \sim 5 \text{ cm yr}^{-1}; \tag{2.14a}$$

as may already have been suspected, we will define

$$d = 700 \text{ km}, \tag{2.14b}$$

as representative of layered mantle convection (or if one likes, the viscous scale height which might control the dynamics: Schubert et al., 1969). The length scale of surface plates is taken as

$$l = 8{,}000 \text{ km}, \tag{2.14c}$$

and then other standard (quoted) values ($\kappa \sim 10^{-2}$ cm s^{-1}, $R \sim 8.3$ J mole^{-1} K^{-1}, $T_a \sim 1{,}500$ K, $E^* \sim 122$ kcal mole^{-1}, $\alpha \sim 3 \times 10^{-5}$ K^{-1}, $g \sim 10$ m s^{-2}, $c_p \sim 0.27$ cal gm^{-1} K^{-1}, $\rho_0 \sim 3.5$ gm cm^{-3}, $V^* \sim 11$ cm^3 mole^{-1}) lead to *typical* values

$$\delta^2 \sim 10^{-2}, \quad D \sim 0.2, \quad \mu \sim 0.5, \quad \varepsilon \sim 1/40; \tag{2.15}$$

particularly

$$D, \mu \lesssim O(1), \quad \varepsilon, \delta^2 \ll 1. \tag{2.16}$$

The ensuing discussion will now proceed precisely on the basis of the asymptotic limits implied by (2.15), i.e. $\varepsilon, \delta \to 0$; $D, \mu \lesssim O(1)$. It should be noted that these arguments apply regardless of whether $\delta^2 \sim 10^{-2}$ or 10^{-4}, for example; it is only in the specific application to the Earth that any quantitative selection is indicated.

Let us first consider the energy equation (2.6) in the light of these estimates. *Since the scales are specifically chosen so that the dimensionless variables are* $O(1)$, we are led to neglect $\delta^2 \nabla^2 \theta$ in (2.6) on the basis that $\delta^2 \ll 1$, and that if $\theta \sim 1$, then we should expect $|\nabla\theta|, |\nabla^2\theta|$, etc. to be $O(1)$ unless this leads to inconsistency. In the case that this is valid, i.e. if $|\mathbf{q}| \sim 1$ *and* $|\nabla^2\theta| \sim 1$, then

$$\mathbf{q} \cdot \nabla\theta - D\mathbf{q} \cdot \nabla p \approx 0 \tag{2.17}$$

(at least in a steady state) and we have the adiabatic temperature profiles

$$\theta = \exp\left[\int_0^p D(p)\, dp\right] \tag{2.18}$$

(we can choose $\theta = 1$ at $p = 0$ by choice of T_a). This is the basis for the assumed adiabatic thermal profile.

The neglect of $\delta^2 \nabla^2 \theta$ in (2.6) constitutes a removal of the highest derivatives of the equation, and a consequent reduction of order. As a result of this, the reduced (hyperbolic) equation (2.17) *cannot* generally satisfy all the prescribed boundary conditions (on top and bottom), and at least one must be ignored (we *could* choose θ_0 to satisfy one of them). As a result of this, our original assumption that $\delta^2 \nabla^2 \theta$ is always small must break down, and this implies that $|\nabla\theta|$ becomes large over a length scale small compared to one, i.e. θ changes rapidly in a thin *boundary layer*. Naturally, since the inconsistency is due to an inability to satisfy boundary conditions, one looks first for such layers near boundaries, but it should be emphasised that (since the problem is non-linear) nothing precludes internal layers or multiply-layered solutions (Kevorkian and Cole, 1981) except possibly our hope that these are less likely, physically, to occur. Furthermore, the occurrence of symmetric upper and lower boundary layers in constant viscosity convection, heated from below (Turcotte and Oxburgh, 1967) is a consequence of the symmetry of the problem, and two boundary layers are not a necessary result of small δ, e.g. when internal heating drives the flow (Peltier, 1981). To re-iterate: one expects boundary layers to occur when $\delta \ll 1$ because of the singular nature of the approximation (2.17), but where and how many these are depends on the particular situation; basal boundary layers, particularly, are not always inevitable, especially in variable viscosity flows. Arguments about 'getting the heat out of the core' are also not germane, since it is quite feasible to have a singular layer in which $\partial\theta/\partial y$ jumps by $O(1)$, but θ jumps only by a small amount (e.g. $O(\delta)$): consider $\theta = \delta \exp[-y/\delta]$ near $y = 0$.

Let us now suppose we are away from any boundary layers or thermal plumes, so that we expect the adiabatic temperature (2.18) to be valid. Substitution of this $\theta = \theta_{ad}$ into (2.7), and recalling the dimensionless viscosity $\eta^* = \eta/\eta_a$, yields a dimensionless adiabatic viscosity

$$\eta_{ad} = \exp\left[\frac{1 + \mu p - \theta_{ad}(p)}{\varepsilon \theta_{ad}(p)}\right]. \tag{2.19}$$

We recall from Table 1 that it is feasible to have functional forms for $\mu(p)$ and $D(p)$ which make η_{ad} nearly constant; however, note that any slight deviation from

these isoviscous forms will lead to a substantial variation of η_{ad} *because of the fact that* $\varepsilon \ll 1$. For example, a variation in $[1+\mu p-\theta_{ad}]/\theta_{ad}$ of $O(\varepsilon \ln(1/\delta))$ will cause a variation of $O(1/\delta)$ in the viscosity. In an asymptotic sense, it is clear that as $\varepsilon, \delta \to 0$, very small departures of θ_{ad} from the isoviscous profile θ_{iso} will cause large variations in η^*: yet the observational data apparently constrains η^* to less than a factor of ten within the lower mantle. It is therefore unrealistic and unreasonable to suppose that μ and D are just precisely such that $\eta_{ad}=$constant, rather it is more pertinent and generic to suppose that even if η_{ad} does not vary substantially (i.e. many orders of magnitude), even small departures of θ_{ad} from θ_{iso} will ensure that η^* will vary by perhaps one or two orders of magnitude. We will return to a detailed discussion of the Earth below but for the moment let us suppose that η^* does so vary.

Now consider the effect of a varying η^* on the velocity. Stress and velocity are related in order of magnitude by

$$\tau \sim \eta^* u_y \tag{2.20}$$

(we will not write full equations as our intention is to discuss scales, although with our choice of d and l, $v \sim 0.1$ and (2.20) accurately represents (2.13)). In order to try and understand how $|\mathbf{q}|$ may vary with η, we must first understand how stress is produced in convection. For this purpose, consider the Turcotte-Oxburgh boundary layer theory of convection (1967). In this situation, shear stress is generated by thermal buoyancy in the thermal plumes at the cell boundaries. Away from these plumes, the interior (isoviscous) fluid experiences a net torque which drives the convection cell. The stress (actually vorticity*) is distributed (by Laplace's equation*) through the cell interior, and there are no internal stress boundary layers. The flow is then determined (by Poisson's equation*), and there are similarly no large velocity gradients. In the absence of large velocity and stress gradients, (2.20) then implies that

$$|\mathbf{q}| \sim \tau/\eta^* \sim 1/\eta^* \tag{2.21}$$

(N.B. we do *not* mean $|\mathbf{q}| \propto 1/\eta^*$).

In other words: if η^* increases, $|\mathbf{q}|$ decreases. We claim to have deduced this, but it is in fact an obvious physical proposition. However, (as was the case with the magnitude of δ^2) it could be rather important for the *quantitative* application of our theory that (2.21) holds rather than, say $|\mathbf{q}| \sim 1/\eta^{*\frac{1}{2}}$. In the present context, we cannot hope to prove (2.21) preferentially, but we can perhaps give some further indication of why it may obtain.

There are only two obvious ways in which (2.21) does not follow from (2.20), in the interior of the convection cell. One is that there are internal stress concentrations. As already outlined, this seems implausible and unlikely. Alternatively, since only strain-rates tend to zero as $\eta^* \to \infty$, one could have a state of 'quasi-rigid' motion, which would be, most likely, a parallel return flow. The trouble with this is that one would then naturally expect stresses in the upwelling plume of comparable magnitude to those in the slab in order to obtain the necessary strain rate to alter the direction of flow from horizontal to vertical: however, it is part of the later argument of this paper that large thermal anomalies at the base of the convecting zone are precluded by virtue of the strong temperature dependence of the viscosity (they would be highly unstable). Consequently, stress in the ascending plume should be an order of magnitude smaller than that in the descending slab. It would seem that the more plausible alternative is a quasi-stagnant zone, as described. So let us now suppose that $|\mathbf{q}|$ decreases as η^* increases, as in (2.21).

If we remain on an adiabat, we can thus expect $|\mathbf{q}|$ to fluctuate. But now re-examine (2.6):

$$\mathbf{q} \cdot \nabla\theta - D\theta \mathbf{q} \cdot \nabla p = \delta^2 \nabla^2 \theta. \tag{2.22}$$

The adiabatic temperature was derived from (2.22) on the basis that $|\delta^2 \nabla^2 \theta| \ll 1$. This is motivated by $\delta^2 \ll 1$, and is valid provided $|\nabla^2 \theta| \lesssim O(1)$ (we are away from boundary layers, i.e. in the interior) *and* $|\mathbf{q}| \sim O(1)$: specifically $|\mathbf{q}| \gg O(\delta^2)$. But if $|\mathbf{q}|$ decreases to $O(\delta^2)$, the adiabatic assumption is not valid, and we are no longer warranted in assuming an adiabatic temperature. We explore the consequences of this statement below. For the moment we observe that if the adiabatic gradient is $0.5\ \mathrm{K\ km^{-1}}$, the isoviscous gradient is $0.7\ \mathrm{K\ km^{-1}}$, and if we take $T \sim 2{,}000$ K, representative of upper mantle conditions, then we can expect non-adiabaticity when $\theta_{ad}-\theta_{iso} \sim 2\varepsilon \ln(1/\delta)$, corresponding to a temperature difference ~ 260 K, which at $0.2\ \mathrm{K\ km^{-1}}$ divergence rate occurs at a depth of 1,300 km, certainly well within the mantle. Actually, this is only a rough order of magnitude, and a glance at Table 1 shows an increase of $\sim 40\,(\sim O(1/\delta^2)?)$ at a depth of ~ 700 km. We note the coincidence, if it is that, that this depth is in the middle of the transition zone, and is commonly taken as the proposed chemically induced barrier separating lower and upper mantle convection (Jeanloz and Richter, 1979).

A Non-Adiabatic Temperature in the Lower Mantle

Let us now examine the depth dependence of the temperature in the mantle in some detail. The discussion essentially centres on sub-oceanic mantle, so that the lithosphere participates actively. Consequently, there is a boundary layer at the surface of dimensionless thickness $O(\delta)$, over which the temperature jumps by $O(1)$. Hence

$$|\partial\theta/\partial n|_{p=0}| \sim O\left(\frac{1}{\delta}\right), \tag{3.1}$$

i.e. the Nusselt number $Nu \sim 1/\delta$. The viscosity decreases by $\exp[O(1/\varepsilon)]$ through the lithosphere, attaining a minimum just outside the lithosphere in the asthenosphere (it attains a minimum since by assumption $d\theta_{ad}/dp < d\theta_{iso}/dp$, at least near $p=0$). For the sake of argument, we suppose this minimum is $\sim 10^{20}$ P (Cathles, 1975): the precise figure is *irrelevant*.

We now consider isoviscous profiles corresponding to this minimum viscosity, and two more, bigger by $O(1/\delta^2)$ and $O(1/\delta^4)$. Specifically, these are for viscos-

* In this Turcotte-Oxburgh isoviscous case

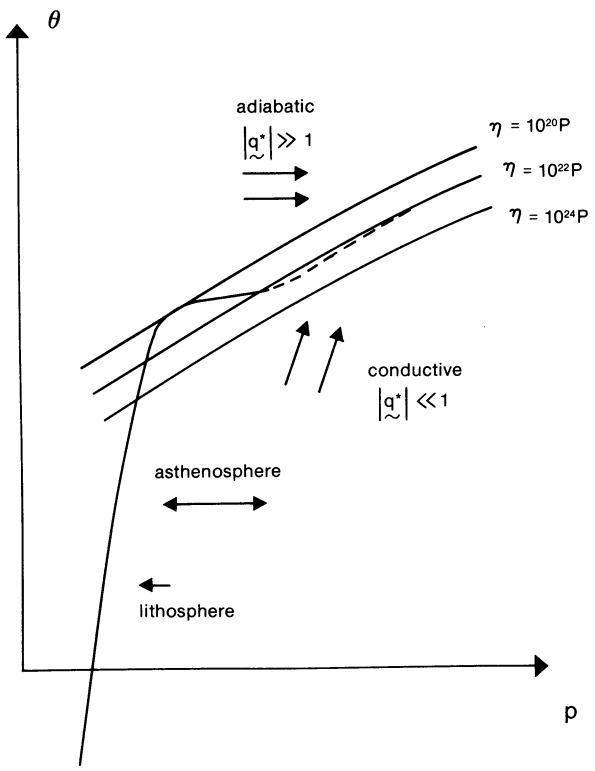

Fig. 1. Control of the temperature by the viscosity. Below the 'asthenosphere' the temperature becomes non-adiabatic and follows approximately the dotted (isoviscous) profile, thereby implying an approximately constant viscosity *and* a more reasonable geotherm in conformation with constraints at the core-mantle boundary

ities $\sim 10^{22}$ P and $\sim 10^{24}$ P, if $\delta \sim 10^{-1}$. Again, these are for illustrative purposes only (see Fig. 1). Choose $\eta_a = 10^{20}$ P, so the three profiles correspond to $\eta^* \sim 1$, $\eta^* \sim 1/\delta^2$, $\eta^* \sim 1/\delta^4$. Then in the asthenosphere, $\eta^* \sim 1$, so $|\mathbf{q}| \sim 1$ and $\theta \approx \theta_{ad}$. We make the (constitutive) assumption that (for small p, at least) $d\theta_{ad}/dp < d\theta_{iso}/dp$. Then as p increases, η^* increases till θ intersects θ_{iso} for $\eta^* \sim 1/\delta^2$. At this point $|\mathbf{q}| \sim \delta^2$, and putting $\mathbf{q} = \delta^2 \mathbf{q}^*$, we have

$$\mathbf{q}^* \cdot \nabla\theta - D\theta \mathbf{q}^* \cdot \nabla p = \nabla^2 \theta, \tag{3.2}$$

$|\mathbf{q}^*| \sim 1$ (if $\tau \sim 1$) and the temperature is not necessarily adiabatic: the question is, what is it? To answer this, we need to solve (3.2), together with the other equations: this would not be easy. However, we can very easily say what the solution is not. Essentially $\eta \sim 10^{20}$ P represents a barrier above which $|\mathbf{q}^*| \gg 1$ ($\gtrsim O(1/\delta^2)$), and hence the temperature there would be adiabatic. Equivalently $\eta \sim 10^{24}$ P represents a barrier below which $|\mathbf{q}^*| \ll 1$ ($\lesssim O(\delta^2)$), and hence in that case, one could ignore the *left* hand side of (3.2) and have a purely conductive profile. Since the heat flux through stagnant zones must equal the heat flux through the surface, one would have the result

$$\frac{\partial\theta}{\partial p} \approx \frac{\partial\theta_{cond}}{\partial p} \sim O\left(\frac{1}{\delta}\right) \tag{3.3}$$

from (3.1). If we make the constitutive assumption that

$$\frac{\partial\theta_{ad}}{\partial p} < \frac{\partial\theta_{iso}}{\partial p} < \frac{\partial\theta_{cond}}{\partial p}, \tag{3.4}$$

then thermal profiles above the $\eta \sim 10^{20}$ P barrier tend to pass below it, while those below the $\eta \sim 10^{24}$ P barrier tend to pass above it, as shown in Fig. 1. Since (3.4) is realistic for the mantle (e.g. $\partial\theta_{ad}/\partial p \sim 0.5$ K km^{-1}, $\partial\theta_{iso}/\partial p \sim 0.7$ K km^{-1}, $\partial\theta_{cond}/\partial p \sim 1.2$ K km^{-1}), assumption of (3.4) leads to the conclusion that the temperature will *self-regulate* itself so that the viscosity lies in a narrow band centred on (in our case) 10^{22} P. We could in fact reasonably restrict this band to be 10^{21} P $< \eta < 10^{23}$ P *below* the asthenosphere. The low viscosity zone $\eta \sim 10^{20}$ P is essential so that there is a viscosity contrast of $O(1/\delta^2)$ across it. The importance of the smallness of ε now becomes manifest. If $\varepsilon \ll 1$, then the width of the θ-band is $O(\varepsilon \ln(1/\delta))$, and θ is therefore quite well-constrained by this restriction.

Since $\theta \approx \theta_{iso}$ below the asthenosphere, we are quite well able to satisfy basal temperature constraints for reasonable V^*, E^*. In fact, using η determined by (1.1) with the same values as Table 1 for A, τ and E^*, we find that (with $\eta = 10^{22}$ P) for $V^* = 4.5$ cm^3 mole^{-1}, $T_b = 2{,}900$ K, for $V^* = 5.4$ cm^3 mole^{-1}, $T_b = 3{,}200$ K, fairly reasonable given uncertainties in E^*, V^* at these depths, as well as ignoring increases due to phase changes and a *small* (in temperature jump) basal thermal boundary layer.

The above idea, that the rheology controls the temperature, is not new, as Tozer (1967, 1972, 1977) has proposed a similar idea; however, apparently (Tozer, 1967) the idea in that form assumed that the interior viscosity was constant (in space), and then stated that this assumed constant viscosity controlled the basal temperature. This essentially deals with the case of an isothermal interior (no adiabatic heating, $D = 0$) and a temperature dependent viscosity (no activation volume, $\mu = 0$). Here we deal with the control of temperature *within the convecting cell* by a non-adiabatic temperature, altogether a different notion: the present discussion would also, for example, be applicable to the case $D = 0$, $\mu \neq 0$.

Although the reasoning leading to Fig. 1 seems elementary and logical, there is one disquieting feature: if the temperature is closely constrained by the rheology, what does the temperature equation solve for? To examine this question we need a simple *model equation* which exhibits the same essential physical process which is of concern. To this end, consider the second order ordinary differential equation

$$V[\theta_z - D\theta] = \theta_{zz}, \tag{3.5}$$

where

$$V = f\left[\frac{\theta - \bar{\theta}(z)}{\varepsilon}\right], \quad \varepsilon \ll 1; \tag{3.6}$$

here z is depth, and we choose boundary conditions such as

$$\theta(0) = \theta_0 \in (0, 1), \quad \theta(1) = 1. \tag{3.7}$$

The velocity V is chosen as in (3.6) for the reason that when $\theta < \bar{\theta}(z)$ (the isoviscous profile of relevance) then

we expect V to decrease (η^* increases) and if $\theta > \bar{\theta}$, V increases; we can think of f as $= 1/\eta^*$, and a measure of fluidity. For example, we might choose $f(\phi) \propto \exp[\phi]$.

Previous discussion in this section suggests the following solution for θ; firstly $\theta \approx \bar{\theta}(z)$ (for large enough z); assuming the adiabat is more slowly increasing than the isoviscous profile $\bar{\theta}$ (as we suppose), then (3.5) implies

$$V = \frac{\bar{\theta}_{zz}}{\bar{\theta}_z - D\bar{\theta}} = \bar{V}(z), \tag{3.8}$$

a given function. Consider first $\bar{V} \neq 0$, i.e. $\bar{\theta}$ is *not* linear in z; then $\bar{V} \sim O(1)$ (generically), and (3.6) gives the first correction to θ as

$$\theta = \bar{\theta}(z) + \varepsilon f^{-1}[\bar{V}(z)]; \tag{3.9}$$

further terms may be found similarly. Secondly, suppose $\bar{V} = 0$; this corresponds to $\bar{\theta} = 1 + \mu z$, μ constant (i.e. V^* constant), and is at first sight puzzling, since by assumption a conductive profile is steeper than an isoviscous one. The resolution, of course, is that $\theta - \bar{\theta}$ is not zero precisely: in fact, choosing

$$f(0) = \varepsilon, \tag{3.10}$$

(as can always be done by shifting $\bar{\theta}$ up or down slightly, e.g. by $\varepsilon \ln(1/\varepsilon)$ if $f(\phi) \propto \exp(\phi)$), putting

$$f(\phi) = \varepsilon g(\phi), \quad g \sim O(1), \tag{3.11}$$

and writing

$$\theta = \bar{\theta}(z) + \varepsilon\phi, \tag{3.12}$$

we find that (3.6), (3.5) and 3.11) give

$$g(\phi)[h(z) + O(\varepsilon)] = \phi_{zz}, \tag{3.13}$$

where

$$h(z) = \bar{\theta}_z - D\bar{\theta} > 0 \quad \text{by assumption,}$$
$$g > 0 \quad \text{is monotonically increasing (e.g. } g = e^{\phi}\text{).} \tag{3.14}$$

We thus solve

$$\phi_{zz} = g(\phi)\, h(z), \tag{3.15}$$

together with boundary conditions at $z = 1$ and $z = c$ on ϕ, where $z = c$ is where the adiabatic asthenospheric solution first intersects the isoviscous profile $\bar{\theta}$. It is easy to prove (almost by inspection) that (3.15) is a well-posed two-point boundary value problem, so that again (3.12) provides the correction to $\bar{\theta}$. Thus in either case, the net effect of the energy equation is to calculate at leading order the $O(\varepsilon)$ correction to the isoviscous temperature profile. If we (as seems reasonable) transmit this back to the real problem, we should infer that $\theta - \theta_{iso} = O(\varepsilon)$ below the asthenosphere, and thus that viscosity variations in the lower mantle truly are no more than $O(1)$, as observed.

Discussion

In this paper we suggest that the temperature profile in the mantle regulates itself in such a way as to produce a relatively constant lower mantle viscosity, and that this temperature is essentially isoviscous, i.e. non-adiabatic, in the lower mantle. A typical geotherm of this type is shown in Fig. 2. Such a geotherm is computed on the basis of fairly elementary reasoning, nevertheless we emphasise that the temperature in the lower mantle may be non-adiabatic, since we propose that the convective velocity there is small ($\lesssim O$(mm/yr)) due to the strong temperature (and pressure) dependence of viscosity. This geotherm seems to fit geophysical constraints better than other (adiabatic) models (e.g. O'Connell and Hager, 1980), and additionally *predicts* a mantle viscosity which is relatively constant *below* the asthenosphere, and a low viscosity zone (asthenosphere) between the lithosphere and lower mantle, in which the viscosity decreases by (say) a factor of 50. Our reasoning is based on a simple scaling analysis of the energy equation, coupled with consideration of a realistic viscosity law.

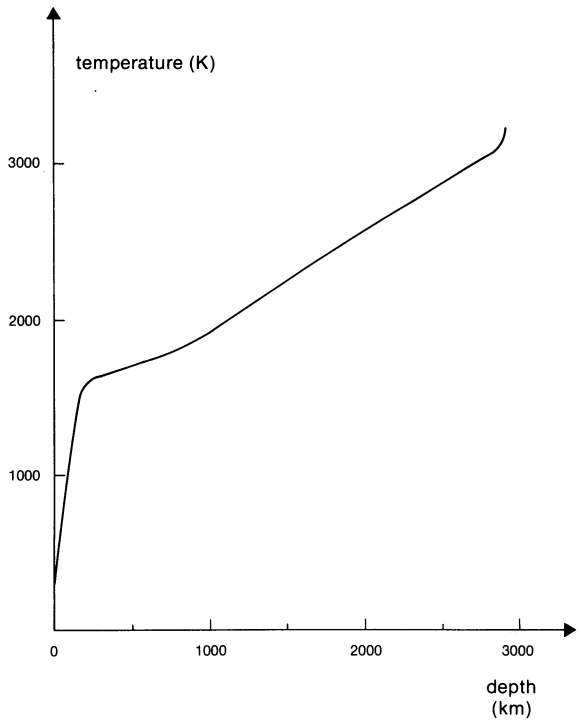

Fig. 2. One possible geotherm for the mantle. This is intended to be schematic, since (for example) it would depend numerically on a full solution of the governing equations, but more importantly on the precise form of V^* and E^* as functions of p and T. We have illustrated a lithospheric thermal boundary layer, a vigorous low viscosity asthenosphere/upper mantle, a less vigorous isoviscous lower mantle, and a small basal thermal boundary layer, in which θ jumps by (probably) $O(\varepsilon)$ in a small region. This basal layer 'gets the heat out of the core'

In the course of our analysis, we are led to reconsider the rôle played by boundary layers and adiabats in vigorous, thermoviscous convection. In supposing that a combination of such thermal profiles can provide a complete understanding of the geotherm is, we suggest, misleading, and in fact, ignoring the effect of a strongly temperature and pressure dependent rheology may lead to gross misconceptions of the nature of mantle convection. We cannot emphasise this too

strongly, since, apart from suggestions of Tozer (1972; 1977), and a variety of numerical computations (Kopitzke, 1979; Schmeling and Jacoby, 1981), much weight has been placed on conclusions of constant viscosity calculations, with only minimal considerations being given to the real rheology (Peltier, 1980).

Part of the concept of this paper has been that Jeanloz and Richter's (1979) argument concerning basal or internal boundary layers is unrealistic since temperature jumps much greater than, say, 200 K across such layers are not feasible, as such jumps entail a viscosity decrease of at least an order of magnitude, which would be expected to be highly unstable. If this is correct, then an explanation of the seismic D'' layer at the base of the mantle in terms of such a comparatively small temperature jump is necessary. Decisive estimates of this jump do not seem available: O'Connell and Hager (1980) quote 300 K, which would be at the upper end of our allowable range.

We have not discussed either phase changes or chemical discontinuities in the mantle. This omission is partly intentional, since the aim is to lay extremely heavy emphasis on the dynamical effect of a varying rheology on the convective style of the mantle, and we actually do not imagine that phase changes, at least, will have a major influence on this. Chemical discontinuities have been invoked (De Paolo, 1981; Anderson, 1982a, b) to explain heterogeneous geochemistry in varying kinds of surface rocks, the idea being that a layered upper and lower mantle would convect separately, consistently with this viewpoint. We do not wish to enter the layering argument here, beyond pointing out firstly, that Peltier (1980) has already observed that increasing the dissipation number D in a constant viscosity fluid can lead to layered convection (he omitted to extend his observation to the mantle), and secondly, the style of convection implied by our discussion already has a 'layering' implicit in it. We have a 'rigid' lithosphere, a 'fluid' asthenosphere (e.g. $\eta \sim 10^{20}$ P, $|\mathbf{u}| \sim 10$ cm yr^{-1}) and a 'sludgy' lower mantle (e.g. $\eta \sim 10^{22}$ P, $|\mathbf{u}| \sim 0.1$ cm yr^{-1}). Whether the circulatory pattern is actually segregated is unclear, but certainly, a direct implication would be that the sampling of lower mantle material at the surface will be comparatively rare. Of course, this is an approximate discussion, and an examination of the origin of thermal plumes/upwellings is required before any specific opinion is stated. We simply wish to point out that variable-viscosity dynamics appears to carry with it a self-imposed style of 'layering' so that arguments about vigorous whole mantle convection (Davies, 1977; O'Connell, 1977) need to be critically re-examined.

In conclusion, some currently held 'truths' concerning mantle convection should be re-evaluated in the light of the implications of a strongly temperature and pressure dependent rheology.

Acknowledgements. This work was started while I was a visitor at Florida State University. I would like to thank Lou Howard and the Geophysical Fluid Dynamics Institute for making my stay there possible, and for providing such a congenial working environment. Particularly I appreciate stimulating discussion on this and other topics with Dave Loper. The paper was actually written while visiting Dave Yuen at Arizona State University, and I would like to thank him for hospitality and support during my stay, and for discussion and encouragement in this and other matters. While there, Francesca Quareni kindly integrated the model equations (3.5)-(3.7) numerically, using $f(\phi) = \exp(\phi)$. With a lowest $\varepsilon = 0.023$, $\theta_0 = 0.2$, she found results consistent with the discussion in the text.

Partial support of the research reported here was supplied by an Exxon Research Fellowship at MIT, and I am grateful to Professor Harvey Greenspan for this award.

References

Anderson, D.L.: Isotopic evolution of the mantle: the rôle of magma mixing. Earth Planet. Sci. Lett. **57**, 1-12, 1982a

Anderson, D.L.: Isotopic evolution of the mantle: a model. Earth Planet. Sci. Lett. **57**, 13-24, 1982b

Anderson, O.L., Sumino, Y.: The thermodynamic properties of the Earth's lower mantle. Phys. Earth. Planet. Int. **23**, 314-331, 1980

Bullen, K.E.: The earth's density. New York: Wiley 1975

Cathles, L.M.: The viscosity of the Earth's mantle. Princeton, N.J.: Princeton University Press 1975

Christensen, U.: Phase boundaries in finite-amplitude convection. Geophys. J. R. Astron. Soc. **68**, 487-497, 1982

Daly, S.F.: The vagaries of variable-viscosity convection. Geophys. Res. Lett. **7**, 841-844, 1980

Davies, G.F.: Whole mantle convection and plate tectonics. Geophys. J. R. Astron. Soc. **49**, 459-486, 1977

De Paolo, D.J.: Nd isotopic studies: some new perspectives on earth structure and evolution. EOS, Trans. Am. Geophys. Union **62**, 137-140, 1981

Dziewonski, A.M., Anderson, D.L.: Preliminary reference Earth model. Phys. Earth Planet. Int. **25**, 297-356, 1981

Elsasser, W.H., Olson, P., Marsh, B.D.: The depth of mantle convection. J. Geophys. Res. **84**, 147-155, 1979

Fowler, A.C.: The depth of convection in a fluid with strongly temperature and pressure dependent viscosity. Geophys. Res. Lett. **9**, 816-819, 1982a

Fowler, A.C.: Implications of scaling and nondimensionalisation for the convection of the Earth's mantle. Preprint, 1982b

Goetze, C.: The mechanisms of creep in olivine. Phil. Trans. R. Soc. Lond. **A 288**, 99-119, 1978

Goetze, C., Brace, W.F.: Laboratory observations of high-temperature rheology of rocks. Tectonophys. **13**, 583-600, 1972

Hewitt, J.M., McKenzie, D.P., Weiss, N.O.: Large aspect ratio cells in two-dimensional thermal convection. Earth Planet. Sci. Lett. **51**, 370-380, 1981

Howard, L.N.: Convection at high Rayleigh number. In: Proc. 11th Int. Cong. Appl. Mech., Munich 1964, H. Görtler, ed.: pp. 1109-1115, Berlin: Springer 1966

Ivins, E.R., Unti, T.W.J., Phillips, R.J.: Large Prandtl number finite-amplitude thermal convection with Maxwell viscoelasticity. Geophys. Astrophys. Fluid Dynamics **22**, 103-132, 1982

Jaoul, O., Poumellec, M., Froidevaux, C., Havette, A.: Silicon diffusion in forsterite: a new constraint for understanding mantle deformation. In: Anelasticity in the Earth, F.D. Stacey, M.S. Paterson, A. Nicholas, eds.: pp. 95-100, Geodynamics Series No. 4. Washington, D.C.: A.G.U. 1981

Jarvis, G.T., Peltier, W.R.: Mantle convection as a boundary layer phenomenon. Geophys. J. R. Astron. Soc. **68**, 389-427, 1982

Jeanloz, R., Richter, F.M.: Convection, composition, and the thermal state of the lower mantle. J. Geophys. Res. **84**, 5497-5504, 1979

Karato, S.: Rheology of the lower mantle. Phys. Earth Planet. Int. **24**, 1-14, 1981

Kevorkian, J., Cole, J.D.: Perturbation methods in applied mathematics. New York: Springer 1981

Kopitzke, U.: Finite-element convection models: comparison of shallow and deep mantle convection, and temperatures in the mantle. J. Geophys. **46**, 97–121, 1979

McKenzie, D.P., Roberts, J.M., Weiss, N.O.: Convection in the Earth's mantle: towards a numerical simulation. J. Fluid. Mech. **62**, 465–538, 1974

Morris, S.: An asymptotic method for determining the transport of heat and matter by creeping flows with strongly variable viscosity; fluid dynamic problems motivated by island arc volcanism. Ph.D. thesis, Johns Hopkins University, Baltimore, 1980

Nataf, H.C., Richter, F.M.: Convection experiments in fluids with highly temperature-dependent viscosity and the thermal evolution of the planets. Phys. Earth Planet. Int. **29**, 320–329, 1982

O'Connell, R.J.: On the scale of mantle convection. Tectonophys. **38**, 119–136, 1977

O'Connell, R.J., Hager, B.H.: On the thermal state of the earth. In: Physics of the earth's interior, A.M. Dziewonski and E. Boschi, eds. Proc. Int. School of Physics, 'Enrico Fermi', Course LXXVII, 270–317. Amsterdam: North-Holland 1980

Olson, P.M., Corcos, G.M.: A boundary layer model for mantle convection with surface plates. Geophys. J. R. Astron. Soc. **62**, 195–219, 1980

Parmentier, E.M., Turcotte, D.L.: Two-dimensional mantle flow beneath a rigid accreting lithosphere. Phys. Earth Planet. Int. **17**, 281–289, 1978

Peltier, W.R.: Mantle convection and viscosity. In: Physics of the Earth's interior, A.M. Dziewonski and E. Boschi, eds. Proc. Int. School of Physics 'Enrico Fermi', Course LXXVII, 361–431. Amsterdam: North-Holland 1980

Peltier, W.R.: Surface plates and thermal plumes: separate scales of the mantle convective circulation. In: Evolution of the Earth, R.J. O'Connell and W.S. Fyfe, eds.: pp. 229–248. Geodynamics Ser. Vol. **5**; Washington, D.C.: A.G.U. 1981

Peltier, W.R., Yuen, D.A., Wu, P.: Postglacial rebound and transient rheology. Geophys. Res. Lett. **7**, 733–736, 1980

Sammis, C.G., Smith, J.C., Schubert, G., Yuen, D.A.: Viscosity-depth profile of the earth's mantle: effects of polymorphic phase transitrons. J. Geophys. Res. **82**, 3747–3761, 1977

Schmeling, H.: Numerische Konvektionsrechnungen unter Annahme verschiedener Viskositätsverteilungen und Rheologien im Mantel. Berichte des Instituts für Meteorologie und Geophysik der Universität Frankfurt am Main, Feldbergstrasse 47, 1980

Schmeling, H., Jacoby, W.: On modelling the lithosphere in mantle convection with non-linear rheology. J. Geophys. **50**, 89–100, 1981

Schubert, G., Spohn, T.: Two-layer mantle convection and the depletion of radioactive elements in the lower mantle. Geophys. Res. Lett. **8**, 951–954, 1981

Schubert, G., Turcotte, D.L., Oxburgh, E.R.: Stability of planetary interiors. Geophys. J. R. Astron. Soc. **18**, 441–460, 1969

Stacey, F.D.: A thermal model of the earth. Phys. Earth Planet. Int. **15**, 341–348, 1977

Stocker, R.L., Ashby, M.F.: On the rheology of the upper mantle. Rev. Geophys. Space Phys. **11**, 391–426, 1973

Tozer, D.C.: Towards a theory of thermal convection in the mantle. In: The Earth's mantle, Gaskell, T.F. ed.: pp. 325–353. London: Academic Press 1967

Tozer, D.C.: The present thermal state of the terrestrial planets. Phys. Earth Planet. Int. **6**, 182–197, 1972

Tozer, D.C.: The thermal state and evolution of the Earth and terrestrial planets. Sci. Prog. **64**, 1–28, 1977

Turcotte, D.L., Haxby, W.F., Ockendon, J.R.: Lithospheric instabilities. In: Island Arcs, Deep Sea Trenches, and Back-Arc Basins, M. Talwani and W.C. Pitman III, eds.: pp. 63–69. Washington, D.C.: A.G.U. 1977

Turcotte, D.L., Oxburgh, E.R.: Finite amplitude convective cells and continental drift. J. Fluid Mech. **28**, 29–42, 1967

Weertman, J.: Creep laws for the mantle of the Earth. Phil. Trans. R. Soc. A**288**, 9–26, 1978

Yuen, D.A., Sabadini, R., Boschi, E.V.: The viscosity of the lower mantle as inferred from rotational data. J. Geophys. Res., **87**, 10745–10762, 1982

Received May 26, 1982; Revised version October 20, 1982
Accepted December 22, 1982

J Geophys (1983) 53:52–58

Journal of Geophysics

The Estimation and Removal of a Linear Drift from Stacked Data

P.L. McFadden[1] and S.C. Constable
Research School of Earth Sciences, Australian National University P.O. Box 4, Canberra, ACT 2600, Australia

Abstract. In exploration systems with digital data acquisition the process of stacking is frequently performed to reduce the requirement for memory space. If, as is often the case, the observations are corrupted by a drift then this drift is not averaged out by the stacking process. The presence of such a drift will frequently cause serious errors in estimation of the signal. A robust method for least squares linear estimation and removal of the drift is presented together with an analysis of the errors involved. Examples with both synthetic and field data are presented to show the improvement in accuracy of signal recovery achieved by drift removal.

Key words: Electrical sounding - Induced polarisation - Statistics - Data processing

Introduction

In the past few years the availability of microchips and minicomputers has had a significant effect in exploration geophysics. It has now become relatively common for exploration measurements in the field to be computer controlled and for "on-site" data processing to be performed. In particular computer equipment is now being used for induced polarisation (I.P.) studies and DC resistivity soundings. Evidently signal processing cannot be applied to a true DC. However, it is possible to use a sinusoidal current with a frequency low enough that the Earth will respond in an entirely resistive manner and then apply signal processing techniques to the sinusoidal signal. I.P. work entails the use of periodic square wave signals.

Typically an electrical measurement (resistivity or I.P.) would then consist of many voltage measurements per cycle of the input current repeated over several cycles. A large memory (which is usually expensive) would be required to record each of the individual voltage measurements and to avoid this the observations are "stacked" to provide a composite or averaged set of observations over a single cycle. The simplest way to achieve this is to perform the voltage measurements at regular intervals in time and to choose this interval such that a single period of the input current (sinusoid or square wave) is an integral multiple of the measurement interval. If a fast Fourier transform (FFT) or discrete Fourier transform (DFT) is then applied to the stacked observations the signal frequency is precisely equal to the fundamental frequency of the transform and so there is no side-lobe leakage or phase shifting of the fundamental frequency due to the finite record length.

Unfortunately electrical measurements are frequently plagued by potential electrode drift or a drift in telluric potentials. As will be shown, a linear drift is not averaged out by the process of stacking many cycles back to a single cycle of the signal and, from the point of view of an FFT or DFT, the drift appears in the stacked waveform as a sawtooth wave with fundamental frequency equal to the signal frequency. Consequently the presence of drift can lead to grossly inaccurate results and so it is vital to remove the drift from the stacked waveform before performing an FFT.

In the process of stacking information is lost and it becomes very difficult to obtain a reliable estimate of the drift for subsequent removal. A rough estimate can be obtained by taking the difference between the first and last points of the stacked waveform. However, this actually makes use of very little information and so is subject to large amount of random error. If a simple least squares linear regression is performed on the stacked waveform this will lead to an *incorrect* estimate of the drift. This is easily seen from the fact that a least squares linear regression applied to one cycle of the function $(A\cos\theta + B\sin\theta)$ will give an estimated linear drift of $(-6B/\pi)$ per cycle, when in fact none exists.

The purpose of this paper is to suggest a simple modification to the real-time stacking process so that relevant information is not lost, thus allowing optimal estimation and removal of a linear drift. An analysis of the statistical properties of this process is presented so that a better understanding of the results can be achieved. Finally some examples of synthetic and actual field data are presented to show how effective the method is.

Formulation of the Problem

The signal may be considered merely as some periodic function $F(\theta)$ such that

$$F(\theta + 2\pi) = F(\theta) \tag{1}$$

and the measurements of $F(\theta)$ are performed at n equally spaced positions per period for N consecutive per-

1 *Present address:* Scripps Institution of Oceanography UCSD, la Jolla, Ca 92093, USA

iods. The period number will always be indexed as i ($i=1$ to N) and the position in the period as j ($j=1$ to n) so that

$$F_{ji}=F(\theta_j+2\pi(i-1))=F(\theta_j),$$
$$\theta_j=\frac{2\pi j}{n}. \tag{2}$$

Evidently there will always be random noise and so any direct measurement of F_{ji} would give an observation f_{ji},

$$f_{ji}=F_{ji}+\varepsilon, \tag{3}$$

where ε has expectation zero and variance σ_f^2. For the present it is assumed that this variance is constant for all i and j. We now assume that any measurement of F_{ji} is corrupted by a linear drift of D per period and a DC offset C. There will also be random noise in the drift and so any direct measurement (i.e. no signal) of D would give an observation d,

$$d\left(\frac{\theta_j}{2\pi}+i-1\right)=D\left(\frac{\theta_j}{2\pi}+i-1\right)+\delta, \tag{4}$$

where δ has expectation zero and variance σ_d^2. Again we assume for the present that this variance is constant.

With this model a particular observation, y_{ji}, of the voltage will be given by

$$y_{ji}=f_{ji}+d\left(\frac{\theta_j}{2\pi}+i-1\right)+C$$
$$=f_{ji}+d\left(\frac{j}{n}+i-1\right)+C. \tag{5}$$

If these observations are stacked in real time to obtain a composite waveform over a single period the resulting observation is obtained by summing over i from 1 to N as

$$\sum_{i=1}^{N} y_{ji}=\sum_{i=1}^{N} f_{ji}+\frac{Njd}{n}+\tfrac{1}{2}N(N-1)d+NC, \tag{6}$$

giving the average values, $\bar{y}_j$ and $\bar{f}_j$, for each stack as

$$\bar{y}_j=\bar{f}_j+\frac{jd}{n}+\tfrac{1}{2}(N-1)d+C. \tag{7}$$

These n observations $\bar{y}_j$ are then the only observations available, as the individual y_{ji} are lost in the stacking process, and so the signal $F(\theta)$ must be estimated from the n values of $\bar{f}_j$ given by

$$\bar{f}_j=\bar{y}_j-\frac{jd}{n}-\tfrac{1}{2}(N-1)d-C. \tag{8}$$

The term $\frac{1}{2}(N-1)d$ may be considered merely as an additional DC offset but the drift still enters through the term (jd/n). Hence the drift must be estimated and removed.

Estimation and Removal of the Drift

In order to simplify the notation the subscript j will now be dropped from double subscripts so that $y_i \equiv y_{ji}$, $f_i \equiv f_{ji}$ and the summation signs are for i from 1 to N unless otherwise specified. Considering a particular stack j an unbiased estimate for the variance in the f_i is given by s_j^2 where

$$(N-1)s_j^2=\Sigma(f_i-\bar{f})^2 \tag{9}$$

where $\bar{f}\equiv\bar{f}_j$. Any drift unaccounted for will inflate this sum and so the drift D may be estimated as that value of d in Eq. (8) which minimises s_j^2. Substituting from Eqs. (5) and (8) into (9) gives

$$(N-1)s_j^2=\tfrac{1}{12}(N^3-N)d^2+[(N+1)\Sigma y_i-2\Sigma i\, y_i]d$$
$$+\Sigma(y_i-\bar{y})^2 \tag{10}$$

where $\bar{y}\equiv\bar{y}_j$. Differentiation with respect to d then gives

$$(N-1)\frac{\partial s_j^2}{\partial d}=\tfrac{1}{6}(N^3-N)d+(N+1)\Sigma y_i-2\Sigma i\, y_i \tag{11}$$

and so $\hat{d}_j$, the value of d for which the above differential is zero (and therefore the value of d which minimises s_j^2), is given by

$$\hat{d}_j=\frac{2\Sigma i\, y_i-(N+1)\Sigma y_i}{\frac{1}{6}(N^3-N)}. \tag{12}$$

Each of the n stacks will lead to an estimate $\hat{d}_j$ and so an overall estimate, $\bar{d}$, of D will be given by the mean value as

$$\bar{d}=\frac{1}{n}\sum_{j=1}^{n} d_j. \tag{13}$$

In summary, in order to remove a linear drift it is necessary to accumulate for each stack j not only the sums of the measurements, Σy_i, but also the sums of the measurements multiplied by the stack number, $\Sigma i\, y_i$. These are then substituted into (12) to give n independent estimates $\hat{d}_j$ of the drift per cycle, D. The overall estimate, $\bar{d}$, of D is then taken as the average of the n values $\hat{d}_j$ (Eq. 13). This value may then be substituted for d in Eq. (8) to remove the effect of the drift. Further, if it is known that the mean of $F(\theta)$ over a cycle is zero then, without loss of generality, C may be chosen as that value which makes the sum of the n values $\bar{f}_j$ (corrected for drift) equal to zero.

Properties of the Drift Estimator

The estimate $\hat{d}_j$ is a linear combination of the observations y_i and consequently it has several useful properties. Using Eqs. (3) and (4) Eq. (5) may be rewritten as

$$y_i=F_i+\varepsilon+D\left(\frac{j}{n}+i-1\right)+\delta+C$$
$$=(F_i+C)+Y_i \tag{14}$$

where Y_i is merely an observation of the drift corrupted by both the noise (δ) in the drift and the noise (ε) in the signal. Substitution of the y_i values in this form into Eq. (12) gives

$$\hat{d}_j=\frac{2\Sigma i\, Y_i-(N+1)\Sigma Y_i}{\frac{1}{6}(N^3-N)}. \tag{15}$$

If we now let $x_i \equiv i$ and recognise that

$$(N+1)=\frac{2}{N}\Sigma i \equiv \frac{2}{N}\Sigma x_i = 2\bar{x} \tag{16}$$

and

$$\tfrac{1}{6}(N^3-N)=2\Sigma\left(i-\frac{N+1}{2}\right)^2 \equiv 2\Sigma(x_i-\bar{x})^2 \tag{17}$$

then

$$\hat{d}_j=\frac{\Sigma(x_i-\bar{x})\,Y_i}{\Sigma(x_i-\bar{x})^2}=\frac{\Sigma(Y_i-\bar{Y})\,x_i}{\Sigma(x_i-\bar{x})^2}. \tag{18}$$

Hence $\hat{d}_j$ is merely the slope of a least squares linear regression of the drift. Expansion of Eq. (15) with the error terms ε and δ shows that the expectation of $\hat{d}_j$ is D and the variance, σ_D^2, of $\hat{d}_j$ is given by

$$\sigma_D^2=\frac{12}{N^3-N}(\sigma_f^2+\sigma_d^2)$$

$$=\frac{12}{N^3-N}\sigma_t^2 \tag{19}$$

where σ_t^2 is the overall variance of the noise. Each of the $\hat{d}_j$ is an independent estimate of D and so an unbiased estimate for the variance σ_D^2 is given by s_D^2 where

$$s_D^2=\frac{1}{n-1}\sum_{j=1}^{n}(\hat{d}_j-\bar{d})^2. \tag{20}$$

Evidently an unbiased estimate for the variance in $\bar{d}$ is given by (s_D^2/n).

If the errors ε and δ are normally distributed then the $\hat{d}_j$ are normally distributed with mean D and variance σ_D^2. Furthermore the estimate s_D^2 will have a chi-square distribution with $(n-1)$ degrees of freedom as

$$\frac{(n-1)s_D^2}{\sigma_D^2}\sim \chi^2_{(n-1)}. \tag{21}$$

Here the symbol "$\sim$" is to be read as "is distributed as".

Finally, the fact that the $\hat{d}_j$ are least squares linear regressions means the overall estimate $\bar{d}$ is fairly robust to deviations from a truly linear drift.

Applications when $F(\theta)$ is a Single Sinusoid

If $F(\theta)$ is a single frequency sinusoid then

$$F(\theta_j)=A\cos\left(\frac{2\pi j}{n}\right)+B\sin\left(\frac{2\pi j}{n}\right) \tag{22}$$

and A and B are given by

$$A=\frac{2}{n}\sum_{j=1}^{n}F(\theta_j)\cos\left(\frac{2\pi j}{n}\right)$$

$$B=\frac{2}{n}\sum_{j=1}^{n}F(\theta_j)\sin\left(\frac{2\pi j}{n}\right). \tag{23}$$

Having corrected the stacked data for the drift the values $\bar{f}_j$ are estimates of $F(\theta_j)$ and so estimates of A and B may be obtained. In terms of understanding the estimates so obtained it is important to investigate the statistical properties of these estimates.

If we define $\bar{\delta}$

$$\bar{\delta}=D-\bar{d} \tag{24}$$

then $\bar{\delta}$ is the error in estimation of the drift and so after correcting the stacked results for the drift there is still a drift of $\bar{\delta}$ per cycle left. We now consider a particular stack j again. In Eq. (10) the term $\Sigma(y_i-\bar{y})^2$ may be expanded as

$$\Sigma(y_i-\bar{y})^2=\Sigma y_i^2-\frac{1}{N}(\Sigma y_i)^2 \tag{25}$$

and so if the sum of the squares of the observations is also kept the value of $\Sigma(f_i-\bar{f})^2$ for each stack may be determined from Eq. (10) after substituting $\bar{d}$ for d. Using Eq. (10) in this manner it follows that

$$\left\langle\left(\frac{\Sigma(f_i-\bar{f})^2}{N-1}\right)\right\rangle=\langle s_j^2\rangle=\sigma_t^2+\tfrac{1}{12}(N^2+N)\langle\bar{\delta}^2\rangle \tag{26}$$

where the notation $\langle z\rangle$ indicates the expectation of z. In the general sense of repeating the whole experiment many times, $\bar{\delta}$ is a random variable and $\langle\bar{\delta}^2\rangle$ is simply the variance of $\bar{d}$, i.e. (σ_D^2/n). Substituting from Eq. (19) then gives

$$\langle s_j^2\rangle=\left(1+\frac{1}{n(N-1)}\right)\sigma_t^2 \tag{27}$$

and so even for fairly small N and n it may be considered that $\langle s_j^2\rangle=\sigma_t^2$. However, for the case of a single experiment (the usual case), $\bar{\delta}$ is not a random variable but a constant and so $\langle\bar{\delta}^2\rangle=\bar{\delta}^2$. From the argument leading to Eq. (27) it is evident that $\frac{1}{12}(N^2+N)\bar{\delta}^2$ will be small compared to σ_t^2 and so for a single experiment it may also be considered that $\langle s_j^2\rangle=\sigma_t^2$.

Using the $\bar{f}_j$ as estimates of $F(\theta_j)$, estimates a and b for A and B are obtained as

$$a=\frac{2}{n}\sum_{j=1}^{n}\bar{f}_j\cos\left(\frac{2\pi j}{n}\right)$$

$$b=\frac{2}{n}\sum_{j=1}^{n}\bar{f}_j\sin\left(\frac{2\pi j}{n}\right). \tag{28}$$

The estimate, s_a^2, for the variance, σ_a^2, of a is given by

$$s_a^2=\frac{4}{n^2N}\sum_{j=1}^{n}s_j^2\cos^2\left(\frac{2\pi j}{n}\right) \tag{29}$$

since (s_j^2/N) is the estimate of the variance in $\bar{f}_j$. Furthermore

$$\langle s_a^2\rangle=\sigma_a^2=\frac{4}{nN}\langle s_j^2\rangle\frac{1}{n}\sum_{j=1}^{n}\cos^2\left(\frac{2\pi j}{n}\right)$$

$$=\frac{2}{nN}\sigma_t^2. \tag{30}$$

Similarly

$$s_b^2=\frac{4}{n^2N}\sum_{j=1}^{n}s_j^2\sin^2\left(\frac{2\pi j}{n}\right) \tag{31}$$

and

$$\langle s_b^2\rangle=\sigma_b^2=\frac{2}{nN}\sigma_t^2=\sigma_a^2. \tag{32}$$

The residual drift $\bar{\delta}$ per cycle affects the estimates a and b so that

$$\langle a\rangle = A; \quad \langle b\rangle = B - \frac{1}{\pi}\bar{\delta}. \tag{33}$$

Consequently a is an unbiased estimate of A but b is not quite an unbiased estimate of B. However, the bias in b is small enough that in practice it may be ignored.

Invoking the central limit theorem the estimates a and b will be normally distributed independent of the original distributions of the noise. Consequently it is a simple matter to obtain error limits for A and B.

Testing for a Non-linear Drift

If the original noise in the signal and the drift is normally distributed then the estimates s_j^2 will each have chi-square distributions with $(N-1)$ degrees of freedom. The average of the n values of s_j^2 will also have a chi-square distribution but with $n(N-1)$ degrees of freedom. However, it is s_a^2 and s_b^2 which are calculated rather than the average of the s_j^2 values. Consequently it is more useful to determine the distribution of these estimates. Reference is made here to s_a^2 but because of the equivalence of s_a^2 and s_b^2 it is immaterial whether we use s_a^2, s_b^2 or $\frac{1}{2}(s_a^2+s_b^2)$.

In determining s_a^2 the individual values of s_j^2 are multiplied by different factors and so the distribution of s_a^2 cannot be exactly chi-square. However, it will be approximately chi-square distributed and because $n(N-1)$ will represent a large number of degrees of freedom this approximation will be very good. Hence we can choose as the approximating chi-square distribution that which has the same mean and variance as the statistic s_a^2. Thus, as a very good approximation,

$$s_a^2 \sim \frac{3}{n^2}\frac{\sigma_t^2}{N(N-1)} X^2_{\frac{2}{3}n(N-1)}. \tag{34}$$

Combining Eqs. (19) and (21)

$$s_D^2 \sim \frac{12\sigma_t^2}{(n-1)(N^3-N)} X^2_{(n-1)}. \tag{35}$$

It then follows from Eqs. (34) and (35) that

$$\frac{s_a^2}{s_D^2}\frac{6n}{N^2-1} \equiv G \sim F[\frac{2}{3}n(N-1),(n-1)], \tag{36}$$

where $F[m_1,m_2]$ is the F distribution with m_1 and m_2 degrees of freedom. The statistic G of Eq. (36) is merely the ratio of σ_t^2 estimated from the scatter in the f_i values to σ_t^2 estimated from the scatter in the individual drift estimates $\hat{d}_j$. Evidently in practice m_1 must be chosen as the integer nearest $2n(N-1)/3$.

If the drift was in fact non-linear then systematic errors due to misfit of the model will cause an apparent inflation of σ_d^2 and so, from Eq. (19), will cause an apparent inflation of σ_t^2 as estimated from scatter in the individual drift estimates. This apparent inflation will also appear in the s_j^2 through σ_t^2 in Eq. (26). However, the second term of Eq. (26), $(N^2+N)\langle\bar{\delta}^2\rangle/12$, will be replaced by the term $(\Sigma(i-\frac{1}{2}[N+1])^2\delta_i^2)/(N-1)$ where the δ_i represent the systematic errors due to misfit of the model. Consequently the second term of Eq. (26) would no longer be small with respect to the first term but would instead be of the same order. Hence if σ_t^2 is estimated from the scatter in the f_j values then this estimate would be inflated substantially more than the estimate of σ_t^2 determined from scatter in the individual drift estimates. Under these conditions the statistic G of Eq. (36) would not have an F-distribution and we would expect an observed value of the statistic to be substantially greater than unity. Thus if the observed value of G exceeds the critical value of the F-distribution then the hypothesis of a linear drift may be rejected.

It is important to recognise that the statistical ability to reject the hypothesis of a linear drift does not invalidate the procedure suggested here for removal of drift. If the random noise in an experiment is very small then a very small amount of non-linearity in the drift will cause rejection of the linear drift hypothesis. Conversely, if the random noise in an experiment is large then a moderate degree of non-linearity in the drift will not cause rejection of the linear drift hypothesis. Equation (28) for estimating A and B is merely the fundamental frequency term of a DFT applied to the data and, as noted previously, in a stacked waveform a linear drift contributes to the power observed in this fundamental frequency. This is a consequence of the stacking process and holds true for a non-linear drift as well. Estimation and removal of the drift as if it were a linear drift will effectively remove most of the apparent power in the fundamental frequency consequent upon stacking a non-linear drift. However, it should be clear from the preceding argument that the estimate of the variance in the result will be artifically inflated.

Examples of Drift Removal

Synthetic data

In order to show the effectiveness of the drift removal process, synthetic data were generated from

$$y_{ji} = A\cos\theta_j + B\sin\theta_j + C + D\left(\frac{\theta_j}{2\pi}+i-1\right) + Q\left(\frac{\theta_j}{2\pi}+i-1\right)^2 + \text{Gaussian noise (variance } \sigma_t^2). \tag{37}$$

Here Q is a quadratic drift per cycle to simulate a non-linear drift and the other terms are as previously defined.

In the first example $A=0$ and there is only a linear drift, with the drift per cycle being twice the signal amplitude. Figure 1 shows the estimated signal and data both before and after estimation and removal of the linear drift. The details of the parameters are given in Table 1. In the second example there is still only a linear drift (but twice that of the first example) and A is now non-zero. The fits are shown in Fig. 2 and the details are given in Table 2. In both examples it may be seen that the presence of a linear drift affects the estimation of B far more than the estimation of A, as is to be expected from Eq. (33) with $\bar{\delta}$ replaced by D. In neither example can the hypothesis of a linear drift be

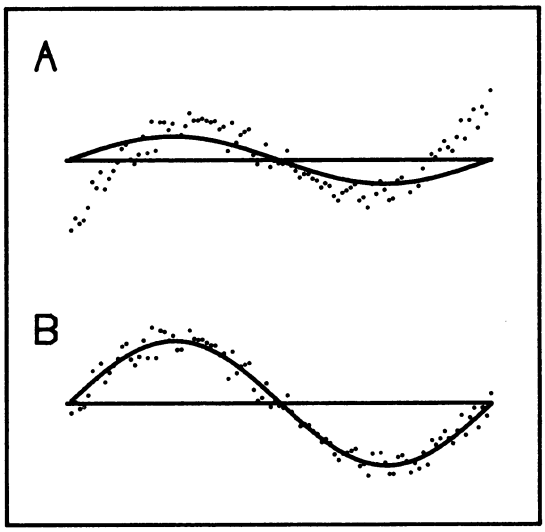

Fig. 1 a and b. Synthetic data with a linear drift. **a** before and **b** after estimation and removal of drift. See Table 1 for details

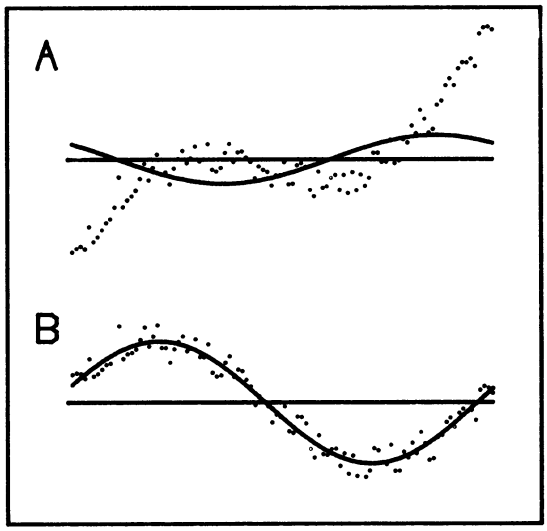

Fig. 2 a and b. Synthetic data with a linear drift. **a** before and **b** after estimation and removal of drift. See Table 2 for details

Table 1. Synthetic data with a linear drift. See also Fig. 1

Actual parameters	Estimated parameters	
	Before drift removal	After drift removal
$A=0.0$	$a=0.0001$ $s_a=0.2720$	$a=-0.020$ $s_a=0.022$
$B=1.0$	$b=0.39$ $s_b=0.27$	$b=1.028$ $s_b=0.022$
$C=2.0$	$c=12.03$	$c=2.03$
$D=2.0$		$\bar{d}=1.998$ $s_D=0.054$
$Q=0.0$		
$\sigma_t=0.5$		$s_1=0.489$ $s_2=0.490$
$n=100$		$G=1.06$
$N=10$		

Notes

1. s_1 is an estimate of σ_t obtained by substituting s_D^2 for σ_D^2 in Eq. (19)
2. $s_2^2=\frac{1}{2}nNs_a^2$ and so s_2 is also an estimate of σ_t (see Eq. 30)
3. Critical value of G at the 95% level of confidence = 1.29

Table 2. Synthetic data with a linear drift. See also Fig. 2

Actual parameters	Estimated parameters	
	Before drift removal	After drift removal
$A=0.25$	$a=0.268$ $s_a=0.543$	$a=0.228$ $s_a=0.023$
$B=1.00$	$b=-0.297$ $s_n=0.544$	$b=0.980$ $s_b=0.023$
$C=1.00$	$c=21.05$	$c=0.973$
$D=4.00$		$\bar{d}=4.012$ $s_D=0.057$
$Q=0.00$		
$\sigma_t=0.50$		$s_1=0.518$ $s_2=0.514$
$n=100$		
$N=10$		$G=0.992$

Notes

1. s_1 and s_2 are as defined in Table 1
2. Critical value of G at the 95% level of confidence = 1.29

rejected (as expected). Both of these examples show that the presence of a linear drift can produce serious errors in signal estimation and that the drift removal process suggested here is very effective in such instances.

In the third example a fairly severe quadratic drift has been used. The fits are shown in Fig. 3 and the details are given in Table 3.

Since a stacked quadratic has even function components the estimation of A is now also affected seriously. As expected, the hypothesis of a linear drift may be rejected and this has some consequences which are of interest.

First of all, the DC component, C, is incorrectly estimated (even after removal of a least squares linear drift), but this is of little importance unless C is itself a desired parameter. Secondly, the noise, s_2, estimated from s_b is much larger than the estimate s_1, from s_D, and both of these are much larger than the actual noise, σ_t. Thus, as expected from the theory, if the hypothesis of a linear drift can be rejected then the calculated errors on the parameter estimates are in fact too large. However, it may be seen from this example that the drift removal process is very robust, the overall amplitude of the signal being estimated to within 2% and the phase to within 0.6° (without any drift removal the amplitude estimate is only 35% of the correct amplitude and the estimated phase would be in error by 39°).

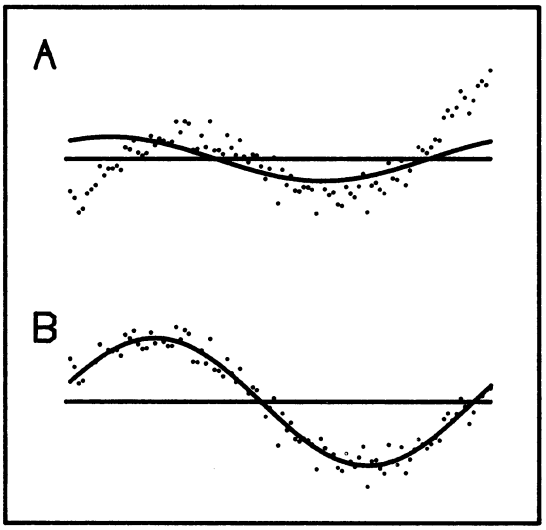

Fig. 3 a and b. Synthetic data with a quadratic drift. **a** before and **b** after linear estimation and removal of drift. See Table 3 for details

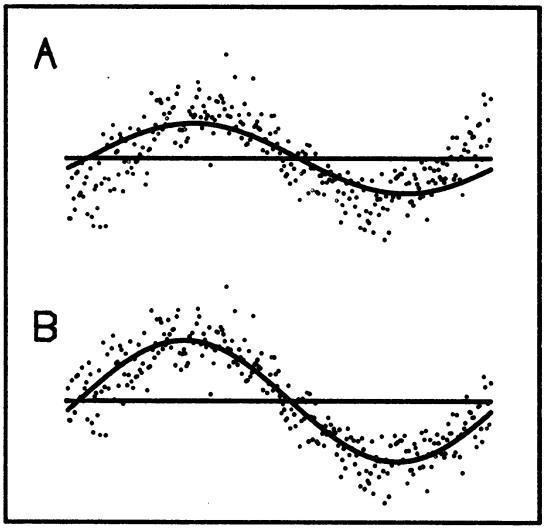

Fig. 4 a and b. Field data. **a** before and **b** after linear estimation and removal of drift. See Table 4 for details

Table 3. Synthetic data with a quadratic drift. See also Fig. 3

Actual parameters	Estimated parameters	
	Before drift removal	After drift removal
$A = 0.25$	$a = 0.290$	$a = 0.265$
	$s_a = 0.351$	$s_a = 0.091$
$B = 1.00$	$b = 0.219$	$b = 1.017$
	$s_b = 0.351$	$s_b = 0.091$
$C = 1.00$	$c = 9.304$	$c = -3.230$
$D = 0.00$		$\bar{d} = 2.504$
		$s_D = 0.159$
$Q = 0.25$		
$\sigma = 0.50$		$s_1 = 1.444$
		$s_2 = 2.035$
$n = 100$		
$N = 10$		$G = 1.979$

Notes

1. s_1 and s_2 are as defined in Table 1
2. Critical value of G at the 95% level of confidence = 1.29
3. If $c' + \bar{d}'i$ is a least squares linear fit to the quadratic drift (before stacking), then $c' = -3.179$ and $\bar{d}' = 2.503$, in excellent agreement with the estimate from the stacked data

Table 4. Field data. See also Fig. 4

Before drift removal	After drift removal
$a = -0.316$ mV	$a = -0.324$ mV
$s_a = 0.438$ mV	$s_a = 76.3$ μV
$b = 1.01$ mV	$b = 1.79$ mV
$s_b = 0.336$ mV	$s_b = 80.6$ μV
$c = -0.930$ V	$c = -0.968$ V
	$\bar{d} = 2.48$ mV
	$s_D = 77.2$ μV
	$s_1 = 3.66$ mV
	$s_2 = 5.41$ mV
	$G = 2.18$

Notes

1. s_1 and s_2 are as defined in Table 1
2. Critical value of G at the 95% level of confidence = 1.16
3. $n = 300$ and $N = 30$

Field Data

It is to be expected that in the real world a truly linear drift would be a rare phenomenon. However, as has already been shown, the drift removal process is robust to non-linearities and therefore provides a very useful tool in the analysis of real data.

Figures 4 and 5 show two examples of field data obtained using a computer controlled electrical sounding system. The details are given in Tables 4 and 5. The input signal is a very low frequency, in-phase sinusoidal current. The recovered voltage signal is very noisy, phase shifted and corrupted by a large drift. In both cases the hypothesis of a linear drift may be rejected but the great improvement in signal recovery after drift removal is immediately apparent.

The final example of real data is quite interesting, the fits being shown in Fig. 6 and the details given in Table 6. Here the noise is very small, a drift is readily apparent and there is a distinct "kink" in the data. Because the noise is small this "kink" appears as a strong non-linearity in the drift and the hypothesis of a linear drift is rejected (very strongly so in this case). Again, the improvement in signal recovery after drift removal is apparent.

Conclusions

A method for removal of a linear drift from stacked data has been presented. In addition it has been shown that the method is robust to non-linearities (because it is a least squares fit) and thus is a useful tool in the analysis of real data.

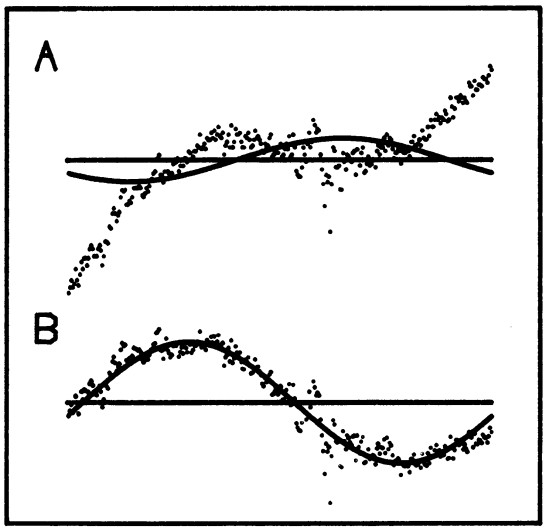

Fig. 5a and b. Field data. **a** before and **b** after linear estimation and removal of drift. See Table 5 for details

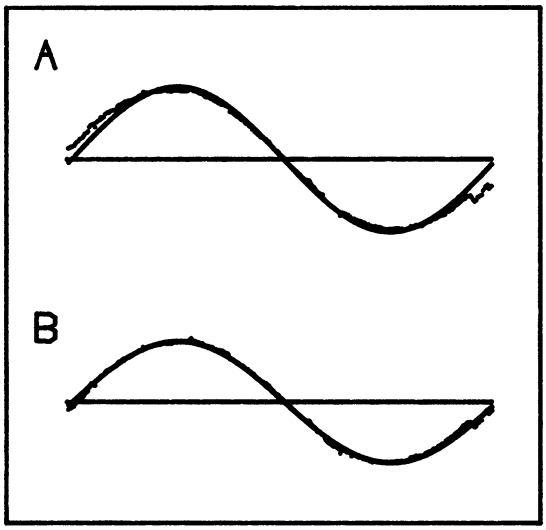

Fig. 6a and b. Field data. **a** before and **b** after linear estimation and removal of drift. See Table 6 for details

Table 5. Field data. See also Fig. 5

Before drift removal	After drift removal
$a = -0.429$ mV	$a = -0.456$ mV
$s_a = 0.688$ mV	$s_a = 6.22$ μV
$b = -0.575$ mV	$b = 1.96$ mV
$s_a = 0.628$ mV	$s_b = 63.0$ μV
$c = -2.07$ V	$c = -2.11$ V
	$\bar{d} = 7.96$ mV
	$s_D = 0.205$ mV
	$s_1 = 1.86$ mV
	$s_2 = 2.44$ mV
	$G = 1.72$

Notes

1. s_1 and s_1 are as defined in Table 1
2. Critical value of G at the 95% level of confidence = 1.17
3. $n = 300$ and $N = 10$

Table 6. Field data. See also Fig. 6

Before drift removal	After drift removal
$a = -0.549$ mV	$a = -0.535$ mV
$s_a = 0.636$ mV	$s_a = 56.6$ μV
$b = 8.02$ mV	$b = 6.71$ mV
$s_b = 0.327$ mV	$s_b = 55.6$ μV
$c = -0.306$ V	$c = -0.285$ V
	$\bar{d} = -4.12$ mV
	$s_D = 74.0$ μV
	$s_1 = 0.672$ mV
	$s_2 = 2.15$ mV
	$G = 10.3$

Notes

1. s_1 and s_2 are as defined in Table 1
2. Critical value of G at the 95% level of confidence = 1.17
3. $n = 300$ and $N = 10$

The process of stacking reduces the required memory space by keeping only the sums of the observations at each stack point rather than retaining all of the individual observations. In order to estimate and then remove a drift the sums of (observations multiplied by cycle number) must also be kept at each stack point. The drift may then be estimated using Eqs. (12) and (13) and then removed by using Eq. (8). Although this doubles the memory required for the same number of stack points the improvement in accuracy of signal recovery fully justifies the process.

In order to perform a statistical analysis of the signal estimation the sums of the squares of the observations at each stack point must also be retained. Again this increases the memory required for a given number of stacks and in many applications it may be felt that this increase in memory requirement is not justified.

Naturally it is possible to obtain a least squares quadratic fit, from stacked data. However, this would require that the sums of (observations multiplied by the square of the cycle number) also be kept for each stack point. Since the simpler process suggested here is robust to non-linearities the increased requirement in memory size is probably not justified.

Finally, it is important to note that the statistical analysis presented here estimates only the precision of a particular measurement. Repeated measurements may show that larger errors are indicated due to a non Gaussian and/or a non stationary noise process. Above all, it must be realised that "geological noise" (the consequence of real geology being more complicated than models used to describe it) cannot be estimated by the processes described here.

Received July 6, 1982; Revised Version January 18, 1983
Accepted January 19, 1983

J Geophys (1983) 53:59–67

Journal of Geophysics

A Study of the Mechanism of Whistler-Triggered VLF Emissions

Toshio Yoshida[1], Jinsuke Ohtsu, and Masashi Hayakawa
Research Institute of Atmospherics, Nagoya University, Toyokawa, Aichi, 442, Japan

Abstract. The conditions for triggering VLF emission by a natural whistler are studied, in terms of the length of interaction between whistler and electron determined by the unperturbed phase variation resulting from the spatial inhomogeneity and wave frequency variation. The computations are performed for a realistic magnetospheric model at $L=4.0$. It is found that we expect the highest probability of VLF emission triggering at an initial frequency slightly above 3 kHz in the whistler spectrum, at a geomagnetic latitude $\sim -15°$ on the upstream side of the electron for the following reasons. (1) The interaction time has a sharp maximum ($\gtrsim 50$ ms) at ~ 3.25 kHz, (2) the interaction time at 3 kHz is very large compared with the phase bunching time for reasonable wave amplitudes over a wide range of resonant electron pitch angles ($\alpha_{eq}=5°$–$60°$), and (3) resonance electron energy at 3 kHz (~ 10–20 keV for $\alpha_{eq}=5°$–$55°$) is less than that at 1,2 and 4 kHz and there is, therefore, a greater flux of electrons available for wave amplification. For the initial frequency $\gtrsim 3$ kHz the variation of the Doppler-shifted wave frequency seen by the electron matches very well with the variation of the resonant electron's gyrofrequency in the inhomogeneous medium, giving rise to the longest interaction time. Our method of analysis would be applicable to the triggering of VLF emissions by other variable frequency waves, in which the ratio of the interaction time to the phase bunching time would be an essential quantity in the wave triggering.

Key words: Whistler-triggered VLF emissions — Whistlers — VLF emissions — Whistler-electron cyclotron interaction — Magnetosphere — Phase bunching

Introduction

Discrete VLF emissions are thought to be generated *around the equator* by cyclotron resonance between whistler mode waves and energetic electrons (Helliwell, 1967; Rycroft, 1972; Gendrin, 1975). Evidence for their equatorial generation includes the observations of banded chorus of Burtis and Helliwell (1969, 1976), who have found that the frequency of chorus is associated with the equatorial gyro-frequency. As further evidence, Maeda (1976) has shown that the missing frequency of two-banded chorus is equal to one half of the equatorial gyro-frequency. In parallel with the studies of naturally generated waves the Siple active experiments using the injected waves with constant frequency (Helliwell, 1977) have yielded a wealth of interesting results on nonlinear whistler instability around the equator, which would also be of great use when interpreting natural discrete emissions.

However, wave-particle interactions in the *off-equatorial* plane have not been thoroughly investigated. Helliwell (1970) has considered a case of linearly changing frequency and has shown simply that the resonance point is situated on the upstream side of the electron when the frequency decreases. A wave with this linearly changing frequency has been added as a triggering signal in the Siple experiment (Miller, 1979), but there has been, as yet, no detailed study on the region and mechanism of wave-particle interactions based on the ramp signal transmissions. Recently Brinca (1981) has proposed a method of enhancing the whistler instability by the use of waves whose frequency is suitably varied so as to compensate the plasma inhomogeneity. In the off-equatorial region the plasma inhomogeneity is greatly enhanced compared with that at the equator so that the region is of great importance in studying the essential points lying in the general wave-particle interactions. Needless to say, the off-equatorial region can be attacked only by the use of variable frequency waves.

In this paper we adopt natural whistlers originating from lightning as a variable frequency wave and elucidate the possible conditions of triggering new emissions by natural whistlers in order to study the mechanism of whistler-triggered emissions. The L value we are concerned with is assumed to be 4.0 where we expect the most frequent occurrence of whistler-triggered emissions (Carpenter, 1968). We study the wave-particle interaction by using the variations of unperturbed phase angle determined by both the spatial inhomogeneity of the medium and wave frequency variation, enabling us to define the "interaction time", with a special reference to its comparison with the bunching time. Then, in order to examine the importance of the ratio of the interaction to bunching time in whistler-triggered

1 *Present address:* Nippon Electric Co. Ltd., Microwave Communications Systems Division, Yokohama, 226, Japan

Offprint requests to: M. Hayakawa

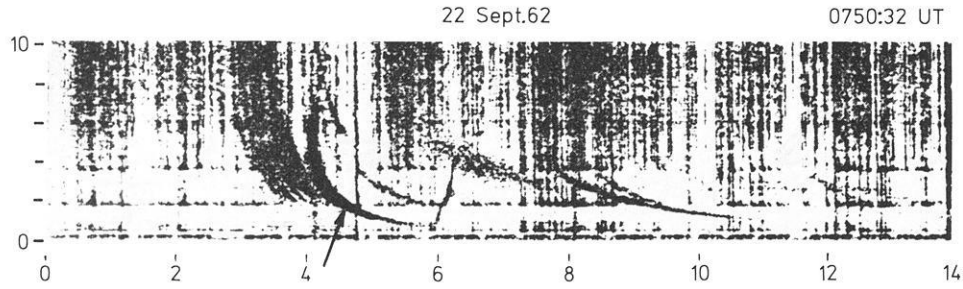

Fig. 1. An example of whistler-triggered emissions (After Helliwell, 1965). The emission shown by an arrow is the one for which the plasma parameters are very similar to those treated in the present paper

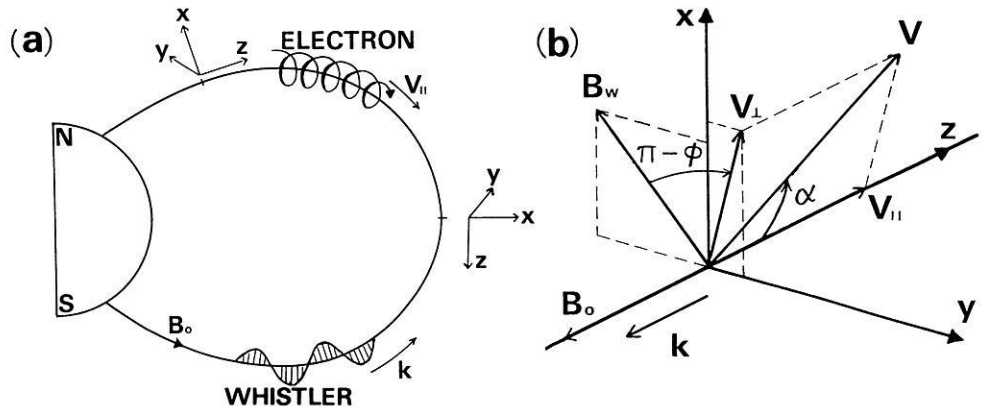

Fig. 2. a Model of interaction between a whistler and an electron. **b** The phase angle ϕ between the electron's perpendicular velocity ($v_\perp$) and the opposite direction of wave magnetic field ($-B_w$). α is the electron's pitch angle

emissions, we calculate the trajectories of electrons in phase space in the presence of a whistler wave with its amplitude being varied over a wide range.

Unperturbed Phase Angle and Bunching Time

Figure 1 shows an example of whistler-triggered hook emission at $L\sim4.0$ (after Helliwell, 1965). The generation of triggered emissions can be roughly divided into two steps. The first step is that the wave amplitude grows usually at the frequency of the triggering or stimulating signal; we expect phase bunching of resonant electrons by the triggering wave. The second step is that emissions are triggered above the frequency of the triggering wave, and we have drastically varying frequency changes. The present paper is concerned only with the first step for the variable frequency wave.

Figure 2a shows the model in which a constant amplitude whistler wave propagating along the magnetic field interacts with a counter-streaming electron on the same field line. The equations of motion of an electron (charge, -e and mass m) travelling in the inhomogeneous medium, in the presence of a whistler wave are given by (Dysthe, 1971; Inan et al., 1978; Matsumoto, 1979),

$$\dot{V}_\parallel = \Omega_w V_\perp \sin\phi - \frac{V_\perp^2}{2B_0}\frac{\partial B_0}{\partial z}, \tag{1a}$$

$$\dot{V}_\perp = -\Omega_w\left(V_\parallel + \frac{\omega}{k}\right)\sin\phi + \frac{V_\perp V_\parallel}{2B_0}\frac{\partial B_0}{\partial z}, \tag{1b}$$

$$\dot{\phi} = (\Omega_H - \omega - kV_\parallel) - \Omega_w\left(V_\parallel + \frac{\omega}{k}\right)\frac{\cos\phi}{V_\perp} \tag{1c}$$

where $\omega(=2\pi f)$=angular wave frequency, k=wave number, B_w=wave amplitude, $\Omega_w = eB_w/m$, $\Omega_H(=2\pi f_H) = eB_0/m$, $v_\parallel$ and $v_\perp$=the electron's parallel and perpendicular velocities, and the phase angle ϕ is defined as an angle between $v_\perp$ and $-B_w$, as shown in Fig. 2b. Equation (1c) implies that as each electron moves through the wave train, ϕ changes because of (1) wave induced longitudinal drift and (2) spatial inhomogeneity of the medium and wave frequency variation. For the conditions we usually meet (not too large wave amplitude and not too small pitch angle; $B_w \lesssim 30\,\mathrm{m}\gamma$ and $\alpha > 5°$ at $L=4$), it is appropriate to neglect the wave term in Eq. (1c) and then it reduces to,

$$\dot{\phi}_u = \Omega_H - \omega - kv_\parallel. \tag{2}$$

The ϕ_u indicates the phase angle under the conditions of extremely small amplitudes ($B_w\sim0$) and is called the "unperturbed phase angle". In this case we have only the last terms in Eqs. (1a) and (1b), which are the differential form of the first adiabatic invariant. We now define a terminology of "unperturbed resonance" as follows. Suppose that an electron resonates with the whistler initially at a specific point on the field line. As the electron travels adiabatically (for $B_w\sim0$), the local electron's gyro-frequency changes in the inhomogeneous medium and the Doppler-shifted wave frequency seen by the electron also changes. If the rates of change of the electron's gyro-frequency and of the wave frequency balance each other, there exists a situation for which ϕ_u is maintained nearly constant with time, this being named the unperturbed resonance. Under the unperturbed resonance condition, we cannot ignore the wave amplitude effect any longer. That is, the resonant electrons may be phase bunched by the $ev_\perp \times B_w$ force

acting along the field line so as to radiate coherently with consequent wave amplification. By taking into account the finite B_w, we have the motion of a simple pendulum for ϕ around $-B_w$. This oscillation can be considered to be the trapping of electrons by the wave, with its period being given by,

$$T=\left(2\pi\frac{m}{e}\frac{v_p}{v_\perp B_w f}\right)^{1/2} \tag{3}$$

where $v_p(=\omega/k)$=wave phase velocity. The electrons whose absolute initial phase is less than 90° will be bunched at $\phi=0°$ after the period of $T/4$. So we will call this $T/4$ the "bunching time", T_B. The smaller the amplitude B_w becomes, the longer duration we require for the unperturbed resonance because of the large T_B. For natural whistlers, it is generally difficult to maintain the unperturbed resonance condition for an absolutely long time, by making a complete match of the variations between the wave frequency and electron's gyro-frequency. If ϕ_u changes very slowly, or we satisfy the unperturbed resonance for as long as possible, we are able to expect a strong wave-particle interaction. Only in this case, is it possible to expect phase bunching of resonant electrons, when we take into account the wave effect. So, the unperturbed phase variation would be of primary interest and will be studied in the following section.

Calculation of Interaction Time Based on the Unperturbed Phase Angle

In the analysis the background plasma is considered to be cold, and the effects of ions and collisions are neglected so the wave number k is given by (Helliwell, 1965),

$$k=\frac{1}{c}\frac{f_p f^{1/2}}{(f_H-f)^{1/2}} \tag{4}$$

where f_p=plasma frequency. We have employed a centered dipole model for the magnetic field and a diffusive equilibrium model (Angerami, 1966) for the cold plasma density. The parameters of the diffusive equilibrium model are chosen so as to yield a realistic model by making the calculated dispersion agree with the experimental one. The parameters for our computations are summarized in Table 1. In the computations $L=4.0$ is selected because whistlers are most numerous at these latitudes (Helliwell, 1965), and correspondingly we frequently observe the whistler-triggered VLF emissions there (Carpenter, 1968).

The "interaction time", T_I is defined as follows.

$$|\Delta\phi_u|=\left|\int_0^{T_I}\dot{\phi}_u dt\right|=\pi/2. \tag{5}$$

This implies that T_I is the time interval for which ϕ_u stays within $\pm\pi/2$ of the exact resonance condition. The value of T_I varies considerably, depending on the position of initiation of resonance, initial wave frequency and electron pitch angle. Given the equatorial pitch angle α_{eq} and initial resonance frequency f_i, we can calculate the variation of ϕ_u for various initial

Table 1. Parameters used for calculations

Field line	$L=4$
Equatorial gyrofrequency	$f_{Heq}=13.65$ kHz
Equatorial cold plasma density	$N_{eq}=420\,\mathrm{cm}^{-3}$ ($f_p=184$ kHz)
Nose frequency	$f_n=5.2$ kHz
Whistler dispersion	$D=110\,\mathrm{s}^{1/2}$
Initial frequency	$f_i=1, 2, 3, 4$ kHz ($\Delta f_i=1$ kHz)
Equatorial pitch angle	$\alpha_{eq}=5, 15, 30, 45, 60°$

geomagnetic latitudes λ_i. The pitch angle at the initial position is obtained by the first adiabatic invariant,

$$\sin\alpha_i=\sin\alpha_{eq}(f_{Hi}/f_{Heq})^{1/2} \tag{6}$$

where f_{Heq}=equatorial gyro-frequency and f_{Hi}=gyro-frequency at the initial position. The initial value $v_{\|i}$ for the electron's parallel velocity is deduced from the resonance condition (or $\omega-kv_\|=\Omega_H$). Then we can determine the electron's total velocity v and energy W, which remain constant in our unperturbed study. As we are interested in triggering around whistler tails as shown in Fig. 1, the initial frequency f_i is chosen to be below the nose frequency. For further details of the calculation procedure, see Appendix.

Now the results of computations are presented. Figure 3 illustrates the variation of ϕ_u for four different initial frequencies for a specific pitch angle of $\alpha_{eq}=30°$. The ϕ_u variation given by a thick line in each panel yields the largest $T_I(T_{Imax})$. In each panel a shift of the initial latitude from that giving the T_{Imax}, even by a small amount, is found to result in remarkably different ϕ_u curves, a typical example of this being seen in the third panel of Fig. 3. This suggests that there is a very restricted range of geomagnetic latitude where we might expect the unperturbed resonance, and its interaction region is far from the equator on the upstream side of the electrons, being significantly different from the case for constant frequency waves. Some of the ϕ_u variations with larger T_I values show conspicuous oscillations as a consequence of a joint effect of the variations of the spatial inhomogeneity and wave frequency, as if they were phase-trapped by the wave.

A summary deduced from Fig. 3 is given in Fig. 4 as the relationship between the interaction time and initial geomagnetic latitude, with initial frequency as a parameter. The variation of frequency of the whistler wave is smaller at lower f_i so that the resonance region limited in latitude should be located in a region of smaller spatial inhomogeneity, or nearer to the equator. Conversely the resonance region would move farther away from the equator for higher f_i. The most important point of Fig. 4 is that the interaction time T_I is a maximum (~ 50 ms) for $f_i=3$ kHz, among various frequencies.

Figures 5 and 6 are a summary of the results of similar computations when the pitch angle is changed. Figure 5 shows how the initial geomagnetic latitude for which we have the T_{Imax} for each f_i varies with pitch angle. Generally speaking, the initial position where the wave-particle interaction is maximized, is located at higher latitudes for smaller pitch angles, and it shifts towards lower latitudes relatively abruptly at pitch an-

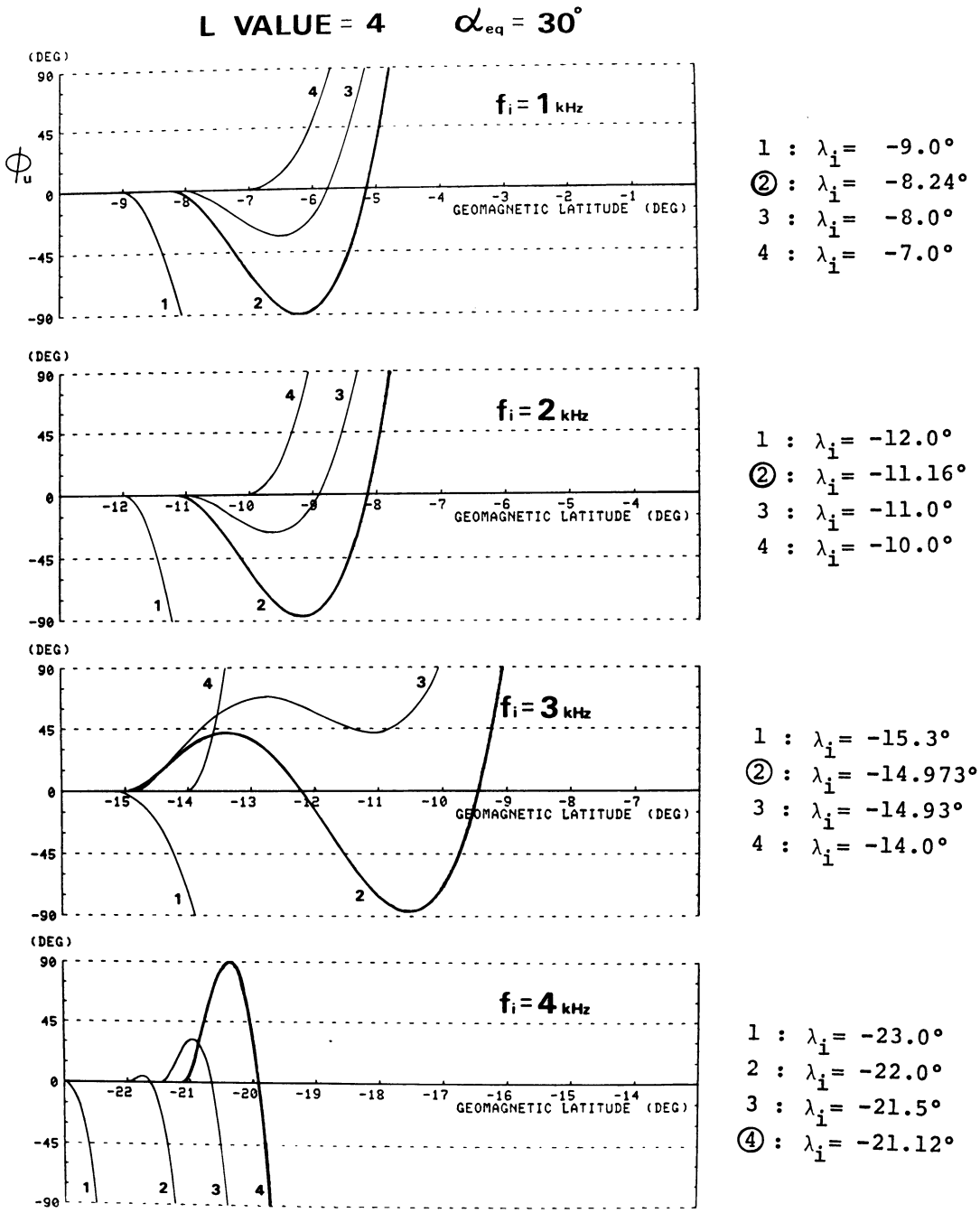

Fig. 3. Variations of unperturbed phase angle ϕ_u starting at various geomagnetic latitudes. Four initial frequencies are studied. A thick curve gives the largest T_I in each panel, and the corresponding initial latitude is described on the right of each panel

gles larger than about 30°. Figure 6 illustrates the resonance energy, as calculated from $\dot{\phi}_u = 0$ in Eq. (2), versus pitch angle for different f_i. This shows that the interaction for $f_i = 3$ kHz requires smaller resonant electron energy (15–25 keV) than for any other f_i.

In Fig. 7 we compare the calculated T_I with the bunching time T_B discussed above to examine the possibility of phase bunching and subsequent triggering emissions. We take the parameters $f_i = 3$ kHz and $\alpha_{eq} = 30°$, these conditions being found to be extremely favorable for triggering emissions because of the maximum T_I as seen in Figure 4 and of the minimum resonant electron energy as in Fig. 6. The broken lines indicate the variation of T_B for different wave amplitudes. In the calculations of T_B we have used the initial values of $v_\perp, f$ and v_p at λ_i. The T_B for an appreciable amplitude such as $B_w = 10\,\mathrm{m}\gamma$ is rather small so that T_{Imax} is much larger than T_B, and the region where T_I exceeds T_B for $B_w = 10\,\mathrm{m}\gamma$ is relatively wide (about 5°) in latitude. With a decrease of wave amplitude down to $B_w = 1\,\mathrm{m}\gamma$, T_B increases up to ~ 14 ms at the geomagnetic latitude of $\sim -15°$, but the maximum $T_I (\sim 50$ ms) is still much larger than the T_B within an extremely restricted region ($\sim 1°$) in latitude. This may suggest that the phase bunching of electrons might be possible with weak whistler amplitude even below $1\,\mathrm{m}\gamma$. This $1\,\mathrm{m}\gamma$

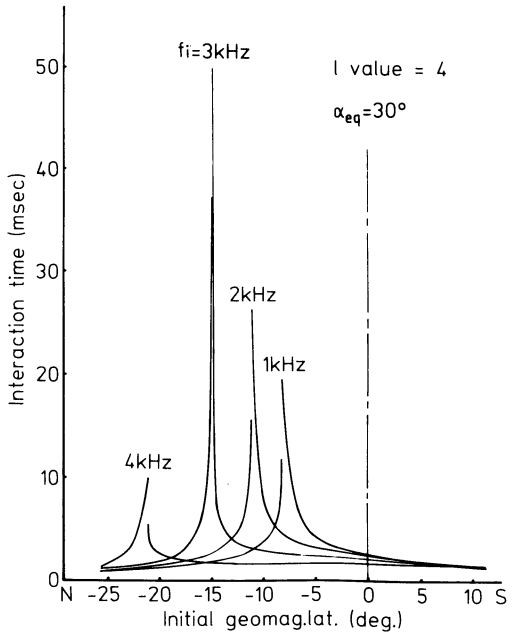

Fig. 4. Relationship between the interaction time and initial latitude with an initial frequency as a parameter. $\alpha_{eq}=30°$

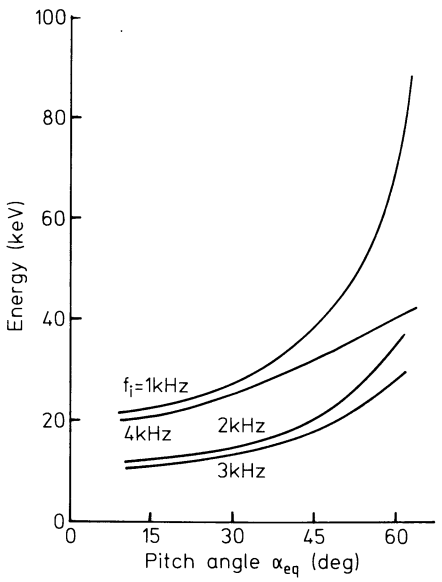

Fig. 6. Resonant electron energy versus pitch angle for different f_i

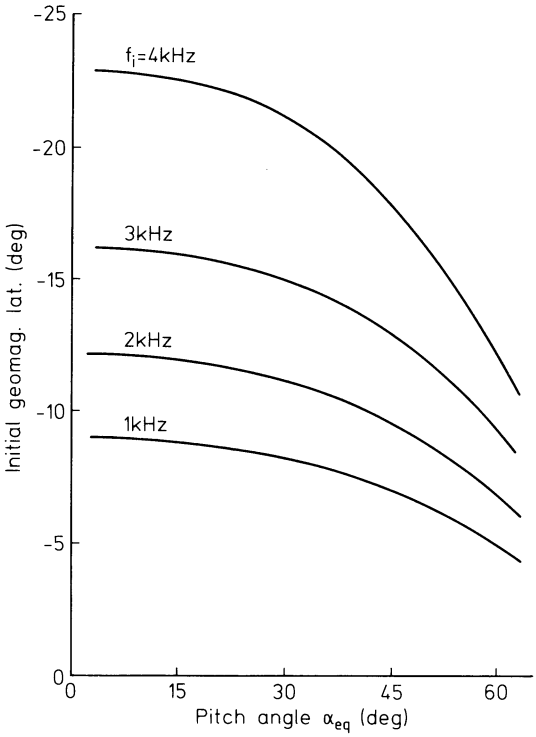

Fig. 5. Initial geomagnetic latitude for which T_I is maximized, versus pitch angle. The initial frequency f_i is a parameter

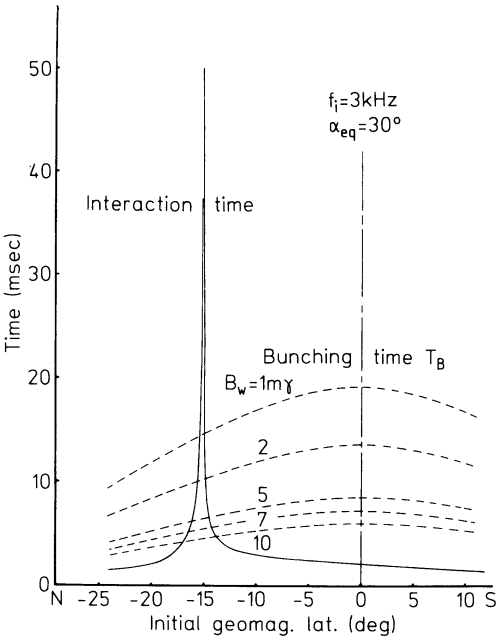

Fig. 7. Comparison between the interaction time and bunching time for various wave amplitudes. $f_i=3$ kHz and $\alpha_{eq}=30°$

(~ 3 mV/m) is a typical value for the intensity of ordinary whistlers at $L\sim 4$ (Helliwell, 1965).

Figure 8 illustrates the relationship of T_{Imax} for each f_i with α_{eq} (solid lines). The broken lines indicate the variation of T_B with pitch angle for a typical $B_w=1$ mγ. Except for the case of $f_i=4$ kHz, the interaction time (T_{Imax}) decreases with an increase of pitch angle. In particular T_{Imax} shows a decrease when the pitch angle is larger than 40°. It is found that T_{Imax} for $f_i=3$ kHz has an extremely large value compared with that for other f_i. The part indicated by thick solid lines corresponds to the region where the condition $T_I > T_B$ is satisfied. A comparison of the maximum interaction times at $f_i=1, 2, 3$ and 4 kHz in Fig. 8 results in Fig. 9, which is a different form of presentation. This figure indicates that T_I is maximised at $f_i\sim 3.25$ kHz. The amplitude of

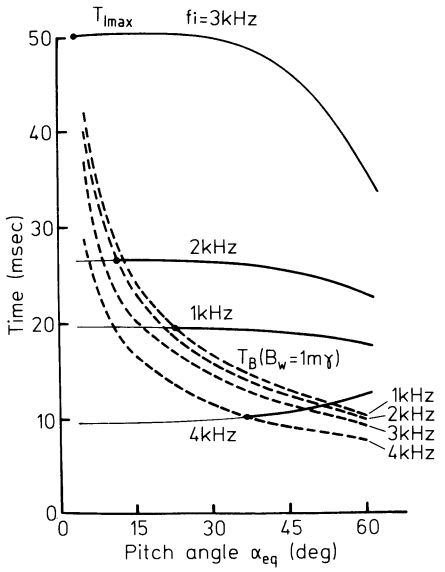

Fig. 8. Maximum T_I (T_{Imax}) versus pitch angle for different f_i and the corresponding variations of T_B for $B_w=1$ m

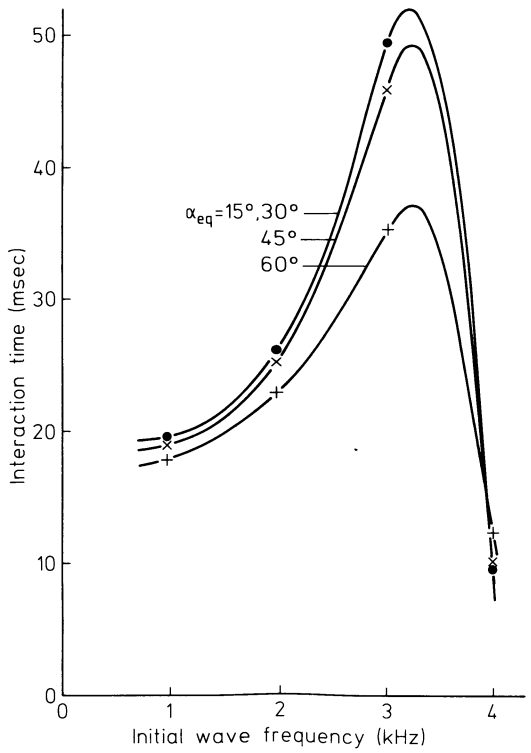

Fig. 9. Relationship of the interaction time with the initial frequency

whistlers at $L\sim4$ is, normally, about 1 mγ as stated above, and so 1 mγ is taken as a reasonable value in Fig. 8. As the condition favorable for triggering VLF emissions by a natural whistler, we require a large difference between T_{Imax} and T_B. In this case it is highly probable that emissions will be triggered by a natural whistler with $f_i=3$ kHz even with small amplitude below 1 mγ. The initial f_i of 3 kHz yields the final whistler frequency of 3.0–1.8 kHz after the interaction, depending on the length of the interaction time; the new emissions will appear at that frequency. This gives the ratio of $f/f_{Heq}=0.22$–0.13. Figure 8 imposes a lower limit on the pitch angle for producing phase bunching, and correspondingly, as shown in Fig. 6, the resonant electron energy increases with increasing pitch angle. So the range of pitch angle appropriate for phase bunching would be in an intermediate range of 30°–45°, as suggested by Helliwell (1967).

Wave Effect and Phase Bunching

The importance of the ratio T_I/T_B discussed in the previous section is quantitatively examined by calculating the trajectories of electrons in phase space based on the complete equations, Eq. (1). Wave amplitude is assumed to be constant over the whole frequency range. Provided that perpendicular velocities of nearly resonant electrons are oriented randomly before they come into resonance with the wave, the actual population can be represented by a sheet of electrons spaced uniformly in phase (Helliwell, 1970; Helliwell and Crystal, 1973). So the test particles are assumed to have initial phases equally spaced at 30° intervals and to be in exact resonance with the wave at λ_i. Since we adopt a test particle approach, our calculations do not include the effects of the electromagnetic fields generated by perturbed electrons. We present the results only for the most promising situation for wave generation, i.e. $f_i=3$ kHz and $\alpha_{eq}=30°$. Figure 10 shows the computed trajectories for 12 electrons which are distributed in initial phase angle ϕ_0 and which start the interaction at $\lambda_i=-15$. For this situation we obtained a larger T_I (25.19 ms). Figure 10a refers to the case of $B_w=1$ mγ and Fig. 10b $B_w=0.3$ mγ. Figure 11 shows similar results for an initial latitude slightly displaced by 0.5° ($\lambda_i=-14.5°$), for which we have obtained a smaller T_I (7.17 ms). Figure 11a is for $B_w=1$ mγ, while Fig. 11b for $B_w=5$ mγ. From Fig. 10a for $B_w=1$ mγ such that T_I is larger than $T_B(\sim12$ ms), it is found that the electrons whose initial phase angle is approximately less than 90° are phase bunched at $\phi\cong0°$ and at $\lambda_i=-13°$. Even if we decrease the wave amplitude down to $B_w=0.3$ mγ (in Fig. 10b), we have the condition $T_I\simeq T_B$, and we can confirm the presence of the phase bunching phenomenon at $\lambda_i=-11°$ at $\phi\simeq-160°$, but not at $\phi\simeq0°$. Figure 11a shows that the variations of ϕ starting at various ϕ_0 indicate nearly the same structures, indicating a negligibly small effect of the wave amplitude. This is because T_I is much smaller than T_B for this amplitude of $B_w=1$ mγ. If we increase the amplitude up to $B_w=5$ mγ, as given in Fig. 11b, we expect that T_I is approximately equal to T_B, and hence the phase bunching is observable at $\lambda_i=-13.5°$ at $\phi\sim80°$, but not at $\phi\simeq0°$. Further increase of wave amplitude so as to satisfy the condition of $T_I>T_B$ is found to result in the phase bunching of resonant electrons at $\phi\simeq0°$. From these results, we may conclude that the electrons are possibly phase bunched only by the wave whose amplitude satisfies the condition of $T_I>T_B$. Hence, the value of T_I deduced from the variation of unperturbed phase angle seems to be of great use in determining the threshold for phase bunching of resonant electrons by a variable frequency wave.

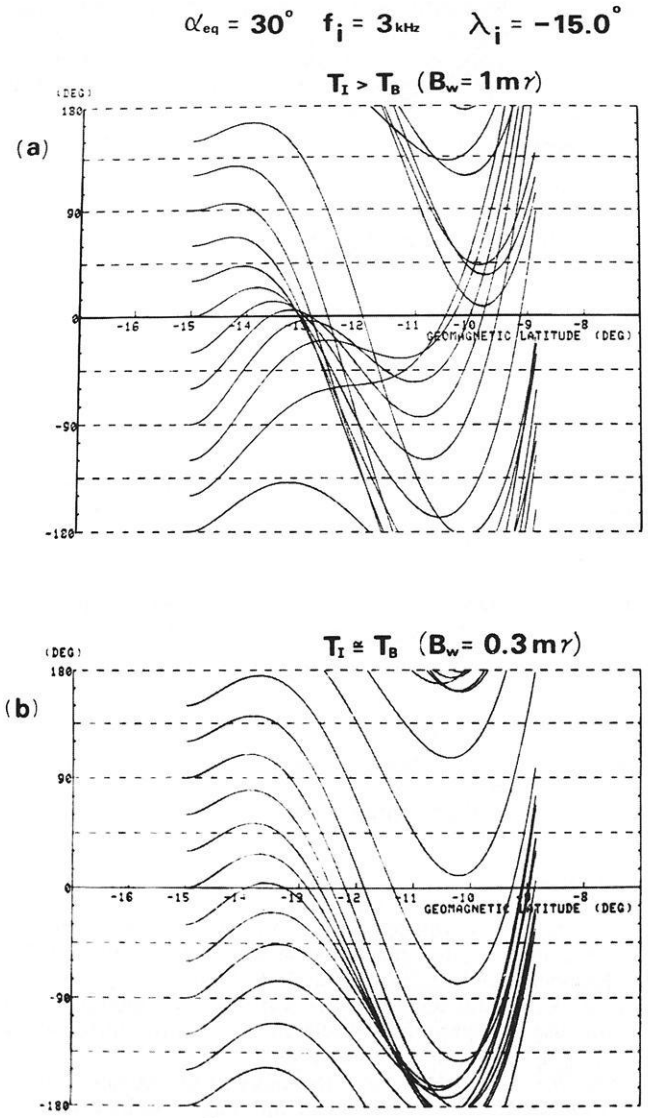

Fig. 10a and b. Variation of phase angle of electrons starting at $\lambda_i = -15$ (large T_I) for **a** $B_w = 1\,\mathrm{m}\gamma$ ($T_I > T_B$), and **b** for a smaller amplitude, $B_w = 0.3\,\mathrm{m}\gamma$ ($T_I \simeq T_B$). $f_i = 3$ kHz and $\alpha_{eq} = 30°$. A random distribution in phase is assumed before the interaction

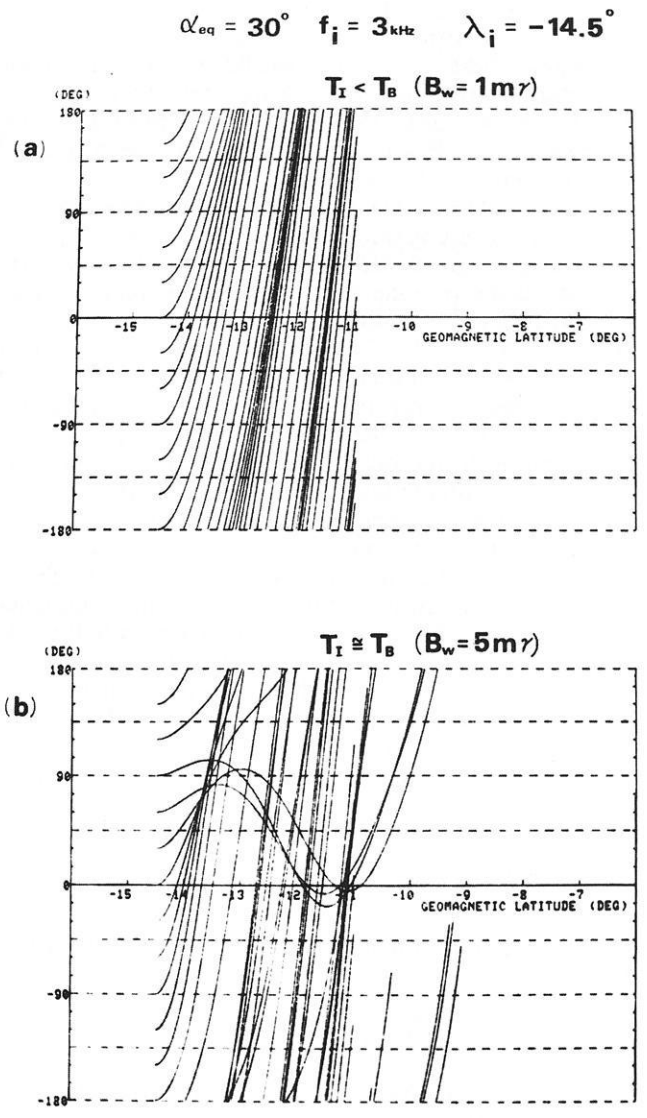

Fig. 11a and b. Variation of phase angle of electrons starting at a slightly displaced initial latitude ($\lambda_i = -14.5°$) (smaller T_I than that in Fig. 10) **a** for a smaller amplitude $B_w = 1\,\mathrm{m}\gamma$ ($T_I > T_B$) and **b** for a considerable amplitude $B_w = 5\,\mathrm{m}\gamma$ ($T_I \simeq T_B$). $f_i = 3$ kHz and $\alpha_{eq} = 30°$

Conclusions and Discussion

In conclusion we first summarize the essential points elucidated in the present paper.

(1) The interaction time defined by the variation of unperturbed phase angle determined by the spatial inhomogeneity of the medium and wave frequency variation is found to be very useful in the study of triggering emissions by a variable frequency wave such as a natural whistler, with special reference to its comparison with the bunching time. This point was quantitatively examined by calculating the trajectories of resonant electrons in phase space in the presence of a wave with variable amplitude. Our method of analysis would be applicable to other variable frequency waves such as linearly changing frequency (ramp) and sinusoidally varying frequency waves in the Siple transmissions.

(2) The computations of interaction times for a realistic model at $L = 4$ have shown that the region where electrons stay in resonance with a natural whistler is extremely restricted in latitude, far from the equator on the upstream side of the electrons. A resonance with initial frequency of 3 kHz would be extremely favorable for triggering VLF emissions compared with other initial frequencies. The interaction region for $f_i = 3$ kHz is located at $-15.89°$ for $\alpha_{eq} = 15°$ and at $-9.34°$ for $\alpha_{eq} = 60°$. The resonant electron energy ranges from 10.77 keV ($\alpha_{eq} = 15°$) to 28.35 keV ($\alpha_{eq} = 60°$). Pitch angles appropriate for phase bunching and subsequent coherent radiation would probably be in the intermediate range, 30°–45°. In the present paper we used initial frequencies 1 kHz apart, but Fig. 9 shows that the maximum T_I is achieved for $f_i \sim 3.25$ kHz, yielding the starting frequency of new emissions at 3.25–3.5 kHz (or

$f/f_{Heq}=0.24$–0.17). The lowest frequencies would be more likely starting frequencies for whistler-triggered emissions. These results seem to be in good agreement with the statistics on the starting frequency by Matsumoto and Kimura (1971), who found the highest occurrence probability at about one sixth the equatorial gyro-frequency ($f/f_{Heq}=0.17$).

Because there have been as yet no theoretical reports on the interaction region and starting frequency of whistler-triggered VLF emissions, we believe that the present results provide new information on these subjects. Although the calculations were performed for a specific L value of 4.0, it is generally accepted that there exists a restricted initial geomagnetic latitude and initial frequency appropriate for triggering emissions by a natural whistler even for other L values. These facts invite attention to the use of whistler spectra in studies of wave-particle interactions. We intend to extend the analyses to other L values, to be compared with experimental results. Furthermore, assuming a realistic distribution of energetic electrons, we will be able to calculate the resonant currents formed by the phase bunched electrons and subsequent coherent wave radiation. In the case of emission triggering at whistler tails, as treated in the present paper, we have a prominent property of a rapid frequency change as in Fig. 1. The mechanism of this drastic frequency change seems to be closely related with the second-order resonance condition (Helliwell, 1967; Nunn, 1974) in which the spatial inhomogeneity plays a key role. As is inferred from the present paper, the interaction region is far from the equator where there is a large spatial inhomogeneity, and this off-equatorial interaction region might result in such a rapid frequency change. This requires further study.

Appendix

In Fig. (A1), t_1 indicates the group delay time traversed by a wave with frequency f_1 during the transition from the starting position z_s (the height of 300 km in the ionosphere) to the position z_1 in the magnetosphere, and is given by

$$t_1=\int_{z_s}^{z_1}\frac{dz}{v_g(f_1)} \tag{A1}$$

where $v_g(f)$ is the group velocity at frequency f. Similarly t_2 is given by

$$t_2=\int_{z_s}^{z_2}\frac{dz}{v_g(f_2)}. \tag{A2}$$

Then, $\Delta t(=t_2-t_1)$ is the time interval the electron travels from z_1 to z_2, which is expressed by

$$\Delta t=\int_{z_1}^{z_2}\frac{dz}{v_{\parallel}}. \tag{A3}$$

Using Eqs. (A1), (A2) and (A3), we obtain the following requation.

$$\int_{z_s}^{z_2}\frac{dz}{v_g(f_2)}-\int_{z_s}^{z_1}\frac{dz}{v_g(f_1)}=\int_{z_1}^{z_2}\frac{dz}{v_{\parallel}}. \tag{A4}$$

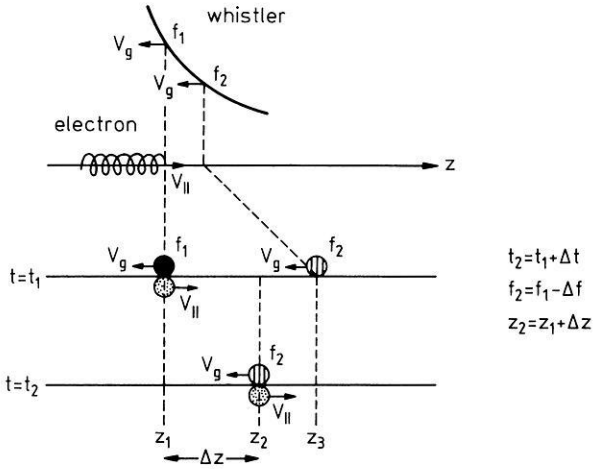

Fig. (A1). Relation between whistler wave packets and resonant electrons between two closely spaced points within the interaction region

Therefore, when we fix the position z_1 and frequency f_1 and we give Δz, we can determine Δf by using a numerical computation. So we can calculate ϕ_u with a step of Δz.

Acknowledgements. The authors wish to express their sincere thanks to Dr. Y. Tanaka of their institute for useful discussions. Thanks are also due to Professors A. Iwai and A. Kimpara for their continual encouragement.

References

Angerami, J.J.: A whistler study of the distribution of thermal electrons in the magnetosphere. Tech. Rept. 3412-7, Radioscience Lab., Standord Univ. 1966

Brinca, A.L.: Enhancing whistler wave-electron interaction by the use of specially modulated VLF wave injection. J. Geophys. Res. **86**, 792–800, 1981

Burtis, W.L., Helliwell, R.A.: Banded chorus—A new type of VLF radiation observation in the magnetosphere by Ogo 1 and Ogo 3. J. Geophys. Res. **74**, 3002–3010, 1969

Burtis, W.L., Helliwell, R.A.: Magnetospheric chorus:occurrence patterns and normalised frequency. Planet. Space Sci. **24**, 1007–1024, 1976

Carpenter, D.L.: Ducted whistler mode propagation in the magnetosphere: A half-gyrofrequency upper intensity cutoff and some associated wave growth phenomena. J. Geophys. Res. **73**, 2919–2928, 1968

Dysthe, K.B.: Some studies of triggered whistler emissions. J. Geophys. Res. **76**, 6915–6931, 1971

Gendrin, R.: Waves and wave-particle interactions in the magnetosphere—A review. Space Sci. Rev. **18**, 145–200, 1975

Helliwell, R.A.: Whistlers and related ionospheric phenomena. Stanford Univ. Press 1965

Helliwell, R.A.: A theory of discrete VLF emissions from the magnetosphere. J. Geophys. Res. **72**, 4773–4790, 1967

Helliwell, R.A.: Intensity of discrete VLF emissions. In: Particles and fields in the magnetosphere, B.M. McCormac, ed. Dodrecht: D. Reidel 1970

Helliwell, R.A.: Active very low frequency experiments on the magnetosphere from Siple Station, Antarctica. Philos. Trans. R. Soc. London Ser. B **279**, 213–224, 1977

Helliwell, R.A., Crystal, T.L.: A feedback model of cyclotron interaction between whistler-mode waves and energetic electrons in the magnetosphere. J. Geophys. Res. **78**, 7357–7371, 1973

Inan, U.S., Bell, T.S., Helliwell, R.A.: Nonlinear pitch angle scattering of energetic electrons by coherent VLF waves in the magnetosphere. J. Geophys. Res. **83**, 3235–3253, 1978

Maeda, K.: Cyclotron side-band emissions from ring current electrons. Planet. Space Sci. **24**, 341–347, 1976

Matsumoto, H.: Nonlinear whistler-mode interaction and triggered emissions in the magnetosphere. In: Wave Instabilities in Space Plasma, P.J. Palmadesso and K. Papadoulos, eds. Dodrecht: D. Reidel, 1979

Matsumoto, H., I. Kimura: Linear and nonlinear Cyclotron instability and VLF emissions in the magnetosphere. Planet. Space Sci. **19**, 567–608, 1971

Nunn, D.: A self-consistent theory of VLF emissions. Planet. Space Sci. **22**, 349–378, 1974

Miller, T.R,: Siple VLF transmitter data 1978: Selected records from Roberval, Canada and ISEE. Tech. Rept. VLF 79-1, Radioscience Lab., Stanford Univ. 1979

Rycroft, M.J.: VLF emissions in the magnetosphere. Radio Sci. **7**, 811–830, 1972

Received November 11, 1982; Revised version January 5, 1983

Accepted January 19, 1983

J Geophys (1983) 53:68–71

Journal of Geophysics

foF2 Response to IMF Sector-Boundary Crossings

Ludmila Třísková
Geophysical Institute, Czechoslovak Academy of Sciences, 141 31 Praha 4, Boční II, 1401, Czechoslovakia

Abstract. An analysis of night-time critical F2-layer frequencies in the equinoxial period of the 19th, 20th and 21st solar cycles has shown that the F2-layer response to sector-boundary crossings represents a response to the change of geomagnetic activity caused by the change of IMF polarity. For boundary crossings of the +/− type, the critical frequencies in both hemispheres in general decrease in March and April, and increase in September and October while the reverse holds for −/+ crossings.

Key words: Solar sector boundary – Interplanetary magnetic field – Ionosphere – Night foF2.

Introduction

Observations have shown that, in the Earth's orbital plane, the interplanetary magnetic field (IMF) is divided into sectors that co-rotate with the Sun. On the average, the nature of this structure is quasi-stationary and it consists alternately of regions with the magnetic field pointing away from (+) and towards the Sun (−), roughly along the Archimedean spiral. These sections, oriented almost opposite to one another, are separated by relatively sharp boundaries. According to results of satellite experiments, these boundaries can be thought of as intersections of the ecliptic plane with a warped global current sheet that surrounds the sun near its equatorial plane (Smith et al., 1978; Behannon et al., 1981).

In recent years, considerable attention has been paid to the effect of the sector-boundary crossing on various geophysical phenomena. The influence of the IMF polarity on geomagnetic activity has been proved in several papers, e.g. Berthelier (1976), the variation of Kp at sector boundaries has been dealt with by Schreiber (1977), the effect of the sector-boundary passage on geomagnetic activity has been studied in detail by Arora and Rangarajan (1981).

The influence of IMF polarity changes on the state of the lower ionosphere can be considered proved, e.g. by Schlegel et al. (1977), Laštovička (1979) Oksman and Ranta (1980), whereas the relation between the sector-boundary crossing and the condition of the F2-layer has not been fully clarified yet. F2-layer phenomena associated with the boundary passage were dealt with by D'Angelo (1980) and Lyon and Bhatanagar (1979), where a decrease of the nighttime foF2 after the boundary crossing is indicated for both types of passage. The influence of the IMF polarity on the nighttime critical F2-layer frequency in the equinoxial period has been demonstrated by Třísková (1982). From that paper it follows that the effect of the sectorial structure of the IMF appears in the F2-region as a response to changes in geomagnetic activity caused by the changes of the IMF polarity. Thus the foF2 response should differ with the type of boundary crossing.

In this paper, foF2 changes during sector-boundary passages are analyzed, taking the type of the boundary and the season of the year into account. The analysis has been made for the equinoxial period at solar cycle maximum when the IMF influence on geomagnetic activity (and hence also on foF2) should be most pronounced.

Experimental Data, Method of Analysis

The average of six hourly values of the critical F2-layer frequency between 00 and 05 h local time was chosen as the characteristic value f_r representing the state of the nighttime F-region on individual days. Vertical sounding data from middle latitudes in the Northern and Southern Hemispheres have been analyzed; the list of ionospheric stations and the time periods for which the data were used is given in Table 1.

Equinoxial periods for three years of the maxima of the 19th, 20th and 21st solar cycle have been examined; the data given by Svalgaard (1975) were taken as the days of boundary crossings for 1957–1959 and 1968–1970, whereas the days of boundary passages for 1979–1981 come from the Solar Geophysical Data (1979, 1981). For northern latitudes, where more data are available, a parallel analysis has been made for data from two stations; the aim was to verify whether the nature of the foF2-variation for boundary crossings of a given type remains the same and whether disturbances or local conditions can be excluded as the possible cause. For three days before and after the sector boundary crossing the average value $\bar{f}_r$ was calculated separately for both boundary types and both equinoxial periods, irrespective of the degree of geomagnetic activity.

Table 2 shows the numbers and types of analyzed crossings. The resultant numbers of events in the individual groups are low; the cause, on the one hand, is that usually not more than two crossings of a given type occurred in a month, and on the other, that not all observed crossings could be analyzed because of the lack of processed data. The f_r-value was not determined if less than four of the six foF2-values on a given day were available and, similarly,

Table 1

Station	Geographic		Invariant latitude	L	Data available
	Latitude	Longitude			
Juliusruh	54.62° N	13.38° E	51.67°	2.60	Sept. 1957–April 1981
Lindau	51.65° N	10.13° E	48.86°	2.31	April 1957–April 1979
Průhonice	49.99° N	14.55° E	46.75°	2.13	Sept. 1958–April 1981
Hobart	42.92° S	147.17° E	−53.60°	2.84	March 1957–March 1959
					March 1969–Oct. 1980
Canberra	35.32° S	149.00° E	−44.86°	1.99	March 27, Oct. 11, 1970

Table 2

Station	Season	Boundary	Number of analyzed crossings			
			1957 to 59	1968 to 70	1979 to 81	in sum
Lindau, Průhonice	March, April	+/−	7	7	4	18
		−/+	5	6	4	15
	Sept., Oct.	+/−	5	7	6	18
		−/+	5	7	5	17
Juliusruh	March, April	+/−	5	7	4	16
		−/+	5	6	4	15
	Sept., Oct.	+/−	7	6	6	19
		−/+	5	7	5	17
Hobart	March, April	+/−	5	7	3	15
		−/+	5	6	2	13
	Sept., Oct.	+/−	5	7	6	19
		−/+	4	7	5	16

a boundary crossing for which the data from less than four of seven subsequent days were available, was omitted. In the Lindau data set, data from the ionospheric station Průhonice were used, beginning with September 1979.

Results and Discussion

The main results are given in Figures 1 and 2 showing the average variation of the characteristic frequency f_r and, therefore, also the variation of the maximum electron density in the F-region in the course of sector-boundary crossings. Figure 1 gives the results obtained for the maxima of the individual solar cycles, whereas Figure 2 shows the average variation of f_r for the whole period under investigation. Average values of characteristic frequencies are normalized here by the value $\bar{f}_r$ (0) for the day of the sector-boundary crossing. It follows from the analysis that the characteristic frequencies decrease in March and April during boundary crossings of the +/− type as well as in September and October for the −/+ crossings, while they increase for crossings of opposite types. The same variation occurred both in northern and southern mid-latitudes; thus it can be concluded that the influence of the sector-boundary crossings on the F2-region is of a global nature.

One should take into account that f_r-variations are affected by several kinds of error. Firstly, they are distorted

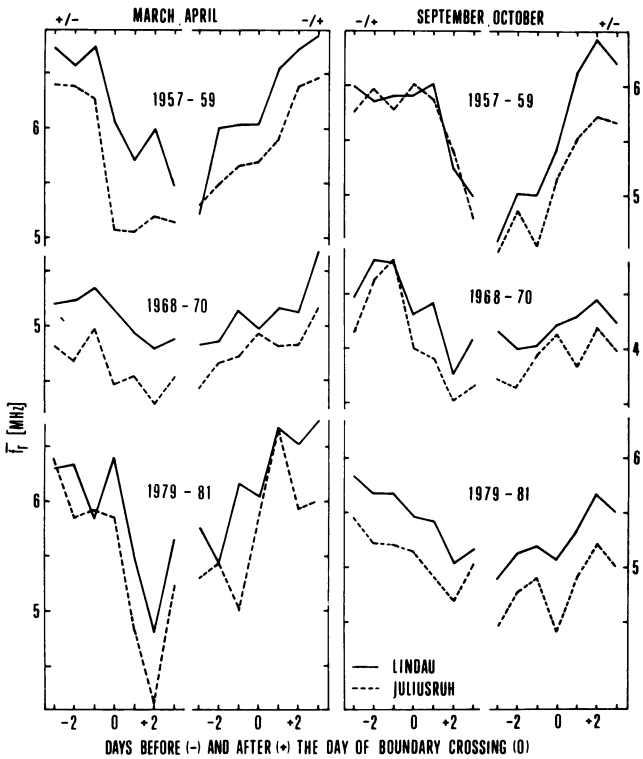

Fig. 1. Average variation of the characteristic frequency at solar cycle maxima in dependence on the season and on the type of the sector boundary crossing

by a low number of events in individual groups as well as by the non-equal numbers of f_r-values for corresponding days before and after the boundary crossing; secondly, the uncertainty in determining the day of the boundary passage plays a role. The date given by Svalgaard (1975) refers to 00 h UT, assuming that the boundary was crossed very probably within ±12 h of this instant. Under the assumption that boundary crossings within this interval are distributed uniformly and that nighttime foF2-values can be influenced only by boundary passages occurring before 03 h local time, then for the Lindau, Průhonice and Juliusruh data the crossing day as given by Svalgaard (1975) can coincide with the day on which its influence is reflected in the nighttime foF2-values in more than half the events. As regards the Hobart data, on the contrary, the influence of the boundary crossing can be expected on the next day in most events. Therefore, normalized variations of $\bar{f}_r$ are

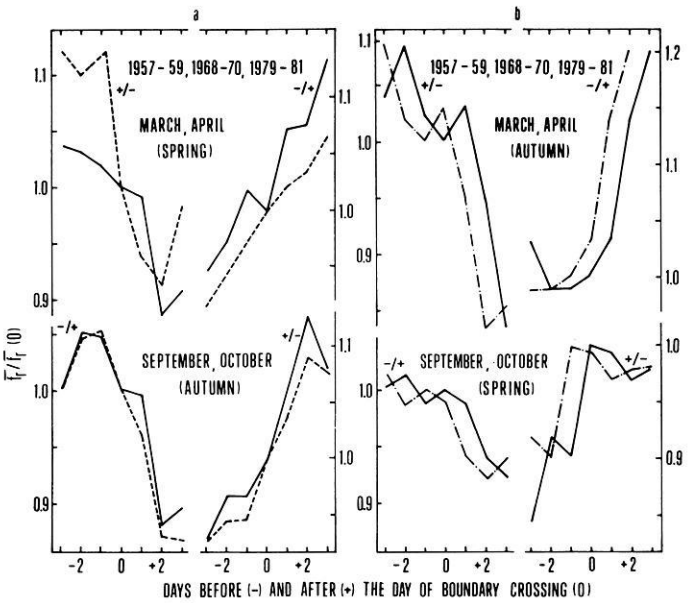

Fig. 2a and b. Average variation of the characteristic frequency in equinoxial periods in dependence on the type of the sector boundary crossing. Calculated for the maxima of the 19th, 20th and 21st solar cycle, normalized by the average characteristic frequency value on the day of the boundary crossing. (**a**) —— Lindau, ----- Juliusruh (**b**) —— Hobart, the crossing day is identical with the date of the zero day in (**a**); –·–·– Hobart, the influence of the boundary crossing delayed by one day with respect to the zero day in (**a**)

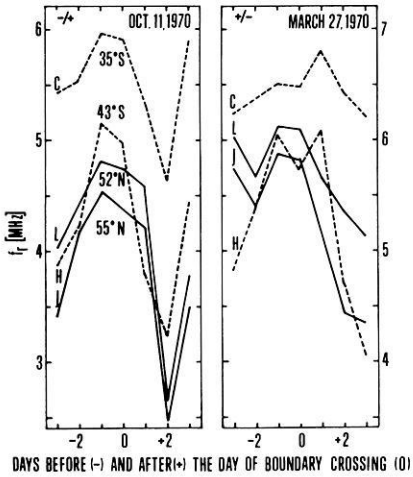

Fig. 3. Variations of the characteristic frequency for sector-boundary crossings at stations C = Canberra, H = Hobart, L = Lindau, J = Juliusruh

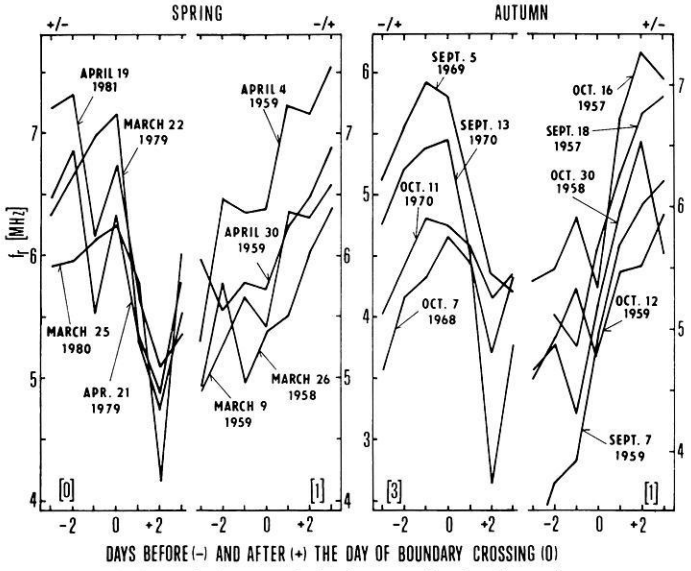

Fig. 4. Variation of characteristic frequencies for boundary crossings of individual types at ionosphere stations Lindau and Průhonice. The dates of boundary-crossing days mark the curves. The numbers in square brackets give the number of crossings in the given group where the f_r-variation showed a different behaviour (not included in the plot)

plotted in Figure 2b for both alternatives. Beside that, the original systematic foF2 variation connected with the boundary crossing can sometimes be added to by large fluctuations associated with sporadic but strong geomagnetic disturbances.

In view of the circumstances described, the credibility of the results given in Figure 1 and 2 has been investigated in two ways. The first was to observe the influence of the same boundary crossing at four stations, two of them in northern and two in southern latitudes. The second dealt with the nature of f_r-variations at one station, always for all events of a given data set.

The F2-layer response at the two pairs of stations was very similar in most cases as demonstrated by f_r-variations in Figure 3; the f_r-variation at one station also shows a very similar pattern in most crossings of the same type, as shown in Figure 4. Despite the occurrence of single variations not behaving according to the laws shown, it can be suggested that conclusions made on the basis of the results contained in Figures 1 and 2 may be considered as valid.

Considering that the critical F2-layer frequencies decrease with increasing magnetic activity, the f_r-variation should correspond to an opposite variation of the A_p-indices. Comparison can be made with results given by Arora and Rangarajan (1981) where an analysis of A_p-variation during sector-boundary crossings is made. As can be seen in Figure 2 of that paper, the A_p-variation at solar activity maximum really shows an increasing tendency for vernal $+/-$ and autumnal $-/+$ crossings (with respect to the Northern Hemisphere) while a decreasing tendency appears for the remaining two types of crossings. Thus the A_p-variation after Arora and Rangarajan and the f_r-variation shown herein confirm that changes of geomagnetic activity caused by the polarity of the departing and incoming sector are decisive for the behaviour of the F2-region during sector-boundary crossings.

The enhancement of geomagnetic activity in the $(-)$ sector in Northern Hemisphere spring and in the $(+)$ sector in autumn can be explained by a stronger interaction between the magnetosphere and the solar wind, when a southward pointing component of the IMF exists. The IMF is supposed to be ordered in the GSEQ (geocentric solar equatorial) coordinate system with the B_z component symmetrically distributed around a zero mean value, while its interaction with the magnetosphere is thought to be ordered in the GSM (geocentric solar magnetospheric) coordinate system. In GSM coordinates, southward fields of the IMF are more probable when the Earth is in a negative sector

in spring and in a positive sector in autumn (e.g. Russel and McPherron, 1973; Berthelier, 1976; Paulikas and Blake, 1976).

The foF2 depression, representing a marked decrease of the F2-layer maximum electron density, on days of enhanced geomagnetic activity is thought to be a consequence of the negative phase of magnetic storms. This negative phase, which occurs at mid-latitudes in summer and at equinoxes, can be caused by composition changes due to the storm circulation (introduction of air with an enhanced molecular gas concentration into the F-region). A detailed study of F-region storm effects and mechanisms has been given e.g. by Rishbeth (1975).

As can be found from Figures 2, 3 and 4, the crossings with a decrease of characteristic frequencies show a pronounced f_r-decrease (and thus foF2 decrease) on the second day after the boundary passage. Attention to the foF2-decrease on two days after the boundary crossing is drawn, for example, by D'Angelo (1980) as to a phenomenon valid for both types of passages in the time interval April to December 1974. This conclusion can be affected by the fact that, in this period, the foF2-decrease for vernal $+/-$ and autumnal $-/+$ crossings was stronger than the frequency increase for other events, so that the former prevailed on the average. This is also indicated by Arora and Rangarajan (1981). For the data set centred around 1974, a different change of magnetic activity appears in the equinoxial period dependending on the season and on the crossing type, but for the annual average these differences are overlapped by a stronger change in the case of an increase in magnetic activity which corresponds to the prevailing change for the foF2-decrease.

Conclusion

From the analysis presented here, it follows that the F-layer response to sector-boundary crossings represents a response to the change of geomagnetic activity caused by these crossings. The response is practically the same in both hemispheres; after boundary crossings of the $+/-$ type, the critical frequencies decrease in March and April, and increase in September and October while the opposite variation appears for $-/+$ crossings. Thus, considering the various physical mechanisms and couplings referring to sector-boundary passages, not only the type of the passage but also the season of occurrence have to be taken into account.

References

Arora, B.R., Rangarajan, G.K.: Temporal variation in the geomagnetic response to IMF sector boundary passage. J. Geophys. Res. **86**, 3369–3374, 1981

Behannon, K.W., Neubauer, F.M., Barnstorf H.: Fine-scale characteristics of interplanetary sector boundaries. J. Geophys. Res. **86**, 3273–3287, 1981

Berthelier, A.: Influence of the polarity of the interplanetary magnetic field on the annual and diurnal variations of magnetic activity. J. Geophys. Res. **81**, 4546–4552, 1976

D'Angelo, N.: On the global scale electrodynamic coupling of high-latitude and low-latitude regions. Can. J. Phys. **58**, 693–696, 1980

Laštovička, J.: Lower ionosphere, lower atmosphere and IMF sector structure in winter. J. Atmos. Terr. Phys. **41**, 995–998, 1979

Lyon, G.F., Bhatangar, V.P.: Response of the mid-latitude ionosphere to solar magnetic sector crossing. Can. J. Phys. **57**, 218–221, 1979

Oksman, J., Ranta, H.: Influence of IMF sector polarity on annual and diurnal variations of absorption in the auroral zone. Planet. Space. Sci. **28**, 1155–1161, 1980

Paulikas, G.A., Blake, J.B.: Modulation of trapped energetic electrons at 6.6 R_E by the direction of the interplanetary magnetic field. Geophys. Res. Lett. **3**, 277–280, 1976

Rishbeth, H.: F-Region storms and thermospheric circulation. J. Atmos. Terr. Phys. **37**, 1055–1064, 1975

Russell, C.T., Mc Pherron, R.L.: Semiannual variation of geomagnetic activity. J. Geophys. Res. **78**, 92–108, 1973

Schlegel, K., Rose, G., Widdel, H.U.: Interplanetary magnetic field polarity changes and D-region radio wave absorption. J Atmos. Terr. Phys. **39**, 101–103, 1977

Schreiber, H.: On the variation of Kp at sector boundaries. J. Geophys. Res. **42**, 437–445, 1977

Smith, E.J., Tsurutani, B.T.: Observations of the interplanetary sector structure up to heliographic latitudes of 160: Pioneer 11. J. Geophys. Res. **83**, 717–724, 1978

Solar Geophysical Data: 423, Part I., 38, November 1979; 441, Part I., 48, May 1981; 448, Part I., 42, December 1981; U.S. Departement of Commerce

Svalgaard, L.: Solar sector boundary crossings, 1957–1975. Solar-terrestrial physics and meteorology: a working document, issued by SCOSTEP secretariat, July, 1975, 72

Třísková, L.: Effects of IMF polarity on the F2-region. J. Atmos. Terr. Phys. **44**, 37–41, 1982

Received May 14, 1982. Revised version December 15, 1982.
Accepted December 15, 1982

J Geophys (1983) 53:72–73

Journal of Geophysics

Letter to the Editor

On the Equivalence of the "Niblett" and "Bostick" Transformations in the Magnetotelluric Method

Alan G. Jones

Geophysics Laboratory, Physics Department, University of Toronto, Toronto, Ontario, Canada, M5S 1A7

Key words: Bostick transformation – Niblett transformation – Magnetotelluric method

Introduction

In the $1D$ interpretation of magnetotelluric data, it is often useful to discover a reasonable first-approximation to the true conductivity-depth distribution beneath the recording location. This may be undertaken in the field, in order to ascertain if the station spacing is satisfactory or whether a greater station density of coverage is required, or at the base laboratory, as a prelude to a more sophistocated $1D$ inversion of the data.

There are three approximations presently in use by workers whose interest lies in the conductivity structure of the earth: (1) the Schmucker ρ^*-z^* scheme (Schmukker, 1970); (2) the Bostick transformation (Bostick, 1977); and (3) the Niblett approximation (Niblett and Sayn-Wittgenstein, 1960). The first two are in widespread use in western Europe and north America, whilst the Niblett approximation appears to be strongly favoured in eastern Europe and the USSR.

Weidelt et al. (1980) have previously detailed the relationship between Schmucker's ρ^*-z^* and Bostick's transformation; it is the purpose of this letter to demonstrate that Bostick's transformation and Niblett's approximation are *very* equivalent - they give *exactly* the same resistivity-depth profiles!

Theory

Both the Bostick transformation and the Niblett approximation are applied to the derived apparent resistivity curve $\rho_a(T)$ only and, as such, may be considered to be superior to Schmucker's ρ^*-z^* when the phase information does not exist or is thought to be unreliable.

The Bostick transformation and the Niblett approximation give a resistivity-depth distribution, $\rho_B(h)$ and $\rho_N(h)$, where h is a "penetration depth" in a half space medium of resistivity equal to the apparent resistivity at that particular period T, defined by

$$h=\sqrt{\frac{\rho_a(T)T}{2\pi\mu_0}}.$$

Note that this penetration depth implies an attenuation factor of approximately $\frac{1}{2}$ instead of the more usual skin depth attenuation of $1/e$.

The "Bostick" resistivity, $\rho_B(h)$, at depth h is given by

$$\rho_B(h)=\rho_a(T)\frac{1+m(T)}{1-m(T)}$$

where $m(T)$ is the gradient of the apparent resistivity curve on a log-log scale, i.e.

$$m(T)=\frac{d\log(\rho_a(T))}{d\log(T)}=\frac{T}{\rho_a(T)}\frac{d\rho_a(T)}{dT}.$$

The "Niblett" transformation gives a conductivity at depth h, $\sigma_N(h)$, from

$$\sigma_N(h)=h\frac{d\sigma_a(T)}{dh}+\sigma_a(T)$$

where $\sigma_a(T)=1/\rho_a(T)$. Obviously

$$\sigma_N(h)=\sqrt{\frac{\rho_a T}{2\pi\mu_0}}\frac{d\left(\frac{1}{\rho_a}\right)}{d\sqrt{\frac{\rho_a T}{2\pi\mu_0}}}+\frac{1}{\rho_a}$$

$$=\sqrt{\rho_a T}\frac{d\left(\frac{1}{\rho_a}\right)}{d\sqrt{\rho_a T}}+\frac{1}{\rho_a}$$

(dependence of ρ_a on T assumed) which, after differentiating by parts, becomes

$$\sigma_N(h)=\frac{-2T}{\rho_a\left(T+\rho_a\frac{dT}{d\rho_a}\right)}+\frac{1}{\rho_a}.$$

Hence, $\rho_N(h)=1/\sigma_N(h)$ is given by

$$\rho_N(h)=\rho_a(T)\frac{\left(1+\frac{T}{\rho_a}\frac{d\rho_a}{dT}\right)}{\left(1-\frac{T}{\rho_a}\frac{d\rho_a}{dT}\right)}$$

$$=\rho_a(T)\frac{1+m(T)}{1-m(T)}.$$

Thus, $\rho_B(h)=\rho_N(h)$ for all depths h.

Vanyan et al. (1980) have previously presented a form of the Niblett transformation involving estimation of the gradient of $\log(\rho_a(T))$ against $\log(\sqrt{T})$, which, after simple manipulation, can now be recognised as also exactly equivalent to the Bostick transformation.

An alternative expression for the Bostick resistivity at depth h has been used by various authors (for example, Weidelt et al., 1980; Goldberg and Rotstein, 1982). This form, given by

$$\tilde{\rho}_B(h)=\rho_a(T)\left(\frac{\pi}{2\phi(T)}-1\right)$$

employs the phase information $\phi(T)$ and is related to the original by Weidelt's "approximate phase" (Weidelt, 1972). The above expression has the advantage of not requiring an estimate of $m(T)$ to be made, but $\tilde{\rho}_B(h)\neq\rho_B(h)$, and hence $\tilde{\rho}_B(h)\neq\rho_N(h)$.

Acknowledgements and Apology. This clarifying letter arose from a discussion between the author and Professor L.L. Vanyan after erroneous comments made by the author about the Niblett approximation during the recent Sixth Workshop on Electromagnetic Induction in the Earth and Moon held at Victoria, B.C., Canada, from 15–22 August 1982. The comments of the author were due to a minor, but unfortunately not insignificant, coding error in the routine that was used to derive the Niblett approximation from synthetic data of known resistivity-depth distribution.

References

Bostick, F.X.: A simple almost exact method of MT analysis. Workshop on Electrical Methods in Geothermal Exploration, U.S. Geol. Surv., Contract No. 14080001-8-359, 1977

Goldberg, S., Rotstein, Y.: A simple form of presentation of magnetotelluric data using the Bostick transformation. Geophys. Prospect. **30**, 211–216, 1982

Niblett, E.R., Sayn-Wittgenstein, C.: Variation of electrical conductivity with depth by the magnetotelluric method. Geophys. **25**, 998–1008, 1960

Schmucker, U.: Anomalies of geomagnetic variations in the south-western United States. Bull. Scripps Inst. Oceanogr., 1970

Vanyan, L.L., Berdichevskiy, M.N., Vasin, N.D., Okulyesskiy, B.A., Shilovskiy, P.P.: On the normal geoelectric profile. Phys. Solid Earth **16**, 131–133, 1980

Weidelt, P.: The inverse problem of geomagnetic induction. J. Geophys. **38**, 257–289, 1972

Weidelt, P., Müller, W., Losecke, W. and Knödel, K.: Die Bostick Transformation. In: Protokoll über das Kolloquium „Elektromagnetische Tiefenforschung", V. Haak and J. Homilius, eds.: pp. 227–230. Berlin-Hannover, 1980

Received November 11, 1982; Revised February 3, 1983; Accepted February 3, 1983

J Geophys (1983) 53:74–76

Journal of Geophysics

Short Communication

On the Generation of Almost Uniform Magnetic Fields Inside Solenoids

J. Watermann
Institut für Geophysik der Universität Göttingen, Herzberger Landstraße 180, D-3400 Göttingen, Federal Republic of Germany

Key words: Single-layered solenoid — Uniform magnetic fields — Least squares fitting — Gradient method iteration

Introduction

Since the first investigations of the magnetic fields of stationary current distributions, the problem of providing almost uniform artificial magnetic fields has touched many branches of physics. For different applications different solutions were found (see, for example, the proposals of Garrett, 1967 and the review of Serson, 1974). Here, the following problem is stated: How can one generate a magnetic field which is as uniform as possible in a long (as compared with its diameter) cylindrical volume, while the length of the field generating device cannot be much longer than that volume but might be much broader for practical reasons?

The weak fields used in some applications, e.g. calibration coils for geomagnetic micropulsation sensors, can best be controlled if a moderate excitation current (about one milliAmp) is allowed. For this, single-layered solenoids with equally spaced turns, of the order of one hundred, are in use. As the axial magnetic field of a uniformly wound solenoid decreases from the center to the ends, the idea of increasing the winding density towards the ends or - more generally - of choosing the winding density as a function of distance from the center is suggested.

In the next section, a numerical method for calculating this winding density function will be presented, and in the last part, the result will be applied to an arbitrarily chosen example.

The Calculation

A single-layered solenoid can be modelled by a series of concentric circular filamentary currents which for practical reasons (easy but precise construction) should have equal radii and carry equal currents. Keeping in mind the symmetry of the solenoid, we choose a cylindrical coordinate system with its centre at the centre of the coil and its z-axis along the central axis.

Let a be the radius of the solenoid and $2z_N$ its length, and let $2N+1$ current filaments be in the (generally not equally spaced) planes $z_n = \text{const.}$ ($n = -N, \ldots, N$). Let us consider now the (longitudinal) field along the z-axis between the limits $-z_{\max}$ and $z_{\max}$ (remarks on the off-axis field will follow later), for which scalar notation can be used. Following Biot-Savart's law, a current strength I in each turn will produce a field at the point z on the axis (SI units used)

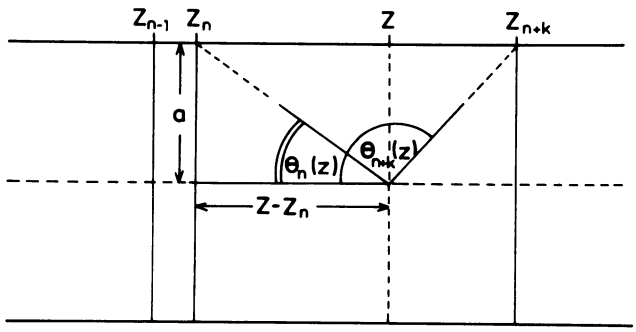

Fig. 1. On the calculation of the magnetic field at the point z on the z-axis caused by circular currents in the planes $z = z_n$ and $z = z_{n+k}$

$$H(z) = \frac{I a^2}{2} \sum_{n=-N}^{N} [a^2 + (z - z_n)^2]^{-3/2}. \tag{1}$$

Let all spatial dimensions be normalized with respect to a and the magnetic field with respect to $I/2a$, and let $\Theta_n(z)$ be the angle between the z-axis and a straight line from z to the filament z_n (see Fig. 1), then we obtain Eq. (1a) instead of (1):

$$H(z) = \sum_{n=-N}^{N} \sin^3 \Theta_n(z) = \sum_{n=-N}^{N} H_n(z). \tag{1a}$$

If $\bar{H}$ denotes the arithmetic mean of the field between the limits $-z_{\max}$ and $z_{\max}$ and

$$D(z) = H(z) - \bar{H} \tag{2}$$

the error at the point z, then the requirement for an almost uniform field between $-z_{\max}$ and $z_{\max}$ means finding the minimum of

$$J_2 = \int_{-z_{\max}}^{z_{\max}} D^2(z)\,dz = z_{\max} \int_{-1}^{1} D^2(z_{\max} \cdot \zeta)\,d\zeta \tag{3}$$

under the condition

$$J_1 = \int_{-z_{\max}}^{z_{\max}} D(z)\,dz = z_{\max} \int_{-1}^{1} D(z_{\max}\cdot\zeta)\,d\zeta = 0 \tag{4}$$

which is identical with taking $\bar{H}$ as the arithmetic mean between the limits $-z_{\max}$ and $z_{\max}$.

(We should use the relative errors instead of the - easier to handle - absolute errors, but we will see later, that $\bar{H}$, once chosen, will hardly be changed by the minimization procedure.) As neither J_2 nor $\partial J_2/\partial z_n$ can be evaluated in analytical form, a numerical integration has to be carried out. $2M+1$ nodes will be chosen in accordance with the integration formula. Let

$$Q = z_{\max} \sum_{m=-M}^{M} g_m D_m^2 \tag{5}$$

be the sum of the absolute squared errors and

$$P = z_{\max} \sum_{m=-M}^{M} g_m D_m \tag{6}$$

be the sum of errors, with $D_m = D(z_{\max}\cdot\zeta_m)$, $\zeta_m (m = -M, \ldots, M)$ being the nodes in the interval $[-1, 1]$ and g_m the respective weights. Writing $\Theta_n^m = \Theta_n(z_{\max}\cdot\zeta_m)$, we find

$$\bar{H} = \tfrac{1}{2} \sum_{m=-M}^{M} g_m \sum_{n=-N}^{N} \sin^3 \Theta_n^m. \tag{7}$$

Minimization of Q and taking into account the symmetries of the problem

$$\begin{aligned} z_{-n} &= -z_n \\ g_{-m} &= g_m \\ \sin\Theta_n^{-m} &= \sin\Theta_{-n}^m \\ \cos\Theta_n^{-m} &= -\cos\Theta_{-n}^m \\ \partial Q/\partial z_{-n} &= -\partial Q/\partial z_n \end{aligned}$$

will lead to a $N+1$-dimensional system of equations $(\bar{n} = 0, \ldots, N)$

$$\begin{aligned} 0 = {} & \frac{1}{6 z_{\max}} \frac{\partial Q}{\partial z_{\bar{n}}} \\ = {} & \sum_{\bar{m}} g_{\bar{m}} \Big[\sum_n \sin^3 \Theta_n^{\bar{m}} - \sum_m g_m \sum_n \sin^3 \Theta_n^m - \frac{g_0}{2} \sum_n \sin^3 \Theta_n^0 \Big] \\ & \cdot \big[\sin^4 \Theta_{\bar{n}}^{\bar{m}} \cos \Theta_{\bar{n}}^{\bar{m}} - \sin^4 \Theta_{-\bar{n}}^{\bar{m}} \cos \Theta_{-\bar{n}}^{\bar{m}} - g_0 \sin^4 \Theta_{\bar{n}}^0 \cos \Theta_{\bar{n}}^0 \\ & - \sum_m g_m (\sin^4 \Theta_{\bar{n}}^m \cos \Theta_{\bar{n}}^m - \sin^4 \Theta_{-\bar{n}}^m \cos \Theta_{-\bar{n}}^m) \big] \\ & + \frac{g_0}{2} \Big[(1 - g_0/2) \sum_n \sin^3 \Theta_n^0 - \sum_m g_m \sum_n \sin^3 \Theta_n^m \Big] \\ & \cdot \big[(2 - g_0) \sin^4 \Theta_{\bar{n}}^0 \cos \Theta_{\bar{n}}^0 \\ & - \sum_m g_m (\sin^4 \Theta_{\bar{n}}^m \cos \Theta_{\bar{n}}^m - \sin^4 \Theta_{-\bar{n}}^m \cos \Theta_{-\bar{n}}^m) \big]. \end{aligned} \tag{8}$$

(Summation index m or $\bar{m}$ has to be taken from 1 to M, and n from $-N$ to N.)

As the non-linear system cannot be solved directly, we try to find a minimum by a gradient iteration procedure, i.e. we start with equally spaced loops, for example, calculate $\partial Q/\partial z_{\bar{n}}$, and find after k steps improved values

$$\begin{aligned} & z_{\bar{n}}^{(k+1)} = z_{\bar{n}}^{(k)} - \kappa \cdot \partial Q/\partial z_{\bar{n}}^{(k)} \\ & \cdot (\bar{n} = 0, \ldots, N;\ k = 1, \ldots) \end{aligned} \tag{9}$$

with a suitable κ. After each step, the new values will be stretched or compressed so that $\pm z_N$ keeps constant to preserve the length of the solenoid and (nearly) the mean field $\bar{H}$. Furthermore, the gradient iteration procedure will guarantee to approach a minimum of Q.

A Numerical Example

Let us consider a solenoid with a length-to-diameter ratio of 5 with 101 turns. We require an almost uniform field along the central 90% of its length. Taking 1001 nodes and using the trapezoidal integration formula, we find the residual sum of squares Q to be decreased to 0.1% of that of equally spaced turn after 78 iterations while the mean field $\bar{H}$ changed less than 5%. Figure 2 compares the relative deviation of the axial field from the field in the center for equally spaced starting values of z_n with that after 78 iterations and after 250 iterations for one half of the cylinder (upper box). The dashed-dotted line marks the 90% region. The (+)/(−) signs indicate positive/negative deviation. Errors of less then 0.1% are supressed for technical reasons: Let the construction errors be normally distributed with a variance of $(\Delta a)^2$ for the radial and $(\Delta z)^2$ for the longitudinal errors of the current filaments. From Eqs. (1) and (1a) we get for the n-th turn

$$\partial H_n/\partial a = (2 - 3\sin^2\Theta_n)\cdot\sin^3\Theta_n.$$

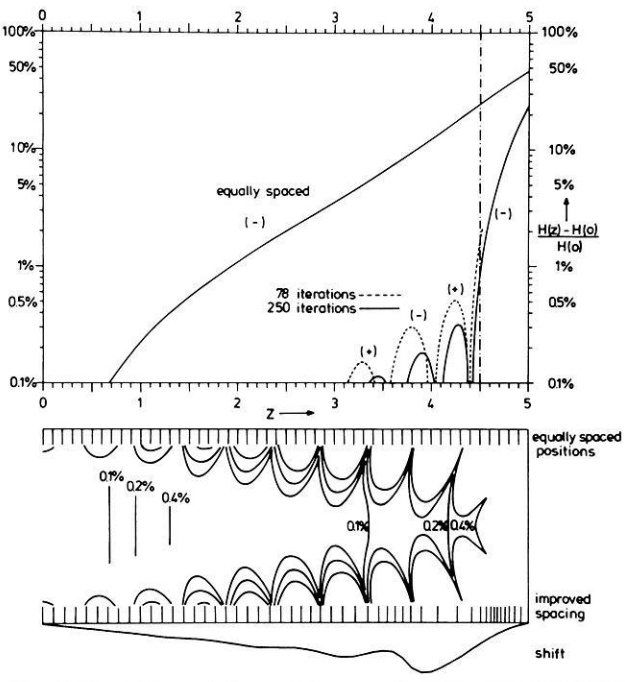

Fig. 2. Deviation of the axial magnetic field component from the field in the coil's center with equally spaced turns and with improved spacing after 78, and 250 iteration steps (upper box). For the last case, envelope of the 0.1%, 0.2%, and 0.4% error regions (lower box) as well as the shift magnitude of each turn (bottom)

Differentiation shows that the error reaches its maximal absolute value at $z=z_n$, decreasing to zero at $|z-z_n| = \sqrt{2}/2$ and increasing again, but only to one fifth of its maximum value before decreasing to zero when $|z-z_n|$ reaches infinity. Therefore, in reasonable cases, the largest error will be found at $z_0=0$:

$$\frac{\Delta H(0)}{\bar{H}} \approx \frac{\Delta a}{\bar{H}} \cdot \left[2 \sum_{n=1}^{N} [(2-3\sin^2 \Theta_n^0) \cdot \sin^3 \Theta_n^0]^2 + 1 \right]^{1/2}. \quad (10)$$

Similarly, we find

$$\partial H_n / \partial z = 3 \sin^4 \Theta_n \cos \Theta_n$$

which is zero for $z=z_n$, but increases quickly to its maximum at $|z-z_n|=0.5$ and decreases again to zero. Therefore, the largest error will be found at $z_0=0$ (in all reasonable cases):

$$\frac{\Delta H(0)}{\bar{H}} \approx \frac{3\Delta z}{\bar{H}} \cdot \left[2 \sum_{n=1}^{N} (\sin^4 \Theta_n^0 \cos \Theta_n^0)^2 \right]^{1/2}. \quad (11)$$

Choosing $a=10$ cm and $\Delta a=\Delta z=0.05$ cm gives a total construction error of $\Delta H(0)/\bar{H} \approx 0.1\,\%$.

The lower box of Fig. 2 shows one half of the solenoid scale-modelled, with equally spaced turns on the the upper boundary, improved spacing on the lower, and the amount of turn shift below. The undulation of the latter is in accordance with the results of Montgomery (1969, p. 260) for compound coils. The vertical lines indicate the 0.1 %-, 0.2 %-, and 0.4 %-error limits for an equally spaced winding, the contours mark the error limits for the improved device, as calculated from the tables of Hart (1967) for the z-component of the magnetic field.

References

Garrett, M.W.: Thick cylindrical coil systems for strong magnetic fields with field or gradient homogeneities of the 6th to 20th order. J. Appl. Phys. **38** (6), 2563–2586, 1967

Hart, Ph.J.: Universal tables for magnetic fields of filamentary and distributed circular currents. New York: American Elsevier Publ. Comp. 1967

Montgomery, D.B.: Solenoid magnet design - the magnetic and mechanical aspects of resistive and superconducting systems. New York: J. Wiley Intersc. Publ. 1969

Serson, P.H.: Compact bias coil systems for geomagnetic measurements. Publ. Earth Physics Branch **44** (10), Ottawa, 1974

Received December 8, 1982
Accepted February 18, 1983

Book Reviews

Landolt-Börnstein. Numerical Data and Functional Relationships in Science and Technology. New Series, Group V, Volume 1, Physical Properties of Rocks (Subvolume a), 373 p. Editor: Angenheister, G., Springer, Berlin, Heidelberg, New York 1982

This is the first volume on geophysical data within the new series of the Landolt-Börnstein table work, which has appeared on the market. Together with Subvolume b it contains laboratory data on physical properties of minerals and rocks, while geophysical "in situ" data of the solid earth are treated in Volume V.2. Compared with the previous edition of 1952 in which Astronomy and Geophysics were sharing one volume the expansion reflects the increasing demand of these data for geophysical data inversion and interpretation.

In contrast to other table works individual chapters begin usually with a rather comprehensive characterization and definition of the respective physical properties and the methods of their measurement. This almost encyclopedic character is, in some chapters, unterlined by key words in bold letters. All text pages are set up as double columns in English and German language simultaneously. This is not only convenient for German speaking users but may also be helpful for transcribing geophysical terms in both directions.

The first chapter, written by a competent petrographer (H.G. Huckenholz) gives an overview, especially for geophysicists, on nomenclature, genesis, composition, and structure of the rocks of the earth. Tables on densities of minerals and rocks at atmospheric pressure (J. Wohlenberg) are followed by an extensive list of high pressure shock wave data (D. Stöffler). A broad and profound section is devoted to quantities such as porosity, permeability, internal surface, and capillarity (J.R. Schopper), which have an important influence on many physical properties of sedimentary rocks. A rather lengthy list of individual porosity data, however, seems to be of limited value only for general use. Thermal properties of rocks under room- and elevated temperature conditions, and radioactive heat production, are thoroughly treated by V. Čermák, L. Rybach, M. Schuch, and supplemented by a short section on melting temperatures of rocks (R. Schmid).

Of course, a full appreciation of the content and completeness of the geophysical table work can only be given after the other volumes have been published. The weight of certain chapters and the preference of the physical units used is somewhat biased by the individual authors. Concerning the data sources used there appears to be a fair balance between European and Anglo-American references which is often not the case. In this respect, but also in stile and content, this book seems to be complementary to other modern table works on physical rock properties.

The arrangement and printing of text, tables and figures are of traditional Springer quality. This, in every respect very "valuable" table work should be available in central scientific libraries, in libraries of geoscience institutes where pure or applied research is carried out but may also be found useful for research in material sciences and civil engineering. A broader distribution, hower, will probably be prevented by its exorbitant price. **H. Berckhemer**

Yuen, C.K., Fraser, D.: Digital Spectral Analysis. CSIRO, Pitman Advanced Publishing Program, San Francisco, London, 1979

This book is a publication of a course of lectures on spectral analysis. It differs from currently available texts on spectral analysis and digital signal processing as it does not require a background in advanced mathematics and communication theory. This volume gives in the early chapters an introduction to mathematical and computational properties of Fourier Transform and Fast Fourier Transform applied to discrete values. Beside the potentials of these methods the limits are also pointed out. The following chapters discribe statistical treatments of discrete time series, e.g. autocorrelation, autoregression, power spectrum etc. Finally the very important technics of windowing, digital filtering and spectrum interpretation which are necessary when applying spectral analysis to real data are introduced. The appendix contains five Fortran computer programs for various transformations.

Since the matter is clearly arranged this book is a rather helpful guide for teaching this subject. Besides that it is a good introduction for students who intend to work in this area. It clearly points out the shortcomings of the various methods. This is of special relevance nowadays, since these functions are available at many computers and nobody should use them blindly. Every one who wants to apply these algorithms to real data needs, however, additional information about the spectral properties of the special data set. **Hermann Lühr**

Swinney, H.L. and Gollub, J.P. (eds.): Hydrodynamic Instabilities and the Transition to Turbulence. Springer, Berlin, Heidelberg, New York, 1981

"Hydrodynamic Instabilities and the Transition to Turbulence" is a collection of eight review articles written by hydrodynamicists and mathematicians for this book. In geophysics and other fields the interest in instabilities and turbulence is rising. A break-through seems to be pending. Freely quoted from the Preface by H.L. Swinney and J.P. Gollub: The transition from laminar flow to turbulent flow has until recently been beyond the reach of theory and experiment. The situation has been changed dramatically by the use of computers in laboratory experiments and in numerical analysis of nonlinear systems. Numerical studies of nonlinear models have also revealed unexpected results, such as chaotic behaviour in a system with only three variables. Another development is the application of new mathematical concepts from the qualitative theory of differential equations. More traditional methods such as bifurcation theory and stability analysis also continue to contribute new insights.

The various chapters include: introductions to the relationships between dynamical systems theory and turbulence (O.E. Lanford: 'Strange attractors and turbulence'; J.A. Yorke and E.D. Yorke: 'Chaotic behaviour and fluid dynamics); a review of hydrodynamic stability and bifurcation theory (by D.D. Joseph); three case studies – convection, rotating fluids, and shear flows (F.H. Busse: Transition to turbulence in Rayleigh-Benard convection; R.C. DiPrima and H.L. Swinney: Instabilities and transition in flow between concentric rotating cylinders; S.A. Maslowe: Shear flow instabilities and transition); a review of geophysical fluid instabilities (by D.J. Tritton and P.A. Davies); and a discussion of instabilities and chaotic behaviour in nonhydrodynamic systems (J.M. Guckenheimer).

The articles are not strictly introductory, but the authors have tried to make their chapters accessible to physicists, mathematicians, geophysicists, and engineers, who may not be specialists in fluid dynamics. Certainly the book provides an introduction to the literature of this rapidly growing field.

The book covers the spectrum from abstract mathematics to empirical observation, but the emphasis is on theory. It does not make easy reading, but it seems important in providing an insight into a complex subject. Up to recently turbulence was thought to be accessible only by statistics. We begin to understand now that turbulence is a property of systems that are sensitive to initial conditions. Such systems are sometimes described by only few parameters and by simple differential equations. The study of such 'simple' systems is an important step toward a deeper insight into nature.

I repeat: a break-through may be pending in understanding turbulence and chaos. It seems to require more sophisticated and

more abstract mathematics than many of us are used to. The book seems to be a good document of the state of the endeavors in that direction and of the developments to come. For everybody interested in the problems of geophysical fluid dynamics I consider the book highly recommendable and for libraries of institutions with any kind of interest in fluid dynamics I consider it a must.

W.R. Jacoby

D.H. Griffiths and R.F. King: Applied Geophysics for Geologists and Engineers (Second edition of "Applied Geophysics for Engineers and Geologists"), Pergamon Press, Oxford, 230 pp., 1981

"Applied Geophysics for geologists and engineers, the elements of geophysical prospecting" is exactly what the title promises. It is (the second revised edition of) a text which originally had been aimed at civil engineers but now gives more attention to the interests of geology students. "The scope of the book has therefore been broadened to include some discussion of geophysical methods used in prospecting for oil and other minerals, even though these methods will be of little or no interest to the civil engineer" "...this being reflected in considerable strengthening of the sections dealing with electromagnetic and induced polarization techniques. However, the bias of the book remains... toward the seismic and resistivity methods which dominate the field of engineering geophysics, and it does not pretend to be a comprehensive textbook...". There are also chapters "Gravity surveying" and "Magnetic surveying", "Geophysical borehole logging" and "Radiometric surveys and remote sensing".

Judging from my experience in teaching geophysics to geology students, I think the book is an excellent compromise between physical explanation, practical application, and theory using mathematical formulation. It describes the geophysical methods very accurately, though so much abbreviated (necessarily so) that only someone with considerable knowledge will realize how much is behind what is actually said. This is, of course, so much better than a description that has become inaccurate by its brevity. The authors generally try to make the problems intuitively understandable with only a minimum of abstract back-up. The book is well illustrated. A brief bibliography is added for those who want to learn more about the various methods; again I find the selection is appropriate for the readership of this book. Finally the book is completed by 12 quesions (followed by brief answers) for the student to work out.

I find this book a highly recommendable text of introcudtory applied geophysics for geologists and engineers, so much that I shall use my next opportunity of teaching such a course to test it in practice.

W.R. Jacoby

Krefelder und Lippstädter Gewölbe – die großen Querstrukturen am Rande des Ruhrkohlenbeckens. 439 Seiten, 83 Abbildungen, 31 Tabellen, 28 Tafeln. Krefeld, Geologisches Landesamt Nordrhein-Westfalen 1982. Fortschritte in der Geologie von Rheinland und Westfalen, Band 30.

Krefelder und Lippstädter Gewölbe sind zwei große Querstrukturen, die das Ruhrkohlenbecken im Westen und Osten begrenzen. Beide Gewölbe stellen Aufragungen älterer Schichten im Karbon der subvariscischen Vortiefe dar, die unter einem Deckgebirge aus Kreide- und jüngeren Schichten verborgen sind. Das Geologische Landesamt Nordrhein-Westfalen hat in Zusammenarbeit mit der Erdölindustrie die Forschungsbohrungen Schwarzbachtal 1 am Südostrand des Krefelder Gewölbes und Soest-Erwitte 1/1a im Lippstädter Gewölbe abgeteuft. Mit diesen Bohrungen wurde beabsichtigt, in den Gewölben einen Einblick in den devonischen und altpaläozoischen Unterbau des Ruhrkohlenbeckens zu erhalten.

Die Ergebnisse dieser Bohrungen regten umfangreiche interdisziplinäre Forschungsarbeiten an, über deren Ergebnisse in dem vorliegenden Band berichtet wird. In 19 Arbeiten ist von 26 Autoren ein umfangreiches Material über das Krefelder und Lippstädter Gewölbe zusammengetragen worden, das auch für die Erforschung der angrenzenden Gebiete von großem Wert ist. Neben regionalgeologischen, tektonischen, petrographischen und geochemischen Arbeiten stehen Forschungsergebnisse von Seismik, Magnetik, Geothermik, Gravimetrie, Magnetotellurik und Geoelektrik. Daß bei der Fülle des Materials der Überblick nicht verloren geht, dafür sorgen eine Einleitung und eine zusammenfassende Arbeit über „geklärte und ungeklärte Probleme" am Ende des Bandes. In einigen Arbeiten wäre es wünschenswert, wenn deutlicher zwischen Modellen, Hypothesen und gesicherten Erkenntnissen unterschieden würde. Das trifft besonders dann zu, wenn Ergebnisse jeweils anderer Fachbereiche als Beweismittel herangezogen werden.

Dieses Buch ist allen Geophysikern, die im Bereich der genannten Strukturen und in den angrenzenden Gebieten arbeiten, als Nachschlagewerk zu empfehlen.

Als Schulbeispiel interdisziplinärer geowissenschaftlicher Forschung dürfte dieser Band aber auch für Studenten von Interesse sein.

K. Knödel

Charles C. Bates, Thomas F. Gaskell, and Robert B. Rice: Geophysics in the Affairs of Man. A Personalized History of Exploration Geophysics and its Allied Sciences of Seismology and Oceanography. XX + 492 pp., Pergamon Press, Oxford, New York, Toronto, Sydney, Paris, Frankfurt, 1982.

The authors present an intriguing review of the history of applied geophysics and allied sciences. Main emphasis is attributed to the role and interaction of men and human organisations as governmental institutions and agencies, scientific organisations (universities and societies) and private (mainly commercial) enterprise. The authors restrict their report, but not exclusively, to Canada, Great Britain and the United States of America with emphasis on the latter. Though it must be admitted that the U.S. have a leading role in applied geophysics, especially seismics, the restriction to the above mentioned countries might have been mentioned already in the title or subtitle.

The book is divided into 9 chapters. Each chapter refers to genuine exploration geophysics for private enterprise, mainly the oil industry, but also to civil and military governmental applications of geophysical methods. Furthermore classical seismology and physical oceanography are two additional topics of most chapters. As to the geophysical methods most attention has been paid to the history of seismics.

After a short glance in Chapt. 1 on what happened before world war I, the authors devote Chapt. 2 to the "roaring twenties" and "the depressing thirties". They describe in detail how the first geophysical contractors developed in the U.S., partly flourished, and partly disappeared. The strong impetus to this development by Mintrop and his Seismos Ltd. company by 1924 is only shortly mentioned*), but more emphasis has been given to the technical progress achieved by the daring first geophysical companies of the U.S., especially to the advent of the reflection seismograph.

Non-seismic methods are also dealt with as Schlumberger's well logging, the torsion balance and the gravimeter, however, not mentioning the Thyssen gravimeter of Seismos Ltd., Germany, one of the first such field proven instruments (1934) of which about 100 pieces were constructed and sold all over the world before world war II.

In Chapt. 3 the development and application of geophysical methods for warfare in world war II is reported on. Detection of enemy artillery, influence mines, e.g. magnetic mines, and geophysical aspects of undersea warfare are the main topics.

Chapters 4 to 6 deal with the time from 1945 to 1970. Tremendous development is going on in exploration seismics. The introduction of magnetic recording, digital recording and processing,

* By the way, Mintrop did obviously not spoil the prices for the arising industry of exploration geophysics in the U.S., if footnote 9 of p. 25 is interpreted in favour of Mintrop

the common reflection point (CRP) method etc. are represented in an intriguing manner, giving due credit to the persons and companies involved.

Aeromagnetics, an offspring of the techniques of world war II's warfare, and other aerogeophysical methods are also duely dealt with.

Considerable attention is paid to the problem of detecting nuclear tests and the Vela Uniform project. Increased oceanographic activity gives rise to the conceptions of ocean spreading and plate tectonics and ensues the deep sea drilling program.

Chapter 7 comprises the 1970s and early 1980s. It deals especially with the problems caused by environmentalists and Opec. During this period the reflection seismic exploration of the crust and upper mantle was initiated by the COCORP effort.

The rest of the book is devoted to "geophysics as a business" (Chapt. 8) and to "personal achievements" of a selection of important geophysicists (Chapt. 9). In Chapt. 8 the history and achievements of 8 most important geophysical contractors are presented. Moreover, an Appendix was devoted to a broader version of the history of GSI and Texas Instruments. Prakla-Seismos GmbH was excluded from this list because it is government-owned as announced in a Note (Table 8.2, p. 301). I myself cannot understand this exclusion since some of the other major companies are owned by large holdings or the majority of shares is owned by government. By the way, it is not quite logical either, to mention Prakla-Seismos GmbH on the table of the eight largest geophysical contractors (p. 301) and to mention Prakla-Seismos GmbH once more on Table 8.7 where smaller seismic acquisition firms are dealt with (p. 343).

If I disregard these and some previous minor objections this book is an excellent presentation of the history of a rather young science, focussing on the human aspects of those persons who were active in promoting their sciences. It was a pleasure for me to read the book and let pass in review all the years when I was active in geophysics (since 1936), and all the persons mentioned, many of whom I know or knew.

Many figures, tables and photos enrich the book. Proper references, a name index and a subject index facilitate to follow up special problems. An index of abbreviations might have been an additional help, though each abbreviation is generally explained when it appears for the first time. **Th. Krey**

Kaufman, Alexander A. and Keller, George V.: The Magnetotelluric Sounding Method, Methods in Geochemistry and Geophysics, Vol. 15, 596 pp., Elsevier Scientific Publishing Company, Amsterdam 1981.

Das große Interesse an geothermischer Energie war Anlaß eines vom U.S. Geological Survey an der Colorado School of Mines geförderten Projektes zur Sicherung des gegenwärtigen Wissensstandes elektromagnetischer Prospektionsmethoden großer Eindringtiefe; speziell solchen zum Explorieren auf geothermische Energie. Einen Teil der Ergebnisse dieser Studie dokumentiert das vorliegende Buch. Nur einen Teil deshalb, weil neben der hierin ausschließlich behandelten Magnetotellurik (MT) auch andere Sondierungsmethoden: Controlled-Source (Time Domain, aktive Audio Magnetotellurik) und Gleichstromverfahren untersucht wurden.

Erklärtes Ziel dieses Buches ist es, eine möglichst umfassende Darstellung des physikalischen und mathematischen Apparates der MT in einem Bande zu geben. Dabei beschränken sich die Autoren auf die ‚klassische MT'; nicht zuletzt deshalb, weil diese Methode auch in fernab gelegenen Gebieten ohne künstliche Anregung auskommt und sie deshalb eine sehr große Verbreitung gefunden hat.

Ausgehend von den Quellen der natürlichen elektromagnetischen Felder wird in didaktisch hervorragender Weise die ganze Theorie der MT entwickelt. Für das Verständnis, besonders des Lernenden, sehr hilfreich sind die durchgängig zahlreichen Graphen für unterschiedliche Horizontalschichtmodelle. Hier wird das Einwirken der verschiedenen Parameter auf den scheinbaren spez. Widerstand und die Phasenbeziehungen besonders anschaulich.

Neben den Fragen nach den Gültigkeitsgrenzen des Modelles ebener Wellen, gerade auch unter dem Aspekt der Kugelgestalt der Erde, werden auf breitem Raum die Probleme der nicht horizontalen Schichtung und die eingelagerter Inhomogenitäten (Zylinder in E- und H-Polarisation) abgehandelt. Hier fehlt auch nicht die Diskussion magnetotellurischer Sondierungskurven über vertikalen Stufen, schräg einfallenden Leitfähigkeitsanomalien, Aufwölbungen oder Grabenstrukturen.

Im Gegensatz zum Vorangegangenen, sind die Themenkreise: Elliptische Polarisation und Impedanztensoren knapp dargestellt. Ebenso wird auch die Signalverarbeitung nur kurz angerissen. Hier findet man Ausführungen zum Dynamikbereich, den erforderlichen Abtastraten und der Meßdauer einer MT-Apparatur. Auch wird eine Übersicht gängiger Filter gegeben. Das aktuelle ‚Remote-Reference'-Verfahren, zur Verbesserung des Signal- zu Rauschverhältnisses, wird, wie auch der sehr große, komplexe Themenbereich der Inversion in nur einem sparsamen Unterabschnitt abgehandelt.

Das Kapitel Meßtechnik stellt unter anderem inzwischen ungebräuchliche E-Feld-Sonden wie auch Magnetometertypen vor. So findet sich neben der Beschreibung des SQUIDs die eines Torsionsmagnetometers mit Vacuumphotozelle und Röhrenverstärker. Ob letzteres noch zum ‚State of the Art' gezählt werden darf?

Ganz entsprechend der Herkunft beider Autoren schließen sich im letzten Abschnitt des Buches einige MT-Fallstudien aus der UdSSR bzw. den USA an: Kamchatka, Moskauer Becken, Kaukasus – The Geysers, Utah Thermal Belt .... Ganz entsprechend zitieren sie in der Literaturliste zur Hauptsache Autoren dieser beiden Lager; wobei die jüngsten Zitate auf 1979 datieren.

Zusammenfassend darf man sagen: Es handelt sich um ein Buch, gleichermaßen geeignet für denjenigen, der sich in die Theorie der MT einarbeiten oder es als Nachschlagewerk benutzen möchte. Da die Autoren das Schwergewicht auf den physikalisch-mathematischen Apparat gelegt haben, läßt das Buch für den Praktiker viele Wünsche offen. Bleibt aber zu hoffen, daß sie sich mit eben solcher Gründlichkeit in einem weiteren Bande der Theorie der hier ausgesparten Themen der Controlled-Source annehmen mögen. **Falko Kuhnke**

Kanasewich, E.R.: Time Sequence Analysis in Geophysics. University of Alberta Press, Edmonton, Canada, 3rd ed., 1981.

The third edition of this excellent textbook has been revised and appreciably extended to 480 pages. Five new chapters have been added as indicated below on subjects which were at most touched very briefly in the earlier editions. A few useful computer subroutines (FORTRAN) have been imbedded in the text. The book costs 30 Dollars (Canadian, I suppose) and for that price it is a real bargain. The quality of the make-up leaves nothing to be desired.

The sequence of subjects treated by the author is as follows: introduction, convolution, Fast Fourier transforms, Laplace transform, transfer function of linear systems, correlation and covariance, power spectrum and periodogram, aliasing, power spectral estimation, joint spectral analysis on two data sets, maximum entropy methods, maximum likelihood methods, properties of filters and minimum delay concept, deconvolution, band pass filters, wave propagation in layered media and filter theory, velocity filters, velocity spectra, polarization analysis, homomorphic deconvolution and cepstral analysis (new), Hilbert transforms (new), digital data acquisition and conversion (new), Walsh transform and data compression (new), and a chapter on generalized linear inverse theory (new). Seven useful appendices on subjects like Fourier transforms, delta functions, Wiener-Hopf equation, stationary time series and white noise, windows, filter stability and the Cooley-Tukey algorithm extend the information contained in the main text appreciably and could as well have been chapters in the book.

The list above looks complete to the scientist or student interested in time series analysis not only in geophysics. But it seems that longperiod seismology in a wide sense is excluded from geo-

physics by the author and this hurts a little. There is not even a single reference to the tricky methods for the analysis of dispersed wave-trains (surface wave seismology), namely time-frequency spectra and the more generally interesting implications of causality of linear systems on the relation between attenuation and dispersion. The modern methods of analysis of a sum of decaying cosinusoids (free oscillations) are not mentioned, although this very field is used as one of the prime examples of the importance of time series analysis in geophysics in the introductory chapter. The book does not contain a single reference to the analysis of tides. This shortcoming is especially sad, because these missing items comprise very interesting types of time series, a treatment of which could make the book very interesting to the nonseismologist. At least there should be references to these methods in the introduction or somewhere else. Of course, the addition of the chapter on generalized linear inverses could be said to contain implicitly some of the not discussed subjects (tides are usually analyzed by least squares).

Besides this obviously biassed look at geophysics from the point of view of an applied or short-period seismologist the book must be highly recommended to the student, the teacher and researcher in time series analysis including geophysics. **Walter Zürn**

Journal of Geophysics Zeitschrift für Geophysik

General Index Volumes 1 (1924)–50 (1982)

Managing Editors

W. Dieminger, G. Müller, J. Untiedt

Editorial Board

K.M. Creer Edinburgh, Scotland
W. Dieminger Lindau, F.R.G.
C. Kisslinger Boulder, Colorado
Th. Krey Hannover, F.R.G.
G. Müller Frankfurt, F.R.G.
G.C. Reid Boulder, Colorado
U. Untiedt Münster, F.R.G.
S. Uyeda Tokyo, Japan

Advisory Board

G. Angenheister, München
A. A. Ashour, Cairo
H.-J. Burkhardt, Berlin
K. Fuchs, Karlsruhe
N. Fukushima, Tokyo
H. Gebrande, München
V. Haak, Berlin
W. Jacoby, Frankfurt a.M.
T. Kirsten, Heidelberg
I. P. Kosminskaja, Moskwa
G. Kremser, Lindau
W. Lowrie, Zürich
St. Müller, Zürich
F. Neubauer, Köln
H. Neugebauer, Clausthal-Zellerfeld
F. Rummel, Bochum
S. Saxov, Aarhus
U. Schmucker, Göttingen
M. Siebert, Göttingen
H. Soffel, München
H. Stiller, Potsdam
P. Weidelt, Hannover
J. Zschau, Kiel

Springer International

Journal of Geophysics – Zeitschrift für Geophysik

This journal was founded by the Deutsche Geophysikalische Gesellschaft on the initiative of L. Mintrop in 1924 as the Zeitschrift für Geophysik and edited by G. Angenheister from Vol. 1–18 (1944). It reappeared in 1954 edited by B. Brockamp from Vol. 19–26 (1960), and edited by W. Dieminger from Vol. 27–33 (1961), and from Vol. 34 (1968) edited by W. Dieminger and J. Untiedt. After Vol. 40 (1970) the title was changed to Journal of Geophysics – Zeitschrift für Geophysik.

Published: Vols. 19–39 by Physica-Verlag, Würzburg, from Vol. 40 by Springer Berlin, Heidelberg, New York, Tokyo.

Copyright

Submission of a manuscript implies that the work described has not been published before (except in the form of an abstract or as part of a published lecture, review or thesis), that it is not under consideration for publication elsewhere, that its publication has been approved by all the authors and by the responsible authorities – tacitly or explicitly – in the laboratories where the work was carried out and that, if accepted, it will not be published elsewhere in the same form, in either the same or another language, without the consent of the copyright holders. By submitting a manuscript, the authors agree that the copyright for their article is transferred to the publisher if and when the article is accepted for publication. The copyright covers the exclusive rights to reproduce and distribute the article, including reprints, photographic reproductions, microform, electronic data-base, video-disks, or any other reproductions of similar nature, and translations.

Photographic reproduction, microform, electronic data-base, video-disks, or any other reproduction of text, figures, or tables from this journal is prohibited without permission obtained from the publisher.

The use of general descriptive names, trade names, trade marks, etc., in this publication, even if the former are not specifically identified, is not to be interpreted as exempt from the relevant protective laws and regulations.

Special Regulations for the USA

The Article Fee Code on the first page of an article in this journal indicates the copyright owner's consent that in the USA copies may be made for personal or internal use, provided the stated fee for copying beyond that permitted by Section 107 or 108 of the United States Copyright Law is paid through the Copyright Clearance Center, Inc., 21 Congress Street, Salem, Mass. 01970, USA.

If a code does not appear, copies of the article may be made without charge, provided permission is obtained from the publisher.

The copyright owner's consent does not extend to copying for general distribution, for promotion, for creating new works, or for resale. Specific written permission must be obtained from the publisher for such copying.

Other Regulations

Authors of this journal can benefit from library and photocopy fees collected by VG WORT if certain conditions are met. If an author lives in the Federal Republic of Germany or in West Berlin it is recommended that he contact Verwertungsgesellschaft WORT, Abteilung Wissenschaft, Goethestraße 49, D-8000 München 2, for detailed information.

Springer-Verlag Berlin Heidelberg New York

Printed in Germany by Universitätsdruckerei H. Stürtz AG Würzburg

© Deutsche Geophysikalische Gesellschaft, Clausthal-Zellerfeld, 1983

General Index Vols. 1–50

For the use of the index:
Please note that in the citations the first figure is the volume number and the second figure the page number. The volumes were published in the following years:

Vol. 1 (1924/25)
Vol. 2 (1926)
Vol. 3 (1927)
Vol. 4 (1928)
Vol. 5 (1929)
Vol. 6 (1930)
Vol. 7 (1931)
Vol. 8 (1932)
Vol. 9 (1933)
Vol. 10 (1934)
Vol. 11 (1935)
Vol. 12 (1936)
Vol. 13 (1937)
Vol. 14 (1938)
Vol. 15 (1939)
Vol. 16 (1940)
Vol. 17 (1941/42)
Vols. 18–20 (1943–1954)
Vol. 21 (1955)
Vol. 22 (1956)
Vol. 23 (1957)
Vol. 24 (1958)
Vol. 25 (1959)
Vol. 26 (1960)
Vol. 27 (1961)
Vol. 28 (1962)
Vol. 29 (1963)
Vol. 30 (1964)
Vol. 31 (1965)
Vol. 32 (1966)
Vol. 33 (1967)
Vol. 34 (1968)
Vol. 35 (1969)
Vol. 36 (1970)
Vol. 37 (1971)
Vol. 38 (1972)
Vol. 39 (1973)
Vol. 40 (1974)
Vol. 41 (1975)
Vol. 42 (1976)
Vol. 43 (1977)
Vol. 44 (1977)
Vol. 45 (1978)
Vol. 46 (1979)
Vol. 47 (1980)
Vol. 48 (1980)
Vol. 49 (1981)
Vol. 50 (1981)

Aase, S., see Storetvedt, K.M., et al. 46:319
Abrahamsen, N., see Saxov, S. 32:455
Achtermann, E., Freden, S.C., Hovestadt, D.: Time Variation of Low Energy Protons in the Inner Radiation Belt 36:27
Achtermann, E., Häusler, B., Hovestadt, D., Scholer, M.: The Solar Particle Event of March 1970 as Observed Over the Polar Cap and in the Radiation Belt with Satellite GRS-A/AZUR 37:211
Ackemann, M.: Untersuchung von Sekundäreffekten der kosmischen Ultrastrahlung bei großen Bleidicken 11:154
Ackerl, F.: Die Ergebnisse der Entwicklung des Schwerkraftfeldes der Erde nach Kugelfunktionen bis zur 16. Ordnung. (Das Geoid, II.) 9:263
Ackerl, F.: Stellungnahme zu dem vorangehenden Aufsatz des Herrn Dr. K. Jung 9:325
Ádám, A., Märcz, F., Verö, J., Wallner, Á., Duma, G., Gutdeutsch, R.: Magnetotelluric Sounding in the Transitional Zone Beetween the Eastern Alps and Pannonian Basin 50:37
Adloff, J.P., see Haïssinsky, M. 34:633
Ahorner, L.: Einige Bemerkungen zum Aufbau der Erdkruste in West-Deutschland auf Grund von Nahbeben-Untersuchungen 33:193
Ahorner, L., Murawski, H., Schneider, G.: Die Verbreitung von schadenverursachenden Erdbeben auf dem Gebiet der Bundesrepublik Deutschland 36:313
Ahorner, L., Rosenhauer, W.: Probability Distribution of Earthquake Accelerations with Applications to Sites in the Northern Rhine Area, Central Europe 41:581
Ahorner, L., Rosenhauer, W.: Seismic Risk Evaluation for the Upper Rhine Graben and Its Vicinity 44:481
Akascheh, B.: Mechanismus des Bebens vom 10. April 1972 in Qir (Iran) 39:1055
Akasheh, B.: Travel Time Residuals in the Iranian Plateau 41:281
Akasheh, B., Eshghi, I., Soltanian, R.: The Iranian Long Period Array (ILPA) 42:159
Akhmetjev, M.A., see Zverev, S.M., et al. 47:191
Aki, K.: Three Dimensional Seismic Velocity Anomalies in the Lithosphere. Method and Summary of Results 43:235
Albert, G.: The Magnetic Anomaly of the Ivrea-Zone 40:283
Albrecht, F.: Der Wärmeumsatz durch die Wärmestrahlung des Wasserdampfes in der Atmosphäre 6:421
Albrecht, F.: Kalorimetrische Filtermessungen der Sonnen- und Himmelsstrahlung in engen Spektralbereichen 12:308
Alekseev, A.S., Mikhailenko, B.G.: The Solution of Dynamic Problems of Elastic Wave Propagation in Inhomogeneous Media by a Combination of Partial Separation of Variables and Finite-Difference Methods 48:161
Alekseev, A.S., see Romanow, M.E. 48:173
Alekseevskaya, M., Gabrielov, A., Gel'fand, I., Gvishiani, A., Rantsman, E.: Formal Morphostructural Zoning of Mountain Territories 43:227
Alfano, L., see Hunsche, U., et al. 49:26
Aliverti, G.: Quantitative Bestimmungen des Luftgehaltes an Radium-Thoriumemanation mittels einer neuen elektrischen Ausströmungsmethode 9:16
Aliverti, G.: Über die indirekten emanometrischen Aliverti- und Gerdien-Methoden 16:284
Alt, E.: Der Stand des meteorologischen Strahlungsproblems 5:385
Alvarez, W., see Lowrie, W. 45:417
Amann, V., see Bangert, W. 44:165
Anders, W.: Untersuchungen von Gesteinen mit ferrimagnetischen Mineralen mittels der Resonanz der Spin-Präzession der die Erscheinung des Ferromagnetismus bewirkenden Elektronen 37:443
Anderson, D.L., see Hart, R.S. 43:503
Anderson, K.A.: Intensity and Energy Spectrum of Electrons Accelerated in the Earth's Bow Shock 40:701
Anderssen, R.S., see Wang, C., et al. 45:129
Andreae, H.: Hydrometrische Verfahren und Fernmeßgeräte, ihre Aufgaben im Dienste der Landeskultur. (H. Pleiss) 28:247
André, D., Baumjohann, W.: Joint Two-Dimensional Observations of Ground Magnetic and Ionospheric Electric Fields Associated with Auroral Currents – 5. Current System Associated with Eastward Drifting Omega Bands 50:194
Andrée, K., Andrée, K.: Die geophysikalische Warte der Albertus-Universität 8:479
Angenheister, A., Pohl, J.: The Remanent Magnetization of the Suevite from the Ries Area (Southern Germany) 30:258
Angenheister, G.: Schallbeobachtungen in Göttingen während der Sprengungen in Jüterbog am 24. Juli 1924 1:20
Angenheister, G.: Das Polarlichtspektrum und die Konstitution der polaren Atmosphäre 1:70

Angenheister, G.: Die Laufzeit des Schalles für große Entfernungen 1:314
Angenheister, G.: Beobachtungen bei Sprengungen 3:28
Angenheister, G.: Nachruf auf Louis Agricola Bauer 8:253
Angenheister, G.: Alfred Wegeners letzte Grönlandfahrt 8:480
Angenheister, G.: Beziehung zwischen Meereshöhe und Schwere in gestörten Gebieten 14:219
Angenheister, G.: Bestimmung einer Grenzfläche durch Laufzeiten oder Richtungswinkel reflektierter Wellen 17:309
Angenheister, G.: Kolloquium zum Thema: Gesteinsmagnetismus 30:37
Angenheister, G., Bunninghoff, A., Beurlen, K., Hildebrandt, K., Wolf, K.L.: Zeitschrift für die gesamte Naturwissenschaft einschl. Naturphilosophie und Geschichte der Naturwissenschaft und Medizin 11:163
Angenheister, G., Consbruch, C. v.: Pulsationen des erdmagnetischen Feldes in Göttingen von 1953–1958 27:3
Angenheister, G., Consbruch, C. v.: Pulsationen des erdmagnetischen Feldes in Göttingen von 1953–1958. II 27:103
Angenheister, G., Huebner, W.: Geology and Allied Sciences. A Thesaurus and a Coordination of English and German Specific and General Terms. Part I, German-English 16:93
Angenheister, G., see Kohlschütter, E., et al. 8:480
Angenheister, G., see RRISP Working Group 47:228
Ansel, A.: Die Alpen im Lichte ihrer Schwerestörung 1:36
Ansel, A.: Erwiderung zum Aufsatz von R. Schwinner [1:166] 1:167
Ansel, A.: Schollengleichgewicht und Schwerestörungen 2:209
Ansel, E.A.: Bemerkungen zu den Ausführungen von H. Jung 6:178
Ansel, E.A.: Erwiderung zu der Arbeit von H. Schmehl 9:261
Ansel, E.A.: Erwiderung zu Apsen: Ausrechnung von Drehwaagebeobachtungen 17:198
Ansorge, J., Mueller, St.: The *P*-Wave Structure of the Uppermost Mantle in Europe Based on Long-Range Explosion Observations 39:385
Antony-Spies, P., see Drisler, J. 41:1
Apps, K.S., see Rostoker, G. 49:163
Apsen, B.: Über die Ausrechnung der zweiten partiellen Ableitungen des Schwerepotentials aus den Drehwaagebeobachtungen nach der Methode der kleinsten Quadrate 17:188
Araschmid, A.: Über die Bündelung von Geophonen in der Refraktionsseismik 28:185
Argence, E.: Methoden zur Bestimmung der wahren Höhen der Ionosphährendichten 20:91
Argence, E.: Kritische Betrachtung der Wellenausbreitung in einem isotropen, absorbierenden Medium 21:1
Argence, E., see Rawer, K. 20:84
Aric, K.: Reflexionsseismische Messungen im Skagerrak 34:223
Ariç, K.: Über die Struktur des Reykjanes-Rückens nach den Ergebnissen reflexionsseismischer Messungen (Brief an den Herausgeber) 36:229
Aric, K., Hirschleber, H.B., Weigel, W.: Ergebnisse seismischer Messungen im Bereich der Großen Meteor-Bank 34:531
Arnold, F., Krankowsky, D., Marien, K.H., Joos, W.: A Mass Spectrometer Probe for Composition and Structure Analysis of the Middle Atmosphere Plasma and Neutral Gas 44:125
As, J.A.: The Compensation Method for Measuring the Components of the Earth's Magnetic Field 39:303
Ashour, A.A.: The Effect of the Earth's Conductivity on Ionospheric Shielding 35:269
Auer, F., Berckhemer, H., Oehlschlegel, G.: Steady State Creep of Fine Grain Granite at Partial Melting 49:89
Axford, W.I., see Ryan, J.M. 41:221

Babuška, V.: Anisotropy in the Upper Mantle Rocks 38:461
Babuška, V.: Anisotropy of v_p and v_s in Rock-Forming Minerals 50:1
Babuška, V., see Pros, Z. 33:289
Babuška, V., see Pros, Z., et al. 35:287
Bachem, H.C., see Makris, J., et al. 39:279
Backus, G., Mulcahy, M.: Phenomenological Representation of Seismic Sources 43:497
Baksi, S.S., see Roy, K.K. 42:521
Balensiefer, E., Büttner, K., Pfleiderer, H., Wetzel, W.: Untersuchungen über die Bodenunruhe auf Sylt 15:337
Balling, N.P.: Geothermal Models of the Crust and Uppermost Mantle of the Fennoscandian Shield in South Norway and the Danish Embayment 42:237
Bamford, D.: Refraction Data in Western Germany – A Time-Term Interpretation 39:907
Bamford, D.: Interpretation of Wide-Angle Reflection Travel-Times in Realistic Crust-Mantle Structures 44:219
Bamford, D., see Kaminski, W., et al. 42:103
Banerjee, S.K., Butler, R.F., Stout, J.H.: Magnetic Properties and Mineralogy of Exposed Oceanic Crust on Macquarie Island 40:537
Bangert, W., Amann, V.: Measurements of the $O_2(^1\Delta_g)$ Height Profile During a Winter Anomaly Event 44:165
Baranskiy, L.N., Troitskaya, V.A., Sterlikova, I.V., Gokhberg, M.B., Ivanov, N.A., Khartchenko, I.P., Münch, J.W., Wilhelm, K.: The Analysis of Simultaneous Observations of Nighttime Pi Pulsations on an East-West Profile 48:1
Baransky, L., see Kangas, J., et al. 46:237
Barcilon, V.: On Impulse Response Data and the Uniqueness of the Inverse Problem 43:139
Bärnreuther, H.: Beobachtung eines Nordlichtes am 3. Januar 1940 16:89
Barnstorf, H., see Neubauer, F.M., et al. 42:599
Barta, G.: Über die Säkularbewegung des magnetischen Zentrums 24:197
Bartels, J.: Nachruf Prof. Nippoldt 12:279
Bartels, J.: Aufschlüsse über die Ionosphäre aus der Analyse sonnen- und mondentägiger erdmagnetischer Schwankungen 12:368
Bartels, J.: Vorankündigung der diesjährigen Tagung der Deutschen Geophysikalischen Gesellschaft vom 20. bis 22. Oktober in Jena 14:48
Bartels, J.: Potsdamer erdmagnetische Kennziffern. I 14:68
Bartels, J.: Potsdamer erdmagnetische Kennziffern. II 14:230
Bartels, J.: Potsdamer erdmagnetische Kennziffern. III 14:272
Bartels, J.: Besprechung erdmagnetischer Registrierungen im Hinblick auf Vorgänge in der Ionosphäre und Wirkungen in der Höhenstrahlung 14:297
Bartels, J.: Aussprachebemerkung zum Vortrag Fanselau (über Filchner) 15:6
Bartels, J.: Potsdamer erdmagnetische Kennziffern. IV 15:214
Bartels, J.: Potsdamer erdmagnetische Kennziffern. V 15:333
Bartels, J.: Sonnenstrahlung und Erdmagnetismus 16:101
Bartels, J.: Die magnetische Großstörung vom 1. März 1941 17:56
Bartels, J.: Potsdamer erdmagnetische Kennziffern. XIII 18:76
Bartels, J.: Potsdamer erdmagnetische Kennziffern. XIV 18:180
Bartels, J., Burger, A.: Potsdamer erdmagnetische Kennziffern. XII 17:317
Bartels, J., Fanselau, G.: Geophysikalischer Mond-Almanach 13:311
Bäte, J., Becker, M., Niederlöhner, U., Papanikas, D.G.: Pitot Pressure Measurements for Atmospheric Density Determination Between 50 and 120 km (Western Europe Winter Anomaly Campaign, January 1976) 44:147
Bauer, S.J., see Lämmerzahl, P. 40:571
Baumgardt, D.R.: Errors in Matrix Element Expressions for the Reflectivity Method 48:124
Baumjohann, W., Greenwald, R.A., Küppers, F.: Joint Magnetometer Array and Radar Backscatter Observations of Auroral Currents in Northern Scandinavia 44:373
Baumjohann, W., see Untiedt, J., et al. 45:41
Baumjohann, W., see Mersmann, U., et al. 45:281
Baumjohann, W., see Küppers, F., et al. 46:429

Baumjohann, W., see Sulzbacher, H., et al. 48:7
Baumjohann, W., see Brüning, K., et al. 49:74
Baumjohann, W., see Wilhelm, K., et al. 49:128
Baumjohann, W., see Gustafsson, G., et al. 49:138
Baumjohann, W., see Inhester, B., et al. 49:155
Baumjohann, W., see André, D. 50:194
Baur, F.: Der gegenwärtige Stand der meteorologischen Korrelationsforschung 5:391
Baur, F.: Über die Notwendigkeit eines großen Beobachtungsstoffes bei statistischen Untersuchungen 9:11
Beblo, M.: Ein transportabler, netzunabhängiger Elektrograph für Dauerregistrierungen des induzierten erdelektrischen Feldes 38:133
Beblo, M., Björnsson, A.: Magnetotelluric Investigation of the Lower Crust and Upper Mantle Beneath Iceland 45:1
Beblo, M., Björnsson, A.: A Model of Electrical Resistivity Beneath NE-Iceland, Correlation with Temperature 47:184
Becker, H.: Magnetic Anomalies (ΔZ) in NE-Iceland and Their Interpretation Based on Rock-Magnetic Investigations 47:43
Becker, H., Förster, H., Soffel, H.: Central Iran Former Part of Gondwanaland? Palaeomagnetic Evidence from Infra Cambrian Rocks and Iran Ores of the Bafq Area, Central Iran 39:953
Becker, H., see Soffel, H., et al. 41:541
Becker, J.J., see Ghazi, A., et al. 37:641
Becker, L.: Die Bewegung der Kontinente und die Köppen-Wegenersche Polkurve 15:379
Becker, M., see Bäte, J., et al. 44:147
Behle, A., Ehrismann, W., Makris, J., Menzel, H., Morelli, C., Rosenbach, O.: Gravimetrische Untersuchungen in den Ostalpen I (Meßgebiet Mittenwald-Innsbruck-Verona) 38:45
Behle, A., Ehrismann, W., Makris, J., Menzel, H., Rosenbach, O., Steinhauser, P.: Gravimetrische Untersuchungen in den Ostalpen II (Meßgebiet Salzburg-Kärnten-Tirol) 38:221
Behle, A., Rohde, J.: Ultrasonic Modelling of a Moving Source 42:131
Behnke, C.: Über Speicherung mehrerer durch Flüssigkeitsfunken erzeugter seismischer Impulse auf einem einzigen magnetischen Tonträger 26:24
Behnke, C., see Giese, P., et al. 33:215
Behrendt, J.C., Bentley, C.R.: Magnetic and Gravity Maps of the Antarctic. (H.A. Roeser) 36:111
Behrens, J.: Refraktionsseismische Messungen auf See 26:161
Behrens, J., Bortfeld, R., Gommlich, G., Köhler, K.: Interpretation of Discontinuities by Seismic Imaging 38:481
Behrens, J., Dresen, L.: Ein experimentelles Verfahren zur Eliminierung von Störsignalen bei modellseismischen Untersuchungen 32:232
Behrens, J., Dresen, L.: Eine Möglichkeit zur Laufzeitbestimmung reflektierter Wellen im Bereich der kritischen Entfernung 35:175
Behrens, J., Dresen, L., Hinz, E.: Modellseismische Untersuchungen der dynamischen Parameter von Kopfwelle und Reflexion im überkritischen Bereich 35:43
Behrens, J., Gommlich, G.: Model Investigations with Respect to the Interpretation of Complicated Seismic Discontinuities 38:659
Behrens, J., Shamina, O.G., Waniek, L.: Interpretation of Discontinuities by Seismic Modelling Methods (Invited Paper) 38:579
Behrens, J., Siebels, J.: Model Investigations on Low Velocity Layers 38:627
Behrens, J., Waniek, L.: Modellseismik (Übersichtsartikel) 38:1
Behrens, J., Weigel, W.: Bemerkungen zu Blubberbeobachtungen bei sprengseismischen Messungen auf See 33:131
Behrens, W.V., see Jung, W. 11:162
Beiersdorf, H., see Heye, D. 39:703
Beinroth, H.J., see Neubauer, F.M., et al. 42:599
Belluigi, A.: Über ein geoelektrisches inverses Problem 21:135
Belluigi, A.: Asymptotische Formeln zur Bestimmung des von einer oder von mehreren Elektroden im geschichteten Boden hervorgerufenen Potentials 23:135, 182
Belluigi, A.: Das skalare durch einen rechteckigen Impuls in einem homogenen Medium erzeugte Potential 24:380
Belluigi, A.: Neue Theorie für elektrische Sondierungen 25:113
Benfield, A.E.: Note on the Variation of Gravity with Depth 13:157
Benndorf, H.: Über die nächsten Aufgaben luftelektrischer Forschung 1:147
Benning, W.: A Comparison of Methods for Computing Surface Densities of the Geopotential from Satellite Altimetry 41:501
Bentley, C.R., see Behrendt, J.C. 36:111
Bentz, A.: Drehwaagemessungen im Ries bei Nördlingen: I. Geologische Einführung 7:1
Bentz, A.: Lehrbuch der angewandten Geologie, Erster Band: Allgemeine Methoden: Kartierung, Petrographie, Paläontologie, Geophysik, Bodenkunde. (H. Menzel) 28:244
Beran, D., Suckfüll, E.: Intensity Measurement of the (1,0) γ-Band of NO at 2,150 Å with a Polarizing Nitric Oxide Photometer 44:155
Beránek, B., Dudek, A.: The Results of Deep Seismic Sounding in Czechoslovakia 38:415
Berckhemer, H.: MARS 66. Eine Magnetbandapparatur für seismische Tiefensondierung 36:501
Berckhemer, H.: A Possible Scattering Mechanism for Lunar Seismic Waves 36:523
Berckhemer, H., Hiller, W.: Kurzperiodische Stationsseismographen mit Trägerfrequenzverstärker und mechanischer Registrierung 26:1
Berckhemer, H., Müller, S., Sellevoll, M.: Die Krustenstruktur in Südwestdeutschland aus Phasen-Geschwindigkeitsmessungen an Rayleigh-Wellen 27:151
Berckhemer, H., Oliver, J.: Zur Deutung seismischer Einsätze mit parallelen Laufzeitkurven 21:152
Berckhemer, H., see Schneider, G., et al. 32:383
Berckhemer, H., see Herminghaus, Ch. 40:341
Berckhemer, H., see Auer, F., et al. 49:89
Bérczi, Sz., see Stegena, L. 40:775
Berg, A.P. van den, Cloetingh, S.A.P.L., Doornbos, D.J.: A Comparison of PKP Precursor Data from Several Seismic Arrays 44:499
Berg, H.: Zur Struktur des erdmagnetischen Störungscharakters 19:12
Berger, R., see Procházková, D., et al. 46:343
Berktold, A.: Erste Auswertung von Messungen des zeitlich variablen erdmagnetischen Feldes entlang eines Profiles vom Oberpfälzer Wald bis zu den Kitzbüheler Alpen 32:492
Bernhardt, F., Philipps, H.: Angenäherte Berechnungen der vertikalen, langwelligen Strahlungsströme G und U in Abhängigkeit von einer vorgegebenen Feuchteverteilung, einer vorgegebenen vertikalen Kohlensäureverteilung und einer vorgegebenen vertikalen Temperaturverteilung (E. Raschke) 33:146
Berroth, A.: Schweremessungen mit zwei und vier gleichzeitig auf demselben Stativ schwingenden Pendeln 1:89
Berroth, A.: Referenzpendelmessungen am Salzhorst Oldau-Hambühren (Hann.) 3:1
Berroth, A.: Beitrag zur Theorie und Praxis der Referenzpendel-Messungen unter Anwendung von Minimumpendeln 8:30
Berroth, A.: Theorie einiger gravimetrischer Instrumente nach dem Prinzip der bifilaren Aufhängung 8:331
Berroth, A.: Eine praktische Möglichkeit der Triangulationsverbindung mit dem amerikanischen Kontinent 9:145
Berroth, A.: Geometrische Lösung der Grundaufgaben der in der Geologie angewandten Seismik 13:87
Berroth, A.: Gravitationsfeld und Oberflächengestalt der Erde und ihre geometrische Festlegung 13:133
Berroth, A.: Numerische Werte der Masse und Dichte der Erde sowie ihrer Hauptträgheitsmomente 18:42

Berroth, A.: Das Lebenswerk des überragenden Meisters der Erdmessung Friedrich Robert Helmert 18:87
Berroth, A.: Über die Lage der physischen Erdpole 18:106
Berroth, A.: Das Schwerefeld des Harzes 18:109
Berroth, A., Schleusener, A.: Erdmagnetische Messungen mit Hilfe der Drehwaage 9:355
Berteussen, K.A.: Crustal Structure and *P*-Wave Travel Time Anomalies at NORSAR 41:71
Berteussen, K.A.: *P* Wave Amplitude Variability at NORSAR 41:595
Beuermann, W.: Untersuchung der Schallausbreitung bei Unterwasserexplosionen 8:1
Beurlen, K.: Mitteilung über die Fachgliederung Bodenkunde (Geologie, Mineralogie, Geophysik) im Reichsforschungsrat 13:131
Bewersdorff, A.: Der Einfluß der Entmischung auf remanente Magnetisierung von Titanomagnetiten 27:215
Beyer, M., see Knoechel, H., et al. 17:57
Bhattacharya, J., Das Gupta, S.C.: On Leaking Modes Coupled with Shear Waves 29:101
Bhimasankaram, V.L.S., see Rao, S.M.V., et al. 44:353
Bibl, K.: Die Ionosphärenschichten und ihre dynamischen Phänomene 19:136
Bibl, K.: Zur Dynamik der Ionosphäre 24:1
Bibl, K., Delobeau, F.: Ionosphärische Beobachtungen während der totalen Sonnenfinsternis vom 30. Juni 1954 21:215
Bilitza, D.: Effective Energy Reception of the Electron Gas per Created Ion Electron Pair 46:35
Bilitza, D., see Spenner, K., et al. 46:57
Bindel, E.: Johannes Kepler. Beiträge zu seinem Lebensbild. (H. Schwentek) 37:755
Binder, O.: Untersuchungen von Intensitätsschwankungen der kosmischen Strahlung im Periodenbereich zwischen 20 und 28 h 35:565
Biot, A.: Remarques sur les Microseismes 1:262
Biquand, D., Prévot, M.: Demagnetization of Viscous Remanent Magnetization in Rocks 37:471
Bird, M.K., see Volland, H., et al. 42:659
Bistricsany, E.: On the Problem of Magnitude Determination 24:153
Biswas, A.: Propagation of Love-Type Waves in Heterogeneous Elastic Layers 42:137
Bitterlich, W., Wöbking, H.: Eine Methode zur direkten Bestimmung der sogenannten „Geometrischen Tortuosität" 36:607
Bitterlich, W., Wöbking, H.: Versuch einer Einteilung von Gesteinen nach gefügekundlichen und elektrischen Größen 36:743
Bjerknes, V.: Leipzig-Bergen, Festvortrag zur 25-Jahrfeier des Geophysikalischen Instituts der Universität Leipzig 14:49
Björnsson, A.: Aufzeichnung und Auswertung erdmagnetischer Pulsationen in Island und Göttingen 35:419
Björnsson, A., Hillebrand, O., Voelker, H.: First Observational Results of Geomagnetic pi2 and pc5 Pulsations on a North-South Profile Through Europe 37:1031
Björnsson, A., see Beblo, M. 45:1, 47:184
Björnsson, A., see Jacoby, W.R., et al. 47:1
Björnsson, A., see Johnsen, G.V., et al. 47:132
Björnsson, S., see RRISP Working Group 47:228
Björnsson, S.B., see Israël, H. 33:48
Blei, D.F.: Natural Electromagnetic Phenomena below 30 kc/s. (G. Lange-Hesse) 31:282
Bleil, U.: Cation Distribution in Titanomagnetites 37:305
Bleil, U., see Petersen, N. 39:965
Bleil, U., see Hornemann, U., et al. 41:13
Bleil, U., see Pohl, J., et al. 41:23
Blinn, L., see Keen, C.E., et al. 47:265
Bloh, J. v., Rammner, R.: Beiträge zur Abschätzung der Leistungsfähigkeit geoelektrischer Meßapparaturen für Gleichstrom-Vierpunktmessungen 34:183
Blohm, E.K., Worzyk, P., Scriba, H.: Geoelectrical Deep Soundings in Southern Africa Using the Cabora Bassa Power Line. Preliminary Results 43:665
Blohm, E.-K., see Homilius, J. 39:441
Blum, R., Bock, G., Fuchs, K., Merkler, G., Widmann, R.: Correlation Between Micro-Activity and Variation of Water Level at the Schlegeis-Reservoir 43:561
Blut, H.: Ein Beitrag zur Theorie der Reflexion und Brechung elastischer Wellen an Unstetigkeitsflächen 8:130, 305
Bock, D., see Rössler, F. 35:485
Bock, G.: Load-Induced Stresses and Their Relation to the Initial Stress Field 48:94
Bock, G., Soffel, H.: Paleomagnetic Investigation on Igneous Rocks from the Rhön, Germany 37:581
Bock, G., see Blum, R., et al. 43:561
Bock, G., see Merkler, G., et al. 49:198
Bock, R.: Über die Schmidtsche Methode der Bestimmung der Parameter von Stabmagneten 4:227
Bock, R.: Theorie einer neuen galvanischen Waage 6:251
Bock, R.: Planung und Verlauf der magnetischen Reichsvermessung 1934/1935 11:357
Bock, R.: Über die Magnetische Reichsvermessung II. Ordnung und ihre ersten vorläufigen Ergebnisse 15:66
Boedecker, G.: An Economically Working Method for Computing the Gravimetric Terrain Correction 41:513
Boesch, A., see Koulomzine, T. 8:166
Böhm, J.: Measurements of MeV-Electrons During the Recovery-Phase of a Polar Magnetic Substorm on March 6, 1970 38:291
Böhnecke, G., see Schulz, B. 12:399
Boldt, B., see Leppin, M. 44:557
Boldyrev, S.A., see Zverev, S.M., et al. 44:283
Bolle, H.-J.: Satellite Techniques for Observing Water Vapor-Height Profiles (Übersichtsartikel) 36:1
Bondaletoff, N., see Koulomzine, T. 10:85
Bonjer, K.-P., Fuchs, K., Wohlenberg, J.: Crustal Structure of the East African Rift System from Spectral Response Ratios of Long-period Body Waves 36:287
Bonjer, K.-P., Kaminski, W., Kind, R.: Seismic Observations in Germany of a 10 t Explosion off Scotland 40:259
Bonjer, K.-P., see Makris, J., et al. 36:387
Bonjer, K.-P., see Müller, G., et al. 44:203
Bonner, F., see Krankowsky, D., et al. 40:601
Booth, D.C., see Jacob, A.W.B. 43:687
Borchers, R., see Widdel, H.U., et al. 44:179
Borisevič, E.S.: Sowjetische Geräte für die Erdbebenregistrierung 33:425
Borm, G.: Über den Schwimmzustand bei sehr großen Massen (Ein Beitrag zur Isostasiefrage) 37:707
Borm, G.: Zur Theorie eines Netzwerkmodells für geoelektrische Analogmessungen 38:791
Borm, G.: Solutions of Boundary Value Problems of Multilayer Analogs of Geoelectrics and Hydrology 39:41
Born, A.: Die Schwereverhältnisse auf dem Meere auf Grund der Pendelmessungen von Prof. Vening Meinesz 1926 3:400
Börsken, N., see Schmidtke, G., et al. 49:146
Bortfeld, R., see Behrens, J., et al. 38:481
Boschi, E., Mulargia, F.: Equation of State of Liquid Iron at the Earth's Core Conditions 43:465
Bose, K.: A Wave Theory for the Generation of *T*-Waves 30:235
Bose, K.: The Vertical Component of *Lg* and *Rg* 30:294
Bose, S.K.: A Wave Theory for the Generation of Love, G and S_a Waves 29:215
Bose, S.K.: Generation of *Lg*-Waves and *S*-Velocity Distribution in the Crust 31:1
Bose, S.K.: Notes on Wave Theories for the Propagation of T-, Lg-, G-Waves and Microseisms from Storms Over Deep Sea 36:193
Bösinger, T., see Novikov, Yu.P., et al. 48:116
Bossolasco, M.: Das Strömungssystem der Luft über Mogadischu 10:360

Bossy, L.: Wave Propagation in Stratified Anisotropic Media. An Algorithm for the Computation of the Reflection and Transmission Coefficients as Well as of the Fields 46:1
Bosum, W.: Erdmagnetische Messungen im Deckdiabasgebiet der Dillmulde und ihre Auswertung 26:144, 177
Bosum, W., Hahn, H.: Diagrams for the Computation of Magnetic Field Components, for Their Transformation into one Another and for Their Upward Continuation (Two-dimensional Case) 32:1
Bosum, W., Kind, E.G.: Die magnetische Anomalie von SOEST 38:749
Bott, M.H.P., Gunnarsson, K.: Crustal Structure of the Iceland-Faeroe Ridge 47:221
Bourmin, V.Yu., see Zverev, S.M., et al. 44:283
Bowen, R.: Paleotemperature Analysis. (P. Zedler) 33:213
Bradenstein, H.J., see Spenner, K., et al. 44:81
Braile, L.W., see Frese, R.R.B. von, et al. 49:234
Bram, K.: New Heat Flow Observations on the Reykjanes Ridge 47:86
Bram, K., Giese, P.: Die Geschwindigkeitsverteilung der P-Wellen in der Erdkruste im Raum Augsburg (Süd-Deutschland). Ergebnisse und Vergleiche zweier seismischer Messungen 34:611
Brand, J.: Beiträge zum Studium der Bodenbewegung nicht seismischen Ursprungs 1:348
Brandsdóttir, B., see Einarsson, P. 47:160
Breyer, F.: Die topographische Reduktion der Lotabweichungen am Nanga Parbat mit Hilfe eines Diagramms 15:229
Breyer, H.: Über die Elastizität von Gesteinen 6:98
Breymann, U.: Magnetotelluric Investigation of a Nearly Circular Saltdome in Northern Germany 42:391
Brinca, A.L.: The Geocyclotron Revisited: Potentialities of Modulated Wave Injection 49:245
Brinkmann, R.: Über petrographisch-geophysikalische Grenzfragen 1:143
Brinkmann, R.: Über einige Beziehungen zwischen Magmenaufstieg und Tektonik 2:138
Brinkmann, R., Born, A.: Der geologische Aufbau der Erde 9:171
Brinkmann, R., Fairshild, H.L.: The Geological Society of America 1888–1930 9:171
Briske, R.: Gemeinschaftliche Arbeit zwischen Seismologen und Baufachmann zur Verringerung von Erdbebenschäden 4:219
Brockamp, B.: Seismische Untersuchungen auf dem Pasterzegletscher. II 7:232
Brockamp, B.: Seismische Beobachtungen bei Steinbruchsprengungen 7:295
Brockamp, B.: Über einige Ergebnisse der vom Geodätischen Institut Kopenhagen durchgeführten seismischen Feldarbeiten in Dänemark 11:89
Brockamp, B.: Zur hypsographischen Kurve des Mondes 26:271
Brockamp, B.: Die Luftdruckschwankungen zu Münster/W., die durch die Explosion einer Bombe am 30.10.1961 über Nowaja Semlja verursacht wurden 28:157
Brockamp, B.: Barographisch-topographische Höhenkurve 28:219
Brockamp, B., Mothes, H.: Seismische Untersuchungen auf dem Pasterzegletscher. I 6:482
Brockamp, B., Rüter, H.: Die Abhängigkeit der elastischen Parameter des Eises von hydrostatischem Druck bis zu 400 bar 35:277
Brockamp, B., Wölcken, K.: Bemerkungen zu den Beobachtungen bei Steinbruchsprengungen 5:163
Brockamp, B., u. Mitarbeiter: Eisseismische Untersuchungen 23:241
Brockhaus, K., Joksch, H.C.: Bestimmung der hypsometrischen Kurve des Mondes aus Beobachtungen von J. Franz 26:9
Brocks, K.: Wechselwirkung Ozean-Atmosphäre (Übersichtsartikel) 38:675
Bromann, P.: Registrierung und Auswertung seismischer Ereignisse. (K. Strobach) 35:103
Broße, B.: Die seismische Bestimmung der Grundwassertiefe 23:236
Bruce, J.P., Clark, R.H.: Introduction to Hydrometeorology. (A. Baumgartner) 33:369
Brückl, E., Fürlinger, W.: Ein Vergleich von geologischen Gefügeaufnahmen mit seismischen Messungen 39:291
Brüning, K., Baumjohann, W., Wilhelm, K., Stüdemann, W., Urban, A., Ott, W., Spenner, K., Schmidtke, G.L., Fischer, H.M.: Application of Different Methods for the Determination of Ionospheric Conductivities from Sounding Rocket Observations 49:74
Brunner, W.: Tägliche Sonnenflecken-Relativzahlen für das 1. Vierteljahr 1938 14:108
Brunner, W.: Tägliche Sonnenflecken-Relativzahlen für das 2. Vierteljahr 1938 14:232
Brunner, W.: Tägliche Sonnenflecken-Relativzahlen für das 3. Vierteljahr 1938 14:274
Brunner, W.: Tägliche Sonnenflecken-Relativzahlen für das 4. Vierteljahr 1938 15:222
Brunner, W.: Tägliche Sonnenflecken-Relativzahlen für das 1. Vierteljahr 1939 15:223
Brunner, W.: Tägliche Sonnenflecken-Relativzahlen für das 2. Vierteljahr 1939 15:336
Brunner, W.: Tägliche Sonnenflecken-Relativzahlen für das 3. Vierteljahr 1939 16:87
Brunner, W.: Tägliche Sonnenflecken-Relativzahlen für das 4. Vierteljahr 1939 16:195
Brunner, W.: Tägliche Sonnenflecken-Relativzahlen für das 1. Vierteljahr 1940 16:196
Brunner, W.: Tägliche Sonnenflecken-Relativzahlen für das 2. Vierteljahr 1940 16:250
Brunner, W.: Tägliche Sonnenflecken-Relativzahlen für das 3. Vierteljahr 1940 16:332
Brunner, W.: Tägliche Sonnenfleckenrelativzahlen für das 4. Vierteljahr 1940 17:70
Brunner, W.: Tägliche Sonnenfleckenrelativzahlen für das 1. Vierteljahr 1941 17:71
Brunner, W.: Tägliche Sonnenfleckenrelativzahlen für das 2. Vierteljahr 1941 17:149
Brunner, W.: Tägliche Sonnenfleckenrelativzahlen für das 3. Vierteljahr 1941 17:230
Brunner, W.: Tägliche Sonnenfleckenrelativzahlen für das 4. Vierteljahr 1941 17:328
Brunner, W.: Tägliche Sonnenfleckenrelativzahlen für das 1. Vierteljahr 1942 17:329
Brunner, W.: Tägliche Sonnenfleckenrelativzahlen für das 2. Vierteljahr 1942 17:330
Brunner, W.: Tägliche Sonnenfleckenrelativzahlen für das 3. Vierteljahr 1942 17:331
Brunner, W.: Tägliche Sonnenflecken-Relativzahlen für das 4. Vierteljahr 1942 18:183
Brunner, W.: Tägliche Sonnenflecken-Relativzahlen für das 1. Vierteljahr 1943 18:184
Brunner, W.: Tägliche Sonnenflecken-Relativzahlen für das 2. Vierteljahr 1943 18:185
Brunner, W.: Tägliche Sonnenflecken-Relativzahlen für das 3. Vierteljahr 1943 18:186
Buchar, E., see Knoechel, H., et al. 17:57
Buchheim, W.: Das magnetische Feld einer geradlinigen Wechselstromleitung auf homogen leitendem Untergrund 19:124
Buchheim, W.: Anwendungen der Methode der induzierten Polarisation an schwedischen Erzlagerstätten 23:26
Budde, E.: Bestimmung des Beweglichkeitskoeffizienten der Radiumemanation in Lockergesteinen 24:96
Budde, E.: Der Beweglichkeitskoeffizient der Radium-Emanation in Lockergesteinen 26:72
Büdeler, W., see Knoechel, H., et al. 17:57
Bullard, E.C.: Note on the Hayford-Bowie Tables for Calculating g 10:318

Bullen, K.E.: An Introduction to the Theory of Seismology. (H. Burkhardt) 31:223
Bunch, A.W.H.: Crustal Development of the Reykjanes Ridge from Seismic Refraction 47:261
Bungers, R.: Zum 2-Schichten-Problem der angewandten Seismik 11:207
Bungers, R.: Bestimmung von Schichtneigungen aus dem Emergenzstrahl bei Sprengungen 11:326
Bungers, R.: Theorie der Schwebungen 12:229
Bungers, R.: Neuere Untersuchungen über Schwingungsformen in der angewandten Seismik 12:347
Bungers, R.: Zur Methodik der Nahbebenbearbeitung 15:160
Bungers, R.: Die Überlagerung zweier Wellen verschiedener Herkunftsrichtung 15:321
Bungers, R.: Die geodätischen, gletscherkundlichen und geographischen Ergebnisse der Deutschen Himalaja-Expedition 1934 zum Nanga Parbat 16:89
Bungers, R.: Analyse eines mikroseismischen Sturmes 17:114
Bungers, R., Baur, E.: Einführung in die Großwetterforschung 17:337
Bungers, R., Jung, K.: Kleine Erdbebenkunde 15:227
Bungers, R., Kähler, K.: Wolken und Gewitter 17:73
Bungers, R., Kirsch, G.: Geomechanik 15:228
Bungers, R., Raethjen, P.: Einführung in die Physik der Atmosphäre 17:336
Bungers, R., Sirk, H.: Einführung in die Mathematik für Chemiker und Naturwissenschaftler 17:73
Bungers, R., Thorade, H.: Ebbe und Flut 17:72
Bungum, H., Risbo, T., Hjortenberg, E.: Precise Continuous Monitoring of Seismic Velocity Variations 43:501
Buntebarth, G.: Modellberechnungen zur Temperatur-Tiefen-Verteilung im Bereich der Alpen und des Alpenvorlandes 39:97
Buntebarth, G.: Über die Größe der thermisch bedingten Bouguer-Anomalie in den Alpen 39:109
Buntebarth, G.: A Short History on the Naming of the Discipline Geophysics 49:247
Burek, P.J.: An Advanced Device for Chemical Demagnetization of Red Beds 37:493
Burger, A.: Potsdamer erdmagnetische Kennziffern 16:85, 185, 247
Burger, A.: Potsdamer erdmagnetische Kennziffern. IX 17:67
Burger, A.: Potsdamer erdmagnetische Kennziffern. X 17:147
Burger, A.: Potsdamer erdmagnetische Kennziffern. XI 17:226
Burger, A., see Bartels, J. 17:317
Burkard, O.: Ein geomagnetischer Längeneffekt der F-Schicht-Ionisation 17:51
Burkard, O.: Studie zum geomagnetischen Effekt der F_2-Schicht 20:75
Burkard, O.: Ionosphärenbeobachtungen zur Sonnenfinsternis am 15. Febr. 1961 29:123
Burkard, O.M.: Statistische Zusammenhänge zwischen Sonnenwind und Ionosphäre 39:739
Burkard, O.M., Rucker, H.: Correction of Graphs Concerning the Chapman-Ferraro Image Method 45:219
Burkhardt, H., Keller, F., Müller, G., Rosenbach, O., Vees, R.: Bemerkungen zur Einsatzmöglichkeit der Magnetband-Refraktionsapparaturen MARS 66 in großen Registrierentfernungen 33:455
Burkhardt, H., Vees, R.: Explosions in Shallow Water for Deep Seismic Sounding Experiments 41:463
Burkhart, K.: Mikropulsationen des Erdstromes und der erdmagnetischen Horizontalkomponenten 21:57
Burkhart, K.: Zur Messung der Inklination mit Kippspule und langperiodischem Galvanometer 23:41
Burmeister, F.: Die Säkularvariation in der Rheinpfalz in den Jahren 1850 bis 1928 6:186
Burmeister, F.: Die Entwicklung der erdmagnetischen Forschung in Bayern 9:236
Burmeister, F.: Über die Bestimmung der Temperatur eines schwingenden Magneten 16:125
Burmeister, F.: Über die Verwendung von Photozellen bei Messungen der Schwingungsdauer von Magneten 18:123
Burmeister, F., Bock, R.: Praxis der magnetischen Messungen 18:193
Busse, F.H.: Bewegungen im Kern der Erde (Übersichtsartikel) 37:153
Busse, F.H.: An Example of Nonlinear Dynamo Action 43:441
Butler, R.F., see Banerjee, S.K., et al. 40:537
Büttner, K., Chromow, S.P.: Einführung in die synoptische Wetteranalyse 17:334
Büttner, K., Linke, F.: Meteorologisches Taschenbuch 8:111, 9:355
Büttner, K., see Balensiefer, E., et al. 15:337
Bykov, A.M., Toptyghin, I.N.: The Theory of Particle Acceleration in Astrophysical Objects Containing Shock Waves and Turbulent Plasma Motions 50:221

Calcagnile, G., Panza, G.F.: Crustal and Upper Mantle Structure Beneath the Apennines Region as Inferred from the Study of Rayleigh Waves 45:319
Calcagnile, G., Panza, G.F., Schwab, F., Kausel, E.: On the Computation of Theoretical Seismograms for Multimode Surface Waves 43:502
Caldwell, J.R., see Spencer, N.W., et al. 40:613
Caloi, P.: The Crust of the Earth, from the Apennines to the Atlantic, Reconstructed in Accordance with the Data Supplied by Seismic Surveys 24:65
Caner, B., Dragert, H.: Instrumentation for Wide-Frequency-Band (0.01 to 100 Millihertz) Geomagnetic Induction Work 38:121
Caputo, M.: Ein graphisches Verfahren für die Berechnung der vertikalen Komponente der Anziehungskraft zylindrischer Körper und dessen Anwendung für die Bestimmung der Gestalt von Gletscherbetten 24:359
Caputo, M.: The Gracity Field of the Earth from Classical and Modern Methods. (G. Müller) 35:214
Carignan, G.R., see Spencer, N.W., et al. 40:613
Carmichael, C.M.: A Test of Paleomagnetic Intensity Methods Using Recent Lavas and Implications for Anomaly Interpretation 40:489
Caspar, M.: Johannes Kepler. (H. Schwentek) 37:754
Cassebaum, H., see Jeske, H., et al. 36:621
Cassell, B.R., Fuchs, K.: Seismic Investigations of the Subcrustal Lithosphere Beneath Fennoscandia 46:369
Casten, U., Hedebol Nielsen, P.: Faeroe Islands – a Microcontinental Fragment? 41:357
Casten, U., Hirschleber, H.: Seismic Measurements in Jutland 1969 37:47
Cermák, V.: Heat Flow of the Bohemian Massif 42:455
Červený, V.: Theory of Elastic Wave Propagation in Inhomogeneous Media (Invited Paper) 38:469
Červený, V.: Accuracy of Ray Theoretical Seismograms 46:135
Červený, V.: Ray Theoretical Seismograms for Laterally Inhomogeneous Structures 46:335
Červený, V., Kozák, J.: Experimental Evidence and Investigation of Pseudospherical Waves 38:617
Červený, V., Pšenčík, I.: Rays and Travel-Time Curves in Inhomogeneous Anisotropic Media 38:565
Červený, V., Zahradník, J.: Amplitude-Distance Curves of Seismic Body Waves in the Neighbourhood of Critical Points and Caustics – A Comparison 38:499
Cevolani, G., Dardi, D.: Zonal Meteor Wind Observations at Budrio, Italy 50:212
Chalmers, J.A.: Atmospheric Electricity. (K. Höschele) 35:213
Chamalaun, F.H., White, A.: Electromagnetic Induction at Dili, Portuguese Timor 41:537
Chamberlain, J.W.: Physics of the Aurora and Airglow. (W. Dieminger) 28:51
Chander, R.: On Tracing Seismic Rays with Specified End Points 41:173
Chang, F.-S., see Knopoff, L. 43:299

Channell, J.E.T.: Dual Magnetic Polarity Measured in a Single Bed of Cretaceous Pelagic Limestone from Sicily 44:613
Channell, J.E.T., Freeman, R., Heller, F.: Magnetic Properties of Swiss Flysch 48:60
Channell, J.E.T., Zanche, V. De, Sedea, R.: Reappraisal of Palaeomagnetism of the Colli Euganei and Monti Lessini Volcanics (Italy) 45:29
Channell, J.E.T., see Heller, F. 46:413
Chapman, C.H., Dey Sarkar, S.K.: A First-Motion Alternative to Geometrical Ray Theory 43:504
Chapman, S.: On the Determination of the Lunar Atmospheric Tide 6:396
Chapman, S.: Ozone and Water Vapor in the Atmosphere 12:377
Chapman, S.: Geophysics and Germany, Men and Enterprises 36:393
Charleton, P., see Rees, D., et al. 50:202
Chatterjee, N.D.: Paläomagnetische Untersuchungen an ladinischen Eruptiven der westlichen Dolomiten, Norditalien 31:90
Choudhury, M.A.: P-Wave Attenuation in the Mantle 38:447
Choy, G.L.: Theoretical Seismograms of Core Phases Calculated by a Frequency-Dependent Full Wave Theory, and Their Interpretation 43:506
Christensen, U.: Numerical Experiments on Convection in a Chemically Layered Mantle 49:82
Christoskov, L.: On the Amplitude Curves of Body Waves for Short Epicentral Distances and Their Oscillatory Character 38:429
Cipa, W.: Kurzbericht über einige erdmagnetische Untersuchungen an Lavaströmen und Tuffschloten in der Vordereifel 21:48
Cisternas, A., Jobert, G.: Extension of Matrix Methods to Structures with Slightly Irregular Stratification 43:59
Čižek, V.: Restoration of the Input Signal of a Linear Dynamic System 39:501
Clark, R.H., see Bruce, J.P. 33:369
Clarke, G.K.C., see Dragert, H. 42:373
Classen, J., see Knoechel, H., et al. 17:57
Cleary, J.R., see Wang, C., et al. 45:129
Cloetingh, S.A.P.L., see Berg, A.P. van den, et al. 44:499
Cloos, E.: Auto-Radio als Hilfsmittel geologischer Kartierung 10:252
Closs, H.: In Memorian Hermann Reich 42:547
Closs, H., Morelli, C.: Seismic Experiments in the Dolomits (Lago Lagorai) to Investigate the Earth's Crust in the Eastern Alpine Area 28:249
Collette, B.J., Verhoef, J., Mulder, A.F.J. de: Gravity and a Model of the Median Valley 47:91
Conrad: Zum Vergleich von Sonnenscheinregistrierungen an Orten mit verschieden geformtem natürlichen Horizont 7:134
Conrad, V.: Der jährliche Gang der Erdbebenhäufigkeiten und sekundär auslösenden Ursachen der Erdbeben 1:191
Conrad, V.: Dynamische Geologie 1:265
Conrad, V.: Die Erdbebenwarten von Deutschland u. Österreich im Jahre 1925 1:285
Conrad, V.: Laufzeitkurven eines alpinen Bebens 2:34
Conrad, V.: Zur Frage des Schemas zur Auswertung von Seismogrammen 2:168
Conrad, V.: Erdbeben, Mondphasen, Sonnenflecken 2:309
Conrad, V.: Das Schwadorfer Beben vom 8. Oktober 1927 4:286
Conrad, V.: Bemerkungen zum Neuseelandbeben vom 16. Juni 1929 5:253
Consbruch, C. v., see Angenheister, G. 27:3, 103
Cook, M.A.: Prehistory and Earth Models (Vorgeschichte und Erdmodelle). (A. Hahn) 34:103
Cormier, V.F., Richards, P.G.: Full Wave Theory Applied to a Discontinuous Velocity Increase: The Inner Core Boundary 43:3
Coroniti, S.C., Dolezalek, H., Israël, H.: On the Electrical Feature of the Upper-Stratosphere and Mesosphere 27:301
Courtot, P., see Procházková, D., et al. 46:343
Courvoisier, L.: Über die Polhöhenschwankungen infolge der Lorentz-Kontraktion der Erde 4:49
Cowley, A.D., see Haurwitz, B. 36:771
Crampin, S.: Seismic Anisotropy – a Summary 43:499
Crampin, S., Kirkwood, S.C.: Velocity Variations in Systems of Anisotropic Symmetry 49:35
Crampin, S., Yedlin, M.: Shear-Wave Singularities of Wave Propagation in Anisotropic Media 49:43
Creer, K.M.: Geophysical Interpretation of Remanent Magnetization in Oxidized Basalts 37:383
Creer, K.M., Hogg, T.E., Readman, P.W., Reynaud, C.: Palaeomagnetic Secular Variation Curves Extending Back to 13,400 Years B.P. Recorded by Sediments Deposited in Lac de Joux, Switzerland. Comparison with U.K. Records 48:139
Creer, K.M., Petersen, N.: Thermochemical Magnetization in Basalts 35:501
Creytz, D. v.: Die Gezeiten- und Luftdruckwirkung im überfluteten Reichenbergschacht 30:140
Critikos, N.A.: Über die Ursachen der mikroseismischen Bodenunruhe von 4 bis 8 sec Periode in Athen 7:22
Critikos, N.A.: Ein Horizontalseismometer für die Aufzeichnung von starken Orts- und Nahbeben 10:265
Cumme, G., Knuth, R., Wagner, C.-U.: A Method for the Interpretation of Ionospheric Absorption Measurements During the Sunrise Effect in the D-Region 36:57
Czechowsky, P.: Berechnung eines Stromsystems in der polaren E-Region (Brief an den Herausgeber) 36:647
Czechowsky, P.: Doppler Shift of Auroral Backscatter Signals 40:229
Czechowsky, P., Kochan, H., Lange-Hesse, G., Lauche, H., Möller, H.G.: Simultane Beobachtungen verschiedener ionosphärischer Phänomene während des erdmagnetischen Sturmes von 31. Oktober bis 2. November 1968 36:77
Czechowsky, P., see Untiedt, J., et al. 45:41

Dahlblom, T.: The Increase of the Temperature Downwards in the Crust of Rocks 14:131
Dahlen, F.A., Smith, M.L.: The Influence of the Core and the Oceans on the Chandler Wobble 43:497
Dainty, A.M., Toksöz, M.N.: Elastic Wave Propagation in a Highly Scattering Medium. A Diffusion Approach 43:375
Damaske, D.: On the Annual Wave of Hemispheric Geomagnetic Activity 45:81
Damaske, D., Meyer, J.: Comment on: On the Sources of the 12-Month Wave in the *an* and *as* Geomagnetic Activity Indices by P.N. Mayaud, J. Geophys. 46, 261–271, 1979 48:54
Damaske, D., see Meyer, J. 49:66
Daragan, S.K.: Design of High Precision Long Period Seismic Channels 39:567
Dardi, D., see Cevolani, G. 50:212
Das Gupta, S.C., see Bhattacharya, J. 29:101
Dasgupta, S.N., see Vincenz, S.A., et al. 39:727, 1067
Das Gupta, S.P.: Effect of Low Velocity Layer in Earthquakes 33:1
Datta, B.K.: Das Spektrum seismischer Wellen bei der Reflexion an einer Übergangsschicht 33:80
David, E.: Materie im Erdinnern 20:1
David, E.: Dynamische Kompressibilität für hohe Drücke 25:239
David, E.: Bemerkung zur Arbeit „Der Zuwachs des Erdradius" von G. Eder 32:173
David, E.: Großmeteoriteneinschläge und Tektite 32:539
Davydova, N.I., Kosminskaya, I.P., Kapustian, N.K., Michota, G.G.: Models of the Earth's Crust and M-Boundary 38:369
Dawes, G.J.K., see Hobbs, B.A. 46:273
Defant, A.: Die Gezeitenströme und die inneren Gezeitenwellen des Atlantischen Ozeans 9:63

Defant, A.: Zur Dynamik des antarktischen Bodenstromes im Atlantischen Ozean 11:50
Defant, A.: Entstehung und Erhaltung der troposphärischen Sprungschicht 12:281
Défourneaux, M., see Müller, W.F. 34:483
Dehmel, G., see Neubauer, F.M., et al. 42:599
Dehmel, G., see Wilhelm, K., et al. 49:128
Deist, H.J., Dohr, G.: Untersuchungen über Perioden von Erdbebenwellen in Abhängigkeit von Herdgebiet und -entfernung 23:34
Delobeau, F., see Bibl, K. 21:215
Demnati, A., Dohr, G.: Reflexionsseismische Tiefensondierungen im Bereich des Oberrheintalgrabens und des Kraichgaues 31:229
Dempewolf, W., see Münch, J. 37:627
Denskat, K.U., Neubauer, F.M.: The Propagation of Plasma Waves in the Jovian Magnetosphere 43:511
Deutsch, E.R., see Radhakrishnamurty, C. 40:453
Deutsch, E.R., see Radhakrishnamurty, C., et al. 45:433
Dey Sarkar, S.K., see Chapman, C.H. 43:504
Dieminger, W.: Erdmagnetismus und Ionosphäre 20:167
Dieminger, W.: In Memoriam Julius Bartels 30:113
Dieminger, W.: „METEOR" Forschungsergebnisse, Reihe A, Nr. 2. Hrsg. Deutsche Forschungsgemeinschaft 33:463
Dieminger, W., Hartmann, G.K.: Problems in the Investigation of Space and Time Dependent Media Exemplified by the Ionosphere 42:447
Dieminger, W., Plendl, H.: Ergebnisse von Dauerregistrierungen der Ionosphäre 14:315
Dieterichs, H.: Ein mechanisch registrierendes Vertikalanemometer und seine Verwendung im Gelände 13:179
Dietrich, G.: Das „ozeanische Nivellement" und seine Anwendung auf die Golfküste und die atlantische Küste der Vereinigten Staaten von Amerika 12:287
Dietrich, G.: In memoriam Karl Brocks 38:811
Dietrich, G., see Wooster, W.S., et al. 35:611
Dietze, G.: Intensität und Polarisation des Zenitlichtes im Laufe der Dämmerung. (Czerwinski) 36:777
Dizioğlu, M.Y.: A Method for Determining True Chargeabilities of Vertical Discontinuities and Its Application to Some Types of Lead-Zinc Ores in Turkey 34:37
Dobberstein, H.: Eichung von Schallempfängern (Undographen und Membranapparate) 11:102
Dobberstein, H.: Eichung von Fernschallempfängern (Undographen und Membranapparate) 11:362
Dobberstein, H.: Ein photoelektrischer Schwingungsmesser 13:123
Doe, B.R.: Lead Isotopes. (I. Wendt) 38:965
Dohr, G.: Perioden der ersten Vorläufer in Göttinger Seismogrammen 21:165
Dohr, G.: Statistischer Nachweis von Gezeiten in Binnenseen, dargestellt am Beispiel des Bodensees 23:256
Dohr, G.: Über die Beobachtung von Reflexionen aus dem tieferen Untergrunde im Rahmen routinemäßiger reflexionsseismischer Messungen 25:280
Dohr, G.: Reflexionsseismische Tiefensondierung (Übersichtsartikel) 38:193
Dohr, G., see Deist, H.J. 23:34
Dohr, G., see Demnati, A. 31:229
Dolezalek, H.: Die Problematik luftelektrisch-synoptischer Betrachtung 24:268
Dolezalek, H.: On the Measurement of Mobility and Conductivity in the Mesosphere 28:239
Dolezalek, H.: Der radioaktive Kollektor bei luftelektrischen Sondierungen 30:43
Dolezalek, H.: On the Measurement of Electric Fields in Space 32:318
Dolezalek, H., Oster, A.L.: Ion-Spectrometer for the Terrestrial Mesosphere and the Atmosphere of Mars 32:163
Dolezalek, H., see Israel, H. 26:77
Dolezalek, H., see Coroniti, S.C., et al. 27:301
Doornbos, D.J., see Vermeulen, J.M. 43:545
Doornbos, D.J., see Berg, A.P. van den, et al. 44:499
Dorman, L.M., see Orcutt, J.A. 43:257
Dose, V., Schmocker, U., Sele, G.: Auroral Lyman-Alpha Emission 42:15
Dragert, H.: A Field Evaluation of Caner's Broad-Band Geomagnetic Induction Instrumentation 40:121
Dragert, H., Clarke, G.K.C.: A Detailed Investigation of the Canadian Cordillera Geomagnetic Transition Anomaly 42:373
Dragert, H., see Caner, B. 38:121
Drecker: Zeitmessung und Sterndeutung in geschichtlicher Darstellung 2:208
Drescher, A.: A Two Channel Rocket Photometer for 5,577 Å Ol Nightglow Measurements 44:173
Dresen, L.: Amplitudenuntersuchungen an seismischen Wellen zur Charakterisierung von Verwitterungsschichten mit vertikalem Geschwindigkeitsanstieg 37:71
Dresen, L., Freystätter, S.: Rayleigh Channel Waves for the In-Seam Seismic Detection of Discontinuities 42:111
Dresen, L., see Behrens, J. 32:232, 35:175
Dresen, L., see Behrens, J., et al. 35:43
Dresen, L., see Freystätter, S. 43:807
Drewes, H., see Schleusener, A., et al. 42:27
Drewes, H., see Torge, W. 43:771
Drimmel, J., Fiegweil, E., Lukeschitz, G.: Macroseismic Intensity Map of Austria for the Swabian Alb Earthquake of September 3, 1978 45:341
Drimmel, J., Gangl, G., Gutdeutsch, R., Koenig, M., Trapp, E.: Modellseismische Experimente zur Interpretation makroseismischer Daten aus dem Bereich der Ostalpen 39:21
Drimmel, J., see Procházková, D., et al. 46:343
Drisler, J., Antony-Spies, P.: Statistical Behaviour of Elastic Waves in a Reverberating Solid 41:1
Drygalski, E. v.: Über Grundeis 11:109
Duckert, P.: Zur Erforschung der höheren Atmosphärenschichten 5:377
Duckert, P.: Ergebnisse der Hörbeobachtungen des Sprengversuchs in Oldebroek am 15. Dezember 1932 10:119
Duckert, P.: Die Wetterlage und die Schichtung der Atmosphäre am 15. Dezember 1932, dem Sprengtag von Oldebroek. 10:127
Duckert, P.: Ergebnisse der Registrierungen von Schallwellen an kreisförmig um den Sprengherd angeordneten Stationen 10:197
Duda, S.J.: Phänomenologische Untersuchung einer Nachbebenserie aus dem Gebiet der Alëuten-Inseln 27:207
Duda, S.J., see Upadhyay, S.K. 48:67
Dudek, A., see Beránek, B. 38:415
Duma, G., see Ádám, A., et al. 50:37
Dumbs, A., see Spenner, K. 40:585
Dunlop, D.J.: Thermal Enhancement of Magnetic Susceptibility 40:439
Dürschner, H.: Über den Reflexionscharakter und die Laufzeitkurven nach Geschwindigkeitslogs 27:188
Dürschner, H.: In Memoriam Ulrich Fleischer 44:281
Dutta, S.: Note on the Propagation of Love-Waves in a Two-Layer Heterogeneous Medium 31:200

Ebel, A.: Zeitliche Variation und Genauigkeit bei der Bestimmung der Höhenveränderlichkeit geomagnetischer Elemente, abgeleitet aus Normalfeldern für Mitteleuropa 34:87
Ebel, A., Hartmann, G., Leitinger, R., Schmidt, G., Schödel, J.P.: Vergleichende Auswertung von Faraday-Effekt-Beobachtungen zweier Empfangsstationen 35:373
Ebert, A., see Haalck, H. 8:409
Edel, J.B.: Dominating Trends of the Anomalies of the Gravity and Magnetic Fields in NE France and SW Germany 40:781

Edel, J.-B.: Palaeomagnetic Study of the Tertiary Volcanics of Sardinia 45:259
Edel, J.B., Fuchs, K., Gelbke, C., Prodehl, C.: Deep Structure of the Southern Rhinegraben Area from Seismic Refraction Investigations 41:333
Edelmann, H.: Methoden der Erzeugung seismischer Energie auf See 34:513
Edenhofer, P., Esposito, P.B., Hansen, R.T., Hansen, S.F., Lüneburg, E., Martin, W.L., Zygielbaum, A.I.: Time Delay Occultation Data of the Helios Spacecrafts and Preliminary Analysis for Probing the Solar Corona 42:673
Eder, G.: Der Zuwachs des Erdradius 31:206
Egedal: Über die Bestimmung der atmosphärischen Mondgezeiten 7:191
Egedal, J.: Über eine Verbindung zwischen den mondentägigen und den sonnentägigen Variationen der magnetischen Deklination 4:155
Egedal, J.: Über die Existenz einer mondentägigen Variation in den Erdströmen 6:157
Egedal, J.: Über die Herleitung des Potentials des täglichen erdmagnetischen Variationsfeldes 6:263
Egedal, J.: Über eine Messung der Bewegung von Pfeilern 8:195
Egyed, E., Stegena, L.: Physical Background of a Dynamical Earth Model 24:260
Egyed, L.: Physik der festen Erde (M. Toperczer) 37:756
Ehmert, A., Revellio, K.: Solare Ultrastrahlung und jonosphärische D-Schicht am 23. Febr. 1956 23:113
Ehrismann, W.: Ein allgemeines Verfahren zur digitalen Berechnung der Schwerewirkung von Modellkörpern 39:131
Ehrismann, W., Leppich, W., Lettau, O., Rosenbach, O., Steinhauser, P.: Gravimetrische Detail-Untersuchungen in den westlichen Hohen Tauern 39:115
Ehrismann, W., see Behle, A., et al. 38:45, 221
Eichler, D., see Ellison, D.C., et al. 50:110
Eichmeier, J.: Die theoretischen Grundlagen und das Auflösungsvermögen von Aspirations-Beweglichkeitsspektrographen für atmosphärische Ionen 34:69
Eichmeier, J.: Beitrag zum Problem der Struktur der atmosphärischen Kleinionen 34:297
Eichmeier, J.: Ionenbahnen in einem platten- und zylinderförmigen Aspirationskondensator bei ebenem bzw. parabolischem Luftgeschwindigkeitsprofil 36:753
Eichmeier, J.: Vergleich der Beweglichkeitsspektren von „natürlichen" Luftionen und der verwendeten Meßverfahren 38:915
Eiden, R., Eschelbach, G.: Das atmosphärische Aerosol und seine Bedeutung für den Energiehaushalt der Atmosphäre (Übersichtsartikel) 39:189
Einarsson, P., Brandsdóttir, B.: Seismological Evidence for Lateral Magma Intrusion During the July 1978 Deflation of the Krafla Volcano in NE-Iceland 47:160
Einarsson, P., see Foulger, G. 47:171
Einarsson, P., see RRISP Working Group 47:228
Einarsson, P., see Gebrande, H., et al. 47:239
Eisemann, E.: Der nächtliche Anstieg der *F*-Schicht der Ionosphäre. Seine Synopsis und Deutung 32:280
Elling, W., see Schwentek, H. 44:27
Ellison, D.C., Jones, F.C., Eichler, D.: Monte Carlo Simulation of Collisionless Shocks Showing Preferential Acceleration of High A/Z Particles 50:110
Embleton, B.J.J., see Schmidt, P.W. 49:20
Enescu, D., see Müller, G., et al. 44:203
Engel, K.H., see Raeuber, A. 33:212
Engelhard, L.: Absorptionszellen-Magnetometer (Übersichtsartikel) 37:1
Engelhard, L.: Geoelektrische und magnetische Messungen im Nördlinger Ries 37:667
Engelhard, L.: Zur Kritik von K. Ernstson an dem Artikel von L. Engelhard über geoelektrische und magnetische Messungen im Nördlinger Ries (Z. Geophys. 37 (4), 667, 1971) (Brief an den Herausgeber) 38:185
Ernst, Rittmann, A.: Vulkane und ihre Tätigkeit 13:348
Ernstson, K.: Bemerkungen zum Artikel von L. Engelhard über geoelektrische und magnetische Messungen im Nördlinger Ries (Z. Geophys. 37 (4), 667, 1971) (Brief an den Herausgeber) 38:183
Ernstson, K.: Geoelektrische Messungen im Nördlinger Ries (Briefe an den Herausgeber) 38:949
Ernstson, K.: The Structure of the Ries Crater from Geoelectric Depth Soundings 40:639
Errulat, F.: Zur Vollendung des siebzigsten Lebensjahres von Herrn Direktor Friedrich Burmeister 26:301
Ertel, H.: Zur Theorie der Maxwellschen Geschwindigkeitsverteilung in turbulenten Strömungen 6:329
Ertel, H.: Polygonale Koordination von Seezufluß und Wasserstand 29:45
Eschelbach, G., see Eiden, R. 39:189
Eshghi, I., see Akasheh, B., et al. 42:159
Eshghi, I., see Sobouti, M., et al. 44:663
Esposito, P.B., see Edenhofer, P., et al. 42:673
Essen, H.-H.: Attenuation Coefficients of Acoustic Normal Modes in Shallow Water 43:569
Essen, H.-H.: Theoretical Investigations on Acoustic Remote Sensing of Ocean Surface Waves 45:183
Essen, H.-H., Hasselmann, K.: Scattering of Low-Frequency Sound in the Ocean 36:655
Essen, H.H., Hirschleber, H.B., Siebert, J.: Geschwindigkeits- und Dämpfungsmessungen an Sedimenten der Nordsee 39:833
Essen, H.-H., Janle, H., Schirmer, F., Siebert, J.: Propagation of Surface Waves in Marine Sediments 49:115
Essen, H.-H., Kebe, H.-W., Siebert, J.: Acoustic Normal Modes Generated by Explosive Sources 41:111
Essers, E., Kappes, T.: Bodenerschütterungen durch Kraftfahrzeuge 3:49
Exner, F.M.: Dynamische Meteorologie 1:263

Faber, S., see Kaminski, W., et al. 42:103
Fabian, P., Libby, W.F.: Ozone in the Atmosphere of Venus (Übersichtsartikel) 35:1
Fabian, P., see Tiefenau, H., et al. 38:145
Fabian, P., see Jessen, W. 39:1023
Faltas, F., see Kamel, M. 12:383
Fanselau, F., Lucke, O.: Über die Veränderlichkeit des erdmagnetischen Hauptfeldes und seine Theorien 22:121
Fanselau, G.: Einfluß des Mondes auf die erdmagnetischen Elemente in Samoa 6:65
Fanselau, G.: Was sagen uns die Parameter eines Magneten? 6:258
Fanselau, G.: Über das elastische Altern von Metallfäden 8:226
Fanselau, G.: Ein neuer Schwingungsmesser 9:93
Fanselau, G.: Erwiderung auf die vorstehende Bemerkung des Herrn Martin 9:170
Fanselau, G.: Über die Homogenität des Magnetfeldes bei symmetrischer Spulenanordnung 9:236
Fanselau, G.: Über den Einfluß der mitschwingenden Luft bei den magnetischen Schwingungsbeobachtungen 12:58
Fanselau, G.: Über Messungen mit dem Quarzfaden-Horizontalintensitätsmagnetometer von la Cour in Potsdam, Seddin und Niemegk 12:192
Fanselau, G.: Einige Bemerkungen zu der magnetischen Störung vom 24. bis 28. April 1937 13:191
Fanselau, G.: Über eine photographische Ableseeinrichtung am Doppelkompaß 13:235
Fanselau, G.: Geophysikalische Arbeiten Prof. Filchners in Inner-Asien 15:1
Fanselau, G.: Vorläufige Ergebnisse der erdmagnetischen Beobachtungen in Niemegk im Jahre 1939 16:181
Fanselau, G.: Vorläufige Ergebnisse der erdmagnetischen Beobachtungen in Niemegk im Jahre 1940 17:213

Fanselau, G.: Vorläufige Ergebnisse der erdmagnetischen Beobachtungen in Niemegk in den Jahren 1941 und 1942 18:78
Fanselau, G.: Über quadratische Mittelwerte des geomagnetischen Potentials 24:320
Fanselau, G., Nippoldt, A.: Erdmagnetismus, Erdstrom und Polarlicht 13:202
Fanselau, G.: In memoriam Otto Lucke 35:615
Fanselau, G., see Bartels, J. 13:311
Fanselau, J.: Einfluß des Mondes auf die erdmagnetischen Elemente in Samoa 6:65
Fechtig, H., see Grün, E., et al. 42:717
Fedtke, C.: Nordlicht 16:88
Fehlhaber, L.: Einfluß außerirdischer Korpuskularströme auf das Magnetfeld der Erde 29:65
Felske, D., see Schmelovsky, K.H. 33:155
Fengler, G.: Progress in Radio Science 1960–1963. Vol 2, Radio and Troposhere 33:294
Ferrari, A., Trussoni, E.: Turbulent Acceleration of Electrons in Extended Extragalactic Radio Sources 50:70
Fertig, J., Müller, G.: Approximate Diffraction Theory for Transparent Half-Planes with Application to Seismic-Wave Diffraction at Coal Seams 46:349
Feussner, K., Friedrichs, H.: Zum Trübungsfaktor 6:159
Fiegweil, E., see Drimmel, J., et al. 45:341
Fiegweil, E., see Procházková, D., et al. 46:343
Fielitz, K.: Elastische Wellengeschwindigkeiten in verschiedenen Gesteinen unter hohem Druck und bei Temperaturen bis 750° C 37:943
Finckh, P., see Herzen, R.P. von, et al. 40:141
Fischer, G.: Die Mitschwinggezeiten der Nordsee, errechnet mit einem Differenzenverfahren 25:186
Fischer, H.-J., see Mühleisen, R., et al. 37:1055
Fischer, H.M., see Brüning, K., et al. 49:74
Fischer, H.M., see Wilhelm, K., et al. 49:128
Fisk, H.W., see Fleming, J.A. 7:74
Flach, D., Große-Brauckmann, W.: Recordings with the Askania Borehole Tiltmeter (Vertical Pendulum) in the Frequency Range of Earth's Free Oscillations 40:355
Flach, D., Große-Brauckmann, W.: An Electronic Filter and Damping System for the Askania Borehole Tiltmeter 41:303
Flach, D., Jentzsch, G., Rosenbach, O., Wilhelm, H.: Ball-Calibration of the Askania Borehole Tiltmeter (Earth Tide Pendulum) 37:1005
Flach, D., Rosenbach, O., Wilhelm, H.: Tidal Analyses of Simultaneous Records Taken by Two Askania Borehole Tiltmeters 37:993
Flathe, H.: In memoriam Franz Hallenbach 32:179
Fleischer, U.: Charakteristische erdmagnetische Baystörungen in Mitteleuropa und ihr innerer Anteil 20:120
Fleischer U.: Shipboard Gravity Measurements 40:1
Fleming, J.A., Fisk, H.W.: On the Distribution of Permanent Repeatstations 7:74
Flemming, G.: Das Klima an Waldbestandsrändern. (K. Höschele) 33:212
Flóvenz, Ó.G.: Seismic Structure of the Icelandic Crust Above Layer Three and the Relation Between Body Wave Velocity and the Alteration of the Basaltic Crust 47:211
Flügge, S.: Handbuch der Physik, Band 47: Geophysik I. (H. Flathe) 28:293
Flüh, E.R., see Meissner, R.O. 45:349
Folkman, Y.: Magnetic and Gravity Investigations of the Dead Sea Rift and Adjacent Areas in Northern Israel 47:34
Forejt, H., see Fritsch, V. 17:217
Formisano, V., Orsini, S.: Acceleration Processes at the Earth's Bow Shock 50:114
Förster, H., see Becker, H., et al. 39:953
Förster, H., see Soffel, H., et al. 41:541
Förtsch, O.: Das Verhalten noch freistehender Brückenpfeiler bei Schwingungen und deren Abhängigkeit vom Untergrund 14:173
Förtsch, O.: Ableitung des von der Frequenz unabhängigen Absorptionskoeffizienten aus Maschinenschwingungen 16:57
Förtsch, O.: Beiträge zur Ausbreitung elastischer Oberflächenwellen 19:59
Förtsch, O.: Ergebnisse seismischer Untersuchungen auf Gletschern der Ostalpen 24:161
Förtsch, O.: Prof. Dr. Hermann Reich zum 75. Geburtstag 32:334
Förtsch, O., Sirk, H.: Einführung in die Mathematik für Chemiker und Naturwissenschaftler 17:337
Foulger, G., Einarsson, P.: Recent Earthquakes in the Hengill-Hellisheidi Area in SW-Iceland 47:171
Franke, A., Gutdeutsch, R.: Macroseismic Estimations of Parameters of Austrian Earthquakes During the Period 1905–1973 40:173
Franke, A., see Seiberl, W., et al. 44:639
Franke, R., see Noßke, G. 24:340
Frankenberger, E., see Wigand, A., et al. 6:458
Franz, J., see Knoechel, H., et al. 17:57
Freden, S.C., see Achtermann, E., et al. 36:27
Freeman, R., see Channell, J.E.T., et al. 48:60
Freiburg, Ch., Kertz, W.: Anordnung von Stabmagneten zur Erzeugung homogener Feldbereiche 26:227
Frese, R.R.B. von, Hinze, W.J., Braile, L.W., Luca, A.J.: Spherical-Earth Gravity and Magnetic Anomaly Modelling by Gauss-Legendre Quadrature Integration 49:234
Freystätter, S., Dresen, L.: Propagation of Rayleigh Channel-Waves in Coal Seams – Modelseismic Investigations 43:807
Freystätter, S., see Dresen, L. 42:111
Fricker, A., see Keen, C.E., et al. 47:265
Fridleifsson, I.B., see Kristjansson, L., et al. 47:31
Friedemann, H.: Von neuen Erfindungen. Meßeinrichtungen für sprengseismische Bodenuntersuchungen 28:47
Friedemann, H.: Patentbericht. Erschütterungsmesser, insbesondere Seismograph 28:155
Friedemann, H.: Von neuen Erfindungen. Verstärkerschaltung zur Reflexionsüberhöhung für seismische Registrierungen 28:239
Friedemann, H.: Von neuen Erfindungen. Anordnung zur Voranzeige bei seismischen Messungen auf See 29:81
Friedemann, H.: Von neuen Erfindungen: Ring für seismische Seemessungen 29:173
Friedemann, H.: Von neuen Erfindungen: Magnetometer zur Messung der Inhomogenitäten des magnetischen Erdfeldes 30:105
Friedrich, M., Torkar, K., Ulrich, S.: A Rocket Borne Experiment to Measure Plasma Densities in the *D*-Region 44:91
Friedrich, V.H., Offermann, D., Trinks, H., Zahn, U. von: The Cryo Mass Spectrometer in the Winter Anomaly Campaign 44:139
Friedrich, W., see Hasse, H., et al. 10:388
Friedrichs: Ein Strahlungskalender 7:349
Friedrichs, H., see Feussner, K. 6:159
Fries†, G., see Israel, H. 20:137
Frisch, W., see Mauritsch, H.J. 44:623
Fritsch, V.: Die Messung der Antennenersatzkapazität in der Funkmutung 14:93
Fritsch, V.: Einiges über die Widerstandsverfahren der Funkmutung 14:260
Fritsch, V.: Die Bedeutung geoelektrischer Faktoren bei der Überprüfung von Blitzableitererden 16:149
Fritsch, V.: Die geoelektrische Untersuchung der Heilwässer in der Umgebung des Neusiedlersees im Burgenland 27:112
Fritsch, V.: Geoelektrische Probleme der elektrischen Bodenverfestigung 32:518
Fritsch, V., Forejt, H.: Die Anwendung des Druckindikators in der Funkmutung 17:217
Fritsch, V., Tauber, A.F.: Geoelektrische Untersuchungen von Salzwasservorkommen 35:161
Fritsch, V., Tauber, A.F.: Zur objektiven Beurteilung der

festigkeitsmechanischen Eigenschaften von Fels durch geoelektrische Messungen 37:293
Fritz, T.A., Williams, D.J.: Wave and Particle Observations by Explorer 45 Pertaining to Wave-Particle Interactions 41:551
Fröhlich, R.K.: Gravity Investigations Over a Salt Structure Near Lübbecke, Northern Germany 37:883
Fröhlich, R.K.: Combined Magnetic and Geoelectrical Investigations Over Lava Flows in the Volcanic Zone of the Laacher See, West Germany 39:263
Frölich, F.: Strukturphysikalische Gesetzmäßigkeiten der Spinelltyp-Oxyde der Erdkruste 22:65
Frölich, F.: Zur magnetischen Stabilität von Erdkrustengesteinen 24:228
Frölich, F., Löffler, H.: Einflüsse auf die Korundtyp-Wechselwirkungen im System Hämatit-Ilmenit 32:26
Frölich, F., Stiller, H., Wagner, Ch.F.: Erfahrungen mit Laborverfahren für Gesteinsuntersuchungen 27:136
Frölich, F., see Stiller, H., et al. 27:89
Frölich, F., see Stiller, H. 30:13
Frölich, F., see Kirsten, G., et al. 33:182
Fuchs, K.: Investigation on the Wave Propagation in Wedge-shaped Media 31:51
Fuchs, K.: Das Reflexions- und Transmissionsvermögen eines geschichteten Mediums mit beliebiger Tiefen-Verteilung der elastischen Moduln und der Dichte für schrägen Einfall ebener Wellen 34:389
Fuchs, K.: On the Properties of Deep Crustal Reflectors 35:133
Fuchs, K.: The Method of Stationary Phase as a Diagnostic Aid in Estimating the Field Pattern of Body Waves Reflected from Transition Zones 35:431
Fuchs, K.: On the Determination of Velocity Depth Distribution of Elastic Waves from the Dynamic Characteristics of the Reflected Wave Field 36:531
Fuchs, K.: The Method of Stationary Phase Applied to the Reflection of Spherical Waves from Transition Zones with Arbitrary Depth-Dependent Elastic Moduli and Density 37:89
Fuchs, K.: The Fine Structure of the Lower Lithosphere – a Possible Marker for Its Vertical Deformation (Briefe an den Herausgeber) 39:313
Fuchs, K.: Synthetic Seismograms of PS-Reflections from Transition Zones Computed with the Reflectivity Method 41:445
Fuchs, K.: Seismic Observations of Structure and Physical Properties of the Subcrustal Lithosphere as Evidence for Dynamical Processes in the Upper Mantle 43:499
Fuchs, K.: Presentation of the Emil Wiechert-Medal to Leon Knopoff, Los Angeles, on March 7, 1978 at Münster 44:567
Fuchs, K., Landisman, M.: Results of a Re-interpretation of the N-S-Refraction Line Adelebsen-Hilders-South in West-Germany 32:121
Fuchs, K., Mayer-Rosa, D., Liebau, F.: Lateral Inhomogeneities of the Earth's Mantle and Their Petrological Interpretation 37:937
Fuchs, K., Schulz, K.: Tunneling of Low-Frequency Waves Through the Subcrustal Lithosphere 42:175
Fuchs, K., see Peterschmitt, E., et al. 31:41
Fuchs, K., see Bonjer, K.-P., et al. 36:287
Fuchs, K., see Makris, J., et al. 36:387
Fuchs, K., see Hirn, A., et al. 39:363
Fuchs, K., see Edel, J.B., et al. 41:333
Fuchs, K., see Blum, R., et al. 43:561
Fuchs, K., see Cassell, B.R. 46:369
Fuchs, K., see Merkler, G., et al. 49:198
Fuckner, J., see Kunow, H., et al. 42:615
Fulks, G., Meyer, P.: Cosmic Ray Electrons in the Atmosphere 40:751
Fuller-Rowell, T.J., see Rees, D., et al. 50:202
Funder, L., see Rössiger, M. 11:75
Fürlinger, W., see Brückl, E. 39:291
Gabrielov, A., see Alekseevskaya, M., et al. 43:227
Galbas, P.A., Marten, W.: Absolute Sonnenstrahlungsmessungen in der freien Atmosphäre im Flugzeug 5:322
Galkin, I.N., Levshenko, V.T., Myachkin, V.I., Nikolayev, A.V.: Inhomogeneity of the Earth with Respect to Physical Processes of Earthquakes 38:455
Gamburzew, G.A.: Grundlagen seismischer Erkundung. (P. Giese) 32:62
Gammelin, P., see Grün, E., et al. 42:717
Gangl, G., see Drimmel, J., et al. 39:21
Gaskell, T.F. (Herausgeber): The Earth's Mantle. (K. Jung) 34:631
Gast, P.: Die hypothesenfreie Bestimmung der Erdfigur mit neuen Hilfsmitteln 9:189
Gebelein, H.: Das abrollende physikalische Pendel 8:272
Gebelein, H.: Störungen von Pendeluhren durch Bodenerschütterungen 9:137
Gebrande, H.: Der Einfluß von Phasenumwandlungen auf Konvektionsströme im Erdmantel 33:297
Gebrande, H., Miller, H., Einarsson, P.: Seismic Structure of Iceland Along RRISP-Profile I 47:239
Gebrande, H., see RRISP Working Group 47:228
Gees, R.H.: Die Wellenausbreitung der Erdbeben vom 20. November 1932 (Nordbrabant) und 7. Juni 1931 (Doggerbank) 13:159
Gehlinsch, E.: Forschungsmethoden über den Zusammenhang zwischen der Sonnenfleckentätigkeit und den erdmagnetischen Störungen 6:271
Geier, S.: Die Berechnung von geoelektrischen Modellkurven bei beliebiger Elektroden-Anordnung auf horizontal geschichteten Medien 24:326
Gelbke, C., see Edel, J.B., et al. 41:333
Gel'fand, I., see Alekseevskaya, M., et al. 43:227
Genschel, G.: Über modellseismische Fallversuche, Fallwerks- und Sprengerschütterungen. Veröffentlichungen des Instituts für Geodynamik Jena, Heft 4 (R. Schick) 33:464
Georgii, W.: Wettervorhersage 1:215
Geranios, A.: The Shape of the Cosmic Ray Modulation Region of the April 30, 1976, Event, as Deduced from HELIOS-1, HELIOS-2, IMP-8, and Neutron Monitor Data 46:171
Geranios, A.: Non-Adiabatic Expansion of Low-Temperature Solar Wind Radial Temperature Gradients 49:192, 50:124
Gerecke, F.: Seismische Registrierungen in Jena. 1. Jan. 1959 bis 31. Dez. 1959. (G. Schneider) 30:48
Gerecke, F.: Seismische Registrierungen in Jena, 1. Januar bis 31. Dezember 1961. (O. Förtsch) 35:214
Gerecke, F., Güth, D.: Seismische Registrierungen der Nebenstationen von Jena: Potsdam, Halle, Plauen und Sonneberg 1958. (G. Schneider) 30:48
Gerecke, F., Müller, H.K.: Messungen auf dem Rhonegletscher 8:65
Gerecke, F., Ramspeck, A.: Boden- und Gebäudeschwingungen in Rastatt nach dem Erdbeben vom 8. Februar 1933 9:342
Gerharz, R.: Appearance of the Atmospheric Scatter Field During a Solar Eclipse 42:163
Gerlach, W.: Diskussionsbemerkung zu dem Vortrag von Herrn F. Linke in der Gesellschaft für Geophysik, Pyrmont, am 13. September 1934 10:345
Gerlach, W.: Die Sprache der Physik. (H. Schwentek) 30:156
Gerlach, W., List, M.: Johannes Kepler – Leben und Werk. (H. Schwentek) 37:754
Gerlach, W., List, M.: Johannes Kepler; Dokumente zu Lebenszeit und Lebenswerk. (H. Schwentek) 37:755
Gernet, A. v.: Überblick über den Gang der magnetischen Vermessung der Ostsee 4:27
Gernet, A. v.: Die Ergebnisse der magnetischen Messungen in der Ostsee in den Jahren 1924 bis 1929 6:216
Gerstenecker, C., see Pelzer, H. 47:166
Geußenhainer, O.: In memoriam Dr. Friedrich Trappe 21:229
Geyh, M.A.: Betrachtungen über ^{14}C-Gemischtproben-datierungen 32:154

Geyh, M.A.: Der Radiokohlenstoff und seine Rolle in der geowissenschaftlichen Forschung (Übersichtsartikel) 37:909
Ghazi, A., Becker, J.J., Kaul, I.K.: Studies on Total Ozone Over Cologne 37:641
Gherzi, E.: Microséismes et Déferlement des Vagues sur les Côtes 1:163
Gherzi, E.: Microséismes et Déferlement des Vagues sur les Côtes 2:159
Gherzi, E.: Le Problème des Microséismes à Groupes 4:147
Gherzi, E.: Note sur des Microséisme Solitaires (Ondes „Z") de Longue Période et sur les Microséisme à Groupes 4:422
Gherzi, E.: Le Problème des Microséismes et le Déferlement des Vagues 10:317
Ghosh, M.L.: Reflection of Love Wave from a Rigid Obstacle 28:223
Gidskehaug, A., see Storetvedt, K.M., et al. 44:317
Giese, P.: Die Geschwindigkeitsverteilung im obersten Bereich des Kristallins, abgeleitet aus Refraktionsbeobachtungen auf dem Profil Böhmischbruck-Eschenlohe 29:197
Giese, P.: Neue Gesichtspunkte zur Gliederung der Erdkruste auf Grund refraktionsseismischer Messungen 32:488
Giese, P.: The Special Structure of the P^MP Traveltime Curve 38:395
Giese, P., Prodehl, C., Behnke, C.: Ergebnisse refraktionsseismischer Messungen 1965 zwischen dem Französischen Zentralmassiv und den Westalpen 33:215
Giese, P., Stein, A.: Versuch einer einheitlichen Auswertung tiefenseismischer Messungen aus dem Bereich zwischen der Nordsee und den Alpen 37:237
Giese, P., see Bram, K. 34:611
Giese, R.H.: Interpretation of the Optical Properties of Interplanetary Dust 42:705
Giesel, W.: Geschwindigkeiten elastischer Wellen und Wärmeleitfähigkeit im Steinsalz 33:9
Giesel, W., see Höhndorf, A., et al. 41:179
Girardin, N., see Jacoby, W.R. 47:271
Gjøystdal, H., see Steinert, O., et al. 41:289
Glaßmeier, K.-H.: Magnetometer Array Observations of a Giant Pulsation Event 48:127
Gloeckler, G., see Scholer, M., et al. 49:186
Gnass, G.: Bestimmung gezeitlicher Änderungen des Schwerevektors hinsichtlich der Tide M_2 aus gleichzeitigen Horizontalpendelbeobachtungen in Pillnitz, Berchtesgaden und Beuthen 16:1
Gockel, H.: Die Fehler bei der Aufnahme der drahtlosen Zeitsignale und Vorschläge zur Verbesserung 13:223
Gockel, H.: Neuere Gangbeobachtungen an Pendeluhren 14:97
Gockel, H.: Erfahrungen bei Störungen von Schwerependel durch Fernbeben 17:41
Godefroy, P., see Procházková, D., et al. 46:343
Goertz, C.K., see Stüdemann, W. 49:123
Gogte, B.S., see Ramana, Y.V., et al. 41:523
Gokhberg, M.B., see Baranskiy, L.N., et al. 48:1
Goldberg: Die Helligkeitsschwankungen des aschgrauen Mondlichtes 7:345
Goldberg, S., Loewenthal, D., Rotstein, Y.: An Improved Algorithm for Magnetotelluric and Direct Current Data Interpretation 50:151
Goldflam, P., Weigel, W., Loncarevic, B.D.: Seismic Structure Along RRISP-Profile I on the Southeast Flank of the Reykjanes Ridge 47:250
Goldflam, P., see RRISP Working Group 47:228
Goldflam, St., Hirschleber, H.B., Janle, P.: A Refined Crustal Model and the Isostatic State of the Scandinavian Blue Road Area 42:419
Goldflam, S., see Snoek, M. 45:107
Goldmann, G., Swerzina, P.: Lichtklimatisches Observatorium Arosa, Nordlichtbeobachtungen im September 1940 17:246
Golikov, Yu., see Kangas, J., et al. 46:237
Gombosi, T., see Richter, A.K., et al. 50:101
Gomez de Llarena, J.: Die neue Isoseistenkante des mitteldeutschen Erdbebens vom 6. März 1872 1:182
Gommlich, G., see Behrens, J. 38:659
Gommlich, G., see Behrens, J., et al. 38:481
Gose, W.A.: Bemerkungen zum Artikel von E. Schenk: „Über die Magnetisierung der Tuffe und Paläosole im Paläovulkan des Vogelsberges" 35:551
Götz, F.W.P., Maier-Leibnitz, H.: Zur Ultraviolettabsorption bodennaher Luftschichten 9:253
Götz, F.W.P.: Zum Nordlicht vom 25.1.1938 14:314
Götz, P.: Diskussionsbemerkung zum Vortrag Kiepenheuer 14:332
Gra, A.: Über die Bestimmung der Gravimeterkonstante bei einem frei hängenden Federsystem 15:49
Grabowski, L.: Kann die Laplacesche Differentialgleichung für das Schwerkraftpotential auch innerhalb der Erdkruste als erfüllt angesehen werden? 10:322
Grabowski, R.: Sondenmessung des statischen elektrischen Feldes in Ionosphäre und Magnetosphäre (Übersichtsartikel) 39:321
Grabowski, R., see Wilhelm, K., et al. 49:128
Graeser, E., Lode, W., Pott, G.: Die Konstruktion gekrümmter Reflexionshorizonte bei gegebener variabler Geschwindigkeitsverteilung im Raum 24:134
Graewe, H.: Atomphysik. (H. Schwentek) 29:315
Graf, A.: Über theoretische Kippisoklinen und Horizontalisodynamen bei Induktionsmethoden 5:331
Graf, A.: Beitrag zur Berechnung von Minimum-Stabpendeln 10:67
Graf, A.: Zur Theorie elastischer Pendel mit besonderer Berücksichtigung des Holweck-Lejayschen Stabpendels 10:73
Graf, A.: Ein neuer statischer Schweremesser zur Messung und Registrierung lokaler und zeitlicher Schwereänderungen 14:152
Graf, A.: Über die Bestimmung der Gravimeterkonstante bei einem frei hängenden Federsystem 15:49
Graf, A.: Großentfernungsmessungen mit dem Askania-Gravimeter in Texas 15:117
Graf, A.: Stellungnahme zur vorstehenden Abhandlung von G. Ising über die Bestimmung der Apparatekonstante bei astasierten Gravimetern 16:31
Graf, A.: Das Problem der Schweremessungen auf See mit Gravimetern 20:208
Graf, A.: Über die bisherigen Erfahrungen und Meßergebnisse mit dem Seegravimeter 23:4
Graf, A.: In memoriam Rudolf Tomaschek 32:181
Graf, A.: Gravimetrische Instrumente und Meßmethoden. (K. Jung) 34:631
Graf, A., see Seblatnig, H. 5:329
Grafarend, E.: Isotropietests von Lotabweichungsverteilungen in Westdeutschland. I 37:719
Grafarend, E.: Isotropietests von Lotabweichungsverteilungen in Westdeutschland. II 38:243
Grafe, A., see Treumann, R., et al. 43:719
Gräfe, H.: Das Nordtiroler Beben vom 8. Oktober 1930. I. Teil 8:144
Gräfe, H.: Das Nordtirol. Beben vom 8. Oktober 1930. II. Teil. Die Kräfte im Herd des Bebens 9:31
Gräfe, H.: Über die Deformation der Erdoberfläche durch Scherungskräfte im Herd von Erdbeben 10:17
Gräfe, H.: Über die Möglichkeit der Messung von Schwerevariationen mit Ausgleichpendeln 11:144
Grandal, B., see Thrane, E.V., et al. 44:99
Grasnick, K.: Ergebnisse der Ozonmessungen in Potsdam während des IGJ und der IGC 1957–1959. (P. Fabian) 29:315
Green, G., see Kunow, H., et al. 42:615
Greenwald, R.A., see Baumjohann, W., et al. 44:373
Greenwald, R.A., see Inhester, B., et al. 49:155
Gregersen, S., see Müller, G., et al. 43:507

Griffiths, D.H., King, R.F.: Applied Geophysics (D. Mayer-Rosa) 33:214
Grimm, H.: Beobachtungen über die Helligkeitsschwankungen des aschgrauen Mondlichtes 7:92
Gringauz, K.I., see Richter, A.K., et al. 50:101
Grosse, S.: Ergebnisse gravimetrischer Regionalvermessungen im Westerzgebirge 24:321
Große-Brauckmann, W., see Flach, D. 40:355, 41:303
Grosser, M.: Entdeckung des Planeten Neptun (R. Schick) 36:777
Groten, E.: Berechnung des Einflusses der Meeresgezeiten auf die Registrierung der Erdgezeiten in Neunkirchen/Siegerland 29:57
Groten, E.: Untersuchung der zeitlichen Variation des Gravimeterfaktors 29:169
Groten, E.: Ein Vergleich von Gravimetermessungen mit Satellitenbeobachtungsergebnissen 34:163
Groten, E.: A New Type of Vertical Gravity Gradiometer 41:321
Groten, E.: Some Problems of Large-Scale Gravity Interpretation 41:659
Groten, E., see Thyssen-Bornemisza, S. 37:747
Grotewahl, M.: Die magnetische Aufnahme der Ostsee mit dem eisenfreien Schiff „Cecilie" 5:255
Grube, C.: Bericht über ein Erdbeben, gefühlt an Bord des Dampfers „Aachen" (Norddeutscher Lloyd) vor Iquique 11:133
Grün, E., Fechtig, H., Kissel, J., Gammelin, P.: Micrometeoroid Data from the First Two Orbits of Helios 1 42:717
Grünthal, G., see Procházková, D., et al. 46:343
Gruschwitz, E.-H.: Experimental Results on the Diurnal Variation of MF-Radiowave Reflections from the Lower Ionosphere 39:779
Gubbins, D.: Energetics of the Earth's Core 43:453
Gubbins, D., see Julian, B.R. 43:95
Gudmundsson, G., Saemundsson, K.: Statistical Analysis of Damaging Earthquakes and Volcanic Eruptions in Iceland from 1550-1978 47:99
Guha, S.: Modellseismische Untersuchungen zur Entstehung der reflektierten Refraktion 32:139
Guilino, G.: Ausbau eines Wechsellichtmonochromators und seine Anwendung zur Messung des Luftleuchtens während der Dämmerung und in der Nacht 31:115
Gunnarsson, K., see Bott, M.H.P. 47:221
Gupta, A., see Kotadia, K.M. 46:23
Gupta, S.P., Prakash, S., Subbaraya, B.H.: Spectral Characteristics of Cross-Field and Two Stream Instability as Revealed by Rocket Borne Studies 43:681
Gustafsson, G., Baumjohann, W., Iversen, I.: Multi-Method Observations and Modelling of the Three-Dimensional Currents Associated with a Very Strong Ps6 Event 49:138
Gutdeutsch, G., Menzel, H.: Bemerkungen zur sogenannten 2-dimensionalen Theorie der Modellseismik 33:200
Gutdeutsch, R.: Über Vielfacheinsätze elastischer Wellen an Schichten 28:11
Gutdeutsch, R.: Über Vielfacheinsätze elastischer Wellen an Schichten, 2. Teil 28:53
Gutdeutsch, R.: Modellseismische Experimente über die Ausbreitung von Rayleighwellen an keilförmigen Schichten 32:372
Gutdeutsch, R.: Über die seismischen Informationen aus Hydrophonregistrierungen 37:273
Gutdeutsch, R., Koenig, M.: Über die Signalgeschwindigkeit gebeugter elastischer Wellen 31:246
Gutdeutsch, R., see Rao, S.H., et al. 25:253
Gutdeutsch, R., see Drimmel, J., et al. 39:21
Gutdeutsch, R., see Franke, A. 40:173
Gutdeutsch, R., see Seiberl, W., et al. 44:639
Gutdeutsch, R., see Ádám, A., et al. 50:37
Gutenberg, B.: Bemerkungen zu den Untersuchungen von Gherzi: Die seismische Bodenunruhe in Zi-ka-wei 1:69, 165
Gutenberg, B.: Der Aufbau der Erdkruste auf Grund geophysikalischer Beobachtungen 1:94
Gutenberg, B.: Neuere Untersuchungen über Gezeiten und ähnliche Meeresbewegungen 1:260
Gutenberg, B.: Untersuchungen zur Frage bis zu welcher Tiefe die Erde kristallin ist 2:24
Gutenberg, B.: Der Aufbau der Erde 2:297
Gutenberg, B.: Zur Frage der Laufzeitkurven 2:305
Gutenberg, B.: Bodenunruhe durch Brandung und durch Frost 4:246
Gutenberg, B.: Nochmals: Zur Frage der Laufzeitkurven 6:57
Gutenberg, B.: Bemerkungen zu der vorstehenden Erwiderung von Herrn G. Krumbach 6:62
Gutenberg, B.: Untersuchungen zur Bodenunruhe in Süd-Kalifornien 21:177
Gutenberg, B.: Spectrum of P and S in Records of Distant Earthquakes 23:316
Güth, D., see Gerecke, F. 30:48
Guya, N.H.: Study of the Spatial Variation of the Magnetic Field Intensity on North-South Profiles in Iran in Comparison with the IGRF Model of 1970 42:277
Guyod, H.: Elektrisches Analogon zur Widerstandsmessung in Bohrungen. (O. Rülke) 29:147
Guyod, H.: Die Bestimmungen des wahren spez. Widerstandes aus elektrischen Bohrlochdiagrammen. (O. Rülke) 29:148
Guyod, H., Pranglin, J.A.: Tafeln zur Bestimmung des wahren spez. Widerstandes aus Bohrloch-Widerstandsmessungen. (O. Rülke) 29:147
Gvishiani, A., see Alekseevskaya, M., et al. 43:227
Gwinner, M.P.: Geologie der Alpen (K. Strobach) 38:963

Haak, V.: Magnetotellurik: Bestimmung der Übertragungsfunktionen in Gebieten mit lateraler Änderung der elektrischen Leitfähigkeit 38:85
Haalck, F.: Ein Universal-Torsions-Magnetometer zur Bestimmung von D, H u. Z 19:1
Haalck, F.: Die Genauigkeit eines modernen Gravimeters 19:21
Haalck, F., Schulze, R.: Die mit dem UTM erreichbare Genauigkeit 26:246
Haalck, H.: Über die Wirkung der Zuleitungen vom Generator zu den Elektroden auf die elektromagnetischen Feldmessungen 5:37
Haalck, H.: Über das Vorhandensein einer magnetischen Wirkung durch rotierende Massen und die Ursache des Erd- und Sonnenmagnetismus 5:359
Haalck, H.: Über die Ursache der erdmagnetischen Störung im Gebiet der Freien Stadt Danzig 6:129
Haalck, H.: Zur Frage der Beschaffenheit des Erdinnern 7:68
Haalck, H.: Ein statischer Schwerkraftmesser 7:95
Haalck, H.: Ein statischer Schweremesser. II 8:17
Haalck, H.: Erwiderung zu T. Schlomka [8:84] 8:88
Haalck, H.: Über die physikalische Natur des magnetischen Rindenfeldes der Erde 8:154
Haalck, H.: Ein statischer Schweremesser. II (Forts.) 8:197
Haalck, H.: Ein Quecksilberneigungsmesser von hoher Empfindlichkeit 8:256
Haalck, H.: Bericht über den gegenwärtigen Stand der Entwicklung des statischen Schweremessers 9:81, 12:356
Haalck, H.: Die Messungsergebnisse mit dem statischen Schweremesser 9:285
Haalck, H.: Messungsergebnisse mit dem statischen Schweremesser auf der Nord- und Ostsee und in Norddeutschland 11:55
Haalck, H.: Verzeichnis der im Jahre 1934 mit dem Statischen Schweremesser auf der Nord- und Ostsee und in Norddeutschland gemessenen Schwerewerte 11:134
Haalck, H.: Der neue statische Schweremesser des Geodätischen Instituts in Potsdam 12:1
Haalck, H.: Über eine neue physikalische Erklärung der Ursache des Erd- und Sonnenmagnetismus und des luftelektrischen Vertikalstromes 12:112

Haalck, H.: Barometrische Höhenmessung bei statischen Schweremessungen mit Hilfe einer praktischen Form des Luftbarometers 12:249
Haalck, H.: Zur Frage nach der Ursache des Erdmagnetismus 13:192
Haalck, H.: Entgegnung auf die Ausführungen von T. Schlomka 13:197
Haalck, H.: Über einige die Physik des Erdinnern betreffende atomtheoretische Beziehungen 14:111
Haalck, H.: Eine Neuberechnung der Dichteverteilung und der davon abhängenden physikalischen Größen im Erdinnern 17:1
Haalck, H.: Das Gleichgewicht der Kräfte im Innern des Erdkerns und die sich daraus ergebenden Folgerungen 17:135
Haalck, H.: Über die Größe der Elastizitätskonstanten und die Fortpflanzungsgeschwindigkeit der Raumwellen im Innern des Erdkerns 18:27
Haalck, H.: Zur Kuhn-Rittmannschen Theorie über die Beschaffenheit des Erdinnern 18:32
Haalck, H.: Die Berechnung von W_{zzz} aus Gravimetermessungen und ihre Bedeutung für die angewandte Geophysik 19:46
Haalck, H., Ebert, A.: Eine elektromagnetische Messungsmethode mit Elektrodenverlegung zur Aufsuchung von Leitfähigkeitsunterschieden im Untergrund 8:409
Haalck, H., Jung, K., Numerov, B.: 4:18
Haas, R., see Israel, H. 28:289
Haase, H.: Jahrbuch für Gewässerkunde Norddeutschlands; Abflußjahre 1926, 1927 und 1928 9:276
Haase, H.: Jahrbuch für die Gewässerkunde Norddeutschlands 10:65
Haase, H., Koehne, W., Friedrich, W.: Ungewöhnliches Steigen des Grundwassers und Überschwemmungen in Senken ohne sichtbaren Abfluß 10:388
Haasemann, L.: zum 80. Geburtstag 13:204
Haddon, R.A.W., see Husebye, E.S., et al. 43:535
Haenel, R.: Heat Flow Measurements in Northern Italy and Heat Flow Maps of Europe 40:367
Haenel, R., Zoth, G.: Heat Flow Measurements in Austria and Heat Flow Maps of Central Europe 39:425
Haenel, R., see Höhndorf, A., et al. 41:179
Hagen, O., see Thrane, E.V., et al. 44:99
Hahn, A.: Erfahrungen mit dem Torsions-Magnetometer Gfz der Askaniawerke, Berlin 24:106
Hahn, A.: Methode zur Interpretation magnetischer Flächenvermessungen durch Berechnung des Oberflächenreliefs einer magnetisierten Schicht 30:154
Hahn, A.: Preface 40:401
Hahn, A.: SI Units in the Field of Geomagnetism 44:189
Hahn, H., see Bosum, W. 32:1
Hahnfeld, I.: Untersuchungen über die elektrische Raumladung und das elektrische Feld am Boden 8:89
Hahnkamm, E.: Betrachtungen über ebene Pendel 10:235
Haimson, B.C., see Voight, B., et al. 47:176
Haïssinsky, M., Adloff, J.P.: Radiochemisches Lexikon der Elemente und ihrer Isotope. (W. Stahl) 34:633
Haldoupis, C.I., Sofko, G.J.: Simultaneous Smoothed Variations of Signal Amplitude and Mean Doppler Shift in 42 MHz Auroral Backscatter 46:63
Haldoupis, C.I., Sofko, G.J.: Overnight Statistical Variation of the North-South Movements of Radio Auroral Irregularities 46:77
Hall, D.H.: Long-Wavelength Aeromagnetic Anomalies and Deep Crustal Magnetization in Manitoba and Northwestern Ontario, Canada 40:403
Hamilton, E.I.: Applied Geochronology. (M.A. Geyh) 34:104
Hammecke, K., Kappler, E.: Eine neue Methode zur Bestimmung der Oberflächentemperatur des Wassers bei Verdampfungsversuchen 19:181
Hänel, R.: Eine neue Methode zur Bestimmung der terrestrischen Wärmestromdichte in Binnenseen 36:725
Hänel, R.: Bestimmungen der terrestrischen Wärmestromdichte in Deutschland 37:119
Hänel, R.: Heat Flow Measurements and a First Heat Flow Map of Germany 37:975
Hänel, R.: Heat Flow Measurements in the Red Sea and the Gulf of Aden 38:1035
Hanner, M., see Leinert, C., et al. 42:699
Hänsel, H.: Einige kritische Bemerkungen zu den Terellaexperimenten von Block 30:182
Hansen, R.T., see Edenhofer, P., et al. 42:673
Hansen, S.F., see Edenhofer, P., et al. 42:673
Hanuš, V., Vaněk, J.: Intermediate Aseismicity of the Andean Subduction Zone and Recent Andesitic Volcanism 42:219
Hanuš, V., Vaněk, J.: Tonga-Lau System: Deep Collision of Subducted Lithospheric Plates 44:473
Hanuš, V., Vaněk, J.: Northern Part of the Tonga Region: A Complicated Subduction Closure 46:385
Harang, L.: Über das Auftreten eines besonderen Nordlichtbogens am 26. Januar 1931 7:271
Harang, L.: Filteraufnahmen von Polarlicht 7:324
Harang, L.: Eine Untersuchung der Polarisation des Nordlichtes 9:162
Hardtwig, E.: Über die Wellenausbreitung in einem visko-elastischen Medium 18:1
Hardtwig, E.: Über die Eintauchtiefe von Rayleigh-Wellen 18:150
Hardtwig, E.: Zur Theorie der Rayleigh-Wellen 18:164
Hardtwig, E.: Über die Entstehung der Mikroseismik 23:83
Hardtwig, E.: Theorien zur mikroseismischen Bodenunruhe. (K. Strobach) 30:157
Hargraves, R.B., Petersen, N.: Notes on the Correlation Between Petrology and Magnetic Properties of Basaltic Rocks 37:367
Harjes, H.-P.: Seismic Waves in Inhomogeneous Media 38:1001
Harjes, H.P., Henger, H.: Array-Seismologie (Übersichtsartikel) 39:865
Harjes, H.-P., Seidl, D.: Digital Recording and Analysis of Broad-Band Seismic Data at the Graefenberg (GRF)-Array 44:511
Harnisch, M., see Kautzleben, H., et al. 43:163
Harris, S.: Temperature Changes Between Torsion Balance Readings in the State of Texas 6:171
Hart, R.S., Anderson, D.L.: Seismic Velocities and Density of an Attenuating Earth 43:503
Harth, W.: Die Beschreibung von VLF-Atmospherics-Parametern mit dem Wait- und Walters-Modell 38:153
Harth, W.: VLF-Atmospherics – Ihre Messung und ihre Interpretation (Übersichtsartikel) 38:815
Hartmann, G., see Ebel, A., et al. 35:373
Hartmann, G.K.: The Effect of Low Energetic Electrons in the Polar Ionosphere 41:233
Hartmann, G.K., see Dieminger, W. 42:447
Hartmann, O.: Zeitschrift für Gletscherkunde und Glazialgeologie, Band V, Heft 1 33:145
Hartmann, W.: Ein detonierendes Meteor über dem Weserbergland am 2. Januar 1934 10:288
Hasegawa, A., see Lanzerotti, L.J. 42:271
Hasegawa, M.: Die Wirkung der obersten Erdschicht auf die Anfangsbewegung einer Erdbebenwelle 6:78
Haser, L., see Möller, G.F. 36:451
Hasler, H.G.: Messung des Ladungsspektrums der primären kosmischen Strahlung während des solaren Minimums 1965 34:469
Hasse, L.: Zum Einfluß von Instrumententrägheit oder Filtern auf die Kreuzkorrelation 34:259
Hasselmann, K.: Application of Two-Timing Methods in Statistical Geophysics 43:351
Hasselmann, K., Wibberenz, G.: Scattering of Charged Particles by Random Electromagnetic Fields 34:353
Hasselmann, K., see Essen, H.-H. 36:655
Haubold, W.: Eine Vorrichtung zur Bestimmung der

Geländekorrektion bei Messungen mit Eötvösschen Drehwaagen 8:446
Haurwitz, B.: In Memoriam Prof. Dr. Ludwig Weickmann 28:50
Haurwitz, B., Cowley, A.D.: A Direct Demonstration of the Lunar Barometric Tide (Brief an den Herausgeber) 36:771
Häusler, B., see Achtermann, E., et al. 37:211
Haussmann, K.: Isogonenkarte des Deutschen Reiches für die Epoche 1925.5, mit 1 Karte 1:129
Haussmann, K.: Messungen im Luftschiff 6:253
Haussmann, K.: Dr. Filchners erdmagnetische Beobachtungen in Zentralasien 1926 bis 1928. Bearbeitet von O. Venske 7:355
Haussmann, K., Burmeister: Erdmagnetische Vermessung der Rheinpfalz 8:478
Hecker, O., see Koenigsberger, J. 1:152
Hedebol Nielsen, P., see Casten, U. 41:357
Hédervári, P.: On the Geophysical Interpretation of the Seismical Greatcircle of the Earth 30:1
Hédervári, P.: Map of Tectonic Flux of Japan 37:135
Hédervári, P.: Energetics of the Development of Lunar Calderas 39:1007
Hedley, I.G.: The Weak Ferromagnetism of Goethite (α-FeOOH) 37:409
Heikkila, W.J., see Untiedt, J., et al. 45:41
Heikkila, W.J., see Opgenoorth, H.J., et al. 48:101
Heiland, C.: Instrumentelle Neuerungen auf dem Gebiet der angewandten Geophysik 1:118
Heiland, C.A.: Possible Causes of Abnormal Polarizations of Magnetic Formations 6:228
Heiland, C.A.: Bemerkungen zu der Arbeit von Herrn Dr. O. Meisser: „Ein neuer Vierpendelapparat für relative Schweremessungen" 6:479
Heiniger, C.: Palaeomagnetic and Rockmagnetic Properties of the Permian Volcanics in the Western Southern Alps 46:397
Heinrich, H.: Elastische Wellen in Eis 31:293
Heinrich, H., Reimer, D., Siemann, H.: Investigation of the Auroral Electrojet 36:399
Heiskanen, W.: Die Airysche isostatische Hypothese und Schweremessungen 1:225
Heiskanen, W.: Schwerkraft und isostatische Kompensation in Japan 3:213
Heiskanen, W.: Die Erdkrustendicke nach den Schwereanomalien 3:217
Heitmann, M.-L., Richter, D., Schumann, D.: Der Wärme- und Wasserhaushalt des Stechlin- und Nehmitzsees (Walk) 36:776
Helbig, K.: Some Integrals of Magnetic Anomalies and Their Relation to the Parameters of the Disturbing Body 29:83
Helbig, K.: Berichtigung zum Artikel „Some Integrals..." [29:83] 29:148
Hellbardt, G.: Seismische Versuche auf einer Eisplatte 21:41
Hellbardt, G.: Über die Grenzempfindlichekit des astatischen Spulenmagnetometers 24:34
Hellenthal, W.: Magnetische Eigenschaften ferromagnetischer Granulate 30:282
Heller, F.: Remanent Magnetization of the Bergell Granite 37:557
Heller, F.: Palaeomagnetism of Upper Jurassic Limestones from Southern Germany 42:475
Heller, F.: Rockmagnetic Studies of Upper Jurassic Limestones from Southern Germany 44:525
Heller, F., Channell, J.E.T.: Palaeomagnetism of Upper Cretaceous Limestones from the Münster Basin, Germany 46:413
Heller, F., Markert, H., Schmidbauer, E.: Partial Self-Reversal of Natural Remanent Magnetization of an Historical Lava Flow of Mt. Etna (Sicily) 45:235
Heller, F., see Markert, H., et al. 42:47
Heller, F., see Scriba, H. 44:341
Heller, F., see Channell, J.E.T., et al. 48:60
Hellmann, K.N., Lippolt, H.J.: Calibration of the Middle Triassic Time Scale by Conventional K-Ar and $^{40}Ar/^{39}Ar$ Dating of Alkali Feldspars 50:73
Hempe, H., see Kunow, H., et al. 42:615
Henger, H., see Harjes, H.P. 39:865
Henriksen, K., Holback, B., Witt, G.: Variations in the Auroral Spectrum at the Latitude of the Polar Cleft 44:401
Hente, B.: A Simple Method for the Evaluation of Whistlers not Requiring the Determination of the Nose Frequency (Briefe an den Herausgeber) 39:855
Hentschel, G.: Bioklimatische Arbeits- und Bewertungsunterlagen für die klimatherapeutische Praxis (Walk) 36:776
Henzel, N., Strebel, O.: Modelluntersuchungen über die Tiefenverlagerung von Fallout in verschiedenen Böden 33:33
Hering, W.: Untersuchungen über den Streufehler der Messungen mit Radiosonde – Modell Freiberg. (R. Roth) 33:370
Herminghaus, Ch., Berckhemer, H.: Ultra Sound Absorption Measurements in Rock Samples at Low Temperatures 40:341
Hernandez, J., see Najid, D., et al. 49:149
Herold, F.: Bemerkung zu Zählrohrmessungen im Gelände 15:182
Herrmann, A.: Grundsätzliche Betrachtungen über piezoelektrische Beschleunigungsmesser 15:31
Herrmann, A., Meisser, O.: Ein piezoelektrischer Beschleunigungsmesser 11:152
Herrmann, R.B.: A Method for Synthesis of the Seismic Coda of Local Earthquakes 43:341
Herzen, R.P. von, Finckh, P., Hsü, K.J.: Heat-Flow Measurements in Swiss Lakes 40:141
Heye, D.: Ein Meßverfahren zur paläomagnetischen Untersuchung von Lockersedimenten im Gelände (Briefe an den Herausgeber) 38:1055
Heye, D., Beiersdorf, H.: Radioaktive und magnetische Untersuchungen an Manganknollen zur Ermittlung der Wachstumsgeschwindigkeit bzw. zur Altersbestimmung 39:703
Heye, D., Meyer, H.: Ein Meßverfahren zur paläomagnetischen Messung an Tiefseesedimentkernen an Bord eines Schiffes 38:937
Hide, R.: The Earth's Core-Mantle Interface Revisited 43:498
Hieblot, J., see Witt, C. de, et al. 30:155
Hieronymus, H.: Eine Zweipolschollen-Hypothese der Kontinentverschiebung 33:453
Hiersemann, L.: Aufzeichnung langperiodischer Bodendeformationen mit einem Strainseismometer 27:18
Hildebrandt, W., see Sebulke, J. 45:409
Hillebrand, O.: Spatial Characteristics of Giant Pulsations 42:257
Hillebrand, O., see Björnsson, A., et al. 37:1031
Hillebrand, O., see Wedeken, U., et al. 46:249
Hiller, W.: (4:)
Hiller, W.: Eine Erdbebenwarte im Gebiete der Schwäbischen Alb 9:230
Hiller, W.: Erdbebenherde und Tektonik im Gebiete der Schwäbischen Alb 11:15
Hiller, W.: Eine einfache und sichere Art der Zeitmarkierung bei mechanisch registrierenden Seismographen 11:19
Hiller, W.: 30 Jahre Deutsche Geophysikalische Gesellschaft. 1922-1952 19:V
Hiller, W.: In Memoriam Dr. Ernst Wanner 22:53
Hiller, W.: Nachruf auf Professor Beno Gutenberg 26:298
Hiller, W.: In Memoriam Ernst Tams 30:49
Hiller, W., see Berckhemer, H. 26:1
Hinz, E., see Behrens, J., et al. 35:43
Hinz, K.: Progress in Oceanography (editor: Mary Sears) 35:440
Hinze, W.J., see Frese, R.R.B. von, et al. 49:234
Hirn, A., Steinmetz, L., Kind, R., Fuchs, K.: Long Range Profiles in Western Europe: II. Fine Structure of the Lower Lithosphere in France (Southern Bretagne) 39:363

Hirschleber, H.B., Lund, C.-E., Meissner, R., Vogel, A., Weinrebe, W.: Seismic Investigations Along the Scandinavian "Blue Road" Traverse 41:135
Hirschleber, H.B., Menzel, H.: Das Amplituden-Ladungs-Gesetz für Sprengungen im Kleinen Belt 32:365
Hirschleber, H.B., see Aric, K., et al. 34:531
Hirschleber, H., see Casten, U. 37:47
Hirschleber, H.B., see Essen, H.H., et al. 39:833
Hirschleber, H.B., see Goldflam, St., et al. 42:419
Hjortenberg, E., see Bungum, H., et al. 43:501
Hobbs, B.A., Dawes, G.J.K.: Calculation of the Effect of the Oceans on Geomagnetic Variations with an Application to the Sq Field During the IGY 46:273
Hoelper, O.: Über die Durchlässigkeit der Atmosphäre für die Sonnenstrahlung 1:251
Hoffmann, U., Stiller, H.: Die Bestimmung der Curietemperaturen von natürlichen Magnetiten mit der Methode der thermodynamischen Koeffizienten 32:267
Hoffmeister, C.: Beobachtung auf der Sternwarte zu Sonneberg 16:89
Hoffrogge, Chr.: Experimentelle Untersuchungen der bodennahen Luftströmungen am Hang und im ebenen Gelände 15:184
Hofmann, H., see Mühleisen, R., et al. 37:1055
Hogg, T.E., see Creer, K.M., et al. 48:139
Höhndorf, A., Haenel, R., Giesel, W.: Geothermal Models of the Ivrea-Zone 41:179
Höhne, W.: Verfahren zur Herstellung trägheitsarmer Thermoelemente und Widerstandsthermometer. (E. Keppler) 29:315
Holback, B., see Henriksen, K., et al. 44:401
Hollinderbäumer, J.: Über die Ortung mikroseismischer Stürme 25:209
Holst, H.: Über Gravitationsmessungen mit der Drehwage auf dem Eise des Titisees 1:228
Homilius, J.: Über die Auswertung geoelektrischer Sondierungskurven im Falle eines vielfach geschichteten Untergrundes 27:287
Homilius, J., Blohm, E.-K.: Modell zur Interpretation der geoelektrischen Tiefensondierung im Rheingraben 1967 39:441
Hopfner, F.: Die Reduktion von Bruns-Bowie 5:300
Hopfner, F.: Bemerkung zu der Arbeit „Über die Bestimmung der Geoidundulationen" von Karl Jung 7:91
Hopfner, F.: Darstellung einer gebietsweise harmonischen Funktion durch eine harmonische Funktion 9:77
Hopfner, F.: Die praktische Lösung der zweiten Randwertaufgabe der Geodäsie 9:277
Hopfner, F.: Die Relativität der Undulationen 10:279
Hopfner, F.: Die potentialtheoretischen Grundlagen der Lehre von der Isostasie 12:24
Hopfner, F.: Stellungnahme zum vorangehenden Artikel K. Jung [12:65] 12:66
Horálek, J., see Plešinger, A. 42:201
Hornemann, U., Pohl, J., Bleil, U.: A Compressed Air Gun Accelerator for Shock Magnetization and Demagnetization Experiments up to 20 kbar 41:13
Hornemann, U., see Pohl, J., et al. 41:23
Horner, F., Lowrie, W.: Paleomagnetic Evidence from Mesozoic Carbonate Rocks for the Rotation of Sardinia 49:11
Hoversten, M., see Quon, C., et al. 46:291
Hovestadt, D., see Achtermann, E., et al. 36:27, 37:211
Hovestadt, D., see Scholer, M., et al. 40:37, 49:186
Hsü, K.J., see Herzen, R.P. von, et al. 40:141
Huang, S.-T.: Bestimmung der Geschwindigkeit, Dämpfung und Absorption von Kompressions- und Scherwellen in Kautschuk 16:213
Hubert, F.: Die Registrierung der durch fallende Gewichte erzeugten Bodenschwingungen mit einem zweimillionenfach vergrößernden Wiechertschen Vertikalseismometer 1:134
Hubert, F.: Die Bodenerschütterungen durch fallende Gewichte 1:197
Hubral, P.: Characteristics of Azimuth Independent Optimum Velocity Filters Designed for Two-Dimensional Arrays 41:265
Hudson, J.A.: Scattered Waves in the Coda of *P* 43:359
Hughes, W.J.: Comment on: Hydromagnetic Waves in a Non-Uniform Plasma by E. Kupfer, J. Geophys. 41, 123–126 (1975) 43:829
Hultqvist, B.: Evidence from Particle Precipitation of Two-Way-Convection in Auroral Latitudes 40:713
Hummel, J.N.: Über die Tiefenwirkung bei geoelektrischen Rahmenmethoden 5:72
Hummel, J.N.: Der scheinbare spezifische Widerstand 5:89
Hummel, J.N.: Modellversuche mit der Viertelwellenmethode 5:104
Hummel, J.N.: Der scheinbare spezifische Widerstand bei vier planparallelen Schichten 5:228
Hummel, J.N.: Theoretische Grundlagen für die Erforschung des Erdinnern mittels Gleichstrom 7:182
Hummel, J.N.: Die Tiefenwirkung der Potentiallinien- und Rahmenmethoden bei geschichtetem Untergrund 7:258
Hummel, J.N.: Der scheinbare spezifische Widerstand (Berichtigung) 8:249
Hummel, J.N.: Die elektrische Leitfähigkeit von Aggregaten in bezug auf die Leitfähigkeiten ihrer Bestandteile 11:92
Hummel, J.N.: Die Messung der elektrischen Strömung im räumlichen Leiter 11:321
Hummel, J.N., Witte, H.: Die gleichzeitige Übertragung verschiedener Signalzeichen mit einem Einfachsender und -empfänger 7:175
Hummel, J.N., see Thyssen, St. v., et al. 13:112
Hummervoll, R.: A Method to Reduce the Measuring Time for Spinner Magnetometers 40:265
Hummervoll, R.: Further Utilization of the Fluxgate Magnetometer in the Palaeomagnetic Laboratory 42:85
Humphreys, W.J.: Physics of the Air. (G. Fischer) 31:114
Hung, R.J., Kuo, J.P.: Ionospheric Observation of Gravity-Waves Associated with Hurricane Eloise 45:67
Hunsche, U., Rapolla, A., Musmann, G., Alfano, L.: Application of Magnetotelluric and DC Electrical Resistivity Methods in the Neapolitan Geothermal Area 49:26
Hurley, P.M. (ed.): Advances in Earth Science (H. Closs) 35:437
Husebye, E.S., Haddon, R.A.W., King, D.W.: Precursors to P'P' and Upper Mantle Discontinuities 43:535
Husebye, S., see Steinert, O., et al. 41:289
Hussain, A.G., see Schult, A., et al. 44:333, 50:16

Ihering, H. v.: Das Klima der Tertiärzeit 3:365
Ilan, A.: Finite-Difference Modelling for P-Pulse Propagation in Elastic Media with Arbitrary Polygonal Surface 43:41
Ilan, A., see Ungar, A. 43:33
Inglada, V.: Cálculo de las Coordenadas del Foco Sismico y del Instante Inicial... 3:195
Inhester, B., Baumjohann, W., Greenwald, R.A., Nielsen, E.: Joint Two-Dimensional Observations of Ground Magnetic and Ionospheric Electric Fields Associated with Auroral Zone Currents. 3. Auroral Zone Currents During the Passage of a Westward Travelling Surge 49:155
Innes, R.T.A.: Variability of the Earth Rotation 1:328
Ipavich, F.M., see Scholer, M., et al. 49:186
Isensee, U.: Plasma Disturbances Caused by the Helios Spacecraft in the Solar Wind 42:581
Ising, G.: Die Bestimmung der Apparatkonstanten bei astasierten Gravimetern (Bemerkung zur Abhandlung von A. Graf „Über die Bestimmung der Gravimeterkonstante bei einem frei hängenden Federsystem".) 16:27
Israël, H.: Ein transportables Meßgerät für schwere Ionen 5:342
Israël, H.: Schwere Ionen der Atmosphäre 7:127
Israël, H.: Emanation in Boden- und Freiluft 10:347
Israël, H.: Die luftelektrische Unruhe 24:277

Israël, H.: Der Diffusionskoeffizient des Radons der Bodenluft 25:104
Israel, H.: On the Sun-Rise Effect of Sferics Activity at 27 kc 26:138
Israël, H.: Der Diffusions-Koeffizient des Radons in Bodenluft 27:13
Israël, H.: Zur Verwendung des radioaktiven Kollektors in der luftelektrischen Meßtechnik 30:152
Israël, H.: Probleme der Gewitterforschung. I. Das Gewitter in heutiger Sicht (K. Höschele) 33:211
Israël, H.: Bemerkungen zum Begriff der „luftelektrisch ungestörten" Zeiten 33:362
Israël, H., Björnsson, S.B.: Radon (Rn^{222}) and Thoron (Rn^{220}) in Soil Air over Faults 33:48
Israel, H., Dolezalek, H.: Zur Vergleichbarkeit luftelektrischer Messungen 26:77
Israel, H., Fries†, G.: Luftelektrische Untersuchungen während der Sonnenfinsternis am 30.6.1954 20:137
Israel, H., Haas, R.: Absorption of Natural Fallout in Soil 28:289
Israël, H., La Riva, C. de: Atmosphärische Radioaktivität und Austausch 33:188
Israël, H., Nix, N.: Thermodynamische Vorgänge im Kondensationskernzähler 32:175
Israël, H., Nix, N.: Ein neues Verfahren zur Untersuchung von Kondensation und Verdampfung an Einzelteilchen von Kleinaerosolen 35:207
Israël, H., Rössler, J.: Zum Sonnenaufgangseffekt im Längstwellengebiet 32:207
Israël, H., Stiller, S.: Climatological Aspects of the Natural Radioactivity 29:51
Israel, H., Süring, R.: Die Wolken 17:158
Israël, H., see Coroniti, S.C., et al. 27:301
Ivanov, N.A., see Shapiro, V.A. 40:435
Ivanov, N.A., see Baranskiy, L.N., et al. 48:1
Iversen, I., see Gustafsson, G., et al. 49:138
Iwers, B., see Kunow, H., et al. 42:615
Izmailov, L.I.: Local Magnetic Anomalies of the Area of the Upper Kolyma River (North-East of the USSR) 40:431

Jacob, A.W.B.: Dispersed Shots at Optimum Depth – An Efficient Seismic Source for Lithospheric Studies 41:63
Jacob, A.W.B., Booth, D.C.: Observation of PS Reflections from the Moho 43:687
Jacob, B., see Kaminski, W., et al. 42:103
Jacobs, J.A.: The Earth's Core and Geomagnetism. (J. Meyer) 30:307
Jacobs, J.A.: Anomalous *P*-Velocities in the Earth's Outer Core 44:675
Jacobs, K.G.: Windmessungen durch Radio-Beobachtungen von Meteorstreifen und Vergleich mit Fading-Drift-Ergebnisse 34:423
Jacoby, W.: Schweremessungen auf Helgoland – Auswertung mit Ausgleichsverfahren 32:340
Jacoby, W.: Zur Berechnung der Schwerewirkung beliebig geformter dreidimensionaler Massen mit digitalen Rechenmaschinen 33:163
Jacoby, W.R.: Isostasie und Dichteverteilung in Kruste und oberem Mantel 39:79
Jacoby, W.R.: Morphology of the Reykjanes Ridge Crest Near 62° N 47:81
Jacoby, W.R., Björnsson, A., Möller, D.: Iceland: Evolution, Active Tectonics, and Structure. A Preface 47:1
Jacoby, W.R., Girardin, N.: The Evolution of the Lithosphere at the Southeast Flank of Reykjanes Ridge from Surface Wave Data 47:271
Jacoby, W.R., Ranalli, G.: Non-Linear Rheology and Return Flow in the Mantle 45:299
Jacoby, W.R., see Thyssen-Bornemisza, S. 37:735
Jacoby, W.R., see RRISP Working Group 47:228
Jacoby, W.R., see Schmeling, H. 50:89
Jaeschke, R.: Upper Atmosphere Winds Deduced from Vapour Trail Drifts 32:394
Jain, A.K., see Klootwijk, C.T., et al. 50:127
Jain, A.R., Sastri, N.S.: The *H* Amplitude of Sudden Commencements of Magnetic Storms at Sabhawala (Dehra Dun) 45:101
Jain, S.C., see Mallick, K. 41:127
Jakuschoff, P.: Das Grundeis 10:308
Jankow, K.: Erdbebenstation in Sofia 12:33
Jankow, K.: Niveauänderungen im Schüttergebiet der Erdbeben in Südbulgarien am 14. und 18. April 1928 14:20
Janle, H., see Essen, H.-H., et al. 49:115
Janle, P.: Structure of Lunar Impact Craters from Gravity Models 42:407
Janle, P.: Investigation of Isostasy by Computing the Correlation Coefficients Between Elevations and Bouguer Anomalies 43:655
Janle, P., Rudloff, R., Schmalfeldt, B., Szelwis, R.: Seawave-Generated Elastic Motions of the North Sea Bottom 41:475
Janle, P., see Goldflam, St., et al. 42:419
Janle, P., see Szelwis, R. 43:623
Janle, P.: A Crustal Gravity Model of the Mare Serenitatis-Mare Crisium Area of the Moon 49:57
Jeffreys, H.: Remarks on the Paper of G. Schmerwitz on Central European Earthquakes 15:168
Jelitto, R.J.: Vorbemerkungen zum Artikel von G. Borm über den Schwimmzustand bei sehr großen Massen (Ein Beitrag zur Isostasiefrage) 37:703
Jensen, P.A., see Kremser, G., et al. 38:851
Jensen, V.N., see Kremser, G., et al. 38:851
Jentsch, M.: Reinterpretation of a Deep-Seismic-Sounding Profile on the Ukrainian Shield 45:355
Jentzsch, G., see Flach, D., et al. 37:1005
Jeremic, M.L.: Some Aspects of Athabasca Oil Sand Behavior, Alberta, Canada 44:651
Jeske, H.: Die Feinstruktur des Brechungsindexfeldes in Höhen zwischen 50 und 2400 m über See 35:529
Jeske, H., Seehars, H.D., Pucher, G., Cassebaum, H.: Observations with Synchronously-Offset Beams on a 77 km Path at 1.8 and 4 cm 36:621
Jessberger, E.K., Reimold, W.U.: A Late Cretaceous ^{40}Ar-^{39}Ar Age for the Lappajärvi Impact Crater, Finland 48:57
Jessen, W., Fabian, P.: Stratospheric Ozone Calculations in a Two-Dimensional Model Including Photochemical and Transport Effects 39:1023
Jobert, G.: On Equivalent Models of Seismic Sources 43:329
Jobert, G., see Cisternas, A. 43:59
Jocksch, H.C.: Die hypsometrische Kurve des Mondes 23:250
Jocksch, H.G.: Statistische Analyse der hypsometrischen Kurve der Erde 21:109
Johnsen, G.V., Björnsson, A., Sigurdsson, S.: Gravity and Elevation Changes Caused by Magma Movement Beneath the Krafla Caldera, Northeast-Iceland 47:132
Johnson, G.L., Pálmason, G.: Observations of the Morphology and Structure of the Sea Floor and West of Iceland 47:23
Johnson, G.L., see Vogt, P.R., et al. 47:67
Joksch, H.C., see Brockhaus, K. 26:9
Jones, A.G.: On the Difference Between Polarisation and Coherence 45:223
Jones, A.G.: Geomagnetic Induction Studies in Scandinavia. I. Determination of the Inductive Response Function from the Magnetometer Array Data 48:181
Jones, A.G.: On a Type Classification of Lower Crustal Layers Under Precambrian Regions 49:226
Jones, A.G.: Geomagnetic Induction Studies in Scandinavia. II. Geomagnetic Depth Sounding, Induction Vectors and Coast-Effect 50:23
Jones, A.G., see Küppers, F., et al. 46:429
Jones, F.C., see Ellison, D.C., et al. 50:110
Joos, W., see Arnold, F., et al. 44:125
Jordan, P.: Die Expansion der Erde. (W. Stahl) 34:634

Jordan, T.H.: Lithospheric Slab Penetration Into the Lower Mantle Beneath the Sea of Okhotsk 43:473
Judd, W.R.: State of Stress in the Earth's Crust. (G. Schneider) 31:225
Juilfs, J.: Zählrohrmessungen der radioaktiven und Ultrastrahlung im Segelflugzeug 18:129
Julian, B.R., Gubbins, D.: Three-Dimensional Seismic Ray Tracing 43:95
Jung, H.: Über die Prüfung der Isostasie durch Schweremessungen 3:381
Jung, H.: Über isostatische Schwereanomalien und deren Beziehung zu den totalen Anomalien 6:173
Jung, H.: Über isostatische Schwereanomalien (Forts.) 7:149
Jung, H.: Berechnung der Laufzeitkurven des anormalen Schalles für windstille Atmosphäre und Vergleich mit der Laufzeitkurve der Oldebroeksprengung vom 15. Dezember 1932 10:186
Jung, H.: Über stereophotogrammetrische Vermessung von Pilotballonbahnen an Berghängen 11:157
Jung, H.: Werbeschrift der Seismos G.m.b.H. 12:35
Jung, H.: Bemerkungen zu den vorstehenden Ausführungen von S.W. Tromp 13:83
Jung, H.: Die Lotabweichungen in der Umgebung des Nanga Parbat und ein Versuch zu ihrer geophysikalischen Deutung 13:205
Jung, H.: Dichtebestimmung im anstehenden Gestein durch Messung der Schwerebeschleunigung in verschiedenen Tiefen unter Tage 15:56
Jung, H.: Beispiele für die Anwendung von Anaglyphen-Raumbildern in der Geophysik 17:339
Jung, H., Behrens, W.U.: Mathematische Methoden für Versuchsansteller auf dem Gebiete der Naturwissenschaften, Landwirtschaft und Medizin 11:162
Jung, H., Ertel, H.: Elemente der Operatorenrechnung mit geophysikalischen Anwendungen 16:255
Jung, H., Gutenberg, B.: Handbuch der Geophysik, Bd. 1, Lief. 1 8:325
Jung, H., Gutenberg, B.: Handbuch der Geophysik 11:160
Jung, H., Hopfner, F.: Physikalische Geodäsie 9:275
Jung, H., Jordan, W., Eggert, O.: Handbuch der Vermessungskunde. 3. Band, 1. Halbband (Landesvermessung, sphärische Berechnungen und astronomische Ortsbestimmung) 16:90
Jung, H., Jordan, W., Eggert, O.: Handbuch der Vermessungskunde 17:338
Jung, H., Kienow, S.: Grundzüge einer Theorie der Faltungs- und Schieferungsvorgänge 18:188
Jung, H., Kleffner, W.: Die Reichskartenwerke mit besonderer Behandlung der Darstellung der Bodenformen 16:254
Jung, H., Kohlschütter, E.: Meßkarte zur Auflösung sphärischer Dreiecke 12:272
Jung, H., Spreitzer, H.: Forschung am Nanga-Parbat 11:271
Jung, H., Tomaschek, R.: Die Messungen der zeitlichen Änderungen der Schwerkraft 10:118
Jung, H., Wüst, G.: Das Meer in volkstümlichen Darstellungen 11:160
Jung, K.: Über die größte mögliche Schwankung der Schwereintensität und die Dichte eines engmaschigen Netzes von Pendelstationen 3:137
Jung, K.: Diagramme zur Bestimmung der Terrainwirkung für Pendel und Drehwage und zur Bestimmung der Wirkung „zweidimensionaler" Massenanordnungen 3:201
Jung, K.: Die Bestimmung von Lage und Ausdehnung einfacher Massenformen unter Verwendung von Gradient und Krümmungsgröße 3:257
Jung, K.: Die Wirkung der Kontinente und Ozeane auf die Differenz $B-A$ der Hauptträgheitsmomente der Erde im Äquator 4:33
Jung, K.: Über den größten möglichen Schwereunterschied 5:65
Jung, K.: Bemerkungen zur Ableitung des größten möglichen Schwereunterschieds 5:118
Jung, K.: Zur Bestimmung von Lage und Ausdehnung einfacher Massenformen unter Verwendung von Gradient und Krümmungsgröße 5:238
Jung, K.: Die Belowsche Methode zur Bestimmung der Wirkung gegebener Massen auf Krümmungsgröße und Gradient, ihre Verallgemeinerung für beliebige Massenformen und ihre Anwendung auf „zweidimensionale" Massenanordnungen 6:114
Jung, K.: Drehwaagemessungen im Ries bei Nördlingen: II. Die Messungen und ihre Ergebnisse 7:6
Jung, K.: Über die Bestimmung der Geoidundulationen aus Schweremessungen 7:81
Jung, K.: Zu der vorstehenden Bemerkung des Herrn F. Hopfner 7:92
Jung, K.: Schwere und Geoid bei Isostasie 8:40
Jung, K.: Die Randwertaufgabe der Geodäsie 8:425
Jung, K.: Bemerkungen zu F. Ackerls Berechnung der Geoidundulationen 9:323
Jung, K.: Über mikroseismische Bodenunruhe und Brandung 10:325
Jung, K.: Einige Zahlen über Normalschwere und Abplattung 11:188
Jung, K.: Bemerkung zur Potentialtheorie des Schwerkraftfeldes 12:65
Jung, K.: Direkte Methoden zur Bestimmung von Störungsmassen aus Anomalien der Schwereintensität 13:45
Jung, K.: Über vollständig isostatische Reduktion 14:27
Jung, K.: Zur Isostasiefrage 15:47
Jung, K.: Die Schwerewirkung von Störungsmassen und ihre Veranschaulichung auf der Einheitskugel 17:276
Jung, K.: Zur Bestimmung der Bodendichte nach dem Nettleton-Verfahren 19:54
Jung, K.: „Schweydarsche" Formeln für die Geländewirkung auf g 20:47
Jung, K.: Betrachtungen zum dreiachsigen Erdellipsoid 20:201
Jung, K.: Wilhelm Schweydar† 26:158
Jung, K.: Schwerkraftverfahren in der Angewandten Geophysik. (O. Rosenbach) 28:246
Jung, K.: Earth Science and Meteoritics. Dedicated to F.G. Houtermans on his sixtieth birthday 33:214
Jung, K.: Neuere Gedanken und Ergebnisse über die Gestalt des Erdkörpers und die Verteilung der Massen im Erdinnern 34:7
Jung, K., Menzel, H., Rosenbach, O.: Gravimetermessungen im Nördlinger Ries 31:7
Jung, K., Schaaf, H.: Gravimetermessungen im Nördlinger Ries und seiner Umgebung, Abschätzung der gesamten Defizitmasse 33:319
Jung, K., see Haalck, H., et al.
Jung, W., Behrens, W.V.: Mathematische Methoden für Versuchsansteller auf dem Gebiete der Naturwissenschaften, Landwirtschaft und Medizin 11:162
Jünger, E., see Winterer, G. 38:1049

Kahle, H.-G.: Abschätzung der Störungsmasse im Nördlinger Ries (Übersichtsartikel) 35:317
Kahle, H.-G.: Deutung der Schwereanomalien im Nördlinger Ries 36:601
Kahle, H.-G., Talwani, M.: Gravimetric Indian Ocean Geoid 39:167
Kahle, H.-G., Talwani, M.: Nachtrag zu „Gravimetric Indian Ocean Geoid" 39:491
Kaikkonen, P.: A Finite Element Program Package for Electromagnetic Modeling 43:179
Kaila, K.U., see Opgenoorth, H.J., et al. 48:101
Kaiser, F., see Knoechel, H., et al. 17:57
Kamel, B.Sc.: The Three Components of Microseismic Disturbance at Kew Observatory. Geophysical Memories No. 66, 1935 11:164
Kamel, M., Faltas, F.: Seismische Bestimmung der Lage einer geneigten ebenen Grenzschicht aus Laufzeiten und Amplituden 12:383
Kaminski, W., Bamford, D., Faber, S., Jacob, B., Nunn, K.,

Prodehl, C.: A Lithospheric Seismic Profile in Britain. II. Preliminary Report on the Recording of a Local Earthquake 42:103
Kaminski, W., see Bonjer, K.-P., et al. 40:259
Kaneoka, I., Kono, M.: $^{40}Ar/^{39}Ar$ Dating of Himalayan Rocks from the Mount Everest Region 49:207
Kangas, J., Pikkarainen, T., Golikov, Yu., Baransky, L., Troitskaya, V.A., Sterlikova, V.: Bursts of Irregular Magnetic Pulsations During the Substorm 46:237
Kangas, J., see Untiedt, J., et al. 45:41
Kangas, J., see Novikov, Yu.P., et al. 48:116
Kanngieser, E., see Torge, W. 47:125
Kapička, A.: The Change of Isothermal Saturation Remanent Magnetization of Basalts as a Result of Cyclic Elastic Deformation 41:633
Kappes, T., see Essers, E. 3:49
Kappler, E., see Hammecke, K. 19:181
Kapustian, N.K., see Davydova, N.I., et al. 38:369
Kapustian, N.K., see Kosminskaya, I.P. 45:159
Karbaum, H.: Anwendungsmöglichkeiten und Pobleme des Salzverdünnungsverfahrens zur Abflußermittlung. (H. Dürbaum) 33:368
Karbaum, H.: Der Niederschlag als Wasserhaushaltsgröße. (Diem) 36:654
Kardeván, P.: Die Verwendung der exponentiellen Periodenverteilung zur Feststellung der Resonanzstellen des Untergrundes aus Registrierungen industrieller Bodenunruhe 37:899
Kaselitz, F.: Ein neuer Integrator zur Berechnung von Schwerewerten 8:191
Kaselitz, F.: Ein neuer Integrator zur Berechung von Schwerewerten (Ergänzung) 8:479
Kasemir, H.W.: Der Gewittergenerator im luftelektrischen Stromkreis. I 25:33
Kasemir, H.W.: Der Gewittergenerator im luftelektrischen Stromkreis. II 25:65
Kaul, I.K., see Ghazi, A., et al. 37:641
Kausel, E., see Calcagnile, G., et al. 43:502
Kautzleben, H.: Über das geomagnetische Normalfeld nach Fanselau 25:143
Kautzleben, H.: Ergänzung zur Arbeit: Über das geomagnetische Normalfeld nach Fanselau 26:41
Kautzleben, H.: Zur Interpretation des geomagnetischen Hauptfeldes als vektorielles Zufallsfeld 33:415
Kautzleben, H., Harnisch, M., Schwahn, W.: The Statistical Description and Interpretation of Geophysical Potential Fields Using Covariance Functions 43:163
Kebe, H.-W., see Essen, H.-H., et al. 41:111
Keen, C.E., Fricker, A., Keen, M.J., Blinn, L.: Reykjanes Ridge Crest Studied by Surface Waves with an Earthquake-Pair Technique 47:265
Keen, M.J., see Keen, C.E., et al. 47:265
Keller, F., see Burkhardt, H., et al. 33:455
Kelly, S.F.: Experiments in Electrical Prospecting 1:262
Kennett, B.L.N.: The Inversion of Long Range Seismic Profiles 43:243
Kent, D.V., see Lowrie, W. 44:297
Keppler, E.: Der Forschungssatellit AZUR 36:457
Keppler, E., Kirsch, E., Mörl, P., Musmann, G., Roßbach, A., Roßberg, L.: Raketenexperiment zur Untersuchung von Nordlichtern 33:346
Keppler, E., Richter, A.K., Richter, K., Umlauft, G., Wilken, B., Williams, D.J.: A Survey on Measurements of Medium Energy Protons and Electrons Obtained with the Particle Spectrometer E 8 on Board of Helios 42:633
Keppler, E., see Richter, A.K. 42:645
Keppler, E., see Kirsch, E., et al. 50:45
Keppler, E., see Richter, A.K., et al. 50:101
Keränen, J.: Über den Vektor der magnetischen Störungen im aperiodischen Verlauf 6:265
Kern, H., Richter, A.: Temperature Derivatives of Compressional and Shear Wave Velocities in Crustal and Mantle Rocks at 6 kbar Confining Pressure 49:47
Kertz, W.: Tages- und jahreszeitliche Variationen des erdmagnetischen äquatorialen Ringstromes 24:210
Kertz, W.: Einführung in die Geophysik. I. (H. Mayer) 38:189
Kertz, W.: Einführung in die Geophysik. II. (H. Mayer) 38:190
Kertz, W., see Freiburg, Ch. 26:227
Kertz, W., see Seiler, E. 33:371
Khartchenko, I.P., see Baranskiy, L.N., et al. 48:1
Khorana, R., see Klootwijk, C.T., et al. 50:127
Kiebitz, F.: Zur Rolle der Heavisideschicht in der drahtlosen Telegraphie 1:122
Kienow, S.: Der Zusammenhang zwischen Spannung und Verformung bei tektonischen Vorgängen 9:204
Kiepenheuer, K.O.: Über den Nachweis der Sonnenstrahlung bei 2150 Å 14:327
Kilchling, K.: Ein dynamisch-elastischer Schweremesser 18:51
Killeen, T.L., see Rees, D., et al. 44:47
Kind, E.G., see Bosum, W. 38:749
Kind, R.: Auswertung seeseismischer Messungen mit einer digitalen Methode unter Anwendung der Theorie der Schallwellenausbreitung im Flachwasser 36:549
Kind, R.: Berechnung der Quellenfunktion einer Explosion im Flachwasser mittels einer Dekonvolutionsmethode (Brief an den Herausgeber) 37:141
Kind, R.: Long Range Propagation of Seismic Energy in the Lower Lithosphere 40:189
Kind, R.: Computation of Reflection Coefficients for Layered Media 42:191
Kind, R.: The Reflectivity Method for a Buried Source 44:603
Kind, R.: Observations of sPn From Swabian Alb Earthquakes at the GRF Array 45:337
Kind, R.: Extensions of the Reflectivity Method 45:373
Kind, R., Müller G.: Computations of *SV* Waves in Realistic Earth Models 41:149
Kind, R., see Hirn, A., et al. 39:363
Kind, R., see Bonjer, K.-P., et al. 40:259
Kind, R., see Müller, G., et al. 43:507
King, D.W., see Husebye, E.S., et al. 43:535
King, R.F., see Griffiths, D.H. 33:214
Kingsley, S.P., see Muller, H.G. 44:39
Kirkwood, S.C., see Crampin, S. 49:35
Kirsch, E.: Raketenexperiment zur Untersuchung von Nordlichtern 36:165
Kirsch, E., Martinic, N., Keppler, E.: Low Energy Solar Particles Observed During the Pre-Phase of Large Particle Events 50:45
Kirsch, E., see Keppler, E., et al. 33:346
Kirsch, E., see Kremser, G., et al. 42:1
Kirsten, G., Vollstädt, H., Frölich, F.: Applications of the Neutron Diffraction Method to Decide Self Reversal and Other Petrological Problems 33:182
Kissel, J., see Grün, E., et al. 42:717
Kist, R., Spenner, K.: Plasmamessungen im Polarlicht-Elektrojet und daraus erschlossene elektrische Felder 36:421
Kist, R., see Neske, E. 40:593
Kizawa, T.: Recordings with Askania Gravimeters Before and After Important Earthquakes (Brief an den Herausgeber) 36:519
Kleinschmidt, E.: Eine neue württembergische Erdbebenwarte 6:370
Kleinschmidt, E.: Zur Flutbewegung der festen Erdkruste 9:197
Kleinschmidt, E.: Erwiderung auf den Aufsatz von R. Tomaschek und W. Schaffernicht: Die Flut der festen Erde 9:308
Klíma, K., see Pros, Z., et al. 35:287
Klöcker, N., Theile, B.: Magnetic ULF-Waves in the Vicinity of Active Auroral Forms 46:229
Klöcker, N., see Wilhelm, K., et al. 49:128
Klootwijk, C.T.: A Note on the Palaeomagnetism of the Late Precambrian Malani Rhyolites Near Jodhpur – India 41:189

Klootwijk, C.T., Jain, A.K., Khorana, R.: Palaeomagnetic Constraints on Allochthony and Age of the Krol Belt Sequence, Garhwal Himalaya, India 50:127
Klostermeyer, J.: Influence of Viscosity, Thermal Conduction, and Ion Drag on the Propagation of Atmospheric Gravity Waves in the Thermosphere 38:881
Klostermeyer, J., see Schödel, J.P., et al. 39:1063
Klußmann, J., see Rao, S.H., et al. 25:253
Knoch, K.: Das unperiodische Element im Tropenklima 6:318
Knoechel, H., Liebermann, K., Merfeld, H., Schindler, G., Buchar, E., Stützer, H., Büdeler, W., Lehr, L., Menze, H., Teichgraeber, A., Franz, J., Classen, J., Leonard, G., Malsch, W., Schilp, E., Kaiser, F., Beyer, M., Tank, Mertins, Scultetus, Lux, J., Wirtitsch: Berichte über das Nordlicht am 1. März 1941 17:57
Knödel, K., Losecke, W., Wohlenberg, J.: A Comparison of Results of Geothermal and Magnetotelluric Investigations in Northwestern Germany 45:199
Knopoff, L.: Relative Errors in Group Velocity Measurements 43:509
Knopoff, L., Chang, F.-S.: The Inversion of Surface Wave Dispersion Data with Random Errors 43:299
Knopoff, L., Zürn, W., Rydelek, P.A., Yogi, T.: Q of Mode $_0S_0$ 46:89
Knopoff, L., see Schneider, G., et al. 32:33
Knopoff, L., see Seidl, D., et al. 32:472
Knopoff, L., see Zürn, W., et al. 48:158, 49:249
Knothe, Ch.: Homogene Dreikomponentenanordnungen für tiefenseismische Untersuchungen 25:67
Knothe, M., see Schmidtke, G., et al. 40:577
Knuth, R., see Cumme, G., et al. 36:57
Kobayashi, K., Nomura, M.: Ferromagnetic Minerals in the Sediment Cores Collected from the Pacific Basin 40:501
Kober, L.: Gestaltungsgeschichte der Erde 2:298
Koch, H., Schminder, R.: Über Sonnenaufgangs- und -untergangserscheinungen im Lang- und Mittelwellenbereich 26:285
Koch, H., Schminder, R., Kürschner, D.: Ein neues automatisches Registriergerät für ionosphärische Driftmessungen 28:281
Koch, H.W., Zeller, W.: Der Einschwingvorgang bei Erschütterungsmeßgeräten 12:220
Koch, K.R.: Geophysical Interpretation of Density Anomalies of the Earth Computed from Satellite Observations and Gravity Measurements 38:75
Kochan, H., see Czechowsky, P., et al. 36:77
Koefoed, O.: The Application of the Kernel Function in Interpreting Geoelectrical Resistivity Measurements (R. Schick) 36:777
Koehne, W., see Hasse, H., et al. 10:388
Koenig, M.: Digitalisierung modellseismischer Signale 35:9
Koenig, M., see Gutdeutsch, R. 31:246
Koenig, M., see Drimmel, J., et al. 39:21
Koenigsberger, J.: Vertikalvariometer für Feldmessungen 1:237
Koenigsberger, J.: Zur Empfindlichkeitsbestimmung von magnetischen Variometern und zur Eichung der magnetischen Felder von Spulen 4:151
Koenigsberger, J.: Zur Anisotropie der physikalischen Parameter von Gesteinen speziell der magnetischen Suszeptibilität 5:62
Koenigsberger, J.: Zur Erforschung der ersten 100 km Erdkruste 5:289
Koenigsberger, J.: Zur Ermittlung ausgedehnter Schichten verschiedener Leitfähigkeit 6:71
Koenigsberger, J.: Über tägliche erdmagnetische Variationen in zwei Alpentälern 6:74
Koenigsberger, J.: Größenverhältnis von remanentem zu induziertem Magnetismus in Gesteinen; Größe und Richtung des remanenten Magnetismus 6:190
Koenigsberger, J.: Gesteinsmagnetismus und Säkularvariation 8:322
Koenigsberger, J., Hecker, O.: Beobachtungen des vertikalen Erdstromes an einem Berge und in der Ebene 1:152
Kohl, E.: Zur Frage der mit dem temperaturkompensierten Magnetsystem erreichbaren Meßgenauigkeit 10:93
Köhler, K., see Behrens, J., et al. 38:481
Köhler, R.: Beobachtungen an Profilen auf See-Eis 5:314
Köhler, R.: Harmonische Schwingungen des Untergrundes 6:123
Köhler, R.: Eine neue Methode der Seismographenprüfung 8:74
Köhler, R.: Die Resonanzmethode als Hilfsmittel bei seismischen Untersuchungen 8:461
Köhler, R.: Formen der Bodenschwingung bei sinusförmiger Anregung 10:386
Köhler, R.: Messung der Schwingungskennziffern und Herabminderung der Erschütterungen in einer Kohlenwäsche 12:148
Köhler, R., Gutenberg, B.: Handbuch d. Geophysik, Bd. 2, Lief. 1 8:109
Köhler, R., Haalck, H.: Lehrbuch der angewandten Geophysik 11:158
Köhler, R., Reich, H.: Angewandte Geophysik für Bergleute und Geologen 10:66
Köhler, R., Sieberg, A.: Erdbebenforschung und ihre Verwertung für Technik, Bergbau und Geologie 10:66
Kohlhörster, W.: Die durchdringende Strahlung in der Atmosphäre 1:215
Kohlhörster, W.: Gammastrahlen an Kaliumsalzen 6:341
Kohlschütter, A., see Pahlen, E. v. d. 7:275, 336
Kohlschütter, E.: Die geodätische Konferenz in Helsingfors im Sommer 1924 1:65
Kohlschütter, E.: Alfred Merz† 1:337
Kohlschütter, E.: Die Invariabilität und Abstimmung von Minimumpendeln 6:466
Kohlschütter, E.: Erwiderung zu Meisser, O. [6:476] 6:478
Kohlschütter, E.: Nachruf auf Alfred Wegener 7:213
Kohlschütter, E.: Vorankündigung der XII. Tagung der Deutschen Geophysikalischen Gesellschaft 12:127
Kohlschütter, E.: Verlag Vieweg 150jähriges Bestehen 12:128
Kohlschütter, E.: 12. Tagung der Deutschen Geophysikalischen Gesellschaft 12:273
Kohlschütter, E.: Bericht über die Tagung der Internationalen Geodätischen Gesellchaft in Edinburgh vom 17. bis 26. September 1936 13:22
Kohlschütter, E.: Beitritt Deutschlands zur IGGV 13:202
Kohlschütter, E.: Bemerkungen zu der Abhandlung „Die hydrostatische Reduktion der Schwerebeobachtungen" von Kurt Wegener 16:233
Kohlschütter, E.: Entgegnung auf die Antwort von Herrn Wegener 16:246
Kohlschütter, E., Angenheister, G., Schütt, R.: Bericht über die zehnte Tagung der Deutschen Geophysikalischen Gesellschaft vom 4. bis 6. Oktober 1932 in Leipzig 8:480
Köhne, K.: Untersuchungen über Feindruckwellen 16:310
Kohnen, H.: Über die Beziehung zwischen seismischen Geschwindigkeiten und der Dichte in Firn und Eis 38:925
Kohnen, H., Westkämper, W.: Palaeosecular Variation Studies of the Brunhes Epoch in the Volcanic Province of the East-Eifel, Germany 44:545
Kolderup, N.H., Krumbach, G.: Das Nordseebeben vom 24. Januar 1927 7:225
Kolhörster, W.: Gammastrahlen an Kaliumsalzen 6:341
Kolhörster, W.: Neuere Untersuchungen über Höhenstrahlung 7:199
Kolhörster, W.: Höhenstrahlung und erdmagnetische Variationen 14:333
Köller, W.: Untersuchungen über Vorgänge an der Schneide beim Schwingen eines Schwerependels 13:269
Kölzer, J.: Beitrag zur Schallausbreitung in der Atmosphäre 4:250
Kölzer, J.: Zur Frage der anomalen Schallausbreitung 10:215

Kölzer, J.: Stand der drahtlosen Meßmethoden 12:306
Kondrat'yev, K.Y.: Radiation Heat Exchange in the Atmosphere. (E. Raschke) 33:146
Kono, M., see Kaneoka, I. 49:207
Kono, M., see Nishitani, T. 50:137
Kopitzke, U.: Finite Element Convection Models: Comparison of Shallow and Deep Mantle Convection, and Temperatures in the Mantle 46:97
Kopytenko, Yu.A., see Novikov, Yu.P., et al. 48:116
Korb, H.G.: Über die Analyse der Schwankungen des Grundwasserspiegels in dem überfluteten Bergwerk Sontra 27:75
Korn, M., Stöckl, H.: Reflection and Transmission of Love Channel Waves at Coal Seam Discontinuities Computed with a Finite Difference Method 50:171
Korschunow, A.: Tiefherdbeben aus Göttinger Seismogrammen 21:113
Korschunow, A.: Mittlerer Tagesgang erdmagnetischer Pulsationen am Geophysikalischen Observatorium zu Fürstenfeldbruck in den Jahren 1960 bis 1962 32:79
Korschunow, A.: Note on the Reliability of Subjective Processing of Geomagnetic Pulsation-Records in the Range Pc 2–Pc 5 42:89
Korte, W.: Beiträge zur experimentellen Seismik 7:57
Korth, A., see Kremser, G., et al. 38:851
Koshkina, T.M., Lagutina, M.V., Shapiro, V.A.: Cohenite Diagnosis in South Urals Ultrabasites 40:565
Kosminskaya, I.P., Kapustian, N.K.: The Wave Field Associated with a Fine Structured Moho in Continents and Oceans 45:159
Kosminskaya, I.P., see Davydova, N.I., et al. 38:369
Kossmat, F.: Die eurasiatischen Kettengebirgsgürtel 2:106
Kotadia, K.M., Gupta, A.: Ionospheric Absorption and Profiles of Electron Density and Loss-Rate in the Lower Ionosphere 46:23
Kotadia, K.M., Patel, B.M.: Ionospheric Absorption of Radio Waves on 1.725 MHz and the Winter Anomaly During Sunspot Minimum 37:1043
Koulomzine, T., Boesch, A.: Abhandlung über die von den Askania-Werken erbaute Vertikal-Feldwaage von Schmidt 8:166
Koulomzine, T., Bondaletoff, N.: Eine neue Methode für sehr präzise magnetische Messungen 10:85
Kozák, J.: Contemporary Possibilities of the Schlieren Method in the Study of Seismic Boundary Phenomena 38:595
Kozák, J., Waniek, L.: Schlierenoptische Untersuchungen an seismischen Gelmodellen mit photometrischer Auswertung des Wellenfeldes 36:175
Kozák, J., see Červený, V. 38:617
Kramm, R., Schlegel, K., Weiss, W.: Partial Reflection Measurements with FM-CW – A Preliminary Investigation (Briefe an den Herausgeber) 38:953
Krankowsky, D., Lämmerzahl, P., Bonner, F., Wieder, H.: The AEROS Neutral and Ion Mass-Spectrometer 40:601
Krankowsky, D., see Arnold, F., et al. 44:125
Krause, F.: Mean-Field Electrodynamics and Dynamo Theory of the Earth's Magnetic Field 43:421
Krauss, I.: The Determination of the Transmissibility of Aquifers from the Transient Motion of the Well-Aquifer System 40:381
Krauss, W.: Methoden und Ergebnisse der Theoretischen Ozeanographie. Band II: Interne Wellen (K. Suchy) 33:210
Krauß, W.: Albert Defant (1884–1974) 43:591
Kravetz, T.P.: Über den Zusammenhang der Erdbeben mit den Polhöhenschwankungen 3:221
Krebs, A.: Strahlenbiologie. (H. Israël) 36:111
Kremser, G.: Ergebnisse erdmagnetischer Tiefensondierung in der Umgebung von Göttingen 28:1
Kremser, G., Korth, A., Saeger, K.H., Jensen, P.A., Jensen, V.N., Taagholt, J.: On the Longitudinal Extension of Electron Precipitation During Magnetospheric Substorms 38:851
Kremser, G., Riedler, W., Kirsch, E.: Short-Time Variations of Solar Particle Fluxes During the August 1972 Events 42:1
Krenzien, E., see Wedeken, U., et al. 46:249
Krige see Tammann, G. 1:371
Krinov, E.L.: Giant Meteorites (K. Jung) 33:369
Kristjansson, L., Fridleifsson, I.B., Watkins†, N.D.: Stratigraphy and Paleomagnetism of the Esja, Eyrarfjall and Akrafjall Mountains, SW-Iceland 47:31
Kristjansson, L., see Vogt, P.R., et al. 47:67
Kropáček, V.: Kinetics of Oxidation Processes in Titanomagnetites 40:329
Kropáček, V., Laštovičková, M.: Changes of Structure, Phase Composition and Electric Conductivity Under High-Temperature Oxidation of Titanomagnetites 48:40
Kroshkin, M.G., see Newell, H., et al. 36:653
Krug, H.D.: Ausbreitung der natürlichen Bodenunruhe nach Aufzeichnungen mit transportablen Horizontalseismographen 13:328
Krumbach, G.: Zur Frage der Laufzeitkurven und der Bearbeitung der Diagramme 1:360
Krumbach, G.: Über die Fortpflanzungsgeschwindigkeit der direkten Longitudinalwellen bei künstlichen Beben 2:30
Krumbach, G.: Zur Frage der Laufzeitkurven. II 5:303
Krumbach, G.: Erwiderung zur vorstehenden Arbeit von Herrn Prof. Gutenberg 6:60
Krumbach, G.: Über die Verwendung langperiodischer Seismometer 14:14
Krumbach, G.: Über ein Stationsseismometer für optische Registrierung 15:17
Krumbach, G.: Grundlagen und Aufbau eines Ortsbebenseismometers mit mechanischer Registrierung 17:281
Krumbach, G., see Kolderup, N.H. 7:225
Krumm, H.-Chr.: Der weltzeitliche Tagesgang der Gewitterhäufigkeit 27:85
Krutikhovskaya, Z.A., Pashkevich, I.K.: Long-Wavelength Magnetic Anomalies as a Source of Information About Deep Crustal Structure 46:301
Kühl, W.: Über die Form der Fernschallwelle 6:358
Kuhn, H.: Studie über das luftelektrische Potentialgefälle und dessen Unruhe unter besonderer Berücksichtigung des Einflusses einer Großstadt 9:238
Kuhn, W.: Zur Theorie der endlichen elastischen Verschiebungen und ihre Anwendung auf isotrope elastische Körper, die unter beliebigen Anfangsverzerrungen stehen 31:159
Kulhánek, O., see Shapira, A., et al. 46:123, 49:243
Kulin, G.: Das Nordlicht 1940 März 24 in Ungarn 16:198
Kundorf, W., Rotter, D.: Über die Anwendung der seismischen Eigenimpulsmethode bei der Erforschung dynamischer Auswirkungen des Gebirgsdruckes 27:35
Kunetz, G.: Einfluß vertikaler Schichten auf elektrische Sondierungen 21:10
Kunkis, A., Ries, G.: Anlage zur Messung und Registrierung der luftelektrischen Elemente mit automatischer Stundenmittelauswertung 30:5
Kunow, H., Witte, M., Wibberenz, G., Hempe, H., Mueller-Mellin, R., Green, G., Iwers, B., Fuckner, J.: Cosmic Ray Measurements on Board Helios 1 from December 1974 to September 1975: Quiet Time Spectra, Radial Gradients, and Solar Events 42:615
Kuo, J.P., see Hung, R.J. 45:67
Kupfer, E.: Hydromagnetic Waves in a Non-Uniform Plasma 41:123
Küppers, F., Untiedt, J., Baumjohann, W., Lange, K., Jones, A.G.: A Two-Dimensional Magnetometer Array for Ground-Based Observations of Auroral Zone Electric Currents During the International Magnetospheric Study (IMS) 46:429
Küppers, F., see Baumjohann, W., et al. 44:373
Küppers, F., see Untiedt, J., et al. 45:41
Küppers, F., see Mersmann, U., et al. 45:281
Küppers, F., see Opgenoorth, H.J., et al. 48:101

Kürschner, D., see Koch, H., et al. 28:281
Kurt, V.G., see Richter, A.K., et al. 50:101

Labitzke, K., Schwentek, H.: Midwinter Warmings in the Stratosphere and Lower Mesosphere and the Behaviour of Ionospheric Absorption 34:555
la Cour, D.: Une Modification de l'Enregistreur à Marche Rapide et à Petite Consommation de Papier de Ad. Schmidt pour l'Application aux Stations de l'Année Polaire 1932–1933 6:255
Lagutina, M.V., see Koshkina, T.M., et al. 40:565
Lal, T., see Negi, J.G. 35:589
Lambert, W.D.: The Hayford-Bowie Table and the Definition of Perfect Isostasy 11:35
Lammers, E., see Musmann, G., et al. 42:591
Lämmerzahl, P., Bauer, S.J.: The AEROS Mission 40:571
Lämmerzahl, P., see Krankowsky, D., et al. 40:601
Landisman, M., see Fuchs, K. 32:121
Landsberg, H.: Über einen Fall angeblicher Erdbebenvorgefühle 8:107
Landsberg, H.: Beitrag zum Thema: Seismische Bodenunruhe 9:156
Landsberg, H.: Das Erdbeben im Fuldagebiet vom 15. Januar 1933 9:234
Landsberg, H.E., Mieghem, J. van: Advances in Geophysics. (H. Burkhardt) 31:111
Lange, K., see Mersmann, U., et al. 45:281
Lange, K., see Küppers, F., et al. 46:429
Lange, O., see Suckstorff, G.A. 14:47
Lange-Hesse, G.: Durchschnittlicher Tagesgang der F1-Schicht-Grenzfrequenzen und seine Abhängigkeit von geographischer Breite und Jahreszeit 25:199
Lange-Hesse, G.: Jahreszeitliche Einflüsse auf die Rückstrahlung ultrakurzer Wellen an Polarlichtern in Mitteleuropa 29:35
Lange-Hesse, G.: Radio-Polarlicht (Übersichtsartikel) 34:323
Lange-Hesse, G., see Czechowsky, P., et al. 36:77
Langlie, Aa., see Storetvedt, K.M., et al. 44:317
Lanzerotti, L.J., Hasegawa, A.: Latitude-Dependent Waves and Impulse-Produced Waves 42:271
La Riva, C. de, see Israël, H. 33:188
Larsen, J.C.: Note on Determining Hourly Mean Values 40:255
Laštovičková, M., see Kropáček, V. 48:40
Latka, R.: Modellrechnungen zur Induktion im elektrisch leitfähigen Untergrund 32:512
Lauche, H.: Observations of the Oxygen Green Line Airglow During the Winter Anomaly Campaign 1975/76 44:35
Lauche, H., see Czechowsky, P., et al. 36:77
Lauterbach, R.: Geomagnetische Messungen an Lamprophyrgängen in der Lausitz 13:291
Lebeau, A., see Witt, C. de, et al. 30:155
Ledersteger, K.: Bemerkungen zu den Geoiden von Ackerl und Hirvonen 10:246
Ledersteger, K.: Über die Minimumeigenschaft der Schwerestörungen 11:23
Ledersteger, K.: Der Einfluß des Kimuragliedes auf die Polkoordinaten 12:48
Ledersteger, K.: Zur Frage der Variabilität der Chandlerschen Periode 13:11
Ledersteger, K.: Polbahn und primäres Z-Glied 14:1
Ledersteger, K.: Wittings Störungen und die Veränderlichkeit der Chandlerschen Amplitude 16:203
Ledersteger, K.: Zur Theorie der Wiechertmodelle 32:310
Lee, A.J., see Wooster, W.S., et al. 35:611
Lee, K.-H., see Quon, C., et al. 46:291
Legg, C.A., see Töpfer, K.D. 40:97
Lehmann, H.-R., see Treumann, R., et al. 43:719
Lehmann, I.: Über die Laufzeitkurve der Phase S_cP_cS 5:259
Lehmann, R.: Die Gestaltung der Erdoberfläche 2:112
Lehr, L., see Knoechel, H., et al. 17:57
Leinert, C., Pitz, E., Hanner, M., Link, H.: Observations of Zodiacal Light from Helios 1 and 2 42:699
Leitinger, R.: Untersuchungen über die Höhenabhängigkeit der halbtägigen gravitationserregten Gezeiten der Atmosphäre 37:835
Leitinger, R., Schmidt, G., Tauriainen, A.: An Evaluation Method Combining the Differential Doppler Measurements from Two Stations That Enables the Calculation of the Electron Content of the Ionosphere 41:201
Leitinger, R., see Ebel, A., et al. 35:373
Leonard, G., see Knoechel, H., et al. 17:57
Leppich, W., see Ehrismann, W., et al. 39:115
Leppin, M.: New Experiments with the Two-Loop Sounding Method 40:113
Leppin, M., Boldt, B.: Analogue Model Experiments for Electromagnetic Induction in Elongated Structures 44:557
Lettau, H.: Invar-Minimumpendel als Magnetstäbe 9:180
Lettau, H.: Das Horizontaldoppelpendel 13:25
Lettau, O., see Ehrismann, W., et al. 39:115
Levshenko, V.T., see Galkin, I.N., et al. 38:455
Levy, G.S., see Volland, H., et al. 42:659
Leydecker, G., see Schmedes, E. 44:277
Libby, W.F., see Fabian, P. 35:1
Lidiak, E.G.: Magnetic Characteristics of Some Precambrian Basement Rocks 40:549
Liebau, F., see Fuchs, K., et al. 37:937
Liebermann, K.: Nordlicht 1940, Januar 3 16:88
Liebermann, K.: Nordlicht 1940, September 26 16:251
Liebermann, K.: Nordlichtbeobachtung 16:333
Liebermann, K.: Bericht über Nordlichter vom 18. bis 22. September 1941 17:249
Liebermann, K., see Knoechel, H., et al. 17:57
Liebscher, H.-J.: Reflexionshorizonte der tieferen Erdkruste im Bayerischen Alpenvorland, abgeleitet aus Ergebnissen der Reflexionsseismik 28:162
Liebscher, H.J.: Deutungsversuche für die Struktur der tieferen Erdkruste nach reflexionsseismischen und gravimetrischen Messungen im deutschen Alpenvorland (Teil I) 30:51
Liebscher, H.J.: Deutungsversuche für die Struktur der tieferen Erdkruste nach reflexionsseismischen und gravimetrischen Messungen im deutschen Alpenvorland (Teil II) 30:115
Lieger, P.F.: Eine im Winter bei mittlerer Breite auftretende Senke des Elektroneninhaltes 35:581
Link, F.: Über den möglichen Zusammenhang zwischen den Polarlichtern vom 25. Januar 1938 und 24. März 1940 16:198
Link, H., see Leinert, C., et al. 42:699
Linke, F.: Verwertung von Sonnenstrahlungsmessungen in Luftfahrzeugen 1:55
Linke, F.: Bemerkung zu R. Stoppel: Untersuchungen über die lokalen Schwankungen des Erdpotentials 5:46
Linke, F.: Einfluß geophysikalischer Vorgänge und Zustände auf den menschlichen Organismus 9:62
Linke, F.: Über einige neue Apparate für Bodenexplorationen und deren etwaige Beziehungen zur Wünschelrutenreaktion 10:342
Linsser, H.: Anwendungsmöglichkeiten transversaler Wellen in der Untertage-Seismik 20:150
Lippmann, H.J.: Erdmagnetische Induktion in Leitfähigkeitseinlagerungen im Untergrund 24:113
Lippolt, H.J., Raczek, I.: Rinneite-Dating of Episodic Events in Potash Salt Deposits 46:225
Lippolt, H.J., see Todt, W. 41:43, 641, 48:18
Lippolt, H.J., see Hellmann, K.N. 50:73
List, M., see Gerlach, W. 37:754, 755
Littrow, J.J. von: Die Wunder des Himmels. (H. Schwentek) 30:155
Litvinenko, I.V., see Zverev, S.M., et al. 47:191, 202
Litvinenko, I.V., see RRISP Working Group 47:228
Livländer, R.: Die kontinentalen Verschiebungen von Amerika und Madagaskar 6:134
Lode, W., see Graeser, E., et al. 24:134
Loewenthal, D., see Goldberg, S., et al. 50:151
Löffler, H., see Frölich, F. 32:26

Löhle, F.: Das Nordlicht vom 29./30. März 1940 nach Beobachtungen in Pommern 16:252
Löhnberg, A., Stern, W.: Ein neuer Weg der karsthydrologischen Forschung durch Anwendung geoelektrischer Methoden 8:283
Loidl, A., Schlegel, K.: Measured and Calculated Secondary Electron Energy Spectra (20–1,500 eV) Above 120 km 41:215
Loidl, A., Schwentek, H.: Mesospheric Molecular Oxygen Density, Pressure and Temperature Profiles Obtained from Measurements of Solar H Lyman-α Radiation 44:107
Loidl, A., Schwentek, H.: Intensity of Solar X-rays in the E Region Measured by Proportional Counters Carried on Rockets 44:117
Loncarevic, B., see RRISP Working Group 47:228
Loncarevic, B.D., see Goldflam, P., et al. 47:250
Lorch, S.: Messung des Wassergehaltes in Böden mit der Neutronensonde 29:261
Lorch, S.: Ein Gerät zur Messung der Geschwindigkeit (Betrag und Richtung) des Grundwassers in einem Bohrloch 33:287
Lorch, S.: Messung zeitlicher Wassergehaltsänderungen im Boden 33:403
Lorenz, D.: Die radiometrische Messung der Boden- und Wasseroberflächentemperatur und ihre Anwendung insbesondere auf dem Gebiet der Meteorologie (Übersichtsartikel) 39:627
Lorenz, H.: Beiträge zur Theorie des Erdaufbaus 14:142
Lorenz, H.: Ermittlung des Zustandes des Erdinnern aus dem Energieinhalt 15:371
Loreta, E.: Nordlicht 16:197
Losecke, W.: Über die Bestimmung von Salzstockgrenzflächen mit Hilfe der Magnetotellurik (Briefe an den Herausgeber) 38:959
Losecke, W., Müller, W.: Two-Dimensional Magnetotelluric Model Calculations for Overhanging, High-Resistivity Structures 41:311
Losecke, W., see Knödel, K., et al. 45:199
Lotze, W.: Mitteilung 1: Schallgeschwindigkeitsmessungen von Eis in Abhängigkeit von Druck und Temperatur 23:243
Love, A.E.H.: Some Problems of Geodynamics, Being an Essay to Which the Adams Prize in the University of Cambridge Was Adjudged in 1911. (K. Jung) 34:632
Løvlie, R., see Storetvedt, K.M., et al. 46:319
Lowrie, W.: Oceanic Basalt Magnetic Properties and the Vine and Matthews Hypothesis 40:513
Lowrie, W., Alvarez, W.: Paleomagnetism and Rock Magnetism of the Pliocene Rhyolite at San Vincenzo, Tuscany, Italy 45:417
Lowrie, W., Kent, D.V.: Characteristics of VRM in Oceanic Basalts 44:297
Lowrie, W., see Horner, F. 49:11
Lubiger, F.: Über die vom Samoa-Observatorium registrierten erdmagnetischen Pulsationen 11:116
Luca, A.J., see Frese, R.R.B. von, et al. 49:234
Lucke, O.: Über die Veränderlichkeit des erdmagnetischen Hauptfeldes und seine Theorien 23:197
Lucke, O.: Über den physikalischen Zustand der Materie im Erdinnern 24:240
Lucke, O.: Bemerkungen zur Dissertation von A. Vogel: Über die Unregelmäßigkeiten der äußeren Begrenzung des Erdkerns 26:50
Lucke, O.: Die dynamischen Gleichungen des Plasmas in der Magnetosphäre 26:105
Lucke, O., Sparrer, H.: Die Gerätekonstante des elektrodynamischen Theodoliten des VEB WTBG, Berlin und die Vermessung der Primärspule mit dem Meßgerät des VEB Carl Zeiß, Jena 24:284
Lucke, O., Wagner, F.Ch.: Die dynamischen Gleichungen in der Magnetosphäre. II 27:257
Lucke, O., see Fanselau, F. 22:121
Ludewig, P., Witte, H.: Radioaktive Messungen im Quellgebiet von Brambach 1:242
Lukeschitz, G., see Drimmel, J., et al. 45:341
Lukeschitz, G., see Procházková, D., et al. 46:343
Lund, C.-E., see Hirschleber, H.B., et al. 41:135
Lüneburg, E., see Edenhofer, P., et al. 42:673
Lüneburg, H.; Dynamik und Sediment-Transport an der Wattoberfläche des Weserästuars 23:57
Lutz, C.W.: Ortsgültige Laufzeitkurven 3:34
Lux, J., see Knoechel, H., et al. 17:57
Lynds, B., see Struve, O., et al. 28:294

Maaz, R., see Ullmann, W. 23:75
Mack, K.: Einige Bemerkungen über Weltbeben und die sogenannten Wiederkehrwellen 2:266
Macke, W., Rennert, P., Rieger, F., Voss, K.: Über die Gestalt und das Schwerefeld der Erde 30:21
Maeda, H., see Takeda, M. 45:209
Magnitskii, V.A.: Problems of Theoretical Seismology and Physics of the Earth's Interior. (R. Schick) 31:226
Mahnkopf, H.: Die Registrierung von Pendelschwingungen mittels kapazitiver Kontakte 5:49
Mainardi, F., Servizi, G., Turchetti, G.: On the Propagation of Seismic Pulses in a Porous Elastic Solid 43:83
Majumdar, R.K., Rao, S.H.: An Alignment Chart for Gravity Elevation Correction (Brief an den Herausgeber) 37:743
Makris, J.: Crustal Structure of the Aegean Sea and the Hellenides Obtained from Geophysical Surveys 41:441
Makris, J., Mavridis, L.N., Menzel, H., Stavrou, A., Veis, G.: The Gravity Field of Attika, the Peloponnese and Kithira, Greece 39:929
Makris, J., Menzel, H., Zimmermann, J., Bonjer, K.-P., Fuchs, K., Wohlenberg, J.: Crustal and Upper Mantle Structure of the Ethiopian Rift Derived from Seismic and Gravity Data (Brief an den Herausgeber) 36:387
Makris, J., Thiele, P., Zimmermann, J.: Crustal Investigation from Gravity Measurements at the Scarp of the Ethiopian Plateau 36:299
Makris, J., Vees, R.: Crustal Structure of the Central Aegean Sea and the Islands of Evia and Crete, Greece, Obtained by Refractional Seismic Experiments 42:329
Makris, J., Zimmermann, J., Bachem, H.C., Ritter, B.: Gravity Survey of South AFAR, Ethiopia 39:279
Makris, J., see Behle, A., et al. 38:45, 221
Mal, A.K.: On the Field of an Electric Dipole in Presence of a Layered Media 28:209
Mallick, K., Jain, S.C.: Time-Domain Electromagnetic INPUT Response of a Conducting Horizontal Thin Sheet 41:127
Malsch, W.: Nordlichtbeobachtung zu Nürnberg am 24. März 1940 16:197
Malsch, W., see Knoechel, H., et al. 17:57
Mälzer, H.: Eine Tintenregistrierung für Seismographen 30:245
Mannweiler, R., see Mügge, R. 17:198
Manson, A.J.: Rotational Hysteresis Measurements on Oxidized Synthetic and Natural Titanomagnetites 37:431
Manson, A.J., O'Donovan, J.B., O'Reilly, W.: Magnetic Rotational Hysteresis Loss in Titanomagnetites and Titanomaghemites – Application to Non-Destructive Mineral Identification in Basalts 46:185
Märcz, F.: Solar Electron Fluxes, Increased Geomagnetic Activity and Ionospheric Absorption Following Selected Flares 45:91
Märcz, F., see Ádám, A., et al. 50:37
Marien, K.H., see Arnold, F., et al. 44:125
Markert, H.: On Some Magnetic and Magneto-Optic Properties to be Studied on Fine Precipitations in Glasses 37:525
Markert, H., Heller, F., Steigenberger, N.: Parabolic Field Dependence of Kinks Occurring in the Logarithmic Time Plots of Viscous Magnetization 42:47
Markert, H., Steigenberger, N.: On the Size Distribution of Submicroscopic Magnetite and Titanomagnetite Fine Particles in Basalt 37:499

Markert, H., Trissl, K.-H., Zimmermann, G.J.: On a High-Frequency Method for the Measurement of Susceptibilities and Hysteresis Losses of Rocks and Minerals Between Nitrogen Temperature and 700° C 40:303
Markert, H., see Heller, F. et al. 45:235
Marsch, E., see Rosenbauer, H., et al. 42:561
Marten, W., see Galbas, P.A. 5:322
Martin, H.: Das photographische Koinzidenzverfahren 5:148
Martin, H.: Die allgemeine Koinzidenzkurve 8:205
Martin, H.: Die Genauigkeit von Pendelkontakten und der Einfluß des Steigrades einer Pendeluhr auf die Schwingungsdauer des Pendels 9:83
Martin, H.: Bemerkung zu der Arbeit von G. Fanselau: „Ein neuer Schwingungsmesser" 9:168
Martin, H.: Zur vorstehenden Erwiderung von G. Fanselau 9:170
Martin, H.: Die Grundlagen zur Beurteilung von Verkehrserschütterungen 12:322
Martin, H.: Untersuchungen am Schütteltisch 12:339
Martin, H.: Ein neuer mechanischer Beschleunigungsmesser 13:241
Martin, H.: Ein neuer Erschütterungsmesser und die Aufzeichnung nicht sinusförmiger Bewegungen 15:24
Martin, H.: Zur Frage Schwingweg-, Geschwindigkeits- oder Beschleunigungsmesser 15:260
Martin, H., see Meisser, O. 3:106, 10:158
Martin, W.L., see Edenhofer, P., et al. 42:673
Martinic, N., see Kirsch, E., et al. 50:45
Mason, S.F.: Geschichte der Naturwissenschaft. (H. Schwentek) 31:224
Masuch, V.: Erdstrahlungsmessungen in Bad Nauheim nach der Gammastrahlenmethode 10:112
Materialzusammenstellung der Schallregistrierungen während der Sprengungen in Oldebroek (Holland) am 15. Dezember 1932 10:145
Mattern, G.: Über „Sferics"-Registrierungen im Frequenzbereich bei etwa 1000 Hz 20:104
Mattern, G.: Über die Whistler-Beobachtungen des Taunus-Observatoriums 25:265
Mattern, G.: Zusammenhänge zwischen Dawn chorus Beobachtungen und den Güteziffern des Funkverkehrs 32:244
Maurer, H., Theile, B.: Parameters of the Auroral Electrojet from Magnetic Variations Along a Meridian 44:415
Maurer, H., see Opgenoorth, H.J., et al. 48:101
Mauritsch, H.J., Frisch, W.: Palaeomagnetic Data from the Central Part of the Northern Calcareous Alps, Austria 44:623
Mäussnest, O.: Anomalien des erdmagnetischen Feldes im Gebiet der jungen Vulkane Südwestdeutschlands 37:573
Mäussnest, O.: Magnetische Feldmessungen in der Hegau-Vulkanprovinz (SW-Deutschland) 38:767
Mavridis, L.N., see Makris, J., et al. 39:929
Mayaud, P.N.: On the Sources of the 12-Month Wave in the An and As Geomagnetic Activity Indices 46:261
Mayer, H.: Bild der Wissenschaft: Die Architektur der Erde 38:189
Mayer, H.: Space Research XI: Proceedings of the thirteenth plenary Meeting of COSPAR 38:191
Mayer, W.G.: Neuberechnung der Blutschen Ergebnisse für Reflexion und Brechung elastischer Wellen an Unstetigkeitsflächen 30:275
Mayer-Rosa, D., Mueller, St.: The Gross Velocity-Depth Distribution of *P*- and *S*-Waves in the Upper Mantle of Europe from Earthquake Observations 39:395
Mayer-Rosa, D., see Fuchs, K., et al. 37:937
Mayer-Rosa, D., see Procházková, D., et al. 46:343
Mayhew, M.A.: Inversion of Satellite Magnetic Anomaly Data 45:119
McKenzie, D., see Richter, F. 44:441
McWhirter, I., see Rees, D., et al. 50:202
Meinardus, W.: Die Temperaturverhältnisse der südlichen Halbkugel 15:94
Meinhold, R.: Geophysikalische Meßverfahren in Bohrungen (D. Emter) 33:370
Meisser, O.: Ermittlung der Tiefe der schwerestörenden Massen mittels Drehwagen 1:32
Meisser, O.: Erhöhung der Beobachtungsgenauigkeit bei relativen Pendelmessungen; Registrierung von Pendelschwingungen 5:145
Meisser, O.: Ein neuer Vierpendelapparat für relative Schweremessungen 6:1
Meisser, O.: Geophysikalische Messungen unter Tage 6:13
Meisser, O.: Bemerkung zu der Arbeit „Die Invariabilität und Abstimmung von Minimumpendeln" von E. Kohlschütter 6:476
Meisser, O.: Bemerkung zu den vorstehenden Ausführungen von Herrn Prof. Dr. C.A. Heiland 6:480
Meisser, O.: Das logarithmische Dekrement von Pendeln 9:88
Meisser, O.: Schneiden- und Unterlagematerial bei invariablen Pendeln für relative Schweremessungen 9:173
Meisser, O.: Zur photographischen Registrierung von Stationsseismometern 10:259
Meisser, O.: Beitrag zur Theorie und Konstruktion von statischen Schweremessern 11:221
Meisser, O.: Tabelle der Normalschwere von 47 bis 56° Breite für sehr genaue relative Schweremessungen 12:63
Meisser, O.: Beiträge zur Konstruktion eines Vertikalseismometers 13:251
Meisser, O.: Zur absoluten Schweremessung 15:41
Meisser, O.: I. Internationale Symposium über rezente Erdkrustenbewegung (21.–26. Mai 1962 in Leipzig). (G. Schneider) 30:111
Meisser, O., Martin, H.: Zur experimentellen Seismik 3:106
Meisser, O., Martin, H.: Beiträge zu den Luftschallmessungen 10:158
Meisser, O., see Herrmann, A. 11:152
Meissner, O.: Einige Bemerkungen zu den Aufsätzen des Herrn Tams über den Einfluß von Sonne, Mond u. Luftdruck auf die vogtländischen Erdbebenschwärme 1:194
Meissner, O.: Zur Frage nach der täglichen Periode der Erdbeben 2:165
Meissner, O.: Über die tägliche und jährliche Periode der mikroseismischen Bewegung in Eskdalemuir und Kew 7:193
Meissner, R.: Der Einfluß von Luftdruckschwankungen auf den Grundwasserstand 19:161
Meissner, R.: Vergleiche seismischer Weitwinkelmessungen in der UdSSR und im bayrischen Molassebecken 33:439
Meissner, R.: Zur Deutung der hypsometrischen Kurven von Erde und Mond 34:99
Meissner, R.: Der gegenwärtige Stand der Mondforschung (Übersichtsartikel) 35:441
Meissner, R.: Viscosity-Depth-Structure of Different Tectonic Units and Possible Consequences for the Upper Part of Converging Plates 40:57
Meißner, R.: Untersuchungen über die Zusammenhänge zwischen Luftdruck und Brunnenspiegel 21:80
Meißner, R.: Fehler und Korrekturen bei seismischen Messungen in Gebieten mit bewegtem Oberflächenrelief 23:287
Meissner, R.O., Flüh, E.R.: Probable Relations Between Seismic Anisotropy and a Fine Structure of the Lithosphere 45:349
Meissner, R.O., Vetter, U.R.: Relationship Between the Seismic Quality Factor Q and the Effective Viscosity η 45:147
Meissner, R., see Vetter, U. 36:225
Meissner, R., see Hirschleber, H.B., et al. 41:135
Meister, F.J.: Schwingungsmessung mittels Trägerstrom 16:105
Meitzner, W.: Magnetische Untersuchungen am Backenberg bei Güntersen 28:137
Meitzner, W.: Gesteinsmagnetische Untersuchungen der Vulkanite im Salinar des hessischen Werra-Kaligebirges 31:273

Meitzner, W.: Zur Anwendung der *Förster*-Sonde bei gesteinsmagnetischen Arbeiten 31:332
Melchior, P.: The Earth Tides (K. Jung) 33:464
Melzner, F., Rabben, H.H.: Elektronendichte-Messungen in der Ionosphäre mit einer neuartigen Hochfrequenz-Impedanzsonde 36:135
Melzner, F., Rabben, H., Rothermel, H.: Messung des Elektronendichteprofils der unteren Magnetosphäre mit einer Höhenforschungsrakete 34:105
Mendel, H.: Die seismische Bodenunruhe in Hamburg und ihr Zusammenhang mit der Brandung 6:32
Menze, H., see Knoechel, H., et al. 17:57
Menzel, H.: Ernst Tams zum 80. Geburtstag 28:51
Menzel, H.: Tiefseekuppen (Übersichtsartikel) 37:595
Menzel, H., see Jung, K., et al. 31:7
Menzel, H., see Peterschmitt, E., et al. 31:41
Menzel, H., see Gutdeutsch, G. 33:200
Menzel, H., see Makris, J., et al. 36:387, 39:929
Menzel, H., see Behle, A., et al. 38:45, 221
Menzel, H., see Hirschleber, H.B. 32:365
Merfeld, H., see Knoechel, H., et al. 17:57
Merkler, G., Bock, G., Fuchs, K.: Correlation Between Seismic Microactivity, Temperature and Subsidence of Water Level at Reservoirs 49:198
Merkler, G., see Blum, R., et al. 43:561
Mersmann, U., Baumjohann, W., Küppers, F., Lange, K.: Analysis of an Eastward Electrojet by Means of Upward Continuation of Ground-Based Magnetometer Data 45:281
Mertins see Knoechel, H., et al. 17:57
Meyer, B., see Rosenbauer, H., et al. 42:561
Meyer, H., see Heye, D. 38:937
Meyer, J.: Über die Richtungsveränderlichkeit des geomagnetischen Induktionspfeiles bei endlicher Leitfähigkeit 34:195
Meyer, J.: The Recurrence Tendency of Geomagnetic Activity During Solar Cycle 20 44:427
Meyer, J., Damaske, D.: On the Origin of the Annual Wave in Hemispheric Geomagnetic Activity 49:66
Meyer, J., see Damaske, D. 48:54
Meyer, O.: In memoriam Friedrich Errulat 35:623
Meyer, P., see Fulks, G. 40:751
Meyer, R.: Haloerscheinungen 1:216
Meyer, R.P., see Steinhart, J.S. 30:158
Meyermann, B.: Die Westdrift der Erdoberfläche 2:204
Meyermann, B.: Die Schrumpfungsgeschwindigkeit des Erdradius aus astronomischen Beobachtungen 4:153
Meyermann, B., Wanach, B., Mahnkopf, H.: Ergebnisse des Internationalen Breitendienstes von 1912,0 bis 1922,7 8:329
Michael, W.: Die Erde, gebremst, beschleunigt, abgelenkt, – erlebt Erdbeben, Taifune, Tornados usw. 9:165
Michota, G.G., see Davydova, N.I., et al. 38:369
Mieghem, J. van, see Landsberg, H.E. 31:111
Miggenrieder, H., see Rosenbauer, H., et al. 42:561
Mikhailenko, B.G., see Alekseev, A.S. 48:161
Milch, W.: Über den Einfluß größerer Teilchen in der Atmosphäre auf das Polarisationsverhältnis des Himmelslichts 1:109
Milch, W.: Über die praktische Verwertbarkeit des Depolarisationsfaktors 1:159
Milch, W.: Zur Frage nach der Konstanz der Solarkonstante 1:377
Mildner, P.: Das Geophysikalische Observatorium der Universität Leipzig 11:329
Militzer, H.: Nahseismische Untersuchungen mit einem Bodenvibrator 27:49
Miller, H., see Gebrande, H., et al. 47:239
Miller, H., see RRISP Working Group 47:228
Mintrop, L.: Über die Ausbreitung an der Erdoberfläche erzeugter periodischer Bodenschwingungen (Maschinenschwingungen) in die Tiefe 18:140
Mintrop, L.: Die Entwicklung der Sprengseismik 19:101
Mironova, V.I., see Zverev, S.M., et al. 44:283
Mitronovas, W.: Global and Regional Phase Velocities of Long-Period Fundamental Mode Rayleigh Waves 43:287
Model, F.: Der neue Schreibpegel in Arkona 15:107
Mögel, H.: Über die Beziehungen zwischen Störungen des Kurzwellenempfanges und den erdmagnetischen Störungen 7:207
Möller, D., Ritter, B.: Geodetic Measurements and Horizontal Crustal Movements in the Rift Zone of NE-Iceland 47:110
Möller, D., see Jacoby, W.R., et al. 47:1
Möller, F.: Advances in Geophysics. Herausgegeben von H.E. Landsberg u. J.V. Mieghem 33:292
Möller, F.: In memoriam Bernhard Brockamp 35:619
Möller, F., see Mügge, R. 8:53
Möller, G.F., Haser, L.: Polarisationsmessungen an künstlichen Bariumwolken 36:451
Möller, H.G., see Czechowsky, P., et al. 36:77
Mongstad Våge, H., see Storetvedt, K., et al. 46:319
Montgomery, M.D., see Rosenbauer, H., et al. 42:561
Mooney, W.D., Prodehl, C.: Crustal Structure of the Rhenish Massif and Adjacent Areas; a Reinterpretation of Existing Seismic-Refraction Data 44:573
Moore, P.: Den Sternen auf der Spur (O. Walk) 38:190
Morelli, C.: Modern Standards for Gravity Surveys 42:171
Morelli, C., see Behle, A., et al. 38:45
Morelli, C., see Closs, H. 28:249
Morfill, G., see Scholer, M., et al. 40:37
Moritz, H.: Least-Squares Collocation and the Gravitational Inverse Problem 43:153
Moritz, J.: Messung von Strahlungsgürtel-Protonen im Energiebereich 0,25–1,65 MeV mit dem Satelliten Azur 37:179
Moritz, J.: Energetic Protons at Low Equatorial Altitudes 38:701
Mörl, P., see Keppler, E., et al. 33:346
Morrison, H.F., see Quon, C., et al. 46:291
Mostaanpour, M.M., see Sobouti, M., et al. 44:663
Mothes, H.: Seismische Dickenmessungen von Gletschereis 3:121
Mothes, H.: Neue Ergebnisse der Eisseismik 5:120
Mothes, H., see Brockamp, B. 6:482
Mueller, St., see Ansorge, J. 39:385
Mueller, St., see Mayer-Rosa, D. 39:395
Mueller-Mellin, R., see Kunow, H., et al. 42:615
Mügge, R.: Über die Stratosphärentemperatur und die Strahlungsbedingungen der oberen Atmosphäre 5:194
Mügge, R.: Bericht über die Versammlung der Deutschen Meteorologischen Gesellschaft in Dresden vom 6. bis 9. Oktober 5:371
Mügge, R.: Das Grundwasser als geophysikalischer Indikator 20:65
Mügge, R., Köppen, W., Geiger, R.: Handbuch der Klimatologie 8:111
Mügge, R., Mannweiler, R.: Über Präzessionsbewegungen zonal driftender Luftringe 17:198
Mügge, R., Möller, F.: Zur Berechnung von Strahlungsströmen und Temperaturänderungen in Atmosphären von beliebigem Aufbau 8:53
Mühleisen, R.: Die luftelektrischen Elemente im Großstadtbereich 19:142
Mühleisen, R.: Sferiks von ozeanischen Gewittern und luftelektrische Feldstärke über dem Atlantik während der Expedition 1965 des deutschen Forschungsschiffes „Meteor" 32:419
Mühleisen, R.: Über atlantische und tropische Gewitter 33:273
Mühleisen, R.: Neue Ergebnisse und Probleme in der Luftelektrizität (Übersichtsartikel) 37:759
Mühleisen, R., Fischer, H.-J., Hofmann, H.: Horizontal Electric Fields in the Ionosphere Derived from Air Electric Measurements 37:1055

Mühlen, W. von zur: Über seismische Oberflächenwellen und ihre Beziehung zum geologischen Aufbau des eurasiatischen Kontinents 10:26
Mühlen, W. von zur: Seismische Bodenunruhe und Brandung 12:97
Mühlhäuser, K.H., see Rosenbauer, H., et al. 42:561
Mühlhäuser, S.: Die Richtung der ersten Bodenbewegung in Stuttgart für die Hauptbebengebiete der Erde 19:76
Mula, A., see Müller, G., et al. 43:507
Mulargia, F., see Boschi, E. 43:465
Mulcahy, M., see Backus, G. 43:497
Mulder, A.F.J. de, see Collette, B.J., et al. 47:91
Müller, E.A.W.: Berechnung der oberen Grenze der in der Ionosphäre möglichen Temperatur aus den Messungen der Ionisierungsschichtdicken 11:126
Müller, F.: Beiträge zur Methode der Radioaktivitätsuntersuchungen in der angewandten Geophysik 7:241
Müller, G.: Theoretical Seismograms for Some Types of Point-sources in Layered Media 34:15, 147, 35:347
Müller, G.: Direct Inversion of Seismic Observations 37:225
Müller, G.: Theoretical Body Wave Seismograms for Media with Spherical Symmetry – Discussion and Comparison of Approximate Methods 39:229
Müller, G.: Fault-Plane Solution of the Earthquake in Northern Italy, 6 May 1976, and Implications for the Tectonics of the Eastern Alps 42:343
Müller, G.: Earth-Flattening Approximation for Body Waves Derived from Geometric Ray Theory – Improvements, Corrections and Range of Applicability 42:429
Müller, G.: Thermoelastic Deformations of a Half-Space – A Green's Function Approach 43:761
Müller, G., Bonjer, K.-P., Stöckl, H., Enescu, D.: The Romanian Earthquake of March 4, 1977. I. Rupture Process Inferred from Fault-Plane Solution and Multiple-Event Analysis 44:203
Müller, G., Kind, R., Mula, A., Gregersen, S.: Amplitudes of Long-Period PcP, SKS and SKKS and the Structure at the Base of the Mantle and in the Outer Core 43:507
Müller, G., see Wachholz, H. 30:127
Müller, G., see Burkhardt, H., et al. 33:455
Müller, G., see Kind, R. 41:149
Müller, G., see Fertig, J. 46:349
Müller, G., see Räkers, E. 50:143
Müller, G., see Temme, P. 50:177
Müller, H.: Störung der Windströmung und des Austausches über einem Gebäude 12:173
Muller, H.G., Kingsley, S.P.: Co-Ordinated Meteor Wind Observations from Sheffield During the January 1976 Winter Anomaly 44:39
Müller, H.J.: Suche nach einer systematischen Änderung im Laufe des Jahres in der Phase der zweiten harmonischen der täglichen Variation der kosmischen Strahlung 37:39
Müller, H.K.: Beobachtung von Sprengungen in drei Komponenten 8:459
Müller, H.K.: Beobachtung der Bodenbewegung in drei Komponenten bei Sprengungen 10:40
Müller, H.K.: Vergleich von Laufzeitkurve und Gang des Emergenzwinkels bei Sprengungen 11:111
Müller, H.K., see Gerecke, F. 8:65
Müller, I.I.: Introduction to Satellite Geodesy. (G. Schneider) 31:281
Müller, I.I.: Soviet Antarctic Expedition. (F. Möller) 31:281
Müller, M.: Geophysikalische Feldmessung mit niederfrequenten Wechselströmen 5:256
Müller, M.: Der Einfluß der Anisotropie der Medien auf die Verteilung elektromagnetischer Wechselfelder verschiedener Frequenz 5:335
Müller, M.: Eine Apparatur zur Erzeugung und Messung niederfrequenter elektromagnetischer Wechselfelder 7:248
Müller, M.: Die experimentelle Bestimmung der Reaktionsgeschwindigkeit aktiver elektrischer Vorgänge im Erdboden 8:423
Müller, M.: Der geophysikalische Nachweis des Zechsteindolomits 10:330
Müller, M.: Die Meßverfahren zur Bestimmung des Dispersionseffektes des Widerstandes von Gesteinsmedien 15:176
Müller, M.: Ergebnisse geoelektrischer Polarisationsmessungen 16:274
Müller, M.: Erzeugung sinusförmiger Wechselströme in dem unter dem Hörbarkeitsbereich liegenden Frequenzgebiet 17:181
Müller, M.: Die Messung der Frequenzabhängigkeit der elektrischen Leitfähigkeit und Dielektrizitätskonstante von Gesteinsproben 18:59
Müller, M.: Die Abnahme der Stromdichte einer elektrischen Doppelquelle mit wachsender Entfernung 18:67
Müller, M., Fritsch, V.: Grundzüge der Funkgeologie 15:226
Müller, M., Fritsch, V. Dr.: Die Messungen von Erdwiderständen 18:193
Müller, M., Fritsch, V. Dr.: Meßverfahren der Funkmutung 18:194
Müller, S., see Berckhemer, H., et al. 27:151
Müller, S., see Schneider, G., et al. 32:33
Müller, S., see Seidl, D., et al. 32:472
Müller, S., see Seidl, D. 42:283
Müller, S., Stein, A., Vees, R.: Seismic Scaling Laws for Explosions on a Lake Bottom 28:258
Müller, W., see Losecke, W. 41:311
Müller, W.F., Défourneaux, M.: Deformationsstrukturen in Quarz als Indikator für Stoßwellen: Eine experimentelle Untersuchung an Quarz-Einkristallen 34:483
Müller-Deile, G.: Einige Notizen über das rumänische Erdbeben vom 10. November 1940 17:33
Münch, J.: Das Auftreten von *pc*-Pulsationen des erdmagnetischen Feldes in Abhängigkeit von der erdmagnetischen Aktivität 31:192
Münch, J., Dempewolf, W.: Die Ablage der Orientierungsrichtung des Satelliten Azur von der Richtung des erdmagnetischen Feldes 37:627
Münch, J.W., see Schödel, J.P. 38:169
Münch, J.W., see Baranskiy, L.N., et al. 48:1
Mundry, E.: Berechnung des gestörten geothermischen Feldes mit Hilfe eines Relaxationsverfahrens 32:157
Mundry, E.: „Meteor" Forschungsergebnisse (Hrsg. Deutsche Forschungsgemeinschaft) 35:439
Mundry, E.: Harmonic Temperature Waves in a Horizontally Layered Medium 40:767
Mundry, E., Worzyk, P.: On the Coastal Effect on Geoelectrical Soundings 45:329
Murawski, H. (Hrsg.): Vom Erdkern bis zur Magnetosphäre (E. Seiler) 36:652
Murawski, H., see Ahorner, L., et al. 36:313
Murthy, G.S., see Radhakrishnamurty, C., et al. 45:433
Murthy, I.V.R., see Rao, B.S.R., et al. 44:257
Murty, B.V.S., see Rao, S.M.V., et al. 44:353
Musmann, G., Neubauer, F.M., Lammers, E.: Radial Variation of the Interplanetary Magnetic Field Between 0.3 AU and 1.0 AU. Observations by the Helios-1 Spacecraft 42:591
Musmann, G., Seiler, E.: Detection of Meridional Currents in the Equatorial Ionosphere 44:357
Musmann, G., see Keppler, E., et al. 33:346
Musmann, G., see Hunsche, U., et al. 49:26
Myachkin, V.I., see Galkin, I.N., et al. 38:455
Myrbach, O.: Ein Beitrag zur Frage, ob Sonnenflecken und Mondphase einen auslösenden Einfluß auf Erdbeben haben 2:217
Myrbach, O.: Die bebenauslösende Wirkung der Sonnenflecken, gezeigt an der sogenannten elfjährigen Periode 4:413

Nagata, T.: Integrated Effect of Repeated Mechanical Shocks on Shock Remanent Magnetization and Shock Demagnetization 40:467
Najid, D., Westphal, M., Hernandez, J.: Paleomagnetism of Quaternary and Miocene Lavas from North-East and Central Morocco 49:149
Nakamura, Y.: Seismic Energy Transmission in an Intensively Scattering Environment 43:389
Nakano, H.: On Rayleigh Waves 1:374
Navarro Neumann, S.: Un Petit Grain Blanc, Enregistré par des Séismographes 7:26
Nedoma, J.: Investigation of Linear Harmonic Field of SH-Waves in a Stratified Inhomogeneous Medium Using the Finite Difference Method 38:529
Negi, J.G., Lal, T.: Deformation of the Shape of Seismic Pulses by a Layer of Non-Uniform Velocity Distributions 35:589
Nergård, A., see Storetvedt, K.M., et al. 44:317
Neske, E., Kist, R.: Impedance Probe. The AEROS-B Electron Density Experiment 40:593
Neske, E., see Sheikh, M.N., et al. 45:113
Neubauer, F.M., Beinroth, H.J., Barnstorf, H., Dehmel, G.: Initial Results from the Helios-1 Search-Coil Magnetometer Experiment 42:599
Neubauer, F.M., see Musmann, G., et al. 42:591
Neubauer, F.M., see Denskat, K.U. 43:511
Neubauer, F.M., see Richter, A.K., et al. 50:101
Neugebauer, H.J.: An Approximation of Inverse System Operators 39:507
Neugebauer, H.J., Neunhöfer, H., Plešinger, A., Ruegg, J.C., Schick, R., Souriau, M., Stöckl, H., Vích, R., Zürn, W.: A Comparison of Different Restitution Methods Using Shake Table Experiments 39:563
Neugebauer, H.J., Tobias, E.: A Study of the Echzell-Wetterau Earthquake of November 4, 1975 43:751
Neumann, W.: Neue Untersuchungen der irregulären geomagnetischen Anomalien bei Berggießhübel in Sachsen 24:332
Neunhöfer, H.: Deconvolution by Reiterative Convolution 39:513
Neunhöfer, H., see Neugebauer, H.J., et al. 39:563
Nevanlinna, H.: The Geomagnetic Field and Its Secular Variation in Finland and Nearby Countries 46:201
Nevanlinna, H., Sucksdorff, C.: Impulse in Global Geomagnetic "Secular Variation", 1977–1979 50:68
Newell, H., Kroshkin, M.G., Priester, W.: Satelliten erkunden Erde und Mond. (B. Theile) 36:653
Niederlöhner, U., see Bäte, J., et al. 44:147
Nielsen, E., see Inhester, B., et al. 49:155
Niemann, H.B., see Spencer, N.W., et al. 40:613
Niethammer, T.: Bemerkungen zum Artikel von K. Jung: „Über vollständig isostatische Reduktion" 14:119
Nikiforov, P.: L'Anomalie de la Gravité de la Région de Kursk 1:373
Nikolayev, A.V., see Galkin, I.N., et al. 38:455
Nippoldt, A.: Die Verteilung der regelmäßigen täglichen Variationen des Erdmagnetismus in Mitteleuropa 5:80
Nippoldt, A.: Unsere heutige Kenntnis über die Verteilung des Erdmagnetismus 5:351
Nippoldt, A.: Wesensgleiche und wesensverschiedene Darstellungen 6:182
Nippoldt, A.: Das Allgemeingeräusch in der Atmosphäre 8:403
Nippoldt, A.: Bericht über die deutschen geomagnetischen und geoelektrischen Beobachtungen während des Internationalen Polarjahrs 1932/33 9:90
Nishitani, T., Kono, M.: Grain Size Effect on the Low-Temperature Oxidation of Titanomagnetite 50:137
Nitze, F.W.: Nächtliche Austauschströmungen in der bodennahen Luftschicht, hergeleitet durch stereophotogrammetrisch vermessene Bahnen von Schwebeballonen 11:247
Nitzsche, P.: The Dependence of Ionospheric Absorption of Radio Waves on Equivalent Frequency, with Special Emphasis on the Winter Anomaly 35:303
Nitzschke, P.: Die Temperaturverhältnisse in der freien Atmosphäre über dem Südpolargebiet im Jahre 1963. (M. Diem) 34:632
Nix, N., see Israël, H. 32:175, 35:207
Nolet, G.: The Upper Mantle Under Western Europe Inferred from the Dispersion of Rayleigh Modes 43:265
Nölke, F.: Geotektonische Hypothesen 1:372
Nomura, M., see Kobayashi, K. 40:501
Noßke, G., Franke, R.: Einige Erfahrungen bei der geoelektrischen Kartierung von Mineralgängen, Spalten und Verschiebungen im Mittelgebirge 24:340
Novikov, Yu.P., Kopytenko, Yu.A., Raspopov, O.M., Bösinger, T., Kangas, J., Ranta, H.: Simultaneous Maxima of Geomagnetic Pulsations and Riometer Absorption on the Afternoon Side of the Auroral Zone 48:116
Novotný, M.: Two Methods of Solving the Linearized Two-Dimensional Inverse Seismic Kinematic Problem 50:7
Novotný, O., see Pěč, K. 38:555
Nowack, E.: Die südalbanischen Erdbeben 1930/31 10:3
Numerov: Graphische Methode der Berechnung der topographischen und der unterirdisch gelagerten Massen bei Schweremessungen 1:367
Numerov, B.: Interrelation Between Local Gravity Anomalies and the Derivatives of the Potential 5:58
Numerov, B.: Gravity observations in the Solikamsk and Berezniaky Districts in the Northern Urals in 1926 and 1927 5:261
Numerov, B.: Results of gravity observations of 1928 near Lake Baskunchak 5:265
Numerov, B.: Results of the general gravity survey in the Emba District 5:268
Numerov, B.: Results of gravitational observations in the region of Grosny in 1928 5:271
Numerov, B.: Results of gravimetric observations on Shuvalovo Lake in winter 1927 and 1928 5:276
Numerov, B., see Haalck, H., et al.
Nunn, K., see Kaminski, W., et al. 42:103

Öcal, N.: Aufbau der Erdkruste in Anatolien 29:227
Öcal, N.: Geometrical Solutions of Fault-Plane Problem of Some of the Destructive Earthquakes Occured in Anatolia in the Period 1938–1955 32:293
O'Donovan, J.B., see Manson, A.J., et al. 46:185
Oehlschlegel, G., see Auer, F., et al. 49:89
Oeser, E.: Messungen der kosmischen Ultrastrahlung zwischen 50° und 7° nördlicher Breite 8:242
Offermann, D.: A Study of the *D*-Region Winter Anomaly in Western Europe, 1975/76 44:1
Offermann, D., see Friedrich, V.H., et al. 44:139
Oliver, J., see Berckhemer, H. 21:152
Oliwa, G.: Die Schwere auf dem Niveausphäroid 24:143
Onuoha, K.M.: A Comparison of the Thermal and Mechanical Structure of the Lithosphere Beneath the Bohemian Massif and the Pannonian Basin 49:212
Opgenoorth, H.J., Pellinen, R.J., Maurer, H., Küppers, F., Heikkila, W.J., Kaila, K.U., Tanskanen, P.: Ground-Based Observations of an Onset of Localized Field-Aligned Currents During Auroral Breakup Around Magnetic Midnight 48:101
Opgenoorth, H.J., see Untiedt, J., et al. 45:41
Opitz, D.: Reflexionsseismische Methoden zur Ermittlung der mittleren Geschwindigkeiten elastischer Wellen im Untergrund ohne Berücksichtigung der Strahlenbrechung. (G. Dohr) 29:145
Orcutt, J.A., Dorman, L.M.: An Oceanic Long Range Explosion Experiment. A Preliminary Report 43:257
O'Reilly, W., Readman, P.W.: The Preparation and Unmixing of Cation Deficient Titanomagnetites 37:321
O'Reilly, W., see Readman, P.W. 37:329
O'Reilly, W., see Manson, A.J., et al. 46:185

O'Reilly, W., see Özdemir, Ö. 49:93
Orsini, S., see Formisano, V. 50:114
Oserezky, W.: Ein Diagramm zur Bestimmung der Differenz der Schwerestörung Δ_g in zwei Beobachtungspunkten 6:69
Osokin, N.N., see Zverev, S.M., et al. 47:191, 47:202
Oster, A.L., see Dolezalek, H. 32:163
Ostermeier, J.B.: Eine hochempfindliche magnetische Feldwaage 9:109
Ott, W., see Spenner, K., et al. 44:81
Ott, W., see Brüning, K., et al. 49:74
Ott, W., see Wilhelm, K., et al. 49:128
Özdemir, Ö., O'Reilly, W.: Laboratory Synthesis of Aluminium-Substituted Titanomaghemites and Their Characteristic Properties 49:93

Paeschke, W.: Experimentelle Untersuchungen zum Rauhigkeitsproblem in der bodennahen Luftschicht 13:14
Pahlen, E. v. d., Kohlschütter, A.: Untersuchungen über die Sonnenkorona 7:275, 336
Palandt, M.: Spectral Analysis of Pc3 and Pc4 Pulsations with Regard to the Dayside Plasmapause Position 45:391
Palazzo, L.: Einige Bemerkungen über erdmagnetische Messungen, welche in Feodossia ausgeführt wurden 6:225
Pálmason, G.: A Continuum Model of Crustal Generation in Iceland; Kinematic Aspects 47:7
Pálmason, G., see Johnson, G.L. 47:23
Pálmason, G., see Voight, B., et al. 47:176
Pálmason, G., see Zverev, S.M., et al. 47:191, 202
Pálmason, G., see RRISP Working Group 47:228
Panza, G.F., see Calcagnile, G., et al. 43:502
Panza, G.F., see Calcagnile, G. 45:319
Papanikas, D.G., see Bäte, J., et al. 44:147
Parasnis, D.S.: Principles of Applied Geophysics. (O. Rosenbach) 30:48
Parasnis, D.S.: The Electric Potential and Apparent Resistivity Due to a Pair of Long Line Electrodes in the Presence of a Vertical Outcropping Vein 30:261
Parasnis, D.S.: Mining Geophysics. (R. Gutdeutsch) 34:422
Parasnis, D.S.: Estimates of *in situ* Thermal Diffusivity of the Ore-Bearing Rocks in Some Drillholes in the Skellefte Field (N. Sweden) Using the Annual Temperature Wave 40:83
Parini, M., see Werner, D. 48:28
Partsch, W.: Ein gravimetrisches Modell der Erdkruste im Gebiet der Ostalpen 37:957
Pashkevich, I.K., see Krutikhovskaya, Z.A. 46:301
Patel, B.M., see Kotadia, K.M. 37:1043
Paterson, W.S.B.: The Physics of Glaciers. (W. Zürn) 36:652
Patzke, W.: Untersuchungen über die Genauigkeit von Pendelmessungen an fester Station 12:253
Paul, A.K.: Electron Density Profiles in Ionosphere and Exosphere. Hrg. J. Frihagen 33:368
Paul, A.K.: Radio Pulse Dispersion in the Ionosphere 46:15
Paul, M.: Über Messungen der Erdbodentemperatur an Salzdomen 11:388
Paul, M.: Erfahrungen mit einem neuen geothermischen Aufschlußverfahren 15:88
Pavlenkova, N.I., see RRISP Working Group 47:228
Pěč, K., Novotný, O.: The Influence of the Low Velocity Zone on Phase Velocities and Amplitudes of Love Waves 38:555
Pellinen, R., see Untiedt, J., et al. 45:41
Pellinen, R.J., see Opgenoorth, H.J., et al. 48:101
Pelster, W.D., see Untiedt, J., et al. 45:41
Pelz, D.T., see Spencer, N.W., et al. 40:613
Pelzer, H., Gerstenecker, C.: Measurements of Distance and Tilt Changes in Fissures in Northern Iceland 47:166
Penndorf, R.: Anomale Schallausbreitung und Ozonosphäre 12:315
Penndorf, R.: Berechnung der Stratosphärentemperatur aus Messungen der atmosphärischen Absorptionskoeffizienten des Ozons 14:88
Perepelitsa, V.A.: Determination of the True Ground Motion by Numerical Integration of Seismograms 39:515
Petelski, E.F.: Transmission of Electric Fields and Photoelectron Fluxes Between Conjugate Ionospheric F2-Regions 41:243
Peters, K., see Soffel, H. 36:589
Peters, K., see Soffel, H., et al. 41:491
Peterschmitt, E., Menzel, H., Fuchs, K.: Seismische Messungen in den Alpen. – Die Beobachtungen auf dem NE-Profil Lago Lagorai 1962 und ihre vorläufige Auswertung 31:41
Petersen, N.: Untersuchungen magnetischer Eigenschaften von Titanomagnetiten im Basalt des Rauhen Kulm (Oberpfalz) in Verbindung mit elektronenmikroskopischer Beobachtung 28:79
Petersen, N., Bleil, U.: Self Reversal of Remanent Magnetization in Synthetic Titanomagnetites 39:965
Petersen, N., see Soffel, H. 32:531, 37:303
Petersen, N., see Creer, K.M. 35:501
Petersen, N., see Hargraves, R.B. 37:367
Petersen, N., see Storetvedt, K.M. 36:569, 42:59, 403
Petri, J.: Versuche zur Registrierung der Helligkeit mittels photographischer Methode für unbemannte Aufstiege 12:129
Pfleiderer, H., see Balensiefer, E., et al. 15:337
Pfotzer, G.: In memoriam Alfred Ehmert 37:751
Pheophylaktov, V.D.: Problems of Noise Suppression and of Stability of Long-Period Seismographs 39:613
Philipps, H., see Bernhardt, F. 33:146
Picard, C.F., Sallantin, J.: Data Seizing and Information Processing. Application to Recognition of High Seismicity Earthquake Areas 43:215
Pícha, J.: Einige Ergebnisse der Erdgezeitenbeobachtungen in der ČSSR 32:352
Picht, J.: Über die Anordnung der Optik bei Lichtschreiber-Registrierapparaten 7:265
Pietsch, D.: Ein Verfahren zur direkten Berechnung der Schichtgeschwindigkeiten in der Reflexionsseismik 20:25
Pikkarainen, T., see Kangas, J., et al. 46:237
Pilipp, W., see Rosenbauer, H., et al. 42:561
Pillans, H., see Struve, O., et al. 28:294
Pitz, E., see Leinert, C., et al. 42:699
Plaumann, S.: Kontinuierliche Schweremessungen im Roten Meer mit einem Askania-Seegravimeter vom Typ Gss 2 nach GRAF 29:233
Plaumann, S.: Schweremessungen auf dem zugefrorenen Steinhuder Meer 30:97
Plaumann, S.: Berechnung der Schwerewirkung beliebig geformter dreidimensionaler Massen mit Hilfe von Auszähldiagrammen 31:327
Plaumann, S.: The Gravity Field of the North Frisian Islands and the Adjacent Mainland 45:343
Plendl, H., see Dieminger, W. 14:315
Plešinger, A.: Synthesis of Feedback Controlled Broadband Modifications of Conventional Seismograph Systems 39:573
Plešinger, A., Horálek, J.: The Seismic Broadband Recording and Data Processing System FBV/DPS and Its Seismological Applications 42:201
Plešinger, A., Vích, R.: On the Identification of Seismometric Systems and the Correction of Recorded Signals for Identified Transfer Functions 38:543
Plešinger A., Wielandt, E.: Seismic Noise at 2 Hz in Europe 40:131
Plešinger, A., see Neugebauer, H.J., et al. 39:563
Plešinger, A., see Sitaram, M.V.D., et al. 48:47
Plomerová, J.: Influence of Station Conditions on Spectra of *P* and *S* Waves 39:603
Plugge, R., see Spenner, K. 46:43
Plugge, R., see Spenner, K., et al. 46:57
Pohl, J.: On the Origin of the Magnetization of Impact Breccias on Earth 37:549
Pohl, J., Bleil, U., Hornemann, U.: Shock Magnetization and Demagnetization of Basalt by Transient Stress up to 10 kbar 41:23

Pohl, J., Soffel, H.: Paleomagnetic Age Determination of the Rochechouart Impact Structure (France) 37:857
Pohl, J., Soffel, H.: Palaeomagnetic and Rock Magnetic Investigations of Tertiary Volcanics in Northern Bavaria 42:459
Pohl, J., see Angenheister, A. 30:258
Pohl, J., see Hornemann, U., et al. 41:13
Pohl, J., see Soffel, H., et al. 41:491
Pohl, W.: Messungen des ultraroten Strahlungsstromes in der freien Atmosphäre 22:1
Pollak, L.W.: Fortschritte in der Anwendung des Lochkartenverfahrens auf geophysikalische Probleme 5:33
Pollak, L.W.: Das Lochkartenverfahren 5:410
Pollak, L.W.: Über den Zusammenhang zwischen Typhusmorbidität (bzw. Typhusmortalität) und Niederschlagsschwankungen nebst einer Kritik der Brücknerschen Klimaperiode 6:377
Popoff, I.: Die erdmagnetische Deklination in Bulgarien 8:164
Popoff, K.: Erdmagnetische Messungen in Bulgarien, Mazedonien, Trazien und in der Dobrudja 6:221
Porsche, H.: General Aspects of the Mission Helios 1 and 2. Introduction to a Special Issue on Initial Scientific Results of the Helios Mission 42:551
Porstendorfer, G.: Automatische elektrische Drehsondierung nach dem Wenner- und Dipolverfahren mit direkter Meßwertregistrierung 26:276
Postránecký, J., see Rihánek, L.V. 25:158
Potemra, T.A., see Sulzbacher, H., et al. 48:7
Pott, G., see Graeser, E., et al. 24:134
Prakash, P.: A Residual Method 27:275
Prakash, S., see Gupta, S.P., et al. 43:681
Prandtl, L., Tollmien, W.: Die Windverteilung über dem Erdboden, errechnet aus den Gesetzen der Rohrströmung 1:47
Pranglin, J.A., see Guyod, H. 29:147
Prévot, M.: A Method for Identifiying Naturally Occuring Titanomagnetites 37:339
Prévot, M., see Biquand, D. 37:471
Prey, A.: Neue Formeln zur Isostasie 3:369
Priester, W., see Newell, H., et al. 36:653
Procházková, D., Schneider, G., Schmedes, E., Drimmel, J., Fiegweil, E., Lukeschitz, G., Vogt, J., Courtot, P., Godefroy, P., Grünthal, G., Mayer-Rosa, D., Berger, R.: Macroseismic Field of the Earthquake of September 3, 1978, in the Swabian Jura 46:343
Prodehl, C.: Auswertung von Refraktionsbeobachtungen im bayerischen Alpenvorland (Steinbruchsprengungen bei Eschenlohe 1958–1961) im Hinblick auf die Tiefenlage des Grundgebirges 30:161
Prodehl, C.: Crustal Structure of the Western United States from Seismic-Refraction Measurements in Comparison with Central European Results 36:477
Prodehl, C., see Giese, P., et al. 33:215
Prodehl, C., see Edel, J.B., et al. 41:333
Prodehl, C., see Kaminski, W., et al. 42:103
Prodehl, C., see Mooney, W.D. 44:573
Pros, V., Babuška, V.: A Method for Investigating the Elastic Anisotropy on Spherical Rock Samples 33:289
Pros, Z., Vaněk, J., Klíma, K., Babuška, V.: Experimentelle Untersuchung des Wellenbildes bei der Ultraschall-Durchstrahlung einer Kugel 35:287
Pruchniewicz, P.G., see Tiefenau, H., et al. 38:145
Pšenčík, I.: Ray Amplitudes of Compressional, Shear, and Converted Seismic Body Waves in 3D Laterally Inhomogeneous Media with Curved Interfaces 45:381
Pšenčík, I., see Červený, V. 38:565
Pucher, G., see Jeske, H., et al. 36:621
Pucher, R.: Untersuchung magnetischer Eigenschaften an der Kontaktfläche zweier benachbarter Gesteinsarten 32:113
Pucher, R.: Magnetic and X-Ray Diffraction Measurements of the Synthetic Spinel System $FeFe_2O_4-MgFe_2O_4-NiFe_2O_4$ 37:349
Quon, C., Vozoff, K., Hoversten, M., Morrison, H.F., Lee, K.-H.: Localized Source Effects on Magnetotelluric Apparent Resistivities 46:291
Rabben, H., see Melzner, F., et al. 34:105
Rabben, H.H., see Melzner, F. 36:135
Raczek, I., see Lippolt, H.J. 46:225
Radhakrishnamurty, C., Deutsch, E.R.: Magnetic Techniques for Ascertaining the Nature of Iron Oxide Grains in Basalts 40:453
Radhakrishnamurty, C., Deutsch, E.R., Murthy, G.S.: On the Presence of Titanomagnetite in Basalts 45:433
Raethjen, H.: Protonenmessungen im Morgensektor der Polarlichtzone bei langsam variierender Absorption kosmischen Rauschens 37:195
Raeuber, A., Engel, K.H.: Untersuchungen über den Verlauf der Massenzunahme bei Kartoffeln (Sol. tuberosum L) in Abhängigkeit von Umwelt- und Erbguteinflüssen (K. Höschele) 33:212
Rahman, A.: A New Type of Wave Discovered in the Schlieren Photographs 31:146
Raikes, S.: Teleseismic Evidence for Velocity Heterogeneity Beneath the Rhenish Massif 48:80
Räkers, E., Müller, G.: The Romanian Earthquake of March 4, 1977 – III. Improved Focal Model and Moment Determination 50:143
Ramana, Y.V., Rao, M.V.M.S., Gogte, B.S.: Pressure Dependence of Elastic Wave Characteristics of Ultramafic Rocks of India 41:523
Ramananantoandro, R.: Estimation of the Dispersion of Compressional Waves in Rocks from Ultrasonic to Seismic Frequencies 46:451
Rammner, R.: Ausgewählte Beispiele geoelektrischer Meßtätigkeit 32:532
Rammner, R., see Bloh, J. v. 34:183
Ramsbeck, A.: Reine Longitudinal- und Transversalwellen im elastisch-homogenen Halbraum 18:21
Ramspeck, A.: Eine Schüttelplatte zur Untersuchung von Seismographen 8:71
Ramspeck, A.: Zusammenhang zwischen Boden- und Gebäudeschwingungen 8:467
Ramspeck, A.: Versuche über Boden- und Gebäudeschwingungen 9:44
Ramspeck, A.: Die Ausbreitungsgeschwindigkeit sinusförmiger elastischer Wellen im Boden 10:387
Ramspeck, A.: Die Verwendung sinusförmiger elastischer Wellen bei der Untersuchung des Baugrundes 12:354
Ramspeck, A.: Wendepunkte in der Laufzeitkurve sinusförmiger Wellen 13:1
Ramspeck, A.: Der Einfluß eines mit der Tiefe veränderlichen Elastizitätsmoduls auf den Weg elastischer Wellen im Boden 15:148
Ramspeck, A., see Gerecke, F. 9:342
Ramspek, A.: Versuche über Boden- und Gebäudeschwingungen 9:44
Ranalli, G., see Jacoby, W.R. 45:299
Ranta, A., see Wedeken, U., et al. 46:249
Ranta, H., see Untiedt, J., et al. 45:41
Ranta, H., see Wedeken, U., et al. 46:249
Ranta, H., see Novikov, Yu.P., et al. 48:116
Rantsman, E., see Alekseevskaya, M., et al. 43:227
Rao, B.S.R., Murthy, I.V.R., Rao, D.B.: Interpretation of Magnetic Anomalies with Fourier Transforms, Employing End Corrections 44:257
Rao, D.B., see Rao, B.S.R., et al. 44:257
Rao, M.V.M.S., see Ramana, Y.V., et al. 41:523
Rao, S.H., Gutdeutsch R., Klußmann, J.: Aufbau einer modellseismischen Apparatur 25:253
Rao, S.H., see Majumdar, R.K. 37:743

Rao, S.M.V., Murty, B.V.S., Bhimasankaram, V.L.S.: Petro-Physical Properties (Density and Magnetic-Susceptibility) and Lithologic Composition of Some Dolerite Dykes of Andhra Pradesh, India 44:353
Rapolla, A., see Hunsche, U., et al. 49:26
Raschke, E.: Die Strahlungsbilanz des Systems Erde-Atmosphäre – neuere Ergebnisse von Satellitenmessungen (Übersichtsartikel) 38:967
Raspopov, O.M., see Novikov, Yu.P., et al. 48:116
Rastogi, R.G.: Some Aspects of the F2 Region at Medium Latitudes of the Northern and Southern Hemispheres 26:217
Rastogi, R.G.: Lunar Tidal Oscillations in H and f_0F_2 at Equatorial Stations 31:27
Rawer, K.: Die traditionellen Meßgrößen für die „sporadische Es-Schicht" 20:188
Rawer, K.: Ionosphären-Messungen bei zwei Raketen-Aufstiegen in der Sahara 32:409
Rawer, K., Argence, E.: Zur Entstehung der E-Schicht der Ionosphäre 20:84
Rawer, K., see Sheikh, M.N., et al. 45:113
Readman, P.W., O'Reilly, W.: Oxidation Processes in Titanomagnetites 37:329
Readman, P.W., see O'Reilly, W. 37:321
Readman, P.W., see Creer, K.M., et al. 48:139
Rees, D.: Winter Anomaly – Trace Constituents Sounding Rocket Campaign. A High Resolution Photometer for Observing Daytime Lithium Releases 44:57
Rees, D., Rounce, P., Killeen, T.L.: Winter Anomaly – Trace Constituents Sounding Rocket Campaign. Daytime Neutral Wind Measurements in the Mesosphere and Lower Thermosphere 44:47
Rees, D., Rounce, P.A., Charleton, P., Fuller-Rowell, T.J., McWhirter, I., Smith, K.: Thermospheric Winds During the Energy Budget Campaign: Ground-Based Fabry-Perot Observations Supported by Dynamical Simulations with a Three-Dimensional, Time-Dependent Thermospheric Model 50:202
Refai, E.: Magnetic Anomalies and Magnetization of Basalts in the Area Around Kemnath (Oberpfalz) 27:175
Regener, E., see Regener, V.H. 40:761
Regener, V.H., Regener, E.: Cosmic Rays Underground and the Interplanetary Magnetic Field 40:761
Regula, H.: Neubearbeitung der Schallbeobachtungen, insbesondere des Geophysikalischen Instituts in Göttingen 8:469
Regula, H.: Schallausbreitung in der Atmosphäre 10:167
Regula, W.: Untersuchungen elastischer Eigenschaften von Gesteinsstäben 16:40
Rehn, H.W.: Transverse Plasma Waves in the Solar Wind Close to the Proton Gyrofrequency 40:269
Reich, H.: Die Bedeutung der neuen geophysikalischen Untersuchungsmethoden für die Geologie nach den bisherigen Erfahrungen 1:120
Reich, H.: Instrumentelle Seismik und Geologie 1:121
Reich, H.: Über eine magnetische Anomalie am Lebasee in Ostpommern 6:207
Reich, H.: Bemerkungen zur angewandten Seismik 9:350
Reich, H.: Ergebnisse erdmagnetischer Untersuchungen im Rheinischen Schiefergebirge 11:344
Reich, H.: Stand der geophysikalischen Reichsaufnahme 15:73
Reich, H.: Über die Ausbreitung seismischer Impulse in der Malmkalkplatte des schwäbisch-fränkischen Juras 20:8
Reich, H.: Über die Nachprüfung von magnetischen Messungen mit dem Lokal-Variometer von J. Wüst und die Feststellung der Ursachen der gefundenen magnetischen Störungen 23:169
Reich, H.: Kurzer Bericht über die Bohrung Wörnitzostheim im Nördlinger Ries 32:200
Reicheneder, K.: Zur Neubestimmung der absoluten Schwere in Potsdam 23:1
Reimer, D., see Heinrich, H., et al. 36:399
Reimer, L.: Magnetische Eigenschaften dünner ferromagnetischer Schichten 24:53
Reimold, W.U., see Jessberger, E.K. 48:57
Reitmayr, G.: Die bevorzugten Polarisationsrichtungen des natürlichen erdelektrischen Feldes im Gebiet des Oberrhein-Grabens 38:103
Reitmayr, G.: An Anomaly of the Upper Mantle Below the Rhine Graben, Studied by the Inductive Response of Natural Electromagnetic Fields 41:651
Reiz, H.: Zum Gedenken an Richard Bock 28:49
Renner, R., Lettau, H.: Atmosphärische Turbulenz 16:99
Rennert, P., see Macke, W., et al. 30:21
Renquist, H.: Über kartographische Darstellung der Seismizität 4:348
Renqvist, H.: Die Erdbeben Finnlands 7:145
Repsold, H.: Ergebnisse der Messungen natürlicher Erdströme bei Göttingen 25:97
Reusche, H.-G.: Ein absoluter magnetischer Theodolit 24:299
Reuter, F.: Ein Hilfsapparat zur harmonischen Analyse 12:29
Revellio, K., see Ehmert, A. 23:113
Reynaud, C., see Creer, K.M., et al. 48:139
Richard, S., see RRISP Working Group 47:228
Richards, P.G.: Seismic Waves Reflected from Velocity Gradient Anomalies Within the Earth's Upper Mantle 38:517
Richards, P.G., see Cormier, V.F. 43:3
Richter, A.K., Keppler, E.: Interaction of Low-Energy (>80 keV) Protons with the January 6 and 8, 1975, Shock Waves: Helios-1 Observations 42:645
Richter, A.K., Verigin, M.I., Kurt, V.G., Stolpovsky, V.G., Gringauz, K.I., Keppler, E., Rosenbauer, H., Neubauer, F.M., Gombosi, T., Somogyi, A.: The 3 January 1978 Interplanetary Shock Event as Observed by Energetic Particle, Plasma and Magnetic Field Devices on Board of Helios-1, Helios-2 and PROGNOZ-6 50:101
Richter, A.K., see Keppler, E., et al. 42:633
Richter, A., see Kern, H. 49:47
Richter, D.: Ein Beitrag zur Bestimmung der Verdunstung von freien Wasserflächen, dargestellt am Beispiel des Stechlinsees (Walk) 36:654
Richter, D., see Heitmann, M.-L., et al. 36:776
Richter, F., McKenzie, D.: Simple Plate Models of Mantle Convection 44:441
Richter, G.: Über die Polarisation von SKS 24:168
Richter, I.: Eine Gradientschicht im obersten Teil der Erdkruste als Wellenleiter von Raumwellen 37:1013
Richter, K., see Keppler, E., et al. 42:633
Riedler, W., see Kremser, G., et al. 42:1
Riedler, W., see Wilhelm, K., et al. 49:128
Rieger, E.: Messungen des elektrischen Feldes in der oberen Atmosphäre (Übersichtsartikel) 37:795
Rieger, F., see Macke, W., et al. 30:21
Ries, G., see Kunkis, A. 30:5
Rietsch, E.: The Maximum Entropy Approach to Inverse Problems. Spectral Analysis of Short Data Records and Density Structure of the Earth 42:489
Rietsch, E.: Extreme Models from the Maximum Entropy Formulation of Inverse Problems 44:273
Rihánek, L.V., Postránecký, J.: Bourky a Ochrana Před Bleskem. (H. Israël) 25:158
Ringdahl, F.: P-Wave Amplitudes and Sources of Scattering in m_b-Observations 43:611
Rink, J.: Thermistore und ihre Anwendung in der Meteorologie. (H.G. Müller) 28:208
Rink, M.: Porengeometrische Untersuchungen an Sedimentgesteinen mit einem Bildanalyseverfahren für Digitalrechner 39:989
Rinnert, K.: Untersuchungen der unteren Ionosphäre mit Hilfe der Längswellenausbreitung über große Entfernungen 38:719
Risbo, T., see Bungum, H., et al. 43:501
Rische, H.: Geschwindigkeitsbestimmung aus reflexionsseismischen Messungen bei Anwendung von Luftschüssen 24:351

Ritchie, A.S.: Chromatography in Geology. (H. Schwentek) 33:463
Ritter, B., see Makris, J., et al. 39:279
Ritter, B., see Möller, D. 47:110
Riuscetti, M., see Schick, R. 39:247
Rixmann, F.: Untersuchungen über die Abhängigkeit der Bodenbewegung bei Sprengungen von der Ladung 11:197
Robel, R.: Die Erdbebenstation Bensberg b. Köln 25:16
Roemer, M.: Das raumzeitliche Verhalten der Hochatmosphäre erschlossen aus Bahnänderungen künstlicher Satelliten (Übersichtsartikel) 35:217
Roemer, M., Wulf-Mathies, C.: Atmospheric Drag Analysis with the AEROS Satellite 40:625
Roeser, H.A.: Magnetic Anomalies of the African Red Sea Shelf and Their Implications for the Anomalies of Atlantic Continental Margin 42:73
Rohde, J., see Behle, A. 42:131
Rohde, M., see Schwehm, G. 42:727
Rohleder, H.P.T.: Bodenknalle in Nordirland 3:43
Rohleder, H.P.T.: Beiträge zur Kenntnis der Erdbebenkunde und seismisch-akustischen Phänomene Nord-Rhodesiens 9:325
Rohleder, H.P.T.: Zur Seismizität Afrikas während der Jahre 1913 bis 1930 13:9
Rohrbach, W.: Über die Dispersion seismischer Oberflächenwellen 8:113
Romanow, M.E., Alekseev, A.S.: A Characteristic Method for Numerical Solution of the Inverse Kinematic Seismic Problems 48:173
Rönicke, G.: Erfahrungen mit luftelektrischen Sondierungen in der freien Atmosphäre 28:105
Rose, G.: Über die Meteor-Ionisation im E-Bereich der Ionosphäre 25:1
Rose, G., Widdel, H.U.: Zur Möglichkeit des direkten Nachweises vertikaler Luftbewegungen im Höhenbereich 75 bis 80 km 35:211
Rose, G., Widdel, H.U.: *D*-Region Radio Wave Propagation Experiments, Their Significance and Results During the Western European Winter Anomaly Campaign 1975/76 44:15
Rose, G., Widdel, H.U.: Payload BI: A Compact and Economic *D*-Region Experiment Package for Use on Small Sounding Rockets 44:65
Rose, G., see Widdel, H.U., et al. 44:179
Rosenbach, O.: Ein Verfahren zur Berechnung des Horizontalgradienten aus Schwerewerten 19:37
Rosenbach, O.: In memoriam Karl Jung 38:347
Rosenbach, O., Schmitt, O.: Programmsteuerung der Empfindlichkeit seismischer Meßapparaturen 29:129
Rosenbach, O., see Jung, K., et al. 31:7
Rosenbach, O., see Burkhardt, H., et al. 33:455
Rosenbach, O., see Flach, D., et al. 37:993, 1005
Rosenbach, O., see Behle, A., et al. 38:45, 221
Rosenbach, O., see Ehrismann, W., et al. 39:115
Rosenbauer, H., Schwenn, R., Marsch, E., Meyer, B., Miggenrieder, H., Montgomery, M.D., Mühlhäuser, K.H., Pilipp, W., Voges, W., Zink, S.M.: A Survey on Initial Results of the Helios Plasma Experiment 42:561
Rosenbauer, H., see Richter, A.K., et al. 50:101
Rosenhauer, W., see Ahorner, L. 41:581, 44:481
Rösler, G.: Supersonic Plasma Flow Between High Latitude Conjugate Ionospheres 41:413
Rossbach, A.: Das Polarlichtspektrum (Übersichtsartikel) 34:535
Rossbach, A.: Die Geokorona und ihre Bedeutung für die Hochatmosphäre 35:557
Roßbach, A., see Keppler, E., et al. 33:346
Rossberg, L.: Über die Pitchwinkelverteilung von Elektronenflüssen mit Energien $E > 40$ keV in der Polarlichtzone 36:151
Roßberg, L., see Keppler, E., et al. 33:346
Rössiger, M.: Beitrag zur Theorie des Blattfederseismographen 8:470
Rössiger, M.: Der charakteristische Verlauf eines erdmagnetischen Sturms nach Potsdamer Registrierungen 14:78
Rössiger, M.: Diskussionsbemerkungen zum Vortrag von H. Jung 15:65
Rössiger, M.: Die experimentellen Grundlagen des Dipol-Induktionsverfahrens 15:83
Rössiger, M.: Diskussionsbemerkungen zum Vortrage von M. Paul 15:93
Rössiger, M., Funder, L.: Die Aufzeichnungen der erdmagnetischen Elementarwellen mittels des Kriechgalvanometers 11:75
Rössiger, M., Funder, L.: Messungen des Ionengehaltes von Grubenwettern 11:75
Rössler, E., Zehle, H.: Feststellung, Ortung und Verfolgung radioaktiver Wolken und deren Einfluß auf die Funkortung. II (H. Kohl) 30:112
Rössler, F., Bock, D.: Messung des diffusen Himmelslichtes mittels Ballonen 35:485
Rössler, J., see Israël, H. 32:207
Rossmann, F.: Über die Funkschwierigkeiten bei den Gronau-Flügen über Grönland 13:71
Rostoker, G., Apps, K.S.: Current Flow in Auroral Forms Responsible for Ps 6 Magnetic Disturbances 49:163
Rostoker, G., see Tighe, W.G. 50:51
Roth, J.F.: Sprengungen in über 4000 m Tiefe 31:50
Rothermel, H., see Melzner, F., et al. 34:105
Rotstein, Y., see Goldberg, S., et al. 50:151
Rotter, D., see Kundorf, W. 27:35
Röttger, J.: Some Properties of Large-Scale Equatorial Spread-*F* Irregularities Interpreted by Influences of Atmospheric Gravity Waves 39:799
Röttger, J.: Evidence for Partial Reflection of VHF Radar Signals from the Troposphere 44:393
Röttger, J., see Schödel, J.P., et al. 39:1063
Rounce, P., see Rees, D., et al. 44:47
Rounce, P.A., see Rees, D., et al. 50:202
Roux, L.: Turbulente Windströmungen auf der rauhen Erdoberfläche 11:165
Röwer, P.: Laufzeitanomalien von P-Wellen, beobachtet an den Stationen Stuttgart und Strasbourg (Brief an den Herausgeber) 36:105
Roy, K.K., Baksi, S.S.: Model Studies on Redox Logging for Minerals 42:521
RRISP Working Group (Angenheister, G., Björnsson, S., Einarsson, P., Gebrande, H., Goldflam, P., Jacoby, W.R., Litvinenko, I.V., Loncarevic, B., Miller, H., Pálmason, G., Pavlenkova, N.I., Richard, S., Solomon, S.C., Weigel, W., Zverev, S.M.): Reykjanes Ridge Iceland Seismic Experiment (RRISP 77) 47:228
Rucker, H., see Burkard, O.M. 45:219
Rudloff, H. v.: Die Schwankungen und Pendelungen des Klimas in Europa seit dem Beginn der regelmäßigen Instrumentenbeobachtung (1670) (M. Diem) 35:103
Rudloff, R., see Janle, P., et al. 41:475
Rudloff, R., see Voppel, D. 47:61
Rudolf, H.: Polarlicht und Luftelektrizität 1:342
Rudolph, H.: Die Energie der Heliokathodenstrahlen in ihrer Beziehung zur fortschreitenden Bewegung der Elektronen in den Polarlichtstrahlen 10:356
Rudolph, H.: Über Versuche zur Theorie des Polarlichts 12:360
Rudolph, H.: Überwiegt positive oder negative Elektrizität in der Ionosphäre der Erde? 12:363
Rudolph, H.: Die negative Aufladung der Ionosphäre der Erde 14:346
Ruegg, J.C., Souriau, M.: Theoretical and Experimental Deconvolution 39:525
Ruegg, J.C., see Neugebauer, H.J., et al. 39:563
Rühmkorf, H.A.: In memoriam Dr. phil. Hubert Lückerath 21:233
Rühmkorf, H.A., see Steinmann, W. 34:457
Rülke, O., see Thyssen, St. v., et al. 13:112

Rülke, O., see Thyssen, St. v. 15:130
Rummel, F.: Studies of Time-Dependent Deformation of Some Granite and Eclogite Rock Samples Under Uni-Axial, Constant Compressive Stress and Temperatures up to 400° C 35:17
Ruprecht, L., see Trappe, F. 15:37
Ruprechtová, L.: Recent Interpretation of the Core Discontinuities 38:441
Rüter, H., see Brockamp, B. 35:277
Ruttner, H.: Nordlicht am 4. April 1942 17:333
Ruttner, H., see Teichgraeber, A. 17:333
Ryaboy, V.Z.: Study of the Structure of the Lower Lithosphere by Explosion Seismology in the USSR 43:593
Ryan, J.M., Axford, W.I.: The Behaviour of Minor Species in the Solar Wind 41:221
Rybach, L.: The Radioactivity of Rocks and Its Influence on the Temperature Field in the Continental Crust 42:93
Rydelek, P.A., see Knopoff, L., et al. 46:89
Rydelek, P.A., see Zürn, W., et al. 48:158, 49:249

Saatsamoinen, P.R.: Modal Approach to Wave Propagation in Layered Media with Lateral Inhomogeneities 43:75
Sabatier, P.C.: On Geophysical Inverse Problems and Contraints 43:115
Sabina, F.J., Willis, J.R.: Scattering of Rayleigh Waves by a Ridge 43:401
Sacks, I.S., Snoke, J.A.: Heterogeneous Velocity Structure at the Base of the Mantle. 2. Observations and Interpretations 43:505
Sacks, I.S., see Snoke, J.A. 43:505
Saeger, K.H., see Kremser, G., et al. 38:851
Saemundsson, K., see Gudmundsson, G. 47:99
Sallantin, J., see Picard, C.F. 43:215
Saltzmann, B.: Theory of Thermal Convection (R. Roth) 33:462
Samson, J.C.: Comments on Polarization and Coherence 48:195
Sandmann, B.: Beobachtungsergebnisse über den Einfluß der „akustischen Umkehrschicht" auf die Schallausbreitung 10:200
Sandmann, B.: Die Bedeutung der Unstetigkeiten im Verlauf der Schallgeschwindigkeit mit der Höhe für die normale und anomale Schallfortpflanzung 10:269
Sandner, W.: Nordlicht 1940. III. 29^d 16:197
Sarma, S.B.S.S., Sharma, M.C.: Winter Anomaly in VHF Absorption Studies Over Delhi 42:541
Sarma, S.B.S.S., Sharma, M.C.: New Methods of Separating F Region Absorption from the Cosmic Radio Noise Absorption 44:385
Sarma, S.B.S.S., see Sharma, M.C. 42:535
Sastri, N.S., see Jain, A.R. 45:101
Sawicky, P.: Die Schwere und Geologie in Kaukasien 7:318
Saxov, S., Abrahamsen, N.: Some Geophysical Investigations in the Faroe Islands 32:455
Schaaf, H., see Jung, K. 33:319
Schäfer, J.: The Diurnal Variation of the Electron Density of the Mid-Latitude Ionospheric D-Region Deduced from VLF-Measurements 42:361
Schäfer, K., see Treumann, R. 43:521
Schaffernicht, W., see Tomaschek, R. 9:125, 199, 309
Schäffner, H.J.: Interpretation von Herdmechanismen durch asymmetrische Dislokationen 27:164
Scheidegger, A.E.: Großtektonische Bedeutung von Erdbebenherdmechanismen 31:300
Scheidegger, A.E.: Isallo Stress Prospecting 32:183
Scheidegger, A.E.: The Tectonic Stress in the Vicinity of the Alps 33:167
Scheidegger, A.E.: Theoretical Geomorphology. (W. Kertz) 36:778
Scheidegger, A.E., see Thrasher, J.E. 29:307
Schenk, E.: Über die Magnetisierung der Tuffe und Paläosole im Paläovulkan des Vogelsberges 34:567
Schenk, E.: Die Magnetisierung von Tuffen und Paläosolen 35:553
Schenk, E.: Zur Problematik der Deutung paläomagnetischer Meßergebnisse auf Grund von Untersuchungen an den Basalten des Paläovulkans Vogelsberg in Hessen 36:359
Schenk, E.: Die Bestimmung des Faktors zur Eliminierung barometrisch bedingter Fluktuationen des Grundwasserspiegels 39:471
Schenk, G.: Die Erde, unser Planet im Weltall. (H. Schwentek) 29:145
Schenk, V., see Waniek, L. 32:482
Schepers, R.: A Seismic Reflection Method for Solving Engineering Problems 41:367
Schepers, R.: High Resolution Near Surface Reflection Measurements Using a Vertical Array Technique 43:791
Scheube, H.G., Untiedt, J.: Magnetische Messungen in der Rhön im Rahmen einer Studienfahrt 31:283
Scheuch, J.: Wärmestromdichtemessungen im Roten Meer zwischen 19° und 26° nördlicher Breite (Gebiet der Laugentiefs) 39:859
Schick, R.: Untersuchungen über die Bruchausdehnung und Bruchgeschwindigkeit bei Erdbeben mit kleinen Magnituden ($M<4$) 34:267
Schick, R.: A Method for Determining Source Parameters of Small Magnitude Earthquakes 36:205
Schick, R., Riuscetti, M.: An Analysis of Volcanic Tremors at South Italian Volcanoes 39:247
Schick, R., Zürn, W.: Criterions of the Restoration of Seismograms in the Frequency Domain 39:541
Schick, R., see Schneider, G., et al. 32:383
Schick, R., see Neugebauer, H.J., et al. 39:563
Schilp, E., see Knoechel, H., et al. 17:57
Schindelhauer, F.: Über Luftstörungen 12:299
Schindler, G., see Knoechel, H., et al. 17:57
Schirmer, F., see Essen, H.-H., et al. 49:115
Schlegel, K., see Kramm, R., et al. 38:953
Schlegel, K., see Loidl, A. 41:215
Schleusener, A.: Beitrag zur Frage der temperaturabhängigen Störung der Gleichgewichtslage der Drehwaagegehänge 9:301
Schleusener, A.: Messungen mit transportablen statischen Schweremessern 10:369
Schleusener, A.: Radius der sphärischen Bouguer-Platte bei Benutzung des üblichen ebenen Bouguer-Faktors 0,0419 mgal/m 19:29
Schleusener, A.: Der größte Ring bei Geländeverbesserungen der Gravimetrie der Lagerstättengeophysik 19:33
Schleusener, A.: In Memoriam Prof. Dr. Dr. h.c. Ludger Mintrop 22:58
Schleusener, A., Torge, W.: Investigation of Secular Gravity Variations in Iceland 37:679
Schleusener, A., Torge, W., Drewes, H.: The Gravity Field of Northeastern Iceland 42:27
Schleusener, A., see Berroth, A. 9:355
Schlomka, T.: Über die Abhängigkeit der Schwerkraft vom Zwischenmedium 3:397, 6:392
Schlomka, T.: Zur Haalckschen Theorie des Erdmagnetismus 8:84
Schlomka, T.: Zur physikalischen Theorie des Erdmagnetismus 9:99
Schlomka, T.: Zur neuen Haalckschen Theorie des Erdmagnetismus 13:126
Schlomka, T.: Erwiderung an Herrn Haalck 13:195
Schlomka, T.: Zur Elektrodynamik des rotierenden Erdmagneten 14:285
Schmalfeldt, B., see Janle, P., et al. 41:475
Schmedes, E., Leydecker, G.: Macroseismic Intensity Map of the Federal Republic of Germany for the Friuli Earthquake of May 6, 1976 44:277
Schmedes, E., see Procházková, D., et al. 46:343
Schmehl, H.: Über den Einfluß der Elastizität des Pendelstativs

auf die Schwingungszeiten zweier gleichzeitig auf demselben Stativ schwingender Pendel 3:157
Schmehl, H.: Die Reduktion der Koinzidenzzeiten von Pendeln zur Berechnung von Schweredifferenzen 5:1
Schmehl, H.: Die Registrierung der Schwingungen eines Schwerkraftpendels mittels hochfrequenter elektrischer Schwingungen und ihre Rückwirkung auf das Pendel 5:53
Schmehl, H.: Ein Beitrag zum Zweipendelverfahren bei relativen Schweremessungen 8:427
Schmehl, H.: Die Mitschwingungsreduktion von Pendelbeobachtungen 9:309
Schmeling, H., Jacoby, W.R.: On Modelling the Lithosphere in Mantle Convection with Non-Linear Rheology 50:89
Schmelovsky, K.H.: Untersuchungen über die tages- und jahreszeitlichen Variationen des Plasmas der äußeren Ionosphäre und ihre theoretische Deutung 27:59
Schmelovsky, K.H.: Untersuchungen über die äußere Ionosphäre und deren regelmäßige Variationen. (H. Kohl) 29:316
Schmelovsky, K.H., Felske, D.: Results from Multifrequency Observations of Electron Density with S 66 Satellite 33:155
Schmerwitz, G.: Erhöhung der Empfindlichkeit der Hebelwaage durch ein Horizontalpendel 7:104
Schmerwitz, G.: Experimentelle Ergänzungen zur Theorie des abrollenden Pendels 8:397
Schmerwitz, G.: Einfluß der Schneidenlagerung auf die Meßgenauigkeit geophysikalischer Instrumente 8:439
Schmerwitz, G.: Nachtrag zur Frage der Schneidenlagerung 9:168
Schmerwitz, G.: Die Wirkungsweise eines Klinographen bei der Aufzeichnung vom Neigungswellen 11:273
Schmerwitz, G.: Der Koppelungsfaktor bei galvanometrisch registrierenden Seismographen 12:206
Schmerwitz, G.: Ausgleichung der besten Stationsbeobachtungen mitteleuropäischer Erdbeben 14:351
Schmerwitz, G.: Die Bedeutung des Ausgleichungsverfahrens für die Auswertung von Nahbeben-Seismogrammen 15:365
Schmerwitz, G.: Berechnung der Dicke der Erdkruste und einiger physikalischer Eigenschaften aus mitteleuropäischen Nahbebenaufzeichnungen 15:268
Schmerwitz, G.: Ausgleichung der *P*-Wellen-Einsätze des Bebens vom 11. Juni 1938 in Belgien 16:119
Schmerwitz, G.: Die Verwechslung des Koordinaten-Nullpunktes mit den Epizentralkoordinaten, die P. Caloi bei der Beurteilung meiner Nahbebenausgleichungen unterlaufen ist 17:40
Schmid, E.: Messungen des Radium-Emanationsgehaltes von Kellerluft 8:233
Schmidbauer, E.: Magnetic Properties of Oxidized Fe-Cr Spinels 35:475
Schmidbauer, E.: Magnetization of Fe-Cr Spinels and Its Application for the Identification of Such Ferrites in Rocks 37:421
Schmidbauer, E.: Electrical Resistivity of Fe-Cr Spinels 37:425
Schmidbauer, E.: Magnetic Hysteresis Loops and Magnetization Versus Temperature Curves of Some Basalt Samples Containing Titanomagnetite Ore Either Single-Phase or with an Intergrowth of Ilmenite Lamellae 41:615
Schmidbauer, E., Veitch, R.J.: Anhysteretic Remanent Magnetization of Small Multidomain Fe_3O_4 Particles Dispersed in Various Concentrations in a Non Magnetic Matrix 48:148
Schmidbauer, E., see Heller, F. et al. 45:235
Schmidt, A.: Das erdmagnetische Außenfeld 1:3
Schmidt, A.: Zur Frage der elektrischen Vertikalströme 1:281
Schmidt, A.: Über die sterntägige Schwankung des Erdmagnetismus 7:134
Schmidt, A.: Zur Frage der hypothetischen sterntägigen Variation 7:198
Schmidt, A.: Inwieweit vermag die Annahme eines sich gleichförmig drehenden magnetischen Erdkerns die Erscheinungen der erdmagnetischen Säkularvariation zu erklären? 8:398
Schmidt, A.: Zum Aufsatz von T. Koulomzine und A. Boesch über die Vertikal-Feldwaage 14:63
Schmidt, G.: Determination of the Height of Ionospheric Irregularities with the Holographic Method 38:891
Schmidt, G., see Ebel, A., et al. 35:373
Schmidt, G., see Leitinger, R., et al. 41:201
Schmidt, H.: Untersuchungen zur photoelektrischen Schwingzeitmessung 21:53
Schmidt, H.: Methoden zur Bestimmung des räumlichen Gradienten des geomagnetischen Feldes 23:273
Schmidt, K.D.: Micrometeoroid Orbits Observable by the Helios Micrometeoroid Detector (E 10) 42:737
Schmidt, O. v.: (4)
Schmidt, O. v.: Theorie der 3-Schichten-Seismik 7:37
Schmidt, O. v.: Brechungsgesetz oder senkrechter Strahl? Eine kritische Studie auf Grund seismischer Arbeiten in Venezuela 8:376
Schmidt, O. v.: Zu vorstehender Arbeit von H. Reich: „Bemerkungen zur angewandten Seismik" 9:354
Schmidt, O. v.: Über den Energietransport bei der Sprengseismik 10:378
Schmidt, O. v.: Sprengseismische Untersuchungen 11:83
Schmidt, O. v.: Zur Theorie der Erdbebenwellen. Die „wandernde Reflexion" der Seismik als Analogon zur „Kopfwelle" der Ballistik 12:199
Schmidt, O. v.: Über Kopfwellen in der Seismik 15:141
Schmidt, P.W., Embleton, B.J.J.: A Geotectonic Paradox: Has the Earth Expanded? 49:20
Schmidt, W.: Strömungsforschung in freier Luft 5:404
Schmidtke, G.: EUV-Laborspektrophotometrie zur Vorbereitung von optischen Flugexperimenten 35:69
Schmidtke, G., Börsken, N., Sünder, G.: Variability of Solar EUV Fluxes and Exospheric Temperatures 49:146
Schmidtke, G., Schweizer, W., Knothe, M.: The AEROS-EUV Spectrometer 40:577
Schmidtke, G.L., see Brüning, K., et al. 49:74
Schmidtke, G.L., see Wilhelm, K., et al. 49:128
Schmidtke, G., see Spenner, K. 39:351
Schmincke, H.-U.: Age and Crustal Structure of the Canary Islands. A Discussion 46:217
Schminder, R., see Koch, H. 26:285
Schminder, R., see Koch, H., et al. 28:281
Schmitt, O., see Rosenbach, O. 29:129
Schmocker, U., see Dose, V. 42:15
Schmucker, U.: Einige Ergebnisse der erdmagnetischen Tiefensondierung in Norddeutschland 24:216
Schneider, G.: Zum Wellencharakter der mikroseismischen Bodenunruhe 25:161
Schneider, G.: Mikroseismik-Ausbreitung in Nord- und Mitteleuropa 27:118
Schneider, G., Müller, S., Knopoff, L.: Gruppengeschwindigkeitsmessungen an kurzperiodischen Oberflächenwellen in Mitteleuropa 32:33
Schneider, G., Schick, R., Berckhemer, H.: Fault-plane Solutions of Earthquakes in Baden-Württemberg 32:383
Schneider, G., see Ahorner, L., et al. 36:313
Schneider, G., see Procházková, D., et al. 46:343
Schneider, W.: Untersuchungen über die seismische Bodenunruhe kurzer Periode 4:103
Schneider, W., Ramspeck, A., Schulze, G.A.: Die Dispersion elastischer Wellen im Boden 15:395
Schnippenköter, J., Weyres, T.: Physik für höhere Lehranstalten 13:201
Schober, M.: The Electrical Conductivity of Some Samples of Natural Olivine at High Temperatures and Pressures 37:283
Schober, M., see Schult, A. 35:105
Schödel, J.P.: On the Existence of Sometimes Considerable Transport Effects in the Nighttime Ionosphere 35:297

Schödel, J.P., Klostermeyer, J., Röttger, J., Stilke, G.: Evidence for Tropospheric-Ionospheric-Coupling by Atmospheric Gravity Waves 39:1063
Schödel, J.P., Münch, J.W.: Methode zur Untersuchung der spektralen Frequenzverteilung von Schwerewellen in der Ionosphäre 38:169
Schödel, J.P., see Ebel, A., et al. 35:373
Scholer, M., Ipavich, F.M., Gloeckler, G., Hovestadt, D.: Simultaneous Observations of Energetic Protons Close to the Bow Shock and Far Upstream 49:186
Scholer, M., Morfill, G., Hovestadt, D.: Statistical Analysis of the Pitch Angle Distribution of Magnetospheric Solar Protons During Geomagnetic Activity 40:37
Scholer, M., see Achtermann, E., et al. 37:211
Schopper, J.R.: Untersuchungen über elektrische und hydraulische Eigenschaften poröser Gesteine 32:525
Schreiber, H.: Ein analytischer Weg zur Bestimmung der Elektronendichte in der Magnetosphäre aus Whistler-Daten 33:110
Schreiber, H.: Ringstromindizes und asymmetrischer Ringstrom 36:679
Schreiber, H.: Spherical Harmonic Analysis of the DS-Field During Magnetic Storms 40:239
Schreiber, H.: On the Variation of Kp at Sector Boundaries 42:437
Schreiber, H.: Correlation of Geomagnetic Activity Indices ap with the Solar Wind Speed and the Southward Interplanetary Magnetic Field 49:169
Schriel, Kukuk, P.: Geologie des Niederrheinisch-Westfälischen Steinkohlengebietes 15:115
Schriel, W., Barth, T.F.W., Correns, C.W., Eskola, P.: Die Entstehung der Gesteine 16:91
Schriel, W., Schneider, O.: Grundbegriffe der Geologie 17:339
Schriel, W., Schneiderhöhn, H.: Lehrbuch der Erzlagerstättenkunde. I. Bd.: Die Lagerstätten der magmatischen Abfolge 17:155
Schröder, A.: Untersuchungen über die Windstruktur und den Bau der Windmeßgeräte 14:198
Schröder, W.: Untersuchungen zur Tunguska-Katastrophe und den hochatmosphärischen Erhellungen vom 30. Juni 1908 (Briefe an den Herausgeber) 38:179
Schubert, J., see Wigand, A., et al. 6:458
Schuch, M.: Beobachtungen von Eigenpotentialen an Torflagerstätten mit verschiedenartigen Elektroden 29:175
Schuch, M., Wanke, R.: Strömungsspannungen in einigen Torf- und Sandproben 33:94
Schuch, M., Wanke, R.: Die seitlichen Variationen elektrischer Strömungsspannung auf kurzen vertikalen Meßstrecken in Mineralböden 34:599
Schuh, F.: Die geologische Bedeutung der Schaffung einer Isanomalenkarte der magnetischen Vertikalintensität von Deutschland 6:235
Schuler, M.: Der Kreisel als Richtungsweiser 1:59
Schuler, M.: Schwankungen in der Länge des Tages 3:71
Schuler, M.: Bemerkungen zu dem Aufsatz von G. Schmerwitz: „Einfluß der Schneidenlagerung auf die Meßgenauigkeit geophysikalischer Instrumente" 9:60
Schult, A.: Über die Magnetisierung der Basaltvorkommen in der Umgebung von Göttingen 29:1
Schult, A.: The Effect of Hydrostatic Pressure on the Compensation Temperature of Magnetization in a Li-Cr-Ferrite 33:458
Schult, A.: Methoden zur Messung von physikalischen Eigenschaften an Gesteinen und Mineralen bei hohem statischem Druck (Übersichtsartikel) 34:227
Schult, A.: The Effect of Pressure on the Curie Temperature of Magnetite and Some Other Ferrites 34:505
Schult, A.: Natural Magnetization of Deep Core Samples of Basaltic Rocks from Brazil 36:267
Schult, A.: On the Strength of Exchange Interactions in Titanomagnetites and Its Relation to Self-Reversal of Magnetization 37:357
Schult, A.: The Magnetization of Core Samples from a Serpentinite Near Erbendorf (Oberpfalz) 40:75
Schult, A.: Palaeomagnetism of Tertiary Volcanic Rocks from the Ethiopian Southern Plateau and the Danakil Block 40:203
Schult, A.: Measurements of Magnetic Total Field Anomalies in the Hon Graben, Libya 40:661
Schult, A.: Self-Reversal Above Room Temperature Due to N-Type Magnetization in Basalt 42:81
Schult, A., Hussain, A.G., Soffel, H.C.: Palaeomagnetism of Upper Cretaceous Volcanics and Nubian Sandstones of Wadi Natash, SE Egypt and Implications for the Polar Wander Path for Africa in the Mesozoic 50:16
Schult, A., Schober, M.: Measurement of Electrical Conductivity of Natural Olivine at Temperatures up to 950° C and Pressures up to 42 kbar (Übersichtsartikel) 35:105
Schult, A., Soffel, H.: Magnetic ΔZ-Profile Across the Hon Graben, Libya (Brief an den Herausgeber) 37:299
Schult, A., Soffel, H.C., Hussain, A.G.: Palaeomagnetism of Cretaceous Nubian Sandstone, Egypt 44:333
Schulz, B.: Theodor Stocks und Georg Wüst: Die Tiefenverhältnisse des offenen Atlantischen Ozeans 12:126
Schulz, B.: Wissenschaftliche Ergebnisse der Deutschen Atlantischen Expedition auf dem Forschungs- und Vermessungsschiff „Meteor" 1925–1927, Bd. VI, 2. Teil, 3. Lieferung 15:114
Schulz, B.: Wissenschaftliche Ergebnisse der Deutschen Atlantischen Expedition auf dem Forschungs- und Vermessungsschiff „Meteor" 1925-1927. III. Band. – Erster Teil. Morphologie des Atlantischen Ozeans. 4. Lieferung: Grundkarte der Lotungen 1:5 Millionen 17:340
Schulz, B.: Wissenschaftliche Ergebnisse der Deutschen Atlantischen Expedition auf dem Forschungs- und Vermessungsschiff „Meteor" 1925–1927. II. Band. – Zweiter Teil. Quantitative Untersuchungen zur Statik und Dynamik des Atlantischen Ozeans. 4. Lieferung: Die relative Topographie einzelner Druckflächen im Atlantischen Ozean von Albert Defant. 5. Lieferung: Die absolute Topographie des physikalischen Meeresniveaus und der Druckflächen, sowie die Wasserbewegungen im Atlantischen Ozean von Albert Defant 17:341
Schulz, B., Böhnecke, G.: Temperatur, Salzgehalt und Dichte an der Oberfläche des Atlantischen Ozeans. Atlas dazu 12:399
Schulz, B., Defant, A.: Ausbreitungs- und Vermischungsvorgänge im antarktischen Bodenstrom und im subantarktischen Zwischenwasser 13:43
Schulz, B., Defant, A.: Schichtung und Zirkulation des Atlantischen Ozeans 13:350
Schulz, B., Defant, A., Helland-Hansen, B.: Bericht über die ozeanographischen Untersuchungen im zentralen und östlichen Teil des Nordatlantischen Ozeans im Frühsommer 1938 16:97
Schulz, B., Neumann, G., Wüst, G., Defant, A.: Aus den wissenschaftlichen Ergebnissen der Internationalen Golfstromunternehmung 1938 17:153
Schulz, B., Schubert, O. v.: Quantitative Untersuchungen zur Statik und Dynamik des Atlantischen Ozeans 12:268
Schulz, B., Schumacher, A.: Monatskarten der Oberflächenströmungen im Nordatlantischen Ozean (5° S bis 50° N) 17:150
Schulz, B., Schumacher, A.: Stereophotogrammetrische Wellenaufnahmen 17:151
Schulz, B., Stocks, Th.: Grundkarte der ozeanischen Lotungen 1:5 Millionen 14:44
Schulz, B., Stocks, Th.: Grundkarte der ozeanischen Lotungen 1:5 Millionen, Blatt SI 2 mit durchsichtigem Deckblatt 15:226
Schulz, B., Wüst, G.: Schichtung und Zirkulation des Atlantischen Ozeans 12:269

Schulz, B., Wüst, G., Defant, A.: Atlas zur Schichtung und Zirkulation des Atlantischen Ozeans, Schnitte und Karten von Temperatur, Salzgehalt und Dichte 12:398
Schulz, G.: Reflexionen aus dem kristallinen Untergrund im Gebiet des Pfälzer Berglandes 23:225
Schulz, G.: Über ein Refraktionsproblem 26:236
Schulz, G.: Der mittlere Fehler bei Geschwindigkeitsberechnungen aus der Krümmung von Reflexionen 28:127
Schulz, K., see Fuchs, K. 42:175
Schulze, E.G.: Magnetische Vermessung einiger tertiärer Eruptivgänge und -stöcke im sächsischen Elbsandsteingebirge 6:141
Schulze, G.A.: Über die Ausbreitung sinusförmiger Bodenbewegung 11:307
Schulze, G.A.: Das elastische Verhalten des Bodens bei sinusförmiger Anregung 12:350
Schulze, G.A.: Veröffentlichungen des Instituts der Deutschen Forschungsgesellschaft für Bodenmechanik (Degebo) an der Technischen Hochschule Berlin 12:395
Schulze, G.A.: Ortung einer Maschine durch ihre Bodenschwingungen 13:119
Schulze, G.A., Koch, H.W., Boedeker, E.: Schwingungen im Bauwesen, bei Fahrzeugen und Maschinen, Schwingungsmessung 13:198
Schulze, G.A.: Veröffentlichungen des Instituts der Deutschen Forschungsgesellschaft für Bodenmechanik (Degebo) an der Technischen Hochschule Berlin, Heft 5. Über Zusammenhänge zwischen Wasserhaushalt der Tonminerale und bodenphysikalischen Eigenschaften bindiger Böden 15:114
Schulze, G.A., Beringer, C.Chr.: Geologisches Wörterbuch 13:238
Schulze, G.A., Dengler, M.: Erkundung von Verkehrswegen in Neuländern 15:115
Schulze, R.: Die modernen Askania-Gravimeter 24:318
Schulze, R.: Strahlenklima der Erde (L. Hasse) 38:352
Schulze, R., see Haalck, F. 26:246
Schumann, D., see Heitmann, M.-L., et al. 36:776
Schumann, R.: Beitrag zur Frage der Eigenschwingungen einzelner Teile des Erdkörpers 11:1
Schumann, R.: Über die Bedeutung der Mittelwasserorte als Punkte am Geoid 11:193
Schumann, R.: Abhängigkeit der „Bahn des Poles" von der Tageszeit der Beobachtung 12:37
Schumann, R.: Über die Polhöhenschwankung in Batavia August 1931 bis September 1936 14:123
Schumann, R.: Numerische Untersuchung über Radiusvektor und Azimut der Polbahn 1890-1938 16:259
Schünemann, H.: Die seismische Bodenunruhe zweiter Art in Hamburg und ihre Ursache. (Wellenperioden 10 bis 40 sec.) 8:216
Schütt, R., see Kohlschütter, E., et al. 8:480
Schwab, F., see Calcagnile, G., et al. 43:502
Schwahn, W., see Kautzleben, H., et al. 43:163
Schwehm, G., Rohde, M.: Dynamical Effects on Circumsolar Dust Grains 42:727
Schweitzer, Ch., Soffel, H.C.: Palaeointensity Measurements on Postglacial Lavas from Iceland 47:57
Schweizer, W., see Schmidtke, G., et al. 40:577
Schwenk, T.: Bewegungsformen des Wassers (H. Schwentek) 33:465
Schwenn, R., see Rosenbauer, H., et al. 42:561
Schwentek, H.: Ähnlichkeiten im jahreszeitlichen Verhalten der Stratosphäre und der D- und E-Schicht der Ionosphäre 34:123
Schwentek, H.: Sonneneruptionseffekte in der Ionosphäre, beobachtet in Lindau zwischen dem 27. Oktober und 2. November 1968 36:127
Schwentek, H., Elling, W.: Behaviour of Ionospheric Absorption in Winter 1975/76 at About 52° N, 9° E 44:27
Schwentek, H., see Labitzke, K. 34:555
Schwentek, H., see Loidl, A. 44:107, 117
Schweydar, W.: Die topographische Korrektion bei Schweremessungen mittels einer Torsionswage 1:81
Schweydar, W.: Über Isostasie 2:145
Schweydar, W.: Die topographische Korrektion bei Schweremessungen mittels einer Torsionswage. II 3:17
Schwinner, R.: Zum Aufsatz von Ansel „Die Alpen im Lichte ihrer Schwerestörung" 1:166
Schwinner, R.: Zur Verwertung der Schwerestörungen für die tektonische Geologie 2:126
Schwinner, R.: Über die Gestalt der Erde 2:214
Schwinner, R.: Zur Deutung der Transversalbeben in den nordöstlichen Alpen 5:16
Schwinner, R.: Über den Horizontalabstand von Pendelstationen 6:111
Schwinner, R.: Mikroseismische Bodenunruhe und Gebirgsbau 9:332
Schwinner, R.: Außenraum und Innenraum. (Schlichtung des Streites um die Schwerkraftreduktion) 10:240
Schwinner, R.: Seismik und tektonische Geologie der Jetztzeit. Eine neue wichtige Aufgabe 17:103
Schwinner, R.: Die Schwere auf den Hawai-Inseln. Über Reduktion, Isostasie und Verwandtes 17:159
Scriba, H., Heller, F.: Measurements of Anisotropy of Magnetic Susceptibility Using Inductive Magnetometers 44:341
Scriba, H., see Blohm, E.K., et al. 43:665
Scultetus, H.R.: Luftelektrische und erdmagnetische Begleiterscheinungen von Erdbeben 8:370
Scultetus see Knoechel, H., et al. 17:57
Seblatnig, H., Graf, A.: Zur Messung der horizontalen Störungskomponente des erdmagnetischen Feldes 5:329
Sebulke, J.: The Theoretical Investigation of Resistivity Methods for Geoelectrical Prospecting in Marine Areas 44:245
Sebulke, J., Hildebrandt, W.: A Theoretical Investigation of the Dipole- and Unipole-Resistivity Methods for Geoelectrical Prospecting in Marine Areas 45:409
Sedea, R., see Channell, J.E.T., et al. 45:29
Seehars, H.D., see Jeske, H., et al. 36:621
Seiberl, W., Franke, A., Gutdeutsch, R., Steinhauser, P.: Correlation Between Magnetic and Gravimetric Data in the East Alpine Area 44:639
Seibold, E., Wiegert, R.: Untersuchungen des zeitlichen Ablaufs der Sedimentation im Malo Jezero (Mljet, Adria) auf Periodizitäten 26:87
Seidel, B.L., see Volland, H., et al. 42:659
Seidl, D.: The Simulation Problem for Broad-Band Seismograms 48:84
Seidl, D., Müller, S.: Seismic Surface Waves 42:283
Seidl, D., Müller, S., Knopoff, L.: Dispersion von Rayleigh-Wellen in Südwestdeutschland und in den Alpen 32:472
Seidl, D., see Harjes, H.-P. 44:511
Seidl, E.: Die Bedeutung technischer Bruch-Formen für die Ermittlung geophysikalischer Störungs-Bereiche, erläutert an der Zone des Roten Meeres 7:117
Seidlitz, v.: Entstehen und Vergehen der Alpen 2:256
Seidlitz, W. v.: Die geophysikalische Reichsaufnahme 10:335
Seiler, E., Kertz, W.: Der polare Elektrojet 33:371
Seiler, E., see Musmann, G. 44:357
Seitz, K.: Altersbestimmung nach der RaD-Methode mit gasförmigen Bleiverbindungen 29:149
Sele, G., see Dose, V. 42:15
Sellevoll, M., see Berckhemer, H., et al. 27:151
Sengpiel, K.-P.: Das induzierte erdelektrische Feld, beobachtet längs zweier Profile durch die bayerische Molasse 32:502
Seret Opzoomer-Talma, S.H., see Voight, B., et al. 47:176
Sergeev, V.A.: High Time-Resolution Correlation Between the Magnetic Field Behaviour at 37 R_E Distance in the Magnetotail Plasma Sheet and Ground Phenomena During Substorm Expansive Phase 49:176
Servizi, G., see Mainardi, F., et al. 43:83

Seyfert, F.: Ein Beitrag zur Prognose phänologischer Daten (H. Schwentek) 33:465
Shamina, O.G.: Model Investigations of Inclusions in Medium 38:609
Shamina, O.G., see Behrens, J., et al. 38:579
Shapira, A., Kulhánek, O., Wahlström, R.: Detection Probabilities for Weak Regional Seismic Events 46:123
Shapira, A., Kulhánek, O., Wahlström, R.: Detection Probabilities for Earthquakes in Sweden 49:243
Shapiro, V.A., Ivanov, N.A.: Investigations of Secular Variation Anomalies in the Middle Ural Region 40:435
Shapiro, V.A., see Koshkina, T.M., et al. 40:565
Sharma, M.C., Sarma, S.B.S.S.: Modelling of the Ionosphere and Comparison of the Calculated and Observed Cosmic Radio Noise Absorption Over Delhi 42:535
Sharma, M.C., see Sarma, S.B.S.S. 42:541, 44:385
Sheikh, M.N., Rawer, K., Neske, E.: Electron Density in the South Atlantic Anomaly Region 45:113
Sickenberg, O.: Jahrbuch für die Gewässerkunde des Deutschen Reiches 17:251
Siebels, J., see Behrens, J. 38:627
Sieberg, A.: Das mitteleuropäische Erdbeben vom 16. November 1911, mit 1 Karte 50 × 46 cm 1:21
Sieberg, A.: Auffälliges Wandern von Erdbebenherden im südlichen Mitteleuropa 2:39
Sieberg, A.: Zur Geologie der Erdbeben im Rheinland 2:278
Sieberg, A.: Über Einsturzbeben 2:286
Sieberg, A.: Erdbeben und andere Erdrindenbewegungen 10:340
Sieberg, A.: Die gesetzmäßige Verteilung der tektonischen Verformungszonen in einer Geosynklinale 11:339
Sieberg, A.: Arbeitsgebiete der Reichsanstalt für Erdbebenforschung in ihren Beziehungen zur Geologie und Bergbau 15:7
Sieberg, A.: Neuere Untersuchungen der Reichsanstalt für Erdbebenforschung über bautechnische Erdbebensicherung 17:84
Siebert, J., see Essen, H.H., et al. 39:833, 41:111, 49:115
Siebert, M.: Die solaren Gezeiten im Barogramm des Juli 1959 25:109
Siebert, M.: Die Zerlegung eines zweidimensionalen Magnetfeldes in äußeren und inneren Anteil mit Hilfe der Cauchyschen Integralformel 28:231
Siebert, M.: Solarer Wind und Halbjahreswelle der erdmagnetischen Aktivität 36:41
Siebert, M.: Comment on: Hydromagnetic Waves in a Non-Uniform Plasma by E. Kupfer (J. Geophys. 41, 123–126, 1975) 41:325
Siedler, G.: Zum Mechanismus des Wasseraustausches zwischen dem Roten Meer und dem Golf von Aden 32:335
Siemann, H., see Heinrich, H., et al. 36:399
Sigurdsson, O.: Surface Deformation of the Krafla Fissure Swarm in Two Rifting Events 47:154
Sigurdsson, S., see Johnsen, G.V., et al. 47:132
Simon, R., see Voight, B., et al. 47:176
Šimša, J.: Approximate Deconvolution of Finite Functions with the Aid of Fourier Series 39:533
Sitaram, M.V.D., Plešinger, A., Vaněk, J.: Maximum Velocity Amplitudes of *P* and *S* Waves from Filtered Broadband Records 48:47
Skovli, G. (ed.): The Polar Ionosphere and Magnetospheric Processes. (H. Maurer) 38:352
Smith, K., see Rees, D., et al. 50:202
Smith, L.P.: Weather Studies (H. Schwentek) 33:462
Smith, M.L., see Dahlen, F.A. 43:497
Snoek, M., Goldflam, S.: Crustal Structure of the Reykjanes Ridge at 63° N Derived from Seismic Measurements 45:107
Snoke, J.A., Sacks, I.S.: Heterogeneous Velocity Structure at the Base of the Mantle. 1. Model 43:505
Snoke, J.A., see Sacks, I.S. 43:505
Sobouti, M., Eshghi, I., Mostaanpour, M.M.: Shamil-Siahou Earthquake "North-East of Bandar-Abbas" of 21st March, 1977 44:663
Soffel, H.: Untersuchungen an einigen ferrimagnetischen Oxyd- und Sulfid-Mineralien mit der Methode der Bitterschen Streifen 29:21
Soffel, H.: Die Sichtbarmachung von Grenzen Weißscher Bezirke von polykristallinem Magnetit mit der Methode der Bitterschen Streifen 30:45
Soffel, H.: Magnetic Domains of Poly Crystalline Natural Magnetite 31:345
Soffel, H.: Stress Dependence of the Domain Structure of Natural Magnetite 32:63
Soffel, H.: Die Beobachtung von Weissschen Bezirken auf einem Titanomagnetitkorn mit einem Durchmesser von 10 Mikron in einem Basalt 34:175
Soffel, H.: The Influence of the Dislocation Density and Inclusions on the Coercive Force of Multidomain Titanomagnetites of the Composition 0.65 Fe_2TiO_4 · 0.35 Fe_3O_4 in Basalts as Deduced from Domain Structure Observations 36:113
Soffel, H.: Die Theorien der thermoremanenten Magnetisierung von Gesteinen (Übersichtsartikel) 36:237
Soffel, H.: The Single Domain – Multidomain Transition in Natural Intermediate Titanomagnetites 37:451
Soffel, H.: The Effect of Radiation with Fast Neutrons on the Saturation Remanence of a Basalt 37:519
Soffel, H.: The Palaeomagnetism of Age Dated Tertiary Volcanites of the Monti Lessini (Northern Italy) and Its Implication to the Rotation of Northern Italy 41:385
Soffel, H.: Rock Magnetism of the Monti Lessini and Monte Berici Volcanites and Age of Volcanism Deduced from the Heirtzler Polarity Time Scale 41:401
Soffel, H.: Pseudo-Single-Domain Effects and Single-Domain Multidomain Transition in Natural Pyrrhotite Deduced from Domain Structure Observations 42:351
Soffel, H.: Reinterpretation of Palaeomagnetism of the Colli Euganei and Monti Lessini (Italy) 45:35
Soffel, H.: Palaeomagnetism of Permo-Triassic Red Sandstones from the Northern Calcareous Alps 45:447
Soffel, H.: Palaeomagnetism of a Jurassic Ophiolite Series in East Elba (Italy) 49:1
Soffel, H., Förster, H., Becker, H.: Preliminary Polar Wander Path of Central Iran 41:541
Soffel, H., Peters, K.: Auswertung von Gravimeter-Messungen in der Münchberger Gneismasse längs eines Profils von Konradsreuth nach Niederlamitz 36:589
Soffel, H., Peters, K., Pohl, J.: Interpretation of a Gravity Profile Across the Southern Part of the Graben, Libya 41:491
Soffel, H., Petersen, N.: Druckabhängigkeit der magnetischen Bereichsstrukturen von natürlichem Magnetit 32:531
Soffel, H., Petersen, N.: Vorwort 37:303
Soffel, H., Supalek, P.: Paläomagnetische Messungen am Basalt des Parkstein bei Weiden (Bayern) 34:287
Soffel, H., see Schult, A. 37:299
Soffel, H., see Bock, G. 37:581
Soffel, H., see Pohl, J. 37:857, 42:459
Soffel, H., see Becker, H., et al. 39:953
Soffel, H.C., see Schweitzer, Ch. 47:57
Soffel, H.C., see Schult, A., et al. 44:333, 50:16
Sofko, G.J., see Haldoupis, C.I. 46:63, 77
Solomon, S.C., see RRISP Working Group 47:228
Soltanian, R., see Akasheh, B., et al. 42:159
Somogyi, A., see Richter, A.K., et al. 50:101
Sorge, E.: Die ersten Dickenmessungen des grönländischen Inlandeises 6:22
Souriau, M., see Ruegg, J.C. 39:525
Souriau, M., see Neugebauer, H.J., et al. 39:563
Sparrer, H., see Lucke, O. 24:284
Speer, J.: Zur Denkschrift „Physik des Erdkörpers" 34:3
Spencer, N.W., Pelz, D.T., Niemann, H.B., Carignan, G.R.,

Caldwell, J.R.: The Neutral Atmosphere Temperature Experiment 40:613
Spenner, K., Bilitza, D., Plugge, R.: Intercomparison Between Aeros Electron Temperature Model and Mean Temperature Profiles of Different Incoherent Scatter Radar Stations 46:57
Spenner, K., Dumbs, A.: The Retarding Potential Analyzer on AEROS-B 40:585
Spenner, K., Ott, W., Bradenstein, H.J.: Plasma Measurements During the Western European Winteranomaly Campaign 44:81
Spenner, K., Plugge, R.: Empirical Model of Global Electron Temperature Distribution Between 300 and 700 km Based on Data from Aeros-A 46:43
Spenner, K., Schmidtke, G.: Energy Transport by Photoelectrons in the Early Morning Ionosphere 39:351
Spenner, K., see Kist, R. 36:421
Spenner, K., see Brüning, K., et al. 49:74
Spenner, K., see Wilhelm, K., et al. 49:128
Sperr, J.: Zur Denkschrift „Physik des Erdkörpers" 34:3
Spickernagel, H.: Results of Height Measurements in Northern Iceland 1965/1977 47:120
Spitaler, R.: Über Erdbeben und tektonische Umgestaltungen der Erdoberfläche durch die Polhöhenschwankungen 2:113
Spitaler, R.: Polschwankungen und Geotektonik 2:191
Spitta, P.: Electromagnetic Scale Model Experiments for the Coastline Effect of Geomagnetic Variations 42:507
Sponheuer, W.: Gebäudeschwingungen beim Erdbebenstoß 13:106
Sponheuer, W.: Über die makroseismischen Verfahren zur Bestimmung der Herdtiefe und ihre Anwendung bei Lockerböden 13:301
Stäger, A.: Elektrische Erscheinungen im Zusammenhang mit vulkanischen Ausbrüchen 1:209
Stahl, P.: Seismische Messungen der französischen Polarexpeditionen in Grönland und Island 19:68
Staudacher, W.: Die Temperatur-Leitfähigkeit von natürlichem Olivin bei hohen Drucken und Temperaturen 39:979
Stavrou, A., see Makris, J., et al. 39:929
Stechhöfer, S.: Erdstrahlungsmessungen mit dem Geiger-Müller-Zählrohr und elektrische Feldstärkemessungen im Gelände 12:68
Stefanescu, S.: Über die magnetische Wirkung einiger heterogener Medien in der elektrischen Bodenforschung 24:175
Stegena, L.: Paleogravity – A Possible Chance for Determination of Paleo-Geographic North 41:535
Stegena, L., Bérczi, Sz.: No Transform Faults on the Moon 40:775
Stegena, L., see Egyed, E. 24:260
Steigenberger, N., see Markert, H. 37:499
Steigenberger, N., see Markert, H., et al. 42:47
Stein, A., see Müller, St., et al. 28:258
Stein, A., see Giese, P. 37:237
Steinert, O., Husebye, S., Gjøystdal, H.: Noise Variance Fluctuations and Earthquake Detectability 41:289
Steinhart, J.S., Meyer, R.P.: Explosion Studies of Continental Structure. (R. Gutdeutsch) 30:158
Steinhauser, P.: Scale Factor Determinations of a LaCoste and Romberg Gravimeter Model D 44:395
Steinhauser, P., see Behle, A., et al. 38:221
Steinhauser, P., see Ehrismann, W., et al. 39:115
Steinhauser, P., see Vincenz, S.A., et al. 39:727, 1067
Steinhauser, P., see Seiberl, W., et al. 44:639
Steinhäusser, H.: Horizontalsicht bei örtlich veränderlicher Trübung und Beleuchtung 10:59
Steinmann, W., Rühmkorf, H.A.: Seismische Messungen zur Salzstockflankenbestimmung. Eine Case History 34:457
Steinmetz, L., see Hirn, A., et al. 39:363
Steinwachs, M.: Interpretation von Mikroerdbebenregistrierungen in Westgriechenland 37:867
Stekloff, W.: Über die Wiederherstellung des Netzes seismischer Stationen von USSR... 2:12
Stelzried, C.T., see Volland, H., et al. 42:659
Stenz, E.: Der große Staubfall vom 26. bis 29. April 1928 in Südosteuropa 6:443
Sterlikova, I.V., see Baranskiy, L.N., et al. 48:1
Sterlikova, V., see Kangas, J., et al. 46:237
Stern, W.: Über Größe und Tiefenwirkung der kapazitiven Beeinflussung eines Leiters durch eine Dishomogenität des Untergrundes. Ein registrierendes Meßgerät 7:166
Stern, W.: Beiträge zur Meßtechnik und Anwendung der Methode des scheinbaren spezifischen Widerstandes 8:181
Stern, W.: Die Bestimmung des Verlaufes geneigter Diskontinuitätsflächen (einfallende Schichtgrenzen und Verwerfungen) durch das Widerstandsverfahren 9:1
Stern, W., see Löhnberg, A. 8:283
Steveling, E.: Erdmagnetische Tiefensondierung mit 9 gleichzeitig registrierenden Pulsationsstationen zwischen Göttingen und Goslar 32:422
Stewart, I.C.F.: Lithospheric Structure and Teleseismic *P*-Wave Reflection Delays Under Fennoscandia and Siberia 49:108
Stilke, G.: Registrierung von Luftdruckwellen im Subschallgebiet 33:147
Stilke, G., see Schödel, J.P., et al. 39:1063
Stille, H.: Grundfragen der vergleichenden Tektonik 1:329
Stiller, H., Frölich, F.: Studies on Rock Forming Magnetic Minerals 30:13
Stiller, H., Frölich, F., Wagner, F.Ch.: Zustandsänderungen in magnetischen Gesteinsproben 27:89
Stiller, H., Vollstädt, H.: Bestimmung ferri- und antiferromagnetischer Curie-Temperaturen mittels Differentialthermoanalyse 31:212
Stiller, H., Wagner, C.: Eine Einrichtung für Ultraschallmessungen an Gesteinen unter hydrostatischem Druck bis 2 kbar 35:97
Stiller, H., see Frölich, F., et al. 27:136
Stiller, H., see Hoffmann, U. 32:267
Stiller, S.: Freiluftisolator für luftelektrische Messungen 30:301
Stiller, S., see Israel, H. 29:51
Stix, M.: Planetary Dynamos 43:695
Stock, H.-G.: Mehrjährige Untersuchungen über den Witterungseinfluß auf die Ertragsbildung von Rotklee und Luzerne (N. Czerwinski) 38:191
Stöckl, H.: A Digital Filter Technique for the Recovery of Ground Motion 39:545
Stöckl, H.: Finite Difference Calculation of Stress Relaxation Earthquake Models 43:299
Stöckl, H., see Neugebauer, H.J., et al. 39:563
Stöckl, H., see Müller, G., et al. 44:203
Stöckl, H., see Korn, M. 50:171
Stolpovsky, V.G., see Richter, A.K., et al. 50:101
Stoppel, R.: Weitere Untersuchungen mit dem Sanford-Elektrometer 10:359
Storetvedt, K.M.: Some Paleomagnetic Problems of Strongly Oxidized Rocks 37:487
Storetvedt, K.M., Mongstad Våge, H., Aase, S., Løvlie, R.: Palaeomagnetism and the Early Magmatic History of Fuerteventura (Canary Islands) 46:319
Storetvedt, K.M., Petersen, N.: On Chemical Magnetization in Some Permian Lava Flows of Southern Norway 36:569
Storetvedt, K.M., Petersen, N.: Postulated Rotation of Corsica Not Confirmed by New Palaeomagnetic Data 42:59
Storetvedt, K.M., Petersen, N.: Reply to the Comments by M. Westphal [42:399] 42:403
Storetvedt, K.M., Svalestad, S., Thomassen, K., Langlie, Aa., Nergård, A., Gidskehaug, A.: Magnetic Discordance in Gran Canaria/Tenerife and Its Possible Relevance to the Formation of the NW African Continental Margin 44:317
Storetvedt, K.M., see Waage, H.L. 39:937
Störmer, C.: Vom Jahre 1922 an im südlichen Norwegen aufgenommene Nordlichtphotogramme 4:261

Störmer, C.: Sonnenbelichtete Nordlichtstrahlen 5:177
Störmer, C.: Wie tief dringen die Polarlichter in die Erdatmosphäre ein? 6:334
Störmer, C.: Kurze Erwiderung auf Vegards Bemerkungen über sonnenbelichtete Nordlichtstrahlen 6:463
Stout, J.H., see Banerjee, S.K., et al. 40:537
Strebel, O., see Henzel, N. 33:33
Strobach, K.: Die neue Erdbebenstation in Hamburg 20:160
Strobach, K.: Zum Studium der mikroseismischen Bodenunruhe in Hamburg 21:190
Strobach, K.: Stereoskopische Vektorregistrierung 23:306
Strobach, K.: Morphologische Untersuchung mikroseismischer Bodenbewegungen nach stereoskopischen Vektorregistrierungen 24:369
Strobach, K.: Entstehung und Charakter der Mikroseismik als Resultantschwingung zahlreicher seismischer Oszillatoren 30:192
Strobach, K.: Kolloquium der Deutschen Forschungsgemeinschaft zum Schwerpunktprogramm: Geophysikalische Erforschung des tieferen Untergrundes Mitteleuropas 30:249
Strobach, K.: Über die Natur der elastischen Wellen der Seegangs-Mikroseismik 35:113
Strobach, K.: Scattering of Seismic Waves and Lunar Seismograms (Brief an den Herausgeber) 36:643
Strobach, K.: Curvature of Island Arcs and Plate Tectonics 39:819
Strowald, J.: Schlierenoptische Untersuchung der Ω-Welle 35:83
Struck, B.: Anwendung von Ultraschall zur Strömungsmessung im Meer 34:415
Struve, O., Lynds, B., Pillans, H.: Astronomie, Einführung in ihre Grundlagen. (G. Elste) 28:294
Stubbe, P.: Atmospheric Parameters from Ionospheric Measurements 39:1043
Stüdemann, W.: Untersuchung der Richtungsverteilung energiereicher Elektronen und Protonen im Morgensektor der Polarlichtzone während erhöhten Teilcheneinfalles 38:863
Stüdemann, W., Goertz, C.K.: Simultaneous Observation of an Intense 65 keV Field-Aligned Proton Beam and ULF-Waves During a Break-up Event 49:123
Stüdemann, W., see Brüning, K., et al. 49:74
Stüdemann, W., see Wilhelm, K., et al. 49:128
Stukenbröker, B.: Ergebnisse von Erdgezeiten-Parallelregistrierungen mit drei Askania-Gravimetern 39:1
Stümke, H.: Rotationssymmetrische Gleichgewichtsstörungen in einer isothermen Atmosphäre nebst einem Modellversuch mit rotierender Flüssigkeit 16:127
Štursa, J.: Influence of Round-Off Errors in Digital Filters 39:551
Stützer, H., see Knoechel, H., et al. 17:57
Stüve, G.: Ergebnisse der aerologischen Messungen... 8:250
Stüve, G., Koschmieder, H.: Dynamische Meterologie 9:170
Subbaraya, B.H., see Gupta, S.P., et al. 43:681
Subrahmanyam, C., Verma, R.K.: Densities and Magnetic Susceptibilities of Precambrian Rocks of Different Metamorphic Grade (Southern Indian Shield) 49:101
Suckfüll, E., see Beran, D. 44:155
Sucksdorff, C., see Nevanlinna, H. 50:68
Suckstorff, G.A.: Die Höhenverteilung der Erd-, Luft- und Höhenstrahlung. Auszug aus der Berliner Dissertation 10:95
Suckstorff, G.A.: Eine transportable Zählrohrapparatur und ihre Anwendung im Gelände 11:95
Suckstorff, G.A.: Institut für Meereskunde: Das Meer in volkstümlichen Darstellungen; II. Teil. Der Luftverkehr über dem Ozean 11:159
Suckstorff, G.A.: Einige Untersuchungen über die Struktur der Richtungsschwankungen des Windes 11:378
Suckstorff, G.A.: Ein mechanisch registrierender Barograph hoher Empfindlichkeit 12:245
Suckstorff, G.A.: Boletin del Observatorio del Ebro: Contribution al Estudio climatológico de la Comarca de Tortosa 14:45
Suckstorff, G.A.: The National Geographic Society-U.S. Army Air Corps Stratosphere Flight of 1935 in Ballon „Explorer II" 14:45
Suckstorff, G.A.: Jahrbuch für die Gewässerkunde Norddeutschlands 14:47
Suckstorff, G.A.: Jahrbuch für die Gewässerkunde Norddeutschlands. Abflußjahr 1936 16:94
Suckstorff, G.A.: Meteorologisches Taschenbuch, 4. und 5. Ausgabe 16:96
Suckstorff, G.A.: Handbuch der biologischen Arbeitsmethoden. Abt. II. Physikalische Methoden 16:199
Suckstorff, G.A.: Vergleich der Aufzeichnung von Luftdruckschreibern und Luftdruckvariographen bei der Schallsprengung am 16. August 1939 in Jüterbog 17:260
Suckstorff, G.A., Baur, F.: Einführung in die Großwetterforschung 13:200
Suckstorff, G.A., Dorno, C.: Das Klima von Agra (Tessin) 11:107
Suckstorff, G.A., Hann-Süring: Lehrbuch der Meteorologie 13:199
Suckstorff, G.A., Israël-Köhler, H.: Das Klima von Bad Nauheim 13:200
Suckstorff, G.A., Kendrew, W.G.: Climate 15:394
Suckstorff, G.A., Lange, O.: Der Einfluß wechselnder Wasserstände auf die Höhenlage von Festpunkten und Bauwerken 14:47
Suckstorff, G.A., Linke, F.: Meteorologisches Taschenbuch, 3. Ausgabe 15:394
Suckstorff, G.A., Maurain, Ch.: Etüde Partique des Rayonnements Solaire. Atmosphärique et Terrestre 14:45
Suckstorff, G.A., Miehlnickel, E.: Höhenstrahlung (Ultrastrahlung) 14:46
Suckstorff, G.A., Reinhold, F.: Regenbeobachtungen, Wasserstands- und Wassermengenmessungen 13:199
Suckstorff, G.A., Robitzsch, M.: Ausführliche barometrische Reduktions- und Höhentafeln 16:200
Suckstorff, G.A., Roschke, G.: Die Malapane, ihr Wasserhaushalt, sowie ihre Flußbett- und Talgestaltung 14:48
Suckstorff, G.A., Schmauss, A.: Das Problem der Wettervorhersage 13:201
Suckstorff, G.A., Schnippenkötter, J., Weyres, T.: Physik für höhere Lehranstalten 13:201
Suckstorff, G.A., Steinhauser, F.: Die Meteorologie des Sonnblicks. 1. Teil 16:95
Suckstorff, G.A., Süring, R.: Die Wolken 12:197
Suckstorff, G.A., Sutcliffe, R.C.: Meteorology for Aviators 16:95
Sulzbacher, H., Baumjohann, W., Potemra, T.A.: Coordinated Magnetic Observations of Morning Sector Auroral Zone Currents with Triad and the Scandinavian Magnetometer Array: A Case Study 48:7
Sünder, G., see Schmidtke, G., et al. 49:146
Supalek, P., see Soffel, H. 34:287
Süring, R.: Der Temperaturverlauf im Sandboden 6:285
Svalestad, S., see Storetvedt, K.M., et al. 44:317
Swerzina, P., see Goldmann, G. 17:246
Szelwis, R., Janle, P.: Analysis of Microseisms Measured on the Isle of Sylt 43:623
Szelwis, R., see Janle, P., et al. 41:475

Taagholt, J., see Kremser, G., et al. 38:851
Takeda, M., Maeda, H.: Effect of the Coastline Configuration of South Indian and Sri Lanka Regions on the Induced Field at Short Period 45:209
Talwani, M., see Kahle, H.-G. 39:167, 491
Tammann, G.: Bemerkungen zur Geochemie 1:23
Tammann, G., Krige: Über die Möglichkeit des Auftretens von Gashydraten in höheren Schichten der Atmosphäre 1:371

Tams, E.: Über die erdmagnetischen Anomalien im Gouvernement Kursk 1:68
Tams, E.: Zur Frage des Einflusses von Sonne und Mond sowie des Luftdrucks auf die Stoßfrequenz der vogtländischen Erdbebenschwärme 1:117
Tams, E.: Bruchlinien und Erdbewegungen in Kalifornien 1:187
Tams, E.: Die Fragen der Periodizität der Erdbeben 2:17
Tams, E.: Erdbeben und Ausbruch des Katmai im Jahre 1912 2:163
Tams, E.: Chart Showing the Change of the Depth of the Sea... 2:205
Tams, E.: Die Frage der Periodizität der Erdbeben 2:207
Tams, E.: Bemerkungen zu der Untersuchung von Herrn Myrbach, ob Sonnenflecken und Mondphase einen auslösenden Einfluß auf Erdbeben haben 3:23
Tams, E.: Die Seismizität der Ozeane und Kontinente 4:245, 321
Tams, E.: Die Seismizität des Südantillenbogens 6:361
Tams, E.: Das Epizentrum des südatlantischen Großbebens vom 27. Juni 1929 6:480
Tams, E.: Der große sibirische Meteor vom 30. Juni 1908 und die bei seinem Niedergang hervorgerufenen Erd- und Luftwellen 7:34
Tams, E.: Einige Korrelationen zwischen seismischer Bodenunruhe in Hamburg und der Brandung in West- und Nordeuropa 9:23
Tams, E.: Einige Korrelationen zwischen seismischer Bodenunruhe in Hamburg und der Brandung in West- und Nordeuropa. II 9:295
Tams, E.: Seismische Bodenunruhe in Hamburg und örtlicher Sturm 11:9
Tams, E.: Die neuen Schweremessungen auf dem Meere und ihre Deutung (Schwere-Expeditionen 1923 bis 1932) 11:235
Tams, E.: Zur Frage der regionalen Verkoppelung von Erdbeben 14:241
Tams, E.: Zur Frage der regionalen Verkoppelung von Erdbeben. II 15:249
Tams, E.: Zur Frage der regionalen Verkoppelung von Erdbeben. III 17:18
Tams, E.: Prof. Richard Schütt zum Gedächtnis 18:85
Tams, E.: Über Gruppenbildung bei Erdbeben in der rheinischen Region 19:92
Tams, E.: Die Erdbeben der Karpathen-Becken (455–1918) von Antal Réthly 21:175
Tams, E.: In Memoriam Prof. Dr. Gerhard Krumbach 22:117
Tams, E., Gutenberg, B.: Handbuch der Geophysik, Bd. 3, Lief. 1 8:327
Tams, E., Sieberg, A.: Erdbebengeographie 9:119
Tank see Knoechel, H., et al. 17:57
Tanskanen, P., see Opgenoorth, H.J., et al. 48:101
Tarantola, A., Valette, B.: Inverse Problems = Quest for Information 50:159
Tárczy-Hornoch, A.: Über die Genauigkeit der berechneten durchschnittlichen Geschwindigkeit bei der seismischen Reflexionsmethode 31:260
Tauber, A.F., see Fritsch, V. 35:161, 37:293
Tauriainen, A., see Leitinger, R., et al. 41:201
Taylor, C., see Voight, B., et al. 47:176
Teichgraeber, A., Ruttner, H.: Nordlicht am 5. März 1942 17:333
Teichgraeber, A., Ruttner, H.: Nordlicht am 4. April 1942 17:333
Teichgraeber, A., see Knoechel, H., et al. 17:57
Temme, P., Müller, G.: Numerical Simulation of Vertical Seismic Profiling 50:177
Terebesi, P.: Aufsuchen versteckter Periodizitäten 9:313
Tesch, H.: Der Einfluß der Elastizität der Schneide und Unterlage eines Pendels auf die Schwingungszeit 16:289
Tetens, O.: Über einige meteorologische Begriffe 6:297
Teupser, Ch., Ullmann, W.: Ein neuer Horizontalseismograph mit galvanometrischer Registrierung 25:272
Teupser, Ch., Ullmann, W.: Ein neuer Vertikalseismograph mit galvanometrischer Registrierung 29:115
Theile, B.: Physics and Chemistry in Space. Vol. 1 38:351
Theile, B.: Physics and Chemistry in Space. Vol. 2 38:351
Theile, B., see Maurer, H. 44:415
Theile, B., see Klöcker, N. 46:229
Theile, B., see Wilhelm, K., et al. 49:128
Thiele, P., see Makris, J., et al. 36:299
Thierbach, R.: Electromagnetic Reflections in Salt Deposits 40:633
Thomassen, K., see Storetvedt, K.M., et al. 44:317
Thorsteinsson, T., see Voight, B., et al. 47:176
Thrane, E.V., Grandal, B., Hagen, O., Ugletveit, F.: Measurements of Lyman-α Extinction and Energetic Charged Particle Precipitation During the European Winter Anomaly Campaign 1975/76 44:99
Thrasher, J.E., Scheidegger, A.E.: On the Connection Between Stress and Displacements in Faulted Regions 29:307
Thyssen, F.: Die Temperaturabhängigkeit der P-Wellengeschwindigkeit in Gletschern und Inlandeisen 33:65
Thyssen, F., Wagenitz, V.: A Method to Resolve Structures in the Earth's Crust and Mantle from Short-Period Teleseismic Signals 39:411
Thyssen, St. v.: Mitteilungen über die neuere Entwicklung des Thyssen-Gravimeters 11:131
Thyssen, St. v.: Relative Schweremessungen an einer tiefen Salzstruktur der norddeutschen Tiefebene 11:212
Thyssen, St. v.: Über die Verwendung verschiedenartiger Explosionen zur Erregung seismischer Wellen 12:86
Thyssen, St. v.: Ein neues piezoelektrisches Vertikalseismometer 14:11
Thyssen, St. v.: Über die Wirkungsweise von einigen feldfähigen Federgravimetern 15:121
Thyssen, St. v.: Drehwaageregistrierungen unter gleichzeitiger Einwirkung elastischer Wellen 16:210
Thyssen, St. v.: Über einige Gravimeter-Vergleichsmessungen 17:75
Thyssen, St. v.: Über die mögliche Beeinflußbarkeit der Drehwaage durch Grundwasserschwankungen 17:279
Thyssen, St. v.: Versuche mit einer neuartigen Schneidenentlastung 18:53
Thyssen, St. v.: Einige Fehlerquellen schneidegelagerter Systeme 18:134
Thyssen, St. v., Hummel, J.N., Rülke, O.: Die Ursachen des seismisch-elektrischen Effektes 13:112
Thyssen, St. v., Rülke, O.: Beschreibung des neuen Gerätes zur Bestimmung der Fortpflanzungsgeschwindigkeit elastischer Wellen in Gesteinsproben und einige Meßergebnisse 15:130
Thyssen-Bornemisza, S.: Eine gravimetrische Untersuchungsmethode für oberflächennahe Dichtestörungen 31:219
Thyssen-Bornemisza, S.: Die gleichzeitige Bestimmung von Horizontalgradienten und W_{zzz} aus drei engen Schwereprofilen 32:58
Thyssen-Bornemisza, S.: Ermittlung örtlicher Horizontalgradienten aus Gravimetermessungen im Nördlinger Ries 32:119
Thyssen-Bornemisza, S.: Depth Estimation from Vertical Gravity Observations 32:242
Thyssen-Bornemisza, S.: Mit einem Seegravimeter bestimmte Horizontalgradienten 33:143
Thyssen-Bornemisza, S.: Possible Improvement of Seismic Signal to Noise Ratio by Vertical Gravity Gradients (Briefe an den Herausgeber) 38:1059
Thyssen-Bornemisza, S.: Technique for Simultaneous Observation of Gravity and Vertical Gradient Data 42:169
Thyssen-Bornemisza, S., Groten, E.: Principle of an Absolute Gravity Meter and Gradiometer System (Brief an den Herausgeber) 37:747
Thyssen-Bornemisza, S., Jacoby, W.R.: Vertical Gradients of Gravity for Areal Density Contrast Exploration 37:735

Thyssen-Bornemisza, St. v.: Taschenbuch der angewandten Geophysik. Herausgegeben von H. Reich u. R. v. Zwerger 18:191
Tiefenau, H., Pruchniewicz, P.G., Fabian, P.: Meridional Distribution of Tropospheric Ozone from Measurements Aboard Commercial Airliners 38:145
Tighe, W.G., Rostoker, G.: Characteristics of Westward Travelling Surges During Magnetospheric Substorms 50:51
Timpe, Chr.: Ein Verfahren zur Bestimmung angenäherter Elektronendichteprofile der unteren Ionosphäre aus Absorptionsmessungen bei 245 kHz, 2,775 MHz und 27,6 MHz 39:753
Tkhostov, B.A.: Initial Rock Pressures in Oil and Gas Deposits. (H.J. Dürbaum) 30:260
Tobias, E., see Neugebauer, H.J. 43:751
Todt, W., Lippolt, H.J.: K-Ar Age Determinations on Volcanics with Known Paleomagnetic Field Parameters. I. Oberpfalz and Oberfranken 40:43
Todt, W., Lippolt, H.J.: K-Ar Age Determinations on Volcanics with Known Paleomagnetic Field Parameters. II. Sachsen 41:641
Todt, W., Lippolt, H.J.: K-Ar Age Determinations on Tertiary Volcanic Rocks: V. Siebengebirge, Siebengebirge-Graben 48:18
Toksöz, M.N., see Dainty, A.M. 43:375
Tollmien, W., see Prandtl, L. 1:47
Tomaschek, R., Schaffernicht, W.: Über die Messung der zeitlichen Schwankungen der Schwerebeschleunigung mit Gravimetern 9:125
Tomaschek, R., Schaffernicht, W.: Die Flut der festen Erde 9:199
Tomaschek, R., Schaffernicht, W.: Bemerkung zu E. Kleinschmidt: Erwiderung....[9:308] 9:309
Tomczak, M., jun.: Über winderzeugte interne Wellen 32:357
Töpfer, K.D.: Über den Einfluß oberflächennaher Störkörper auf geoelektrische Widerstandsmessungen 36:345
Töpfer, K.D.: Zur Berechnung des spez. Widerstandes von reinen unverfestigten Sanden 38:773
Töpfer, K.D.: Representation and Interpretation of Resistivity Mapping Data in Groundwater Prospecting in Zambia 42:147
Töpfer, K.D.: Provisional Seismicity Map of the Republic of Zambia and Its Preliminary Interpretation 42:225
Töpfer, K.D.: Relation of Gravity to Elevation in Zambia 43:581
Töpfer, K.D.: Improved Technique for Rapid Interpretation of Gravity Anomalies Caused by Two-Dimensional Sedimentary Basins 43:645
Töpfer, K.D., Legg, C.A.: Geophysical Exploration for Groundwater in the Lusaka District, Republic of Zambia 40:97
Toptyghin, I.N., see Bykov, A.M. 50:221
Torge, W.: In Memoriam Alfred Schleusener 44:679
Torge, W., Drewes, H.: Gravity Variations with Time in Northern Iceland 1965–1975 43:771
Torge, W., Kanngieser, E.: Gravity and Height Variations During the Present Rifting Episode in Northerm Iceland 47:125
Torge, W., see Schleusener, A. 37:679
Torge, W., see Schleusener, A., et al. 42:27
Torkar, K., see Friedrich, M., et al. 44:91
Torkar, K.M., see Urban, A., et al. 50:189
Trapp, E., see Drimmel, J., et al. 39:21
Trappe, F., Ruprecht, L.: Die Anwendung der seismischen Reflexionsmethode zur Untersuchung von Salzstöcken im Harzvorland 15:37
Tregub, F.S.: Relation Between P-Wave Amplitudes and Discontinuities in the Earth's Crust 38:407
Treumann, R.: Induktionspfeile über ideal horizontalen Schichtungen 33:285
Treumann, R., Grafe, A., Lehmann, H.-R.: A Note on the Post-Rosenbluth Quasilinear Diffusion Coefficient in the Ring Current Region 43:719
Treumann, R., Schäfer, K.: Statistical Theory of Electromagnetic Induction in Thin Sheets 43:521
Trinks, H., see Friedrich, V.H., et al. 44:139
Trippler, K.: Bericht über Untersuchungen zur β-Aktivität der bodennahen Atmosphäre 32:102
Trippler, K.: Natürliche Radioaktivität in Abhängigkeit von der Temperaturschichtung und der Windgeschwindigkeit 36:687
Trissl, K.-H., see Markert, H., et al. 40:303
Troitskaya, V.A., see Kangas, J., et al. 46:237
Troitskaya, V.A., see Baranskiy, L.N., et al. 48:1
Trommsdorff, F.: Untersuchungen über die natürliche Bodenunruhe (Mikroseismik) mit transportablen Dreikomponentenstationen 15:304
Trommsdorff, F.: Ergänzende Bemerkung zu „Der Zusammenhang zwischen Bodenunruhe und Zyklonen" von S.W. Visser 16:331
Trommsdorff, W.: Der Meteorfall bei Stadt Rehburg am 2. Januar 1934 10:296
Trommsdorff, W., Heide, F.: Kleine Meteoritenkunde 11:108
Tromp, S.W.: Das Gesetz von Helmholtz und seine Anwendung auf Geotektonik 13:78
Tromp, S.W.: Antwort auf die kritischen Bemerkungen von H. Jung 13:85
Trussoni, E., see Ferrari, A. 50:70
Tryggvason, E.: Subsidence Events in the Krafla Area, North Iceland, 1975–1979 47:141
Tuchel, G.: Zur Frage der Geländekorrektion bei Drehwaagemessungen 10:346
Tucker, P.: Stirred Remanent Magnetization: A Laboratory Analogue of Post-Depositional Realignment 48:153
Turchetti, G., see Mainardi, F., et al. 43:83
Tye, R.P.: Thermal Conductivity (J. Scheuch) 39:863
Tzu, C.-W.: Eine einfache Methode zur Bestimmung der magnetischen Suszeptibilitäten von Gesteinen in schwachen Feldern 16:160

Ugletveit, F., see Thrane, E.V., et al. 44:99
Uhink, W.: Quarzuhren 12:21
Uljanin, W.: Ein Universal-Induktionsmagnetometer 6:435
Uller, K.: Die geführten elastischen Zweimittelwellen 4:259
Uller, K.: Die wahre Kugelwelle 7:108
Ullmann, W., Maaz, R.: Zur Frage der „scheinbaren" und „wirklichen" Neigung 23:75
Ullmann, W., see Teupser, Ch. 25:272, 29:115
Ulrich, S., see Friedrich, M., et al. 44:91
Umlauft, G., see Keppler, E., et al. 42:633
Ungar, A., Ilan, A.: Propagation of Elastic Waves in Vertically Inhomogeneous Media 43:33
Untiedt, J.: Über die direkte Aufzeichnung erdmagnetischer Vektogramme 24:125
Untiedt, J., Pellinen, R., Küppers, F., Opgenoorth, H.J., Pelster, W.D., Baumjohann, W., Ranta, H., Kangas, J., Czechowsky, P., Heikkila, W.J.: Observations of the Initial Development of an Auroral and Magnetic Substorm at Magnetic Midnight 45:41
Untiedt, J., see Scheube, H.G. 31:283
Untiedt, J., see Küppers, F., et al. 46:429
Upadhyay, S.K., Duda, S.J.: Source Parameters of Earthquakes from the Himalayan Region 48:67
Urban, A., Torkar, K.M., Wilhelm, K.: Energy Dispersion and Acceleration of Low Energy Protons and Their Relation to Electrons During an Auroral Breakup 50:189
Urban, A., see Brüning, K., et al. 49:74
Urban, A., see Wilhelm, K., et al. 49:128

Vajk, R.: Mapping of Faults by Isogams 9:151
Valette, B., see Tarantola, A. 50:159
Vaněk, J.: Seismological Evidence on Discontinuities in the Mantle (Invited Paper) 38:355

Vaněk, J., see Pros, Z., et al. 35:287
Vaněk, J., see Hanuš, V. 42:219, 44:473, 46:385
Vaněk, J., see Sitaram, M.V.D., et al. 48:47
Vees, R., see Müller, St., et al. 28:258
Vees, R., see Burkhardt, H., et al. 33:455
Vees, R., see Burkhardt, H. 41:463
Vees, R., see Makris, J. 42:329
Vegard, L.: Die sonnenbelichteten Nordlichtstrahlen und die Konstitution der höheren Atmosphärenschichten 6:42
Vegard, L.: Bemerkungen zu der Erwiderung von Störmer 7:196
Veis, G., see Makris, J., et al. 39:929
Veitch, R.J., see Schmidbauer, E. 48:148
Vening Meinesz, F.A.: Die Schwerkraft auf dem Meere 9:75
Venske, O.: Die innere Genauigkeit von Inklinationsmessungen mit dem Erdinduktor 6:248
Verhoef, J., see Collette, B.J., et al. 47:91
Verigin, M.I., see Richter, A.K., et al. 50:101
Verma, R.K., see Subrahmanyam, C. 49:101
Vermeulen, J.M., Doornbos, D.J.: Mantle Heterogeneity and Mislocation Patterns for Seismic Networks 43:545
Verö, J.: Über einige Ergebnisse des Erdstrom-Observatoriums bei Nagycenk in Ungarn 24:307
Verö, J., see Ádám, A., et al. 50:37
Vetter, U., Meissner, R.: Überprüfung der Isostasie durch tiefenseismische Sondierungen (Brief an den Herausgeber) 36:225
Vetter, U.R.: Stress and Viscosity in the Asthenosphere 44:231
Vetter, U.R., see Meissner, R.O. 45:147
Vích, R.: Bilateral Deconvolution 39:557
Vích, R., see Plešinger, A. 38:543
Vích, R., see Neugebauer, H.J., et al. 39:563
Vigneresse, J.L.: Linear Inverse Problem in Gravity Profile Interpretation 43:193
Vigneresse, J.L.: Damped and Constrained Least Squares Method with Application to Gravity Interpretation 45:17
Vincenz, S.A., Steinhauser, P., Dasgupta, S.N.: Paleomagnetism of Upper Cretaceous Ignimbrites of Jamaica 39:727
Vincenz, S.A., Steinhauser, P., Dasgupta, S.N.: Errata zu: Paleomagnetism of Upper Cretaceous Ignimbrites on Jamaica 39:1067
Visser, S.W.: Der Zusammenhang zwischen Bodenunruhe und Zyklonen 16:329
Vlaar, N.J.: On the Excitation of the Earth's Seismic Normal Modes 43:502
Voelker, H.: Beobachtungen von pt's auf einer Stationskette von Nordskandinavien bis Deutschland 32:434
Voelker, H., see Björnsson, A., et al. 37:1031
Voelker, H., see Wedeken, U., et al. 46:249
Vogel, A.: Laufzeitanomalien von am äußeren Erdkern reflektierten Erdbebenwellen und deren Korrelation zum Schwerkraft- und Nicht-Dipol-Magnetfeld der Erde 26:273
Vogel, A., see Hirschleber, H.B., et al. 41:135
Vogel, R.: Über die Struktur des meteorischen Nickeleisens und ihre Bedeutung für die Bildung der Meteorite 1:273
Voges, W., see Rosenbauer, H., et al. 42:561
Vogler, G.: Die Grenzen der Anwendung von Erdungsmessern für Aufgaben in der angewandten Geophysik 24:184
Vogler, G.: Ursachen emanometrischer Anomalien 26:57
Vogt, J., see Procházková, D., et al. 46:343
Vogt, P.R., Johnson, G.L., Kristjansson, L.: Morphology and Magnetic Anomalies North of Iceland 47:67
Vogt, W.: Radiologische Untersuchungen im Radiumbad Brambach 11:29
Voight, B., Simon, R., Thorsteinsson, T., Pálmason, G., Taylor, C., Seret Opzoomer-Talma, S.H., Haimson, B.C.: Rock Stress in an Icelandic Thermal Area, with Implications on Stresses in the Oceanic Lithosphere 47:176
Voigt, G.-H.: A Three Dimensional, Analytical Magnetospheric Model with Defined Magnetopause 38:319
Voigt, G.-H.: Calculation of the Shape and Position of the Last Closed Field Line Boundary and the Coordinates of the Magnetopause Neutral Points in a Theoretical Magnetospheric Field Model 40:213
Voit, H.: Über die Erzielung möglichst großer innerer und absoluter Genauigkeit bei der Analyse von Horizontalpendel- und Gravimeterbeobachtungen 16:16
Volland, H.: Modelle erdmagnetisch induzierter Ströme im inhomogenen Erdinnern 24:222
Volland, H.: The Flat Earth Approximation of the Theory of LF-Propagation 32:127
Volland, H., Bird, M.K., Levy, G.S., Stelzried, C.T., Seidel, B.L.: Helios-1 Faraday Rotation Experiment: Results and Interpretations of the Solar Occultations in 1975 42:659
Vollstädt, H., see Stiller, H. 31:212
Vollstädt, H., see Kirsten, G., et al. 33:182
Voppel, D.: Ein Spulentheodolit zur Messung der erdmagnetischen Komponenten mit dem Protonenmagnetometer 35:151
Voppel, D., Rudloff, R.: On the Evolution of the Reykjanes Ridge South of 60° N Between 40 and 12 Million Years Before Present 47:61
Voss, K.: Über die Gestalt und das Schwerefeld der Erde. II 31:313
Voss, K.: Über die Gestalt und das Schwerefeld der Erde. III 32:216
Voss, K., see Macke, W., et al. 30:21
Vozoff, K., see Quon, C., et al. 46:291
Vrkljan, V.S.: Zur Frage des neuen Hagenschen Beweises für die Drehung der Erde 7:360

Waage, H.L., Storetvedt, K.M.: The Devonian Geomagnetic Axis Relative to the Orcadian Basin, N. Scotland 39:937
Wachholz, H., Müller, G.: Über einen Zusammenhang von Bruchfestigkeit und Schallgeschwindigkeit bei gefrorenen Erdschichten im Hinblick auf den Gefrierschachtbau 30:127
Wagenitz, V., see Thyssen, F. 39:411
Wagner, A.: Zur Theorie der Häufigkeitsverteilung von Fehlern in der Ebene mit besonderer Berücksichtigung der Windvektoren 5:366
Wagner, A.: Zur Frage der Schwankungen der allgemeinen Zirkulation 5:399
Wagner, A.: Über die Feinstruktur des Temperaturgradienten längs Berghängen 6:310
Wagner, C., see Stiller, H. 35:97
Wagner, C.-U., see Cumme, G., et al. 36:57
Wagner, F.Ch.: Die Stabilität einiger Serpentinitproben aus Granulitgebirge von Sachsen 33:262
Wagner, F.Ch., see Stiller, H., et al. 27:89
Wagner, F.Ch., see Frölich, F., et al. 27:136
Wagner, F.Ch., see Lucke, O. 27:257
Wagner, J.J.: Rockmagnetic Studies on Ophiolites from Montgenevre (French-Italian Alps) 37:589
Wahlström, R., see Shapira, A., et al. 46:123, 49:243
Wallner, Á., see Ádám, A., et al. 50:37
Wanach, B.: Ein Beitrag zur Frage der Kontinentalverschiebung 2:161
Wanach, B.: Eine fortschreitende Lagenänderung der Erdachse 3:102
Wang, C., Cleary, J.R., Anderssen, R.S.: The Effect of Earth Structure on Radial Oscillations 45:129
Waniek, L.: Model Studies of Wave Propagation in Low Velocity Layers with Sharp Boundaries 38:647
Waniek, L., Schenk, V.: Modellseismischer Beitrag zur Deutung des Krustenaufbaues in der bayerischen Molasse 32:482
Waniek, L., see Kozák, J. 36:175
Waniek, L., see Behrens, J. 38:1
Waniek, L., see Behrens, J., et al. 38:579
Wanke, R., see Schuch, M. 33:94, 34:599
Watkins†, N.D., see Kristjansson, L., et al. 47:31
Weaver, J.T.: On the Separation of Local Geomagnetic Fields 30:29

Wedeken, U., Hillebrand, O., Krenzien, E., Ranta, A., Ranta, H., Voelker, H.: Cosmic Noise Absorption Events and Magnetic Pulsation Activity During Substorms 46:249
Wegener, A.: Die äußere Hörbarkeitszone 1:297
Wegener, A.: Bemerkungen zu H. von Iherings Kritik der Theorien der Kontinentverschiebungen und der Polwanderungen 4:46
Wegener, A.: The Origin of Continents and Oceans (H. Cloos) 35:556
Wegener, K.: Geophysikalische Forschungen der beiden letzten Jahre in den Polargebieten 8:419
Wegener, K.: Der vergessene Krakatau 11:127
Wegener, K.: Die Ozonfrage 12:124
Wegener, K.: Die Temperatur am Boden des grönländischen Inlandeises 12:166
Wegener, K.: Die absolute Schweremessung 13:68
Wegener, K.: Die Erhaltung der Gebirge 14:270
Wegener, K.: Bemerkungen zu dem vertikalen Gradienten der Schwere 15:247
Wegener, K.: Die Laufgeschwindigkeit c der Longitudinalwellen als Funktion der Temperatur 15:390
Wegener, K.: Die hydrostatische Reduktion der Schwerebeobachtungen 16:33
Wegener, K.: Antwort auf die Bemerkungen Herrn Kohlschütters zu der Abhandlung: „Die hydrostatische Reduktion der Schwerebeobachtungen" 16:244
Weger, N., Slutzki, E.: Das statistische Experiment als Untersuchungsmethode 11:394
Wehner, H.: Erdmagnetische Säkularvariation und die Orientation alter Kultbauwerke 4:18
Weichert, D.H.: Short-Period Spectral Discriminant for Earthquake-Explosion Differentiation (Brief an den Herausgeber) 37:147
Weickmann, L.: Die dominierende Luftdruckwelle des strengen Winters 1928/29 6:291
Weidelt, P.: Zur Tiefenlage und Größe des Dichtemaximums der induzierten Erdströme 35:191
Weidelt, P.: The Electromagnetic Induction in Two Thin Half-Sheets 37:649
Weidelt, P.: The Inverse Problem of Geomagnetic Induction 38:257
Weidelt, P.: Electromagnetic Induction in Three-Dimensional Structures 41:85
Weidelt, P.: Extremal Models for Electromagnetic Induction in Two-Dimensional Perfect Conductors 49:217
Weigel, W.: Crustal Structure Under the Ionian Sea 40:137
Weigel, W., see Behrens, J. 33:131
Weigel, W., see Aric, K., et al. 34:531
Weigel, W., see RRISP Working Group 47:228
Weigel, W., see Goldflam, P., et al. 47:250
Weinberg, B.: Die Größenordnung der lokalen magnetischen Variationen und die Methodologie der magnetischen Aufnahmen 5:321
Weinberg, K.: Beitrag zur Methodologie der Rekonstruktion der Deklinationsverteilung für ältere Zeiten 7:192
Weinrebe, W., see Hirschleber, H.B., et al. 41:135
Weiss, W., see Kramm, R., et al. 38:953
Wellmann, H.: Über die Untersuchung der Perioden der Nachläuferwellen in Fernbebenregistrierungen auf Grund Hamburger und geeigneter Beobachtungen 1:74
Wenzel, F., Zürn, W.: Numerical Investigation of the Spectral Resolving Power of Burg's Maximum Entropy Method 48:121
Werner, D., Parini, M.: The Geothermal Anomaly of Landau/Pfalz: An Attempt of Interpretation 48:28
Werner, F.: Die Temperaturkompensation bei Torsions-Magnetometern 19:8
Werner, K.: Verhalten der Luftdämpfung und Bestimmung des Dämpfungsgrades bei Seismographen und Erschütterungsmessern 11:288
Westkämper, W., see Kohnen, H. 44:545
Westphal, M.: Comments on: Postulated Rotation of Corsica Not Confirmed by New Palaeomagnetic Data by K.M. Storetvedt and N. Petersen, J. Geophys. 42, 59–71, 1976 42:399
Westphal, M., see Najid, D., et al. 49:149
Wetzel, W., see Balensiefer, E., et al. 15:337
Weyres, T., see Schnippenköter, J. 13:201
Whipple: The action of wind on seismographs 4:417
White, A., see Chamalaun, F.H. 41:537
Wibberenz, G.: Interplanetary Magnetic Fields and the Propagation of Cosmic Rays 40:667
Wibberenz, G., see Hasselmann, K. 34:353
Wibberenz, G., see Kunow, H., et al. 42:615
Widdel, H.U., Rose, G., Borchers, R.: Payload B III – an Instrument Package for the Measurement of Conductivity, Concentration and Mobility of Positive and Negative Ions in the Mesosphere 44:179
Widdel, H.U., see Rose, G. 35:211, 44:15, 65
Widmann, R., see Blum, R., et al. 43:561
Wiechert, E.: Seismische Untersuchungen 1:14
Wiechert, E.: Entfernungsberechnungen von Orten auf der Erde bei kleineren Abständen 1:177
Wiechert†, E.: Seismische Beobachtungen von Steinbruchsprengungen 5:159
Wieder, H., see Krankowsky, D., et al. 40:601
Wiegert, R., see Seibold, E. 26:87
Wielandt, E.: Ein einfacher elektronischer Entzerrer für Seismometer 36:763
Wielandt, E.: Noise in Electronic Seismograph Systems 39:597
Wielandt, E.: Astatic Vertical Pendulum Supported by a Leaf Spring 41:545
Wielandt, E., see Plešinger, A. 40:131
Wienert, K.: Friedrich Burmeister zum 75. Geburtstag 31:227
Wienert, K.: In memoriam Friedrich Burmeister 36:233
Wiese, H.: Tiefentellurik 21:74
Wiese, H.: Über erdmagnetische Absolut- und Vergleichsmessungen 23:63
Wigand, A.: Die Feinstruktur des luftelektrischen Feldes 5:319
Wigand, A., Schubert, J., Frankenberger, E.: Ein neues Verfahren der luftelektrischen Raumladungsmessung 6:458
Wilckens, F.: Die Grundlage der Eigenpotentialmethode 21:25
Wilckens, F.: Elektrokinetische Grenzflächenerscheinungen im Bereich oberflächennaher Erdschichten 23:46
Wilhelm, H.: Das zeitliche Verhalten des erdmagnetischen Quadrupolfeldes von 1835 bis 1965 35:517
Wilhelm, H.: Eine säkulare Schwingung des erdmagnetischen Quadrupolfeldes als Ursache einer Änderung der Erdrotation 36:697
Wilhelm, H.: Upper Mantle Structure and Global Earth Tides 44:435
Wilhelm, H., see Flach, D., et al. 37:993, 1005
Wilhelm, K.: Remote Sensing Experiment for Magnetospheric Electric Fields Parallel to the Magnetic Field 43:731
Wilhelm, K.: Auroral Particle Fluxes in the Ionosphere 46:151
Wilhelm, K.: On the Relation Between Magnetic Field-Aligned Electrostatic Electron Acceleration and the Resulting Auroral Energy Flux 49:69
Wilhelm, K., Klöcker, N., Theile, B., Ott, W., Spenner, K., Grabowski, R., Wolf, H., Stüdemann, W., Dehmel, G., Fischer H.M., Schmidtke, G.L., Baumjohann, W., Riedler, W., Urban, A.: Observation of Field-Aligned Current Sheets Above Discrete Auroral Arcs 49:128
Wilhelm, K., see Baranskiy, L.N., et al. 48:1
Wilhelm, K., see Brüning, K., et al. 49:74
Wilhelm, K., see Urban, A., et al. 50:189
Wilip, J.: Emergenzwinkel, Unstetigkeitsflächen, Laufzeit 1:74
Wilip, J.: Eine Bemerkung zu W. Stekloff „Über die Herstellung des Netzes seismischer Stationen von USSR..." 2:159
Wilip, J.: Experimentelle Prüfung von Verspätungsfragen bei der galvanometrischen Registriermethode 7:219
Wilken, B., see Keppler, E., et al. 42:633

Williams, D.J., see Fritz, T.A. 41:551
Williams, D.J., see Keppler, E., et al. 42:633
Willis, J.R., see Sabina, F.J. 43:401
Winckler, J.R.: Investigation of Electron Dynamics in the Magnetosphere with Electron Beams Injected from Sounding Rockets 40:729
Winterer, G., Jünger, E.: Messung der Horizontalkomponente der elektrostatischen Feldstärke in der niederen Atmosphäre (Briefe an den Herausgeber) 38:1049
Wirtitsch see Knoechel, H., et al. 17:57
Witt, C. de, Hieblot, J., Lebeau, A.: Geophysics: The Earth's Environment. (G. Hartmann) 30:155
Witt, G., see Henriksen, K., et al. 44:401
Witte, H.: Laufzeitkurve und Ausbreitung der elastischen Raumwellen im Erdinnern 8:453
Witte, H., see Ludewig, P. 1:242
Witte, H., see Hummel, J.N. 7:175
Witte, M., see Kunow, H., et al. 42:615
Wöbking, H., see Bitterlich, W. 36:607, 743
Wohlenberg, J., see Bonjer, K.-P., et al. 36:287
Wohlenberg, J., see Makris, J., et al. 36:387
Wohlenberg, J., see Knödel, K., et al. 45:199
Wölcken, K.: Bericht über den jetzigen Stand der Untersuchung über die durchdringende Höhenstrahlung 5:151
Wölcken, K.: Messungen der Ultrastrahlung (durchdringende Höhenstrahlung) zwischen 57 und 67° nördl. Breite 7:267
Wölcken, K.: Schalluntersuchungen im Polargebiet 10:222
Wölcken, K.: Vergleich zwischen der Intensität der kosmischen Ultrastrahlung über Grönland und über Deutschland 10:300
Wölcken, K., see Brockamp, B. 5:163
Wolf, H.: Ausgleichungsrechnung nach der Methode der kleinsten Quadrate. (L. Hasse) 35:215
Wolf, H., see Wilhelm, K., et al. 49:128
Wooster, W.S., Lee, A.J., Dietrich, G.: Redefinition of Salinity 35:611
Wörner, H.: Zur Frage der Automatisierbarkeit der Bevölkerungsangaben durch Verwendung von Strahlungsgrößen. (M. Diem) 34:633
Worzyk, P.: Schlumberger-Messungen mit niederfrequentem Wechselstrom über Lockersedimenten mit tonigen Liegendschichten 39:461
Worzyk, P., see Blohm, E.K., et al. 43:665
Worzyk, P., see Mundry, E. 45:329
Wulf-Mathies, C., see Roemer, M. 40:625
Wüst, G.: Die Ausbreitung des antarktischen Bodenwassers im Atlantischen und Indischen Ozean 11:40
Wüst, G.: Die Stratosphäre des Atlantischen Ozeans 12:287
Wustelt, J.: Die Temperaturschwankungen in der Klimareihe von Jena und ihre Beziehungen zur Witterungskunde und zur Klimageschichte Europas. (O. Baumgartner) 29:146
Wyss, M.: Hawaiian Rifts and Recent Icelandic Volcanism: Expressions of Plume Generated Radial Stress Fields 47:19

Yamamoto, R.: Sur les Bases Nouvelles de la Sismophysique et sur la Constitution Interne du Globe Terrestre 1:214
Yaroshevskaya, G.A., see Zverev, S.M., et al. 47:191, 202
Yedlin, M., see Crampin, S. 49:43
Yogi, T., see Knopoff, L., et al. 46:89
Young, D., Zürn, W.: Tidal Triggering of Earthquakes in the Swabian Jura? 45:171

Zahn, U. von, see Friedrich, V.H., et al. 44:139
Zahradník, J., see Červený, V. 38:499
Zanche, V. De, see Channell, J.T., et al. 45:29
Zech, G.: Veränderungen der magnetischen Eigenschaften von Basaltsäulen seit dem Tertiär 34:53
Zehle, H., see Rössler, E. 30:112
Zeller, W., see Koch, H.W. 12:220
Zenker, H.: Untersuchungen über Klima und Bioklima des Tals von Bad Berka. (P. Zedler) 33:213
Zimmermann, G.J., see Markert, H., et al. 40:303
Zimmermann, J., see Makris, J., et al. 36:299, 387, 39:279
Zink, S.M., see Rosenbauer, H., et al. 42:561
Zirkler, J.: Solare Korpuskularstrahlung – weiche Komponente der Höhenstrahlung 18:126
Zoth, G., see Haenel, R. 39:425
Zuidam, Van: Orbital Photography As Applied to Natural Resources Survey. (O. Walk) 38:192
Zürn, V.: Statistische Untersuchungen über langperiodische Pulsationen des erdmagnetischen Feldes 32:448
Zürn, W., Knopoff, L., Rydelek, P.A.: High Precision Measurement of the Frequency of Mode $_0S_0$ 48:158
Zürn, W., Knopoff, L., Rydelek, P.A.: Correction to: High Precision Measurement of the Frequency of Mode $_0S_0$. J. Geophys. (1980) 48:158–160 49:249
Zürn, W., see Schick, R. 39:541
Zürn, W., see Neugebauer, H.J., et al. 39:563
Zürn, W., see Young, D. 45:171
Zürn, W., see Knopoff, L., et al. 46:89
Zürn, W., see Wenzel, F. 48:121
Zverev, S.M., Boldyrev, S.A., Bourmin, V.Yu., Mironova, V.I.: Weak Earthquakes in the Northern Part of the Rift Zone of Iceland 44:283
Zverev, S.M., Litvinenko, I.V., Pálmason, G., Yaroshevskaya, G.A., Osokin, N.N.: A Seismic Crustal Study of the Axial Rift Zone in Southwest Iceland 47:202
Zverev, S.M., Litvinenko, I.V., Pálmason, G., Yaroshevskaya, G.A., Osokin, N.N., Akhmetjev, M.A.: A Seismic Study of the Rift Zone in Northern Iceland 47:191
Zverev, S.M., see RRISP Working Group 47:228
Zygielbaum, A.I., see Edenhofer, P., et al. 42:673

J Geophys (1983) 53:127–130

Journal of Geophysics

Improvements to Layer Matrix Methods

R. Kind and R.I. Odom [1]
Seismologisches Zentralobservatorium, Krankenhausstrasse 1, 8520 Erlangen, Federal Republic of Germany

Abstract. The problem of numerical instabilities at high frequencies is solved for the case of a source of $P-SV$ waves buried in a layered halfspace. The solution is to compute the high frequency layer matrices by multiplication of low frequency layer matrices. It is only required to compute the problematic exponential terms for a small frequency increment. A normalization is applied. A new analytical solution of the layer matrix equation is also given. This solution separates completely the treatment of the layers below and above the source.

Key words. Haskell matrices – Delta matrices – Numerical instabilities – Theoretical seismograms.

Introduction

Haskell layer matrix methods for the propagation of elastic waves in layered media have a wide range of application. However, numerical instabilities are a problem at high frequencies for phase velocities smaller than layer velocities. This problem requires improvements. Another problem is the large amount of computer time required for these methods. The Haskell layer matrix methods are an essential part of the reflectivity method for the computation of theoretical seismograms. Fuchs (1968) and Fuchs and Müller (1971) have developed this method. Dunkin (1965) and Watson (1970) have contributed to improvements in accuracy and speed of the Haskell layer matrix methods. Kind (1978) has published a computer program which was faster than earlier versions. An error in that program for the case of transmission was corrected by Baumgardt (1980). Abo-Zena (1979) has reformulated the layer matrix multiplication, resulting in improved computational accuracy. Kennett and Kerry (1979) and Woodhouse (1981) have developed different formulations of the buried source problem. Besides the reflectivity method, layer matrix methods are also used in mode summation methods for the computation of theoretical seismograms (Harvey, 1981).

1 *Present address:* Department of Geological and Geophysical Sciences, Princeton University, Princeton, New Jersey 08540, USA
Offprint requests to: R. Kind

The Layered Halfspace with a Buried Source

We consider $P-SV$ plane wave propagation in a layered halfspace with a free surface. The source, represented by a discontinuity of the displacement-stress vector, is buried in the medium, and we are interested in the surface displacements. A layer n is bounded above by the interface $n-1$ and below by the interface n. The displacement-stress vector T_n of the interface n is related to T_{n-1}, the corresponding vector of the interface $n-1$, by the relation $T_n = B_n \cdot T_{n-1}$, where B_n is the Haskell layer matrix of layer n. The displacement-stress vectors are 4×1 matrices, and the Haskell matrices are 4×4 matrices. For a stack of layers the Haskell matrix is simply the product of the individual Haskell layer matrices. The displacement-stress vector is continuous at each interface, except at the source interface m, where we have $T_m^+ = T_m^- + S$. The plus or minus sign denotes location of T just below or above the interface m. S describes the displacement-stress vector of the source. This results in $T_k = B \cdot S + B \cdot T_m^-$, where k indicates the lowermost boundary, and B is the product of all Haskell matrices below the source. T_m^- can now be carried to the free surface, leading to $T_m^- = A \cdot T_0$, where A is the product of the Haskell layer matrices above the source, and $T_0 = (u, w, 0, 0)$ is the displacement-stress vector of the free surface with zero stress components, and the radial and vertical displacements u and w. Now we have

$$T_k = B \cdot (A \cdot T_0 + S). \tag{1}$$

This is the basic equation relating the displacement-stress vector at the free surface to that at the lowermost boundary and to that of the source. T must be expressed by the potential coefficients for up- and downgoing waves in the halfspace, because we want to set these coefficients for upgoing waves equal to zero. This means we want no source at infinity. We have $T_k = E_k \cdot K_k$, where K_k is the vector of the potential coefficients and E_k is a matrix relating these two vectors. The elements of E_k, of the Haskell matrices, and of the source vector S for some sources can be found in Harkrider (1964). Kind (1979) gave the elements of S for a dislocation source. For only downgoing waves we have $K = (K_1, K_1, K_2, K_2)$, where K_1 and K_2 are the potential coefficients for P and SV waves, respectively. Then

we may write

$$\begin{pmatrix} K_1 \\ K_1 \\ K_2 \\ K_2 \end{pmatrix} = E_k^{-1} \cdot B \cdot \begin{pmatrix} W \\ X \\ Y \\ Z \end{pmatrix} \tag{2}$$

and

$$\begin{pmatrix} W \\ X \\ Y \\ Z \end{pmatrix} = A \cdot \begin{pmatrix} u \\ w \\ 0 \\ 0 \end{pmatrix} + S. \tag{3}$$

First we solve (2) for W and X. In order to do that we multiply (2) with the matrix F, defined by

$$F = \begin{pmatrix} 1 & -1 & 0 & 0 \\ 0 & 0 & 1 & -1 \end{pmatrix}.$$

Multiplication with F means subtraction of row 2 from row 1, and of row 4 from row 3. Using $P = F \cdot E_k^{-1} \cdot B$, we obtain

$$\begin{pmatrix} 0 \\ 0 \end{pmatrix} = P \cdot \begin{pmatrix} W \\ X \\ Y \\ Z \end{pmatrix} \tag{4}$$

P is a two row, four column matrix. The solution of (4) for W and X is

$$\begin{aligned} &-(P_{11} \cdot P_{22} - P_{12} \cdot P_{21}) \cdot W \\ &\quad = Y(P_{13} \cdot P_{22} - P_{12} \cdot P_{23}) + Z(P_{14} \cdot P_{22} - P_{12} \cdot P_{24}) \\ &-(P_{11} \cdot P_{22} - P_{12} \cdot P_{21}) \cdot X \\ &\quad = Y(P_{11} \cdot P_{23} - P_{13} \cdot P_{21}) + Z(P_{11} \cdot P_{24} - P_{14} \cdot P_{21}). \end{aligned} \tag{5}$$

Now we recognize that the coefficients in (5) are subdeterminants of the P matrix (Dunkin, 1965). They form a delta matrix. A good explanation of delta matrices can be found in Zurmühl (1964). All possible 2×2 subdeterminants of the 2×4 P matrix form a 1×6 delta matrix R with the following convention for the indices:

$$R_{1t} = P \begin{pmatrix} 12 \\ lm \end{pmatrix} = P_{1l} \cdot P_{2m} - P_{1m} \cdot P_{2l}$$

where $t = 1, 2, 3, 4, 5, 6$ corresponds to the pair $lm = 12$, 13, 14, 23, 24, 34. With these definitions we obtain from (5)

$$\begin{aligned} R_{11} \cdot W &= R_{14} \cdot Y + R_{15} \cdot Z \\ -R_{11} \cdot X &= R_{12} \cdot Y + R_{13} \cdot Z. \end{aligned}$$

Rewriting this equation we obtain:

$$\begin{pmatrix} W \\ X \end{pmatrix} = \begin{pmatrix} C_{11} & C_{12} \\ C_{21} & C_{22} \end{pmatrix} \cdot \begin{pmatrix} Y \\ Z \end{pmatrix} = C \cdot \begin{pmatrix} Y \\ Z \end{pmatrix} \tag{6}$$

where the elements of C follow from the previous equation. The elements of the delta matrix R are also given by Harkrider (1970), for example. We have $R_{14} = R_{13}$, therefore $C_{22} = -C_{11}$. Since the delta matrix of a product matrix is equal to the product of the individual delta matrices, we can compute layer delta matrices and multiply them through the layers. This procedure is more stable numerically than the multiplication of Haskell matrices.

Now we need to solve Eq. (3). Rewriting (3) we have

$$\begin{aligned} \begin{pmatrix} W \\ X \end{pmatrix} - \begin{pmatrix} S_1 \\ S_2 \end{pmatrix} &= A_1 \begin{pmatrix} u \\ w \end{pmatrix} \\ \begin{pmatrix} Y \\ Z \end{pmatrix} - \begin{pmatrix} S_3 \\ S_4 \end{pmatrix} &= A_2 \begin{pmatrix} u \\ w \end{pmatrix} \end{aligned} \tag{7}$$

with the column vector $S = (S_1, S_2, S_3, S_4)^T$ and

$$A_1 = \begin{pmatrix} A_{11} & A_{12} \\ A_{21} & A_{22} \end{pmatrix}, \quad A_2 = \begin{pmatrix} A_{31} & A_{32} \\ A_{41} & A_{42} \end{pmatrix}.$$

From (6) and (7) we obtain

$$(C \cdot A_2 - A_1) \begin{pmatrix} u \\ w \end{pmatrix} = \begin{pmatrix} S_1 \\ S_2 \end{pmatrix} - C \begin{pmatrix} S_3 \\ S_4 \end{pmatrix}. \tag{8}$$

The solution of this equation leads directly to the desired surface displacements. Equation (8) is a new solution of Eq. (1), which separates the treatment of the layers below and above the source completely. The solution of (8) requires the computation of $\det(C \cdot A_2 - A_1)$. This determinant can be computed in two different ways. In the first way it may be obtained from the elements of C, A_2 and A_1. Secondly it may also be computed using delta matrices. Using the first method, the accuracy of (8) is not better than the accuracy of the solution by Kind (1978). The second method improves the accuracy considerably.

Computing the determinant in terms of delta matrices, we may define the 2×2 matrix

$$V \cdot A \cdot I = C \cdot A_2 - A_1 \tag{9}$$

with

$$V = \begin{pmatrix} -1 & 0 & C_{11} & C_{12} \\ 0 & -1 & C_{21} & C_{22} \end{pmatrix}.$$

A is still the Haskell product matrix of all layers above the source, and I is the two columns, four rows unit matrix, containing a one in the 11 and 22 element and zeros elsewhere. From (9) it follows that for the computation of $\det(C \cdot A_2 - A_1)$ we may multiply the reduced 5×1 delta matrix of I with the reduced 5×5 delta matrix of A for each layer above the source. Finally we must multiply the resulting 5×1 column vector with the 1×5 row vector of the reduced delta matrix derived from V. This procedure allows the direct computation of the desired determinant without using the squares of the elements of the Haskell matrix A. The solution of (8) still requires the computation of the first two rows of A. But there elements appear only linear in (8), no squares of these elements are present anymore.

Now we summarize what matrix multiplications are required for the solution of (8): Below the source we need the 1×5 row vector of the reduced product delta matrix to obtain C. Above the source we need the 5×1 column vector of the reduced product delta matrix to

compute the determinant in (8). And secondly we need above the source the 4×2 column vectors of the product Haskell matrix. The elements of this matrix are still in (8). Above the source appear the Haskell elements as quotients with the determinant. The appearance of these quotients in (8) is very important for the normalization. Without normalization the accuracy of the solution of (8) is much reduced. The normalization below the source is simple. Some care is needed above the source, because delta and Haskell matrix elements must be normalized there with the same constant. Above the source a normalization is only possible if the determinant is computed from delta matrices. The additional computation of the required Haskell matrix elements causes no problems.

The solution of Eq. (1) given by Harkrider (1964) did not use delta matrices and was therefore only good for fast phase velocities. Harkrider (1970) used delta matrices but the stability of his second solution was also by far not sufficient. Kind (1978) and Wang and Herrmann (1980) found another solution, which was more stable but still not satisfying. But the solution of (8) is much more stable in connection with the method described in the next section.

A Second Improvement of the Problem of Numerical Instabilities

The Haskell matrices contain exponential factors with the argument

$$P = \pm i\omega/c \cdot r \cdot d$$

with circular frequency ω, imaginary unit i, layer thickness d, phase velocity c and the vertical wavenumber $\omega/c \cdot r$, where $r^2 = c^2/v^2 - 1$. The P- or S-velocity in the layer is v. For a phase velocity larger than the layer velocity P is imaginary and the exponential factor is only a phase term, causing no numerical problems. For a phase velocity smaller than the layer velocity, r is imaginary and P is real. In this case the absolute value of P increases with frequency, layer thickness and inverse phase velocity. The elements of the Haskell matrices use linear combinations of the exponential functions with positive and negative arguments P. The accuracy limit of a digital computer is soon reached for increasing P, when $\exp(P)$ and $\exp(-P)$ are added. The use of delta matrices avoids unnecessary operations with these exponentials, but it is in principle no solution to the problem. We also have no fundamental solution, but we suggest the following method, which is a practical solution:

It is known that the numerical problems may be reduced by subdividing thick layers. That means we may replace a thick layer, which causes problems, by two or more thinner layers and multiply their layer matrices in order to obtain the layer matrix of the thick layer. This procedure reduces the numerical problems. The layer thickness in the layer matrix is only contained in the argument P of the exponential term, where it appears as a product with the frequency. Therefore, a high frequency can be treated in exactly the same manner as a large layer thickness. That means we may obtain the layer matrix for a high frequency by computing layer matrices for lower frequencies and by multiplication of these lower frequency matrices. The sum of the lower frequencies must be equal to the high frequency, exactly as in the case of layer thicknesses. As a consequence we only have to compute a layer matrix for the frequency increment $\Delta\omega$, and then obtain layer matrices for frequencies which are multiples of the frequency increment, by matrix multiplication. This method is applicable for cases where layer matrices for an equidistant set of frequencies are required. This is for example the case for the computation of theoretical seismograms with the reflectivity method. The computation time is not increased with this method, if the computer program is set up carefully, even for large numbers of frequencies.

Now a few more details of the computation of layer product matrices should be discussed. We have three independent variables, which lead in the computer program to three loops. These three variables are the slowness (or the wavenumber), frequency and the layer index. Keeping in mind the method for the solution of the numerical problems just described, we find the following order of the loops over the three variables practical. First we keep the slowness fixed (this is the outermost loop), then we keep the layer index fixed (middle loop), and compute the layer matrices for a set of frequencies (innermost loop). This has also the advantage that frequency independent terms may easily be kept outside the innermost loop. A computer program has been written using the described methods. The program is applying the matrix multiplication in the frequency loop (for slow phase velocities) and has about the same speed as the complex version of the program published by Kind (1976), but its accuracy is much better. A speed factor of about two may be gained by keeping the frequency independent terms outside the innermost frequency loop (not possible for slow phase velocities with matrix multiplication in the frequency loop). Almost another factor of two may be gained on some computers, when the complex operations in the innermost loop are replaced by real and imaginary operations. In test runs we have checked the accuracy of the new method for frequencies up to 100 Hz, layer thicknesses up to 30 km and phase velocities smaller than 0.5 km/s and found for all these cases no indication of numerical instabilities on our Hewlett Packard 1000 minicomputer. The computations were carried out in single precision mode, where the HP 1000 has six decimal digits accuracy. We have attempted to run Abo Zena's (1979) case with a method similar to his method on a HP 1000 with no success. For the method suggested in this paper, his case was no problem at all for the same machine. It should be mentioned that Abo Zena's method is also considerably slower, because it does more matrix multiplications.

Conclusions

The most important result of this research is a practical solution for the problem of numerical instabilities. The new method computes high frequency layer matrices by a multiplication of lower frequency matrices. This implies that the method is most useful if layer matrices of

a set of equidistant frequencies are required. The method also applies a normalization to avoid overflow. It was attempted to apply this method without the use of delta matrices. This attempt was not successful, so delta matrices must be used where the results can be expressed in terms of delta matrices. The above technique is not slower than earlier techniques and its accuracy is much better. It is a solution for practically all frequencies, layer thicknesses and phase velocities used in seismology. It is clearly more accurate and also faster than Abo Zena's (1979) method.

As a second result a new analytical solution was found for the case of a buried source in a layered medium. This solution improves the computational speed especially for deep sources. Applying these new methods and a number of other improvements in the programming technique, we developed new layer matrix programs, which are up to four times faster than our earlier versions and much more accurate.

Acknowledgements. This research was supported by the Deutsche Forschungsgemeinschaft and by the Alexander-von-Humboldt-Stiftung. We also wish to thank Gerhard Müller for reading the manuscript.

References

Abo-Zena, A.M.: Dispersion function computations for unlimited frequency values. Geophys. J.R. Astron. Soc. **58**, 91–105, 1979

Baumgart, D.R.: Errors in matrix element expressions for the reflectivity method. J. Geophys. **48**, 124–125, 1980

Dunkin, J.W.: Computation of modal solutions in layered media at high frequencies. Bull. Seismol. Soc. Am. **55** (2), 335–358, 1965

Fuchs, K.: The reflection of spherical waves from transition zones with arbitrary depth-dependent elastic moduli and density. J. Phys. Earth **16** (Special Issue), 27–41, 1968

Fuchs, K., Müller, G.: Computation of synthetic seismograms with the reflectivity method and comparison with observations. Geophys. J.R. Astron. Soc. **23**, 417–433, 1971

Harvey, D.J.: Seismogram synthesis using normal mode superprosition in the locked mode approximation. Geophys. J.R. Astron. Soc. **66**, 37–69, 1981

Harkrider, D.G.: Surface waves in multilayered elastic media, I. Rayleigh and Love waves from buried sources in a multilayered elastic halfspace. Bull. Seismol. Soc. Am. **54**, 627–679, 1964

Harkrider, D.G.: Surface waves in multilayered elastic media, Part II. Higher modes spectra and spectral ratios from point sources in plane layered earth models. Bull. Seismol. Soc. Am. **60**, 1937–1987, 1970

Kind, R.: Computation of reflection coefficients for layered media. J. Geophys. **42**, 191–200, 1976

Kind, R.: The reflectivity method for a buried source. J. Geophys. **44**, 603–612, 1978

Kind, R.: Extensions of the reflectivity method. J. Geophys. **45**, 373–380, 1979

Kennett, B.L.N., Kerry, N.J.: Seismic waves in a stratified halfspace. Geophys. J.R. Astron. So **57**, 557–583, 1979

Wang, C.Y., Herrmann, R.B.: A numerical study of *P*-, *SV*-, and *SH*-wave generation in plane layered media. Bull. Seismol. Soc. Am. **70**, 1015–1036, 1980

Watson, T.H.: Fast computation of Rayleigh wave dispersion in a layered halfspace. Bull. Seismol. Soc. Am. **60**, 161–166, 1970

Woodhouse, J.: Efficient and stable methods for performing seismic calculations in stratified media. In: Physics of the earth's interior (Proceedings International School of Physics, Enrico Fermi) Dziewonski and Boschi, eds.: pp. 127–151.North-Holland Publ. Co. 1981

Zurmühl, R.: Matrizen und ihre technischen Anwendungen. Berlin: Springer-Verlag 1964

Received March 25, 1983

Accepted June 20, 1983

J Geophys (1983) 53:131–140

Journal of Geophysics

Archaeomagnetic Investigations in Egypt: Inclination and Field Intensity Determinations

A.G. Hussain
Helwan Institute of Astronomy and Geophyscis, Helwan, Cairo, Egypt

Abstract. The intensities of the geomagnetic field (F_a), the inclinations (I) and, in one case, the declination (D) in Egypt at times between 3000 years B.C. and 1400 A.D. were determined from archaeomagnetic measurements and found to be: $F_a = 370$ to 430 μT at 3300–2900 B.C., $I = 65.1°$ to 61.2° at 1600–1450 B.C.; $F_a = 600$ μT with $I = 66.7°$ at 1400 B.C.; $F_a = 430$ μT with $I = 47.7°$ at 350–150 B.C.; $F_a = 580$ μT with $I = 45°$ at 100–50 B.C.; $F_a = 564$ μT with $I = 32.6$ and $D = -3°$ around 150 A.D.; $F_a = 372$ μT at 210 A.D.; $F_a = 540$ μT with $I = 52°$ at 1173 A.D. and $F_a = 470$ μT with $I = 54.9$ at 1450 A.D.

In order to have data and hence curves suitable for correlation with the data measured for Egypt, all the archaemagnetic data (F_a, D and I) measured from samples in an area limited by 3° East and West and 30° North of Egypt have been reduced to an Egyptian middle latitude and longitude (28.0 °W; 30.6 °E). These reduced data are in agreement with the results of this paper and with the direct observations of the geomagnetic field in Egypt during the 19th and 20th centuries.

Key words: Egypt – Archaeomagnetism – Secular variation

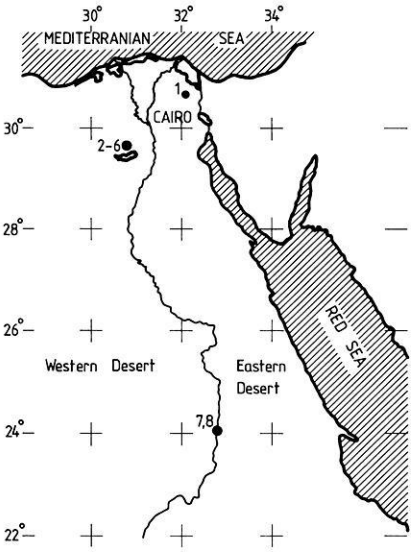

Fig. 1. A sketch map of Egypt showing the sampling sites

Introduction

Archaemagnetic data are necessary for understanding the secular variation of the geomagnetic field and could be used for evaluating different secular variation models. They also have several archaelogical applications including the possibility for use as a dating technique (Aitken, 1974).

The conditions for the study of the secular variation of the geomagnetic field from archaeological samples are better in Egypt than elsewhere, since the historical archaeological record from pre-historic through Pharaonic, Greco-Roman and Islamic ages is well preserved due to a favorable climate and well determined ages due to the tremendous works of the institutions of Egyptology all over the world. Only few archaeomagnetic studies, however, have been done in Egypt (Athavale, 1969; Games, 1980).

For this study samples were collected from Monshaat Abu Omar (3100–2990 B.C.), Madi (1800–1500 B.C. and 250–100 B.C.), Kiman Faris (1400 B.C. and 150 B.C.), Kom Oushim (150 A.C.) and Simon Bin Hadra and Matta Monastries (1200–1400 A.C.). Figure 1 is a sketch map showing these localities (for more details see Tables 1–4).

Present address: Institut für Allgemeine und Angewandte Geophysik, Theresienstr. 41-IV, 8000 München 2

Experimental Procedure and Data Reduction

Palaeointensity

The palaeointensity measurements are often made on homogeneously burnt ceramics or bricks (e.g. Aitken, 1974). Recently Games (1980) determined the palaeointensity from fired materials and has also developed a method for determination of the ancient geomagnetic field from air dried bricks with applications to samples from Egypt. He claimed that his method reached the same results as from fired materials. For the present paper we collected ceramic and brick samples from archaeologically well dated areas. Most of the ceramic samples are from thick walls of wheat containers and oven plates with thicknesses more than one inch. Several samples were cored from each sherd or brick and cast in plaster of Paris if necessary. The cylindrically shaped samples have a typical diameter of 2.5 cm, thicknesses of 0.8–2.45 cm and weights of 5–17.8 grams. A coordinate system was set up on each sherd or brick so that all samples from a sherd or a brick could be oriented relative to one another to within less than ±2°. This provides a mean

Table 1. The palaeointensity of the geomagnetic field in Egypt

Site	Location		Sample Nr.	Age years	Temp. interval °C	n	r^2	F_a in 10^{-1} mT	F_a	F_a/F_p	VDM in 10^{22} A m^2
Monshaat Abu Omar	30.8°N 32.0°E	ceramic	147-4/2	3100 B.C.	150–500	10	0.93	0.424	0.43	1.02	10.0
		ceramic	147-4/2	3100 B.C.	0–500	10	0.92	0.424			
		ceramics	147-4/3	3100 B.C.	0–500	10	0.92	0.456			
		ceramics	298/2	3300 B.C.	0–550	11	0.94	0.448	0.46	1.08	10.54
		ceramics	298/3	3300 B.C.	0–550	11	0.98	0.472			
		ceramics	127-10/1	3000–3100 B.C.	150–500	8	0.99	0.345	0.37	0.87	8.29
		ceramics	127-10/2	3000–3100 B.C.	150–500	8	0.99	0.396			
		ceramics	642/1	3300–2900 B.C.	250–550	6	0.98	0.376	0.38	0.88	8.51
		ceramics	642/2	3300–2900 B.C.	200–550	7	0.98	0.375			
Kiman Faris, Fayoum	29.5°N 30.6°E	ceramics	KF/3/Sh	1400–1350 B.C.	50–550	11	0.99	0.584	0.60	1.41	10.2
		ceramics	KF/2/Sh	1400–1350 B.C.	0–550	12	1.0	0.584			
		ceramics	KF/5/1	1400–1350 B.C.	0–550	12	0.97	0.632			
		bricks	KF/1/2-1	100–50 B.C.	0–550	11	0.99	0.608			
		bricks	KF/1/2-4	100–50 B.C.	0–550	12	1.0	0.576			
		bricks	KF2/3/2-2	100–50 B.C.	100–550	10	0.99	0.552	0.58	1.36	11.45
		bricks	KF2/3/2-3	100–50 B.C.	0–550	12	0.99	0.592			
		ceramics	KF/3/Sh	1400–1350 B.C.	50–550	11	0.99	0.584	0.60	1.41	10.2
		ceramics	KF/2/Sh	1400–1350 B.C.	0–550	12	1.0	0.584			
		ceramics	KF/5/1	1400–1350 B.C.	0–550	12	0.97	0.632			
		bricks	KF/1/2-1	100–50 B.C.	0–550	11	0.99	0.608			
		bricks	KF/1/2-4	100–50 B.C.	0–550	12	1.0	0.576			
		bricks	KF2/3/2-2	100–50 B.C.	100–550	10	0.99	0.552	0.58	1.36	11.45
		bricks	KF2/3/2-3	100–50 B.C.	0–550	12	0.99	0.592			
		bricks	KF5/3/2	100–50 B.C.	0–550	12	0.99	0.576			
		bricks	KF3/4/5	350–150 B.C.	350–550	5	0.95	0.496			
		ceramics	KF3/7/1	350–150 B.C.	200–550	8	0.97	0.400	0.43	1.01	8.11
		ceramics	KF3/7/2	350–150 B.C.	200–550	8	0.95	0.408			
Kom Oushim Fayoum	29.54°N 30.6°E	bricks	KO5/3/2	128–159 A.D.	50–550	11	0.99	0.536	0.52	1.21	11.55
		bricks	KO5/3/7	128–159 A.D.	150–550	10	0.99	0.515			
		bricks	KO7/5/1	117 A.D.	0–550	12	0.98	0.646	0.646	1.5	13.86
		bricks*	KO7/10/2	210 A.D.	450–550	3	0.90	0.372	0.372		8.53
		ceramics	KO8/2/1	147–170 A.D.	0–550	12	0.97	0.520	0.504	1.18	
		ceramics	KO8/2/4	147–170 A.D.	250–550	7	0.98	0.488			
		bricks	KO6/7/1	117–200 A.D.	200–550	8	0.98	0.589			
		bricks	KO6/7/6	117–200 A.D.	200–550	8	0.97	0.612	0.608	1.40	10.4
		bricks	KO6/7/7	117–200 A.D.	150–550	8	0.98	0.623			
		ceramics	KO8/1/1	147–170 A.D.	100–550	10	0.99	0.549	0.562	1.31	12.7
		ceramics	KO8/1/2	147–170 A.D.	150–550	9	0.99	0.576			
Anba Simon Bin Hadra Monastry	24.0°N 32.8°E	bricks	Had 1/1	1173 A.D.	0–600	13	0.97	0.504	0.54	1.26	10.2
		bricks	Had 1/3	1173 A.D.	0–550	11	0.98	0.544			
		bricks	Had 2/1	1173 A.D.	0–600	12	0.99	0.528			
		bricks	Had 2/2	1173 A.D.	100–500	9	0.98	0.542			
		bricks	Had 3/2	1173 A.D.	100–550	10	0.96	0.512			
		bricks	Had 3/4	1173 A.D.	0–600	11	0.99	0.563			
		ceramics	Had 4/2	1173 A.D.	100–550	10	0.97	0.536			
		ceramics	Had 4/6	1173 A.D.	100–550	10	0.99	0.568			
Anba Matta El-Miskin Monastry	24.0°N 32.8°E	ceramics*	Mat 1/1	ca. 1450 A.D.	150–575	9	0.97	0.616	0.61	1.42	10.4
		ceramics*	Mat 1/6	ca. 1450 A.D.	100–450	8	0.99	0.599			
		bricks	Mat 2/1	ca. 1450 A.D.	150–600	7	0.97	0.384			
		bricks	Mat 2/3	ca. 1450 A.D.	200–550	8	0.98	0.446			
		bricks	Mat 3/1	ca. 1450 A.D.	0–600	13	0.98	0.472			
		bricks*	Mat 3/4	ca. 1450 A.D.	150–550	9	0.99	0.575			
		bricks	Mat 4/2	ca. 1450 A.D.	150–550	9	0.98	0.434	0.47	1.10	9.6
		bricks	Mat 4/3	ca. 1450 A.D.	100–600	10	0.97	0.512			
		bricks	Mat 5/1	ca. 1450 A.D.	150–600	11	0.94	0.528			
		bricks	Mat 5/6	ca. 1450 A.D.	0–600	13	0.94	0.536			
		bricks*	Mat 5/7	ca. 1450 A.D.	200–550	8	0.97	0.616			

n = Number of data used for NRM versus PTRM plots; r = Standard deviation; F_a = Ancient field intensity; F_p = Present field ($= 0.427 \times 10^{-1}$ mT); VDM = Virtual dipole moment; * = The result is not consistent

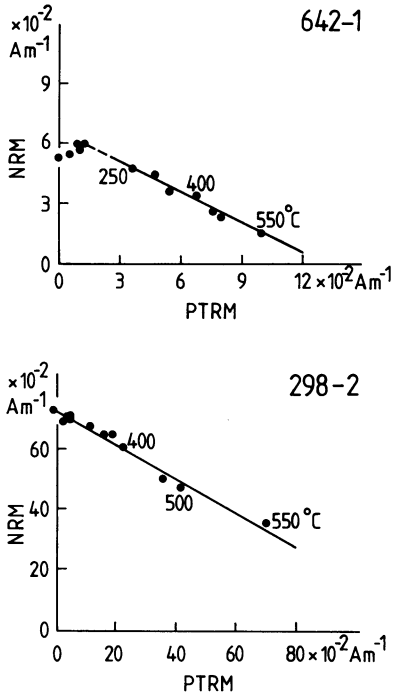

Fig. 2. NRM versus PTRM plots for two samples from Monshaat Abu Omar (3300–2900 B.C.). *Full line*: least square fit

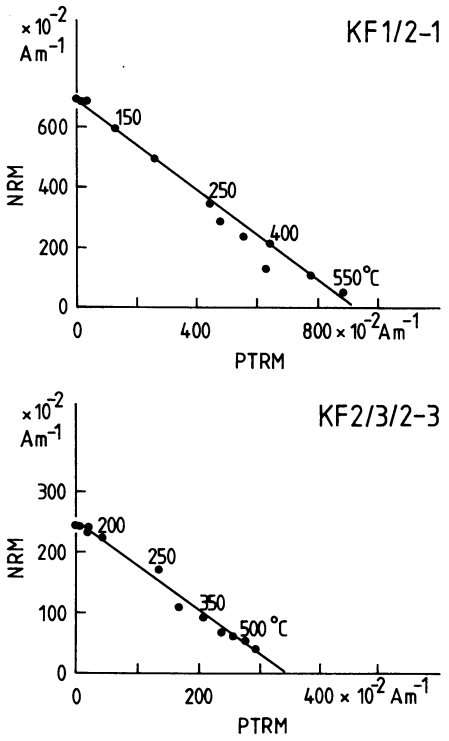

Fig. 3. NRM versus PTRM plots for two samples from Kiman Faris. *Full line*: least square fit

for checking the directional consistency of magnetization for samples from the same sherd or from the same brick. A double heating palaeointensity experiment (Thellier and Thellier, 1959) is used: A coordinate system is given to the sample. The sample is heated to a temperature I in a Schonstedt non-magnetic furnace and held at that temperature for 30 min. The sample is then shifted within few seconds to a cooling chamber with laboratory field F_{lab} of known strength and direction exactly parallel to one of the coordinates of the sample (e.g. Z-axis). After cooling to room temperature within 30–45 min while holding the sample in F_{lab} the magnetization is then measured. This magnetizations:

$J+(T)=J_{NRM}(T)+J_{PTRM}(T, T_0)$;
where T: maximum heating temperature
and T_0: room temperature.

The sample is then reheated to T and cooled in F_{lab} but with the direction of the field reversed by 180°, while the sample direction remains constant. The magnetization is again measured and then:

$J-(T)=J_{NRM}(T)-J_{PTRM}(T, T_0)$.

Vector addition and subtraction of the two measurements at the same T yield the natural remanent magnetization NRM(T) remaining after heating to T and the partial thermoremanent magnetization PTRM(T, T_0) gained by cooling from T to room temperature T_0 in the presence of F_{lab}. All heating is done in air. If NRM is plotted against PTRM (each point corresponding to a particular temperature), the result is a linear relationship (Figs. 2 to 6). The palaeointensity F_a is given by:

$F_a=-b\,F_{lab}$;
where b is the (negative) slope of the straight line.

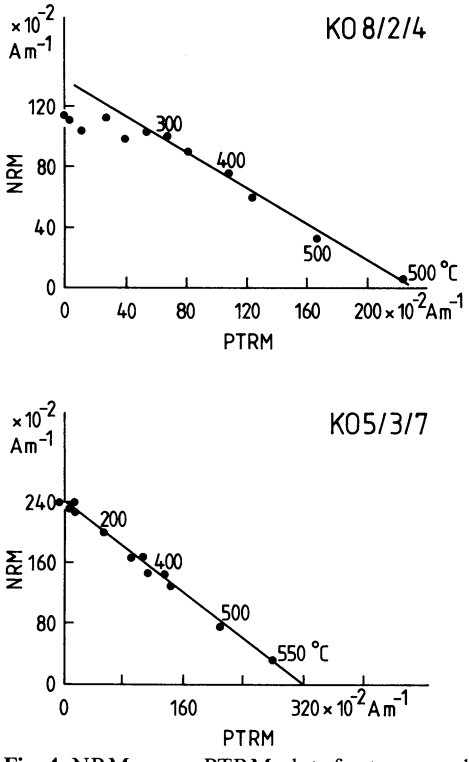

Fig. 4. NRM versus PTRM plots for two samples from Kom Oushim. *Full line*: least square fit

$F_{lab}=0.8\times10^3$ A m^{-1} has been used throughout the experiments. The samples were generally heated in successive steps of 50 °C up to 550–650 °C. Most of the NRM-PTRM plots were linear over a large part of the entire temperature range used, mainly between 150 and 550 °C. Possible causes

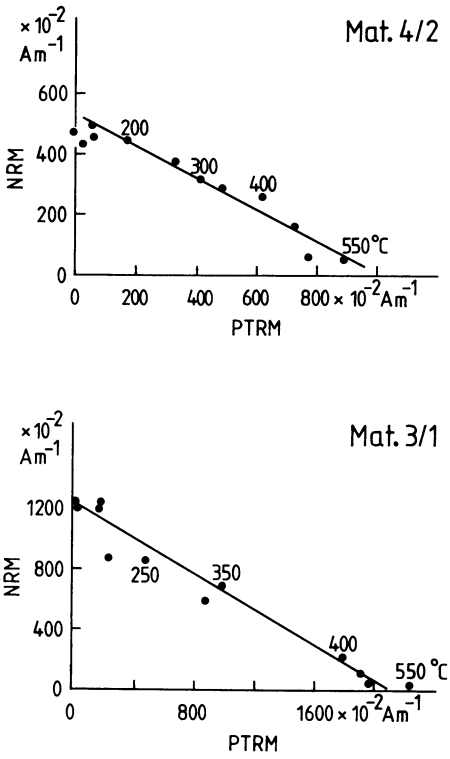

Fig. 5. NRM versus PTRM plots for two samples from Matta El Meskin Monastry. *Full line*: least square fit

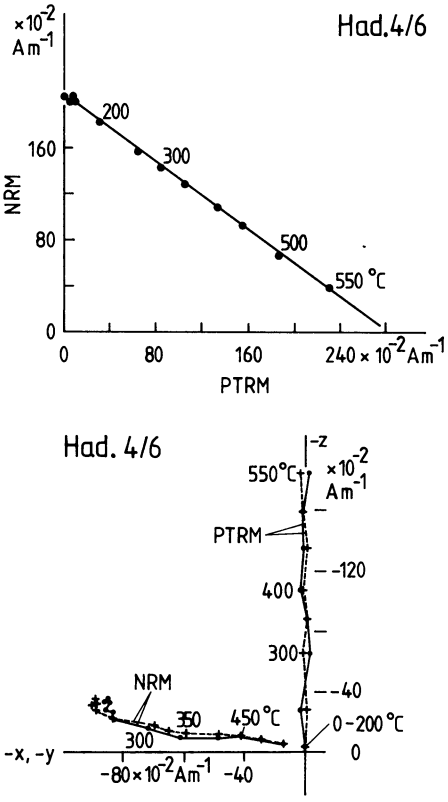

Fig. 6. *Upper part*: An example for NRM versus PTRM plots for a sample from Simon Bin Hadra Monastry. *Full line*: least square fit. *Lower part*: a vector diagram showing the variation of PTRM and NRM directions during heating and cooling processes of the same sample. All data are accepted

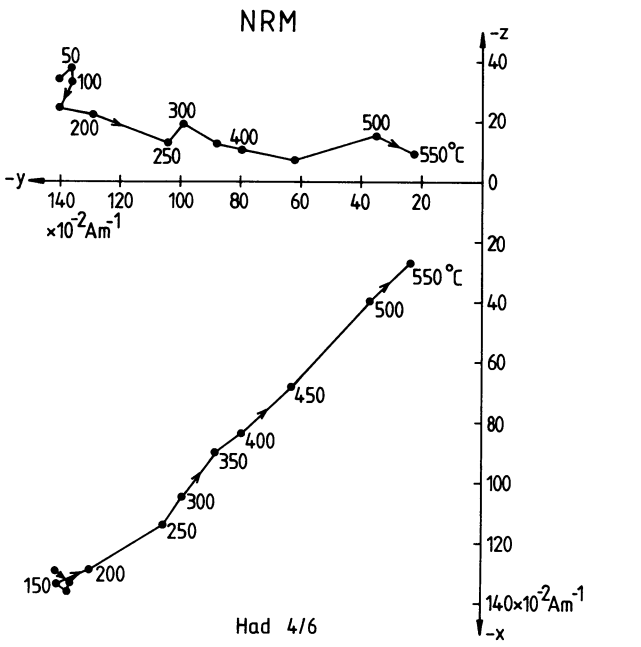

Fig. 7. Zijderveld diagram for the same sample as in Fig. 6. The viscous magnetization is negligible with respect to the NRM and hence all the data are accepted

of nonlinearity at low temperatures are viscous remanent magnetization or heating of the pottery subsequent to manufacture. Nonlinearity at high temperatures (found for only two samples at temperatures 550–650 °C) was possibly connected with a secondary chemical remanence, or with mineralogical changes during heating. Using two or three samples from the same sherd or brick is helpful in locating temperature intervals where the data appear reliable and common inflection points which might indicate a transition from useful to extraneous data. Directions of both NRM and PTRM with increasing temperature during the palaeointensity experiment were also noted and used in selection of the appropriate data subset. The samples were cooled from temperatures of more than 300 °C to room temperature in 45 min which means that the rate of cooling is much more than the possible rate during manufacture. This may lead to an overestimation of the palaeointensity of about 10–15%, sometimes even to 25% (Fox and Aitken, 1980; Walton, 1982). However, systematic investigations of that kind have not been made with the material which we used.

Figures 6 to 10 show vector diagrams of these directions. The directions of PTRM are always along the Z-axis (direction of F_{lab}) while the directions of NRM tend always towards the zero point. The viscous magnetization has been cleaned at temperatures between 50 and 200 °C (Figs. 7 and 9).

The slope of the NRM versus PTRM plots and hence the palaeointensity is determined by a least squares method. We used a least squares method where both ordinate and absissa have the same weighting for each data point. The virtual dipole moment (VDM) was calculated as:

$$\mathrm{VDM} = \tfrac{1}{2} F_a R^3 (1 + 3\cos^2 I)^{1/2};$$

where R is the Earth's radius ($= 6.371 \times 10^6$ m),
I is the inclination of the geomagnetic field at the respective ages and F_a is the field intensity measured (Table 1).

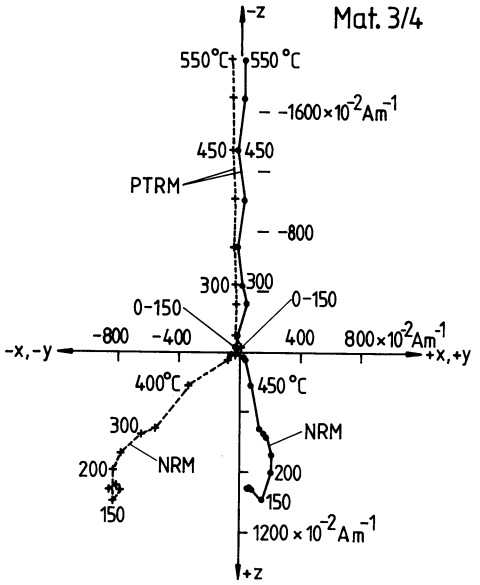

Fig. 8. Vector diagrams of PTRM and NRM for a sample from Matta El Meskin Monastry. *Crosses*: *Y–Z* plots, *points*: *X–Z* plots

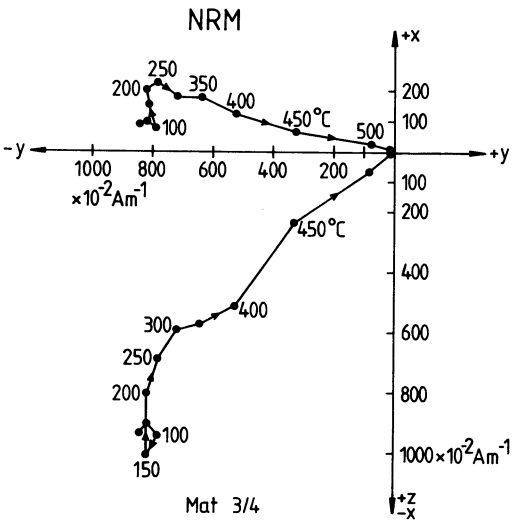

Fig. 9. Zijderveld diagram for the same specimen as in Fig. 8. The viscous magnetization as been removed at temperatures between 200 and 250 °C

The results of the palaeointensity measurements are summarised in Table 1 and represented in Fig. 11a, b.

Measurements of Susceptibility and Anisotropy of Susceptibility

Rogers et al. (1979) have claimed that ceramics possess an anisotropy of susceptibility with maximum parallel and minimum perpendicular to the wall of a ceramic sherd. Therefore, one has to pay attention to whether the magnetization of a sample in one direction is different from that in the other and hence the measured palaeointensity. To overcome this difficulty we collected the samples from thick ceramics and bricks. The susceptibilities then measured using a susceptibility bridge for all samples cored out of the sherds and bricks. These measurements were made along two perpendicular axes for each sample. The susceptibilities

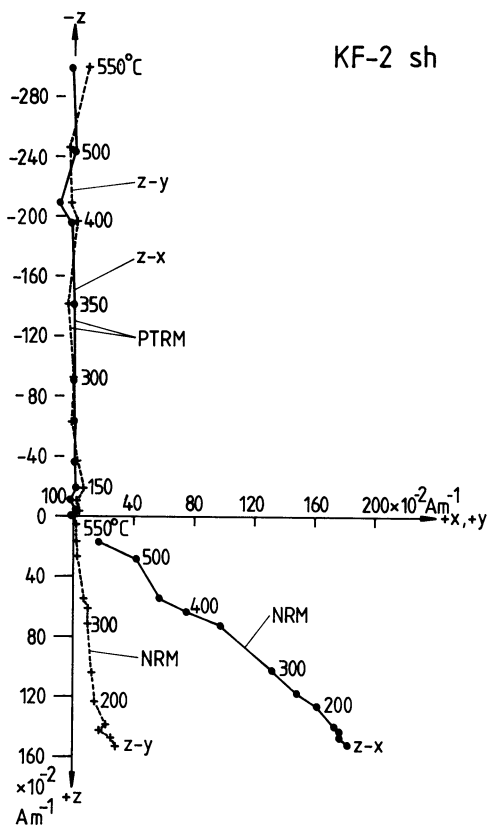

Fig. 10. Vector diagrams for the PTRM and NRM for a sample from Kiman Faris. No viscous magnetization is observed. *Crosses*: *Y–Z* plots, *points*: *X–Z* plots

of samples taken from a sherd do not differ too much from each other (see Table 2) and they seem to be isotropic. Later, some pilot samples were also subjected to anisotropy of susceptibility measurements using a Kapa-bridge type KLY-2 which is of much higher sensitivity and no effective anisotropy has been measured (Table 2). This may indicate that such thick ceramics and bricks do not possess significant anisotropy of susceptibility as detected by Rogers et al. (1979) and that it is preferable to carry out the palaeointensity measurements using such thick ceramics and bricks.

Palaeoinclination Measurements

These measurements are only possible when ceramic sherds are parts of specially shaped pottery. We collected about ten samples from each age such as parts from oven plates, large and wide fired containers, vases of large dimensions and special forms and the like. Field evidence and ornamentation lead the archaeologists and ceramicists, who were present during sampling, to the conclusion that these objects must have been baked standing upright on a horizontal surface. Bricks have been collected from buildings of known ages. The inclination could be also measured from bricks because of the regular way in which they were stacked while being baked.

In laboratory work, these sherds and bricks have been placed in positions representing exactly their positions during baking and then cast in plaster of Paris. A coordinate system was assigned to each sample. Cylindrical samples of 2.5 cm diameter were then cored from these samples and

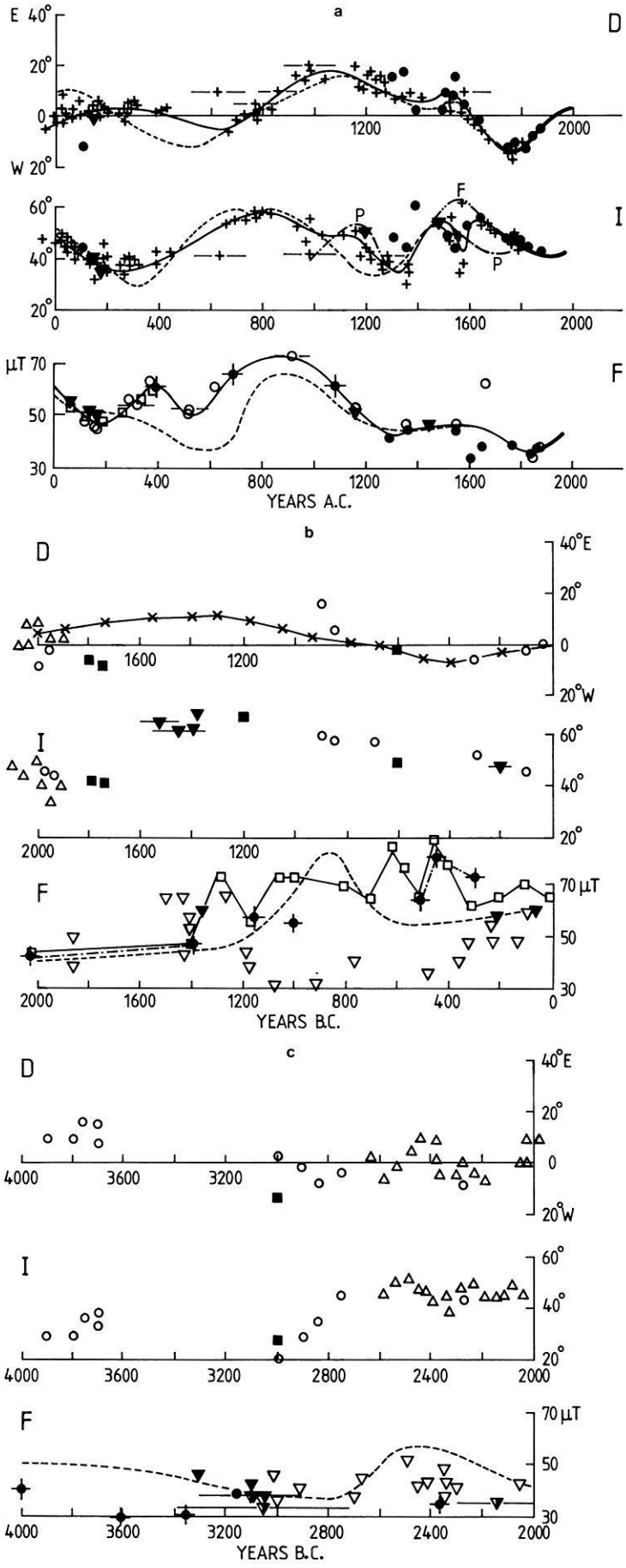

Fig. 11a–c. All the data reduced to Egypt and the results of this paper are represented in these Figures. **a** for the time interval zero A.D. to present, **b** for zero to 2000 years B.C. **c** for the time interval from 2000–4000 B.C. The letters at the side of each Figure denote: *D*: Declination (*upper part* of the curves; *E* = East and *W* = West). *I*: Inclination (*middle part* of the Figures), *F*: Palaeointensity (*lower part*). Thick lines at the end of **a** represent the observations in Egypt in the 19th and 20th centuries (Fahim and Gouda Hussain, 1977), *solid circles*: data reduced from Etna (Tanguy 1970, 1975), *open circles*: data reduced from South-Eastern Europe (Kovacheva 1976, 1977; Kovacheva and Veljovich, 1977), *solid squares*: data reduced from Turkey (Becker, 1979), *open squares*: data reduced from Athens (Walton, 1979), *solid triangle with downward head*: results of this paper, *open triangle with downard head*: data for Egypt (Games, 1980), *half open triangle with head downward*: data for Egypt (Athavale, 1969), *open triangle with upward head*: data reduced from Iran (Kawai et al., 1972), *crosses*: data reduced from Western Europe (Thellier, 1981), *crosses with solid circles*: data reduced from Ukraine and Moldavia (Rusakov and Zagniy, 1973a, 1973b), *continuous curve with "x"*: data reduced from England (Thompson, 1973), *P* in the middle part of **a**: this curve reduced from Poland (Czyszek 1976), while *F*: this part of the curve is after Thellier (1981). The continuous curves of **a** (upper, middle and down) represent the reduced data of the secular variation for Egypt during the last 2000 years

Table 2. Magnetization, susceptibility and anisotropy of susceptibility measurements

Sample No.	Type	$\bar{J}$ 10^{-5} A m^2 kg^{-1}	n	σ_J	$\bar{x}$ 10^{-9} m^3 kg^{-1}	σ_x	Anisotropy of susceptibility measurements (normalized)			
							X	Y	Z	Remarks
Mat 1	cer.	24.9	10	1.4	415.9	15.1				(1)
Mat 2	br.	33.5	10	3.5	128.2	10.1		1.03	0.98	(2)
Mat 3	br.	87.2	8	9.7	276.5	15.1		0.98	1.04	(2)
Mat 4	br.	47.3	7	7.6	272.7	12.6	1.003	1.001	0.996	(3)
Mat 5	br.	143.4	13	5.7	324.2	15.1				(1)
Had 1	br.	73.7	14	3.9	426.0	18.8	1.010	1.003	0.987	(3)
Had 2	br.	90.5	8	6.9	661.0	18.8				(1)
Had 3	br.	43.0	5	5.3	338.0	15.1				(1)
Had 4	cer.	9.3	5	0.8	125.7	8.8	1.011	1.024	*0.964*	(3)
Had 5	cer.	30.4	2	–	287.8	–		1.02	*0.98*	(2)
KO 5-3	br.	15.4	15	0.9	123.2	18.8				(1)
KO 6-5	br.	9.9	2	–	39.0	–	1.002	0.993	1.005	(3)
KO 6-7	br.	9.7	16	2.8	228.7	20.1				(1)
KO 7-10	br.	10.3	7	1.2	227.5	8.8				(1)
KO 8-2	cer.	14.2	4	–	170.9	–		1.02	*0.98*	(2)
KO 8-3	cer.	7.5	8	0.5	84.2	7.5	0.967	0.966	*1.087*	(3)
KF 2-Sh	cer.	16.0	4	0.8	145.8	8.8				(1)
KF 3-Sh	cer.	16.6	22	0.8	118.2	10.1				(1)
KF 4-1	cer.	38.4	2	–	561.7	–	1.042	0.979	*0.979*	(3)
KF 3-7	cer.	20.0	5	1.1	372.0	12.6				(1)
KF 1-2	cer.	38.0	5	2.2	366.9	11.3				(1)
KF 5-2	br.	17.6	4	1.2	51.5	7.5	1.008	0.985	1.007	(3)
M 2-3	cer.	22.1	3	–	601.9	–	1.005	1.032	*0.982*	(3)
M 4-5	br.	12.3	5	0.4	168.4	10.1	0.994	1.007	1.000	(3)

$$\sigma_J \text{ and } \sigma_\Omega = \sqrt{\frac{\sum_{i=1}^{n} (\bar{x} - x_i)^2}{n(n-1)}};$$

where $\bar{x}$ is the mean value of specific magnetization $\bar{J}$ and specific susceptibility $\bar{x}$, resepctively and x_i represents the individual values of J and x, repectively.

(1) The susceptibility was measured using a susceptibility bridge along three axis (X, Y and Z; whereas the Z axis is along the axis of the cylindrical sample). No anisotropy of susceptibility was observed.

(2) The sample were cored parallel to the wall of the sherd and perpendicular to it. The susceptibility was then measured using the same bridge as in (1).

(3) The anisotropy of susceptibility was measured using a Kapa-bridge type KLY-2.

Minimum susceptibility is in the direction perpendicular to the wall (underlined values in columns 8 to 10; these values are normalized i.e. divided by the mean value). Anisotropy of susceptibility ranges between zero and 12%

cut into specimens of 2.5 cm length. The directions of magnetization were then measured using a spinner magnetometer. The directions of magnetization of samples from a sherd or a brick were compared and found to possess small angles of confidence. Table 3 summarizes these measurements and they are represented in Figs. 11 a–c.

Other Measurements of Directions (D and I)

Samples were collected from some ovens in Karanis (Kom Oushim), Fayoum. These samples were oriented prior to removal by an exactly horizontal surface of plaster of Paris and the magnetic North was then marked on this surface. These samples were then cast in plaster of Paris and cut into cubes of 6 cm length. The directions of magnetization (both D and I) were measured using a special type of large-sample spinner magnetometer. All samples are from only one age (150 years A.C.). Table 4 contains the results of these measurements and the mean value of the direction of the geomagnetic field in Egypt at this age. This is also represented in Fig. 11 a.

Discussion

In this work, we tried to have the best conditions suitable for determination of the palaeointensities and palaeoinclinations of the geomagnetic field from archaeomagnetic measurements. The archaeological sites, from which the samples were collected, have been thoroughly studied by Egyptologists and ceramicists (e.g. Boak et al., 1931, 1933; Bresciani, 1968 and others). This enabled the trained archaeologists, who accompanied us during sampling, to determine the ages of these samples (specially with the aid of ceramicists) with an accuracy of a few tens of years. We have been able to select the most proper samples suitable for these measurements from a large variety of ceramic material. The thick ceramic sherds and bricks were found to possess negligible anisotropy of susceptibility and they are of homogeneous magnetization and susceptibility (Table 2) and hence they are the most suitable material for palaeointensity measurements.

Only one sample out of 50 was found to have nonlinearity of NRM versus PTRM plots. The vector diagrams repre-

Table 3. Palaeoinclinations of the geomagnetic field in Egypt

Location	Sample Nr.	Ages		$\bar{I}$	n	α_{95}	k	Reliability factor
Kom	5/3	147–	br.	36.0	19	1.2	699.4	a
Oushim	6/7	170	br.	37.3	17	0.9	1,537.6	a
29.54°N	6/5	A.D.	br.	25.0	2	–	–	a–c
30.6°E	8/1		cer.	33.6	6	1.5	1,422.8	a
	8/2		cer.	28.5	4	3.6	298.3	b
	7/10		br.	33.4	7	7.1	55.9	a–b
	7/5		br.	30.0	4	3.9	327.5	a–b
	11		br.	24.1	7	10.1	38.1	c
	8/3		cer.	34.3	8	3.3	286.1	a–b
	1/1		br.	32.3	15	1.5	586.5	b
	2/1		br.	22.7	15	1.9	399.8	b
	3/1		br.	29.2	10	4.4	95.6	b
	7/4		br.	41.7	1	–	–	c–d
Mean of all (except those with consistency factor c and d): $\bar{I}=30.7$, $N=11$, $A_{95}=2.8$, $K=267.5$								
Kiman	3/4	150–	br.	50.6	13	1.6	642.9	a
Faris	4/3	250	br.	45.2	11	2.8	271.4	a
29.5°N	4/2	B.C.	br.	35.5	2	14.0	19.7	b–c
30.6°E	5/4		br.	45.3	4	3.0	927.2	a
	3/7		cer.	68.0	5	7.6	102.7	d
	5/8		br.	43.4	2	–	–	c
	5/6		br.	34.0	3	11.9	60.5	b–c
	5/2		br.	50.2	6	4.1	266.6	a–b
	2/3		br.	54.4	7	4.4	147.4	b
	5/3		br.	42.2	7	1.1	2,936.4	a–b
	5/1		br.	48.4	7	2.5	593.8	a
	4/1		br.	22.3	2	–	–	c–d
	1/5		br.	24.9	1	–	–	d
Mean of those with consistency factor a–c: $\bar{I}=47.7$, $N=9$, $A_{95}=2.75$, $K=406.7$								
Kiman	10	ca.	cer.	70.2	17	3.1	118.6	b
Faris	4	1400	cer.	67.8	9	4.1	128.0	a–b
29.51°N	3	B.C.	cer.	66.6	3	11.2	122.6	b
30.6°E	5		cer.	61.6	6	6.2	118.6	a–b
	7		cer.	60.8	5	11.1	48.8	b
	3/7		cer.	68.9	5	7.6	102.7	b
	1		cer.	72.5	9	3.1	118.6	c
Mean of all: $\bar{I}=66.7$, $N=7$, $A_{95}=3.2$, $K=350$								
Lahoun,	L_1	1550–	cer.	61.7	7	8.6	49.9	a
Fayoum	L_2	1350	cer.	61.6	5	3.8	414.0	a
29.53°N		B.C.						
30.6°E	Mean of L_1 and L_2: $\bar{I}=61.7$							
Biahmo,	B_2	1550–	cer.	60.3	4	4.2	472.1	a
29.48°N	B_5	1350	cer.	61.7	2	–	–	b
30.59°E		B.C.						
Mean of B_2 and B_5: $\bar{I}=61.2$								
Madi,	2/1	1600–	cer.	66.2	12	4.3	90.0	a
Fayoum,	2/10	1450	cer.	73.4	4	2.0	1,267.1	a–b
29.47°N	1/5	B.C.	cer.	68.2	4	3.8	334.5	a
30.6°E	3/4		cer.	51.8	5	3.0	422.2	b
	1/3		cer.	69.8	2	–	–	b
	1/1		cer.	61.8	4	4.8	364.1	b
	3/5		cer.	56.4	4	2.4	1,426.4	a
	3/1		cer.	71.6	5	2.6	853.8	a
	2/5		cer.	74.4	4	4.5	411.2	a
	4/5		cer.	66.1	6	1.0	4,567.2	a
	4/6		cer.	59.7	2	11.8	450.4	c
Mean of all: $\bar{I}=65.1$, $N=11$, $A_{95}=4.1$, $K=125.8$								

Table 3 (continued)

Location	Sample Nr.	Ages		$\bar{I}$	n	α_{95}	k	Reliability factor
Anba	1	ca.	br.	47.6	14	1.8	409.3	a
Simon	2	1200	br.	41.0	11	1.3	1,032.0	a
Bin	3	A.D.	br.	65.4	11	1.3	1,045.9	a–b
Hadra	4		cer.	59.7	8	2.7	336.9	a–b
Monastry	5		cer.	51.5	1	–	–	c
	6		cer.	47.5	1	–	–	c
	7		cer.	51.5	6	4.0	217.3	b–c
Mean of all: $\bar{I}=52.0$, $N=7$, $A_{95}=6.1$, $K=98.8$								
Matta	1	1450–	cer.	67.1	14	1.5	588.8	a
El-	2	1500	br.	74.3	10	4.5	95.6	a–b
Meskin	3/1	A.D.	br.	47.4	8	3.3	224.2	a–b
Monastry	3/2		br.	45.7	3	3.4	561.2	b
	4		br.	58.7	8	4.8	106.6	a
	5		br.	47.2	14	1.0	1,381.0	a
	6		br.	44.8	4	1.2	3,599.0	a–b
Mean of all: $\bar{I}=54.9$, $N=7$, $A_{95}=8.9$, $K=47.1$								

$\bar{I}$ = Mean inclination measured from specimens cored out of a sample (column 5); n = Number of specimens, α_{95} and k are Fisherian statistical parameters (the directions of magnetization of specimens from a sample are nearly of the same declination, e.g. within ±2°), $\bar{I}$ mean of all samples

Table 4. Mean direction of the geomagnetic field (D and I) in Egypt at 150 years A.D. (Location: 29.5°N, 30.6°E)

Sample Nr.	$\bar{D}$ (°)	$\bar{I}$ (°)	n	α_{95}	k
KO 1	−11.2	33.2	17	3.86	86.23
KO 2	−12.7	23.4	15	7.48	27.1
KO 3	− 9.4	40.8	29	5.28	26.7
KO 8	11.7	24.3	6	4.54	218.3
KO 9	no consistent results				
KO 10	5.3	31.2	3	6.7	338.5
KO 11	no consistent results				
KO 13	−2.6	40.6	28	0.83	1,074.96
Mean of all: $\bar{D}=3.0°$, $\bar{I}=32.6°$, $N=6$, $A_{95}=9.5$, $K=50.72$					

senting the behavior of the direction of NRM and PTRM during heating and cooling processes are useful for selecting the data subset suitable for NRM versus PTRM plots. The PTRM vector diagrams (Figs. 6, 8 and 10) show that the PTRM is always parallel to the direction of F_{lab}, while the NRM vector diagrams (Figs. 6–10) are useful in determining the extraneous data subset where the viscous magnetization is effective. In most of our samples the viscous magnetizations have been removed at temperatures between 50 °C and 250 °C. Sometimes the intensity of the viscous magnetization is much smaller than the NRM so that it does not effect the linearity of the NRM versus PTRM plots.

Unfortunately no determinations have been made for the directions of the geomagnetic field in Egypt in historic times. Only two papers have been published concerning the palaeointensity of the geomagnetic field in Egypt: one by Athavale (1969) in which he measured the palaeointensity from two sample sets of uncertain ages (one for an

age between 3400–2700 B.C. and the other for an age between 2300–1700 B.C.) and the other paper by Games (1980) in which he determined the palaeointensity between 3000 B.C. and 0 B.C. using air dried bricks as well as fired ceramics and bricks. We tried to measure the magnetization of some samples from recent air dried bricks using a spinner magnetometer and we found that their magnetizations are less than 10^{-4} A m^{-1}.

To make correlations with our results, we used all the data obtained from archaeomagnetic measurements in an area close to Egypt so that the non-dipole part of the geomagnetic field can be minimized. The directions of the geomagnetic field (D and I) measured from samples from Western Europe (collected by Thellier, 1981), South-Eastern Europe (Kovacheva, 1976, 1977), Turkey (Becker, 1979), Cyprus (Tanguy, 1970), Iran (Kawai et al., 1972) and Ukraine and Moldavia (Rusakov and Zagniy, 1973a and b) were reduced to a mean site in Egypt. These pairs of archaeomagnetic D and I data together with their respective site localities (latitudes and longitudes) were used to calculate the pole positions of the geomagnetic field at their respective ages (for equations for calculating the pole position of the geomagnetic field from D, I, latitude and longitude of sampling site see, for example, McElhinny, 1973). From these pole positions the directions of the geomagnetic field (D and I) were calculated for Egypt (latitude 28.0 °N, longitude 30.6 °E). These reduced data are represented in Figs. 11 a–c.

The palaeointensities of the geomagnetic field measured at Athens (Walton, 1979), South East Europa (Kovacheva, 1977; Kovacheva and Veljovich, 1977), Ukraine and Moldavia (Rusakov and Zagny, 1973a and b), Czechoslovakia (Bucha, 1967, 1970) and Italy (Tanguy, 1975) have also been reduced to Egypt. Walton (1982) stated that his previous results are overestimated by 15–25%. However, this has no serious effect on our conclusions. The virtual dipole moment equation was used for such reduction.

$$F_{Egypt} = F_{site} \left(\frac{1 + 3\cos^2 I_{site}}{1 \times 3 \cos^2 I_{Egypt}} \right)^{1/2}.$$

These reduced palaeointensity data are represented in Figs. 11 a–c, lower parts.

The observations of the geomagnetic field (F, D and I) made in Egypt in the 19th and 20th centuries (Fahim and Gouda Hussain, 1977), represented as thick lines in the last part of Fig. 11 a, coincide with the reduced data which may indicate a suitable method of reduction. Our results from this paper are also in good agreement with these reduced data.

The periodicity of the geomagnetic field of 2800 years suggested by Thompson (1973) and Bucha (1967) cannot be seen in our data.

The secular variation curves, especially for the period zero to 2000 years A.C. (Fig. 11 a), are suitable for rough chronological estimates. Many more measurements of samples from Egypt for ages along the whole historic column are needed for the enrichment of the data and hence the production of curves suitable for chronology.

Acknowledgments. We are greatly thankful to the Egyptian archaeologists who accompanied me during sampling, specially Mr. Ali Bazeidy, inspector of archaeology of El Fayoum Area and Mr. Ahmed Mousa of Sakkara and Pyramids Areas. Thanks are also due to Dr. Strauss, Institute of Egyptology of the University of Munich for providing the samples from Monshaat Abu Omar.

The measurements were made partyly in the Institut für Allgemeine und Angewandte Geophysik, University of Munich and partyly in the Helwan Institute of Astronomy and Geophysics, Helwan, Cairo. We are thankful to Prof. Dr. G. Angenheister, Prof. Dr. H. Soffel, Prof. Dr. A. Schult and Dr. H. Becker from the first Institute and to Prof. Dr. M. Fahim, Prof. Dr. H. Deebes and Dr. A. Gh. Hassaneen from the second one. Special thanks are due to Prof. Dr. H. Soffel for kindly reading the manuscript.

References

Aitken, M.J.: Physics and Archaeology, 2nd. edt. Oxford: Clarendon Press 1974

Athavale, R.N.: Intensity of the geomagnetic field in pre-historic Egypt. Earth Planet. Sci. Lett. **6**, 221–224, 1969

Becker, H.: Archaeomagnetic investigations in Anatolia from prehistoric and hittite sites. Proceedings of the 18th. International Symp. on Archaeometry and Archaeological prospection, Archaeo-Physico **10**, 382–387, 1979

Boak, A.E.R.: Karanis, The temples, coin hoards, botanical and zoological reports, seasons 1924–1931. Univ. Michigan Press, 1933

Boak, A.E.R., Petersen, E.E.: Karanis, topographic and architectural report of excavations during seasons 1924–1928. Univ. Michigan Press, 1931

Bresciani, E.: Messione die scavo Medinet Madi (Fayoum-Egitto), Rapporto preliminiare della campagne di scavo 1966 e 1967, 1968 (also other unpublished reports of the Institute of Egyptology Univers. Milano for 1968 and 1969 from Foraboschi, D.)

Bucha, V.: Intensity of the Earth's magnetic field during archaeological times in Czechoslovakia. Archaeom. 10, 12–25, 1967

Bucha, V.: Evidence for changes in the Earth's magnetic field intensity. Phil. Trans. R. Soc. Lond. **A 269**, 47–55, 1970

Czyszek, W.: Archaeomagnetism, a preliminary report. Publ. Inst. Geophys. Pol. Acad. Sci. **76**, 59–70, 1976

Fahim, M., Gouda Hussain, A.: The secular variation of the geomagnetic field at Helwan, Egypt. Helw. Observ. Bull. **139**, 1–19, 1977

Fox, J.M.W., Aitken, M.J.: Cooling-rate dependence of thermoremanent magnetization. Nature **283**, 462–463, 1980

Games, K.P.: The magnitude of the archaeomagnetic field in Egypt between 3000 and 0 B.C. Geophys. J. R. Astron. Soc. **63**, 45–56, 1980

Kawai, N., Hirooka, K., Nakajima, J., Tokieda, K., Tosi, M.: Archaeomagnetism in Iran. Nature **236**, 223–225, 1972

Kovacheva, M.: Archaeomagnetic investigations of some pre-historic sites in Bulgaria. Archaeom. **18**, 99–106, 1976

Kovacheva, M.: Archaeomagnetic investigations in Bulgaria: Field intensity determinations. Phys. Earth. Planet. Inter. **13**, 355–359, 1977

Kovacheva, M., Veljovich, D.: Geomagnetic field variations in South-Eastern Europe between 6500 and 10 years B.C. Earth Planet. Sci. Lett. **37**, 131–138, 1977

McElhinny, M.W.: Palaeomagnetism and plate tectonics, Cambridge Uni. Press 1973

Rogers, J., Fox, J.M.W., Aitken, M.J.: Magnetic anisotropy in ancient pottery. Nature **277**, 644, 1979

Rusakov, O.M., Zagniy, G.F.: Intensity of the geomagnetic field in the Ukraine and Moldavia during the past 6000 years. Archaeom. **15**, 275–285, 1973a

Rusakov, O.M., Zagniy, G.F.: Archaeomagnetic secular variation study in the Ukraine and Moldavia. Archaeom. **15**, 153–157, 1973b

Tanguy, J.C.: An archaeomagnetic study of mount Etna: The magnetic direction recorded in lava flows subsequent to the twelfth Century. Archaeom. **12**, 115–128, 1970

Tanguy, J.C.: Intensity of the geomagnetic field from recent Italian

lavas using a new palaeointesnity method. Earth Planet. Sci. Lett. **27**, 314–320, 1975
Thellier, E.: Sur la direction du champ magnétique Terrestre en France durant le deux derniers millenaires. Phys. Earth Planet. Inter. **24**, 89–132, 1981
Thellier, E., Thellier, O.: Sur l'intensité du champ magnétique terrestre dans le passé historique et géologique. Ann. Géophys. **15**, 285–376, 1959
Thompson, R.: Palaeolimonology and palaeomagnetism. Nature **242**, 182–184, 1973
Walton, D.: Geomagnetic intensity at Athens between 200 B.C. and 400 AD. Nature **277**, 643–644, 1979
Walton, D.: Errors and resolution of thermal techniques for obtaining the geomagnetic intensity. Nature **295**, 512–515, 1982

Received November 30, 1982; Revised version March 17, 1983; Accepted April 12, 1983

J Geophys (1983) 53:141–143

Journal of Geophysics

Magnetostatic Energy of Spherical Two-Domain Particles and the Upper Single-Domain Particle Size in Magnetite

R.J. Veitch

Laboratoire de Pétrophysique, Département de Minéralogie de l'Université, 13, rue des Maraîchers, 1211 Genève 4, Switzerland

Abstract. Calculations have been made of the magnetostatic energy of a spherical particle divided by a single 180° domain wall. The results suggest that for magnetite there may be no jump from a uniformly magnetized state to a two domain configuration at a particular particle size, but that the uniform magnetization is preferred for particles $\lesssim 60$ nm in diameter, and distinct domains may appear in particles with diameters $\gtrsim 150$ nm.

Key words: Rock magnetism – Single domain particles – Magnetic domains – Magnetite.

The presence of sub-microscopic magnetic particles in rocks (e.g. Evans and Wayman, 1970, 1974), makes a knowledge of the single-domain size-range, and the properties of particles just larger than single domains, important for palaeomagnetism. Butler and Banerjee (1975) applied Amar's model (Amar 1957, 1958a, 1958b) of a two-domain particle to rectangular parallelepipeds of magnetite, and concluded that the upper limit to the single-domain size-range for magnetite is set by the transition to a two domain configuration with a single 180° domain wall. In Amar's calculation of the magnetostatic energy of the two-domain system, the wall is treated as a uniformly magnetized slab of thickness equal to the effective width of the domain wall, and having the same intensity of magnetization as the neighbouring domains. This overestimates the magnetostatic energy of the wall.

A variation of the calculation, with a different estimate of the magnetostatic energy, is applied here to spherical magnetite particles. Butler and Banerjee preferred the form of a parallelepiped as being more realistic for naturally occuring grains. It is however interesting to see the effect of the change from cubic to spherical shape, while synthetic particles produced by milling may indeed be closer to spherical than cubic form.

Consider a 180° wall of width $2x$ symmetrically dividing a particle of radius R. The volume occupied by the wall is then $2\pi(R^2x - x^3/3)$. Following Amar (1957) the wall energy per unit area (σ) is given by $(\sigma_0/2)(2x/\delta_0 + \delta_0/2x)$ where σ_0 and δ_0 are the wall energy per unit area and the wall width in bulk material. As a first approximation a wall energy per unit volume ($\sigma/2x$) and a total wall energy (E_w) may be calculated.

$$E_w \approx \frac{\pi}{x}\left\{R^2x - \frac{x^3}{3}\right\}\left\{\frac{\sigma_0}{2}\right\}\left\{\frac{2x}{\delta_0} + \frac{\delta_0}{2x}\right\}.$$

The values of σ_0 and δ_0 used by Butler and Banerjee (1975) have been taken: $\sigma_0 = 0.8 \times 10^{-3}\,\mathrm{Jm}^{-2}$, $\delta_0 = 150$ nm.

In the case where the domain wall is considered as having the same intensity of magnetization as the two domains, the magnetostatic problem can be simplified by imagining the wall magnetization rotated through 90° in the plane of the wall so as to be parallel to the magnetization of one of the domains. As the interactions with the two domains are equal and opposite this does not change the magnetostatic energy, and the problem becomes that treated by Néel (1944). Figure 2, curve A, shows the reduced magnetostatic energy (magnetostatic energy of the particular configuration divided by that of the same particle uniformly magnetized) versus reduced wall thickness (x/R) obtained from Néel's solution.

An improved model for calculating the magnetostatic energy is shown in Fig. 1. The wall is divided in halves, in each of which the magnetization is represented by two components of intensity $2/\pi$ times the saturation magnetization. These two components are parallel and perpendicular, respectively, to the magnetization of the neighbouring domains.

Expanding the resulting surface charge distribution in terms of Legendre polynomials (the method used by Néel, 1944 and described by Carey, 1971), and satisfying the boundary conditions at the surface of the sphere for the internal and external potentials, leads to a series solution for the magnetostatic energy E_m. Carey's paper describes the procedure in detail. An important point is that because there is no net interaction between the mutually perpendicular components of magnetization, the energy can be calculated as the sum of two terms, one due to the components parallel and antiparallel to the domain magnetizations, and one due to the net magnetization of the wall.

The magnetostatic energy is given by

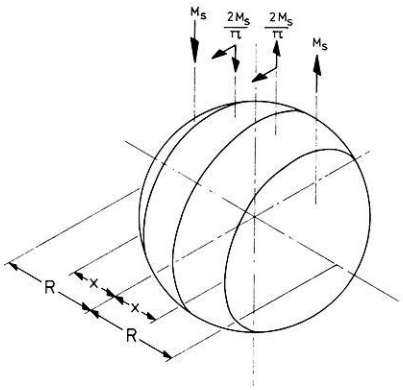

Fig. 1. Spherical particle divided by à 180° domain wall. In the two domains the magnetizations are $+M_s$ and $-M_s$. The rotation of the magnetization in the wall is approximated by giving each half a mean magnetization $2/\pi\ M_s$ parallel to that in the neighbouring domain

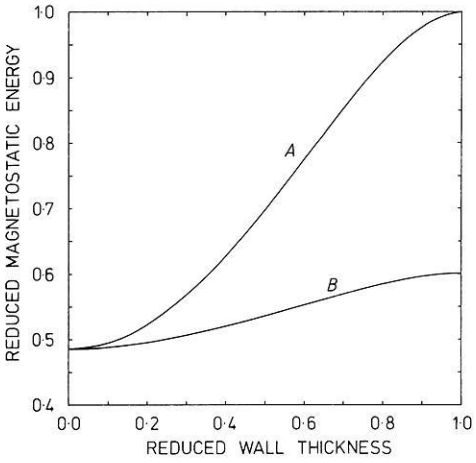

Fig. 2. Reduced magnetostatic energy (magnetostatic energy divided by the magnetostatic energy of a uniformly magnetized sphere of the same size) versus reduced wall thickness (wall thickness divided by diameter of sphere). Curve *A* is for a domain wall carrying magnetization M_s perpendicular to domain magnetizations. Curve *B* refers to the magnetization scheme in Fig. 1. (The energies were calculated to 35 terms in the series expansions)

$$E_m = \tfrac{8}{9}\pi^2 M_s^2 R^3 E_r \qquad \text{(c.g.s.)}$$
$$= \tfrac{2}{9}\pi \mu_0 M_s^2 R^3 E_r \qquad \text{(S.I.)}$$

where R is the radius of the sphere, M_s the spontaneous magnetization within the domains, and E_r the reduced magnetostatic energy given by

$$E_r = \frac{\gamma^2}{\pi^2}(3-\gamma^2)^2 + \frac{9}{8}\sum_{n=2}^{\infty}\frac{n(n+1)}{(2n+1)^2}\{a_n^2 + b_n^2\},$$

$$a_n = \left(\frac{2}{\pi} - 1\right)(1+(-1)^n) \cdot \left\{\frac{P_n(\gamma) - P_{n-2}(\gamma)}{2n-1} - \frac{P_{n+2}(\gamma) - P_n(\gamma)}{2n+3}\right\} - \frac{4}{\pi}\left\{\frac{P_n(0) - P_{n-2}(0)}{2n-1} - \frac{P_{n+2}(0) - P_n(0)}{2n+3}\right\},$$

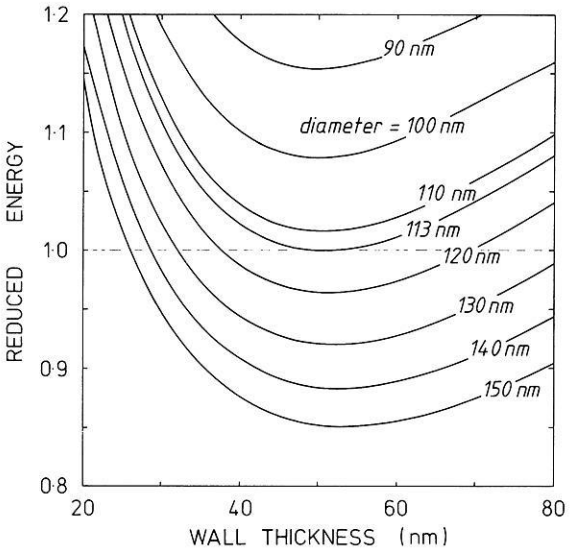

Fig. 3. Reduced energy versus wall thickness for two-domain magnetite particles of various diameters. The magnetostatic energy is taken from Curve *A* of Fig. 2

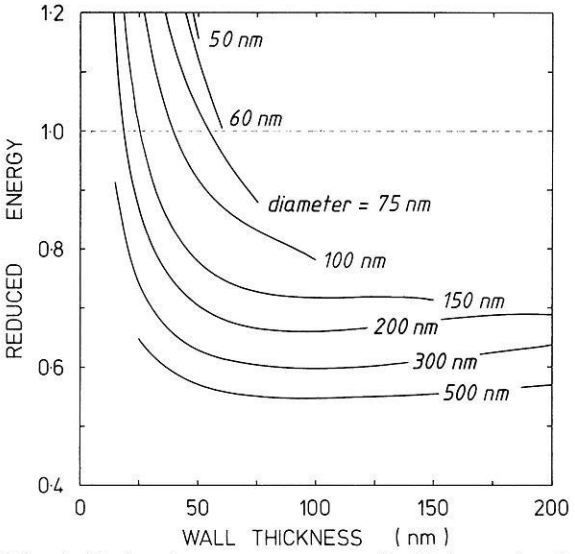

Fig. 4. Reduced energy versus wall thickness for 2-domain magnetite particles of diameters 50 nm to 500 nm. The magnetostatic energy is that of Curve *B*, Fig. 2

$$b_n = \frac{2}{\pi}((-1)^n - 1)\left\{\frac{P_n(\gamma) - P_{n-2}(\gamma)}{2n-1} - \frac{P_{n+2}(\gamma) - P_n(\gamma)}{2n+3}\right\},$$

$$\gamma = x/R.$$

E_r is plotted as a function of γ in Fig. 2, curve *B*.

Summing the wall and magnetostatic energies and then dividing by the magnetostatic energy of a single domain particle of the same size gives the total reduced energy, which is plotted as a function of wall thickness for various particle diameters in Figs. 3 and 4. The results of the simpler model of the wall magnetization are shown in Fig. 3, while Fig. 4 refers to the model of Fig. 1 and the above equation for E_m. From Fig. 3 it is seen that for particles greater than 113 nm there is a

domain wall thickness for which the total reduced energy is less than one, and the two-domain state is stable. Taking the ratio of wall area to particle volume as the critical parameter, this transition size agrees exactly with the value 76 nm obtained by Butler and Banerjee (1975) when they carried out the equivalent calculation for cubic particles. Quite a different picture appears in Fig. 4 however. Here the single domain state is energetically favoured for particles smaller than 60 nm, but two distinct domains do not appear until the particles are larger than 150 nm, intermediate sized particles being filled by the wall itself.

Although the above calculations are not rigorous they do suggest that the upper size limit to single domain behaviour in equidimensional magnetite may not be a direct transition to a two-domain configuration, but rather to a domain wall like magnetization as proposed by Dunlop (1973).

References

Amar, H.: On the width and energy of domain walls in small multidomain particles. J. Appl. Phys. **28**, 732–733, 1957

Amar, H.: Size dependence of the wall characteristics in a two-domain iron particle. J. Appl. Phys. **29**, 542–543, 1958a

Amar, H.: Magnetization mechanism and domain structure of multidomain particles. Phys. Rev. **111**, 149–153, 1958b

Butler, R.F., Banerjee, S.K.: Theoretical single-domain grain size range in magnetite and titanomagnetite. J. Geophys. Res. **80**, 4049–4058, 1975

Carey, R.: Magnetostatic energies of spherical particles. J. Phys. D: Appl. Phys. **4**, 1624–1629, 1971

Dunlop, D.J.: Thermoremanent magnetization in submicroscopic magnetite. J. Geophys. Res. **78**, 7602–7613, 1973

Evans, M.E., Wayman, M.L.: An investigation of small magnetic particles by means of electron microscopy. Earth Planet. Sci. Lett. **9**, 365–370, 1970

Evans, M.E., Wayman, M.L.: An investigation of the role of ultra-fine titanomagnetite intergrowths in palaeomagnetism. Geophys. J.R. Astron. Soc. **36**, 1–10, 1974

Néel, L.: Effet des cavités et des inclusions sur le champ coercitif. Cah. Phys. **25**, 21–44, 1944

Received December 20, 1982; Revised April 28, 1983;
Accepted May 4, 1983

J Geophys (1983) 53:144–148

Journal of Geophysics

Irreversible Changes of Anisotropy of Magnetic Susceptibility of Rocks due to Uniaxial Pressure

Aleš Kapička
Geophysical Institute, Czechoslovak Academy of Sciences, Boční II. 1401, 141 31 Praha 4, Czechoslovakia

Abstract. The irreversible changes of anisotropy of magnetic susceptibility of basalt rocks due to uniaxial pressure up to 250 MPa have been investigated. As a result of the irreversible pressure changes of the domain structure of ferrimagnetic minerals, the degree of anisotropy as well as the shape of the ellipsoid of susceptibility in rocks with initial isothermal remanent magnetic saturation polarization changes systematically. The qualitative behaviour of the changes of the degree of anisotropy is determined by the superposition of shape and domain effects. The magnitude of the pressure-induced changes of anisotropy of susceptibility depends on the stability of the domain structure which can be characterized by the coercive force of the rocks, and on the orientation of the saturated remanence with respect to the uniaxial pressure.

Key words: Rock magnetism – Anisotropy of magnetic susceptibility – Effect of pressure on magnetic properties

Introduction

A knowledge of the physical essence of the changes of the magnetic properties of rocks and minerals due to applied pressure provides a base for interpreting the tectonomagnetic changes observed in seismically active regions, as well as for interpreting certain local anomalies of the geomagnetic field. In experimental and theoretical work, besides the study of the pressure changes of various types of remanent magnetic polarization, attention has also been given to the changes of the magnetic susceptibility of rocks, particularly those due to the effect of directional uniaxial pressure (Kapica,1955; Nagata, 1966; Ohnaka et al., 1968) and to a lesser extent also to the effect of hydrostatic pressure (Nullman et al., 1978).

Uniaxial pressure on ferrimagnetic minerals is responsible for an additional uniaxial anisotropy with the effective anisotropy constant $\sim\frac{3}{2}\lambda\tau$, where λ is the magnetostriction coefficient and τ the stress (Kneller, 1962). The anisotropy constant depends on whether compressive stress or tensile stress is involved, and on the nature of the magnetostriction of the ferrimagnetic minerals. The theoretical interpretation of the changes of susceptibility of rocks due to uniaxial pressure, which is founded on the mechanism of rotation of the vector of spontaneous magnetization in separate domains (Stacey, 1962; Nagata, 1966), agrees well with experimental results obtained from specimens which have been subjected to pressures of the order of tens of MPa. In order to explain the pressure changes of susceptibility of samples in their initial undeformed state, however, we must also take into account the mechanism of irreversible discplacements of domain walls due to external stress (Kinoshita, 1968). Thus, the changes of magnetic susceptibility in rocks, subjected to pressure in the Earth's crust, may be considerably different from those observed on repeatedly deformed specimens.

Most measurements of the pressure changes of susceptibility were carried out parallel ($\chi^{\parallel}$) and perpendicular ($\chi^{\perp}$) to the uniaxial pressure. In view of the different magnitudes of the irreversible changes of directional susceptibilities $\chi^{\parallel}$ and $\chi^{\perp}$ after the stress has stopped acting on the samples (Kapica, 1955; Nagata, 1970), we may also assume irreversible anisotropy changes of magnetic susceptibility of rocks as a result of external pressure. However, no systematic study has been conducted in this respect. From the author's earlier paper (Kapička, 1981) it follows that re-ordering of the domain structure of ferrimagnetic minerals due to the magnetic field results in relatively large irreversible changes of anisotropy of magnetic susceptibility of rocks. The nature of these changes is closely associated with the degree of anisotropy and with the orientation of the ellipsoid of susceptibility due to the shape effect, and the ambient magnetic field relative to each other.

In order to throw light on the question of the extent to which irreversible changes of the domain structure, caused by applied mechanical stress, affect the anisotropy of magnetic susceptibility, changes of anisotropy of basaltic rocks due to uniaxial pressure are studied systematically in the present paper.

Experimental Procedure

The measurements were carried out on Tertiary basaltic rocks from the Bohemian massif, some of whose mechanical and magneto-mechanical properties had already been investigated (Kapička, 1978). Their ferrimagnetic fraction consisted of titanomagnetites with various degrees of oxidation. The basalts studied had different degrees of anisotropy of magnetic susceptibility due to the shape effect (ranging from isotropic to specimens with the degree of anisotropy of $\sim$4%) as well as considerably different values of the coercive force (Table 1). The cubic specimens, $2\times2\times2$ cm, were cut so that their surfaces were perpendicular to the directions of maximum, intermediate and minimum susceptibili-

Table 1. Degree of anisotropy P, coercive force H_c and grain size of the magnetic fraction for specimens in natural state

Specimen no.	P	H_c [10^2 A m^{-1}]	Grain size of magnetic fraction [mm]
211	1.019	60	0.015–0.05
219	1.038	62	0.07 –0.2
231	1.042	23	0.01 –0.07
235	isotropic	227	0.007–0.015

ty in their natural state. The opposite pressure surfaces were ground plane-parallel with an accuracy of 0.02 mm. The specimens were deformed by uniaxial pressure in a hydraulic press with end-pieces of the same cross-section as the sample. Paper inserts were placed between the specimen and the platens. The pressure range was 0–250 MPa, which is in the region of elastic deformation of basalts. The increment of the applied stress was constant ~ 8 MPa s^{-1}. The magnetic saturation of the specimens (J_{rs}) was carried out in a field of $\sim 40 \times 10^4$ A m^{-1}. The magnetic susceptibility was always measured before and after applying the pressure with a KLY-1 AC bridge (Jelínek, 1973) in a weak magnetic field of 80 A/m. The susceptibility anisotropy and its parameters were determined from measurements of fifteen directional susceptibilities with the aid of the Aniso program (Jelínek, 1972). The usual parameters were used to decribe the anisotropy: the degree of anisotropy was characterized by the parameter $P=\chi_1/\chi_3$, the shape of the susceptibility ellipsoid by the parameters $F=\chi_2/\chi_3$ and $L=\chi_1/\chi_2$, $\chi_1 \geqq \chi_2 \geqq \chi_3$ being the maximum, intermediate and minimum susceptibility of the specimens. To determine whether the differences observed between the directional susceptibilities are substantial as compared to the observation errors, i.e. whether the specimens are anisotropic or isotropic, the F-test (Jelínek, 1972) was used. The changes in the shape of the ellipsoid due to pressure were represented with the aid of an $L-F$ diagram in which the line passing through the origin at an angle of 45° separates the points referring to oblate ellipsoids of susceptibility from those referring to prolate ellispoids. The changes in the orientation of the

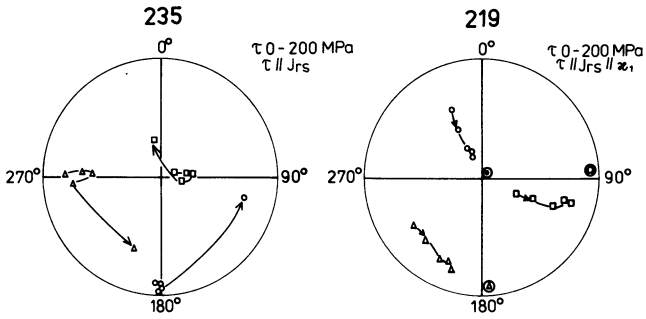

Fig. 2. Changes of orientation of the axes of maximum (△), intermediate (□) and minimum (○) susceptibility due to 50-MPa incremental pressure changes, J_{rs} orientation −180°. The orientation of the major axes of the ellipsoid under natural conditions (specimen 219) is encircled. Equal-area projection, lower hemisphere

major axes of the susceptibility ellipsoid were illustrated with the aid of stereographic projection.

Experimental Results

The irreversible changes of the degree of anisotropy P due to stress τ for specimens 211, 219, 231 and 235 with initial isothermal remanent magnetic saturation polarization (J_{rs}) are shown in Fig. 1. Due to the ordering of the domain structure by the magnetic field, the degree of anisotropy of the specimens with J_{rs} differs from that of the specimens in the natural state, when it is only determined by the shape effect. In each case, the uniaxial stress was applied parallel with J_{rs}. The basalts could be divided into three groups according to the behaviour of $P=f(\tau)$: (*a*) Those which do not display systematic changes of the degree of anisotropy over the whole range of stresses, regardless of the orientation of J_{rs} and of the original susceptibility ellipsoid with respect to one another (231); (*b*) Specimens 219 and 211 in which the systematic changes of the degree of anisotropy depend on the orientation of the ellipsoid and on J_{rs} with increasing stress (decrease of P with increasing τ if J_{rs} is parallel to χ_3, and an increase if J_{rs} is parallel to χ_1). The absolute values of the changes of P are $\sim 3\%$; (*c*) Isotropic specimens in the natural state (235) in which

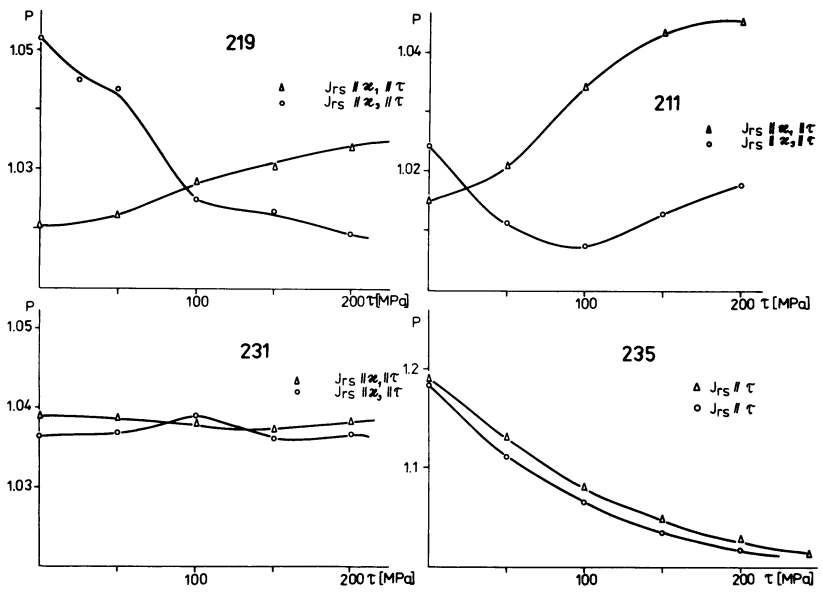

Fig. 1. Irreversible changes of the degree of anisotropy P due to uniaxial pressure τ for specimens with isothermal remanent magnetic saturation polarization in directions χ_1 and χ_3

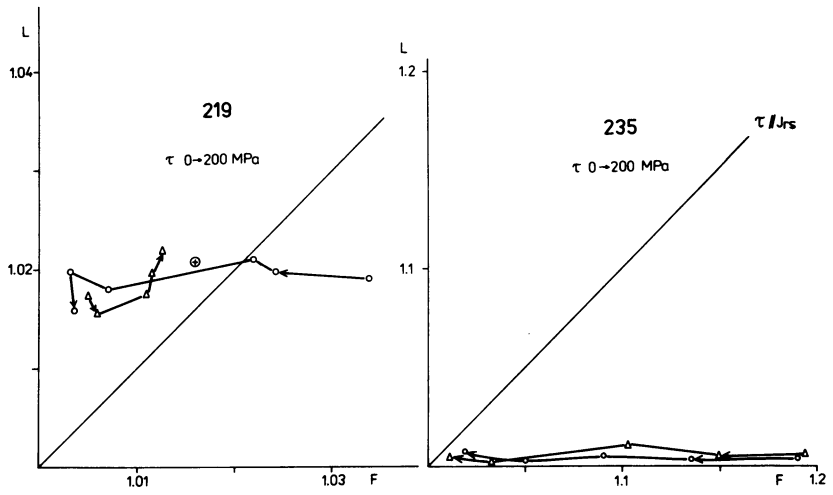

Fig. 3. Irreversible changes of the shape of the susceptibility ellipsoid due to pressure with J_{rs} in the direction of χ_1 (△), χ_3 (○). ⊕ – specimen 219 in original condition

the degree of anisotropy P due to the domain effect decreases with increasing stress for any direction of saturation. The absolute changes of P are ~18%. In all cases the changes of the degree of anisotropy are reversible in the sense that approximately the same anisotropic condition results from repeated saturation in the same direction.

Figure 2 shows the changes of orientation of the principal axes of susceptibility for specimens 235 and 219 as a function of stress. The (*a*) group of specimens displayed no change of orientation of the susceptibility ellipsoid over the whole range of stresses. The (*b*) and (*c*) type specimens display a quite similar tendency of changes: the direction of the minimum susceptibility is gradually changed by the increasing stress (in increments of 50 MPa) from that of the initial saturation remanent magnetic polarization until it is perpendicular to J_{rs}, the tendency of the changes of χ_1 being the opposite. The degree to which the orientation of the major axes of the ellipsoid changes, depends on the degree of anisotropy of the basalts due to the shape effect and it is largest for the isotropic specimens in the natural state.

The changes of the shape of the susceptibility ellipsoid due to uniaxial pressure for the specimens representing type (*b*) and (*c*) basalts are illustrated in the $L-F$ diagram in Fig. 3. The specimens of group (*b*) have qualitatively different changes of shape of the susceptibility ellipsoid with increasing stress for directions of the initial J_{rs} (and τ) parallel with χ_3 and χ_1. In the first case, the oblate ellipsoid changes to the prolate, in the second, the ellipsoid remains prolate for all stresses τ. But the changes of shape of the ellipsoid of specimen 235, which was isotropic before acquiring J_{rs}, are always characterized by a decrease of the parameter F which is analogous to the case of J_{rs} parallel to χ_3 of the anisotropic specimen 219. However, the isotropic condition is not achieved even for the highest values of τ, i.e. the curve of the gradual changes as a whole is located in the field of oblate ellipsoids.

The magnitude of the irreversible pressure changes of anisotropy depends on the orientation of the uniaxial stress τ and of the direction of the initial J_{rs} of the specimens with respect to one another. Figure 4 shows the changes of the degree of anisotropy $P=f(\tau)$ when the pressure is applied parallel and perpendicular to J_{rs}. Whereas the J_{rs}-direction was the same in both cases (e.g., parallel to χ_3 with specimen 219), the stress was applied along the direction of χ_3, on the one hand, and along the direction of χ_1, on the other. From the figure we can see that repeated magnetic saturation of the same specimen in the same direction, following deformation by pressure τ_{max} ~250 MPa, generates the same degree of anisotropy (see degrees of anisotropy for $\tau=0$ denoted as ● and ⊙). Whereas considerable changes in the degree of anisotropy take place by applying τ parallel to J_{rs} (a decrease of P by 3–16%), if the pressure is applied perpendicularly the initial degree of anisotropy remains practically constant, relatively small changes being observed only for high stress values.

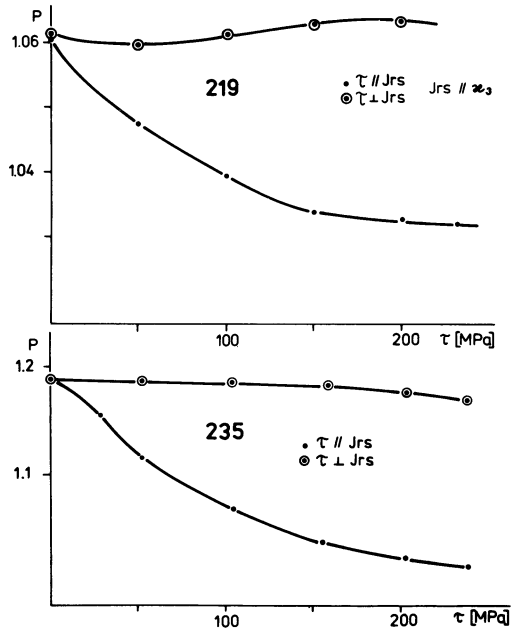

Fig. 4. Irreversible changes of the degree of anisotropy P due to pressure τ for parallel and perpendicular orientation of J_{rs} and τ

The pressure changes of anisotropy of magnetic susceptibility were compared with the changes due to the re-ordering of the domain structure of ferrimagnetic minerals by an AC magnetic field. An example of the functions $P=f(\tau)$ and $P=f(\tilde{H})$ for one basalt with its initial J_{rs} in the direction of χ_3 is shown in Fig. 5. The gradual change to the "antiparallel" domain structure was achieved by applying the AC field $\tilde{H}$ to the sample in stationary position ($\tilde{H}$

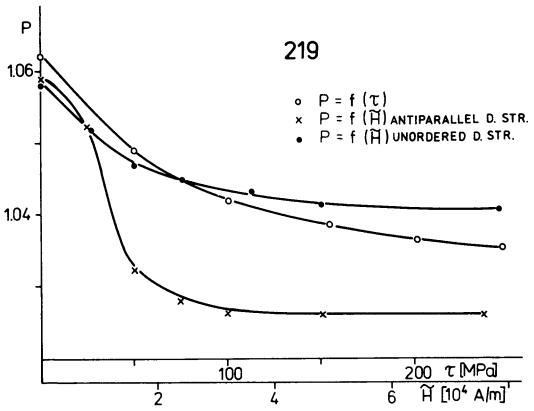

Fig. 5. Comparison of changes of the degree of anisotropy P due to pressure τ with the changes due to the re-ordering of the domain structure of the specimens caused by field $\tilde{H}$

parallel to J_{rs}), the change to the "unordered" domain structure by applying the AC field to the specimen rotating about three mutually perpendicular axes. The pressure changes of the domain structure, resulting in a change of the degree of anisotropy, are more of the nature of an "unordered" structure although deviations may be observed under stresses exceeding 150 MPa. If uniaxial pressure is applied, stabilization of the degree of anisotropy, which already occurs at AC magnetic field intensities of about $3\text{–}4 \times 10^4$ A m^{-1}, is not observed for stresses τ up to 250 MPa.

Discussion

The results presented above indicate that the anisotropy of magnetic susceptibility of basaltic rocks containing cation-deficient titanomagnetites, depends not only on the shape effect, i.e. on the degree to which the ferrimagnetic grains in the rock are ordered, but also on the domain structure of these minerals. If p is the concentration of the ferrimagnetic minerals, the directional susceptibility is then given by [Janák, 1977]

$$\chi = \frac{p\,\chi_i}{[1+(1-p)N\,\chi_i]}, \tag{1}$$

where χ_i is the intrinsic susceptibility of the ferrimagnetic mineral and N the effective value of the demagnetization factor. If we restrict ourselves to the elastic deformation in which irreversible changes of shape and orientation of ferrimagnetic grains do not occur in basalts, the observed changes of the directional susceptibilities and of the susceptibility anisotropy are caused by changes of the intrinsic susceptibility of ferrimagnetic grains.

The domain effect contributes to the overall anisotropy in that the minimum of directional susceptibility is associated with the direction of preferred orientation of the domains (i.e. the domains with magnetization in the J_{rs}-direction prevail) (Fig. 2). If we assume that the reversible susceptibility is due to the mechanism of reversible motion of domain walls (e.g. Kneller, 1962) the observed effect is caused by the 180° domain walls being in much more stable potential gaps after magnetic saturation, which decreases their mobility. The real domain structure of ferrimagnetic grains even in the case of saturation remanence, however, is not formed just by the simple structure of the 180°-walls in the direction of J_{rs} as a result of minimization of the overall energy; indeed closure domains with 71°-walls are formed in the first place (Bhathal and Stacey, 1969). The directional susceptibility perpendicular to the ordered domain structure is then determined by the mobility of these walls rather than by the rotation of the vector of spontaneous magnetization in the main domains.

Irreversible changes of the domain structure and, consequently, also irreversible changes of the susceptibility anisotropy occur as a result of external pressure. The qualitative differences in the functions $P=f(\tau)$ for various directions of J_{rs} in the specimens (Fig. 1) are due to the superposition of the shape and domain effects (Kapička, 1981).

The magnitude of the irreversible pressure changes of the susceptibility anisotropy varies from basalt to basalt and depends on the stability of their domain structure with respect to the weak AC field in which the susceptibility is being measured. The contribution of the domain effect is substantial in specimens with a hihger coercive force which is indicative of a considerable concentration of potential barriers restricting the mobility of domain walls (groups *a* and *b*). These basalts display a much larger stability of the domain walls in saturated condition than after pressure has been applied, when the domain walls are located in other potential gaps, energetically more advantageous. Specimen 235 with a conspicuously higher coercive force contains a considerably non-stoichiometric titanomagnetite characterized by a high degree of oxidation (Kropáček and Kapička, 1979). In specimens with small coercive force (group *c*) the stability of the domain structure in saturated state even after re-ordering by mechanical stress is practically the same and, therefore, the domain effect has a negligible influence on the susceptibility anisotropy.

The pressure changes of susceptibility anisotropy also depend substantially on the direction in which the uniaxial pressure is acting relative to the J_{rs} in the specimens. When τ was perpendicular to J_{rs}, practically no changes of the degree of anisotropy were observed even for quite large stresses τ (Fig. 4). Although the stress distribution close to the pressure surfaces of the specimens may be affected by the contact between the specimen and the press platens, we may assume that the stress acting in the direction of the applied uniaxial pressure is dominant in the sample as a whole. The various orientations of the stress and of the direction of the preferred ordering of the domains in the initial saturated state are responsible for the directional dependence of the pressure changes determined experimentally.

If we consider the stress field round the dislocations to represent a substantial part of the potential barriers limiting the motion of domain walls (Kinoshita, 1968; Carmichael, 1968), we find that the dislocation slip in certain crystallographic planes is caused by the applied stress. In cubic crystals with a spinel structure (magnetite, titanomagnetite) the slip planes are planes {111} with the slip direction [110]. The interaction energy of the stress field of the dislocation with the domain wall depends on the orientation of the slip plane and domain wall with respect to one another, and if an edge dislocation is involved, the appropriate relation reads (Vicena, 1955):

$$\Delta E = \tfrac{3}{4}\delta\lambda\, Gb\frac{1+\gamma}{1-\gamma}\sin\omega, \tag{2}$$

where δ is the width of the domain wall, λ is the magnetostriction coefficient, G the modulus of rigidity, γ Poisson's ratio, b Burgers vector and ω the angle between the slip plane of the dislocation and the perpendicular to the domain wall. For basaltic rocks containing titanomagnetites without crystallographic texture, homogeneously distributed throughout a non-magnetic matrix, one may assume that:

a the slip planes {111} are uniformly distributed in all directions;

b the component of the shear stress in the slip plane and slip direction, which is decisive for the motion of the dislocation, is largest if the applied stress is parallel to the slip plane.

The magnitude of the interaction energy of the dislocation with a 180°-system of domain walls in magnetically saturated condition depends on the angle ω characterizing the position of the dislocation slip plane in and domain walls with respect to one another. The stress applied perpendicular to the domain walls causes the dislocations which do not form effective potential barriers, fixing the positions of these walls, to move in the first place. Dislocations with non-zero interaction energy ΔE may only be re-ordered by stress oriented in another direction, the most effective being the stress parallel to the ordered domain structure.

The differences in the magnitude of the changes of degree of rock anisotropy due to uniaxial pressure and to the magnetic field are caused by slightly different mechanisms of both effects. The applied field affects the position of the domain walls directly. Assuming a constant distribution of potential barriers, the applied stress however affects it indirectly via the changed dislocation configuration and the changes in the distribution of the internal stress fields associated with it. If the applied stress is sufficiently large, the resultant domain pattern has the nature of a disordered structure because it is controlled by the distribution of the easy directions of magnetization [111] which can be considered as uniform in specimens without marked texture. The observed behaviour of the changes of the degree of anisotropy due to pressure, which is analogous to the changes of P due to the effect of the AC field on rotating specimens, i.e. to the change from directional ordering of domains to a disordered condition, also corresponds to this.

The investigation of irreversible changes of anisotropy of magnetic susceptibility due to pressure has proved that the contribution of the domain effect to the overall anisotropy in some rocks is substantial. In interpreting the pressure changes of susceptibility, or of its anisotropy, this effect should be considered together with the mechanism of rotation of the vector of spontaneous magnetization (e.g. Nagata, 1970) due to the applied stress.

References

Bhathal, R.S., Stacey, F.D.: Field-induced anisotropy of magnetic susceptibility in rocks. Pure Appl. Geophys. **76**, 123–129, 1979

Carmichael, R.S.: Remanent and transitory effects of elastic deformation of magnetite crystals. Phil. Mag. **17**, 911–927, 1968

Janák, F.: The determination of the content of ferromagnetic minerals in rock sample. Sbor. geol. věd UG. **14**, 153–162, 1977

Jelínek, V.: Statistická teorie měření anizotropie magnetické susceptibility hornin a její aplikace. Report ÚUG, Brno 1972

Jelínek, V.: Precision AC bridge set for measuring magnetic susceptibility and its anisotropy. Studia Geophys. Geod. **17**, 36–48, 1973

Kapica, S.P.: Magnetic properties of eruptive rocks under mechanical stresses (in Russian). Izv. AN SSSR, Geophys. Ser. **6**, 489–504, 1955

Kapička, A.: Změny magnetických vlastností bazaltů vlivem jednoosého tlaku. Ph.D. thesis, GFÚ ČSAV, Praha, 1978

Kapička, A.: Changes of anisotropy of the magnetic susceptibility of rocks induced by a magnetic field. Studia Geophys. Geod. **25**, 262–273, 1981

Kinoshita, H.: Studies on piezo-magnetization (II) – Change in the initial susceptibility of fine grain assemblage of ferromagnetics due to uniaxial compression. J. Geomagn. Geoelec. **20**, 75–83, 1968

Kneller, E.: Ferromagnetismus. Berlin, Göttingen, Heidelberg: Springer-Verlag 1962

Kropáček, V., Kapička, A.: Changes of stability of remanent magnetization with concentration of vacancies in titanomagnetites. Studia Geoph. Geod. **23**, 168–173, 1979

Nagata, T.: Magnetic susceptibility of compressed rocks. J. Geomagn. Geoelec. **18**, 73–80, 1966

Nagata, T.: Anisotropic magnetic susceptibility of rocks under mechanical stresses. Pure Appl. Geophys. **78**, 110–122, 1970

Nullman, A.A., Shapiro, V.A., Maksimovski, S.I., Ivanov, N.A., Kim, J., Carmichael, R.S.: Magnetic susceptibility of magnetite under hydrostatic pressure and implications for tectonomagnetism. J. Geomagn Geoelec. **30**, 585–592, 1978

Ohnaka, M., Kinoshita, H.: Effect of axial stress upon initial susceptibility of an assemblage of fine grains of $Fe_2TiO_4 - Fe_3O_4$ solid solution series. J. Geomagn. Geoelec. **20**, 107–110, 1968

Stacey, F.D.: Theory of the magnetic susceptibility of stressed rocks. Phil. Mag. **7**, 551–556, 1962

Vicena, F.: O vlivu dislokací na koercitivní sílu ferromagnetik. Czech. J. Phys. **5**, 492–510, 1955

Received May 7, 1982; Revised version April 11, 1983;
Accepted May 20, 1983

J Geophys (1983) 53:149–154

Journal of Geophysics

The 1977–1979 Geomagnetic Impulse: Its Induction Effect and Dependence on Magnetic Activity

H. Nevanlinna
University of Helsinki, Department of Geophysics, Fabianinkatu 24 A, SF-00100 Helsinki 10, Finland and
Finnish Meteorological Institute, Division of Geomagnetism, Box 503, SF-00101 Helsinki 10, Finland

Abstract. All-day and quiet-day annual means from 39 globally distributed observations were used to study further the 1977–1979 secular variation impulse. For the rising part (1977–1978) of the impulse the first order external and internal spherical harmonic coefficients for all-day secular variation were found to be 18 nT/a and 1.3 nT/a, respectively. For the decaying part (1979–1980) these values were 50% lower. A clear difference, up to 50%, was found between all-day and quiet-day amplitude. The difference was largest in H near the equator and in Z at high latitudes where observed amplitudes did not fit well with a distant ring-current field. These differences were probably due to more localized current systems such as equatorial and auroral electrojets. Using a spherical conductivity model of the Earth with a homogeneous inducing external field which grows and decays exponentially, a range from 5 S/m to 20 S/m was found for the electrical conductivity of the upper mantle down to 1,500 km.

Key words: Geomagnetic impulse – Secular variation – Magnetic activity – Induction

Introduction

Nevanlinna and Sucksdorff (1981) showed that in the late '70s there was a sudden enhancement (impulse) in the global "secular variation". The impulse started at the end of 1977 and ended at the beginning of 1980. Using the first order spherical harmonic (SH) coefficients they showed that the impulse was of external origin, probably due to a magnetospheric ring-current.

The observed annual means used by Nevanlinna and Sucksdorff (1981) mainly concerned the rising part (1977–1978) of the impulse. The decaying part (1979–1980) is analyzed in this paper. The effect of magnetic activity on the impulse amplitude is studied by means of all-day and quiet-day means from 39 observatories all around the globe.

Estimates of the electrical conductivity of the upper mantle are obtained by calculating the induction of an exponentially rising and decaying external impulse field on a homogeneous and spherical Earth with a constant electrical conductivity.

The Data

The data used were annual means of Z and H components for all-days and quiet days from 1973 to 1981 from 39 geomagnetic observatories listed in Table 1. To separate the impulse from long-term internal secular variation, a quadratic polynomial in time was fitted to the annual secular variation values for each observatory. The rising (1978–1977) and decaying (1980–1979) years were excluded from the fit (see Fig. 1). The amplitude of the impulse was then obtained by subtracting the polynomial value from the corresponding value for the differences 1978–1977 (rising part) and 1980–1979 (decaying part). As an example, Fig. 1 shows annual differences and the polynomial values of the Z component for the Nurmijärvi observatory ($\phi = 60°30'$ N, $\lambda = 29°39'$ E).

To calculate the first-order internal and external SH coefficients $\dot{g}_{1i}$ and $\dot{g}_{1e}$, respectively, the amplitudes ($\Delta\dot{Z}$ and $\Delta\dot{H}$) of the impulse at different geomagnetic colatitudes were fitted to the following equations:

$$\Delta\dot{Z} = C\cos\theta, \qquad \Delta\dot{H} = S\sin\theta \tag{1}$$

where

$$C = \dot{g}_{1e} - 2\dot{g}_{1i}, \qquad S = -(\dot{g}_{1e} + \dot{g}_{1i}) \tag{1'}$$

where θ is the geomagnetic colatitude. Using these equations, $\dot{g}_{1i}$ and $\dot{g}_{1e}$ can be calculated as follows:

$$\dot{g}_{1i} = -(C+S)/3, \qquad \dot{g}_{1e} = (C-2S)/3. \tag{1''}$$

Table 2 shows the values of C and S obtained by the least-squares fit. Also shown are the calculated values of $\dot{g}_{1i}$ and $\dot{g}_{1e}$.

The SH coefficients in Table 2 show the dominant external character of the impulse: the ratio external/internal is roughly 10. It can also be seen from Table 2 that the amplitudes C, S and $\dot{g}_{1i}, \dot{g}_{1e}$ for the rising part

Table 1. List of geomagnetic observatories used in the determination of the impulse amplitudes. ϕ is geographic latitude and λ east longitude, θ is geomagnetic colatitude

Observatory	Coordinates		
	ϕ	λ	θ
New Aalesund	78.9°N	11.9°E	14.8°
Bear Island	74.5	19.0	19.1
Leirvogur	64.2	338.3	20.0
Barrow	71.3	203.4	21.2
Tromsö	69.7	18.9	23.2
Cape Chelyuskin	77.7	104.3	23.8
College	64.9	212.2	25.1
Loparskaya	68.6	33.3	26.5
Dixon	73.6	80.6	27.1
Lerwick	60.1	358.8	27.8
Dombås	62.1	9.1	28.0
Tixie	71.6	129.0	29.6
Sitka	57.1	224.7	29.7
Eskdalemuir	55.3	356.8	31.8
Nurmijärvi	60.5	24.6	32.4
Rude Skov	55.8	12.5	34.4
Newport	48.3	242.9	34.7
Wingst	53.8	9.1	35.7
Niemegk	52.1	12.7	38.0
Moscow	55.5	37.3	39.4
Fredericksburg	38.2	282.6	40.4
Boulder	40.1	254.8	40.8
Odessa	46.8	30.9	46.6
Tucson	32.2	249.2	49.3
Memambetsu	43.9	144.2	55.9
Kakioka	36.2	140.2	63.9
Honolulu	21.3	202.0	68.6
Hyderabad	17.4	78.6	82.6
Guam	13.6	144.9	85.9
Huancayo	12.0S	284.7	90.5
Tsumeb	49.2	17.6	108.4
Hermanus	34.4	19.2	123.6
South Georgia	54.3	323.5	134.3
Port Alfred	46.4	51.9	141.6
Argentine Islands	65.3	295.7	143.7
Port-Aux-Francaise	49.4	70.2	147.6
Dumont Durville	66.7	140.0	165.6
Mirny	66.6	91.0	167.0
Vostok	78.5	106.9	179.5

of the impulse are roughly twice as large as for the decaying part. There is also a clear difference in amplitude between all-days and quiet-days, especially in the H component, where the difference is about 50% near the equator. In Z, the difference is largest at high northern and southern latitudes. Note that g_{1i} has the wrong sign for quiet-day means. This is partly due to inaccuracies in amplitude determinations, partly due to a rather high disturbance level of Z at high latitudes even during quiet days. This produces higher $\dot{Z}$ amplitudes (C) at high latitudes than $\dot{H}$ amplitudes (S) near the equator, thus $C+S$ in Eq. (1″) will be positive.

There is also a slight correlation between yearly secular variation and differences in magnetic activity index A_k as shown in Fig. 1 for the Nurmijärvi observatory. ΔA_k fluctuates in the same manner as the yearly secular variation during 1977–1979. However, changes in ΔA_k are not exceptionally larger than in earlier

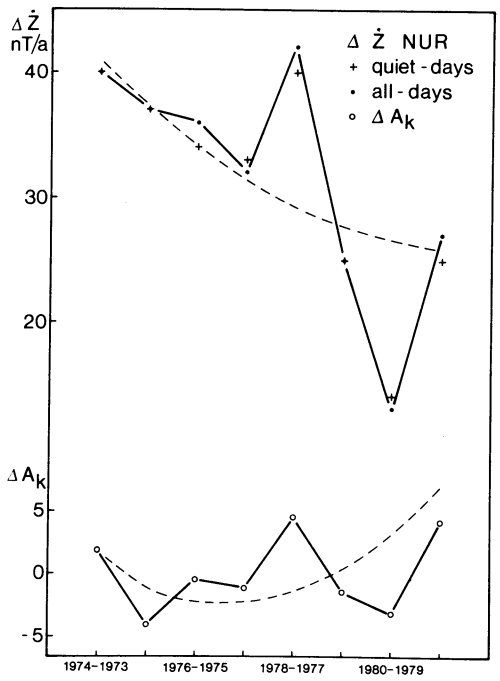

Fig. 1. *Top:* Yearly secular variation (all-days and quiet-days) of the Z component as observed at the Nurmijärvi Observatory. The broken line depicts all-day secular variation smoothed by a 2nd degree polynomial. *Below:* Differences in yearly means of the A_k-index and their smoothed values (broken line)

years. Note that Voppel (1982) has recently reported a correlation between yearly secular variation and changes in the A_p index.

Figures 2 and 3 show the observed amplitudes $\Delta\dot{H}$ and $\Delta\dot{Z}$ for each observatory. It can be seen that $\Delta\dot{Z}$ and $\Delta\dot{H}$ have opposite signs during the rising and decaying parts.

Induction by an External Magnetic Impulse

In this section the electrical conductivity of the upper mantle is estimated using the SH coefficients of the 1977–1979 impulse shown in Table 2. The assumption is that the Earth is a homogeneous sphere with a radius R_e. Inside the Earth there is a concentric conducting sphere (radius qR_e; $0 \leqq q \leqq 1$) with constant conductivity σ. The inducing external magnetic field is assumed to be a uniform field in the direction of the dipole axis of the Earth corresponding thus to the field of a distant equatorial ring-current. During the rising part of the magnetic impulse the external field $B = g_{1e}(t)$ increases exponentially with a time constant a^{-1} (see Fig. 5) as follows:

$$g_{1e}(t) = E_0[1 - \exp(-a\,t)] \tag{2}$$

where E_0 is the value of g_{1e} when $t = \infty$. At moment $t = t'$, the external field starts to decay with the same time constant as in Eq. (2); thus

$$g_{1e}(t) = E'_0 \exp[-a(t-t')]; \quad t \geqq t' \tag{2'}$$

where

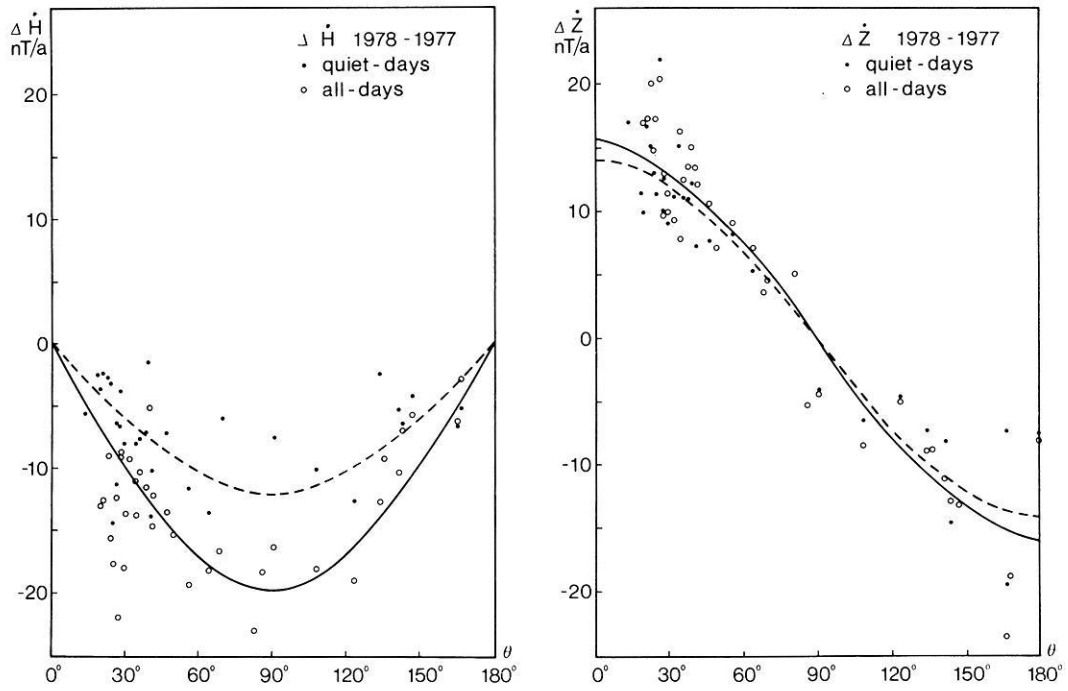

Fig. 2. All-day and quiet-day amplitudes ($\Delta\dot{Z}, \Delta\dot{H}$) of the rising part of the impulse as a function of dipole colatitude θ. Solid (broken) lines are the least-squares fits (see Eq. 1) of all-days (quiet-days)

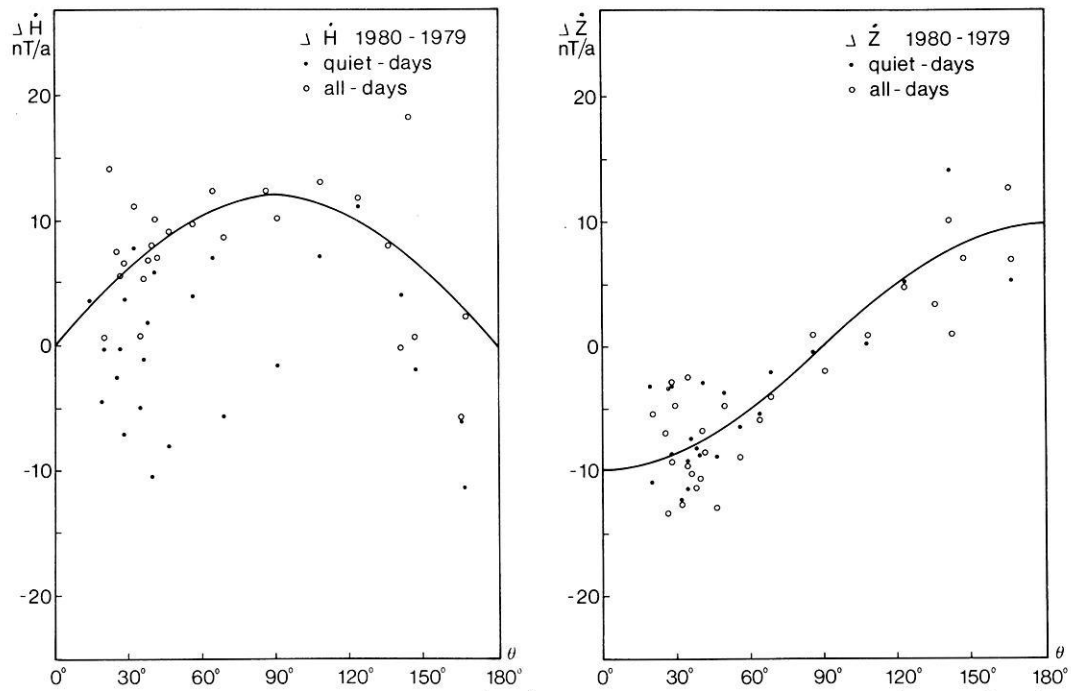

Fig. 3. All-day and quiet-day amplitudes ($\Delta\dot{Z}, \Delta\dot{H}$) of the decaying part of the impulse as a function of dipole colatitude θ. The solid line is the least-squares fit of all-day amplitudes (see Eq. 1)

$$E_0' = E_0[1-\exp(-a\,t')]. \tag{2''}$$

According to Chapman and Bartels (1940; Vol. II, p. 748), the induced magnetic field (g_{1i}) at the Earth's surface induced by any field $g_{1e}(t)$ can be written as follows:

$$g_{1i}(t) = \Phi(0)\,g_{1e}(t) + \int_0^t g_{1e}(t-u)\,(d\Phi(u)/du)\,du \tag{3}$$

where the function Φ is defined by

$$\Phi(u) = 3q^3 \sum_{s=1}^{\infty} \alpha_s \exp(-u/\alpha_s A) \tag{3'}$$

where

$$\alpha_s = (s\,\pi)^{-2}; \qquad A = \sigma\,\mu_0\,q^2\,R_e^2. \tag{3''}$$

Table 2. Amplitudes (C, S) and spherical harmonic coefficients (g_{1i}, g_{1e}) with standard deviations. Q denotes quiet-day and A all-day values, N is the number of observations used. The unit is nT/year

	Rising part 1977–1978				Decaying part 1979–1980			
	C	N	S	N	C	N	S	N
Q	14.0 ± 3.4	29	-12.2 ± 2.9	30	–	–	–	–
A	15.7 ± 3.5	39	-19.7 ± 3.9	34	-9.9 ± 3.1	28	11.9 ± 6.1	28
	g_{1e}		g_{1i}		g_{1e}		g_{1i}	
Q	12.8 ± 1.5		-0.6 ± 2.2		–		–	
A	18.4 ± 1.7		1.3 ± 2.8		-11.2 ± 2.3		-0.7 ± 4.2	

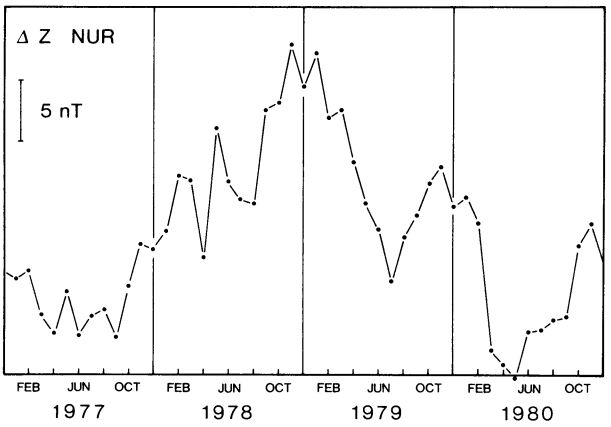

Fig. 4. All-day monthly values of the Z component at the Nurmijärvi Observatory after removing long-term secular variation

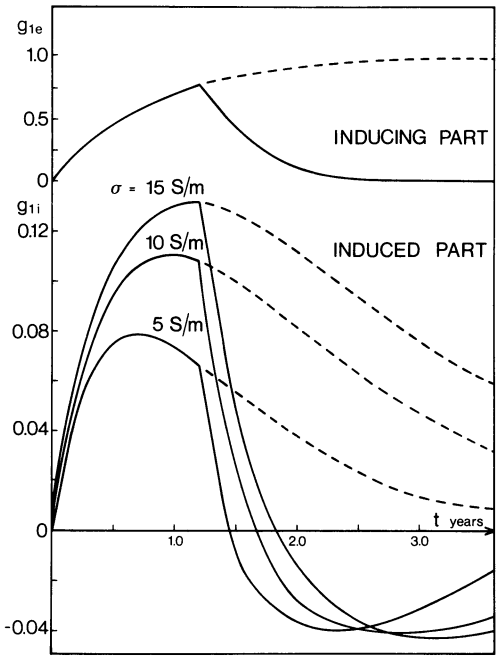

Fig. 5. *Top:* The exponential growth and decay of the inducing external magnetic field g_{1e}. The broken line shows the external field without decay. The values of $g_{1e}(t)$ are normalized so that 1.0 corresponds to $g_{1e}(\infty) = E_0$, see Eq. (2). *Below:* The induced part (g_{1i}) of the magnetic field as a function of time (t) when the conductivity (σ) is 5 S/m, 10 S/m and 15 S/m. Broken lines show the induced field when the external field alone grows

Using the exponential growth Eq. (2) of the impulse when $t \leqq t'$, Eq. (3) leads to:

$$g_{1i}(t) = 3q^3 E_0 \sum_{s=1}^{\infty} \alpha_s^2 [\exp(-t/\alpha_s A) - \exp(-a\,t)]/(\alpha_s - (Aa)^{-1}). \quad (4)$$

The solution of Eq. (3) when $t \geqq t'$ can be obtained if the integration in Eq. (3) is carried out first from $u = 0$ to $u = t - t'$ with g_{1e} from Eq. (2′) and then from $u = t - t'$ to $u = t$ with g_{1e} from Eq. (2). If the value of g_{1i} when $t \geqq t'$ is denoted by $g_{1i}(t)_{t \geqq t'}$, the solution of Eq. (3) is

$$g_{1i}(t)_{t \geqq t'} = g_{1i}(t) - g_{1i}(t - t'). \quad (5)$$

Note, that $g_{1i}(t)$ increases if the rising time of the impulse shortens (i.e., $a^{-1} \to 0$). Then we obtain from Eqs. (3) and (4)

$$\lim_{a \to \infty} g_{1i}(t) = E_0 \Phi(t); \quad t \leqq t' \quad (6)$$

Thus, at the moment $t = 0$, g_{1i} approaches its maximum value $(1/2)\, g_{1e}(0)\, q^3$ (because $q^{-3} \Phi(0) = 3 \sum_s (\pi s)^{-2} = 1/2$) which is independent of the conductivity.

Figure 4 shows details of the impulse based on monthly means of the Z component as observed at the Nurmijärvi observatory. It can be seen that the impulse started roughly in October 1977 and was at a maximum in December 1978 to January 1979, some 1.2 years later. The inducing external field (Eqs. (2) and (2′)) approximates to the observed global magnetic impulse in 1977–1979 when its time constant is fixed 10 months $(= a^{-1}$ in Eq. (2)). The model external field in Fig. 5 grows when $0 \leqq t \leqq t' = 1.2$ years and decays exponentially when $t \geqq t'$. Figure 5 also shows the induced part (g_{1i}) when $\sigma = 5$, 10 or 15 S/m. The radius of the conducting sphere is chosen to be $0.9\, R_e$, which is the same as in other studies with the same conducting model (e.g. Yukutake, 1965). The induced field in Fig. 5 grows rapidly after the onset of the external field. The maximum is attained in 0.5 to 1.2 years and the corresponding maximum amplitude is $0.08 E_0$ to $0.13 E_0$ (depending on the conductivity chosen), which is less than 30% of an infinitely rapid $(a^{-1} = 0)$ impulse (see Eq. (6)).

Table 3. Values of $\dot{g}_{1i}$ caused by changes in an exponential inducing field g_{1e}, as calculated for different values of the conductivity (σ) using a spherical conductivity model (radius $0.9\,R_e$). The unit is nT/year

	$\sigma=5$ S/m	$\sigma=10$ S/m	$\sigma=15$ S/m	obs.	
$\dot{g}_{1i}$	2.0	3.1	3.8	1.3	Rising part (1977–1978)
	−0.7	−1.8	−2.4	−0.7	Decaying part (1979–1980)
$\dot{g}_{1e}$	18.4	18.4	18.4	18.4	Rising part (1977–1978)
	11.2	11.2	11.2	11.2	Decaying part (1979–1980)

When the decay of the external field starts at $t=t'$, the induced field decreases to negative values within about 0.5 years. The decay is much slower than the growth because 3 years after the onset of the inducing field, the induced field is still more than 30% of its maximum value.

Table 3 shows values of $\dot{g}_{1i}$ and $\dot{g}_{1e}$ as calculated from Eqs. (2), (2′) and (5). These values are differences between successive one-year mean values of g_{1i} and g_{1e}, respectively. In Fig. 5, g_{1e} varies between 0 and 1, but for Table 3, $\dot{g}_{1e}$ was normalized to correspond to the observed 1978–1977 difference 18.4 nT/a. Using this normalization we get the value 11.2 nT/a for the difference 1980–1979, which is the same as observed (see Table 2).

As can be seen in Table 3, induction with the conductivity value 5 S/m seems to produce $\dot{g}_{1i}$ values which fit rather well with the observed ones. However, if we include the error limits of observed $\dot{g}_{1i}$ shown in Table 2, conductivity values up to 20 S/m are inside the error range.

Figure 6 was drawn to estimate the depth range in which induction occurs. It shows the attenuation of the induced currents in the conducting sphere as a function of the penetration depth. The current density (j) at different depths can be calculated from the following equation which is a modified formulation of Eq. (88) by Chapman and Bartels (1940; Vol. II, p. 746)

$$j=3E_0(\sigma/8\pi)q^2R_e^2r^{-3}\sin\theta\Big[F(k^2r^2)k^{-2}\cdot\exp(-a\,t)/\sinh(k^2q^2R_e^2)+2\sum_{s=1}^{\infty}F(k_s^2r^2)\exp(-t/\alpha_s A)/[(k^2-k_s^2)F(k_s^2q^2R_e^2)]\Big] \quad (7)$$

where

$$k^2=\mu_0\sigma a,\qquad k_s^2=(\pi s)^2q^{-2}R_e^{-2},\qquad F(x)=\cosh(x)-x^{-1}\sinh(x). \quad (7')$$

Figure 6 shows the current density j 0.5 years after the onset of the magnetic impulse. It can be seen that at a depth of 1,000 km 400 km inside the conducting sphere, the current density is roughly 50% of its surface value, and the attenuation is almost the same for all conductivity values studied here. At a depth of 1500 km only 10% of the current is left. Thus, we can conclude that the mean conductivity of the upper mantle down to 1,500 km is 5...20 S/m. This estimate of mantle conductivity is of the same order as found by several other methods by various authors and summarized by Price (1967).

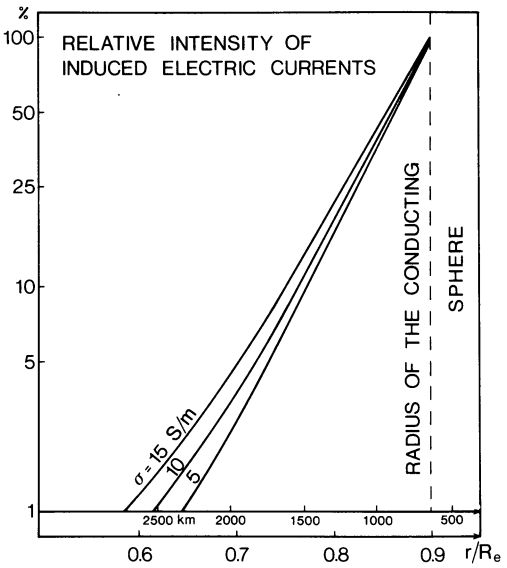

Fig. 6. Attenuation of electric currents as a function of depth 0.5 years after the onset of the impulse. At the surface of the conducting sphere at $0.9\,R_e$ the intensity of the current is normalized to 100%

Discussion

The present study on the 1977–1979 geomagnetic impulse shows that the impulse had up to 50% larger amplitudes for all-day means than for quiet-days. The difference is largest in the H component near the equator and in the Z component at high latitudes. All-day annual means differ at the maximum 10 nT/a from the corresponding quiet-day values. Thus, in studies on internal secular variation, quiet-day means are preferable as they are not as contaminated by external sources. But quiet-day values also seem to contain enough external contamination to make them unreliable, at least during some years, for the study of the internal secular variation.

Consideration of the reason for the 1977–1979 impulse is beyond the scope of this paper. The impulse, as observed on Earth's surface, behaves like an enhancement in the magnetospheric ring-current. However, at high latitudes and near the equator, the observed amplitudes of the impulse do not fit the idealized distant ring-current field. These discrepancies are probably due to more localized sources such as polar and equatorial electrojets.

External magnetic impulses like the one studied here, are useful in studies on electrical conductivity of the mantle. Unfortunately, the large scatter in impulse amplitudes at different observatories and the uneven distribution of observatories between the hemispheres make conductivity estimates uncertain. The conduc-

tivity range obtained in this study, 5 ... 20 S/m, for the upper 1,500 km of the mantle supports earlier results presented in the literature.

Acknowledgements. The author expresses his gratitude to the magnetic observatories listed in Table 1 for their valuable contribution in sending the annual and monthly mean values used in this study. This study received financial support from the Sohlberg's Delegation of the Finnish Scientific Society, which is gratefully acknowledged.

References

Chapman, S., Bartels, J.: Geomagnetism II. Oxford Univ. Press 1940

Nevanlinna, H., Sucksdorff, C.: Impulse in global "secular variation", 1977–1979. J. Geophys. **50**, 68–69, 1981

Price, A.T.: Electromagnetic induction within the Earth. In: Physics of the Geomagnetic Phenomena I, S. Matsushita and W. Campbell, eds.: pp. 235–295. New York and London: Academic Press 1967

Voppel, D.: On the external part of the geomagnetic secular variations of *D* and *H* at Wingst observatory. Dt. Hydrogr. Z. **35**, 169–176, 1982

Yukutake, T.: The solar cycle contribution to the secular change in the geomagnetic field. J. Geomagn. Geoelectr. **17**, 289–310, 1965

Received March 11, 1983; Revised version June 20, 1983
Accepted June 21, 1983

J Geophys (1983) 53:155–162

Journal of Geophysics

Observation of Gravity Changes During the Passage of Cold Fronts

T. Müller[1] and W. Zürn[2]

Geophysical Institute, University of Karlsruhe, Hertzstr. 16, D-7500 Karlsruhe, Federal Republic of Germany

Abstract. Clear observations of small but abrupt changes in gravity during the passage of cold fronts are reported. Instrumental effects can be ruled out by special experiments. Simple models for the atmosphere show that the direction and the order of magnitude of the observed effects can be explained by changes in gravitational attraction of the sensor mass by the atmosphere or by downward acceleration of the ground due to the increasing air pressure. This is additional evidence for the high importance of meteorological causes for long-period seismic noise.

Key words. Gravity changes - Cold front - Seismic noise

Introduction

Meteorological phenomena are well known to be a major source of noise in measurements of ground motion. Research in earth tides has identified several physical mechanisms by which meteorological variables cause signals on gravity-, tilt- and strainmeter records (e.g. Slichter et al., 1979; Warburton and Goodkind, 1977; Große-Brauckmann, 1979; Herbst, 1976; Zschau, 1979; Agnew, 1979). Seismologists have also studied noise from meteorological sources and have concluded that these dominate at periods longer than about 40 s (e.g. Sorrells, 1971; Sorrells et al., 1971; Ziolkowski, 1973). Kisslinger (1960) studied seismograms showing effects associated with the passage of tornadoes.

This paper presents further evidence for the importance of meteorological noise in seismic records especially in the free mode band. Simple models of cold fronts help to understand the measured effects.

Observations

The LaCoste-Romberg Earth-Tide gravimeter ET 19 at Schiltach Observatory ($\varphi = 48° 20' N$, $\lambda = 8° 19' E$; Mälzer, 1976) is equipped with electrostatic feedback and is very similar to the IDA instruments (Agnew et al., 1976). Its output is bandpass filtered for the recording of seismic mantle waves and free modes of the Earth. The frequency response of this system is identical to the UCLA ultralong-period seismometer described by Nakanishi et al. (1976). The cutoff periods (−3 dB) are 120 and 7,200 s, respectively, for this channel and its response to a step in gravity (vertical acceleration) is shown in Fig. 1. The output signal is recorded digitally as well as on a monitor chart recorder with a speed of 2 or 3 cm/h. Temperature, precipitation and the variations of local atmospheric pressures inside and outside the mine are recorded on analog charts at 3 cm/h. The interior of the mine is separated from the outside by an airlock (Heil, 1983).

With very few exceptions (instrumental gliches once or twice per year) transient disturbances on the filtered output of the gravimeter are clearly correlated with barometric pressure changes outside the mine. Sinusoidal barometric pressure waves produced sinusoidal oscillations of the gravity record provided the frequency was in the filter passband. Steplike changes in barometric pressure produced signals resembling closely the free

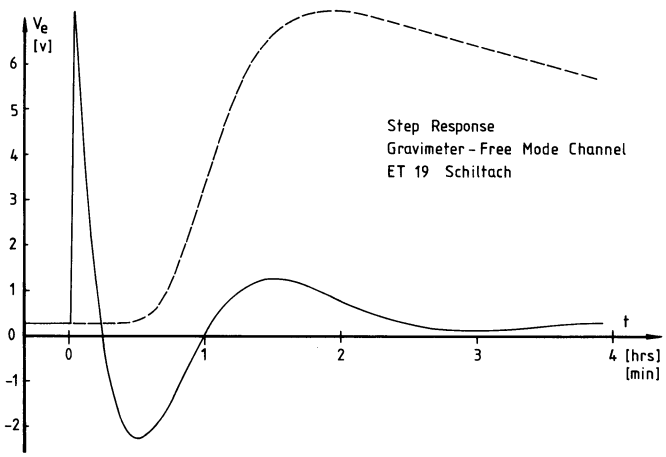

Fig. 1. Response of the free mode channel of LaCoste-Romberg tidal gravimeter ET 19 with electrostatic feedback. A sudden decrease in gravity of 10 μgal was simulated by instantaneously adding 110 mV to the feedback voltage. The step occurred at most one second after $t = 0$. Time scale in hours for solid line, in minutes for broken line

1 Present address: Prakla-Seismos, Postfach 510530, D-3000 Hannover 51, Federal Republic of Germany

2 Permanent address: Schiltach Observatory, Heubach 206, D-7620 Wolfach, Federal Republic of Germany

Offprint requests to: W. Zürn

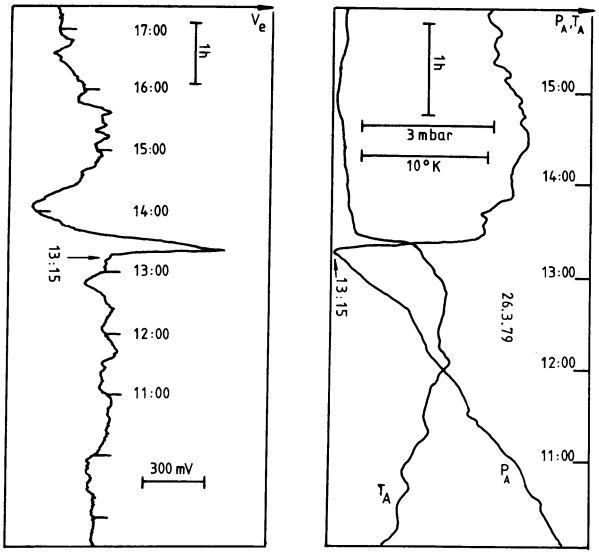

Fig. 2. Cold front passage on 26 March 1979. Simultaneous analog records of external pressure p_A, temperature T_A (*right*) and gravimeter output voltage V_e (*left*). In the center of the passband the sensitivity is 805 mV/μgal. Different time scales were used and time is increasing from bottom to top

mode channel's step response. Figures 2 to 5 and 11 show examples. The more the pressure change resembles a step, the closer the gravimeter output looks like the response to a step in gravity (Fig. 1). Figures 2, 3 and 4 show selected signals associated with the passage of cold fronts. The weather maps for times bracketting our signals confirm, that in each case a cold front was indeed moving through SW-Germany.

The polarity of the pulses always corresponded to a decrease in gravity when outside pressure increased. In Fig. 3 the detrimental effect of such a cold front pulse on the recording of free oscillations of the earth excited by an earthquake about 14 h earlier is demonstrated.

Figures 4 and 5 show more complicated behaviour of atmospheric pressure associated with thunderstorm activity. Every large disturbance has its clear counterpart in the gravity record. Figure 6 shows, for comparison, the signals in three components from the very-long period channels of Wielandt-Streckeisen seismometers (Wielandt and Streckeisen, 1982). The signals on the horizontal components are about ten times larger than on the vertical components. Figure 11 shows a fine example of quasiperiodic pressure variations and their effect on gravity due to the pressure wave from the

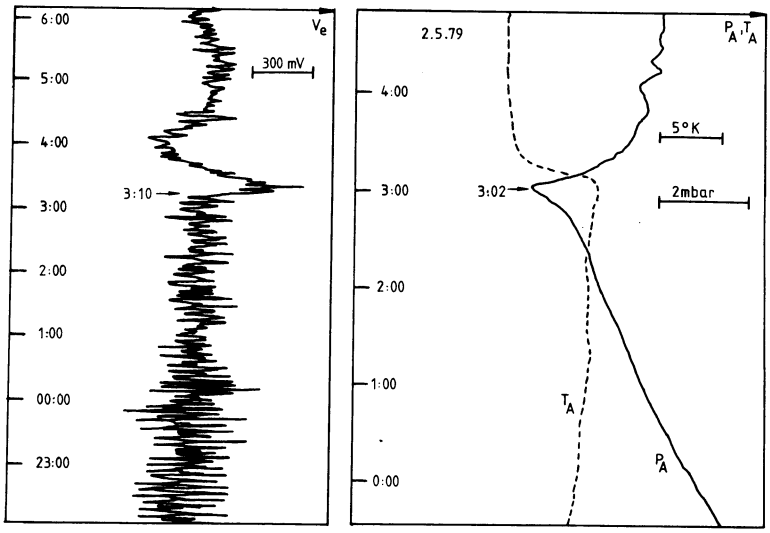

Fig. 3. Cold front passage on 2 May 1979. Simultaneous analog records of external and internal pressures p_A, p_i and temperature T_A (*right*) and gravimeter output voltage V_e (*left*). Different time scales were used and time increases from bottom to top. The cold front effect is superimposed on decaying free oscillations of the Earth excited by an earthquake in the Loyalty Islands region ($m_b = 7.2$; Origin time 13:03:37.1, 1 May)

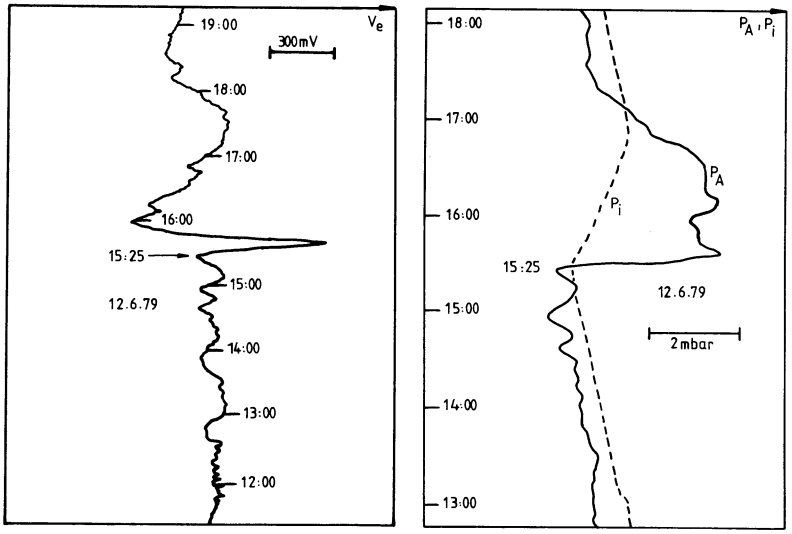

Fig. 4. Same as Fig. 2 and 3 for cold front passage on 12 June 1979. Note the difference in gravimeter response to the rise and fall-off of pressure. The reaction to the rise is a step-response, while the reaction to the fall-off is very smooth. The time scale of the fall-off is a factor of five larger than for the rise and most of its energy lies outside the passband of this channel

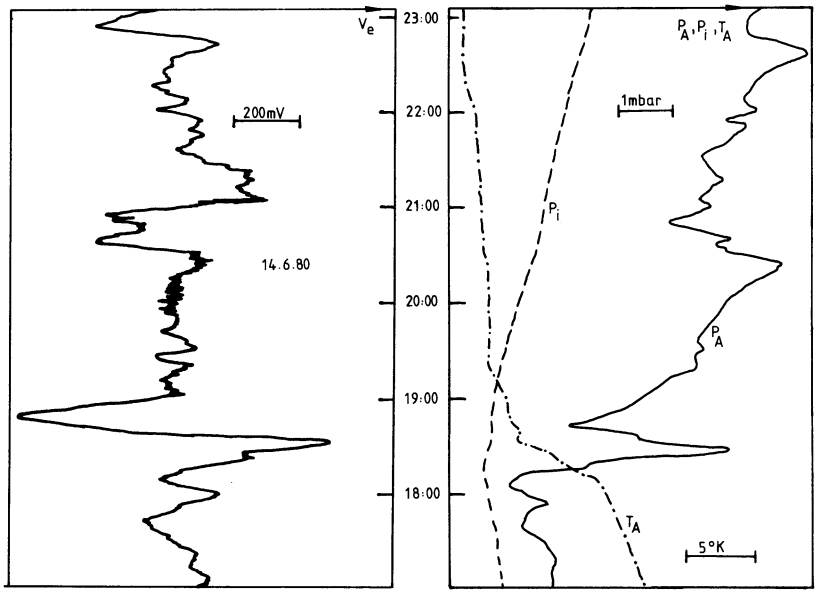

Fig. 5. Same as Figs. 2, 3 and 4 for cold front passage on 14 June 1980 associated with thunderstorms. Correlation between p_A and V_e is quite clear. The records of p_i and p_A demonstrate the lowpass properties of the air-lock

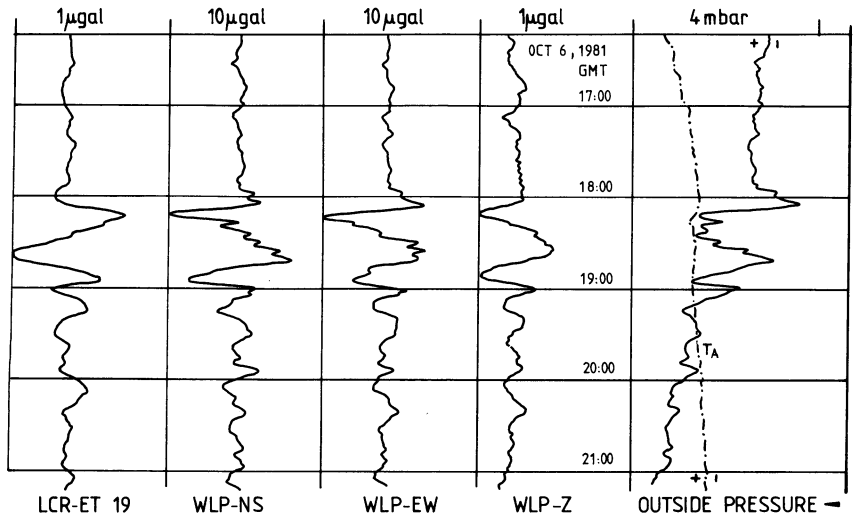

Fig. 6. Simultaneous records of outside pressure p_A and temperature T_A (analog, *right*) and bandpassed vertical and horizontal accelerations (reproduced from digital tape). The traces denoted WLP are from three Wielandt-Streckeisen seismometers (very long period channels). Scales are only valid for center of passbands, different scales for vertical and horizontal components are used. Polarity is reversed between WLP-Z and LCR-ET 19 and small differences in the response of these two vertical components are due to differences in the transfer functions of these instruments

Mount St. Helens eruption of May 1980 (see also Ritsema, 1980; Bolt and Tanimoto, 1981; Bath, 1982).

On Figs. 4 and 5 the temporal variation of inside pressure p_i can also be seen. There are at most minute changes of pressure near the instruments and we demonstrate in the next section that these cannot cause the observed effect.

The direct output of the gravimeter (tidal channel) has 70 times less amplification (at much larger bandwidth), therefore we could not detect the pressure induced transients on the tide records. Also we could never detect pulses during the passage of warm fronts, in this case pressure changes very smoothly.

Gravimeter Sensitivity to Ambient Air Pressure Changes

A variety of physical mechanisms could allow variations in ambient air pressure to produce apparent gravity variations at the output of the instrument: deformation of the instrument case, thermal deformations caused by pressure-induced temperature variations, imperfect sealing and buoyancy compensation etc. Two types of experiments were performed to detect such a sensitivity to ambient air pressure.

An air-lock with a time constant of about 4 h (Heil, 1983) separates the interior of the mine from the outside. Fast pressure variations are reduced appreciably in the interior (see Figs 3, 4 and 6), while slow pressure variations are only slightly attenuated and delayed in phase.

When outside pressure (p_A) changes steadily for some time this phase lag leads to small, time-dependent pressure differences across the air-lock. If, in this situation, both doors of the lock are opened, inside pressure p_i changes to outside pressure immediately. In this way steps Δp_i of a few mbars can be produced at constant p_A. Such tests were carried out several times with steps of $\Delta p_i \sim 2$–7 mbars without any indication of a response of the instrument, one example is shown in Fig. 7.

Another test was performed by opening the valves of two large cylinders of compressed air in the interior

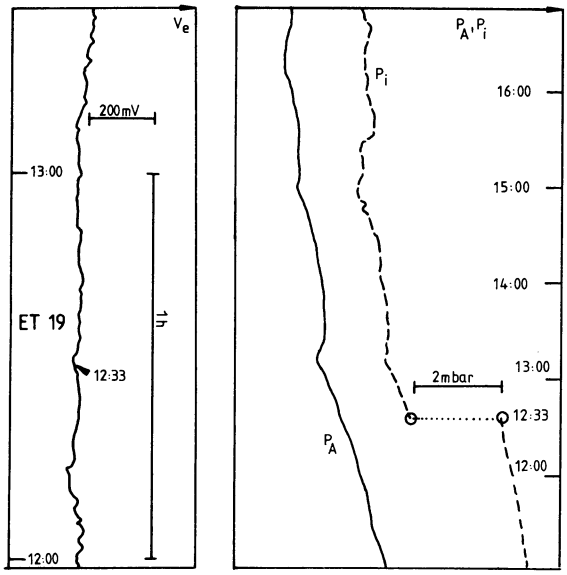

Fig. 7. Same as Fig. 2, 3, 4 and 5 for air-lock test at 12:33 GMT. There is no reaction in the gravity record for this step in p_i of about 2 mbar

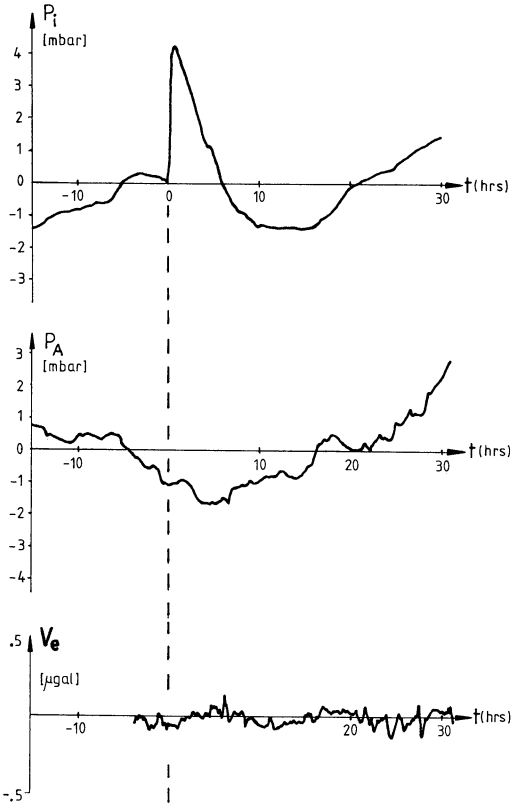

Fig. 8. Release of compressed air in the interior of the mine. Simultaneous records of inside and outside pressure, p_i and p_A and gravimeter output converted to μgal. Gravimeter does not react visibly, although the rise time of the transient in p_i is 30 min, in the passband of the free mode filter

with the air-lock closed. This caused a quick rise in inside pressure and a slow drop because of the long time-constant of the air-lock (for more details see Heil, 1983). As is seen in Fig. 8 the gravimeter did not respond to this pulse in Δp_i either.

For changes of outside pressure of the same order of magnitude there clear signals. Therefore instrumental sensivity to ambient air pressure can be ruled out as an explanation of the observations. These must be due to Newtonian attraction and/or crustal deformation by the changing atmosphere.

Models of Cold Fronts

Contributions to gravity from Newtonian attraction and crustal deformation by air masses were evaluated for the temporal change of density in an otherwise constant layer of air by Slichter et al. (1979), for moving vertical circular cylinders of air (pressure cells) by Warburton and Goodkind (1977), Block and Moore (1966) and Müller (1981) and for spherical harmonic distribution of air pressure by Spratt (1982). In all cases it turned out that for a gravimeter the effect of Newtonian attraction is 5 to 10 times larger than the effect of crustal deformation. However, all these models appear inadequate to describe the transient effects of moving fronts.

Our models consist of two isothermal air masses above ($z>0$) a rigid Earth separated by either a sharp vertical plane or a sharp hyperbolic surface. The gravimeter rests at $x=x_A$, $y=z=0$. The density of each air mass is assumed to vary with height z according to:

$$\rho(z)=\rho_0 \exp(-z/H) \tag{1}$$

where $H=7.99\cdot 10^3$ m is the scale height used. The models are depicted in Fig. 12.

The two air masses differ only by their densities ρ_0 at ground level (ρ_+-cold air, ρ_--warm air). The intersection of the front with the surface is x_F with cold air at $x \leqq x_F$. The models are two-dimensional, no model property depends on y; the front later moves in the positive x-direction with speed v_F. The gravitational attraction of this atmosphere at the site of the gravimeter (gravity positive downward):

$$g(x_A) = -G \int_{z=0}^{\infty} \int_{x=-\infty}^{\infty} \int_{y=-\infty}^{\infty} \frac{\rho_0(x) \exp(-z/H)\, z\, dx\, dy\, dz}{([x-x_A]^2+y^2+z^2)^{3/2}} \tag{2}$$

where G is the gravitational constant.

In our first model the front is a vertical plane ($x=x_F$). In this case the integral Eq. (2) can be evaluated analytically. The result is (see Appendix):

For $x_F-x_A=a \geqq 0$

$$g(x_A) = -2GH\rho_+ \cdot \left\{\pi + \left(1-\frac{\rho_-}{\rho_+}\right)\left\{\mathrm{ci}\left(\frac{a}{H}\right)\sin\left(\frac{a}{H}\right) + \mathrm{si}\left(\frac{a}{H}\right)\cdot\cos\left(\frac{a}{H}\right)\right\}\right\}, \tag{3a}$$

and for $x_F-x_A=a \leqq 0$

$$g(x_A) = -2GH\rho_+ \cdot \left\{\pi\frac{\rho_-}{\rho_+} - \left(1-\frac{\rho_-}{\rho_+}\right)\left\{\mathrm{ci}\left(\frac{|a|}{H}\right)\sin\left(\frac{|a|}{H}\right) + \mathrm{si}\left(\frac{|a|}{H}\right)\cos\left(\frac{|a|}{H}\right)\right\}\right\}, \quad (3b)$$

where

$$\mathrm{ci}(x) = \int_x^\infty \frac{\cos u}{u}\,du,$$
$$\mathrm{si}(x) = -\int_x^\infty \frac{\sin u}{u}\,du \quad (4)$$

are modified cosine and sine integrals. The functions $g(x_A)$ is symmetrical about the point $x_A = x_F$, $g(x_F) = -GH\pi(\rho_+ + \rho_-)$ and has the asymptotic values $-2GH\pi\rho_-$ for $x_A \gg x_F (a \ll 0)$ and $-2GH\pi\rho_+$ for $x_A \ll x_F (a \gg 0)$. The latter expressions correspond to the gravitational attraction at the bottom of either an isothermal atmosphere (Eq. (1)) with infinite extent or a homogeneous atmosphere ($\rho = \mathrm{const} = \rho_0$) with finite vertical extent H.

The second model uses a more realistic shape of the front, which is now a branch of a hyperbola given by:

$$x_F(z) = -a_1[(1 + z^2/a_2^2)^{1/2} - 1] + x_F(0) \quad (5)$$

where a_1, a_2 are parameters of the hyperbola describing the slope $s = a_1/a_2$ for large z and the distance a_1 between the intersections with the ground level of the hyperbola and its asymptote ($2a_1$: transverse axis, $2a_2$: conjugate axis of hyperbola). This simulates how the cold air near the front is underlying the less dense warm air. A typical slope is $s = 100$ (Liljequist and Cehak, 1979). For this model the final integration over z (Eq. (A4)) has to be done numerically, because $x_F = x_F(z)$. The step size used was $\Delta z = 25$ m and the integration was truncated at an altitude of 30 km. This truncation leads to an error of about 10% in the total signal for an infinite isothermal atmosphere, our model is physically doubtful at this level anyway. The curvature of the front near ground level, defined by a_1 and a_2 has a strong influence on the gravity signal, because it modifies the abruptness with which cold air replaces warm air directly above the gravimeter. We chose $a_1 = 300$ km by comparison with meteorological literature (Liljequist and Cehak, 1979).

Both models result in a function which depends on the relative positions of the front and the gravimeter $x_F(0) - x_A$. If the front moves with velocity v_F along the x-direction, the gravimeter senses a gravity variation with time $\Delta g(x_A, t)$ in Fig. 9 and 10. These time functions were convolved with the step response of the instrument (Fig. 1) to yield its output signal $V_e(t)$. Figure 9 and 10 show results for the vertical and hyperbolic front models, respectively. Typical front velocities are of the order of 10 to 20 ms^{-1} (Müller, 1981). As Fig. 9 shows the speed of the front is an important factor for the amplitude of the transient because of the limited bandwidth of the instrument.

The amplitude of the pulse for a given model depends linearly on the density difference at ground level $\Delta\rho = \rho_+ - \rho_-$. For the observed transients the observed

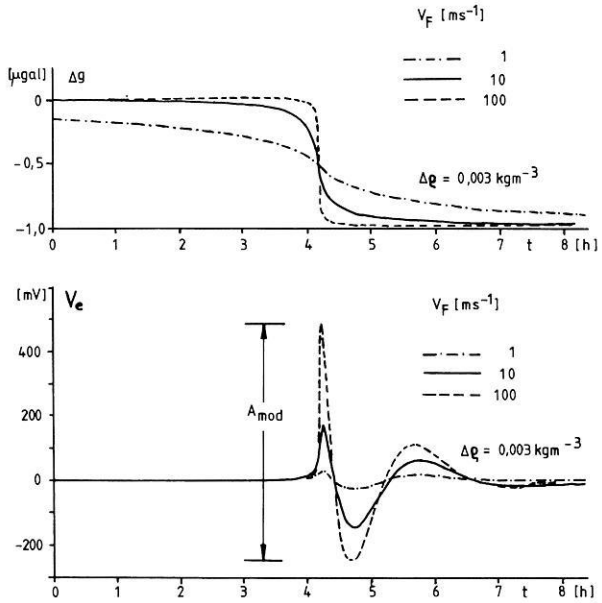

Fig. 9. Cold front model with vertical plane boundary. Top: change of gravity as sensed by the gravimeter mass as a function of time computed for $\Delta\rho = 0.003$ kg m^{-3} and three different front speeds. Corresponding signals at the free mode output are shown at the bottom (805 mV/μgal). Amplitudes A_{mod} are used in Table 1

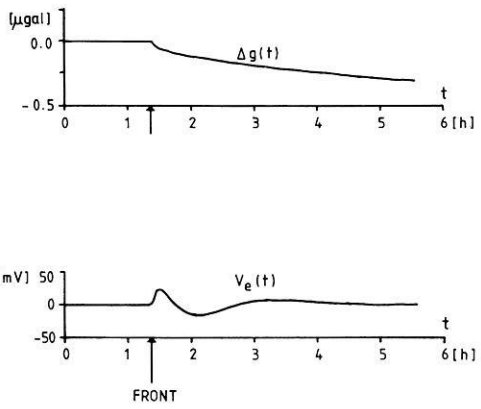

Fig. 10. Cold front model with hyperbolic front using $\Delta\rho = 0.003$ kg m^{-3}, $v_F = 10$ ms^{-1}, $s = 100$ and $a_1 = 3 \cdot 10^5$ m. Otherwise same as Fig. 10. The amplitude of the signal in this case is much lower than for the model in Fig. 9

pressure increase and temperature drop at the passage of the front were used to compute $\Delta\rho$ from the ideal gas law:

$$P_A/\rho_0 = R \cdot T_A. \quad (7)$$

In Table 1 we compare measured peak-to-peak amplitudes A_{obs} for clear cold front passages (like in Fig. 2 and 3) with amplitudes computed as described above for the hyperbolic model using $v_F = 10$ ms^{-1}, $a_1 = 300$ km and $s = 100$ and $\Delta\rho$ computed by Eq. (7). The ratio of observed to computed amplitudes is close to one in all cases. Of course, this agreement must be considered to be somewhat fortuitous because of the assumptions and simplifications implied in the model. But this clearly shows that Newtonian attraction alone

Table 1. Comparison of observed and computed peak-to-peak amplitudes of gravimeter response to cold front passages with simple temporal pressure changes. Δp, ΔT and A_{OBS} are observed data; Δp is computed using the ideal gas law Eq. (7) and A_{MOD} is computed as described in the text for the hyperbolic front model ($\Delta\rho$, $s=100$, $a_1=3\cdot10^5$ m, $v_F=10\,\mathrm{ms}^{-1}$)

Date	Δp_A [mbar]	$-\Delta T_A$ [°K]	$\Delta\rho$ [kg·m^{-3}]	A_{obs} [mV]	A_{mod} [mV]	A_{obs}/A_{mod}
16Mar 1978	2.1	5.7	0.030	525	630	0.83
26 Mar 1978	2.9	4.2	0.024	615	504	1.22
11 Sep 1978	2.7	5.0	0.028	645	588	1.10
9 Mar 1979	2.7	3.5	0.016	495	336	1.47
26 Mar 1979 (Fig. 2)	3.3	7.5	0.041	960	856	1.12
2 May 1979 (Fig. 3)	2.4	6.2	0.032	720	672	1.07
15 Dec 1979	1.7	3.2	0.018	500	378	1.32
2 Apr 1980	1.3	2.7	0.014	380	294	1.29

can account for shape, amplitude and polarity of the observations.

Other contributions to the gravity change sensed by the gravimeter are produced by downward displacement of the surface of the Earth by increasing air pressure:

a) downward motion of the gravimeter in the Earth's gravity field, $\Delta g=-\Delta z\cdot(\partial g/\partial z)_0$;

b) downward displacement of the equipotential surfaces of the Earth's gravity field due to the displaced masses;

c) the inertial effect on the gravimeter mass by the downward acceleration, $\Delta g=(d^2\Delta z/dt^2)$.

The first effect causes an increase, the last two a decrease in gravity. From the observations it is clear that either Newtonian attraction or effects *b* and *c* overwhelm effect *a*. At periods much less than one hour, effect *c* is larger than effect *a* for any displacement, given the gradient of gravity is not much larger than 300 μgal/m. For these reasons the inertial effect (*c*) only must be considered as an alternative explanation, at least for higher frequencies.

For the cold front passages it is impossible to estimate the peak downward acceleration of the ground from the local pressure record. However, an estimate for the quasi-sinusoidal pressure variations in Fig. 11 can be derived. Sorrels (1971, Eq. (24)) has calculated the vertical displacement at the surface of an isotropic, homogeneous elastic halfspace (Lamé parameters λ, μ) due to a pressure wave of amplitude P_0, frequency $\omega_0/2$ and speed C_0 propagating in *x*-direction under the assumption that $C_0 \ll v_s, v_p$ (elastic velocities of the halfspace)

$$W=\frac{C_0 P_0(\lambda+2\mu)}{2\mu(\lambda+\mu)}\frac{1}{|\omega_0|}\cdot\exp(i\omega_0(t-x/C_0)). \tag{8}$$

The peak acceleration is then:

$$|\Delta g_{\max}|=\left|\frac{d^2w}{dt^2}\right|_{\max}=C_0\omega_0 P_0\frac{\lambda+2\mu}{2\mu(\lambda+\mu)}. \tag{9}$$

From Fig. 11 we get for the largest signal with $\lambda=\mu$, $\mu=2.3\cdot10^{10}\,\mathrm{kg\,m^{-1}\,s^{-2}}$ (granite $V_p=5.2\cdot10^3\,\mathrm{ms}^{-1}$, $\rho=2.6\cdot10^3\,\mathrm{kgm}^{-3}$), $P_0=0.23\cdot$mbar, $C_0=308\,\mathrm{ms}^{-1}$,

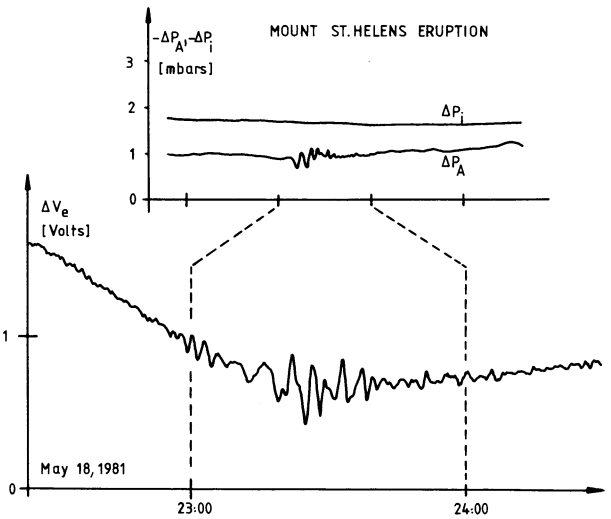

Fig. 11. Simultaneous records of p_A and V_e (805 mV/μgal) on 18 May 1980. The pressure wave from the eruption of Mount St. Helens can clearly be seen on the pressure and gravity records. The first arrival corresponds to a velocity of 308 m s^{-1} along the great circle. The wave train arriving shortly before 23:00 GMT is probably Rayleigh wave R_2 from an earthquake in Yugoslavia ($m_s=5.8$, *O.T.* 20:02:57.5); the long period trend is from nonlinear gravimeter response to R_1 of that quake

$2\pi/\omega_0=4.33$ min a peak-to-peak acceleration of 0.56 μgal. The observed amplitude is 426 mV$_{pp}$, corresponding to 0.53 μgal. Again this very good agreement is somewhat fortuitous because of simplifications. A more realistic crustal model would reduce the theoretical acceleration appreciably.

For warm fronts the pressure records never showed fast changes and neither were gravity signals observed. Although the same total pressure change might occur, it does so much more slowly and therefore the corresponding gravity signals do not come through the passband of the filter with measureable amplitude. This was confirmed by model calculations (Müller, 1981).

Figure 5 and 6 show very complicated frontal passages associated with thunderstorms. In those cases our models are much too simple. In this case additional effects may contribute to the gravity signal, which are

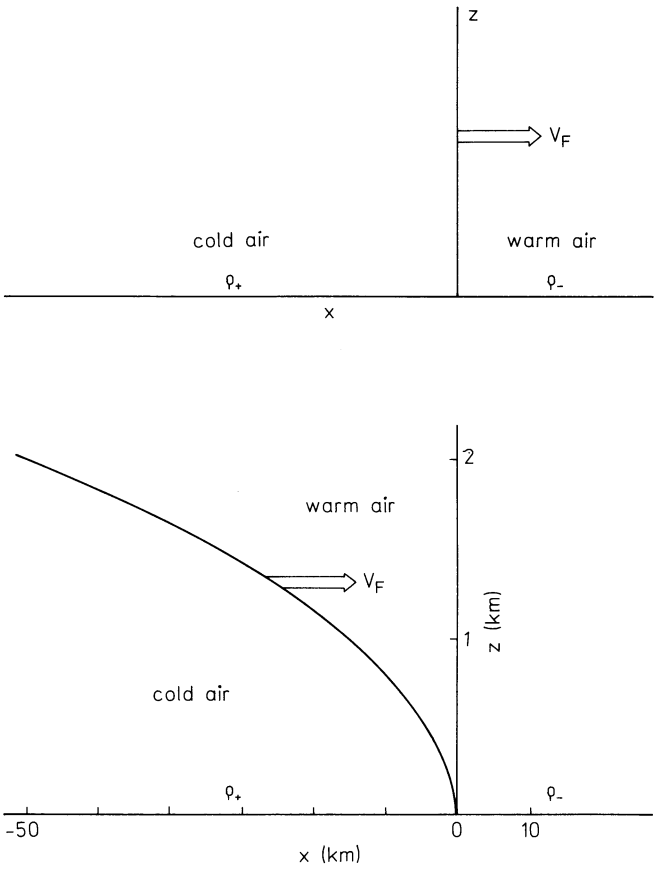

Fig. 12. Two cold front models used in calculations. Note difference in vertical and horizontal scale for hyperbolic front

very hard to estimate: such as vertical motion of air masses, turbulence and heavy rains.

Conclusions

The observed pressure-correlated gravity transients during the passage of cold fronts at the Schiltach underground observatory can be explained in shape, polarity and magnitude by the direct gravitational attraction of the sensor mass by air masses of different densities. The only competing mechanism at higher frequencies ($\gtrsim$4 mHz) is the inertial effect due to vertical acceleration of the ground by the pressure changes. Since our signals were clearly above the normal vertical seismic noise level in the free mode band, we conclude that this noise is caused by the same effects at more moderate amplitudes of pressure or density variations in the atmosphere. Therefore the quality of a record from such an instrument, for example from the IDA-network, depends on local weather. One cannot expect, on average, top-quality vertical seismic records at very long periods from stations where the weather is notoriously bad in terms of frequent large fluctuations in barometric pressure.

For horizontal seismic noise at these frequencies the situation is even worse. According to Große-Brauckmann (1979) the contribution to tilts of the deformation effect is dominant over the gravitational attraction. The latter is of the same order of magnitude for vertical and horizontal instruments, therefore long period horizontal seismic noise should be larger than vertical noise, when caused by the atmosphere. This is demonstrated in Fig. 6, where pressure-correlated signals are ten times larger for horizontal components.

Our simple models cannot be used to prove definitely that Newtonian attraction is the dominant mechanism for the cold front signals in gravity. But since we had to over-estimate the inertial effect to match the observed amplitude at rather high frequency and because this effect decreases linearly with decreasing frequency we feel that Newtonian attraction is highly likely to be dominant. The rise-times of the pressure signals in all cases were larger than the period for which the inertial effect became comparable. The relative importance of the mechanisms must be site-dependent due to the changing crustal structure and topography of the surface could have an influence also. Therefore it is not possible to draw conclusions of more general nature, but we have demonstrated that Newtonian attraction could explain the observed signals and that appreciable contributions must be expected from the inertial effect due to the deformation of the crust.

Appendix: Derivation of Eq. (3)

Equation (2) has to be solved in the case of the vertical front with

$$\varrho_0(x)=\begin{cases}\varrho_+ & x<x_F \text{ cold, denser air}\\ \varrho_- & x_F<x \text{ warm air.}\end{cases} \tag{A1}$$

The integration over coordinate y results in:

$$\int_{y=-\infty}^{+\infty}[(x-x_A)^2+y^2+z^2]^{-3/2}\,dy = 2[(x-x_A)^2+z^2]^{-1}. \tag{A2}$$

Then the integral over x is:

$$\int_a^b[(x-x_A)^2+z^2]^{-1}\,dx=\frac{1}{z}\operatorname{atan}\left(\frac{x-x_A}{z}\right)\Big|_a^b. \tag{A3}$$

The principal values have to be taken for the atan-function as $a\to-\infty$ and $b\to+\infty$.

$$\begin{aligned}g(x_A)&=-2G\int_{z=0}^{\infty}\exp\left(-\frac{z}{H}\right)\left[\varrho_+\left(\operatorname{atan}\frac{x_F-x_A}{z}+\frac{\pi}{2}\right)\right.\\&\quad\left.+\varrho_-\left(\frac{\pi}{2}-\operatorname{atan}\frac{x_F-x_A}{z}\right)\right]dz\\&=-2G\left\{\frac{\pi}{2}(\varrho_++\varrho_-)\int_{z=0}^{\infty}\exp\left(-\frac{z}{H}\right)dz\right.\\&\quad\left.+(\varrho_+-\varrho_-)\int_0^{\infty}\exp\left(-\frac{z}{H}\right)\operatorname{atan}\frac{x_F-x_A}{z}\,dz\right\}\end{aligned}$$

$$\begin{aligned}g(x_A)&=-2G\left\{\frac{\pi}{2}(\varrho_++\varrho_-)H\right.\\&\quad\left.+(\varrho_+-\varrho_-)\int_{z=0}^{\infty}\exp\left(-\frac{z}{H}\right)\operatorname{atan}\frac{x_F-x_A}{z}\,dz\right\}\end{aligned} \tag{A4}$$

and by partial integration using the abbreviation $a = x_F - x_A$

$$g(x_A) = -2G\left\{\frac{\pi}{2} H(\rho_+ + \rho_-) - H(\rho_+ - \rho_-) e^{-z/H} \operatorname{atan} \frac{a}{z}\Big|_0^\infty - H(\rho_+ - \rho_-) a \int_0^\infty \frac{\exp(-z/H)\,dz}{z^2 + a^2}\right\}. \quad \text{(A5)}$$

At this point the cases $a > 0$ and $a < 0$ must be distinguished for two reasons. Firstly the second term is:

$$\lim_{z \to 0} \left(\operatorname{atan} \frac{a}{z}\right) = \begin{cases} \pi/2 & a > 0 \\ 0 & a = 0 \\ -\pi/2 & a < 0. \end{cases}$$

Secondly the third term can be interpreted as a Laplace Transform if $\mathrm{Re}(a) > 0$, $\mathrm{Re}(s) > 0$ (Erdélyi et al., 1954):

$$L\{(t^2 + a^2)^{-1}\} = -\frac{1}{a}\{\mathrm{ci}(as) \cdot \sin(as) + \mathrm{si}(as) \cdot \cos(as)\}$$

where $\mathrm{ci}(x)$, $\mathrm{si}(x)$ are defined in Eq. (4). Hence for $a > 0$ and $s = 1/H$, Eq. (3a) and for $a < 0$, Eq. (3b) result. For $a = 0$ $g(x_A) = -GH\pi(\rho_+ + \rho_-)$.

Acknowledgements. We would like to thank H. Otto and W. Großmann for maintenance of the instrumentation and the air-lock and for help with the active experiments. Drs. D. Emter, G. Müller, E. Wielandt and H. Wilhelm made many helpful comments on the manuscript. Discussions with Drs. H. Dieterich, Frankfurt and F. Fiedler, Karlsruhe helped us to understand meteorological phenomena a little better. E. Heil and E. Wielandt provided material for Fig. 6 and 8. P. Illich helped with the figures and H. Gadau typed the manuscript. The Deutsche Forschungsgemeinschaft supported this research under grants Zu 35/1-4 and B5-SFB 108. All this is gratefully acknowledged.

References

Agnew, D.C., Berger, J., Buland, R., Farrell, W., Gilbert, F.: IDA network for very long period seismology. EOS (Trans. Am. Geophys. Un.) **57**, 180–188, 1976

Agnew, D.C.: Strain tides at piñon Flat: analysis and interpretation. Ph. D. Thesis, University of California at San Diego, 1979

Bath, M.: Atmospheric waves from Mount St. Helens. EOS (Trans. Am. Geophys. Un.) **63**, 193, 1982

Block, B., Moore, R.D.: Measurements in the Earth mode frequency range by an electrostatic sensing and feedback gravimeter. J. Geophys. Res. **71**, 4361–4375, 1966

Bolt, B.A., Tanimoto, T.: Atmospheric oscillations after the May 18, 1980 eruption of Mount St. Helens. EOS (Trans. Am. Geophys. Un.) **62**, 529, 1981

Erdélyi, A., Magnus, W., Oberhettinger, F., Tricomi, F.G.: Tables of integral transforms, Vol. I. New York : McGraw-Hill, 1954

Große-Brauckmann, W.: Untersuchungen der Bodenunruhe im Periodenbereich von 2 min–1 h mit dem Askania Bohrlochneigungsmesser. Ph. D. Thesis, Clausthal Techn. University, 1979

Heil, E.: Erfahrungen mit einem Vertikalextensometer im Observ. Schiltach. Ph. D. Thesis, Karlsruhe University, 1983

Herbst, K.: Interpretation von Neigungsmessungen im Periodenbereich oberhalb der Gezeiten. Ph. D. Thesis, Clausthal Tech. University, 1976

Kisslinger, C.: Seismograms associated with the near passage of tornados. J. Geophys. Res. 65, 721–728, 1960

Liljequist, G.H., Cehak, K.: Allgemeine Meteorologie, 385 pp., Vieweg und Sohn, Braunschweig, 1979

Mälzer, H.: The Observatory. In: Proc. Seventh Int. Symposium Earth Tides (Ed. Szadeczky-Kardoss), 725–727, Schweizerbart'sche Verlagsbuchhandlung, Stuttgart, 1976

Müller, T.: Die Untersuchung von langperiodischen Schweresignalen beim Durchzug von Wetterfronten. Diploma Thesis, Karlsruhe University, 1981

Nakanishi, K.K., Knopoff, L., Slichter, L.B.: Observation of Rayleigh wave dispersion at very long periods. J. Geophys. Res. **81**, 4417–4421, 1976

Ritsema, A.R.: Observation of St. Helens eruption. EOS (Trans. Am. Geophys. Un.) **61**, 1201, 1980

Slichter, L.B., Zürn, W., Syrstad, E., Knopoff, L., Smythe, W.D., Uffelman, H.: Long period gravity tides at the South Pole. J. Geophys. Res. **74**, 6207–6212, 1979

Sorrells, G.G.: A preliminary investigation into a relationship between long-period seismic noise and local fluctuations in the atmospheric pressure field. Geophys. J.R. Astron. Soc. **26**, 71–82, 1971

Sorrels, G.G., McDonald, J.A., Der, Z.A., Herrin, E.: Earth motion caused by local atmospheric pressure changes. Geophys. J.R. Astron. Soc. **26**, 83–98, 1971

Spratt, R.S.: Modelling the effect of atmospheric pressure variations on gravity. Geophys. J.R. Astron. Soc. **71**, 173–186, 1982

Warburton, R.J., Goodkind, J.M.: The influence of barometric-pressure variations on gravity. Geophys. J.R. Astron. Soc. **48**, 281–292, 1977

Wielandt, E., Streckeisen, G.: The leaf-spring seismometer-design and performance. Bull. Seismol. Soc. Am. **72A**, 2349–2368, 1982

Ziolkowski, A.: Prediction and suppression of long-period non-propagating seismic noise. Bull. Seismol. Soc. Am. **63**, 937–958, 1973

Zschau, J.: Air pressure induced tilt in porous media. In: Proc. Eighth Int. Symp. Earth Tides Bonatz, Melchior, eds.: pp. 418–433, Bonn, 1979

Received April 27, 1983; Revised version June 20, 1983
Accepted June 20, 1983

J Geophys (1983) 53:163–169

Journal of Geophysics

Determination of the Steady State Temperature Gradient and of the Thermal Diffusivity in a Shallow Borehole near Braunschweig (F.R.G.)

W. Kessels

Gesellschaft für Strahlen- und Umweltforschung mbH, Institut für Tieflagerung, Theodor-Heuss-Straße 4, D-3300 Braunschweig, Federal Republic of Germany

Abstract. In a shallow borehole of 50 m depth, drilled into a clay subsurface and located on the premises of the Biologische Bundesanstalt (Federal Institute for Biological Research) at Braunschweig, measurements of temperature as a function of depth were made from 1978–1980.

The observed temperatures were corrected for disturbances caused by known temperature variations at the surface, adopting different values of thermal diffusivities a^2. The value selected as the final one was that which gave the most linear dependence of the corrected temperature with depth. The corresponding vertical temperature gradient was used, together with a known value of heat capacity, to determine the heat flow density at the site near Braunschweig. a^2 was found to be $8.5 \cdot 10^{-3}$ cm^2/s in accordance with published values. In the same manner temperature profiles were evaluated from different depth intervals at different times. It was found that, in order to determine the geothermal temperature gradient reliably, a borehole of at least 25 m depth was required in this case. In correcting the time-dependent temperature disturbance the depth interval from 0 to 10 m should be excluded.

Key words: Geothermal temperature – Determination of thermal diffusivity – Meteorological temperature disturbances

Introduction

The determination of the geothermal temperature gradient and of the heat flow density is an important prospecting method and is described in detail in various monographs and textbooks (e.g. Kappelmeyer and Hänel, 1974; Buntebarth, 1980). In this connection reference must be made to applications in hydro-geology concerning the determination of the increased heat flow density above salt domes and also to applications in areas with increased radiogenic and chemical heat production. Knowledge of the terrestrial heat flow density is also important in the discussion of geodynamical problems.

In evaluating temperature profiles made in boreholes, three problems are generally of importance:

1. Topographic corrections must be applied to the temperature profiles (Blackwell et al., 1980).

2. For the determination of heat flow density it is preferable to use a thermal conductivity measured in situ (e.g. Musmann and Kessels, 1980).

3. Especially in the case of shallow boreholes, temperature variations penetrating from the surface into the ground must be eliminated (Lee, 1977).

To investigate this third problem in particular, temperature measurements were made from 1978–1980 in a borehole 50 m deep on the property of the Biologische Bundesanstalt at Braunschweig. In the clay encountered here, hydrological temperature disturbances can almost certainly be excluded. It was the aim of this investigation to find the minimum depth of a shallow borehole required for determining the heat flow density.

Lovering et al. (1963) and Lee (1977) corrected observed temperature profiles under the assumption of a harmonic annual temperature wave. Lee (1977) described a procedure to obtain the gradient of the temperature from a temperature profile measured at a fixed point of time.

In contrast, the temperature correction presented in this paper is in addition performed for temperature variations with periods other than annual. The correction is restricted to influences from the past 100 years. For this period the mean annual temperatures yield disturbances of the gradients of up to 30 K/km at a depth of 18 m (Kessels, 1980). Paleoclimatic corrections are not applied.

Kappelmeyer (1957) has shown that in extremely shallow boreholes (depth $\leqq 2$ m) the geothermal heat flow density cannot be measured. Near the surface, the heat flow density caused by the annual temperature wave is much greater than the heat flow density from depth. The magnitude of the heat flow density near the surface is also determined by the micro-climatic conditions in the near environment and by the geological conditions near the surface (Geiger, 1961; Kessels, 1980).

Lovering et al. (1963) demonstrated that determining the geothermal heat flow density over depths which are subject to the annual temperature wave may also have advantages over determinations in deep boreholes. This is because, in shallow boreholes, the time-dependent temperature field can be used to determine the in situ thermal diffusivity, a^2. Using a suitable assumption for the heat capacity ρc,where ρ denotes density and c denotes specific heat, the thermal conductivity λ can then be derived from:

$$a^2 = \frac{\lambda}{\rho c}$$

Lovering et al. (1963) determined the thermal diffusivity by using the point of intersection of two temperature profiles recorded at different times.

Lee (1977) determined the thermal diffusivity and the temperature gradient by a transformation of variables which transforms the non-linear temperature distribution of the annual wave in the subsurface into a linear relation. The latter is then fitted to the measured data by minimizing the standard deviation.

In the present investigation the thermal diffusivity was determined by a trial and error method, namely by calculating theoretical subsurface temperatures from measured surface temperatures together with an assumed value of the thermal diffusivity and comparing it to the temperatures observed in the borehole.

The thermal diffusivity yielding the best correspondence between the theoretical and the observed temperature profiles was taken as the final value.

In performing heat flow density measurements at the Laacher See (Eifel region, F.R.G.), Musmann and Kessels (1980) showed a good consistency between the thermal diffusivities determined in situ and those determined by fitting temperature profiles. In the measurements made at Braunschweig the surface temperatures did not have to be inferred from the air temperature since at this location the Deutscher Wetterdienst (Meteorological Service of the F.R.G.) has recorded the surface temperatures directly and continuously since 1954. The case where geothermal prospecting is to be done in an area where no direct surface temperature measurements are available was discussed in detail by Kessels (1980) and applied in the measurements at the Laacher See.

Along with the evaluation of a^2 by fitting the calculated temperatures to those observed, a proposal by Hänel (1980) for the determination of the steady state temperature gradient was considered. According to Hänel (1980) a relatively stable temperature gradient between 40 and 50 K/km may be determined from the mean surface temperature and the mean temperature at the deepest point of the borehole, both taken over two years.

Method of Analysis

The procedure presented here, which is described in more detail in Kessels (1980), assumes the subsurface to be homogeneous and isotropic, which implies that the thermal diffusivity is a constant.

The total temperature field T which depends on depth z and time t can be thought of as being split up into two parts according to

$$T(z,t) = T_s + gz + T'(z,t) \tag{1}$$

where the first two terms represent the steady-state geothermal temperature field characterized by the mean surface temperature T_s and the normal temperature gradient g, and where T' denotes the time-dependent temperature component to be eliminated by calculation. This component is caused by deviations of the surface temperature $T(0,t)$ from the long-term mean value T_s and vanishes at any depth if averaged over a long time.

For the correcting calculation usually only mean surface temperatures (mean daily, monthly, and annual surface temperatures) are available. We therefore consider the effect of a constant temperature disturbance T'_{si} imposed at the surface between times t_i and t_{i+1} in the past where $t_i < t_{i+1} < t$. According to Carlslaw and Jaeger (1959; cf. also

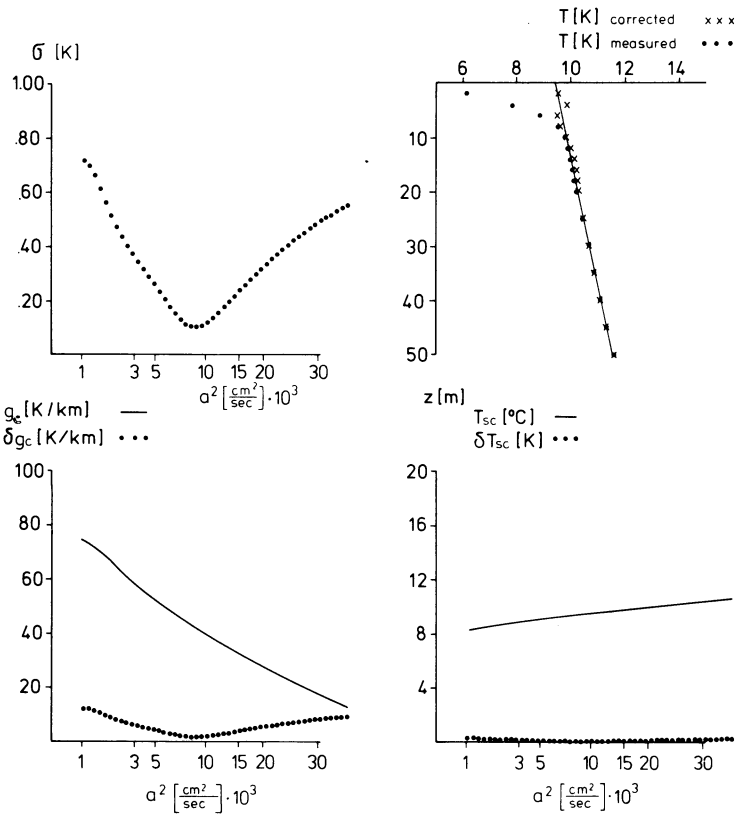

Fig. 1. Example of correction of temperatures T measured in the borehole between 2 and 50 m depth on 22 February 1980, adopting different values for the thermal diffusivity a^2. σ is the standard deviation between the corrected temperatures as depending on depth and the best fitting straight line for any value of a^2. This line is shown in the upper right diagram for $a^2 = 8.9 \cdot 10^{-3}$ cm^2/s, at which value σ adopts a minimum (*upper left*). At the bottom the parameters of the best-fitting straight lines $T_c(z) = T_{sc} + g_{cz}$ are shown together with their probable errors as function of a^2. The finally adopted value of a^2 and the corresponding values of g_c and T_{sc} are indicated by the minimum of $\sigma(a^2)$

Buntebarth, 1980, p. 27) we get for the corresponding temperature disturbance at depth z and time t

$$T'(z,t)=T'_{si}\left[\Phi\left(\frac{z}{\sqrt{2}a\sqrt{t-t_{i+1}}}\right)-\Phi\left(\frac{z}{\sqrt{2}a\sqrt{t-t_i}}\right)\right] \quad (2)$$

where ϕ is the Gaussian error function

$$\Phi(x)=\sqrt{\frac{2}{\pi}}\int_0^x e^{-\frac{\xi^2}{2}}d\xi.$$

For the total time-dependent temperature disturbance we get, by summing up over all surface temperature variations in the past:

$$T'(z,t)=\sum_{i=1}^{n}T'_{si}\left[\Phi\left(\frac{2}{\sqrt{2}a\sqrt{t-t_{i+1}}}\right)-\Phi\left(\frac{2}{\sqrt{2}a\sqrt{t-t_i}}\right)\right]. \quad (3)$$

With this equation the known temperature history at the surface can be used to calculate the temperature disturbance in the subsurface for any adopted value of the thermal diffusivity a^2 and then to subtract it from the temperatures measured in the borehole. An incorrect value adopted for the thermal diffusivity will result in a nonlinear relationship between temperature and depth.

However, if the thermal diffusivity is chosen correctly, the correction will result in a linear temperature curve, around which the measured values will scatter only according to the instrumental errors of measurement.

A best-fit straight line is placed through the points of the corrected depth function (the same procedure may be applied even in the case when an incorrect thermal diffusivity is assumed), of which the standard deviation σ is then determined. σ will be minimal at the correct value of the thermal diffusivity.

In Fig. 1 the application of this procedure is demonstrated for the case of the temperature observations made in the borehole between 2 and 50 m depth. The diagram at the upper left shows that σ as a function of the adopted values of a^2 has a distinct minimum. The diagram at the upper right on the other hand shows the uncorrected temperatures as well as the optimally corrected temperatures (at minimum standard deviation). In the lower two diagrams the parameters of the best-fitting straight lines are shown as functions of a^2. These lines have the mathematical form

$$T_c(z)=T_{sc}+g_c z \quad (4)$$

which corresponds to the first two terms in Eq. (1). The subscript c indicates that these temperatures and parameters have been obtained after correction. Of course, it is hoped that T_{sc} and g_c come close to the true values T_s and g (cf. Eq. (1)) if the optimal value for a^2 has been used in the correction. The lower diagrams in Fig. 1 also give the probable errors δT_{sc} and δg_c of the parameters T_{sc} and g_c, respectively (for more details see Kessels, 1980).

Analysis of Observations 1978–1980

The procedure of analysis outlined above may be applied to data from any time t and even from any depth interval, which will be done in the following.

It should be mentioned that the measurements made from April 1978 to March 1979 were carried out with a fixed probe chain, whereas the later measurements from April 1979 to May 1980 were made with a single probe lowered into the borehole. For determining the geothermal gradient the latter method proved to be of advantage.

The example shown in the upper right part of Fig. 1 indicates that the time-dependent disturbance of the temperature field in the top few meters of the borehole cannot

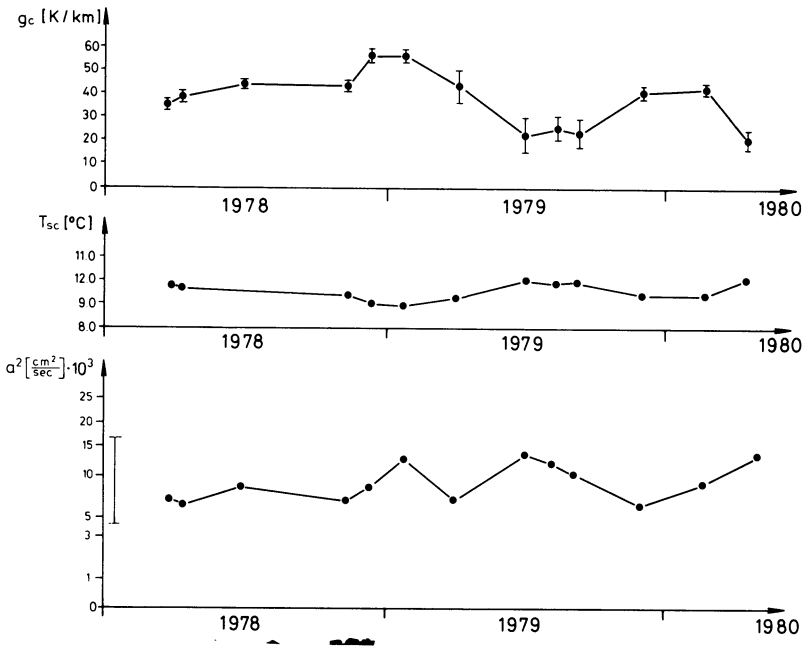

Fig. 2. Final results attained by the procedure as indicated in Figure 1 for different times. Data from the whole depth interval 2–50 m was used

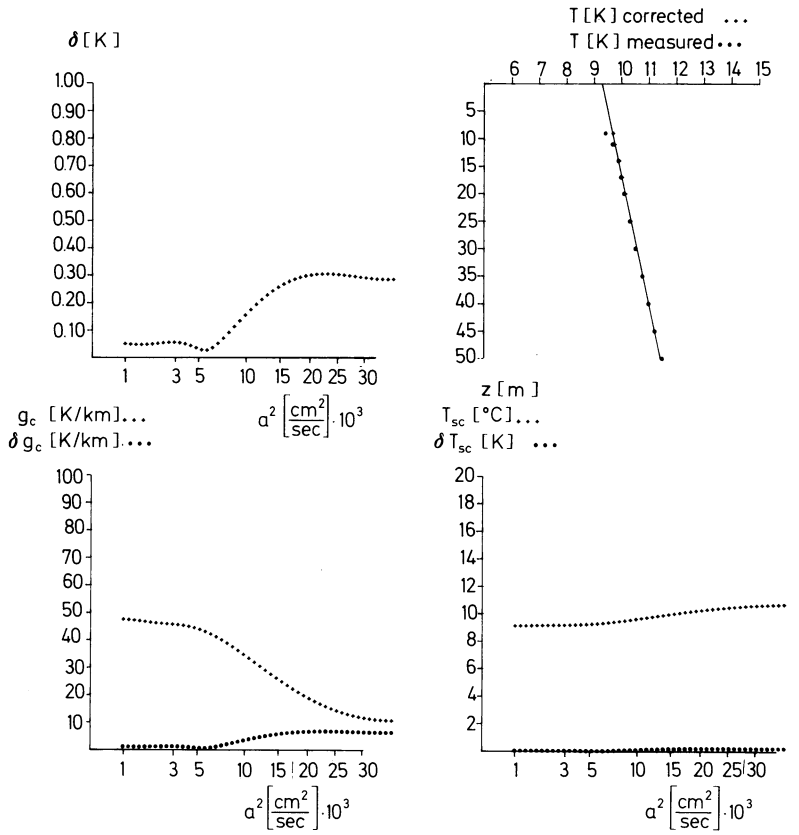

Fig. 3. Example of correction of temperatures T measured in the borehole between 10 and 50 m depth on 29 June 1979. Otherwise as Fig. 1, with the exception that $a^2 = 5.5 \cdot 10^{-3}$ cm^2/s in the optimal case here

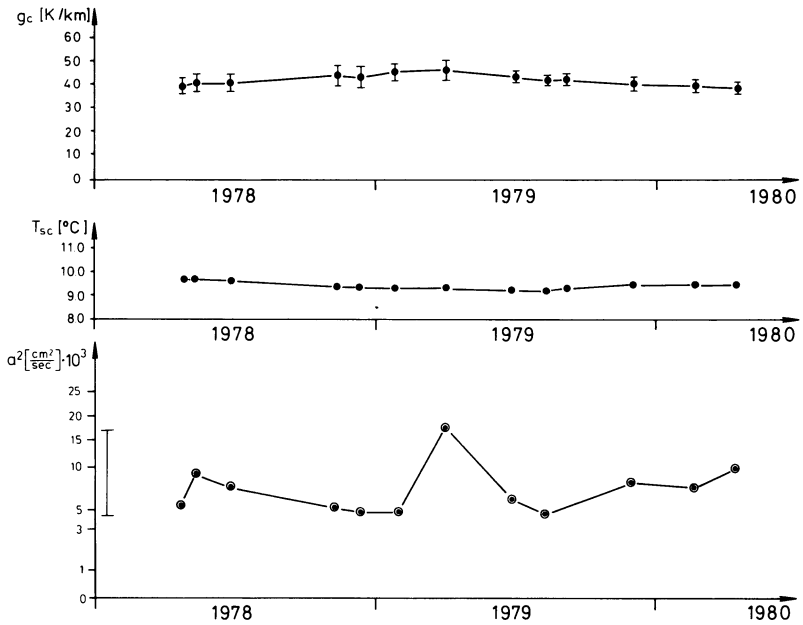

Fig. 4. Final results attained by the procedure as indicated in Figure 1 for different times. Data from the depth interval 10–50 m was used

be eliminated with sufficient accuracy, in accordance with, for example, Kappelmeyer (1957) and Lee (1977). Inhomogeneities in the subsurface, hydrological influences and the inaccuracy of meteorological data are not accounted for by the correction procedure in this depth range.

The diagram at the lower left of Fig. 1 shows that the gradient g_c determined depends heavily on the value of the thermal diffusivity used for the calculation, which implies that its final value adopted will be affected by some error.

The optimal value of the thermal diffusivity seems to be rather well defined due to the sharp minimum in the curve $\sigma(a^2)$ (Fig. 1, upper left). However, it is strongly influenced by the upper depth range, since in the upper few meters of the subsurface the temperature variations of the past few months are especially effective. This means that the thermal diffusivity determined is effectively the thermal diffusivity of the top few meters of the subsurface for a time interval of a few months prior to the measurement by a time-dependent thermal diffusivity.

Figure 2 shows the time-dependent results correspond-

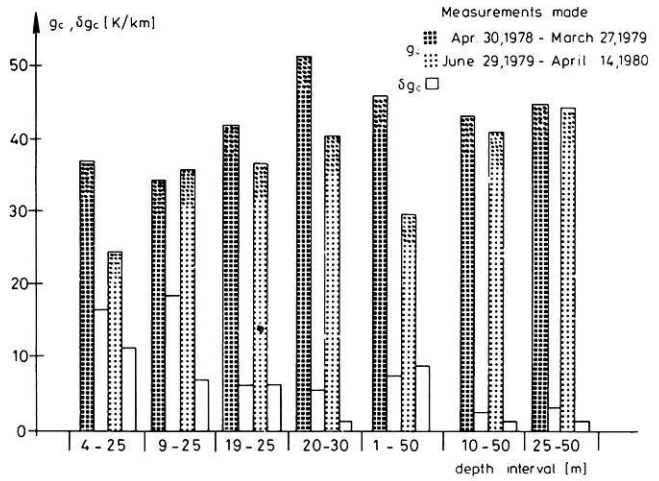

Fig. 5. Mean temperature gradients g_c as determined over different depth intervals with errors δg_c from scatter when g_c values at different times are considered

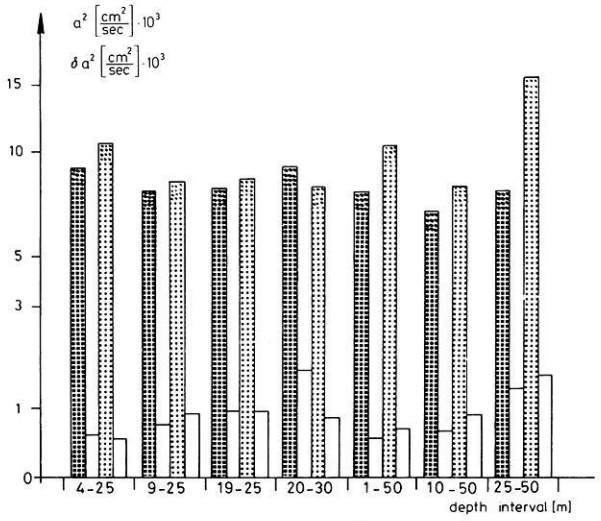

Fig. 6. Mean thermal diffusivities a^2 as determined over different depth intervals with errors δa^2 from scatter when a^2 values at different times are considered

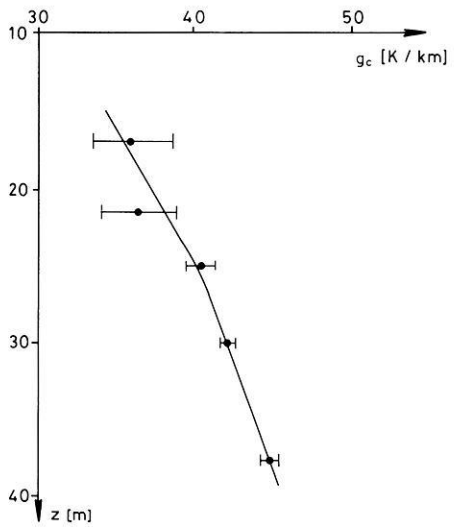

Fig. 7. Mean geothermal gradients g_c over different depth intervals at borehole site

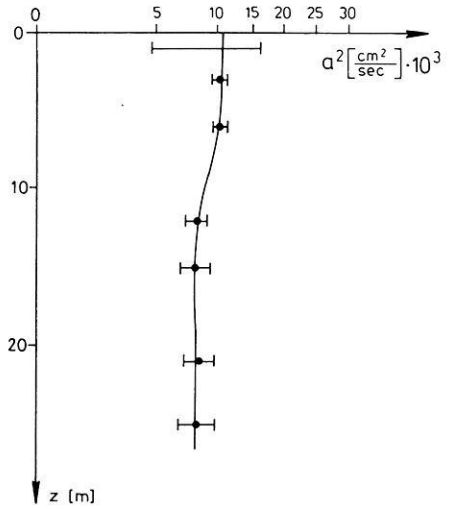

Fig. 8. Mean thermal diffusivities a^2 over different depth intervals at borehole site

ing to the values finally adopted for a^2, T_{sc} and g_c (cf. Fig. 1), where again the data from the whole depth interval 2–50 m have been used. All thermal diffusivities determined were found to be in the range known for the thermal diffusivities of clay. This range is indicated by the barred line to the left in the lower diagram (Kappelmeyer and Hänel, 1976).

The errors of the g_c values attained are greatly diminished if the upper 10 m are excluded from the analysis (Fig. 5).

For the case that the near surface temperature field (less than 10 m depth) is not included in the evaluation, the time-dependent temperature field $T'(z,t)$ (see Eq. 1) is much smaller. The result is that in the evaluation the minimum of the standard deviation, which serves to determine the thermal diffusivity, is much less distinct. A comparison of the upper left diagrams of Figs. 1 and 3 shows this clearly. The result is a smaller error of the thermal diffusivity for the depth interval 2–50 m than for the depth interval 10–50 m. This can be seen in Fig. 6. This is even more pronounced for the depth interval 25–50 m, as is also shown in Fig. 6.

For determining the temperature gradient the effect of the error of the temperature gradient is opposed to the effect of the error of the thermal diffusivity. In this case including the near-surface temperature measurements in the evaluation leads to a significant change of the corrected gradient with respect to thermal diffusivity and thus to a large error. This is evident from a comparison of Figs. 1 and 3. Comparing the different depth intervals in Fig. 5 also shows this clearly.

In Fig. 5 the results of the determination of the gradient g_c for all depth intervals are shown. As in Fig. 6, where all results for the thermal diffusivities are presented, the results are given separately for measurements with the chain probe and for the later ones with the lowerable probe. The errors indicated are not determined from the errors of the individual measurements but from the scattering around the mean values of the total time interval evaluated. These errors proved to be greater than the errors found by applying error calculations to the errors of the individual measurements. Taking into account only those depth intervals

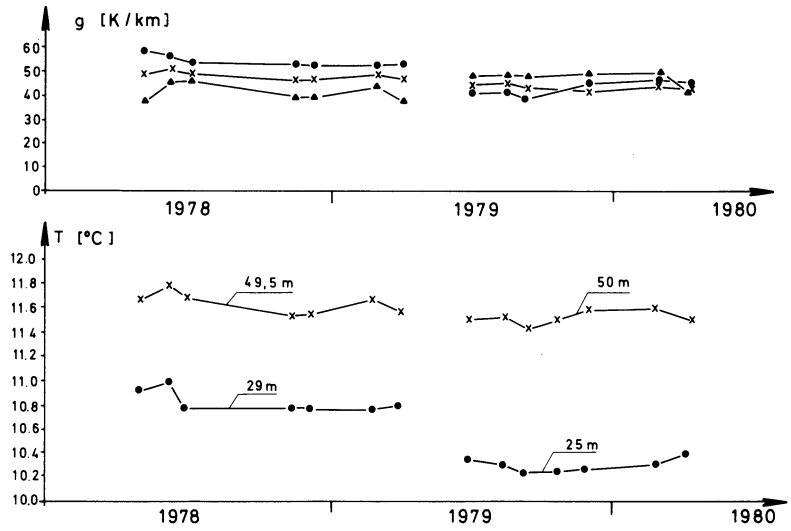

Fig. 9. Temperature gradients $g = \Delta T/z$ (*upper part*) calculated from the differences ΔT between temperatures T observed at depths z (*lower part*) and an adopted mean surface temperature of 9,2° C. *Full circles*: $z = z_1 = 29$ m or 25 m, respectively, with temperatures T_1. Crosses: $z = z_2 = 49.5$ m or 50 m, respectively, with temperatures T_2. In addition, gradients $(T_2 - T_1)/(z_2 - z_1)$ are shown, for comparison (*upper part, triangles*)

where gradients could be determined reliably, the steady state gradient can be plotted with respect to depth in the borehole. Figure 7 shows that the gradient in the top layers of the subsurface is smaller than in deeper layers. A similar profile drawn for the thermal diffusivity (Fig. 8) shows that the thermal diffusivity in the top layers is greater than in deeper layers. Altogether this indicates a tendency towards constant heat flow density as a function of depth. With the gradient and the thermal diffusivity determined by the methods outlined, the heat flow density may be calculated if the heat capacity ρc is known (Kappelmeyer and Hänel, 1974). If a value of 2.29 J/cm K is assumed for the heat capacity ρc, the heat flow density for the depth interval 1–25 m is found to be 89 ± 14 mW/m^2, whereas for the deeper interval 25–50 m it is 81 ± 15 mW/m^2. The mean heat flow density for both intervals is thus 85 ± 11 mW/m^2. This value is slightly larger than the one given by Hänel (1980) for the region of Braunschweig. This may be due to a positive heat flow anomaly connected with a salt dome (Nußberg) which is about 1 km from the borehole.

This holds particularly, since the values of Hänel are corrected for paleoclimatic effects. Such effects in our case result in an increase of the heat flow density.

The temperature data collected for this investigation was also used for testing an evaluation method proposed by Hänel (1980). Hänel proposes to determine the gradient by taking the differences between temperature values at the greatest depth of the borehole and the mean temperature at the surface. This method has the advantage that it can be performed quickly and that the temperature disturbance by drilling at the greatest depth of the borehole is already negligible a short time after the drilling is finished. Evaluation by taking differences was performed here for temperature data from the depths 50 m and 25 m, or 49.5 m and 29 m. The results are shown in Fig. 9. For the long-term mean surface temperature a value of 9.2° C was used. This value is the sum of the mean air temperature at Braunschweig given in meteorological yearbooks as 8.8° C, and the difference between surface and air temperature given by Kessels (1980) as 0.4° C.

As is shown in Fig. 9 this procedure yields relatively good results for the gradients. It must be considered that in the case of the 25 m evaluation an error of 0.1° C in the surface temperature already leads to an error of 4 K/km for the gradient. This means that the error stemming from an incorrect assumption of the long-term mean surface temperature in determining the gradient is considerable.

Concluding Considerations

The measurements made at the Biologische Bundesanstalt show that in shallow boreholes of 25 m depth or more the steady state geothermal gradient and the conductive heat flow density can be determined. In order to obtain the temperature field at greater depths by extrapolation it must be taken into account, however, that the usual model considerations must be applied. These must take into account not only the topography of the surface (Blackwell et al. 1980) but also the homogeneity and heat production of the subsurface as well as hydrological temperature disturbances. The latter are especially significant for shallow boreholes and are well suited for hydrological investigations.

In addition it should be remarked that the method proposed and applied here to correct the time-dependent temperature field is, when applied to shallow boreholes, well suited to determine the long-term mean surface temperature.

Acknowledgements. I thank Prof. W. Kertz for giving me the opportunity to carry out these investigations at the Institut für Geophysik und Meteorologie. I further thank the Biologische Bundesanstalt for making available a test site on its premises and the Deutscher Wetterdienst for data on air and surface temperatures. Last but not least my thanks are due to Dr. Musmann and Dipl.-Phys. John for their advice and assistance.

References

Blackwell, D.D., Steele, J.L., Brott, C.A.: The Terrain Effect on Terrestrial Heat Flow. J. Geophys. Res. **85**, 4757–4772, 1980

Buntebarth, G.: Geothermie. Berlin, Heidelberg, New York: Springer Verlag 1980

Carslaw, H.S., Jaeger, J.C.: Conduction of heat in solids. 2nd Ed. Oxford: Clarendon 1959

Geiger, R.: Das Klima der bodennahen Luftschicht. 4. Aufl. Braunschweig: Fr. Vieweg & Sohn 1961

Hänel, R. et al.: Atlas of subsurface temperatures in the European Community. Hannover: Schäfer Druckerei 1980

Kappelmeyer, O.: The use of near surface temperature measurements for discovering anomalies due to causes at depth. Geophys. Prospect. **3**, 239–258, 1957

Kappelmeyer, O., Hänel, R.: Geothermics with special reference to application. Geoexploration Monographs, Series 1, No. 4. O. Rosenbach, C. Morelli, eds. Berlin, Stuttgart: Gebr. Borntraeger 1974

Kessels, W.: Die Bestimmung des stationären Temperaturgradienten und des geothermischen Wärmeflusses aus Flachbohrungen. Diss. Naturwiss. Fak. Techn. Univ. Carolo-Wilhelmina, Braunschweig 1980

Lee, T.: On shallow-hole temperature measurements – a test study in the Salton Sea geothermal field. Geophysics **42**, No. 3, 572–583, 1977

Lovering, T.S., Goode, H.D.: Measuring geothermal gradients in drill holes less than 60 feet deep. East Tintic District, Utah. U.S. Geol. Surv. Bull. **1172**, 1963

Musmann, G., Kessels, W.: An in situ thermal conductivity probe. – Advances in European geothermal research, Commission of the European Communities. A.S. Strub, P. Ungemach, eds. Dordrecht: D. Reidel Publ. Co. 1980

Received February 10, 1983; Revised Version May 24, 1983
Accepted May 27, 1983

J Geophys (1983) 53:170–181

Journal of Geophysics

A Case Study of the Response of the Magnetosphere to Changes in the Interplanetary Medium

G. Rostoker[1,2], W. Baumjohann[2,3], and C.T. Russell[4]

[1] Institute of Earth and Planetary Physics and Department of Physics, Universtiy of Alberta, Edmonton, Canada T6G 2J1 (permanent address)
[2] Institut für Geophysik der Westfälischen Wilhelms-Universität, Corrensstraße 24, D-4400 Münster, Federal Republic of Germany
[3] Now at: Max-Planck Institut für Physik und Astrophysik, Institut für Extraterrestrische Physik, D-8046 Garching, Federal Republic of Germany
[4] Institute for Geophysics and Planetary Physics, University of California, Los Angeles, California 90024 USA

Abstract. The general response of the magnetosphere to the various solar wind parameters is now generally understood. However, the many deviations found for individual cases via à vis the norm show an incomplete knowledge of the relative role of each of the solar wind parameters presently thought to be of importance in predicting the level of the solar-terrestrial interaction. This study presents a detailed analysis of world-wide ground based magnetometer data together with information on the plasma and magnetic field properties of the interplanetary medium and magnetosheath obtained from the ISEE 1 and 2 and IMP 8 spacecraft. The event in question featured an interval of relatively stable southward IMF followed by a sharp northward turning. During the interval of southward IMF there were occasional transient northward turnings with significant substorm expansive phase activity appearing to be triggered by these transient northward turnings. The final northward turning of the IMF was associated with an episode of strong magnetospheric substorm expansive phase activity after which the level of high latitude magnetic activity decayed to a low level. Evidence is presented that the driven system auroral electrojets begin to decay at the time of the northward turning of the IMF even as the substorm expansive phase activity is initiated in the midnight sector. The collapse of the substorm current wedge during the final decay of high latitude activity is traced in some detail and it is shown that this collapse occurs progressively from east to west in a series of impulsive episodes. The results reported above are discussed in the context of energy dissipation in the magnetosphere-ionosphere system through direct input of solar wind energy and through unloading of the magnetotail.

Key words: Substorm – Electrojet – Interplanetary Fields

Introduction

Over the past decade, a considerable amount of research has been carried out in an effort to understand better the way in which energy from the interplanetary medium enters the earth's magnetosphere and the way in which the magnetosphere is coupled to the ionosphere where the energy is eventually degraded to heat. The work of Axford and Hines (1961) and Dungey (1961) provided a theoretical basis which caused researchers to investigate some correlation between the solar wind parameters and the interplanetary magnetic field and the level of geomagnetic activity in the high latitude regions (which was the indicator of the amount of energy being dissipated in the ionosphere). Fairfield and Cahill (1966) and Rostoker and Fälthammar (1967) were the first to find positive correlations between the interplanetary magnetic field (IMF) and interplanetary electric field (respectively) and the level of geomagnetic activity. Both studies indicated that when the interplanetary magnetic field had a southward component, energy transfer between the solar wind and the magnetosphere took place more efficiently than when the IMF had a northward component. Since these early studies, it has become clear that the coordinate system in which the IMF is ordered is of importance with the GSM (geocentric solar magnetospheric) coordinate system being a more physically reasonable one in which to organize the IMF data than the GSE (geocentric solar ecliptic) system in which the original IMF data were analysed. Furthermore, it is now recognized that the azimuthal B_y component of the IMF has some impact on the modulation of the high latitude cleft (DPY) current system which in turn influences the rate at which energy can be dissipated in the sunlit high latitude ionosphere. At the present time, more comprehensive indices are being developed which give a physically meaningful parameter with which to describe the amount of energy entering the magnetosphere from the solar wind. The two parameters most frequently utilized at the present time are ε (Perreault and Akasofu, 1978) and $V_s B_z$ (V_s being the solar wind velocity and B_z the component of the IMF antiparallel to the earth's dipole field lines in the magnetospheric equatorial plane).

A major question at the present time is how the energy deposited in the magnetosphere from the solar wind is stored and dissipated. In particular, there is a considerable body of evidence (cf. Caan et al., 1977; Pellinen et al., 1982; Rostoker et al., 1982) which suggests that a significant amount of energy stored in the magnetotail during an episode of southward IMF may be released suddenly into the ionosphere at the time when the IMF experiences a northward turning of either a transient or a more long-lived nature. Thus, while some portion of the energy entering the magnetosphere from the solar wind is dissipated directly in the ionosphere (i.e. the driven system of Akasofu, 1981),

there is also a significant amount of energy stored in the magnetotail which can continue to drive the auroral electrojet system even after the energy entering the magnetosphere has been cut off through a reconfiguration of the IMF. Rostoker et al. (1982) have dealt with this problem and have suggested that when the IMF experiences a southward turning, the magnetotail must store some of the increased energy flowing into the magnetosphere. In this way the magnetotail can come into equilibrium with the changed plasma and field properties of the magnetosheath in which it is immersed. Correspondingly when, after a period of southward IMF, the interplanetary magnetic field experiences a northward turning, the magnetotail must reconfigure and give up energy so as to again come into equilibrium with the surrounding magnetosheath environment. In this paper we shall examine in some detail the response of high latitude current systems, on a global basis, to a well defined northward turning of the IMF.

Rostoker and Fälthammar (1967) first pointed out that the product of the solar wind velocity V_s and the north-south component of the IMF B_z (viz. the azimuthal component of the interplanetary electric field) was the relevant parameter to consider when trying to evaluate the amount of energy entering the magnetosphere from the interplanetary medium. (The point here is that, if the velocity of the solar wind is zero, no magnetic field is brought up to the front of the magnetosphere and therefore no merging of IMF and earth magnetic field lines can take place.) However, most researchers studying the solar-terrestrial interaction usually present only the IMF when attempting to establish the level of flow energy into the magnetosphere. One might expect that the flow of energy into the magnetosphere might be regulated, on occasion, purely by changes in solar wind velocity. That this should be the case is evident from the presence of the product of V_sB_z in both the interplanetary electric field parameter favored by some researchers (e.g. Baker et al., 1981) and the ε parameter favored by others (e.g. Akasofu, 1979, 1981). While, as pointed out above, reductions in this energy flow may act to trigger substorm expansive phases, we are able to show in this paper, using ISEE plasma and magnetic field data, that expansive phases may be initiated at times of little apparent change in either V_s or B_z.

Finally we note that the recovery of the magnetosphere from an episode of substorm activity yields an excellent opportunity to study the time constants of the magnetosphere as a whole. There has been a tendency in the past to involve the entire magnetosphere in each substorm perturbation. (For example, one school of thought contends that each substorm involves a neutral line which extends across the entire width of the tail resulting in large sections of the plasma sheet disappearing downstream after the formation of a near-earth neutral point (cf. Nishida and Nagayama (1973) and Hones (1979).) Certainly it appears that, at ionospheric levels, the substorm expansive phase occurs as the development of discrete filaments localized in both latitude and longitude which appear further and further to the west during the course of a substorm. This implies that each element of a substorm has a relatively small scale-size compared to the overall dimensions of the magnetotail and that different regions of the magnetotail can be activated at different times during the course of a substorm disturbance (cf. Rostoker and Camidge, 1971; Sergeev, 1974; Wiens and Rostoker, 1975; Baumjohann et al., 1981). The question then arises as to whether this structured behaviour of the magnetosphere during the substorm expansive phase is also evident during the recovery phase of the disturbance. In this paper we shall present, in detail, a global picture of the decay of the substorm current wedge after the final northward turning of the IMF alluded to earlier in the text. We shall show that the recovery phase can, in fact, proceed in a structured fashion and not as the smooth decay of all the relevant current systems on a global basis.

The Event of 12 December 1977: the Data and their Interpretation

This interval is part of a data set which was first studied at CDAW 1 in late 1978 and for which the data acquisition and distribution was organized by the Steering Committee for the IMS. The period of time we shall present is 0000–0800 on 12 December 1977. (All times given in this paper are in UT unless otherwise specified.) For this period, data from three satellites were available to describe conditions in the interplanetary medium and in the magnetosheath. These were the IMP 8 spacecraft and the ISEE 1 and 2 satellites, both equipped with plasma detectors and fluxgate magnetometers. At the time of the final northward turning IMP 8 was approximately 26 R_E in front of the earth and 17 R_E on the dusk side of the sun-earth line. At the start of the interval under study, ISEE 1 and 2 were inside the magnetopause, however by $\sim$0300 they entered the boundary layer and by $\sim$0345 they crossed the dawnside magnetopause and began to monitor the magnetosheath. ISEE 1 and 2 acted as magnetosheath monitors for the balance of the interval under study. Figure 1 shows the magnetic field data for IMP 8, Fig. 2 shows the magnetic field data from ISEE 1 and Fig. 3 shows the plasma data for ISEE 1 (which, at the time, was separated from ISEE 2 by less than 0.2 R_E). We shall refer back to these Figures as we proceed to identify the responses of the electric current systems to changes in the interplanetary medium. However, it is worthwhile at this point to identify some of the important features of the interplanetary particle and field parameters over the period of interest.

From the IMP 8 data, it is clear that the IMF was dominantly southward for the period 0000–0500 UT after which it was completely northward. During this interval, there were three well separated brief northward turnings of the IMF at $\sim$0030, 0130, and 0220. The separation time between these turnings is, in each case, greater than the approximate L/R time constant of $\sim$50 min for the magnetotail currents associated with the driven system (Rostoker and Boström, 1976) so that for each of these cases, if a substorm had been excited it would have had time to have substantively decayed. Apart from a brief excursion towards the north (although the IMF retained its southward direction throughout) the IMF B_z at IMP 8 reached a steady magnitude of $\sim$10 nT which it maintained for slightly over one hour before the northward turning of 0500 alluded to earlier took place. The total IMF strength over the interval 0000–0500 showed an irregular increase from $\sim$5 nT to $\sim$15 nT, with each of the short-lived northward turnings referred to above being accompanied by a drop in total field strength. The final northward turning at 0500 was also accompanied by a decrease in the total field strength of the IMF.

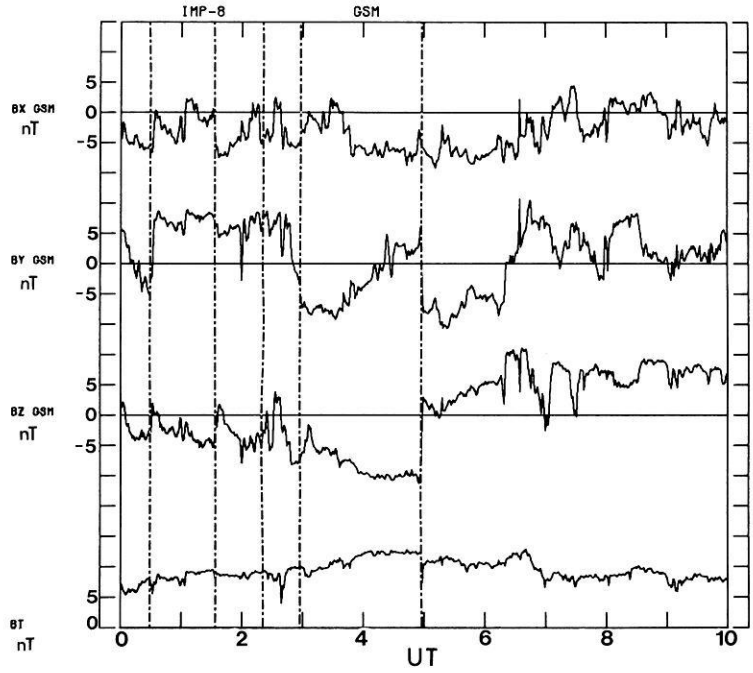

Fig. 1. The components of the interplanetary magnetic field plotted in solar magnetospheric coordinates together with the total field strength as measured by the IMP 8 spacecraft. At the start of the interval under study the satellite was 27 R_E in front of the earth and 17 R_E on the dusk side of the sun-earth line. The reader's attention is drawn to the transient northward turnings of the IMF at ~0030, ~0130, ~0230, ~0300 and the final northward turning at ~0458

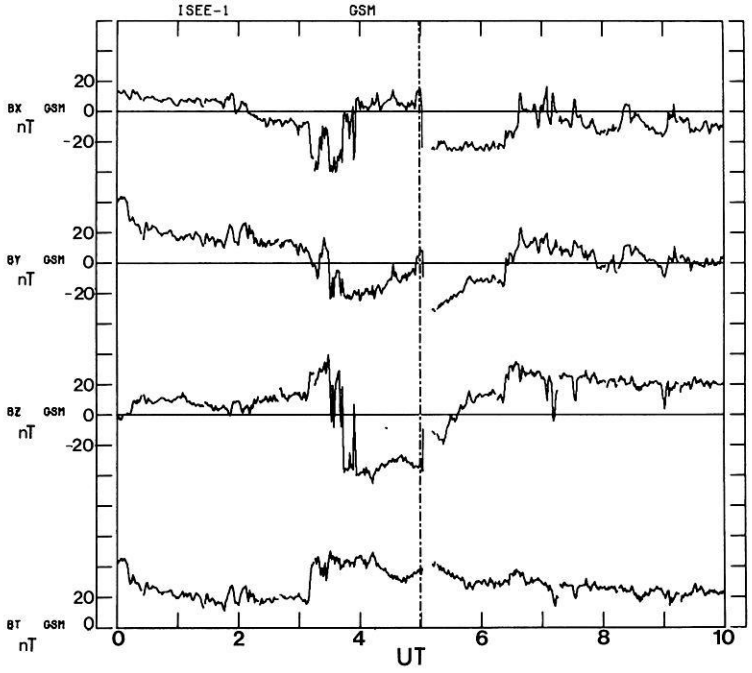

Fig. 2. The components of the magnetic field plotted in solar magnetospheric coordinates together with the total field strength as measured by the ISEE 1 spacecraft (see Russell (1978) for details of the ISEE fluxgate magnetometers). Until shortly after 0300 the satellite is in the magnetosphere. At that time the satellite enters the boundary layer near the dawn meridian and it emerges into the magnetosheath slightly before 0400. The reader is directed to the northward turning of the magnetosheath field just prior to 0500 at approximately the same time as the northward turning detected by IMP 8

The ISEE 1 and 2 satellites were in the magnetosphere until ~0345, after which they were in the magnetosheath. From the time they left the magnetosphere to the time of the 0500 northward turning of the IMF, the ISEE 1 satellite detected a steady southward IMF B_z component with a magnitude of ~30 nT (about a factor of 3 greater than the southward B_z measured at IMP 8 over the same period of time). Of great interest is the fact that the 0500 northward turning at ISEE 1 had a somewhat different structure than that observed at IMP 8. In particular, the IMF B_z component at IMP 8 became northward over a period of less than 5 min. In contrast, at ISEE 1 the B_z component went from about −35 nT of −10 nT at 0500 but did not become completely northward until the time of a second sharp northward turning at ~0520. The fact that the two satellites did not observe the same fine structure in the 0500 northward turning should serve as a warning to researchers trying to use data from a single satellite to correlate with terrestrial activity.

One final point of interest in the IMF data relates to the interval of time starting shortly after 0400, at which time the strength of the magnetosheath magnetic field (Fig. 2) and the velocity of the magnetosheath plasma appeared to decline noticeably (Fig. 3). During this interval

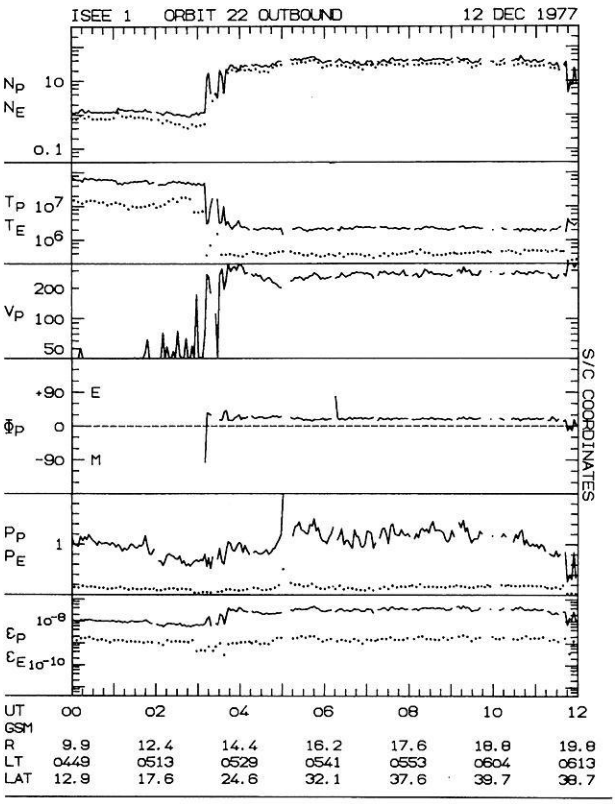

Fig. 3. Plasma parameters measured by the ISEE 1 spacecraft. N_e and N_p are the electron and proton number densities (cm^{-3}) respectively; T_e and T_p are the electron and proton temperatures (K) respectively; V_p is the proton bulk speed ($km \cdot s^{-1}$) and ϕ_p the azimuth direction of that bulk flow (0° being the sunward direction); p_e and p_p are the electron and proton thermal pressures (10^{-8} dynes $\cdot cm^{-2}$) respectively; ε_e and ε_p are the electron and proton energy densities (ergs $\cdot cm^{-3}$) respectively. The reader's attention is drawn to the magnetosheath bulk velocity which is $\sim$350 km s^{-1} at 0400 and which drops steadily over the following hour reaching $\sim$240 km s^{-1} by the time of the final northward turning of the magnetic field at $\sim$0500

the strength and direction of the IMF, as measured in the interplanetary medium by IMP 8, was not changing significantly. The changing plasma and magnetic field in the magnetosheath suggested that there must have been a change in solar wind velocity at the IMP 8 orbital position, however this was found not to be the case. The apparent discrepancy between the IMP 8 and ISEE data will be discussed later in the text.

We now proceed to present the changes in magnetospheric and ionospheric current systems occurring over the time interval 0000–0700 UT for which the interplanetary and magnetosheath conditions were described above. Our data will be presented in the form of individual magnetograms, stackplots of array data where such were available and latitutde and longitude profiles of magnetometer array data where some useful information could be effectively displayed using this latter format. We shall attempt to build up a complete picture of the various types of global activity occurring over the interval of time in question and in the following discussion section we shall interpret the various correlations in terms of the physics of the solar-terrestrial interaction.

The interval of five hours leading up to the start of the UT day 12 December 1977 featured continual activity which had subsided somewhat in the hour 2300–2400. Around 0030 on 12 December a substorm onset was detected in the Scandinavian sector (Fig. 4) – this substorm onset coincided with the northward turning of the IMF noted earlier (Fig. 1). A major episode of substorm activity was activated at $\sim$0130 in the Atlantic Ocean sector (Fig. 5) as was clearly observed at Leirvogur (Iceland) and at Narssarssuaq (Greenland). Again this substorm onset coincided with a northward turning of the IMF (described earlier) which took place after an interval of about one hour of rather strong ($\sim$3–5 nT) southward IMF. After some recovery had taken place following this latter event, a further substorm intensification occurred near 0230 (best seen at Narssarssuaq). This was relatively close in time to the third northward turning of the IMF referred to earlier. A further northward turning of the IMF shortly after 0300 is clearly associated with a further substorm intensification best observed at Leirvogur (Fig. 5). All this activity took place while ISEE 1 and 2 were in the magnetosphere, and it is with this last substorm development shortly after 0300 that these two satellites entered the boundary layer of the magnetosphere. Inspection of low latitude magnetograms for these first few hours of 12 December reveals that only the 0130 substorm could be classified as being of global impact. Figure 6 clearly shows a marked enhancement of the asymmetric ring current over the longitude range stretching from Kakioka to Tuscon across the afternoon sector. Further to the east, San Juan detects the classical positive *H*-component increase associated with the growth of the substorm current wedge for both the 0130 and $\sim$0300 substorm expansive phases. In summary, the interval of time from 0000–0400 more or less confirms the typical characteristics of the response of the magnetosphere to the changes in the north-south component of the IMF identified by Caan et al. (1977), Rostoker et al. (1982) and Pellinen et al. (1982); namely, after some reasonable amount of southward IMF is brought up to the front of the magnetosphere, a northward turning of the IMF leads to the onset of a magnetospheric substorm expansive phase.

The period of time from 0400–0500 also features an onset of substorm expansive phase activity, but in this case the IMF both outside the bow shock (IMP 8) and in the magnetosheath (ISEE 1 and 2) is relatively stable and strongly southward. The substorm expansive phase activity initiated around 0420, while not being particularly large, is typical in its character both on the local and global scale. The onset is most clearly identifiable in the Atlantic and Scandinavian sectors and there is a clear growth in asymmetric ring current stretching westward from San Juan to Kakioka. The sharpness of the electrojet onset seen in the Scandinavian sector (Fig. 4a) strongly suggests that the negative *H*-component bays are associated with an explosive increase in current strength rather than simply an increase in the strength of the driven system. This particular expansive phase onset is of interest because there is no identifiable change in the strength of the north-south component of the IMF with which to associate it. There are no particular significant fluctuations of the solar wind velocity or number density over the interval 0400–0500 as measured by IMP 8 (Table 1) so that the incoming solar wind momentum flux and electromagnetic field do not exhibit any fluctations which might be claimed to trigger the observed expan-

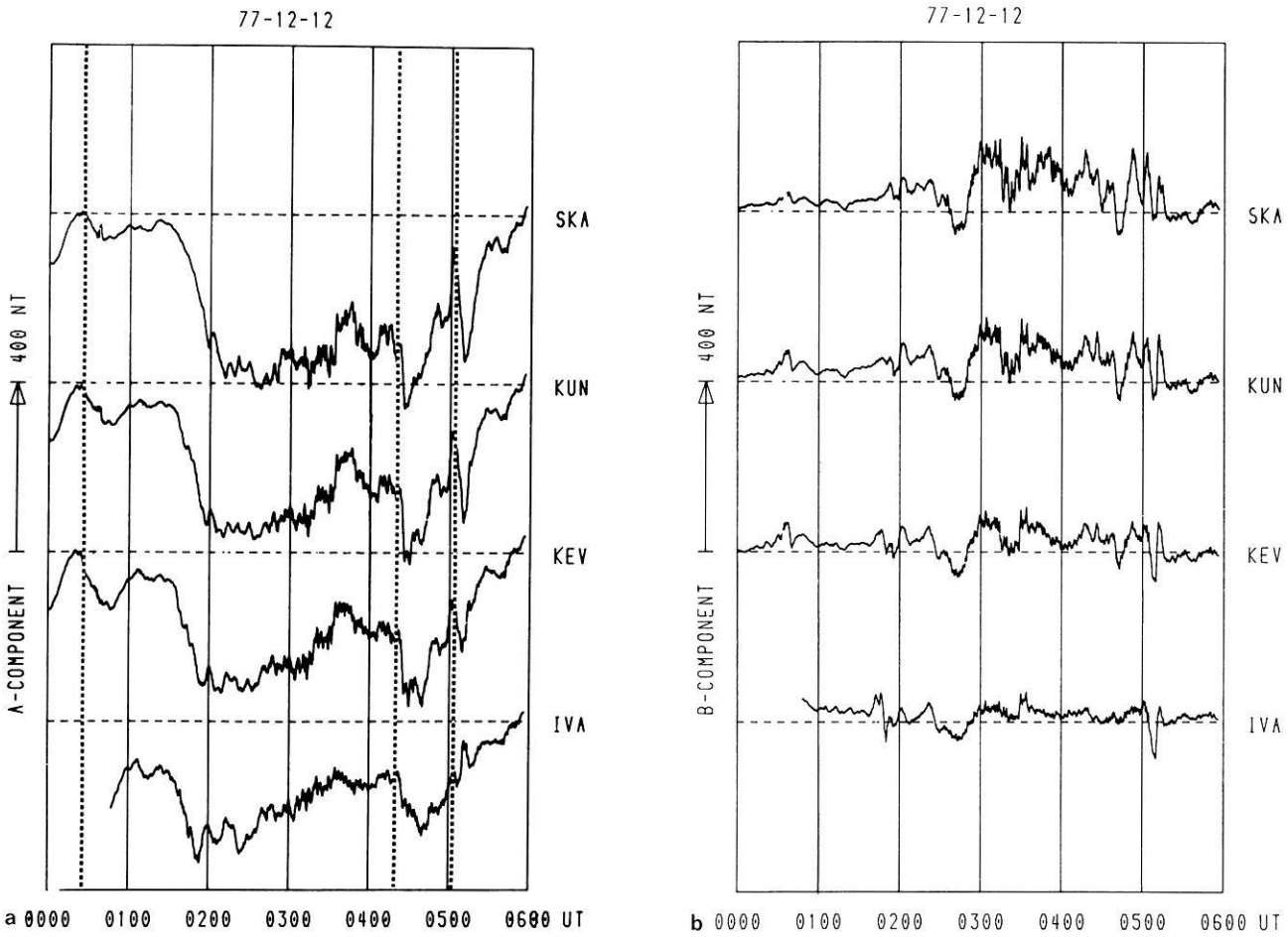

Fig. 4a and b. Stackplot of magnetograms form a meridian line of magnetometers located in eastern Scandinavia. **a** The north-south component of the perturbation field. **b** The east-west component of the perturbation field. The coordinates and code names of the stations are given in Appendix A

sive phase onset. The only possible interplanetary parameter which shows any unusual behaviour around the time of the expansive phase onset is the B_y component of the IMF which reverses polarity from negative to positive (Fig. 1). The behaviour of the magnetosheath plasma during the interval 0400–0520 is rather interesting although somewhat difficult to understand. The components of the plasma bulk velocity shown in Table 2 have been provided through the courtesy of Dr. C. Huang (University of Iowa). Perhaps the most significant feature here is the marked decrease in the Z-component of the magnetosheath bulk flow velocity around the time of the onset of the substorm expansive phase. The change in this component of the flow velocity coincides with the switch in polarity of the B_y component of the IMF from negative to positive. The return of B_y to negative values is accompanied by the return of the Z-component of the magnetosheath bulk flow to its previously high values prior to 0420. One further point of interest is that the spectrograms from the University of Iowa LEPEDEA indicate that after ~0420 there is a steady increase in the flux of sunward streaming particles in the magnetosheath. The presence of these sunward streaming particles influences the calculation of the bulk velocity of the magnetosheath plasma making the anti-sunward flow of plasma appear to be at a lower velocity than it really is (C. Huang, priv. comm.). It is difficult, at this time, to decide whether the change in the character of the magnetosheath plasma is influential in triggering the observed substorm activity or whether, on the other hand, it is stochastically triggered substorm activity which causes a reconfiguration of the magnetosphere leading to changes in the magnetosheath flow. Finally, it cannot be ruled out that the substorm onset observed at ~0420 was triggered internally and that the changes in the magnetosheath flow properties were completely unrelated to the substorm activity. Our observations do, however, suggest that further studies should be undertaken to establish if there are normally responses of magnetosheath flow to substorm onsets in the magnetosphere.

We now come to the northward turning at 0500 which is associated with the largest substorm expansive phase effect recorded over the interval studied in this paper. There are several points which we wish to bring to the attention of the reader regarding the morphology of this event. The first point relates to the interpretation of positive H-component disturbances in the auroral oval. On first sight, the positive movement of H-component at the auroral oval station of Leirvogur at 0500 (Fig. 5) would appear to indicate that the northward turning of the IMF at that time had initiated recovery of the magnetosphere. This would be exactly the wrong interpretation, as the sub-auroral stations of Ottawa, Whiteshell and Victoria (Fig. 8) clearly indicate

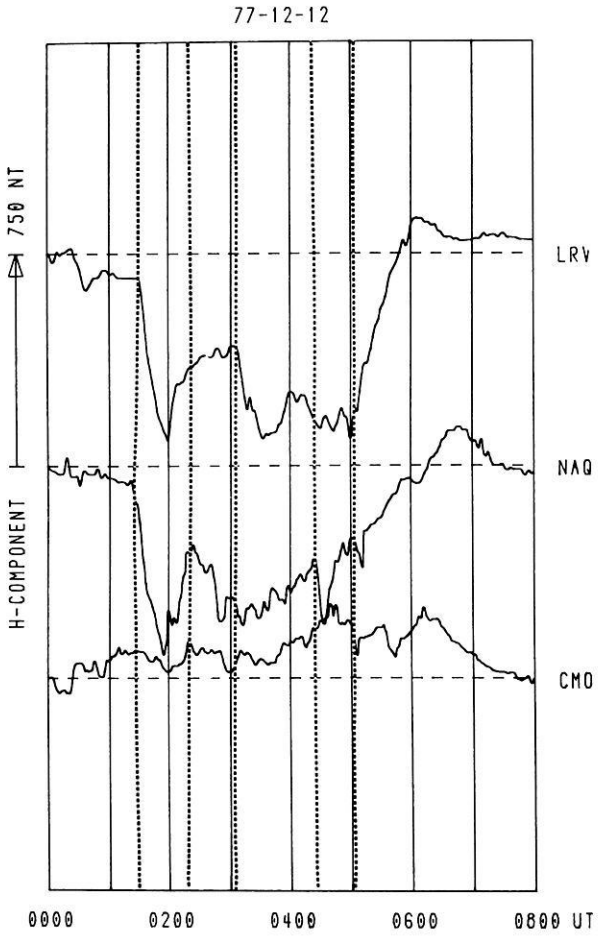

Fig. 5. *H*-component magnetograms from the auroral zone stations of Leirvogur, Narssarssuaq and College for the interval 0000–0800 on 12 December 1977. The coordinates and code names of the stations are given in Appendix A

Table 2. Components of magnetosheath plasma bulk velocity[a] obtained from the ISEE-1 LEPEDEA for the interval 0400–0520 on 12 December 1977

Time (UT)	V_x km·s^{-1}	V_y km·s^{-1}	V_z km·s^{-1}	V km·s^{-1}
0400	−358	−96	175	410
0402	−337	−87	166	386
0404	−323	−78	138	360
0406	−311	−85	110	341
0409	−314	−98	117	349
0411	−305	−95	132	346
0413	−273	−79	94	299
0415	−296	−105	97	329
0417	−307	−88	102	335
0419	−310	−88	116	342
0422	−304	−82	99	330
0424	−315	−84	81	336
0426	−295	−88	74	317
0428	−292	−90	69	313
0430	−292	−88	71	313
0432	−286	−88	72	308
0434	−293	−79	74	312
0437	−297	−85	82	320
0439	−291	−87	72	312
0441	−274	−83	64	293
0443	−278	−93	68	301
0445	−272	−106	62	298
0447	−269	−98	66	294
0449	−257	−96	53	279
0451	−263	−104	59	289
0454	−259	−102	58	284
0456	−254	−101	52	278
0458	−243	−86	63	265
0510	−267	−56	132	303
0512	−265	−59	145	308
0515	−262	−57	144	304
0517	−266	−59	141	307
0519	−266	−53	135	303

[a] Velocity components given in the GSM Coordinate System

Table 1. 5 min average values of the interplanetary plasma and magnetic field[a] parameters for the interval 0400–0520 on 12 December 1977

Time (UT)	B_x (nT)	B_y (nT)	B_z (nT)	V_s (km·s^{-1})	n_s (cm^{-3})
0400	−6.6	−3.5	−9.7	462	11.7
0405	−6.7	−2.5	−10.1	461	11.7
0410	−6.0	−1.2	−10.2	467	12.1
0415	−6.9	−0.8	−10.2	462	11.8
0420	−5.5	2.9	−10.1	485	11.5
0425	−6.1	−0.6	−10.5	468	12.0
0430	−6.2	2.9	−10.3	483	10.0
0435	−6.3	3.0	−10.1	470	10.1
0440	−7.3	2.1	−9.7	464	9.1
0445	−7.1	1.8	−9.7	460	9.3
0450	−6.2	2.4	−10.2	469	13.1
0455	−4.9	0.0	−5.0	469	11.5
0500	−6.7	−8.0	2.0	464	14.1
0505	−7.7	−7.3	1.4	463	12.2
0510	−8.3	−6.8	0.0	455	12.6
0515	−4.4	−10.0	9.0	477	15.1
0520	−4.5	−10.3	1.5	478	15.0

[a] Field magnitudes given in the GSM coordinate system

the development of a large substorm expansive phase at ~0505 as do the Alberta array stations further to the north (Fig. 7). The large negative *D*-component perturbation at Ottawa indicates that the western edge of the substorm current wedge is well to the west of Ottawa, while the positive *D*-component and rather weak response in the *H*-component at both Victoria and Newport (magnetogram not shown here) show the western edge of the wedge to be east of the Alberta array at the time of onset. The extremely large negative *Z*-component perturbation at Whiteshell associated with the substorm expansive phase effect in question strongly suggests that this station is near the equatorward edge of a substorm westward electrojet whose peak intensity is ~500 nT a few degrees further north. Note that, based on the above observations, one would conclude that the AE (or AL) index, which would be dominated by the Leirvogur contribution at ~0500, would decrease markedly after that time completely masking the fact that a major substorm expansive phase effect had taken place.

The question then arises as to why the westward electrojet near dawn (as reflected in the Leirvogur data) decreases in strength at the same time as the substorm current wedge is activated in the midnight sector. An answer to this question can be found in the results of Rostoker et al. (1982)

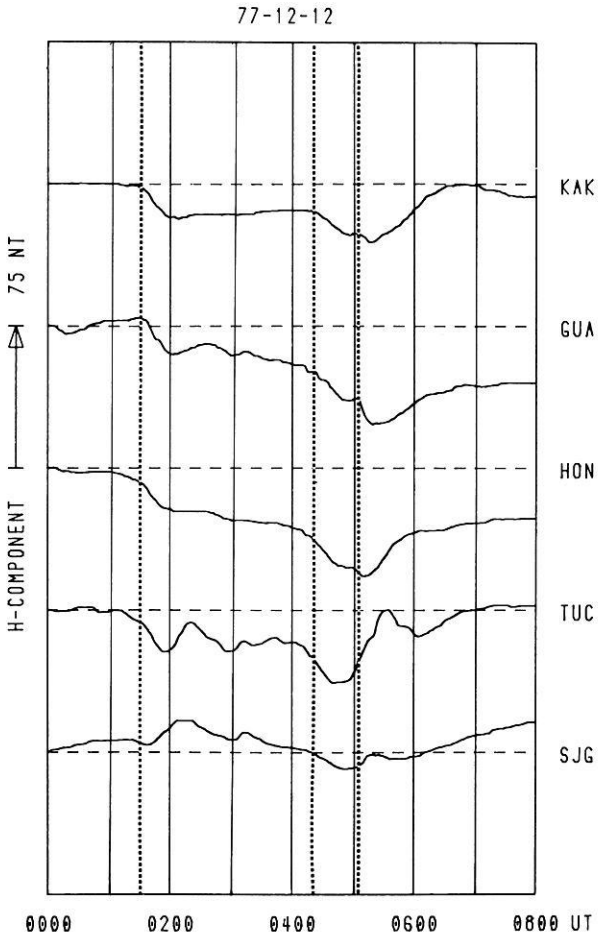

Fig. 6. *H*-component magnetograms from selected low latitude stations ranging from Kakioka in the west to San Juan in the east. The coordinates and code names of the stations are given in Appendix A

who suggested that, in conjunction with a northward turning of the IMF, a significant amount of magnetotail current (which is closing along the high latitude magnetotail boundary) is rerouted – some into the outer ring current belt (of which the cross-tail plasma sheet current is a component) and some directly into the ionosphere forming the substorm current wedge. In this way, some of the energy stored in the magnetotail magnetic field is deposited in the ionosphere where it is dissipated through Joule heating and through collisions of primary auroral particles with atmospheric constituents. The outer ring current belt is coupled to the auroral electrojets of the driven system (Akasofu, 1979, 1981) by field-aligned currents flowing into the auroral oval ionosphere across the noon sector and out of the ionosphere around the region of the Harang discontinuity in the pre-midnight quadrant (Hughes and Rostoker, 1977, 1979). The magnetic perturbations associated with this driven system produce the signature of the asymmetric or partial ring current (Cummings, 1966; Fukushima and Kamide, 1973). The ionospheric electrojets of the driven system and of the substorm current wedge are maximal at quite different local times with the driven system westward electrojet peaking late in the dawn sector (Allen and Kroehl, 1975) and the substorm current wedge peaking near midnight. Based on these considerations, we would suggest that the recovery of the negative *H*-component bay at Leirvogur signals the decline of the strength of the driven system due to the substantial decrease in solar wind energy entering the magnetosphere marked by the northward turning of the IMF. The substorm current wedge, on the other hand, responds to the release of magnetotail energy triggered by the northward turning of the IMF by markedly intensifying. It is quite clear that the maximum auroral electrojet strength associated with the substorm current wedge is attained near 0530 (see Whiteshell in Fig. 8) well after the entry of solar wind energy had been strongly reduced. We would contend that the energy powering the substorm current wedge is derived from the magnetotail during the expansive phase activity after 0500. The portion of the tail current rerouted into the ionosphere is clearly evident in the magnetic effects of the substorm current wedge. The low latitude stations (Fig. 6) show a strengthening of the asymmetric ring current (see e.g. the negative *H*-component perturbations at Guam and Kakioka in comparison to the response at San Juan) marking the temporary storage of the remainder of the tail energy which was redistributed through the rerouting of the magnetotail closure current of the magnetotail boundary. (See Fig. 17 of Rostoker et al. (1982) for a complete presentation of the current configuration in the magnetotail.)

The remaining points which we wish to discuss regarding the 0500 northward turning of the IMF and the ensuing change in magnetospheric substorm activity pertain to the manner in which the magnetosphere recovers to the ground state. Since the northward direction of the IMF persists for several hours after the 0500 northward turning, this would appear to be an excellent opportunity to study the recovery characteristics of the magnetosphere from a state of relatively strong activity.

The first point we wish to note is that the expansive phase breakup activity initiated at 0505 did not terminate immediately but carried on for approximately one hour with intermittent intensifications (as can be seen from the fact that the eastward electrojet in the College sector did not begin to decay until after ~0610). Since the IMF was clearly northward during this period of time, we conclude that the energy for these substorm intensifications continues to be derived from the magnetotail through the release of stored energy. Even during the substorm current wedge intensifications, the driven system electrojets continue to decay as reflected by the decay of the negative *H*-component bays recorded at Leirvogur and Narssarssuaq (Fig. 5) and the eastward electrojet strength as detected in the evening sector by Sitka (Fig. 8). The decaying driven system electrojets result from the reduction of the velocity of plasma convection in the magnetosphere, with the kinetic drift energy of the plasma being converted through MHD generator mechanisms to the electrical energy needed to account for the dissipation of energy in the ionosphere through Joule heating (Rostoker and Boström, 1976).

A second point which we find very striking is the rapidity with which the ionospheric electrojet currents associated with the substorm current wedge can decay in a given region of space. We see this most clearly in the Alberta array magnetograms (Fig. 7) where, just prior to 0600, the *H*-component of the auroral zone east-west line magnetograms recovers to pre-substorm values within ~15 min. This is a factor of ~8 less than the time constant of the driven system as evaluated by Clauer et al. (in press 1983)

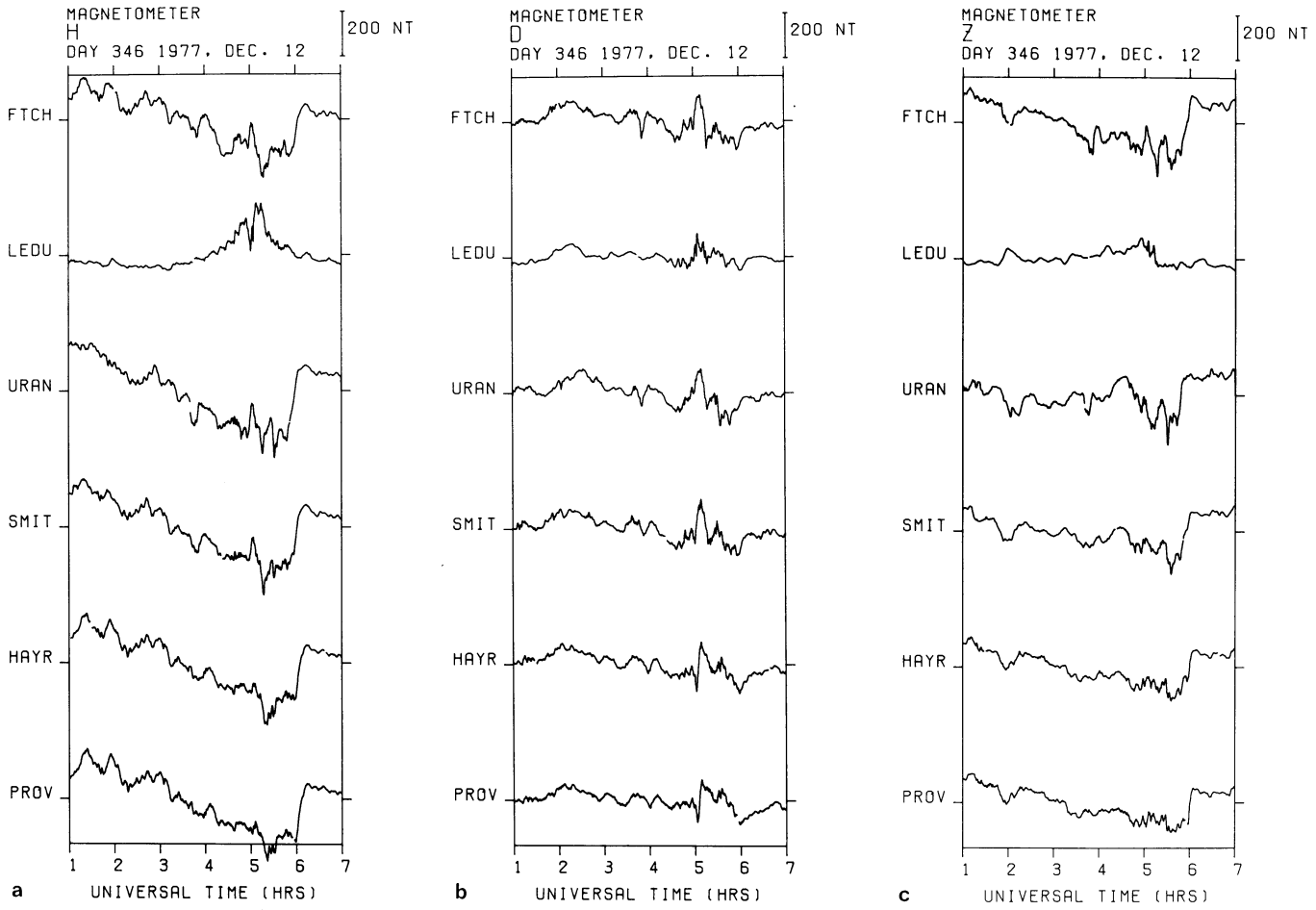

Fig. 7a–c. Stackplot of magentograms from the Alberta array, **a** the *H*-component, **b** the *D*-component, **c** the *Z*-component. The coordinates and code names of the stations are given in Appendix A. The stations URAN, SMIT, HAYR and PROV lie along a common line of geomagnetic latitude over a longitudinal range of ~12° at 67.3° N. The southernmost station of LEDU is dominated by the eastward electrojet associated with the driven system while the stations further north are strongly influenced by the substorm current wedge

and demands that the scale size of the substorm current wedge be considerably smaller than that of the driven system. Furthermore, since the convective drift velocity of the magnetotail plasma varies on the time scale of the driven system, this suggests that the sharp reduction in ionospheric electrojet current flow must be due to a reduction in ionospheric conductivity as suggested some time ago by Gurnett and Akasofu (1974). The effects of the driven system are also seen in the Alberta sector as reflected in the behaviour of the eastward electrojet most easily seen in the *H*-component magnetogram from the lowest latitude station of Leduc. Aside from a brief positive spike in the *H*-component which is associated with the passage of the westward travelling surge over the Alberta array shortly after 0500, the recording provides a measure of the decay of the eastward electrojet (which has a time constant of the order of that expected for the driven system).

The final point which we wish to deal with relates to the details of the decay of the substorm current wedge which had built up from the time that the IMF turned northward shortly before 0500. On the time scale of Fig. 7, the decay of the current wedge appears to be simultaneous at all the Alberta array auroral zone stations. However, when we expand the time scale for these data (Fig. 9) we find that the recovery is quite structured with sudden episodes of decay occurring at approximately 10–15 min intervals. What is most interesting is that the decay is observed first at the easternmost edge of our overall IMS array (LYN) and last at the westernmost edge (NOW). It appears to be the case that the substorm current wedge collapses from east to west across our array. Our earlier observation that the decay of the substorm current wedge occurs as a consequence of a reduction in ionospheric conductivity can now be understood in the context of the following picture of the lifetime of a substorm electrojet system.

Earlier studies of multiple onset substorms (Wiens and Rostoker, 1975; Pytte et al., 1976; Baumjohann et al., 1981) suggested that the typical development of such a disturbance involved the sequential onset of several substorm electrojet elements, each one further to the north and often west of the previous one. The ensemble of these current elements makes up the substorm current wedge and each element can co-exist with the elements formed earlier and later in the sequence. If each element has roughly the same characteristic lifetime, one would expect the first element in the sequence (namely the most eastern one) to decay

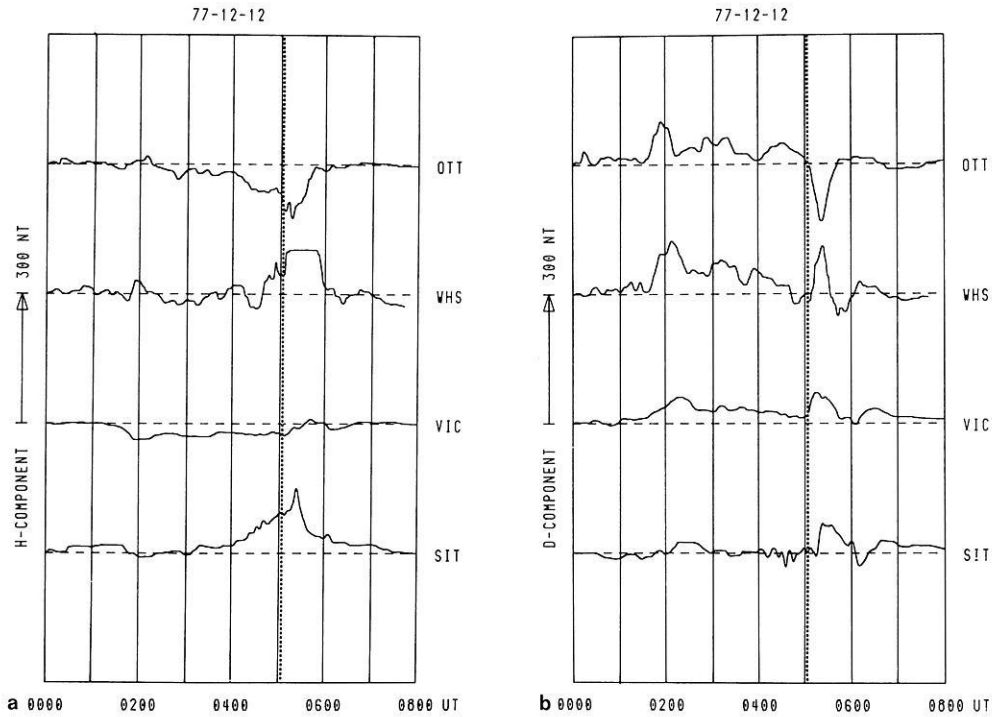

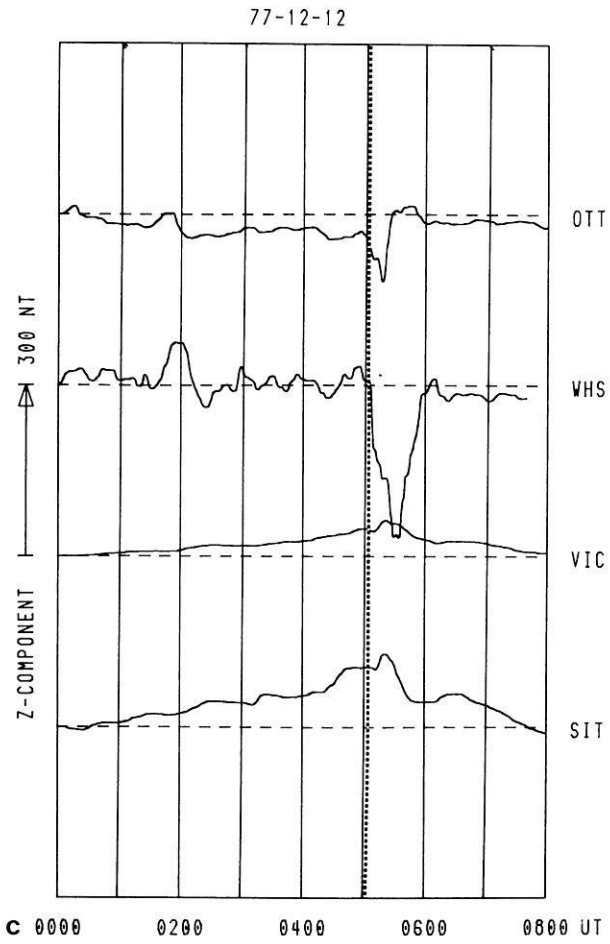

Fig. 8a–c. Stackplot of magnetograms from selected sub-auroral observatories for the interval 0000–0800 on 12 December 1977. **a** The *H*-component, **b** the *D*-component, **c** the *Z*-component. The flat portion of the WHS *H*-component trace from ~0510–0550 indicates saturation on the scale of the magnetogram utilized. The coordinates and code names of the stations are given in Appendix A. The data shown here can be used to establish the azimuthal extent of the substorm current wedge

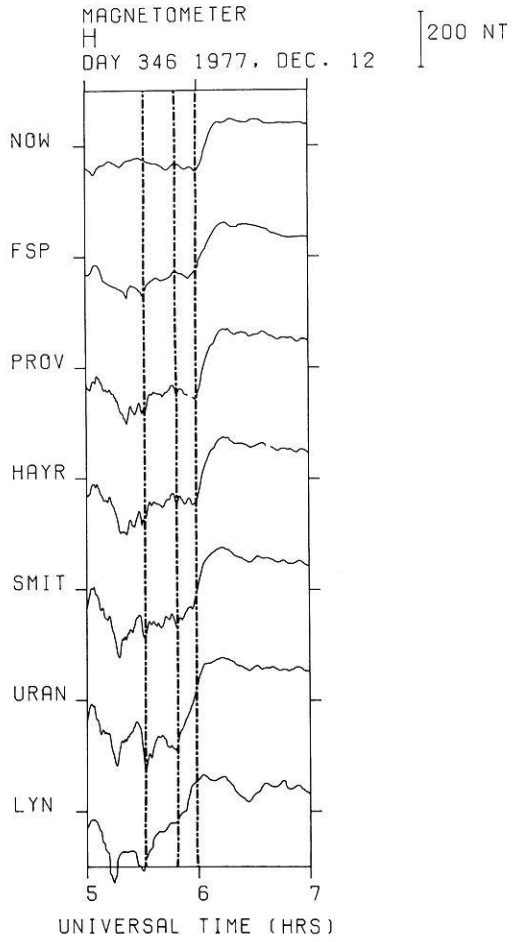

Fig. 9. *H*-component data for the interval 0500–0630 recorded at several stations lying along the auroral oval in the North American sector from LYN in the east to NOW in the west. The coordinates and code names of the stations are given in Appendix A. Note the impulsive character of the substorm recovery with LYN recovering well in advance of the recovery at NOW

first. In this framework we can now understand why the substorm current wedge collapses from east to west across our array. Insofar as the physical processes leading to the development of an electrojet element are concerned, we associated the onset with the sudden activation of the acceleration region at ~ 1 R_E altitude due to the growth of field-aligned current densities to above $\sim 10^{-6}$ A m^{-2} (see Akasofu, 1981 and Pellinen et al., 1982 among others). The crossing of this current density threshold accounts for the sudden precipitation of keV electrons into the ionosphere characteristic of the development of discrete auroral forms at the onset of an auroral breakup. Equally, we believe that when the current density of the field-aligned current drops below $\sim 10^{-6}$A m^{-2}, the acceleration can terminate as suddenly as it turned on. This would happen sequentially with the electrojet element which began the sequence being the first to suddenly disappear. In this manner, we can understand both the east-to-west collapse of the substorm current wedge and the rapidity which the decay of each electrojet element exhibits.

Summary of Results

The International Magnetospheric Study involved the cooperative acquisition of ground based and satellite data using an array of instrumentation which was far superior to anything available in the past for the study of global processes in the magnetosphere. Our study has taken advantage of the availability of this superior data base to deal with the problem of the development and decay of magnetospheric substorm activity on both a global and a local scale. Our major findings are as follows:

(1) We provide further evidence that northward turnings of the IMF, after periods of southward IMF have allowed energy to be stored in the magnetotail, can trigger significant substorm expansive phase activity, the energy for which is derived from the magnetotail. Although there has been evidence presented in the past for such an influence of the IMF on substorm activity, there have been some doubts expressed as to the strength of the correlations presented. Even for the case of isolated substorms, where the correlation has been presented recently by Rostoker (in press, 1983), the question has arisen as to whether or not isolated substorms have the same characteristic behaviour as more typical substorms which occur during intervals of more turbulent IMF when the field is never northward or southward for more than a few minutes at a time. In this study we have presented three instances where the IMF fluctuated northward after sustained intervals of southward directed field. These three instances occurred in an interval of less than four hours, and in each case we were able to point to their correlation with the onset of enhanced expansive phase activity. Thus, even for our more complex event, which certainly cannot be thought of as an isolated substorm, the effect of northward turnings of the IMF as a trigger for substorm expansive phase activity seems clear. In addition, we have noted that substorms can be triggered even under conditions when the north-south component of the IMF is relatively constant and the solar wind velocity and number density are unchanging (as typified by the 0420 substorm expansive phase onset). While the possibility of changes in the B_y component of the IMF triggering substorms such as the 0420 event are not ruled out, it appears that there may be substorm onsets which are triggered internally within the magnetosphere rather than externally. Further studies are needed to provide a clearer picture of the influence of fluctuations in the interplanetary medium plasma and field as a trigger for magnetospheric substorm expansive phases.

(2) We have studied in detail the behaviour of the magnetosphere-inosphere current systems in response to a sharp northward turning of the IMF followed by a period of sustained northward field of the order of a few hours. In this case we have provided convincing evidence that at least some substorm expansive phase activity can be driven by the unloading of magnetotail energy stored during the growth of the driven system. Our case study has shown the great danger in using *AE* or *AL* to define the presence or absence of substorm expansive phase activity, since these indices are very often dominated by the effects of the driven system rather than the substorm current wedge.

(3) We have shown that, following the reduction of energy flow from the solar wind into the magnetosphere, the substorm current wedge can grow at the same time as the driven system is decaying. This demonstrates the need to take great care in correlating increases and decreases in auroral current systems with changes in the level of the solar-terrestrial interaction.

(4) We have shown that the decay of the substorm cur-

rent wedge occurs as the sequential sudden collapse of segments of the ionospheric electrojet. The decay starts at the most eastern edge of the wedge and proceeds westward until the entire electrojet has disappeared. We have pointed to a threshold effect in the current denstiy of upward field-aligned current as a possible explanation of the sudden turning on of the electrojet elements which constitute the substorm current wedge and the equally sudden turning off of these electrojet elements.

We conclude by noting that a great deal of data (i.e. from an adequate array of ground stations and suitably equipped satellites) must be analysed in order to be able to minimize the ambiguity in the interpretation of the behaviour of the magnetosphere-ionosphere current systems in response to changes in the interplanetary medium. Many studies of the kind we have reported here must be carried out in the future for different interplanetary plasma and field environments before most of the suggestions made in this paper can be placed on a firm basis. The data base acquired during the International Magnetospheric Study is now available for these much needed detailed studies of the various ways in which the magnetosphere can respond to changes in the interplanetary medium.

Appendix A. Geomagnetic coordinates and code names of stations used in this study

Station Name	Code Name	Geomagnetic	
		Latitude (°N)	Longitude (°E)
Alberta Array			
Leduc	LEDU	60.6	302.9
Fort Chipewyan	FTCH	66.3	303.1
Uranium City	URAN	67.4	304.3
Fort Smith	SMIT	67.3	300.0
Hay River	HAYR	67.3	294.3
Fort Providence	PROV	67.5	292.0
Scandinavian Array[a]			
Ivalo	IVA	65.0	109.9
Kevo	KEV	66.2	110.6
Kunes	KUN	66.8	110.8
Skarsvag	SKA	67.6	111.0
Additional High Latitude Stations			
Leirvogur	LRV	70.2	71.0
Narssarssuaq	NAQ	71.0	37.0
Lynn Lake	LYN	66.0	315.6
Norman Wells	NOW	69.2	278.8
College	CMO	64.6	256.5
Fort Simpson	FSP	67.2	287.2
Sub-Auroral Stations			
Ottawa	OTT	54.6	247.1
Whiteshell	WHS	58.6	323.1
Victoria	VIC	54.2	293.0
Sitka	SIT	60.0	275.3
Low Latitude Stations			
Kakioka	KAK	26.0	206.0
Guam	GUA	4.0	212.9
Honolulu	HON	21.1	266.5
Tucson	TUC	40.4	312.2
San Juan	SJG	29.6	3.1

[a] Coordinates of the Scandinavian stations are given in revised geomagnetic coordinate system

Acknowledgements. We thank H. Maurer (TU, Braunschweig) for putting the digital recording of the Scandinavian magnetometer data at our disposal. We gratefully acknowledge Environment Canada (Atmospheric Environment Service) and Transport Canada (Telecommunications Branch) for their assistance in setting up and operating the stations in the Alberta array. The authors gratefully acknowledge Dr. G. Paschmann (Max-Planck-Institut für Physik and Astrophysik, Garching, F.R.G.), Dr. L.A. Frank and Dr. C. Huang (University of Iowa) for providing the ISEE plasma flow data and for helping in the interpretation. The IMP 8 plasma and magnetic field data were provided by WDC-A-R and S though the courtesy of Dr. J.H. King. Standard magnetometer data used in this study were supplied by WDC-A for Solar Terrestrial Physics and Dept. of Energy, Mines and Resources (Earth Physics Branch) of Canada. The work of W.B. was supported financially by grants from the Deutsche Forschungsgemeinschaft while that of G.R. was supported by the Natural Sciences and Engineering Research Council of Canada. G.R. further gratefully acknowledges financial assistance from the Deutscher Akademischer Austauschdienst while on leave at Universität Münster. The work of C.T.R. was supported by the National Aeronautics and Space Administration under Research Contract NAS5-25772. This research is part of the International Magnetospheric Study.

References

Akasofu, S.-L.: What is a magnetospheric substorm? In: Dynamics of the Magnetosphere. S.-I. Akasofu ed: pp. 447–460. Dordrecht-Holland: D. Reidel Publ. Co. 1979

Akasofu, S.-I.: Energy coupling between the solar wind and the magnetosphere. Space Sci. Rev. **28**, 121–190, 1981

Allen, J.H., Kroehl, H.W.: Spatial and temporal distributions of magnetic effects of auroal electrojets as derived from AE indices. J. Geophys. Res. **80**, 3667–3677, 1975

Axford, W.I., Hines, C.O.: A unifying theory of high latitude geophysical phenomena and geomagnetic storms. Can. J. Phys. **39**, 1433–1464, 1961

Baker, D.N., Hones, E.W., Jr., Payne, J.B., Feldman, W.C.: A high resolution study of interplanetary parameter correlations with AE. Geophys. Res. Lett. **8**, 179–182, 1981

Baumjohann, W., Pellinen, R.J., Opgenoorth, H.J., Nielsen E.: Joint two-dimensional observations of ground magnetic and ionospheric electric fields associated with auroral zone currents: Current systems associated with local auroral break-ups. Planet. Space Sci. **29**, 431–447, 1981

Caan, M.N., McPherron, R.L., Russell, C.T.: Characteristics of the association between the interplanetary magnetic field and substorms. J. Geophys. Res. **82**, 4837–4842, 1977

Clauer, C.R., McPherron, R.L., Searls, C.: Solar wind control of the low-latitude asymmetric magnetic disturbance field. J. Geophys. Res, in press 1983

Cummings, W.D.: Asymmetric ring current and the low latitude daily variation. J. Geophys. Res. **71**, 4496–4503, 1966

Dungey, J.W.: Interplanetary magnetic field and the auroral zones. Phys. Res. Lett. **6**, 47–48, 1961

Fairfield, D.H., Cahill, L.J., Jr.: Transition region magnetic field and polar magnetic disturbances. J. Geophys. Res. **71**, 155–169, 1966

Fukushima, N., Kamide, Y.: Partial ring current models for worldwide geomagnetic disturbances. Rev. Geophys. Space Phys. **11**, 795–853, 1973

Gurnett, D.A., Akasofu, S.-I.: Electric and magnetic field observations during a substorm on February 24, 1970. J. Geophys. Res. **79**, 3197–3200, 1974

Hones, E.W., Jr.: Plasma flow in the magnetotail and its implications for substorm theories. In: Dynamics of the Magnetosphere. S.-I. Akasofu, ed: pp. 545–562. Dordrecht-Holland: D. Reidel Publ. Co. 1979

Hughes, T.J. Rostoker, G.: Current flow in the magnetosphere and ionosphere during periods of moderate activity. J. Geophys. Res. **82**, 2271–2282, 1977

Hughes, T.J., Rostoker, G.: A comprehensive model current system for high latitude magnetic activity 1. The steady state system. Geophys. J. **58**, 525–569, 1979

Nishida, A., Nagayama, N.: Synoptic survey for the neutral line in the magnetotail during the substorm expansion phase. J. Geophys. Res. **78**, 3782–3798, 1973

Pellinen, R.J., Baumjohann, W., Heikkila, W.J., Sergeev, V.A., Yahnin, A.G., Marklund, G., Melnikov, A.O.: Event study on pre-substorm phases and their relation to the energy coupling between solar wind and magnetosphere. Planet. Space Sci. **30**, 371–388, 1982

Perreault, P.D., Akasofu, S.-I.: A study of geomagnetic storms. Geophys. J. **54**, 547–573, 1978

Pytte, T., McPherron, R.L., Kokubun, S.: The ground signatures of the expansion phase during multiple onset substorms. Planet. Space Sci. **24**, 1115–1132, 1976

Rostoker, G.: Triggering of expansive phase intersifications of magnetospheric substorms by northward turnings of the interplanetary magnetic field. J. Geophys. Res., in press 1983

Rostoker, G., Fälthammar, C.-G.: Relationship between changes in the interplanetary magnetic field and variations in the magnetic field at the earth's surface. J. Geophys. Res. **72**, 5853–5863, 1967

Rostoker, G., Camidge, F.P.: The localized character of magnetotail magnetic fluctuations during polar magnetic substorms. J. Geophys. Res. **76**, 6944–6951, 1971

Rostoker, G., Boström, R.: A mechanism for driving the gross Birkeland current configuration in the auroral oval. J. Geophys. Res. **81**, 235–244, 1976

Rostoker, G., Mareschal, M., Samson, J.C.: Response of dayside net downward field-aligned current to changes in the interplanetary magnetic field and to substorm perturbations. J. Geophys. Res. **87**, 3489–3510, 1982

Russell, C.T.: The ISEE 1 and 2 fluxgate magnetometers. I.E.E.E. Trans. on Geoscience Electronics **GE-16**, 239–242, 1978

Sergeev, V.A.: On the longitudinal localization of the substorm active region and its changes during the substorm. Planet. Space Sci. **22**, 1341–1343, 1974

Wiens, R.G., Rostoker, G.: Characteristics of the development of the westward electrojet during the expansive phase of magnetospheric substorms. J. Geophys. Res. **80**, 2109–2128, 1975

Received January 27, 1983; Revised version June 7, 1983
Accepted June 21, 1983

J Geophys (1983) 53:182–197

Journal of Geophysics

Substorm Time Sequence and Microstructure on 11 November 1976*

A.G. Yahnin[1], V.A. Sergeev[2], R.J. Pellinen[3], W. Baumjohann[4], K.U. Kaila[3], H. Ranta[5], J. Kangas[6] and O.M. Raspopov[1]

[1] Polar Geophysical Institute, Kola Branch Acad. Sci. USSR, Apatity, 184200, USSR
[2] Institute of Physics, University of Leningrad, Leningrad 198904, USSR
[3] Finnish Meterological Institute, Division of Geomagnetism, Box 503, SF-00101 Helsinki 10, Finland
[4] Institut für Geophysik der Universität Münster, Correnstraße 24, D-4400 Münster, FR Germany
Present address: Max-Planck-Institut für Physik und Astrophysik, Institut für Extraterrestrische Physik, D-8046 Garching, FR Germany
[5] Geophysical Observatory, SF-99600 Sodankylä, Finland
[6] Department of Physics, University of Oulu, Linnanmaa, SF-90570 Oulu 57, Finland

Abstract. Two substorms of different character are studied by means of data recorded on 11 November 1976 both on the ground and in the solar wind. The first, rapid and widespread substorm occurred at the end of a period of almost constant, intense magnetospheric convection. The second, weak, shortlived and localized substorm was preceeded by variable magnetospheric convection that was obviously controlled by changes in the interplanetary magnetic field. In spite of the large differences in the extent and strength of the substorms, obvious similarities in their temporal development were found. Prior to both substorms, growth-phase-type energetic electron precipitation was recorded. During the expansion phases, each impulsive arc brightening as well as each auroral arc formation at the leading edge of the auroral bulge was accompanied by a burst of energetic electron precipitation, by a burst of Pi pulsations and by an impulsive change of the equivalent ionospheric currents recorded in the auroral zone. At mid-latitudes a sharp change in the amplitude and phase of Pi2 pulsations was observed. The fine structure observed represents discrete steps in the development of the expanding auroral bulge, that were separated by 1–3 min from each other. Details of the bulge development and of the altitudes of different auroral structures within the bulge are given. The role of variations in the interplanetary magnetic field on the development of the substorms is discussed.

Keywords: Auroral absorption – Auroral altitude – Auroral bulge – Convection bay – Growth phase – Interplanetary magnetic field – Microsubstorm – Multiple onset – Pi2 – PiB – Substorm

Introduction

The concept of magnetospheric substorm (Akasofu, 1968), being historically a large step towards an understanding of magnetospheric disturbances, does not contain (both in the initial and modified form; Akasofu, 1977; McPherron, 1979) a detailed description of the development of different ionospheric and magnetospheric phenomena during a substorm. Hence, one of the most important and urgent tasks in magnetospheric physics is to learn more about the time sequence and the phenomenology of substorms (Roederer, 1977).

Three recent findings seem to be of special importance in this respect. First, it was established that intense magnetic disturbances (on the global scale) and bright discrete auroral arcs can occur for long times without any signatures of substorm expansion both on the ground and in the magnetotail (Kokubun et al., 1977; Sergeev, 1977; Pytte et al., 1978a; Fairfield et al., 1981). These observations were explained as a manifestation of enhanced magnetospheric convection (for a more comprehensive discussion see Sergeev and Tsyganenko, 1980).

Second, it was recognized that common expansion related features, observed both on the ground and in the magnetotail, may repeat several times with durations of 5–10 min and repetition intervals between 5 and 30 min. These individual events, called microsubstorms (Sergeev, 1974) or substorm intensifications (Rostoker et al., 1980), correspond to time intervals of explosive energy dissipation from the magnetotail into the ionosphere (Sergeev, 1981). Each event seems to be fairly localized both in the magnetotail and in the ionosphere (Wiens and Rostoker, 1975; Clauer and McPherron, 1974; Sergeev, 1974; Vorobjev and Rezhenov, 1973; Saito et al., 1976; Pytte et al., 1976a, b, 1978b; Sergeev and Yahnin, 1979a; Baumjohann et al., 1981).

Third, the last result that has to be mentioned in this context is the fine structure of each microsubstorm. Sergeev and Yahnin (1979b) have recently shown that auroral expansions usually proceed through formation of new structures at the poleward border of the auroral bulge. Signatures of similar step-like processes were found in balloon X-ray measurements (Pytte et al. 1976c; Melnikov et al., 1978), in cosmic noise absorption recordings and in Pi2 pulsation data (Sergeev et al., 1978), as well as in magnetic field variations recorded in the magnetotail (Sergeev, 1981).

* Main results of this study were presented at the Second Workshop on IMS Observations in Northern Europe held at Bad Lauterberg, Federal Republic of Germany, 1978

Offprint requests to: A.G. Yahnin

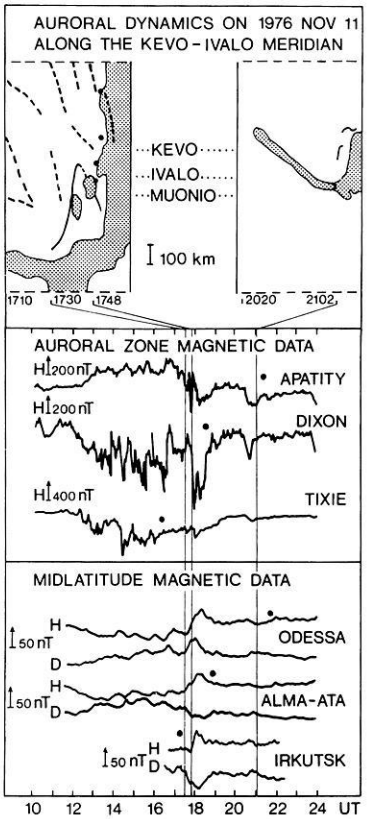

Fig. 1. Position of auroras (*dots:* diffuse and irregular auroras; *lines* and *thick points:* discrete auroras) along the Ivalo meridian under the assumption of 100 km height of auroras (*top panel*); magnetograms of a few auroral zone (*center panel*) and mid-latitude stations (*bottom panel*) for 11 November 1976. Black dots in the magnetograms denote local magnetic midnight at the respective stations

In our opinion, to proceed further in the studies on substorm time sequence the following necessary steps have to be taken:

1) To document more precisely the local features of the whole magnetospheric substorm;

2) To study more extensively the relationship between local and global substorm features;

3) To check the consistency of the phenomenological models proposed for the different types of disturbances (e.g. intense isolated substorms, prolonged intense disturbances, small and localized substorms).

These three aspects form the main topic of the present study. Our data were recorded by extensive networks of all-sky cameras, riometers, induction magnetometers and by a two-dimensional array of magnetometers operated in the Northern Europe during the International Magnetospheric Study, IMS, 1976–79. Balloon X-ray measurements were made during one of the events. The whole data set provides an opportunity to study local substorm features with a time resolution better than one minute. The information on the global magnetic effects and mid-latitude Pi2 pulsations were obtained from standard observatory data.

The two substorms under examination are not "typical" in the "classical" sense (intense, isolated, duration about 1 h). The expansion phase of the first event started at 1730 UT (Fig. 1) at the end of an interval of prolonged and intense auroral zone activity. The second event, starting at about 2100 UT was preceded by a bay-like disturbance of 30 min duration in the auroral zone and at mid-latitudes that looked like an isolated substorm, but, as we shall show later, was just a worldwide magnetic bay occurring during the substorm growth phase (Pellinen et al., 1982). No evident worldwide effects were observed during the subsequent weak, short-lived and fairly localized expansion phase.

Instrumentation and Methods of Data Handling

The main observation sites, their coordinates and instrumentation are listed in Table 1.

In addition to the standard magnetic observatory data rapid-run magnetograms and pulsation recordings (0.01–0.2 Hz) from Borok, Kaliningrad and Lovozero were available for the analysis. Pulsation recordings in a higher frequency range (0.1–2 Hz) were made at Kevo, Sodankylä, Oulu and Nurmijärvi. For the second event data of the Scandinavian Magnetometer Array (SMA) were also available. The locations of the SMA stations and details on the instrumentation can be found in Küppers et al. (1979).

A description of the Finnish riometer chain used in this study is given in Ranta (1978).

On 11 November 1976 all-sky cameras were operated at Esrange (near Kiruna), Kevo, Ivalo and Muonio at a speed of 1 frame/min. Technical data on the Finnish all-sky cameras are given in Hyppönen et al. (1974). The positions of auroral forms were calculated from simultaneous all-sky photographs by fitting the digitized lower border of an auroral arc from two different stations, using the position and altidues as variable parameters (for details see Kaila, 1981).

Details of the SAMBO-76 campaign and the balloon data used in this study can be found in Zhulin et al. (1978) and Melnikov et al. (1978). Three balloons were located at latitudes between Ivalo and Sodankylä and longitudes between Muonio and Ivalo during the second event (see Fig. 8b).

Interplanetary magnetic field (IMF) data obtained by the IMP-8 satellite, were available for the entire period.

Observations

On 11 November 1976 two separate auroral substorms were recorded in the Scandinavian region from 1730–1800 UT and from 2030–2110 UT. Below, these substorms will be treated in the following way: Mid-latitude magnetic bays (McPherron et al., 1973; Sergeev, 1974; Wiens and Rostoker, 1975) and Pi2 pulsations (Saito et al., 1976) will be analyzed to study the global features of these substorms. According to Rostoker et al. (1980) these data give information about both strong and weak expansions occurring in any local time sector. Local features will be studied by investigating in detail the auroral zone data recorded in the Scandinavian sector. The discrete events observed during the expansion phases are summarized in Table 2.

Time Interval 1730–1800 UT

Global features. In general, between 1200–1900 UT the level of magnetic activity in the auroral zone is rather high as can be deduced from Fig. 1. However, between 1630–1730 the Pi2 activity is low at Lovozero, Borok and Kaliningrad (data not shown here) and there are no sharp magnetic

Table 1. Permanent or temporary stations from which data have been used in the present study

Station	Symbol	Geogr. Coord.		Corr. geom. coord.[a]		Type of instrument
Alma-ata	AAA	43°15′N	76°55′E			M
Apatity	APA	67 33	33 20			M
Borok	BOX	58 02	38 20	53.5°N	113.8°E	M(2) P
Boulder	BOU	40 08	254 46	49.2	316.1	M
Dixon	DIK	73 33	80 34			M
Evenes	EVE	68 31	16 46			M
Fredericksburg	FRD	38 12	282 37	50.3	355.7	M
Honolulu	HON	21 19	202 00	21.7	267.8	M
Irkutsk	IRT	52 10	104 27	46.9	176.0	M
Ivalo	IVA	68 36	27 29			AR
Kaliningrad	KNG	54 48	20 30			M(2)P
Kevo	KEV	69 45	27 01			APR
Kiruna	KIR	67 50	20 25			AM
Lovozero	LOZ	67 58	30 05			M(2)P
Mattisdalen	MAT	69 51	22 55			M
Mikkelvik	MIK	70 04	19 01			M
Minsk	MNK	54 30	27 53	49.3	103.2	M
Muonio	MUO	68 02	23 34			AM
Nattavaara	NAT	66 45	21 00			M
Novosibirsk	NVS	54 51	83 15	50.6	153.1	M
Nurmijärvi	NUR	60 31	24 39			P
Odessa	ODE	46 47	30 53			M
Oulu	OUL	65 06	25 29			PR
Petropavlovsk	PET	52 58	158 15	45.4	225.2	M
Ritsemjokk	RIJ	67 42	17 30			M
Rovaniemi	ROV	66 33	25 50			R
San Juan	SJG	18 07	293 51	31.0	6.6	M
Sodankylä	SOD	67 22	26 38			MPR
Sverdlovsk	SVD	56 44	61 04	52.0	133.6	M
Tixie	TIK	71 35	129 00			M
Vadsö	VAD	17 06	29 39			M
Valentia	VAL	51 56	349 45	51.3	72.2	M
Vladivostok	VLA	43 41	132 10	36.8	203.3	M

A = all-sky camera, M = magnetometer, M (2) = normal and rapid-run magnetometers, P = induction magnetometer, R = riometer

[a] Corrected geomagnetic coordinates for 1980.0 epoch geomagnetic field after Tsyganenko (1979) are given for the stations in Figs. 2 and 3

bays at mid-latitudes (see Fig. 1). The mid-latitude magnetic H and D variations (quiet level from 5–6 November 1976 subtracted) shown in Fig. 2, upper panel, resemble the conditions of intense stationary magnetospheric convection reported by Sergeev (1977).

Figure 1 shows that there are two pronounced magnetic bays starting at mid-latitudes at 1730 and 1748 UT. Also Fig. 7a indicates that these bays are associated with two separate Pi2 trains recorded at Borok and Kaliningrad. The mid-latitude magnetic H and D variations given in Fig. 3 are typical for an intense substorm expansion phase (McPherron et al., 1973; Akasofu, 1977) and for successive separate microsubstorms (Sergeev, 1974; Pytte et al., 1976a). According to Sergeev (1978) the positions of the positive and negative maxima in the ΔD curve correspond to the longitudes of the western and eastern edges of the auroral bulge. Hence, the auroral bulge in the first expansion is within 100–150° corrected geomagnetic longitude and in the second expansion within 70–200°. The shape of the ΔD curve in the second case indicates that two new current wedges appear both eastwards and westwards of the first expansion region. The interplanetary magnetic field data (Fig. 4), show strong fluctuations between 1700–1800 UT, B_z being southwards (<0) during periods of auroral activity. The second auroral activation in particular, which starts at 1748 UT, seems to coincide within one minute with the sharp southward turning of the IMF.

Auroral zone phenomena. All-sky pictures from the first substorm are shown in Fig. 5a. The lower borders of distinct auroral structures have been digitized and replotted on geographical maps in Fig. 5b (Kaila, 1981). The shaded ovals on the maps give the effective antenna beams (at auroral altitudes) of the Finnish riometer chain from which the data are displayed in Fig. 6. Figure 7a presents the recordings of low-frequency magnetic pulsations from both the auroral zone (LOZ) and the mid-latitudes (BOX and KNG), while Fig. 7b shows a sonagram of the high-frequency pulsation component recorded in the auroral zone (KEV).

The first substorm can be divided into two microsubstorms starting at 1730 and 1748 UT (for details see Table 2). The first microsubstorm is preceded by typical pre-onset features like enhanced absorption (Pytte et al., 1976d; Ranta, 1978; Ranta et al., 1981) (Fig. 6) and auroral structures moving southwards with an average speed of 180 m/s. The absorption maximum reaches Rovaniemi at 1720 UT where the poleward boundary of diffuse aurora is also located by that time.

At 1729:30 UT a Pi2 onset is recorded at mid-latitudes

Table 2. Timing of events in different phenomena appearing during substorm expansion phases

No.	Time UT	Relation to substorm phases	Mid-latitude magnetic bay	Mid-latitude Pi2	Auroral development in Scandinavia	Cosmic noise absorption and X-rays	Appearance of PiB's
1	1730	Onset of first microsubstorm	Sharp bay onset	Onset at 1729:30 UT	Rapidly westward traveling "auroral horn" appears in the south-eastern sky, altitude 92 ± 2 km	Absorption starts to increase at 1732 UT in ROV under the "auroral horn"	No PiB
2	1735	The micro-substorm continues	The bay continues to develop	Intensification and phase change occur at 1734:30 UT	Brightening of the "horn", appearance of ripples	Onset of slow rise in absorption in SOD	PiB at 1734 UT, most distinctly at OUL
3	1738	The micro-subsorm continues	The bay continues to develop	Distinct intensification at 1737 UT	WTS appears in the eastern horizon, altitude 86 ± 3 km	Onset in IVA and KEV	PiB after 1737 UT
4	1745	The micro-substorm continues	The bay continues to develop	Onset of weak pulsations	Formation of a new faint discrete arc on the poleward edge of auroral bulge, altitude 97 ± 2 km	Weak onset in SOD	PiB at 1745 UT only at KEV
5	1748	Onset of second micro-substorm	Sharp change in bay pattern	No intensification, change in phase at 1747:30 UT	Brightening of the poleward edge of auroral bulge, altitude 85 ± 5 km	Onsets in IVA and KEV (sharp)	PiB at 1748 UT
6	1750	The micro-substorm continues	The bay continues to develop	Intensification	Formation of new bright discrete arcs (altitudes 73 ± 2 and 83 ± 2 km) on the poleward edge of auroral bulge	Intensification in absorption in KEV	PiB at 1750 UT
7	1752	The micro-substorm continues	The bay continues to develop	Intensification	Intensification in luminosity in the north (altitudes between 79 ± 2 and 90 ± 4 km) and decrease in the zenith as seen from MUO	Absorption in KEV reaches a maximum (6 dB)	PiB at 1752 UT
8	2102	Onset of a small microsubstorm	–	–	Brightening and activation of discrete arc, altitude 105 ± 3 km	X-ray enhancement starts at 2101:30 UT	PiB's appear in KEV, SOD
9	2103	The micro-substorm continues	–	Onset of Pi2 at 2102:30 UT	Formation of a bright discrete arc, altitude 98 ± 2 km	X-ray spikes detected by balloons 1 and 2	PiB's appear in KEV, SOD
10	2105	The micro-substorm continues	–	Intensification at 2105 UT	Formation of a bright discrete arc (at 2106 UT) altitude 103 ± 3 km	X-ray enhancement starts at balloon 3 at 2104. Enhancement starts at all balloons at 2105 UT	PiB's appear in KEV, SOD

(Fig. 7a). At Kevo no Pi activity is observed (Fig. 7b) at this moment. A discrete auroral arc propagates from the east along the poleward boundary of the diffuse band south of Muonio (Fig. 5a). This arc, which we call „auroral horn" is located at a considerably lower altitude (92 ± 2 km) than the diffuse band (approximately 105 km).

At 1732 UT the western edge of the horn reaches the Rovaniemi riometer (Fig. 5b), which records an enhancement in absorption (point "1" in Fig. 6). Between 1734 and 1735 UT both Pi2 intensification, phase change, and a small Pi burst (PiB), seen most distinctly at Oulu, are observed (marked as "2" in Figs. 7a and b). These are related to the intensification of the horn brightness (Fig. 5a) and to the minor enhancement in absorption at Sodankylä ("2" in Fig. 6).

The horn is followed by a westward travelling surge (WTS) that appears at 30° E longitude at 1739 UT. The appearance of the surge is related both to a strong intensification of Pi pulsations and to a start of PiB at Kevo (Figs. 7a, b). The altitude of the surge is 86 ± 3 km, which explains the abrupt onset of absorption at Ivalo when the surge moves over ("3" in Fig. 6). The region of energetic

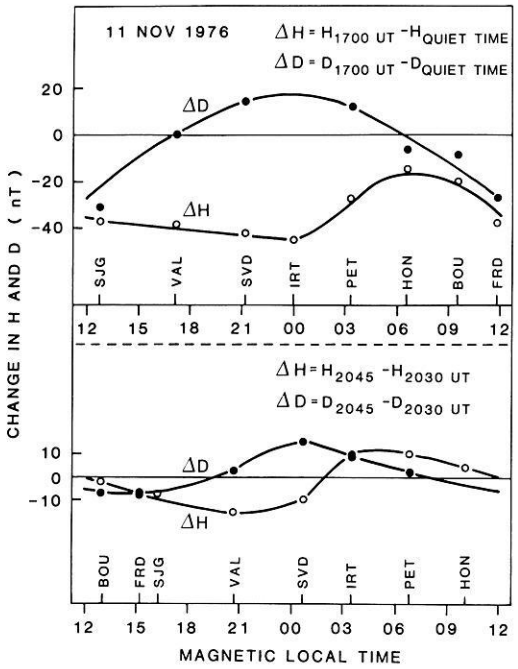

Fig. 2. Longitudinal profiles of mid-latitude magnetic disturbances, showing their patterns during the period of intense worldwide disturbances (top panel) and changes during the convection bay, which started at 2030 UT (bottom panel)

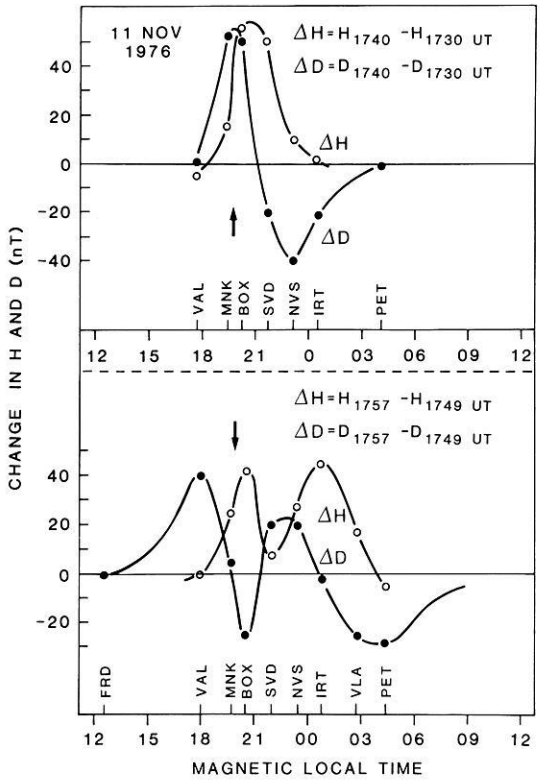

Fig. 3. Longitudinal profiles of mid-latitude bay-like disturbances, related to two intense microsubstorms, started at 1730 and 1748 UT. The arrows denote the meridian of Ivalo

precipitation within the surge seems to be fairly localized since the absorption enhancements at Kevo and Sodankylä remain on moderate levels.

The first microsubstorm ends with the disappearance of the surge. During the passage of the surge the bright auroral arcs that form the auroral bulge propagate some 300 km polewards. Before the second microsubstorm the brightness of the auroras in the bulge region decreases.

At 1745 UT a new faint arc appears polewards of the bulge (Figs. 5a, b). This is associated with a clear onset of a weak Pi2 train at mid-latitudes ("4" in Fig. 7a) and a weak PiB enhancement observed only at Kevo (Fig. 7b). The altitude of the arc is 97 ± 2 km which is of the same order as the altitude of the bulge. Fig. 5b shows that the arc is located between Kevo and Ivalo riometers, which do not record any enhancement in auroral absorption. However, there is a slow absorption enhancement at Sodankylä by this time ("4" in Fig. 6).

The second microsubstorm starts at 1748 UT with a brightening of the poleward edge of the auroral bulge (Fig. 5a). In spite of the abrupt enhancement in auroral intensity there is no change in Pi2 amplitude at mid-latitudes, only the phase seems to change ("5" in Fig. 7a). PiB activity starts at Kevo (Fig. 7b) and the auroral absorption starts to rise both at Ivalo and Kevo (Fig. 6). The poleward edge of the bulge descends to 85 ± 5 km while brightening.

At 1750 UT two new bright arcs (altitudes 73 ± 2 and 83 ± 2 km) appear polewards of the bulge edge (Figs. 5a, b). Since these low-altitude arcs form within the Kevo riometer antenna beam an abrupt absorption enhancement ("6" in Fig. 6) is recorded. At the same time Pi activity intensifies both at mid-latitudes and in the auroral zone (Fig. 7a, b).

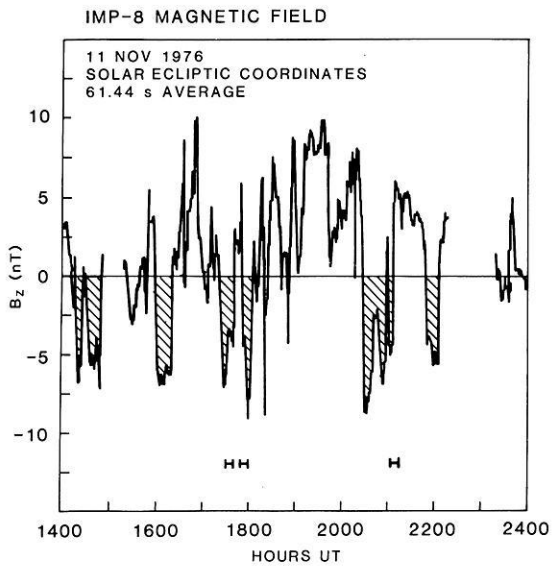

Fig. 4. B_z component of the interplanetary magnetic field in solar-ecliptic coordinates. Southward orientations are indicated by shading. Horizontal bars at the bottom indicate periods of microsubstorms

At 1752 UT a WTS is located to the north-west of Kevo (Fig. 5b). The altitudes of the surge and the arcs over Kevo range between 80 and 90 km (see Table 2). The highest absorption value (6 dB) is recorded at Kevo at this time ("7" in Fig. 6). Also the Pi activity both at mid-latitudes and in the auroral zone reaches a maximum (Figs. 7a, b).

MUONIO
11 NOV 1976
1727-1754 UT

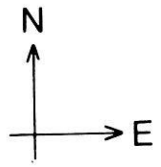

1727-1733 1734-1740 1741-1747 1748-1754

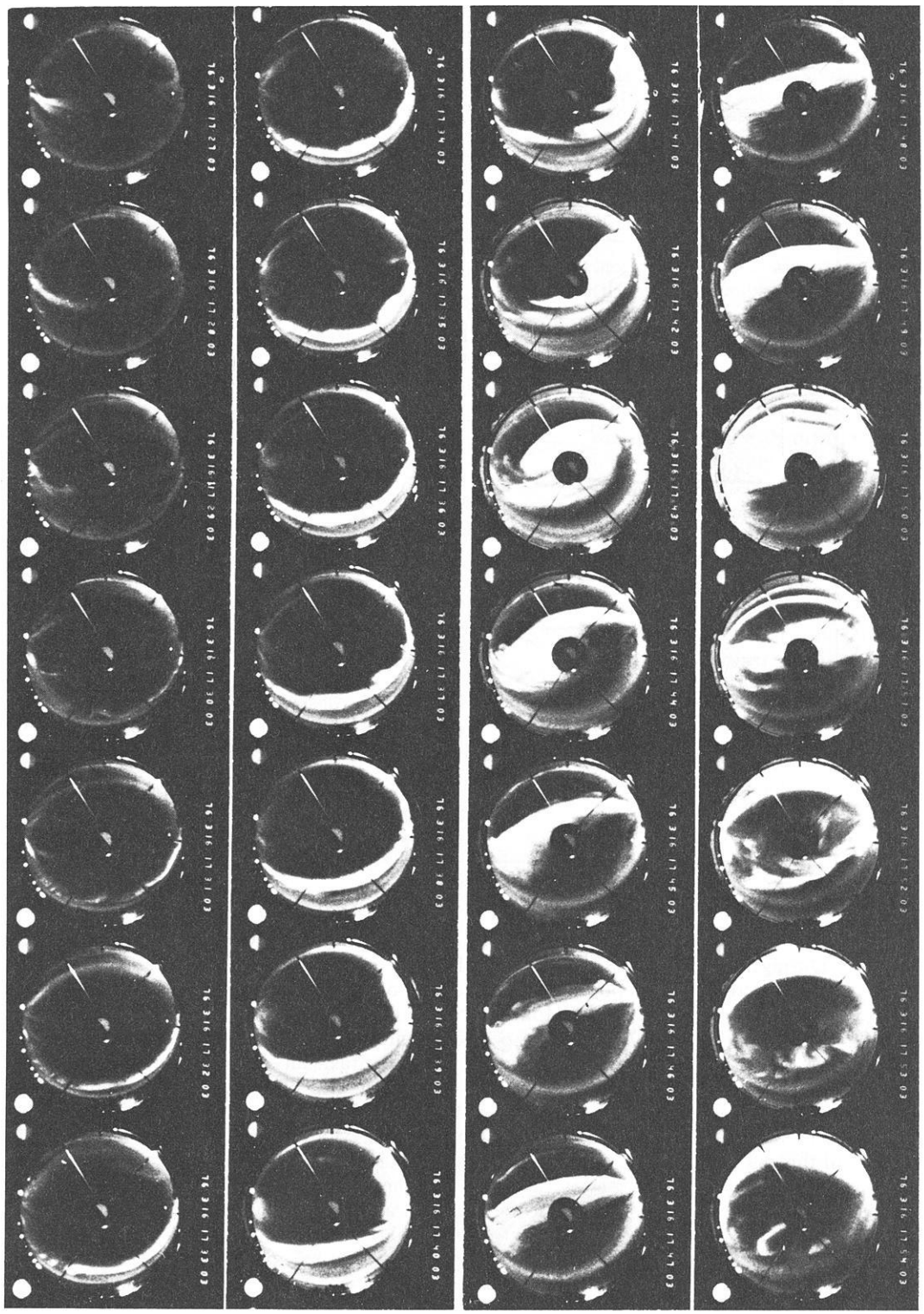

Fig. 5a

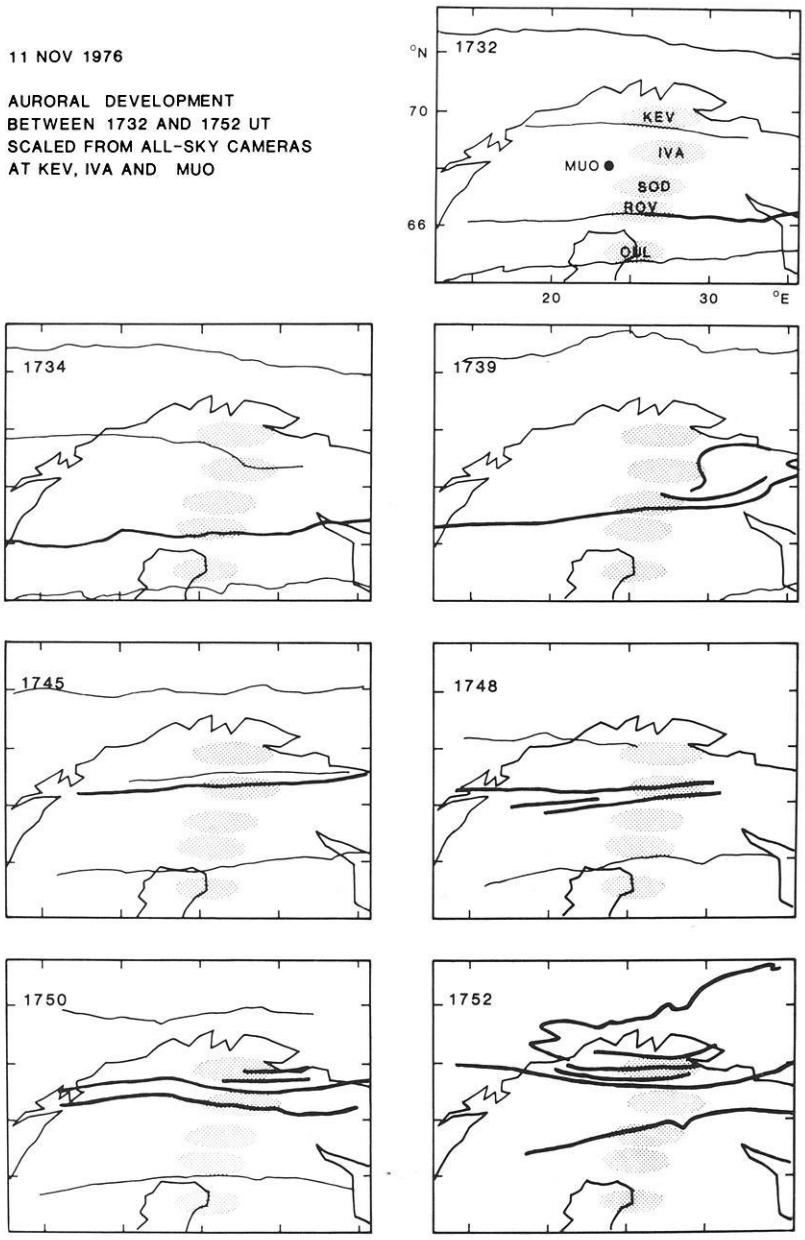

Fig. 5. a All-sky camera pictures recorded at Muonio around the two microsubstorms initiated at 1730 and 1748 UT. **b** Digitized all-sky camera pictures rectified and mapped in geographic coordinates. The lower border altitudes of the arcs are given in the text and Table 2. Shaded ovals indicate effective riometer antenna beams at 100 km altitude

During this second microsubstorm the auroral bulge propagated 600 km polewards. During both microsubstorms faint equatorward drifting arcs were observed polewards of the expanding bulge.

Time Interval 2030–2110 UT

Global features. A thorough description of this event is given in Pellinen et al. (1982), here we will only summarize the results essential to the scope of this paper.

Figure 1 shows a negative magnetic bay starting to develop at the midnight-morning auroral zone stations some half an hour prior to the substorm onset at about 2100 UT. The development is world-wide and associated with a rapid southward turning of the interplanetary magnetic field (Fig. 4). The maximal magnetic disturbance ($AE \sim 500$ nT) is reached at 2045 UT. According to Pellinen et al. (1982) the development observed on the ground is well correlated with variations in the solar wind-magnetosphere energy coupling function ε (Akasofu, 1981).

The pattern of the mid-latitude magnetic variations, as follows from Fig. 2 (lower panel), is similar to the one for the period of intense convection before 1700 UT (Fig. 2, upper panel), but drastically differs from the patterns of substorm expansion, e.g. Fig. 3. During the whole period between 2030 and 2200 UT we are unable to discover any expansion-type behaviour in the mid-latitude data. The only signature is detected in the very sensitive (0.5 nT/mm), rapid-run (90 mm/h) magnetogram (data not shown here) of the Kaliningrad observatory at 2102 UT, but the effect is extremely weak.

During the one and half hour period prior to 2030 UT there are no signatures of mid-latiude Pi2 pulsations both near midnight and in the morning sector. The interplanetary magnetic field is northward directed during the whole period (Fig. 4). A Pi2 onset is detected at 2102 UT, and a weak

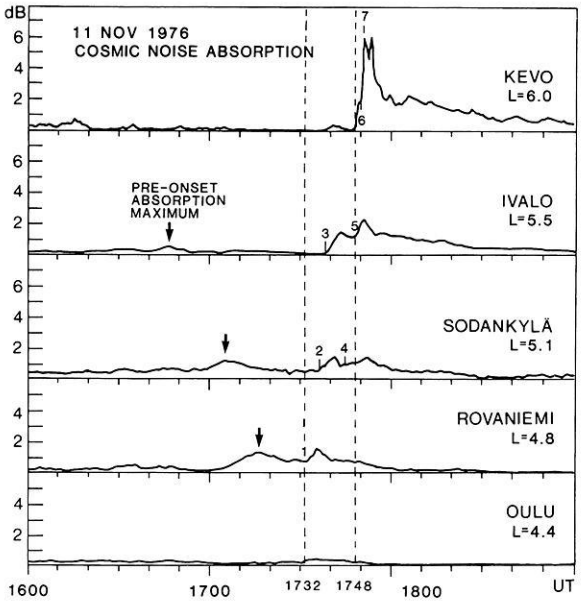

Fig. 6. Data from the Finnish riometer chain during the first expansion event. Numbers, marking the onsets of distinct rises in cosmic noise absorption, correspond to the numbers in Table 2 (see the text for details)

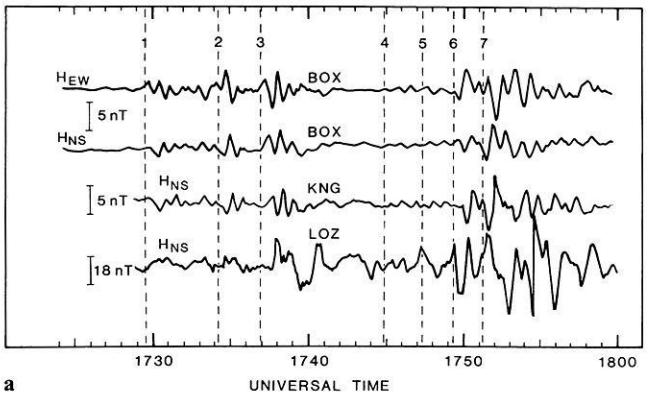

a

pulsation train appears at 2137 UT. No auroral zone magnetic effects are detected during these two substorm intensifications except at stations within the Scandinavian area (Fig. 9). No enhancement in cosmic noise absorption is detected by the Danish high-latitude riometer network during these events (Stauning and Christiansen, 1978). We shall focus our attention on the earlier one of these two short and weak expansions since it occurs in the Scandinavian sector.

Auroral zone phenomena. During this time interval stations in the Scandinavian region are located in the region of westward electrojet close to magnetic midnight (Pellinen et al., 1982). At 2030 UT, a faint auroral arc appears in the northern sky of Kevo (Fig. 1) and then drifts equatorwards until 2058 UT, when the motion stops between Ivalo and Sodankylä (Figs. 8a and 8b). The average altitude of the arc is 102 ± 3 km both at 2057 and at 2100 UT.

At the onset of the magnetic bay at 2030 UT a small increase in auroral absorption is seen in the Kevo recording (Fig. 9). The subsequent decrease in absorption at Kevo and the simultaneous increase over Ivalo indicates equatorward movement of the absorption region.

Three balloons of the SAMBO-76 campaign drifted over the region between Ivalo and Sodankylä (see Fig. 8b). Their recordings (Fig. 9) show variations in X-ray intensity that are similar to the absorption at Ivalo, but the pre-break-up intensity maximum occurs near 2058 UT, 3 min later than the absorption maximum at Ivalo. The balloon detector aperture is about 100 km wide at 100 km altitude in the ionosphere. The combined riometer and balloon data suggest that the latitudinal width of the energetic electron precipitation region is of the order of 100 km, and the equatorward drift speed is 100 m/s. Comparison of the absorption recordings made at Ivalo and Sodankylä with the X-ray intensity recordings leads to the conclusion that the equatorward motion stops at 2058 UT – 4 min before the break-up, in good correlation with the behaviour of the auroral arc.

The high-frequency component of the Pi pulsations is shown in Fig. 10b by the dynamic spectrum made from the Kevo recordings. No PiB activity appears before 2102 UT. The same holds for all the Finnish stations from Kevo to Nurmijärvi.

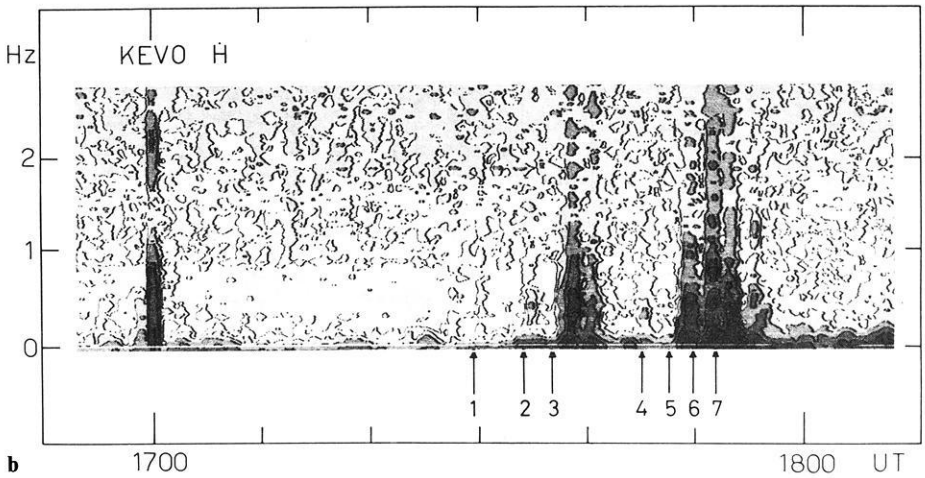

b

Fig. 7. a Mid-latitude and auroral-zone induction magnetograms for the first time interval. **b** Dynamic spectrum of Pi pulsations recorded at Kevo. The numbers 1–7 refer to the same times as in Fig. 7a. The intensity grey-scale is for qualitative purposes only

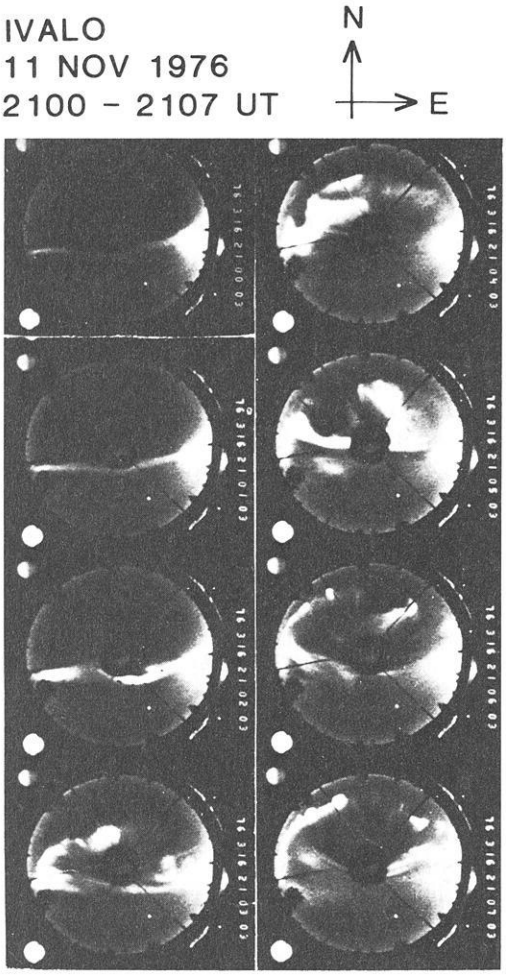

a

At 2102 the arc becomes considerably brighter. In contrast to the substorms between 1730–1800 UT the altitude of the brightening arc seems to ascend at this moment being 105 ± 3 km along the brightest forms. At 2103 UT a new bright arc appears polewards of the previous one, developing a surgelike structure over Kiruna (Figs. 8a and 8b). The average altitude of the surge is 98 ± 2 km. At 2104 and 2105 UT a deformation of the poleward border of the bulge with apparent eastward motion takes place over the observing area. The brightest parts of the eastward travelling surge (possibly a small Ω-band according to Akasofu, 1974) seem to be at an altitude of 103 ± 3 km. Weak glow is visible polewards of the bulge at 2105 UT and one minute later a new distinct bright arc forms in the glow region (altitude about 100 km). At 2106 UT the Ω-band becomes smaller and decreases in intensity. The altitude remains close to 100 km all the time.

The arc located over the Norwegian coast (2107 UT, Fig. 8b) is the last signature of this moderate auroral break-up, which is rather local (about 250 km in poleward expansion) and short in duration (6 min). The longitudinal extent of the auroral expansion is only about 1 h in magnetic local time at 2104–2105 UT.

The auroral break-up at 2102 UT initiates a brief increase in auroral absorption at Ivalo and Kevo (Fig. 9), located by this time near the eastward expanding auroral

Fig. 8. a All-sky photographs from Ivalo during the local break-up, initiated at 2102 UT. **b** Mapped all-sky camera data corresponding to the all-sky pictures presented in Fig. 8a. Shaded ovals indicate riometer antenna beams and the three rings around Sodankylä the effective recording areas (at 100 km altitude) of balloon X-ray counters. The dots at EVE, MAT and VAD give sites of the three magnetometers from which data are presented in Fig. 9

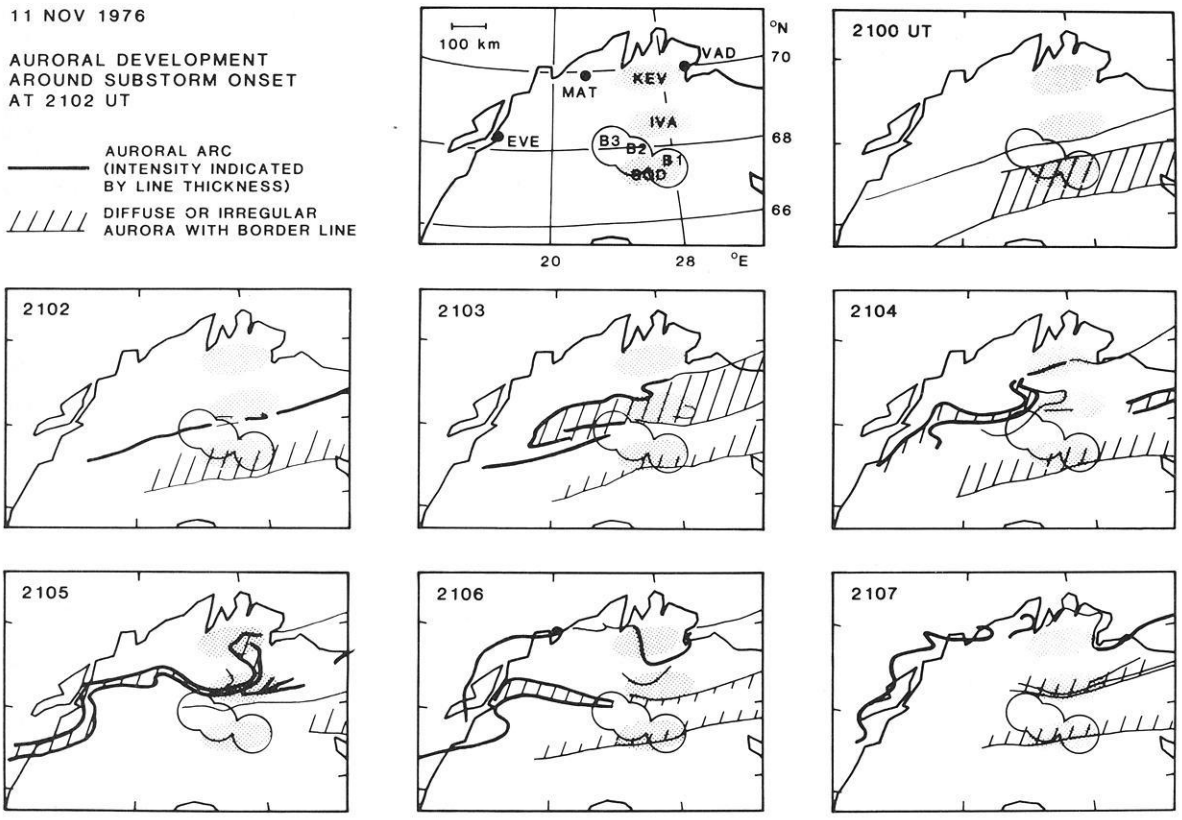

b

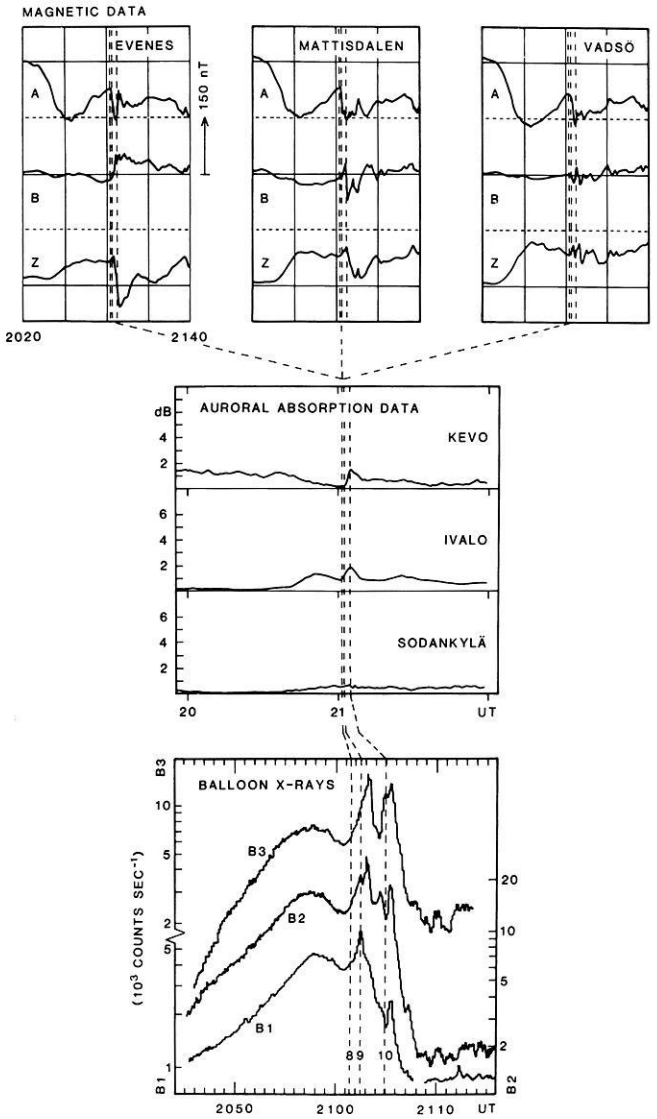

Fig. 9. Magnetic data from Evenes, Mattisdalen and Vadsö (top panels), riometer recordings of the Finnish chain (center) and counting rates of the X-ray detectors at the three balloons shown in Fig. 8b. The X-ray energy ranges are for $B_1 > 25$ keV and for B_2 and B_3 30–40 keV. (data from Melnikov et al. 1978) (bottom panel)

bulge. The impulsive character of the X-ray data recorded in this event is typical for an auroral break-up (Pytte et al., 1976c; Melnikov et al., 1978). The first abrupt onset at 2102 UT (8) is recorded by all three balloons. The first peak at 2102:30 UT is observed only by the two southernmost balloons (B1 and B2) while the second peak at 2103 UT (9) appears over balloons B2 and B3. The first peak obviously corresponds to the auroral activation within the discrete arc and the second peak to the formation of the auroral bulge.

At 2104–2105 UT the Ω-band moves across the poleward sky oof Ivalo. Before it reaches the longitude of Ivalo minor X-ray activity peaking at 2104:30 UT is recorded at balloon 2 and then probably propagates polewards to be recorded by balloon 3 some half a minute later. The exact correlation of this event with aurora is impossible due to the slow recording speed of the all-sky camera. It is possible that local irregularities in the energetic electron precipitation related to Ω-bands cause these impulses (Oksman, 1981). At 2105–2106 UT a new arc forms polewards of the bulge. Impulsive X-ray bursts are recorded at all balloons during this time (10).

A Pi2 onset is detected both at auroral and mid-latitudes between 2102 and 2103 UT ("9" in Fig. 10a). An increase in Pi2 amplitude around 2105 UT (10) is evident at the mid-latitude stations and in the auroral zone (Lovozero) even if the data are more disturbed there. Two PiB's can be identified starting at 2103 (9) and 2105 UT (10) (Fig. 10b). There are no signatures of these pulsations at Oulu and Nurmijärvi.

Again Pi pulsations appear simultaneously with increases in electron precipitation as inferred from the auroral and riometer recordings (see Table 2). A remarkable feature is the total absence of magnetic pulsations during the growth phase before 2102 UT in spite of the clear electron precipitation activity. Similar observations have been reported earlier by Wedeken et al. (1979).

Data from 24 instruments of the SMA (temporal resolution 10 s) are available for this period. Details of the evolution of the current pattern over Scandinavia from 2030 UT to 2100 UT can be found in Pellinen et al. (1982). Gradual changes occur in the westward electrojet intensity during the equatorward movement. Prior to the substorm expansion onset, during the convection bay, the maximal horizontal magnetic disturbance is about 150 nT in contrast to the $\sim$70 nT disturbance being added to the background field during the substorm expansion (see the data in Fig. 9 — top panels).

The pattern of changes in the equivalent currents over Scandinavia from the moment of expansion onset towards its end (Fig. 11) displays a very complex distribution of magnetic disturbances (both in intensity and orientation of the vectors), differing in each part of the magnetometer array. Therefore we analyzed the magnitude of the total horizontal disturbance after the expansion onset by subtracting from it the horizontal magnetic field recorded at 2101 UT in different parts of the expansion current system. Additionally the disturbance amplitude was averaged over a few "typical" stations, as also shown in Fig. 11. In spite of some minor differences, the data consistently show two major increases in disturbance level, starting at 2102:30 UT and between 2104:30 and 2105:00 UT, in good coincidence with the other data mentioned above. In addition we constructed the differential current patterns for each activation, i.e. from 2102:30 till 2104:00 and from 2104:30 till 2106:00. Both of these were found to have a current distribution similar to the summary current system in Fig. 11, but during the second activation the whole current system was displaced polewards in comparison to the first one, being in accordance with the poleward shift of active aurora (data not presented here).

Discussion

The discussion covers three major topics. First we shall discuss the regularities found in the substorm fine structure. As the second question we shall treat the relationships between the different expansion signatures reported above. The third question deals with the problem of whether the global disturbances observed prior to and during the expansion phases are due to external or primarily internally oper-

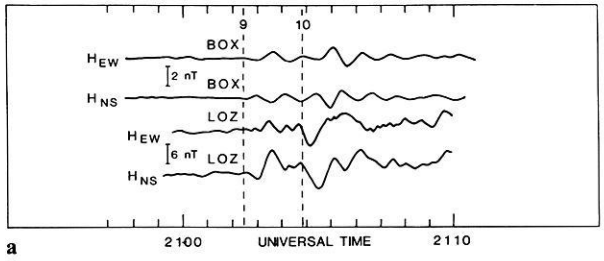

a

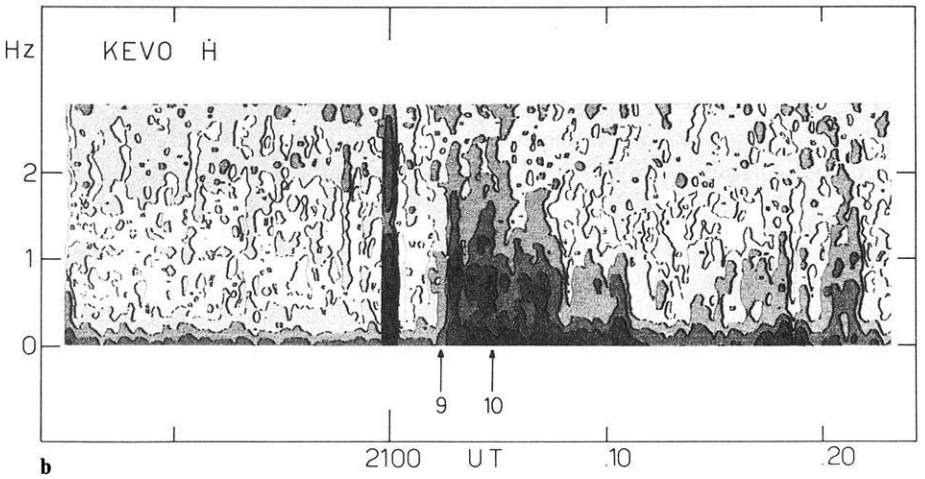

b

Fig. 10a and b. The same as in Fig. 7a and b for the second substorm event

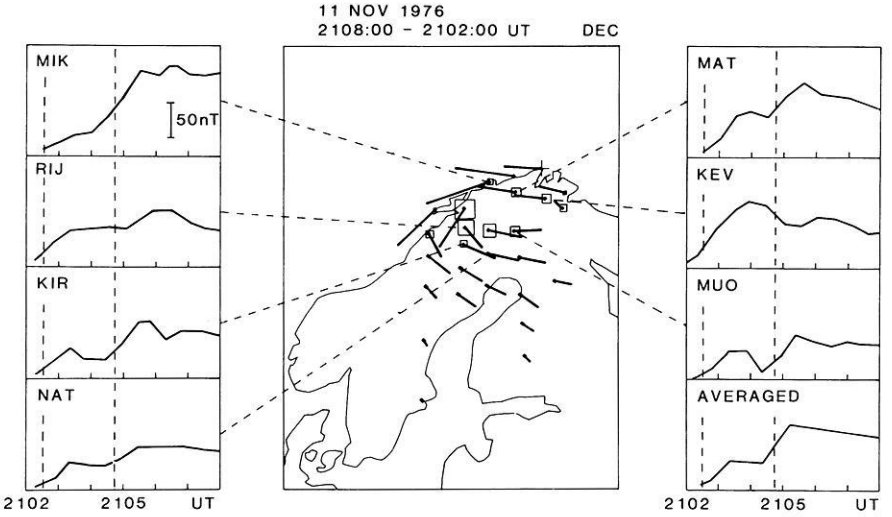

Fig. 11. A change of equivalent current system during the period of local break-up (from 2102 UT to 2108 UT) and the change in magnitude of the horizontal magnetic disturbance at a few stations of the SMA. The averaged data have been taken from the seven other panels framing the map

ating magnetospheric processes. At present the debate on this field is highly controversial (Akasofu, 1981; Fairfield et al., 1981).

Substorm Intensifications: Microsubstorms and Their Fine Structure

Rostoker et al. (1980) defined the substorm expansion phase as "the ensemble of the onset plus all intensifications up to the time of maximum poleward expansion of the substorm-disturbed region". The observations presented in this paper well support this view.

There seem to be two different time scales embeded in the discrete substorm structure. In the first intensive substorm the intervals of auroral expansion last for 5–10 min and they are clearly separated by quiet periods. The active periods are identified by well-separated Pi2 trains and mid-latitude magnetic bay intensifications. In the literature these discrete activations are called microsubstorms (Sergeev, 1974) or multiple onsets (Wiens and Rostoker, 1975; Pytte et al., 1976a, b). Another time scale (repetition interval about 2 min), which we consider as a new element of substorm morphology, appears both in intensive and weak microsubstorms. The most obvious presentation of this type of discrete fine structure can be found in Figs. 7b and 10b where the PiB spikes are repeated approximately in 2 min (see also Table 2). In some earlier studies these spikes were found to be associated with auroral break-ups and intensifications of auroral arcs (Heacock, 1967; Kangas et al., 1979; Bösinger et al., 1981). Our study supports these observa-

tions. Each effective brightening of an auroral arc or even a formation of a new faint arc in the vicinity of the auroral bulge is associated with PiB in the auroral zone. At mid-latitudes simultaneous changes in Pi2 characteristics (amplitude, phase, and period) are observed. Each optical activation is also accompanied by a simultanous increase in energetic electron precipitation (monitored by riometers and balloons) and by step-like changes in ionospheric equivalent currents.

The fact that mid-latitude Pi2 recordings are associated with phenomena observed only locally in the auroral zone leads to the conclusion that some large-scale (substorm) mechanisms have to operate in the background, since the responses detected at distances comparable to the dimension of the bulge itself, cannot be caused only by changes in small-scale features within the bulge. This conclusion is supported by Sergeev (1981) who found that simultaneous abrupt changes in Pi2 characteristics at widely spaced (1,000–2,000 km) mid-latitude stations coincided with sharp impulsive variations in the magnetic field of the far tail (30 R_E). Hence, the observed fine structure of microsubstorms must follow from steplike changes in the geometry of the whole auroral bulge (Sergeev an Yahnin, 1979b) and/or from the intensification of the total precipitation in the bulge region. The above results lead to the conclusion that the microsubstorm fine structure is part of the entire substorm mechanism.

Substorm Signatures and Their Relationships

An obvious result of our study is that all expansion signatures, even small details, are strictly grouped in time. However, details in their relations differ, apparently because of the different origin of the phenomena involved. First we shall point out some morphological features. A southward-moving "particle arc" which causes riometer absorption precedes both substorm onsets. The cosmic noise absorption curves from Rovaniemi (Fig. 6) and Ivalo (Fig. 9) look quite similar. The pre-onset absorption maxima are over 1 dB in both cases. Two conclusions can be drawn from these data. First, the strength of the forthcoming substorm seems to be correlated with the location of the southernmost latitude of the pre-onset absorption (lower latitudes lead to more intense expansions). Second, the pre-onset absorption region seems to have a long east-west extension (Ranta et al., 1981) since in our cases the absorption development is independent of whether the substorm is triggered far in the east (first case) or in our immediate environment (second case).

Our results show that after the substorm onset an "auroral horn" propagates with high speed away from the triggering area approximately along the poleward edge of the pre-substorm particle arc. The horn keeps its arc structure while the disturbed auroras that follow are shaped in forms which can be identified as westward travelling surge (Akasofu et al., 1965) and (eastward travelling) Ω-band (Akasofu, 1974). Our observations suggest that the propagation speeds of these large-scale forms are less than the speed of the auroral horn. Supporting examples can be found in the extensive ASC data set collected in Finland during the IMS.

In the present study the following estimates for the lower border altitudes of different auroral structures have been obtained:

Equatorward diffuse band	105–110 km
Faint arcs poleward of the bulge	100–110 km
Auroral horn	90 km
Surge	80– 90 km
Arcs formed near the poleward boundary of bulge	75– 90 km

These numbers show that the auroral horn, westward travelling surge, and the new bright arcs near the poleward boundary of auroral bulge are caused by electrons of higher energy than the discrete and diffuse auroras outside the bulge region. The auroral absorption recordings show that impulsive precipitation of energetic electrons is associated with these low-altitude structures. This conclusion is valid even in the second substorm (mainly for balloon X-rays), where the auroral altitudes are considerably higher ($\sim$100 km – see Table 2).

PiB events seem to be associated with pronounced changes in auroral arcs (Table 2). However, no PiB appears at the onset of mid-latitude Pi2 at 1730 UT. The first PiB event starts at 1734 UT (most distinctly at Oulu, Table 2) when the horn has propagated beyond the Oulu meridian and starts to brighten. This leads to the conclusion that PiB penomena can be observed only in the MLT sector occupied by active aurora but the localization is not as limited as for the burst-like precipitation of energetic electrons. These observations agree with those reported by Parkhomov et al. (1976) who show that a PiB can be observed simultaneously over a longitudinal distance of 30° and it may propagate westward with a speed of 2–10° min^{-1}.

As mentioned above, a significant correlation was found between the times of discrete auroral zone phenomena and the abrupt changes in the intensity (or phase) of Pi2's at mid-latitudes. Details of the response are not the same when comparing, for instance, with the response of PiB pulsations. In particular, Pi2 intensity seems to be influenced much more by the formation of new auroral structures than by brightening of previously existing ones. This can be seen e.g. by comparing points 4 and 5 in Table 2: formation of a faint discrete auroral structure slightly polewards of the bulge causes pulsations of the same amplitude as during the subsequent strong brightening of the bulge's edge. Also point 8 in Table 2 supports the conclusion since auroral brightening does not generate Pi2 pulsations until the formation of a new structure of similar intensity. These results are in accordance with the examples presented by Sergeev et al. (1978) and Sergeev (1981).

Our observation that the mid-latitude Pi2 pulsations and the onset of a magnetic bay occur simultaneously with the appearance of the "auroral horn" in the auroral zone contradicts the results reported by Kawasaki and Rostoker (1979). Based only on auroral zone data from one meridian, they argued that the arc brightening and substorm onset, particularly the onset of Pi2, do not coincide. Pashin et al. (1982) have shown that in the auroral zone there is an intimate connection between the positions of the Pi2 (PiB) maximum and the auroral bulge. Hence, if the auroral bulge develops outside the field of view of the all-sky camera (as in our first event) Pi2 (PiB) pulsations do not appear under the auroral horn, which can also be identified as "arc brightening", until the horn starts to become disturbed. It is also possible that the pulsations associated with the auroral horn have very small amplitude and are

confined to the horn area. This feature is supported by the auroral zone data recorded at Lovozero (LOZ in Fig. 7a). Kawasaki and Rostoker (1979) analyzed pulsation data recorded only at one auroral zone station which also may lead to wrong conclusion, e.g. at 1734 UT in our case (Table 2) PiB appears only weakly at Kevo (Fig. 7b) but more distinctly at Oulu.

The mid-latitude magnetic bay seems to be very sensitive to the current intensity and to the longitudinal dimensions of the current wedge. In our second event (around 2100 UT) both the size of the bulge and the total current through it are so small that the disturbance is not distinguishable in a normal mid-latitude magnetogram. According to Pellinen et al. (1982) the current wedge is 2 h wide in MLT and carries a total current of 250 kA which would create about 4 nT maximal disturbance in magnetic H and D components at 40° geomagnetic latitude. This numerical value is below the resolution of standard magnetic data.

Relationship Between IMF Variations, Magnetospheric Convection and Substorms

In spite of the entirely different intensities and scales of the two substorms reported here their general signatures are similar and coincide with those of a "typical substorm". An equatorward moving high-energy precipitation region which, according to Pytte and West (1978), can be regarded as a signature of growth phase, is observed to appear 30–60 min before both expansion phases. The expansion phases develop through brightening an poleward expansion of auroras, abrupt increases in energetic electron precipitation, and appearance of irregular magnetic pulsations both in the auroral zone and at mid-latitudes.

The basic difference in the substorms can be found in the behaviour of magnetospheric convection prior to the onsets. Features of convection can be deduced from worldwide magnetic field recordings. In both cases a two-cell current system (for details see Pellinen et al., 1982) is observed at high latitudes. At mid-latitudes the magnetic disturbance is of partial DR (disturbed ring current) type (Fig. 2, see also Sergeev, 1977). In the first case convection is intense but stable before the onset. The IMF is mainly northwards but fluctuating (Fig. 4). In the second case, an obvious convection intensification prior to the expansion phase is associated with a clear southward turning of the IMF.

The relationship between convection development and substorm processes observed both in the magnetosphere and in the ionosphere appears to be complicated and indirect. In the literature the following examples can be found:

(a) Convection enhancement caused by southward turning of the IMF leads to substorm growth phase and expansion (typical substorm development explored by many authors, see the review by McPherron, 1979).

(b) Strong convection during a stable southward IMF can proceed for a few hours without any significant substorm development (Sergeev, 1977).

(c) Strong expansion preceded by a growth phase can occur within a prolonged period of intense stationary convection and southward IMF (Pytte et al., 1978a).

(d) Strong expansion can be initiated when convection fades at a northward turning of the IMF (Caan et al., 1977).

(e) Substorm expansions may occur without any signatures of convection under northward IMF (substorms along a contracted auroral oval: Akasofu et al., 1973).

An obvious consequence of the complex relationship between convection and substorm is that the use of AE or DR indices, without any further investigation, may lead to wrong conclusions in determining the time of different substorm phases, since they are sensitive to current systems associated both with magnetospheric convection and subsorm expansion. This is well demonstrated in our events. The AE index values recorded during the first expansion phase differ only insignificantly from the values recorded during the growth phase and the several preceding hours (data not presented here). The AE index for the second event reaches a rather intense value (500 nT) during a relatively short interval, about half an hour preceding the subsorm onset. The expansion, strictly confined both in time and space, shows no response at all in the AE index.

The fact that growth phase development is usually associated with enhanced magnetospheric convection (McPherron, 1979) suggests that an external convection electric field is applied to the ionosphere and to the magnetotail. One typical feature of the growth phase, besides the ground-based features described above, is the enhancement of magnetotail current. In rare situations, where the convection is stationary during a stable southward directed IMF (which means no change in external influence) the behaviour of magnetotail current seems to be varying. There may appear growth and expansion-like changes in the tail magnetic field (Pytte et al., 1978a) or, on the contrary, prolonged periods without any changes (Sergeev, 1977). This leads to the conclusion that the relationship between the imposed electric field and the evolution of the tail current intensity is complicated, and that a simple correspondence between enhanced convection and the growth-phase features (classified as "typical" behaviour) can be considered as an exceptional case.

The weakness of the second substorm expansion cannot be explained by the absence of magnetic field energy stored in the magnetotail. The fact that, during the intense large-scale convection prior to the onset, the auroral oval is expanding together with the equatorward moving high-energy particle arc, confirms the idea of growing tail current intensity during the growth phase. Also the estimates of energy balance made by Pellinen et al. (1982) support this view. One possible explanation is that the substorm is triggered by an external influence at the moment when the magnetotail conditions are far from the threshold of a large-scale instability. This may lead to a current instability in a localized region of the plasma sheet but not to a large-scale process in which most of the stored energy is released. Northward turning of the IMF seems to be the reason for the external influence (Fig. 4, see also Pellinen et al. 1982).

Caan et al. (1977) have studied the association of substorm expansions with the northward turning of the IMF. The results obtained by Caan et al. are confirmed in a more detailed study by Dmitrieva and Sergeev (in press 1983) which shows that IMF reversals, brief northward excursions, and fluctuations are effective in substorm triggering. Dmitrieva and Sergeev (1983) also found a class of spontaneous expansions that started without any simultaneous changes in the IMF or in the dynamic pressure of the solar wind. In events triggered by southward turning of the IMF they found a simple quantitative relationship between the duration of growth phase, τ, and VB_s (V = speed of the

solar wind, and B_s = magnitude of the southward component of the IMF),

$$\tau V B_s \simeq 9 \cdot 10^4 \text{ nT min km s}^{-1}.$$

The constancy of this value can be interpreted as a constant flux of magnetic energy added to the magnetotail, which changes the tail towards the state of marginal instability. In our second substorm $\tau = 30$ min, $V = 500$ km/s, and $B_s = 5$ nT, which means that $\tau V B_s \simeq 7 \cdot 10^4$ nT min km/s, only slightly below the value given above. In the light of this result the previous explanation for the small scale of the expansion is not completely satisfactory.

In our first event the IMF makes sharp southward turnings around the onset times of the two microsubstorms (1730, 1748 UT) (see Table 2 and Fig. 4). This suggests that external influence may play an important role even in these cases. However, it is impossible to make reliable estimates of the propagation delays of these changes between the satellite and the magnetopause, which makes the treatment of the causal relationship rather vague.

In conclusion of this section we suggest that there is no simple relationship between gross-scale variations of convection intensity and substorm processes in the magnetotail. Furthermore, a transition towards enhanced energy dissipation in the tail (expansion phase) is complicated by the influence of short-term variations in the IMF and solar wind parameters.

Conclusions

1) The conditions of the two substorms analyzed in this work differ from a typical substorm. The first one is associated with a prolonged, stable and intense convection during fluctuating IMF. In the second case a convection enhancement is initiated by a southward turning of the IMF at the beginning of substorm growth phase. Based on these observations we infer that the intensity of convection itself does not define conclusively the state of the magnetotail (steady or non-steady). Therefore the AE and DR indices may be misleading in determing the substorm phases. Our second event supports this view: the substorm expansion that follows after the intense convection during the growth phase, is weak, short-lived and localized.

2) In spite of the uncommon nature of the two substorms clear growth and expansion phase signatures can be distinguished in the ground-based data. Before both onsets, a southward moving absorption band is observed. The strength of the forthcoming substorm seems to be correlated to the southernmost location of the absorption band: lower latitudes lead to more intense expansions.

Substorm onsets are followed by bright auroral arcs ("auroral horns") propagating with high speed along the poleward boundary of the pre-existing diffuse auroral band. These arcs are precursors to the auroral bulges coming into the field of view a few minutes later. The appearance of the auroral horn coincides with the magnetic disturbances (bay, Pi2) starting at mid-latitudes. The PiB's in the auroral zone are delayed until the appearance of the auroral bulge.

The auroral structures appearing within or near the bulge are produced by higher energy particles than the auroras farther away from the bulge.

3) The substorms can be divided into separate microsubstorms that seem to have a systematic fine structure. Microsubstorms last for 5–10 min and are separated by quiet periods. Intensifications (fine structure) in each microsubstorm are repeated approximately each 2 min. Both the microsubstorm onsets and intensifications are observed in the auroral zone and mid-latitude Pi2 pulsation data.The three microsubstorms reported here are all associated with rapid variations in the IMF.

4) Mid-latitude Pi2 pulsations are sensitive to changes in the auroral phenomena. Formation of a weak new auroral structure near the auroral bulge causes pulsations of the same amplitudes as a strong brightening of the bulge edge. Since the pulsation recordings are made at distances comparable to the dimensions of the bulge itself it is concluded that a large-scale substorm mechanism has to be responsible for these observations. In principle, this means that the formation of new auroral structures or the brightening of existing ones has to correspond to impulsive field variations in the distant magnetotail.

5) PiB phenomena can be observed only in the MLT sector occupied by active aurora (auroral bulge). The brightening of the most equatorward arc and onset of PiB need not coincide in the auroral zone at substorm onset but, most obviously, there is a one-to-one correspondence between arc brightening and Pi2 pulsations.

Acknowledgements. The magnetic field data of the IMP-8 satellite (Drs N.F. Ness and R.P. Lepping as principal investigators), used in this study, were kindly provided by Dr. J. Vette through WDC-A (Rockets and Satellites) and plotted into the present form by Dr. W. Heikkila. We are grateful to Drs. W. Heikkila, C. Sucksdorff and J. Untiedt for valuable comments and fruitful discussions. We owe thanks to K. Lehto and H. Opgenoorth who treated the all-sky film data. We are indebted to T. Roldugina, M. Holeva, T. Suortti and A. Jokinen for their help in preparation of text and figures. The SMA observations were obtained in cooperation with several Scandinavian institutions and were supported financially by the Deutsche Forschungsgemeinschaft. The work by A.G. Yahnin, R.J. Pellinen, K.U. Kaila, H. Ranta, J. Kangas and O.M. Raspopov was supported financially by the Finnish-Soviet Committee on co-operation in science and technology. The comments and suggestions made by our referees proved to be very valuable during the final prepartion of this paper.

References

Akasofu, S.-I.: Polar and magnetospheric substorms. Dordrecht: D. Reidel, 1968

Akasofu, S.-I: A study of auroral displays photographed from the DMSP-2 satellite and from the Alaska meridian chain of stations. Space Sci. Rev. **16**, 617–725, 1974

Akasofu, S.-I.: Physics of magnetospheric substorms. Dordrecht: D. Reidel, 1977

Akasofu, S.-I.: Energy coupling between the solar wind and magnetosphere. Space Sci. Rev. **28**, 121–190, 1981

Akasofu, S.-I., Kimball, D.S., Meng, C.-I.: The dynamics of the aurora II: westward traveling surges. J. Atmos. Terr. Phys. **27**, 173–187, 1965

Akasofu, S.-I., Perreault, P.D., Yasuhara, F., Meng, C.-I.: Auroral substorms and the interplanetary magnetic field. J. Geophys. Res. **78**, 7490–7508, 1973

Baumjohann, W., Pellinen, R.J., Opgenoorth, H.J., Nielsen, E.: Joint two-dimensional observations of ground magnetic and ionospheric electric fields associated with auroral zone currents: current systems associated with local auroral breakups. Planet. Space Sci **29**, 431–447, 1981

Bösinger, T., Alanko, K., Kangas, J., Opgenoorth, H., Baumjohann, W.: Correlations between PiB type magnetic micropulsations, auroras and equivalent current structures during two isolated substorms. J. Atmos. Terr. Phys. **43**, 933–945, 1981

Caan, M.N., McPherron, R.L., Russel, C.: Characteristics of the association between the interplanetary magnetic field and substorms. J. Geophys. Res. **82**, 4837–4840, 1977

Clauer, C.R., McPherron, R.L.: Mapping the local time – universal time development of magnetospheric substorms using midlatitude magnetic observations. J. Geophys. Res. **79**, 2811–2819, 1974

Dmitrieva, N.P., Sergeev, V.A.: Spontaneous and triggered substorm onsets and duration of substorm growth phase. Geomagn. Aeronom. (in Russian), **22**, in press 1983

Fairfield, D.H., Lepping, R.P., Hones, E.W., Bame, S.J., Asbridge, J.R.: Simultaneous measurements of magnetotail dynamics by IMP spacecraft. J. Geophys. Res. **36**, 1396–1414, 1981

Heacock, R.R.: Two subtypes of type Pi micropulsations. J. Geophys. Res. **72**, 3905–3917, 1967

Hyppönen, M., Pellinen, R.J., Sucksdorff, C., Torniainen, R.: Digital all-sky camera. Finn. Met. Inst., Technical Report No. 9, 26, 1974

Kaila, K.U.: Three-dimensional mapping of the aurora from digitized all-sky pictures. Finn. Met. Inst., Technical Report No. 25, 38, 1981

Kangas, J., Pikkarainen, T., Golikov, Yu., Baransky, L., Troitskaya, V.A., Sterlikova, V.: Bursts of irregular magnetic pulsations during the substorm. J. Geophys. **46**, 237–247, 1979

Kawasaki, K., Rostoker, G.: Auroral motions and magnetic variations associated with the onset of auroral substorms. J. Geophys. Res. **84**, 7113–7122, 1979

Kokubun, S., McPherron, R.L., Russel, C.T.: Triggering of substorms by solar wind discontinuities. J. Geophys. Res. **82**, 74–86, 1977

Küppers, F., Untiedt, J., Baumjohann, W., Lange, K., Jones, A.G.: A two-dimensional magnetometer array for ground-based observations of auroral zone currents during IMS. J. Geophys. **46**, 429–450, 1979

McPherron, R.L., Russel, C.T., Aubry, M.P.: Satellite studies of magnetospheric substorms on August 15, 1968 (9). J. Geophys. Res. **78**, 3131–3147, 1973

McPherron, R.L.: Magnetospheric substorms. Rev. Geophys. Space Phys. **17**, 657–681, 1979

Melnikov, A.O., Khrustchinsky, A.A., Zhulin, I.A., Kornilov, I.A., Lazutin, L.L., Raspopov, O.M., Riedler, V.K., Sakharov, Ya.A., Tagirov, V.R., Treilhou, J.-P.: X-ray burst structure of breakup and Pi2 geomagnetic pulsations. In: "Dynamical processes and structure of auroral magnetosphere (SAMBO experiment)" (in Russian), Ed. Kola Branch Acad. Sci. USSR, Apatity, 28–42, 1978

Oksman, J.: Riometer chain in Finland. Proceedings of the Finnish-American Auroral Workshop. Ed. L. Jalonen and T. Nygren. Sodankylä Geophysical observatory, Report No. 37, 42–48, 1981

Pashin, A.B., Glassmeier, K.H., Baumjohann, W., Raspopov, O.M., Yahnin, A.G., Opgenoorth, H.J., Pellinen, R.J.: Pi2 Magnetic pulsations, auroral break-ups, and the substorm current wedge: a case study. J. Geophys. **51**, 223–233, 1982

Parkhomov, V.A., R.A. Rakhmatulin, S.I. Solovjev and T.N. Polynshkina: The azimuthal drift of PilB source. In: Issledovaniya po geomagnetizmu, aeronomii i fizike Solntsa, Moscow, Nauka, **39**, 33, 1976

Pellinen, R.J., Baumjohann, W., Heikkila, W.J., Sergeev, V.A., Yahnin, A.G., Marklund, G., Melnikov, A.O.: Event study on pre-substorm phases and their relation to the energy coupling between solar wind and magnetosphere. Planet. Space Sci. **30**, 371–388, 1982

Pytte, T., McPherron, R.L., Kokubun, S.: The ground signatures of the expansion phase during multiple-onset substorms. Planet. Space Sci. **24**, 1115–1132, 1976a

Pytte, T., McPherron, R.L., Kivelson, M.G., West, H.I., Hones, E.W.: Multiple-satellite studies of magnetospheric substorm: Radial dynamics of the plasma sheet. J. Geophys. Res. **81**, 5921–5933, 1976b

Pytte, T., Trefall, H., Kremser, G., Tanskanen, P., Riedler, W.: On the morphology of energetic (>30 keV) electron precipitation at the onset of negative magnetic bays. J. Atoms. Terr. Phys. **38**, 757–773, 1976c

Pytte, T., Trefall, H., Kremser, G., Jalonen, L., Riedler, W.: On the morphology of energetic (>30 keV) electron precipitation during the growth phase of magnetospheric substorm. J. Atoms. Terr. Phys. **38**, 739–755, 1976d

Pytte, T., West, H.: Ground-satellite correlations during pre-substorm magnetic field configuration changes and plasma sheet thinning in the near-earth magnetotail. J. Geophys. Res. **83**, 3791–3804, 1978

Pytte, T., McPherron, R.L., Hones, E.W., West, H.I.: Multiple-satellite studies of magnetospheric substorms: Distinction between polar magnetic substorms and convection-driven negative bays. J. Geophys. Res. **83**, 663–679, 1978a

Pytte, T., McPherron, R.L., Kivelson, M.G., Hones, E.W., West, H.I.: Multiple-satellite studies of magnetospheric substorms: Plasma sheet recovery and the poleward leap of auroral zone activity. J. Geophys. Res. **83**, 663–678, 1978b

Ranta, H.: The onset of an auroral absorption substorm. J. Geophys. Res. **83**, 3893–3899, 1978

Ranta, H., Ranta, A., Collis, P.N., Hargreaves, J.K.: Development of the auroral absorption substorm: studies of pre-onset phase and sharp onset using an extensive riometer network. Planet. Space Sci. **29**, 1287–1313, 1981

Roederer, J.G.: Global problems in magnetospheric plasma physics and prospects for their solution. Space Sci. Rev. **21**, 23–72, 1977

Rostoker, G., Akasofu, S.-I., Forster, J., Greenwald, R.A., Kamide, Y., Kawasaki, K., Lui, A.T.Y., McPherron, R.L., Russel, C.T.: Magnetospheric substorms – definitions and signatures. J. Geophys. Res. **85**, 1663–1668, 1980

Saito, T., Sakurai, T., Koyama, Y.: Mechanism of association between Pi2 pulsations and magnetospheric substorm. J. Atmos. Terr. Phys. **38**, 1265–1269, 1976

Sergeev, V.A.: The discrete activations of the magnetosphere during the substorm explosive phase. Proc. of STP Symposium, Sao Paulo, Brazil. Ed. by Brazilian Organizing Committee, v. 2, 22–58, 1974

Sergeev, A.V.: On the state of magnetosphere during prolonged periods of southward oriented IMF, Phys. Solariterr., Potsdam, N 5, 39–50, 1977

Sergeev, V.A.: On the relation between the Birkeland system of field-aligned currents and the geometry of auroral bulge, in "Geomagnetic Research" (in Russian), N 23, 52–58, 1978

Sergeev, V.A.: High resolution correlation between the magnetic field behaviour at 37 R_E distance in the magnetotail plasma sheet and ground phenomena during substorm expansive phase. J. Geophys. **49**, 176–185, 1981

Sergeev, V.A., Yahnin, A.G., Raspopov, O.M.: On the space-time structure of the explosive phase of the microsubstorm, in "Dynamical processes and structure of auroral magnetosphere" (SAMBO experiment) (in Russian). Ed. Kola Branch Acad. Sci. USSR, Apatity, 42–54, 1978

Sergeev, V.A., Yahnin, A.G.: A correspondence of the substorm expansive phase signatures, in "Geomagnetic Research" (in Russian), N 24, 78–89, 1979a

Sergeev, V.A., Yahnin, A.G.: The features of auroral bulge expansion. Planet. Space Sci. **27**, 1429–1440, 1979b

Sergeev, V.A., Tsyganenko, N.A.: The Earth's magnetosphere. (in Russian) Moscow: Nauka 1980

Stauning, P., Christiansen, B.: Polar riometer absorption data 1 July–31 December, 1976. Ionlab Report, R-49, 1978

Tsyganenko, N.A.: The subroutines and tables for the calculation of geomagnetic field. WDC-B report, Moscow, 1979

Vorobjev, V.G., Rezhenov, B.V.: Progressive westward displacements of the region of the auroral substorm localization in

conjunction with impulsive variations of the magnetic field. Inst. Ass. Geomag. Aeron. Bull. **34**, 441–449, 1973

Wedeken, U., Hillebrand, O., Krenzien, E., Ranta, A., Ranta, H., Voelker, H.: Cosmic noise absorption events and magnetic pulsation activity during substorms. J. Geophys. Res. **46**, 249–259, 1979

Wiens, R.G., Rostoker, G.: Characteristics of the development of the westward electrojet during the expansive phase of the magnetospheric substorms. J. Geophys. Res. **80**, 2109–2128, 1975

Zhulin, I.A., Lazutin, L.L., Riedler, W.K. et al.: Experiment SAMBO-76, in "Dynamical processes and structure of the auroral magnetosphere" (in Russian). Ed. Kola Branch Acad. Sci., USSR, Apatity, 3–24, 1978

Received May 17, 1982; Revised version March 15 and May 10, 1983
Accepted May 20, 1983

J Geophys (1983) 53:198–200

Journal of Geophysics

Short Communication

Experimental Data on Electric Field and Electron Density Dependence of Auroral E-Region Drift Turbulence and Radar Backscatter

M.V. Uspensky[1], W. Baumjohann[2,3], R.J. Pellinen[4], and G.V. Starkov[1]

[1] Polar Geophysical Institute, Vladimirskaya 17, 183023 Murmansk, USSR
[2] Institut für Geophysik der Universität Münster, D-4400 Münster, Federal Republic of Germany (former address)
[3] MPI für Physik und Astrophysik, Institut für extraterrestrische Physik, D-8046 Garching, Federal Republic of Germany (present address)
[4] Finnish Meteorological Institute, Division of Geomagnetism, SF-00101, Helsinki 10, Finland

Key words: Radar aurora amplitude – Electron density

Introduction

Haldoupis et al. (1982), Uspensky et al. (1983) and Starkov et al. (1983) have recently found that the 140 MHz backscatter amplitude in the auroral ionosphere depends mainly on the mean electron density (height-integrated conductivity) in the *E*-layer. A similar relationship for the 46 MHz band was also found by Leinonen et al. (in press 1983). In principle, this can be explained by only a slight dependence of the relative level of *E*-region drift turbulence $<(\Delta N/N)^2>$ in the auroral ionosphere on ionospheric parameters, viz. electric field and mean electron density.

However, up to now, quantitative evidence for such a backscatter amplitude – electron density relationship is restricted to the few events which have so far been analyzed. Therefore, the aim of this short note is to add some more data to that data set. Furthermore, we will compare measurements made in the evening and morning sectors, where the conditions for irregularity excitation might be different.

Electron Density Fluctuations

The volume cross-section in the Born approximation, which is a quantitative measure of the auroral backscatter, is a function of the relative level of the ionospheric wave tubulence due to the Farley-Bunemann and gradient drift instabilities (Fejer and Kelley, 1980). The wave turbulence equals the mean fractional electron density fluctuations $<(\Delta N/N)^2>$ or – which is the same – the level of the ionospheric drift turbulence. Using the turbulence level the backscatter cross-section equation can be written:

$$\sigma_v(k) = 32\pi^4 r_e^2 N^2 <(\Delta N/N)^2> f(k) \qquad (1)$$

where k is the wave number, $f(k)$ the fluctuation power spectra, $\iiint f(k) d^3k = 1$ and r_e is the classical electron radius.

Let us consider here $f(k)$ as a stable statistical function of its parameters, viz. aspect angle, azimuth or propagation angle (André, 1980) and wave number (Chestnut, 1968). Then one can study the behaviour of the ionospheric turbulence level by utilizing radar backscatter data

$$<(\Delta N/N)^2>^{1/2} \sim \sqrt{\sigma_v}/N \qquad (2)$$

if one knows the mean electron density N in the backscatter region.

To solve Eq. (2) Uspensky et al. (1983) substituted N by the height-integrated Hall conductivity Σ_H. The latter was derived by dividing the upward continued external magnetic field (calculated from the Scandinavian Magnetometer Array data; Küppers et al., 1979) by the ionospheric electric field from the STARE measurements (Greenwald et al., 1978). The same method is used in the present paper. The backscatter amplitude used is that measured by the Finland STARE radar corrected for aspect and azimuth angle and slant range dependence.

Data from Morning and Evening Sectors

We will show data for two intervals: 15 March 1978, 0100-0119 UT (morning sector) and 16 March 1978, 1800-1814 UT (evening sector). A full geophysical description of these events can be found in Uspensky et al. (1982, 1983), but we should note that both events occur during pre-substorm and thus relatively smooth and stable ionospheric conditions.

Figure 1 shows two histograms for the ionospheric electron density turbulence as a function of electric field amplitude in the morning and evening sectors. These histograms were constructed from STARE electric field and backscatter amplitudes averaged over a four point meridional strip running along the x-axis of the Kiruna coordinate system (Küppers et al., 1979). The mean longitude of this strip is 19 °E and the longitudinal range covers 2°. The backscatter amplitudes have been corrected for the 7.5 dB/deg aspect angle anisotropy and slant range dependence. The aspect angle changes along the strip equally for morning and evening events from 0° to 0.6°. The average azimuth angle is always close to 90°. However, the data have still been corrected for azimuth angle dependence by using Eq. (2) of Starkov et al. (1983).

From Fig. 1 one can easily see that there is no strong dependence of ionospheric electron density turbulence on electric field amplitude and that there is at least no simple

Offprint requests to: W. Baumjohann

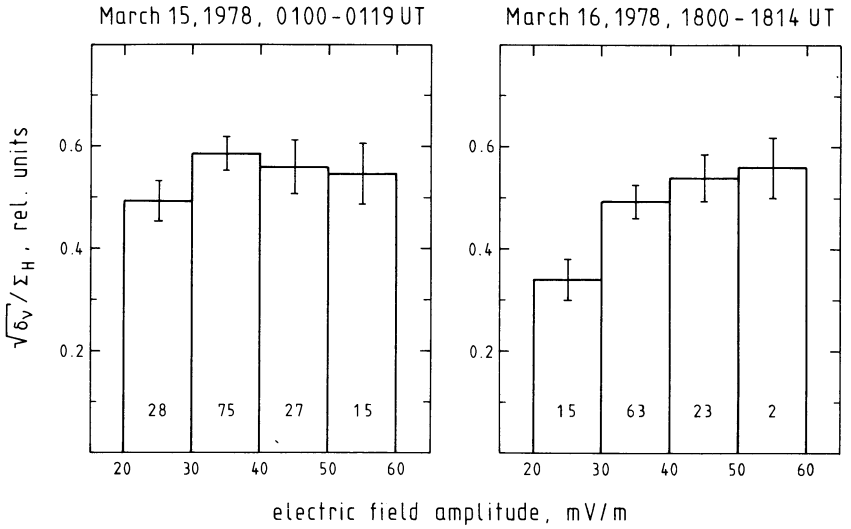

Fig. 1. Corrected STARE backscatter amplitudes from the Finland radar normalized by the height-integrated Hall conductivities as a function of electric field amplitude for the two events discussed. The bars give standard deviations and the numbers in the histogram boxes give the number of associated data samples

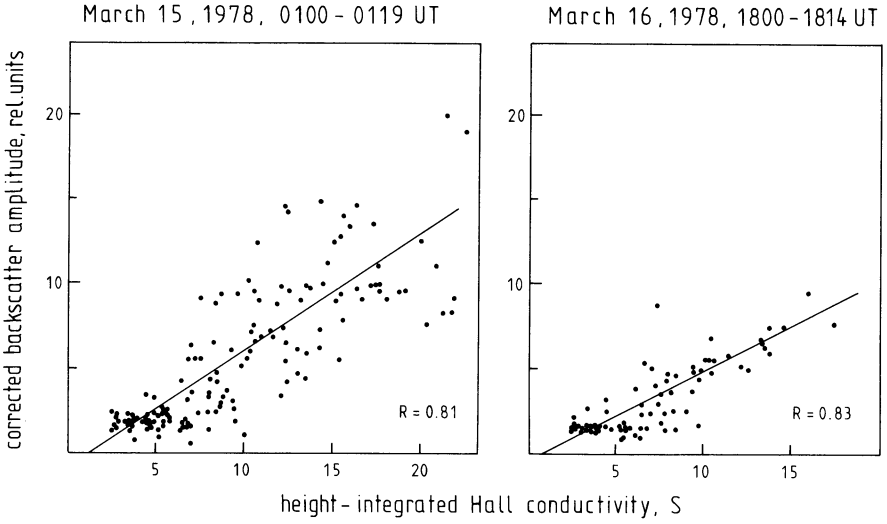

Fig. 2. Corrected Finland STARE backscatter amplitudes as a function of the height-integrated Hall conductivities. The heavy line gives the linear regression line. Note that both data sets exhibit a conductivity/electron density threshold for radar backscatter of about 1 S/0.25·10^5 cm^{-3}

linear relationship between those two quantities. For both events there is a saturation of the turbulence when the electric field amplitude reaches 30–40 mV/m. Note that the saturation level is approximately the same in the morning and evening ionopshere.

Note further, that the independence and saturation of the *E* region turbulence becomes even more pronounced if we take into account the recent findings by Nielsen and Schlegel (in press 1983). These authors found that the electric fields estimated from the STARE data are increasingly too low when the real ionospheric electric field exceeds 35 mV/m.

Figure 2 gives a scatter diagram of the STARE backscatter amplitudes as a function of height-integrated Hall conductivities (the latter being averaged in a similar way to the STARE quantities). In spite of some scatter there is a clear linear dependence of the backscatter amplitude on the height-integrated Hall conductivity and thus mean electron density with a correlation coefficient of about 0.8. The regression lines have very similar slopes for both morning and evening sector events. Both data sets also exhibit a similar electron density threshold (about $0.25 \cdot 10^5$ cm^{-3} for the regression line crossing the abscissa and $0.5 \cdot 10^5$ cm^{-3} for the existence of radar backscatter). A similar threshold was found earlier by Tsunoda and Presnell (1976) for 398 MHz backscatter data ($0.5 \cdot 10^5$ cm^{-3}). We believe that these electron density thresholds are an inherent property for the *E* region Farley-Buneman turbulence.

In conclusion our results confirm that the recently observed (nearly) linear relationship between backscatter amplitude and mean electron density, as well as the independence of the fractional electron density variations from the electric field magnitude (Haldoupis et al., 1982; Uspensky et al., 1983; Starkov et al., 1983; Leinonen et al., in press 1983) hold both in the evening and morning sector ionosphere. This is also supported by the linear relationship found earlier between radar amplitude and ionospheric current density (e.g. Greenwald et al., 1975; Siren et al., 1977; Baumjohann et al., 1978; Mareschal et al., 1979) which is apparently a special case of the more common linear relationship between radar amplitude and mean electron density in the backscattering region.

Acknowledgements. The authors are indepted to Drs. R.A. Greenwald and E. Nielsen for the STARE data. This work was financially supported by the Deutsche Forschungsgemeinschaft (W.B.) and the Finnish-Soviet Committee on cooperation in science and technology (M.U., R.P., G.S.).

References

André, D.: Radarmessungen von Plasmawellen in der polaren Ionosphäre. Dissertation Math.-Naturwiss. Fak., Georg-August-Universität, Göttingen, 1980

Baumjohann, W., Greenwald, R.A., Küppers, F.: Joint magnetometer array and radar backscatter observations of auroral currents in Northern Scandinavia. J. Geophys. **44**, 373–383, 1978

Chestnut, W.: Low frequency waves and irregularities in the auroral ionosphere as determined by radar measurements. In: Low frequency waves and irregularities in the ionosphere, N. D'Angelo, ed.: pp. 173–191. Dordrecht: D. Reidel 1968

Fejer, B.G., Kelley, M.C.: Ionospheric irregularities. Rev. Geophys. Space Phys. **18**, 401–454, 1980

Greenwald, R.A., Ecklund, W.L., Balsley, B.B.: Radar observations of auroral currents. J. Geophys. Res. **80**, 3635–3641, 1975

Greenwald, R.A., Weiss, W., Nielsen, E., Thomson, N.F.: STARE: A new radar auroral backscatter experiment in northern Scandinavia. Radio Sci. **13**, 1021–1039, 1978

Haldoupis, C., Nielsen, E., Goertz, C.K.: Experimental evidence on the dependence of 140-Megahertz radar auroral backscatter characteristics on ionospheric conductivity. J. Geophys. Res. **87**, 7666–7670, 1982

Küppers, F., Untiedt, J., Baumjohann, W., Lange, K., Jones, A.G.: A two-dimensional magnetometer array for ground-based observations of auroral zone electric currents during the International Magnetospheric Study (IMS). J. Geophys. **46**, 429–450, 1979

Leinonen, J., Kangas, J., Kustov, A.V., Stepanov, G.S., Uspensky, M.V.: PiC magnetic pulsations and variations of ionospheric electric field and conductivity. J. Atmos. Terr. Phys. **45**, in press 1983

Mareschal, M., McDiarmid, D.R., McNamara, A.G.: Some properties of diffuse radio aurora at high aspect angles. J. Geophys. Res. **84**, 6687–6690, 1979

Nielsen, E., Schlegel, K.: A first comparison of Stare and Eiscat electron drift velocity measurements. J. Geophys. Res. **88**, in press 1983

Siren, J.C., Doupnik, J.R., Ecklund, W.L.: A comparison of auroral currents measured by the Chatanika radar with 50 MHz backscatter observed from Anchorage. J. Geophys. Res. **82**, 3577–3584, 1977

Starkov, G.V., Oksman, J., Uspensky, M.V., Kustov, A.V.: On the dependence of radar amplitude on ionospheric electron density. J. Geophys. **52**, 49–52, 1983

Tsunoda, R.T., Presnell, R.I.: On a threshold electric field associated with the 398-MHz diffuse radar aurora. J. Geophys. Res. **81**, 88–96, 1976

Uspensky, M.V., Greenwald, R.A., Kaila, K., Kustov, A.V., Pellinen, R.R., Pudovkina, E.V., Raspopov, O.M., Starkov, G.V.: Eastward motion of radar aurora and auroral loops in the morning sector. In: Studies of the high-latitude ionosphere and magnetosphere, O.M. Raspopov, ed.: pp. 41–55. Leningrad: Nauka 1982 (in Russian)

Uspensky, M.V., Pellinen, R.J., Baumjohann, W., Starkov, G.V., Nielsen, E., Sofko, G., Kaila, K.U.: Spatial variations of ionospheric conductivity and radar auroral amplitude in the eastward electrojet region during pre-substorm conditions. J. Geophys. **52**, 40–48, 1983

Received March 18, 1983; Revised version June 1, 1983
Accepted June 1, 1983

J Geophys (1983) 53:201–202

Journal of Geophysics

Letter to the Editor

Comments on "On the Thermal State of the Earth's Mantle" by A.C. Fowler

U. Christensen
Institut für Meteorologie und Geophysik, Feldbergstrasse 47, 6000 Frankfurt 1,
and Max-Planck-Institut für Chemie, Saarstrasse 23, 6500 Mainz, Federal Republic of Germany

In this paper A.C. Fowler deals with convective systems with strongly temperature- and pressure-dependent viscosity and an isoviscous gradient which is steeper than the adiabatic temperature gradient, as it is thought to apply to the Earth's mantle. His suggestion is that below a certain depth the temperature gradient switches from adiabatic to essentially isoviscous and superadiabatic. This seems to be a reasonable possibility in a general context provided the convective system has sufficient depth-extent. However, the proposition that it happens at the boundary between upper and lower mantle in the Earth and requires a lower mantle viscosity of about 10^{22} Poise is untenable. In the following I shall indicate several of the weak points and supply an additional argument why the conclusion is wrong.

(1) Although the author discusses this point at some length it is not clear how he can choose a depth range of $d=700$ km for calculating $\delta^2=\kappa\cdot l/U\cdot d^2$ (Eq. 2.8), while he wants to find out about the convective state of the whole or lower mantle. The reason that the obvious choice $d=$ 3000 km does not lead to the desired result is not very convincing. If some form of layered convection is expected due to chemical or viscosity stratification or any other reason one might apply $d=700$ km, but only to draw conclusions concerning the properties of convection in the upper layer. The ratio of $|q|$ versus δ^2 (Eq. 2.22) measures the relative importance of advective versus conductive heat transport, which depends critically on the length scale over which this transport has to take place. When it is taken for granted that at 700 km depth in the mantle the (scaled) velocity has dropped to that value of δ^2 which is calculated from $d=700$ km, then advection is still the dominant process for scales in excess of this value, i.e. for whole or lower mantle dimensions. Concerning the thermal state of the *whole* mantle the 'obvious choice' for d is the only appropriate one, irrespective of the convective style which eventually emerges.

(2) Essential to the whole analysis is the assumption 2.21, namely that the local velocity is inversely proportional to the local viscosity in different parts of the convective system – at least on an order-of-magnitude scale. This appears reasonable at first but it does not seem to hold for convection. The author's arguments in defence of this relation are not conclusive. Stress and vorticity are confused. These quantities behave very differently – especially in a variable viscosity fluid. Unlike vorticity stress is not distributed via a Poisson's equation and internal stress concentrations (thought to be improbable by Fowler) may in fact occur. If any relation like 2.21 makes sense, one might try with a more relaxed formulation

$$|q|\sim 1/\eta^{\beta}$$

where β has to be determined from numerical or laboratory experiments with variable viscosity. No special emphasis has been laid on this point in the various publications, however, a re-analysis of the available data suggests that the dependence is rather weak. For convection with layered viscosity at the marginal stability state (Davies, 1977) a velocity difference of one order of magnitude relates to a viscosity contrast of 10^4. In a model with temperature-dependent viscosity (McKenzie, 1977) the typical difference in velocity is at most a factor of two between regions with a viscosity contrast of more than an order of magnitude. In Torrance and Turcotte's model (1971) with p,T-controlled rheology a change of one order of magnitude in velocity seems to relate to two orders of magnitude in viscosity (as far as can be deduced from the packing of stream lines in their figures), suggesting $\beta\simeq 0.5$. In a re-examination of a variety of models with variable and partially non-Newtonian rheology (Christensen, 1983) regarding this point, I find the range for β to be 0.3–0.6. Although a comprehensive study of the q versus η dependence is missing, it seems that Fowler's assumption of β equal 1 cannot be the general rule. A lower value of β would imply that larger viscosity and temperature variations can occur within the flow.

(3) In order to arrive at $\eta=O(10^{22}\mathrm{P})$ for the lower mantle (when accepting the rest of the analysis) one has to start out with an asthenospheric minimum viscosity of 10^{20} Poise as that value which controls the plate- or scaling-velocity of 5 cm/a. The analysis of plate-driving forces shows that there is hardly any viscous drag at the bottom of a plate (e.g. Forsyth and Uyeda, 1975; Davies, 1978). This implies that the asthenospheric viscosity is fairly irrelevant for the velocity of the plate, which is thought to be controlled by localized forces like 'trench resistance'. The asthenospheric viscosity is therefore only a lower bound to that value which can be related to the chosen scaling velocity. The higher this value is the higher also becomes the lower mantle viscosity.

(4) Fowler's proposed model has a lower mantle which is superadiabatic by about 0.2 K/km and has a viscosity of $O(10^{22}\mathrm{P})$. With these and some other standard values ($\alpha=1$–$3\cdot10^{-5}\ \mathrm{K}^{-1}$, $\kappa=1$–$2\cdot10^{-6}\ \mathrm{m}^2\ \mathrm{s}^{-1}$, $d=2000$ km) one calculates the local Rayleigh-number for the subsystem of the lower mantle

$$Ra = \frac{\alpha g \rho d^4 \partial T/\partial z}{\kappa \eta}$$

to be of the order of 10^6, suggesting that this layering is highly unstable. It is true that supercritical Rayleigh-number alone is not sufficient since the lower mantle is embedded into the larger circulation which might suppress local instability – although this seems hard to believe with the local Rayleigh-number being 1000 times supercritical. I suggest, as a reasonable stability criterion, a comparison of the characteristic time for the large-scale flow to pass once through the lower mantle with the (*e*-folding) growth-time of a disturbance. The former is estimated with the velocity of 1 mm/a assumed by the author to be in excess of 1 Ga, while the latter can be estimated from linearized theory for an aspect-ratio-one disturbance in a constant-viscosity fluid with stress free boundaries:

$$\tau = \frac{d^2}{\kappa} \frac{4\pi^2}{(Ra - Ra_c)}.$$

Using the previous data one arrives at τ less than 10 Ma. Even when it is taken into account that the viscosity in the lower mantle is not entirely constant but is bounded by 10^{21} and 10^{23}Poise and that the upper bound rather than the average might control the growth time, τ is still much lower than 1 Ga. Therefore it seems impossible that the proposed temperature- and viscosity distribution exists for any sufficient length of time (after having once been established). This defeats Fowler's thesis independently from the other criticism.

Both the more realistic lower value for δ^2 (point 1 of this discussion) and the weak dependence of velocity on local viscosity (point 2) widen the range of permissible viscosity and temperature variations in a convecting mantle. I recently showed (Christensen 1983) that convection in a power-law fluid with stress exponent 3 can be represented by Newtonian convection with activation energy and volume reduced by a factor of one half or less. If this applies to the mantle, the band of permissible temperatures around an isoviscous profile has to be doubled once more. In this light it appears very doubtful that the breakdown of the convective regime proposed by Fowler ever occurs in an essentially adiabatic mantle above the core mantle boundary.

References

Christensen, U.: Convection in a variable viscosity fluid: Newtonian versus power-law rheology. Earth Planet. Sci. Lett. **64**, 153–162, 1983

Davies, G.F.: Whole mantle convection and plate tectonics. Geophys. J.R. Astron. Soc. **49**, 459–486, 1977

Davies, G.F.: The role of boundary friction, basal shear stress, and deep mantle convection in plate tectonics. Geophys. Res. Lett. **5**, 161–164, 1978

Forsyth, D., Uyeda, S.: On the relative importance of the driving forces of plate motion. Geophys. J.R. Astron. Soc. **43**, 163–200, 1975

Fowler, A.C.: On the thermal state of the earth's mantle. J. Geophys. **53**, 1983

McKenzie, D.P.: Surface deformation, gravity and convection. Geophys. J.R. Astron. Soc. **48**, 211–238, 1977

Torrance, K.E., Turcotte, D.L.: Thermal convection with large viscosity variations. J. Fluid Mech. **47**, 113–125, 1971

Received February 4, 1983; Accepted February 6, 1983

J Geophys (1983) 53:203–205

Journal of Geophysics

Reply

A.C. Fowler
Department of Mathematics, Massachusetts Institute of Technology, Cambridge, MA 02139, USA

At the outset, let me note that Dr. Christensen is willing to accept the *idea* of a superadiabatic lower mantle, and, since the expression of the idea was the main point of my paper, I might let the issue rest there. However, Dr. Christensen claims that even if the idea could *in principle* be valid, it is inapplicable to the Earth, as the numbers do not come out right. To an extent, this contention must remain a matter of interpretation, since my argument is (necessarily, at this stage) only a semi-quantitative one. On the other hand, I actually think that each of the four arguments he advances against my conclusions is wrong and insupportable, and so I will here try to elaborate why I think this to be so.

(1) The Depth Scale

At issue is the choice of an "upper mantle" depth scale $d_u (= 700\,\text{km}$, say) rather than a "lower mantle" scale $d_l (= 3{,}000\,\text{km}$, say). The choice of $d_u = 700\,\text{km}$ (or 500 km or 1,000 km) is actually not made because it "[leads] to the desired result", but because of other considerations (Fowler, 1982a, b) which suggested that an upper mantle vigorous convection was more likely; but in fact, it is clear from the argument in my paper (Fowler, 1983), and its conclusion, that the natural depth scale turns out to be d_u, where d_u is the depth at which the 'switch' from adiabatic to isoviscous is supposed to take place.

However, the clearest rebuttal may be to do as Dr. Christensen asks, and scale the vertical coordinate with $d_l \approx 3{,}000\,\text{km}$. With reference to Fowler (1983), we will denote the corresponding $\delta = \delta_l$, etc. Now let us proceed with the argument of the paper. Since $\delta_l \lesssim \delta_u$ (δ_u computed using a putative d_u), we still have an adiabatic sub-lithospheric temperature $\theta \approx \theta_{\text{ad}}$ (given by (2.18) of Fowler, 1983), and corresponding $\eta \approx \eta_{\text{ad}}$. Accepting (for the moment) that $|\mathbf{q}| \sim 1/\eta$ (see point (2) below), then the transition depth from adiabatic to isoviscous will be at a *dimensionless* (with d_l) depth such that

$$\eta_{\text{ad}} = \exp\left[\frac{1+\mu p-\theta_{\text{ad}}}{\varepsilon\theta_{\text{ad}}}\right] \sim \frac{1}{\delta_l^2}, \tag{1}$$

where

$$\theta_{\text{ad}} = \exp\left[\int_0^p D(p)\,dp\right] \approx 1 + Dp \tag{2}$$

for constant D and small enough p (this does not affect the argument); this can be adequately approximated by

$$(\mu - D)\,p \sim 2\varepsilon \ln\frac{1}{\delta_l}, \tag{3}$$

for ε small enough (as is being assumed, i.e. $\varepsilon \to 0$). If we assume rather that $|\mathbf{q}| \sim 1/\eta^b$ (e.g. $b \leqq 1$), then (3) is

$$(\mu - D)\,p \sim \frac{2}{b}\varepsilon \ln\frac{1}{\delta_l}. \tag{4}$$

It is instructive to write (4) dimensionally, denoting the value of the depth determined by (4) as d_u. Then (2.5), (2.8), (2.9) and (2.10) of Fowler (1983), together with a lithostatic pressure, lead to

$$\frac{d_u}{d_l} \sim \frac{2\varepsilon}{b}\left[\frac{d_l}{d_1}\right]^{-1} \ln\left[\frac{d_l}{d_2}\right], \tag{5}$$

where

$$d_1 = \left[\frac{\rho_0 g V^*}{E^*} - \frac{\alpha g}{c_p}\right]^{-1},$$
$$d_2 = (\kappa l/U)^{\frac{1}{2}}; \tag{6}$$

for the Earth, we compute $d_1 \approx 2{,}300\,\text{km}$, $d_2 \approx 50\,\text{km}$, with usual parameters. If we assume (as the problem suggests) $d_l \gg d_2$, $d_l \sim d_1$, $\varepsilon \ll 1$, then (5) implies that firstly $d_u < d_l$, and in addition for *larger* d_l, d_u/d_l actually *decreases*. This is true for mantle-type values of $\varepsilon \lesssim 1/20$, $d_l \approx d_1$, $d_l/d_2 \approx 60$, and remains so even if we take $b \approx 1/2$, as recommended by Dr. Christensen (see point (2)). But if $d_u < d_l$, in particular if $d_u \ll d_l$, then since this will imply a restriction of vigorous convection to a shallow depth range $\lesssim d_u$, it means that d_u *is* the correct scale for isolating the adiabatic-isoviscous transition.

The subsequent argument in my paper is essentially a *reductio ad absurdum*, and I cannot offhand see any logical fault in it. Dr. Christensen's further comment is that if $|\mathbf{q}| \sim \delta^2$ at the transition zone (this is δ_u^2), then advection must dominate in the lower mantle, since *its* relevant (dimensionless) depth scale is $y \sim \delta_u/\delta_l$ (compared to the upper mantle): i.e., in the lower mantle one should write

$$y = (\delta_u/\delta_l)\,y^*, \qquad \mathbf{q} = \delta_u^2 \mathbf{q}^*, \tag{7}$$

leading to

$$\mathbf{q}^* \cdot \nabla\theta \ldots = (\delta_l/\delta_u)^2 \nabla^2 \theta, \tag{8}$$

so that adiabaticity is still assumed (since $\delta_l \ll \delta_u$); however this is not the appropriate conclusion: rather, one concludes that (7) is inappropriate for the lower mantle, and some other scaling is relevant. My argument is that once $|\mathbf{q}|$ *gets* to $O(\delta_u^2)$, adiabaticity is no longer guaranteed, and the rest of the argument consists of looking at Fig. 1: I do not offer any precise scaling appropriate to the lower mantle. This was why I considered the *model* problem (3.5), in order to try and understand what the equations could mean in an isoviscous régime.

(2) Velocity-Viscosity Relation

The point at issue here is whether $|\mathbf{q}| \sim 1/\eta^b$ as η increases, with $b=1$ (my assumption), or $b<1$. The outcome does not affect the argument, but only its quantitative interpretation, particularly if one feels constrained by independent mantle viscosity estimates (e.g. Cathles, 1975). Dr. Christensen contends that my 'arguments to defend this relation [that $b=1$] are not conclusive'. On the contrary, I hardly need to defend it, since it is explicitly written in the constitutive relation, particularly in its lubrication theory form (as is *a posteriori* relevant here, for shallow aspect ratio flows). Rather, if $b<1$, one would need sound numerical evidence to establish any other *asymptotic* value of b, and even then some convolved theoretical argument to explain it.

But such numerical evidence as there is does not lend itself to any *quantitative* relation about a purported value of b, beyond the general premise that $|\mathbf{q}|$ generally decreases with η. McKenzie's (1977) results treat a highest viscosity contrast of 110, in an order-one aspect ratio; Torrance and Turcotte's (1971) results are also for an order-one aspect ratio, free slip boundary conditions; Davies' (1977) model is of *marginally* unstable *linear* modes in a *piecewise discontinuous* viscous model. I might accept qualitative indications from these papers (e.g. the appearance of stagnant zones in Torrance and Turcotte's results): but it is hardly realistic to take any quantitative conclusions from them. I might even quote Davies (1977) in my own favour: although a viscosity contrast of 10^4 gives very little velocity contrast, a contrast of 10^5 gives a totally stagnant 'lower mantle'! But the result is simply not quantitatively relevant in the present context. Concerning Dr. Christensen's own recently obtained results, I am unable to comment; in view of his other adduced 'evidence', however, I am for the moment inclined to remain skeptical.

As for stress and vorticity, the stress generated by thermal plumes in high Rayleigh number constant viscosity convection is actually equal to the (viscosity times the) vorticity (Roberts, 1979). I am well aware what stress and vorticity are. Dr. Christensen suggests internal stress concentrations "may in fact occur". Since internal (in a steady state) means away from plumes (upwellings, downwellings) and thermal (top and bottom) boundary layers, I am enthusiastic to hear how he is going to do this.

(3) Asthenospheric Viscosity

The choice of a controlling function for asthenospheric viscosity is actually made on the basis of a separate analysis (Fowler, 1982b), but in the present context it is clear that it is the appropriate self-consistent choice of viscosity scale. I do not say that the plate *velocity* is controlled by the asthenospheric viscosity (see Eq. (2.14a) and preceding discussion), but in view of the purported nature of the flow, one needs substantial return flow in the upper mantle. This requires the balance (2.12) or (2.20), so that one can have $\int_0^{d_u} u\,dz \approx 0$, thus conserving mass. The *shear rate* is controlled by the asthenospheric viscosity. The plate-driving analyses of Forsyth and Uyeda (1975) and Davies (1978) are *kinematic* discussions of plate forces, with nothing to say about sub-lithospheric dynamics; they are not of relevance in the present context.

(4) Lower Mantle Instability

At issue here is whether the proposed super-adiabatic lower mantle is unstable, not in a normal dynamic sense (e.g. boundary layer plumes, or oscillatory instabilities which do not alter the *basic* structure), but in a catastrophic sense, in the same way (and analogously to the situation) that a conductive temperature profile is catastrophically unstable when the Rayleigh number is large.

Firstly, the Rayleigh number criterion applies to *linear* instability of a motionless, conducting state. Since this does not pertain here, one had better discuss the use of large 'Rayleigh' number somewhat adeptly. This, Dr. Christensen acknowledges. Nevertheless, the use of linear stability theory to analyse a slowly varying basic state can be justified (in principle, by the method of multiple scales: Kevorkian and Cole, 1981) provided the growth or decay time of instability is much faster than the slowly varying time scale: this is called the frozen time hypothesis, and has been used in convection studies by Robinson (1976), amongst others. Unfortunately, Dr. Christensen's linear stability results do not concern the problem at hand: (i) he assumes a constant viscosity *fluid* (exactly what I do not have); (ii) his basic state is one of *no* motion (also exactly what I do not have).

Nevertheless, suppose that in some sense, the result is correct; that is, an infinitesimal disturbance to the lower mantle starts to grow very fast. Let us imagine that this disturbance consists of an initial upward movement of a parcel of fluid which is slightly lighter than its surroundings. If the instability is *fast*, then the parcel's temperature changes adiabatically. Correspondingly, its viscosity changes 'adiabatically', and consultation of Fig. 1 in Fowler (1983) reveals that its viscosity increases rapidly and exponentially, whereas the driving stress (the excess buoyancy compared to its surroundings) increases slowly and linearly. Viscosity wins, and the parcel velocity becomes quickly limited. In fact it becomes limited to a value such that the viscosity stays roughly constant. In other words, I am suggesting that any purported rapid linear instability that *might* occur is effectively limited at small finite

amplitude by the temperature dependence of viscosity, and in fact that this amplitude is just that which I in any case propose that the lower mantle should have. A similar case of effective stability appears in the glaciological context (Fowler and Larson, 1980), where it is computed explicitly.

The discussion above is certainly no proof, but it does at least consider the problem in its correct physical context. I would not claim that the lower mantle *is* necessarily stable, but Dr. Christensen's claim that this argument 'defeats [my] thesis' is an inflated one.

Much of my viewpoint, as expressed above, is based on the notion that the ideas are self-consistent, and 'hang together'. To a geophysicist, this may seem a circular way of reasoning, but anybody who is at all familiar with the methods of singular perturbation theory will recognise this self-consistency as the hallmark of the procedure, and a sign that it 'works'. I would not guarantee that the proposed geotherm is necessarily of the correct form, and there are certainly problems (the 'how do you get the heat out of the core?' question may be one), but I haven't been able to find anything better, which is itself not in contradiction to the assumed equations describing the flow.

References

Cathles, L.M.: The viscosity of the earth's mantle. Princeton University Press, Princeton, N.J., 1975

Davies, G.F.: Whole mantle convection and plate tectonics. Geophys. J. R. Astron. Soc. **49**, 459–486, 1977

Davies, G.F.: The role of boundary friction, basal shear stress, and deep mantle convection in plate tectonics. Geophys. Res. Lett. **5**, 161–164, 1978

Forsyth, D., Uyeda, S.: On the relative importance of the driving forces of plate motion. Geophys. J. R. Astron. Soc. **43**, 163–200, 1975

Fowler, A.C.: The depth of convection in a fluid with temperature and pressure dependent viscosity. Geophys. Res. Lett. **9**, 816–819, 1982a

Fowler, A.C.: Implications of scaling and nondimensionalisation for the convection of the earth's mantle. Preprint, 1982b, submitted to J. Fluid Mech.

Fowler, A.C.: On the thermal state of the earth's mantle. J. Geophys. **52**, 000–000, 1983

Fowler, A.C., Larson, D.A.: Thermal stability properties of a model of glacier flow. Geophys. J. R. Astron. Soc. **63**, 347–359, 1980

Kevorkian, J., Cole, J.D.: Perturbation methods in applied mathematics. New York: Springer 1981

McKenzie, D.P.: Surface deformation, gravity and convection. Geophys. J. R. Astron. Soc. **48**, 211–238, 1977

Roberts, G.O.: Fast viscous Bénard convection. Geophys. Astrophys. Fluid Dyn. **12**, 235–272, 1979

Robinson, J.L.: Theoretical analysis of convective instability of a growing horizontal thermal boundary layer. Phys. Fluids **19**, 778–791, 1976

Torrance, K.E., Turcotte, D.L.: Thermal convection with large viscosity variations. J. Fluid Mech. **47**, 113–125, 1971

Received May 9, 1983; Accepted May 9, 1983

Book Reviews

Ben-Menahem, A.; Singh, S.J.: Seismic Waves and Sources 1981. 307 figs. XXI, 1108 pages. Berlin-Heidelberg-New York: Springer-Verlag

Seismic Waves and Sources is a profund and comprehensive treatise on the generation and propagation of seismic waves. It has been designed both as a textbook and as a handbook for graduate students and scientists working in seismology and related branches of earth sciences. Evolving from a long-time cooperation between the two authors, it presents the mathematical theory of seismic fields in a self-contained way from basic principles to actual scientific problems.

The material is arranged in ten chapters and a part containing the appendices. Within each chapter the topics are aligned from fundamental problems and basic models to questions of growing complexity and applications to the real earth. Frequently general results are illustrated by worked out examples. Each chapter is followed by a bibliography which however is never complete by far. The reader appreciates the authors' intention to offer a theory which is self-explanatory and does not need support from other sources. Consequently there are almost no references in the text which may sometimes be felt as a deficiency.

Chapter 1 is a short recapitulation of basic facts of continuum mechanics. Special regard is payed to the seismic field equations in lossfree verticaly heterogeneous media.

Chapter 2 recalls the classical solutions of the wave equation in cartesian and orthogonal curvilinear coordinates. Vector spherical harmonics are introduced as the basic eigenvector system of a vector field described in spherical coordinates, and the decomposition of the solution of the vector Helmholtz equation in Hansen vectors is demonstrated by a variety of examples.

Wave interaction with plane discontinuities is the main subject of *Chapter 3*. The reflexion and refraction of body waves, the dispersion of surface waves as a consequence of the heterogeneity of the medium and the spectral response of a multilayered crust to incident body waves from below are investigated. The matrix method is introduced and the inverse problem for surface waves is discussed.

Chapter 4 is of central importance as a basic description of the theory of seismic sources relating the force or the displacement of the source to the displacement, stress and strain at the observation point. The inhomogeneous Navier equation is solved by determining the corresponding Green's dyadic. Many examples of special sources are discussed as illustrations of the general results. Single and dipolar point sources with stress and displacement dislocations are considered. The corresponding displacement fields are expanded in terms of spherical and cylindrical eigenvectors. Extended sources are described by the kinematic source model.

Another highlight for the specialized reader is *Chapter 5* which is devoted to the determination of surface wave amplitudes for a vertically inhomogeneous earth model. The numerical algorithms for the calculation of amplitudes and of phase and group velocities are presented. Terrestrial interferometry evolved from the study of the interference pattern of surface waves caused by the Doppler-effect of a moving source. These earthquake and source radiation studies have been one of Ben-Menahem's important original contributions to seismology.

The free oscillations of the earth are analysed in *Chapter 6*. For different types of sources the oscillations of a homogeneous elastic sphere are determined and the field equations for a radially inhomogeneous self-gravitating sphere are derived. By numerical integration the eigenperiods and spectral amplitudes for different source types are determined. The effects of rotation of the earth and of the time-function and the extension of the source are discussed.

Ray theory as geometric elastodynamic approximation of wave theory is the subject of *Chapter 7*. On the basis of the eikonal equation and the ray amplitude equation applications of ray theory to a radially heterogeneous earth are described. For weakly heterogeneous media asymptotic wave theory with WKBJ-solutions is applied, and the limits of applicability of ray theory for example at a caustic are investigated. The computation of theoretical seismograms is demonstrated and normal mode and ray solutions are compared.

In *Chapter 8* another asymptotic approximation of wave theory is developed, i.e. the representation of body waves and surface waves by normal modes. Asymptotic solutions of the normal mode equations are sought. The ray-mode correspondence is checked for simple earth models. Also the normal mode expansion is used for the computations of diffracted waves in the shadow zone. For a spherical earth model the rainbow expansion of reflection and transmission coefficients is introduced in order to describe the interaction of a spherical wave front with a spherical boundary. With this tool at hand problems involving diffraction and tunneling of waves are solved.

Chapter 9 gives a view on waves generated by explosions and earthquakes which propagate in the earth's hydrosphere and atmosphere, i.e. sound waves, gravity waves, seiches, tsunamis, and atmospheric acoustic-gravity waves. Moreover the generation of elastic surface waves by infrasonic atmospheric waves is considered. For a stratified atmosphere with uniform layers waves generated by a point source are calculated by a matrix formalism similar to the corresponding seismic algorithm. Other subjects are the resonant coupling of atmospheric waves and internal ocean gravity waves and the excitation of Rayleigh waves by atmospheric explosions.

Chapter 10 accounts for anelasticity effects in seismic wave propagation. After a short introduction to the physics of linear anelastic media the three-dimensional propagation of seismic pulses in a slightly attenuating medium is discussed. Consequences of causality regarding dispersion and attenuation are explained. Finally the attenuation of body waves, surface waves, and free oscillations in the earth is discussed.

In the *Appendices* useful functional relations and techniques are described, e.g. generalized functions, special functions, generalized spherical harmonics, asymptotic solution of the Helmholtz equation, calculus of dyadics, etc.

After the publication of Aki's and Richard's »Quantitative Seismology« every textbook on the same subject will naturally be in competition. A comparison shows that in »Seismic Waves and Sources« the theoretical aspects are dominant whereas »Quantitative Seismology« has a broader range of applications. My impression is that »Seismic Waves and Sources« as a basic treatise on theoretical seismology will become a standard tool in seismic research and teaching. Its outstanding importance is a consequence of the fact that the theory is developed from the basic laws and that all results are completely derived in the text.

Sometimes the mathematical formalism is overwhelming and the physics seems to disappear behind a mathematically painted vail. Also, some of the material of the chapters 7 and 8 could have been presented in a different but more logical context. This, however, does not diminish the indisputable value of this book which eventually fills a gap which has painfully been felt in the past.

H. Wilhelm

Structure of transition zone, edited by S. Asano. Advances in Earth and Planetary Sciences, 8. Supplement Issue to Journal of Physics of the Earth. D. Reidel Publishing Company/Dordrecht, Boston, London 1980, 184 pp.

I do not know what you would expect to find in a book with the title "Structure of Transition Zone"? I expected to find everything about the transition from the Upper to the Lower Mantle. I was actually misled: this book is a more or less loose conglomer-

ate of individual contributions to the special transition from the Pacific Plate to the Asian Continent. Why then this quite general title which promisses an even quite general treatment of the problem? The answer will remain a secret to the editor. If you would propose a title like "Structure of a Subduction Zone" in order to avoid confusion with the afore mentioned transition zone then you would probably touch the most delicate problem of this book published in 1980: The hypothesis of plate tectonics (e.g. page 77)! Here you find the USSR point of view mixed with the Western look. Soviet and Japanese authors are mixed, and so are the conclusions they draw from their geophysical measurements. And quite symbolically Big Old Beloussov is watching as one of the authors of the very last contribution all his fellows in front of him.

On page 53 the Japanese author H. Okada begins: "An island arc is one of the most important test field of the plate tectonics hypothesis." He concludes: "The present study will contribute to refinements and modifications of the mechanisms of the subduction and the magma genesis associated with the plate." On page 77 we may read: "We do not consider the focal zone to be a descending lithospheric plate, but we suggest it to be a dipping domain of stress release that occur due to the interaction of the crust-mantle megablocks of Eurasia and Pacific." The author: R.Z. Tarakanov, USSR.

It's typical: Nowhere in this book there is even the slightest attempt to listen and to talk to the "other side". Once while reading the book I had the strong feeling to read ghost stories. Because human stories should contain at least a minimum of community. It is not the difference of geophysical data, what I hope, but it is the difference of looking at the data.

And I became thoughtful because I remembered Heinrich von Kleist: If you look through a red glass the world appears to be red, if you look through a blue glass the world appears to be blue; since we do not know the colour of the glass we are looking through all our life we never will know how the world looks.

Is there no way to distinguish between wright and wrong? There cannot be two truths: I remember the philosopher Karl Popper who argues that any true scientific theory should display that item which would falsify this theory.

What could be the critical point of the theory of plate tectonics or the theory of fixism of the USSR-scientists.

It would have been an interesting frame for this issue, much more justifying this edition than just the existence of the Japan-USSR Scientific Cooperation Program and the existence of extensive research work done by the USSR scientist which has never been published by an English written journal.

The book includes 5 seismological, 3 geophysical and geological, 2 geothermal, 3 geomagnetic and 1 geodetic studies. Some of the contributions are of high quality, some of less. I recommend this book for the library of your institute.

Volker Haak

Electromagnetic induction in the earth and moon, edited by Ulrich Schmucker. Advances in Earth and Planetary Sciences 9. D. Reidel Publishing Company/Dordrecht-Boston-London, 1980, 196 pp.

This book is a non-book, and I can give you no real book review. Actually, it is a supplement issue to the Journal of Geomagnetism and Geoelectricity. This issue contains review papers and contributed papers given during the IAGA Scientific Assembly in Seattle 1977 and during the Workshop of Electromagnetic Induction of the Working Group I-3 in Murnau in Bavaria 1978. The title of this non-book is indeed the denomination of this IAGA working group I-3. The title therefore is also a non-title since it does not specify the content of this issue.

Nevertheless this collection of papers is of very high quality: I recommend it to all thinkers and workers in the field of electromagnetic induction for their private and public library. Why this?

Because the topics of the papers group around two "gravity-centers" of interest, firstly around oceanic induction and conductivity studies and secondly around studies of the upper mantle. Both themes have never been treated so extensively in the past. And since the editor and the authors have treated it so well I must recommend it to all specialists of electromagnetic induction.

What should you know about the content of the book? Of course you should know all titles and all authors since it resembles more a luxurious journal, i.e. a collection of papers, than a book. Instead of it I will tell you just my present favourites and their first author:

C.S. Cox et al.: Atlantic Lithosphere Sounding.

J.H. Filloux: North Pacific Magnetotelluric Experiments.

W.D. Parkinson: Induction by Sq.

J.C. Larsen: Electromagnetic Response Functions from Interrupted and Noisy Data.

A.A. Kovtun et al.: Deep Conductivity Distribution on the Russian Platform from the Results of Combined Magnetotelluric and Global Magnetovariational Data Interpretation.

J. Pěčová et al.: Remarks on spatial Distribution of Long Period Variations in the Geomagnetic Field over European Area.

Of course, at some time later or for somebody else, quite different papers would be favoured, e.g.:

R.C. Hewson-Browne et al.: Induction in Arbitrarily Shaped Oceans II: Edge Correction for the Case of Infinite Conductivity.

B.A. Hobbs et al.: The Effect of a Simple Model of the Pacific Ocean on Sq Variations.

If I would continue in this way, you would learn to know the complete content. However this is not necessary: If you are thinking and working in the wide field of electromagnetic induction then you MUST buy this issue in each case, as well for your private library as well for the Library of your institution.

Volker Haak